An ***IPRF*** Research Report

Innovative Pavement Research Foundation

Airport Concrete Pavement Technology Program

Report IPRF-01-G-002-05-2

JOINT LOAD TRANSFER IN CONCRETE AIRFIELD PAVEMENTS:

FINAL REPORT

Programs Management Office
9450 Bryn Mawr Road
Rosemont, IL 60018

August, 2011

An ***IPRF*** Research Report

Innovative Pavement Research Foundation

Airport Concrete Pavement Technology Program

Report IPRF-01-G-002-05-2

JOINT LOAD TRANSFER IN CONCRETE AIRFIELD PAVEMENTS:

FINAL REPORT

Lead Investigator and Author

Christopher R. Byrum, PhD, PE

Principal Investigators

Starr D. Kohn, PhD, PE (decd)
Chuck A. Gemayel, PE
Shiraz Tayabji, PhD, PE

Contributing Authors
Phillip J. Barton, PE
Dan Ye, PhD, PE
Ray Rollings, PhD, PE
Anastasios, M. Ioannides, PhD, PE
Rohan W. Perera, PhD, PE

Programs Management Office
9450 Bryn Mawr Road
Rosemont, IL 60018

PREFACE

This report has been prepared by the Innovative Pavement Research Foundation (IPRF) under the Airport Concrete Pavement Technology Program. Funding is provided by the Federal Aviation Administration (FAA) under Cooperative Agreement Number 01-G-002. Dr. Satish Agrawal is the Manager of the FAA Airport Technology R&D Branch and the Technical Manager of the Cooperative Agreement. Mr. Jim Lafrenz is the IPRF Cooperative Agreement Program Manager.

The IPRF and the FAA thank the Technical Panel that willingly gave of their expertise and time for the development of this report. They were responsible for the oversight and the technical direction. The names of those individuals on the Technical Panel follow.

Mr. Stan Herrin, P.E.	**Crawford, Murphy, and Tilly, Inc.**
Dr. Wayne Seiler, P.E.	**All About Pavements, Inc.**
Mr. Gary Harvey, P.E.	**Othon, Inc.**
Dr. David Brill, P.E.	**FAA Technical Advisor**

The contents of this report reflect the views of the authors who are responsible for the facts and the accuracy of the data presented within. The contents do not necessarily reflect the official views and policies of the FAA.

ACKNOWLEDGEMENTS

The project team would like to acknowledge the contributions by the staff of the following:

- Federal Aviation Administration
- Airport Authorities that supported the field testing

The contents of this report reflect the views of the authors, who are responsible for the facts and the accuracy of the data presented. The contents do not necessarily reflect the official views and policies of the FAA. This report does not constitute a standard, specification, or regulation.

TABLE OF CONTENTS

LIST OF TABLES

Table **Page**

LIST OF FIGURES

Figure **Page**

ACRONYMS AND ABBREVIATIONS

AC	= Advisory Circular
AC	= Asphalt Concrete
AGG	= Aggregate Interlock
ASTM	= American Society for Testing of Materials
CT	= Cement Treated
DIA	= Denver International Airport
DCI	= Dowel-Concrete Interaction coefficient
DOT	= Department of Transportation
ERDC	= Engineering Research and Development Center
FAA	= Federal Aviation Administration
FAARFIELD	= pavement thickness design software by FAA
FEAFAA	= multi-slab finite element method model by FAA
FEM	= Finite Element Method
FWD	= Falling Weight Deflectometer
GPS3	= General Pavement Study Three for the FHWA LTPP project
ILSL2	= Finite element analysis software by Ioannides et al
ILLIBACK	= slab interior load back-calculation software by Ioannides et al
IPRF	= Innovative Pavement Research Foundation
LEDFAA	= FAA's Layered Elastic Design procedure
LT	= Percent of free-edge stress transferred
LTE	= Load Transfer Efficiency
LTPP	= Long Term Pavement Performance
MEPDG	= Mechanistic-Empirical Pavement Design Guide
NAPTF	= National Airport Testing Facility
PCC	= Portland-Cement Concrete
PCI	= Pavement Condition Index
SCI	= Structural Condition Index
USAF	= United States Air Force
WWII	= World War Two

CHAPTER 1. INTRODUCTION

This research was performed under the Innovative Pavement Research Foundation (IPRF) in cooperation with the Federal Aviation Administration (FAA) as project number IPRF-01-G-002-05-2. The project was initiated in the fall of 2007 and was completed in the summer of 2011. The work was led by Soil and Materials Engineers, Inc. with team members: Chris Byrum (Lead Investigator and Author), Phillip Barton (Lead Field Evaluation Engineer), Starr Kohn (initial Principal Investigator-deceased), Rohan Perera (Pavement Damage Modeling) and Chuck Gemayel (Co-Principal Investigator), in close partnership with Fugro Consultants with team members; Dan Ye (Finite Element Method Structural Analysis) and Shiraz Tayabji (Co-Principal Investigator), and with the technical assistance and guidance of project consultants Ray Rollings and Anastasios Ioannides.

1.1 BACKGROUND INFORMATION

A majority of the heavy duty pavement areas that support large aircraft are constructed with jointed portland-cement concrete (PCC) slabs. This research project is focused on the evaluation of the structural behavior of in-service jointed PCC slabs, in the context of new state of the art structural analysis and pavement thickness design tools being developed by the FAA. The heavy duty airfield concrete slabs evaluated for this study ranged from about 14 to 22 inches in thickness. The large concrete placements for airfield operations areas are significant investments, costly to construct and maintain. These concrete placements typically have a 15-40 year life cycle. Concrete slabs are typically sawed or formed into squares or rectangles having dimensions between about 15 and 30 feet. The behavior of the joints between slabs in terms of their ability to transfer heavy aircraft wheel loads from slab to slab is complex and is the focus of this research.

Historically, the stress reduction effects from structural joints built into concrete pavement slabs have not been directly simulated in structural analysis procedures used for pavement thickness design by the FAA (FAA AC 150/5320 versions 6D and 6E). Instead, simplified "free-edge" loading structural analysis is performed using single-slab models without joints and with loads placed along the un-restrained edge of the slab. These "free-edge" stress analysis results are then empirically calibrated using a long ago established standard 25% stress reduction factor to account for the ability of joints to transfer load and reduce slab bending stress. The 75% of free-edge stress values that come from these procedures are used in empirically calibrated damage algorithms for design of slab thickness for airfield pavements (US Army Corps of Engineers 1946; Parker et al., 1979; Rollings 1989; Brill, 2010).

Although the principles and research behind the existing design methods are sound, the current methodologies without joints are simplified and do not capture some complex slab action and joint behaviors observed in the field. For example, jointed concrete slabs constructed at the National Airfield Pavement Test Facility (NAPTF) developed corner-cracking and top of slab cracking, instead of the slab edge load, bottom of slab cracking traditionally assumed as the basis of design. This top of slab cracking was attributed to unusually large upward warping developing in slabs in the relatively dry zero-precipitation inside environment at the NAPTF test

facility (Guo et al., 2002). Some large variations in joint behavior related to thermal curling and seasonal average slab temperature variation were measured at the Denver International Airport (DIA) instrumented pavement research test site (Rufino et al., 2004). Results from these two test sites and other structural analysis studies provided new measurements and insights that caused the airfield design community to question existing simplified 25% reduction methods and seek a more accurate analysis engine for design methods, ultimately leading to this research project.

Advances in computer speed and structural analysis software, have encouraged FAA to develop modern design methods and pavement analysis software. The modern analysis procedures allow for, and in fact require, detailed simulation of the structural behavior of joints. Current design methods for airfield pavements do not directly account for daily and annual changes in joint behaviors related to temperature variations or traffic related deterioration of joint load transfer ability. A better understanding of how these variations affect stress and strain in heavy duty airfield pavements can be obtained using the modern pavement analysis tools. Naturally, the joint behavior idealizations embedded in these new tools need to be calibrated to behave like real joints. Measurements of real joint responses reveal some complex behaviors, and joint behavior can change significantly over a typical 24-hour slab thermal curling cycle. The calibration of the joint models used in modern pavement analysis tools and the study of real joint behavior, as measured at in-service airfields across the USA was the focus of this research project.

This research was accomplished in part by developing an advanced on-site structural response evaluation procedure including: heavy-weight falling weight deflectometer (FWD) deflection measurements, slab curling analysis using slab end slope measurements, and measuring changes in joint openings, from mid-morning to early-afternoon at each test site. Test procedures were repeated from morning to afternoon to capture daily thermal effects on slab and joint response. This intensive 8-10 hour on-site evaluation procedure is non-destructive and requires no cutting or coring. This mechanistic response evaluation procedure was performed on eleven different heavy-duty airfield test sites spread across different climate zones.

The detailed evaluations of real pavement systems have highlighted some key differences between real joint behavior and how joints have typically been represented in pavement structural analysis routines. Figure 1.1 shows an image of a joint cross section highlighting key aspects of real joint behavior that are not easy to simulate using currently available analysis tools. Once a joint fully cracks, an opening will form as the ends of the slabs pull apart. The purpose of a joint load test is to characterize a fault shaped deformation, as shown. In addition, slabs will typically develop some slight differential settlements, which will cause small vertical offsets to develop between the slabs crack face roughness features. These offsets may not be visible to the eye, but they are visible in load test data obtained from both sides of a joint. In highway slabs, the high speed directional traffic causes enhanced differential settlements and vertical faults can grow to large sizes as vertical grooves are ground into the aggregate interlock crack faces. Vertical faults generally do not become large at airfield sites but the off-set slack still exists, visible as significant differences in joint load test responses for loading on opposing sides of the same joint. Load transfer is typically higher when loading the lower slab. Load transfer is lower when loading the higher slab due to this off-set slack effect. The joint opening size can change dramatically from summer to winter, ranging from completely closed to completely open at sites in regions having large thermal variation. Steel dowel bars and tie bars

are often placed across the joints to resist the off-set slack and differential settlement effects, and keep joints more effective or stiffer during cold weather. Traffic essentially grinds the crack face roughness away over time, and can loosen any dowels or tie bars placed across joints. In general, the joint opening size, the roughness and stiffness of the crack face contact, and the amount and type of steel present across the joint control how load is transferred from slab to slab through the joint.

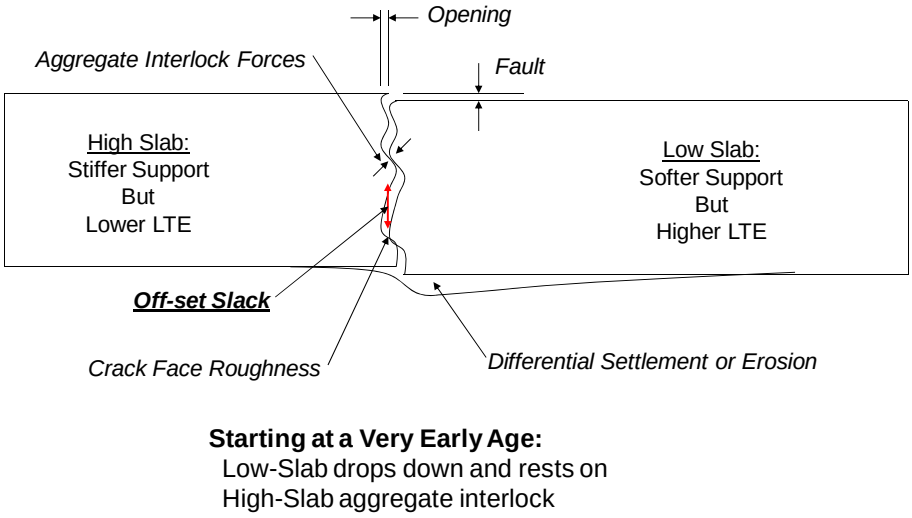

FIGURE 1.1. IMAGE SHOWING KEY ASPECTS OF REAL CONCRETE PAVEMENT JOINT BEHAVIOR THAT ARE DIFFICULT TO ACCOUNT FOR IN JOINT STRUCTURAL BEHAVIOR MODELS; DIFFERENTIAL SETTLEMENT OFF-SET SLACK AND JOINT OPENING EFFECTS

The most important structural analysis concept regarding joint load transfer is the concept of vertical shear stiffness along a line/fault feature. Springs are often used to represent stiffness of a point in space. For example, consider a vertical spring having a 1-Dimensional spring constant, k_{spring}, equal to 100 pounds per inch (lb/in) of vertical displacement. Now arrange a long horizontal line of these individual point vertical springs spaced at 1 inch intervals like small dowel bars along an imaginary joint line. The effective "2-Dimensional Line Stiffness" constant, k_J, for this joint line is 100 pounds per inch of line load per inch of vertical deflection along the line (lb/in/in or psi). This 2-D line stiffness with a unit of pounds per inch of load per inch of deflection is the primary "Joint Stiffness" parameter of interest to this study. Now take many of these lines with 1 inch spring spacing, and space them at 1 inch intervals oriented into a 1-inch horizontal grid pattern, with each vertical spring having 1 square inch of horizontal tributary area on the grid. The magnitude of this "3-Dimensional Area Stiffness" constant is 100 pounds per square inch of tributary area load, per inch of vertical deflection (psi/in). This is the common dense liquid subgrade spring constant well known to pavement engineers often referred to as the modulus of subgrade reaction *k*-value. So, the 1-D, 2-D, and 3-D example stiffness values and units are 100 lb/in, 100 lb/in/in, and 100 lb/in/in/in respectively for the point spring, and the 1 inch spacing line and 1-inch area grid made from the point springs. The amount of joint line vertical stiffness present controls the amount of load transferred through the joint. The subgrade

area springs and slab thickness control the overall joint deflections. The joint line stiffness springs and the subgrade area stiffness springs are completely un-related in design and construction. But these two parameters significantly interact to affect the total force transferred through a joint. Joint line stiffness and the subgrade area spring stiffness values can be estimated using deflection measurements obtained in the field with the FWD.

An extensive literature review revealed no existing methods for directly calculating a value of line-type joint stiffness from FWD joint load test measurements. Ingenious methods for backcalculating an apparent joint stiffness were available (Ioannides et al., 1996; Skarlatos 1949; Skarlatos and Ioannides, 1998; Armaghani et al., 1986), but no methods for direct calculation of joint stiffness were found. Therefore, a new way of measuring pavement joint line stiffness directly from FWD joint load test deflection data was developed for this study. This new method uses an analysis of the geometry of the deflection of the FWD sensors for a joint load test and extracts apparent joint stiffness without needing a backcalculation routine or an assumed subgrade support value at the joint. This new method now allows a closer look than has been previously possible at how thermal variations, slack and looseness affect joints. When using the FWD to evaluate joint stiffness, it is best to consider joint stiffness with the following relation:

$$k_J = k_{J\text{-}D/s} + k_{J\text{-}AGG} + k_{J\text{-}Base} \text{ , lb/in/in or psi}$$

where,

k_J = Total measured stiffness for a pavement joint, lb/in/in.
$k_{J\text{-}D/s}$ = Stiffness from point devices (dowels, ties,…) with stiffness, D, spacing, s.
$k_{J\text{-}AGG}$ = Stiffness contribution from PCC slab crack face aggregate interlock.
$k_{J\text{-}Base}$ = Apparent joint stiffness contribution caused by elastic solid base effects.

As a result of the new joint stiffness calculation procedure, a new method for backcalculating the apparent edge support subgrade stiffness value using FWD joint load test data was made possible. Previously, the Skarlatos/Ioannides Edge Stress Equations or FEM software were being used to backcalculate apparent total joint stiffness. The new method for direct calculation of total joint stiffness now allows these same Skarlatos/Ioannides Equations or FEM software to be used in a new way: to backcalculate the effective modulus of subgrade reaction along the joint lines, somewhat inverse to what has been done in the past. These methods are described in detail later in the report. These two new methods in combination with existing subgrade stiffness backcalculation procedures for mid-slab load tests allow a direct comparison of edge support relative to mid-slab support at a site, through an index called the *Slab Support Ratio*.

Use of the new comprehensive on-site mechanistic evaluation procedure has resulted in a database of FWD load test and backcalculation information for airfield concrete slabs in the 14 to 22 inch thickness range, for a wide range of joint conditions and types. The test site database and measured site responses are presented in a way that will be useful for calibration of jointed FEM results to the real measurements.

1.2 HOW JOINTS HAVE BEEN CONSIDERED IN AIRFIELD PAVEMENT DESIGN

In FAA pavement thickness design methodologies, the magnitude of load transfer across pavement joints has been accounted for using the standard 25% stress reduction factor applied to the free-edge stress calculations. These approaches were based on a series of field studies such as Lockbourne #1 and Lockbourne #2 in Ohio (Parker et al., 1979; Brill, 2010) where slab bending strain at the edges of slabs was measured using strain gage instrumentation and load transfer studied in detail. Based on these past studies, suitably designed and constructed joints have been globally assumed to be capable of reducing the maximum stress level in the slab edge caused by a wheel load to 75% of the free edge stress value. This simplifying global assumption for the effectiveness of joints allowed the complex behavior associated with joints to be eliminated from the thickness design idealization and process. Seasonal or daily thermal effects on slab stress or joint behavior are also not directly considered in current or past thickness design methods. PCC pavement slab damage formulae have been calibrated to this "*flat-slab free-edge stress*" analysis approach using field test sites. This "75% of free edge stress" concept is currently used as the basis of pavement thickness design for FAA in AC 150/5320 version 6E.

The current slab damage algorithms used as the basis of FAA thickness design are statistically calibrated with empirical constants such that they can predict observed deterioration patterns, while assuming the 25% stress reduction was present. So regardless of whether or not the currently assumed 75% global joint effectiveness factor was slightly too high or slightly too low, these statistical calibration factors in the final damage model can compensate for, and mask out this general bias type estimation error. The current FAA design philosophy can be considered a simplified mechanistic-empirical design procedure. For this type of design process, it is more important that the analysis engine generate trend shapes that match reality. Small errors in the magnitudes of any statistical bias can be calibrated out of final damage formulae provided the analysis engine is producing realistic trend shapes. It is more difficult to compensate for "trend shape" type errors caused by an inaccurate analysis engine. The 25% reduction factor procedure became well established by the mid 1900s. In the late 1900s and up to current, advanced non-destructive field evaluation devices and techniques, along with modern computer based structural analysis capabilities revealed new insights on slab and joint behaviors. Several studies in the late 1900s that used the new tools, along with the recent detailed NAPTF and DIA slab structural analysis studies and others have put this initial simplified "75% of free-edge stress" design approach into question, leading to this study.

1.3 FAA ANALYTICAL PROCEDURES FOR JOINTED SLABS (FAARFIELD and FEAFAA)

In the true spirit of advanced mechanistic analysis methodologies, the FAA has been developing modern finite element method (FEM) structural analysis tools to replace the Westergaard free edge stress equations and layered elastic half-space methods (Brill, 1998; Kawa et al. 2002; Brill, 2010). There are two primary FEM representations that are currently supported by FAA: a single 30 ft by 30 ft flat-slab free-edge configuration being used for thickness design in the version 6E FAARFIELD, and a more detailed jointed arrangement, having up to nine-slabs, and ability to simulate curling. The more advanced jointed FEM software is being used more as a research and analysis tool and is called FEAFAA. The single slab unjointed configuration in

FAARFIELD is the basis of the new design procedure released with FAA AC 150/5320-6E. The single-slab FEM configuration places individual gear configurations on the edge of the single slab and calculates free edge stress. The current official design procedure is based on 75% of 3-D FEM free-edge stress values determined for various aircraft wheel loads. The enhanced version of FEAFAA can have up to nine slabs connected by linear elastic joints (stiffness is a constant lb/in/in value).

In year 1998, two FAA research reports were issued summarizing detailed 3-D FEM model development studies (Brill, 1998; Hammons, 1998). Both of these studies showed that joint stiffness parameters have a strong effect on stress calculations from FEM analyses, and ended up having a significant focus on joint parameters. Hammons (1998) used a 3-D ABAQUS FEM approach to simulate the behavior of small scale jointed slabs. This research focused on two key factors affecting LTE_{δ}, de-bonding of the slab to base interface bond, and cracking of treated base materials. Cracking of the treated base was considered to be a primary factor affecting load transfer deterioration observed by Hammons (1998). Hammons discussed the different joint options available in ABAQUS and noted the JOINTC element was used. Brill (1998) introduced a 3-D FEM procedure for jointed slab analysis based on the NIKE3D FEM software. This UNIX based 9-slab FEM arrangement could simulate cracked and uncracked base, and elastic solid or springs subgrade idealizations. Both Hammons (1998) and Brill (1998) anticipated significantly more loss of load transfer ability for cracked versus uncracked base assumptions. The current FAA thickness design guide FAA AC 150/5320-6E is based on a single-slab FEM configuration that evolved from the original 9-slab FEM arrangement developed in Brill (1998).

Figures 1.2-1.4 show some highlights obtained from the FAA web site for the single slab FEM configuration that was the basis of FAA AC 150/5320-6E. Figure 1.2 shows the general mesh shape for the single-slab FAARFIELD model and shows one of the key findings to date. A key finding is that decreasing slab size causes a reduction in calculated free edge stress compared to the infinite slab edge case like the Skarlatos/Ioannides equations. A slab with 30-ft dimensions was used in FAARFIELD, which results in slightly reduced edge stress for weak subgrade and no significant change in edge stress for stiff subgrade, compared to infinite slab assumptions. This plot is showing how greater slab rotations, occurring for shorter slabs, reduces stress levels in the slab edges caused by edge loading, while overall deflections increase and more of the load is taken by the subgrade. By the time the simulated slab edges are 40 feet long, the single slab FAARFIELD configuration is behaving like a Skarlatos/Ioannides infinite edge would. This 30-ft by 30-ft panel is the single-slab simplified mechanistic analysis engine used to estimate free-edge stresses caused by different aircraft gears. Figure 1.3 shows the typical wheel load positions analyzed to obtain a stress value for a given landing gear simulation. Figure 1.4 shows the slab damage regression algorithm form used to estimate the number of passes of aircrafts needed to cause failure for a given slab stress value. The parameters a, b, c, d, F'_s, and F_c are empirical regression or calibration factors applied to the mechanistic stress analysis results in order to solve the thickness design problem for airfield pavements using the mechanistic-empirical design philosophy (Brill, 2010). This research is focused on how real joint behaviors affect the stress values that should be used in calibrated damage procedures.

Discretized Model – Slab Size

30ft X 30ft slab size selected for FAARFIELD

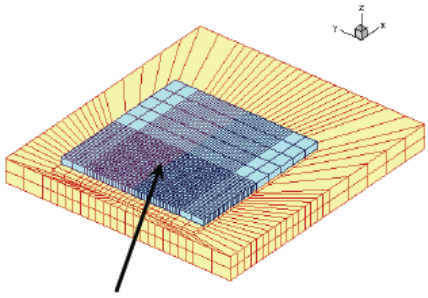

SLAB Size for model

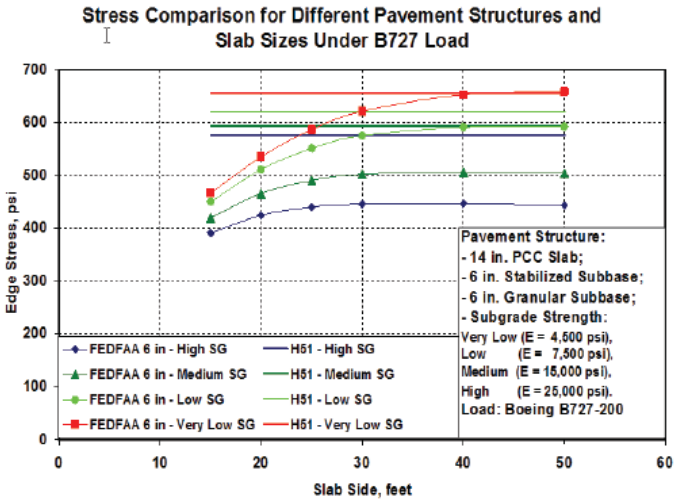

FIGURE 1.2. IMAGE SHOWING THE GENERAL SHAPE OF THE SINGLE SLAB FEM CONFIGURATION IN FAARFIELD AND SOME FEM ANALYSIS RESULTS SHOWING HOW SHORTER SLAB LENGTH CAUSES A REDUCTION IN FREE EDGE TENSILE STRESS

FAArfield – Gear Alignment on slab edge

- FAARFIELD either places the gear perpendicular or parallel to the edge of a slab.
- FAARFIELD makes this determination.

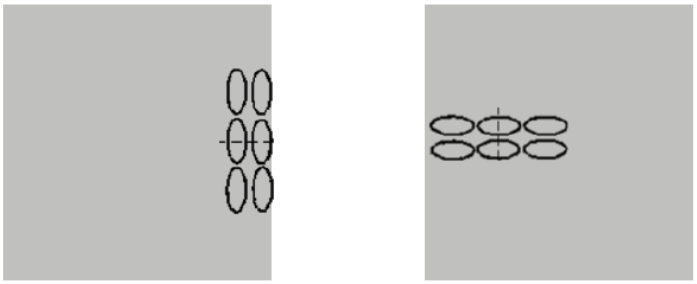

FIGURE 1.3. AN EXAMPLE OF AIRCRAFT GEAR LOAD POSITIONS COMPARED IN THE FAARFIELD SINGLE-SLAB FEM PROCEDURE TO OBTAIN THE MAXIMUM SLAB EDGE STRESS

Rigid pavement failure model in FAARFIELD

$$\frac{DF}{F_c} = \left[\frac{F_s' bd}{\left(1-\frac{SCI}{100}\right)(d-b)+F_s' b}\right] \times \log C + \left[\frac{\left(1-\frac{SCI}{100}\right)(ad-bc)+F_s' bc}{\left(1-\frac{SCI}{100}\right)(d-b)+F_s' b}\right]$$

DF = design factor, defined as the ratio of concrete strength R to computed stress
C = coverages
SCI = structural condition index, defined as a subset of the pavement condition index (PCI) excluding all non-load related distresses from the computation
a, b, c, d = parameters
F'_s = compensation factor for high quality and stabilized base
F_c = calibration factor

FIGURE 1.4. GENERAL FORM OF THE SLAB DAMAGE REGRESSION ALGORITHM USED WITH THE STRESS ESTIMATES FROM THE VERSION 6E FAARFIELD SINGLE-SLAB FEM CONFIGURATION TO ESTABLISH DESIGN SLAB THICKNESS

In general, the stress values used in the damage calculations have over time evolved from:

1. Early methods based on Westergaard Interior Stress
   ⇩
2. 75% of the Westergaard Free Edge Stress,
   ⇩
3. Empirically Adjusted Layered Elastic Basin Stress (LEDFAA),
   ⇩
4. 75% of the FAARFIELD single slab FEM model free edge stress (version 6E).
   ⇩
5. THE FUTURE (FEAFAA) - Perhaps the direct calculation of top and bottom of slab maximum bending stresses using the calibrated 9-slab FEM model using sophisticated joint model algorithms and full combined aircraft gear configurations.

This research project is situated right between items 4 and 5 listed above with the overall goal of taking a major step towards item 5 with respect to understanding and simulating real joint behaviors, while developing a scheme that is useful in the single slab analysis framework of item 4. It is necessary to quantify and understand real joint load transfer behavior if joints are directly being represented in a multi-slab structural analysis. The highway design community has moved into using structural analysis approaches that do include joints embedded in the Mechanistic-Empirical Pavement Design Guide (MEPDG) thickness design procedures. The FAA is also proceeding with direct modeling of joints and slabs with the NIKE 3-D based jointed FEAFAA computer program.

1.4 PROBLEM STATEMENT AND KEY QUESTIONS LEADING TO THIS STUDY

The Request for Proposal (RFP) issued by the Innovative Pavement Research Foundation (IPRF) included the following research problem statement:

> *The design protocols used to determine rigid airfield pavement thickness include an assumption that there is stress (load) transfer at the joint equal to 25%. It is also understood that for most of the calendar year the load transfer efficiency is much higher. However, depending upon the season, there may be conditions when the efficiency is lower than the assumed value.*
>
> *Random field studies have been accomplished at select airports but there has been no intent to use those studies to evaluate the sensitivity of the load transfer efficiency with respect to the variables that directly influence the quantitative value. It is known that some of the variables that influence load transfer efficiency include subbase support, joint design (plain, tied and dowelled), construction quality, ambient environment ….*
>
> *Understanding the impact of sensitivity of the variables could significantly influence the choice of boundary conditions used for the thickness design of airfield pavements. If the variables that influence load transfer efficiency are documented, it is possible that the selection of the joint transfer efficiency could be introduced into the design protocol at the macro scale.*

The IPRF RFP also included a list of questions that in general presents the basis for this study of joint load transfer behavior, as follows:

- What is the genesis of the assumption that a partial load transfer of the load at a joint reduces flexural stress by 25%?
- What were the variables examined that resulted in the adoption of the 25% value?
- What variables used in the development of the current 25% assumption are valid and applicable to pavement design as it exists today?
- How sensitive are the pavement thickness design protocols being used to the assumed load transfer variables?
- Do the minimum design requirements dictate the thickness requirement?
- Is it feasible to dictate the use of a "short duration" period of low load transfer for the design?
- Under what conditions is there a difference in load transfer efficiency for a dowelled, tied, and plain contraction joint?
- On a contraction joint, does the depth of saw cut impact the value of load transfer efficiency?
- Is there an ambient environment regime where load transfer efficiency is nearly constant?
- Is there an ambient temperature environment when load transfer efficiency has a minimum value?

- Can ambient environment be a design variable? If so, what are the conditions that must be satisfied before a reasonable value for load transfer can be assigned?
- What are the variables that affect the quantitative value of load transfer efficiency and are those variables equally significant?
- If not equally significant, what variables can be ignored for the purpose of assigning a value for load transfer?
- Is there a simple technique that can be employed to determine when aircraft gear configuration will significantly influence the quantitative value of load transfer efficiency?
- Is there sensitivity in the thickness computation that is a result of the interaction between gear configuration, slab curling, slab warping, slab size and load transfer for a given set of variables?
- What metric is best used to define and simulate joint load transfer when data are collected using an FWD?
- When using the FWD is it necessary to correct for slab bending?
- What dynamic loading is required to evaluate load transfer efficiency?

1.5 RESEARCH APPROACH AND SUMMARY OF REPORT CONTENTS

Clearly the list of questions regarding joint load transfer that initiated this research project is broad in scope. In order to thoroughly evaluate these questions, the following tasks and milestones were accomplished:

- Completed an extensive literature review regarding joint load transfer and the history of the 25% factor.
- Recognized that joint stiffness is the key mechanistic parameter used in modern pavement structural analysis tools, and that it controls load and stress transfer characteristics of joints.
- Recognized there was no pre-existing method for measuring joint stiffness directly, and developed a way of calculating joint stiffness directly from FWD joint load test data.
- Recognized this new joint stiffness determination procedure allowed new ways of backcalculating apparent modulus of subgrade reaction at joints for a field test site.
- Performed thirteen (13) detailed full day mechanistic pavement evaluations at heavy-duty jointed concrete airfield pavement test sites across the country using the FWD and other supporting tools.
- Performed a detailed analysis of FWD data from the DIA instrumented test site, the NAPTF CC2 test strip study, and thinner highway test sites.
- Documented the range of joint stiffness and load transfer efficiency values expected for slabs between about 8 and 22 inches in thickness.
- Documented the effects of slab curling and temperature changes on joint stiffness and load transfer behavior.
- Developed a comprehensive joint stiffness estimation tool that can yield joint stiffness versus average slab temperature for a wide range of joint design scenarios.
- Matched FEM software outputs and Skarlatos/Ioannides slab edge closed-form responses to the measured load transfer response from test sites.

- Performed load transfer sensitivity studies for load area size and multiple wheel gears using the calibrated FEM and Skarlatos/Ioannides algorithms.
- Established simplified methods for estimating an effective load transfer value for a joint design considering climate variations and the FAA slab damage procedure.
- The test site properties and FWD load test database is provided in a format that will be useful to other researchers and can be extended with additional site evaluations.

Chapter 2 of this report provides more detailed information regarding joint load transfer behavior, the FWD load test device, and the history of the long used 25% free-edge stress reduction factor. Chapter 3 describes the field test sites, the non-destructive tests and data, and provides examples of slab joint and pavement system behavior as measured in the field. Examples of how to analyze the various types of field data are provided. Chapter 4 presents a summary of the field test site measurements and overall joint behaviors observed at the test sites. Chapter 5 provides numerical joint behavior models that reasonably reproduce the measured joint behaviors from test sites. Simplified methods are provided for establishing a sites characteristic joint stiffness response curve. A comprehensive joint behavior simulation procedure is also provided, which can predict a pavement design's joint stiffness behaviors as a function of average slab temperature and several other key pavement design parameters. Chapter 6 summarizes the study of how various site design factors affect load transfer, LT, in pavement systems as viewed through calibrated FEM simulations of varying joint stiffness, curling, load types, and other key design parameters. Chapter 7 summarizes the research and provides recommendations for implementation of the findings and follow-up studies. Appendix A provides a summary database of overall site average parameters and general information, and the detailed compilation of the field measurements and response data for the test sites. Appendix B is a separate report not included here and consists of the full literature review document developed during the first phase of this study.

CHAPTER 2. KEY DEFINITIONS AND LITERATURE REVIEW SUMMARY

This section provides a brief summary of the key definitions and past research regarding joint load transfer behaviors described in this report. A detailed literature review was developed as a separate appendix to this report. Only key references and summary information are included in this main report for the project.

2.1 PCC PAVEMENT JOINT LOAD TRANSFER DEFINITIONS

The study of load transfer across joints and cracks in PCC pavements has been intensive in the past with a large body of literature available. There are many different measures of joint load transfer that have been used. There are, however, three primary definitions for load transfer at a pavement joint or crack that are most relevant, as follows:

$$\text{Deflection Load Transfer Efficiency } (LTE_\delta) = \left(\delta_U \Big/ \delta_L\right) \quad (1)$$

$$\text{Stress Load Transfer Efficiency } (LTE_\sigma) = \left(\sigma_U \Big/ \sigma_L\right) \quad (2)$$

$$\text{Percent of Free-Edge Stress Transferred (LT)} = \left((\varepsilon_F - \varepsilon_L) \Big/ \varepsilon_F\right) \quad (3)$$

Where,

δ_L = Deflection of the loaded side of the joint
δ_U = Deflection of the unloaded side of the joint
σ_L = Bending stress in the loaded slab
σ_U = Bending stress in the unloaded slab
ε_U = Bending strain in the unloaded slab edge at the joint
ε_L = Bending strain in the loaded slab edge at the joint
ε_F = Bending strain for "Free-Edge" loading conditions

There has been some inter-mixing of these definitions in past literature that can cause some confusion to readers not aware of the differences. Current technology and equipment can accurately measure slab edge deflections and deflection load transfer efficiency using nondestructive load tests. However, accurately measuring the stress or strain in concrete slabs is quite difficult. Theoretical slab models or real slabs instrumented with strain gauges are necessary to get estimates of stress or change in stress, which is directly related to measurable strain.

The "Percent of Free Edge Stress Load Transferred (LT)" concept evolved in direct support of airfield pavement design and is related to testing of instrumented slabs using embedded strain gages focused on measuring slab edge bending strain. Often, the free-edge strain was not actually measured but was assumed to be equal to the sum of the loaded slab strain and the unloaded slab strain measured for a joint load test. It is this percentage reduction LT concept that is the primary focus of this research. Reported LT values typically have ranged in magnitude from 0 to 50%. In the past, measurements of strain in the unloaded slab have been

assumed to be equal to the magnitude of the strain reduction in the loaded slab. This research has found this is generally not true when significant curling is present. LT is best defined as: the percentage reduction of the free-edge load bending stress magnitude caused by the joint load transfer effect, or more specifically, joint stiffness.

The Load Transfer Efficiency (LTE) concepts are different than LT and have evolved more with a focus on the ability to measure real joint deflections, and comparing real joint deflections with more recent FEM type theoretical simulation of pavements, where joints are actually being incorporated in the slab structural analysis. Both of the LTE values can range from 0 to 100%.

2.2 TYPICAL JOINT TYPES AND CHARACTERISTICS

Since the beginning of jointed concrete pavement construction, joint details have evolved from initially being simple in the early 1900s, to being rather exotic during the mid 1900s, and now over the last few decades, back to being relatively simple and basic. During the mid 1900s the industry went through a phase of trial and error research using many unusual load transfer devices (Teller and Sutherland, 1936; Van Breeman and Finney, 1950). Most of these bizarre, often patented joint load transfer devices proved too costly relative to effectiveness when compared to the simple round steel dowel bar. The industry is currently using mostly round steel dowels and segments of standard deformed steel reinforcing bar (tie-bars) as joint load transfer devices. Refer to document FAA AC 150/5320-6D for pavement joint details commonly used in FAA Portland cement concrete designs representing the test sites evaluated for this study. The following paragraphs provide detailed descriptions of joint types, with their corresponding joint identification codes from version FAA AC 150/5320-6E shown in parentheses:

- ***Aggregate Interlock Joint (Type-D dummy joint)*** - A thermal or shrinkage contraction joint with no load transfer devices, that forms after the concrete is placed and through a partial depth saw-cut or preformed groove. These joints can open and close significantly from summer to winter. Any load transfer ability for this joint type is developed in vertical shear through the crack face roughness, historically referred to as *aggregate interlock*. Loss of joint load transfer ability related to temperature and crack opening size is almost entirely related to apparent looseness or slack that develops between the crack faces. This slack can result in very low load transfer for small loads, and progressively increasing load transfer percentage for increasing load size. If the crack face that forms is very smooth, just a slight joint opening will result in rapid loss of load transfer ability. If the crack face is very rough, a greater joint opening change will be required before load transfer ability is lost. An irregular random crack with no steel reinforcement will behave structurally like an aggregate interlock joint. Load transfer will range from zero for large joint openings typical with very cold temperatures, to very high when slab crack faces compress together during hot weather.

- ***Doweled Contraction Joint (Type-C doweled joint)*** - This joint is also a thermal or shrinkage contraction joint that forms after the concrete is placed, and through a partial depth saw-cut or preformed groove, but now has smooth steel dowels installed generally at the mid-depth position in the slab thickness. If the joint opening is small, both the crack face aggregate interlock and the steel dowel are available to contribute to load

transfer. When the crack is fully open, all load transfer is developed through the embedded dowel. Doweled joints tend to maintain a relatively constant and higher level of load transfer during cold weather. The dowels may develop increasing looseness or slack over time causing loss of load transfer ability, to the point where the joint behaves as an aggregate interlock joint without dowels.

- ***Doweled Construction Joint (Type-E doweled joint)*** - Same as a doweled contraction joint, but this type typically has a relatively smooth formed face, and dowels are either drilled and grouted into the face after the concrete sets, or are set into holes in forms and the fluid concrete placed around the dowels. There is less aggregate interlock available for load transfer with this joint type compared to a doweled contraction joint. Some European contractors have used a sine-wave shaped form having three or four smooth shaped waves with about 1 to 2 inch amplitude to encourage better construction joint face interlock.

- ***Tied Contraction Joint (Type-B hinged joint)*** - Same as a doweled contraction joint but deformed steel bars are spaced along the saw cut or groove line. This joint is restrained to opening and is supposed to stay closed. There is typically less steel area across the joint face compared to a doweled detail, but by keeping the joint closed, the aggregate interlock remains effective in cold weather. The deformed bar actually acts to somewhat resist contraction type crack formation in a saw cut or groove placed over the bars. Testing has shown that many of these joints were not cracked after many years of service.

- ***Thickened-Edge Isolation Joint (Type-A thickened edge joint)*** - This joint type is used at all outer free edges of airfield concrete placements. FAA requires a 25% increase in thickness (2 in minimum) tapered over a full slab length or a minimum of 10 feet.

- ***Anchored Construction Joint-*** Similar to a tied construction joint, but load transfer is developed with drilled and grouted anchors such as red-heads or hook-bolts. These joints are more common for low-traffic rehabilitations and retrofits and are generally not used for new construction designs, or in heavy traffic areas.

- ***Doweled Expansion Joint (Old FAA Type-A doweled joint, No Longer Used)*** - Relatively rare, these joints were sometimes used in large area placements to relieve potential very high compressive stresses in the heat of the summer from thermal expansion. The least costly versions are like a doweled construction joint, but also add a compressible fiber-board joint filler placed between the slab faces. If present, these joints will represent a very small percentage of the joints at a pavement site. Because there is a large joint opening between concrete slabs, steel dowels with a significant non-embedded length between slabs must develop all load transfer.

- ***Tied Construction Joint (Old FAA Type-E hinged butt joint, No Longer Used)*** - Same as a doweled construction joint but deformed steel bars are spaced along the form face. This joint is supposed to be restrained to opening and is supposed to stay closed. There is typically less steel area per foot across the joint face compared to a doweled detail.

- ***Keyed Construction Joint (Old FAA Type-C keyed joint, No Longer Used)*** - A non-reinforced joint relying on a formed keyway shape for the joint face to develop joint stiffness. Although not common in new construction due to observed poor performance, this joint type is currently present at many airfields.

- ***Keyed-Tied Construction Joint (Old FAA Type-E hinged keyed joint, No Longer Used)*** - Same as a keyed construction joint but having deformed steel bars to prevent joint opening.

Current version 6E added a steel reinforced edge expansion joint detail, and eliminates all keyed joints in the group of standard recommended joints for FAA designs. Doweled construction joints are currently the only type of construction joint recommended for heavy load airports.

2.3 RECENT TRENDS IN JOINTING PATTERNS

Joint pattern and slab dimension characteristics for the test sites generally met requirements for FAA designs provided in the FAA AC 150/5320-6D. In the 1995 version 6D, there was a table recommending maximum slab lengths of 25 feet for thicker PCC slabs on unbound aggregate bases. For stabilized bases, maximum slab lengths were recommended to be less than 4 to 6 times the radius of relative stiffness for the slab and foundation system and an equation was provided. In the 2002 changes to version 6D, a new note appeared in the jointing requirements stating that joint spacing for all sites should be less than 20 feet unless the design engineer had good reason to allow longer joints. The 2002 version 6D recommended that joint spacing for stabilized bases be less than 5 times the radius of relative stiffness. In the current version 6E, joint spacing tables are provided for both stabilized and non-stabilized bases and no reference to radius of relative stiffness is present. The 6E tables limit all joint spacing values to be less than 20 feet. So, in version 6E, 20-ft maximum joint spacing is presented as a requirement and not a recommendation as it was in previous versions.

In general, the trend over time for joint spacing has been to use smaller and smaller joint spacing. Use of shorter panels will generally result in smaller average joint openings and smaller changes in joint openings while in-service, keeping aggregate interlock at higher magnitudes. At a point however, smaller slabs will begin to want to rotate under load more compared to larger slabs, for a given wheel load or gear load magnitude. The optimum slab size is large enough to resist excessive rotation or punching stress along joint lines under the design loads, but small enough to keep joint openings and curl or warp deflections smaller.

In airfield pavements, a great percentage of the older joints in-service are aggregate interlock joints without load transfer devices for the sawed transverse contraction joints across the paving lanes. Reinforcements were initially more used for longitudinal joints between paving lanes. An increasing percentage of newer designs used doweled and tied transverse contraction joints. Currently, load transfer devices are generally placed at the mid-depth position in the slab thickness. When the steel is at the neutral axis position for slab bending, it will act more like a pure rotational hinge, and the PCC cover thickness over the top and bottom of the dowel bar is maximized. Many older designs in northern freeze climates used steel welded wire fabric or deformed bar mat reinforcement in the slabs. Some designs required the mesh steel to be placed

unusually close to the top of slab, with only 3-4 inches of cover, perhaps in an attempt to resist upward slab warp.

2.4 HISTORY OF THE 25% FACTOR AND RELATED TEST SITES

The FAA slab thickness design procedures have evolved along the same general philosophy as military airfield design. The unprecedented size of military aircraft used in World War II (WWII) forced the US military to become actively involved in development of appropriate design and construction criteria for airfields. Since the 1940s the military played an active role in the airfield pavement arena as military aircraft continued to evolve (Rollings 2003, Ahlvin 1991, Lenore and Remington 1972). The FAA general design philosophy followed the military practices and only fairly recently have there been much divergence in design methodologies and requirements.

In a series of tests during WWII, Corps of Engineers investigators established the current framework for military airfield rigid pavement design that included such salient features as: the Westergaard approach, which was used to determine strains and stresses in airfield pavement; critical stresses were assumed to be caused by edge-loading adjacent to the joints; slow moving or stationary aircraft were recognized to cause higher stresses than rapidly moving aircraft; the importance of controlling non-load related curling stress was recognized; repetitions of load were an important design factor; properly designed joints could reduce free edge strain by transferring load from one slab to another; and, expansion joints were a source of weakness unless proper load transfer was designed for the joint. Following WWII through the Cold War and into the War on Terrorism, military airfield pavement design continued to evolve to meet changing needs and used theoretical development, small scale model tests, full-scale accelerated traffic tests, instrumented in-service pavements, and observation of airfield performance to support the evolution of design concepts (e.g., Rollings 2003, Rollings and Pittman 1992, Ahlvin 1991, Rollings 1989, Rollings 1981, Hutchinson and Vedros 1977, Ahlvin et al. 1971, Hutchinson 1966, Sale and Hutchinson 1959, Mellinger and Carlton 1955).

Throughout the development of the military rigid airfield design procedure, the ability of properly constructed joints in the pavement to transfer loads between slabs has been recognized and has been a fundamental part of the military rigid airfield pavement design criteria. Initial tests at Lockbourne during WWII suggested that 25% was an appropriate design value for load transfer, LT, which could be used for properly designed joints (US Army Corps of Engineers 1946). The performance of various joint designs during the Lockbourne No. 2 full-scale accelerated traffic tests in the 1940s (Ahlvin 1991, Sale and Hutchinson 1959, US Army Corps of Engineers 1950a and 1950b) were assessed from strongest to weakest as:

1. Doweled contraction joint
2. Doweled construction joint
3. Keyed construction joint with tie bar
4. Contraction joint
5. Keyed construction joint
6. Doweled expansion joint
7. Free edge expansion joint

These studies also found there were no advantages to using other structural shapes in lieu of conventional round, smooth dowel bars.

A theoretical treatment of the load transfer issue was also developed by a doctoral student of Professor Westergaard under contract with the Army Corps of Engineers, but it received little attention until the mid 1990s (Skarlatos 1949, Skarlatos and Ioannides, 1998 , Ioannides and Hammons 1996). This closed-form theoretical approach is used extensively in this report.

The experience gained at the Lockbourne tests and the follow-on full-scale accelerated traffic tests at Sharonville found the 25% load transfer to be adequate for design and probably conservative for doweled joints, but details and quality of joint construction were recognized as critical to obtaining high levels of load transfer (unpublished minutes of All-Division Meeting on Doweled Joints, US Army Engineer Ohio River Division Laboratories, September 1958, available at ERDC Technical Library, Vicksburg, MS). The early Corps of Engineers design policy concerning load transfer was articulated by Hutchinson (1966) as:

> *From these studies* (full-scale test tracks, theoretical studies, model studies, in-service pavement assessments)*, the decision was made to use three types of load transfer devices: (a) keys and keyways constructed in the joints during construction; (b) dowels, consisting of round smooth steel bars or pipe, one end of which would be bonded in the concrete and the other end left unbonded; and (c) the interlock provided by a natural crack occurring shortly after concrete was placed. ... each demonstrated that it would provide at least 25 percent load transfer and maintain slab alignment. ... In addition, the difference between the maximum stress from edge and interior loading is only about 25 percent; hence any device that reduces the edge stress by more than 25 percent then makes the interior loading condition critical.*

In the event that these approved load-transfer capable joint designs were not used, a thickened edge joint 25% thicker than the design thickness was required. This thickened edge effectively reduced stresses along the critically loaded slab edge.

In the late 1950s, the Sharonville Heavy-Load test tracks were built to assess design criteria for 325,000 lb twin-tandem gears representing a 700,000 lb aircraft. These test tracks received some initial trafficking, but changing priorities led to halting the traffic, and the results were never formally reported (Ahlvin 1991, Rollings 1987). Some of this trafficking suggested that keys might not be adequate under such heavy gear loads, and the Multiple-Wheel Heavy-Gear Load Tests conducted in the 1960s for aircraft exceeding 600,000 lb confirmed that keys were inadequate under heavy aircraft loads (Ahlvin 1991, Ahlvin et al. 1971, Grau 1972). A later assessment of keyed joints in civil airports reached a similar conclusion (Barenberg and Smith 1979). The military initially restricted keys to more lightly loaded pavements on favorable subgrades, but then abandoned them all together for new construction leaving the saw-cut contraction joint and doweled construction joint as the default joints for USAF airfield pavements (Rollings 1981, Rollings 1989, Department of Defense 2001). Thickened edge, expansion, and doweled contraction joints can be used for special circumstances.

The early Corps of Engineers investigations collected strain measurements on the loaded and unloaded side of the joint to define load transfer, LT. Their load transfer measurements of in-service airfield pavements are particularly germane. A summary of these measurements is shown in Table 2.1. The key joint measurements are too limited to allow one to draw any conclusions. The doweled construction joint measurements reveal that on average the measured load transfer exceeded the 25% used in design, but there is much variation in the data. Three of the test sites, Dow, Lockbourne and McCoy, fail to average the design allowance, and Lockbourne fails to have a single measurement equal to 25%. In contrast, Ellsworth and Lincoln do not have a single measurement below 25% and had average LT values of 40.6 and 36.5% respectively. While the in-service doweled joints appear to generally meet the 25% design allowance, there is much variation. This could easily reflect factors such as variation in construction technique or temperature at the time of the test.

TABLE 2.1. SUMMARY OF LOAD TRANSFER FROM STRAIN MEASUREMENTS ON IN-SERVICE USAF AIRFIELDS (ROLLINGS 1981, BASED ON DATA FROM US ARMY CORPS OF ENGINEERS 1959 AND GRAU 1979)

Location	Modulus of Subgrade Reaction, kPa/cm	Pavement Thickness, cm	Number of Measure-ments	Load Transfer, %[a]		
				Range	Mean	Coefficient of Variation,%
Doweled Joints						
Beale AFB, CA	580	58	15	16.7-52.3	32.8	32
Dow AFB, MI	950	48	16	0.0-35.7	10.5	94
Ellsworth AFB, SD	580	58	16	30.4-50.0	40.6	12
Hunter AFB, GA	475	46	15	18.2-42.9	27.4	28
Lincoln AFB, NE	180	53	16	27.8-50.0	36.5	19
Lockbourne AFB, OH	200	30	11	7.4-23.7	15.8	37
March AFB, CA	270	41	15	20.0-47.4	32.0	24
McCoy AFB, FL	610	46	14	14.3-35.7	24.2	25
Tyndall AFB, FL	430	20-25	10	15.6-46.8	30.4	30
		Overall	128	0.0-52.3	28.1	43
Keyed Joints						
Lincoln AFB, NE	180	53	2	35.9-36.1	36.0	-
McCoy AFB, FL	610	46	2	35.9-38.6	37.3	-
		Overall	4	35.9-38.6	36.6	-

Note: 1 kPa/cm = 0.369 lb/in^2/in, 1 cm = 0.3937 in
a. Calculated from measured strains on loaded and unloaded edges of joint.

Table 2.2 is a compilation of Corps of Engineers load transfer data based on strain measurements, and estimates based on joint deflections during full-scale traffic tests and from in-service pavements. This data emphasizes that although properly designed joints can achieve the 25% design allowance for load transfer, there is much variation, and sometimes this is met, and sometimes it is not. Joints without load transfer devices consistently fail to meet the design allowance (e.g., the Lockbourne "free" or butt joint). The mean of the keyed joint barely meets the 25% design allowance for load transfer presaging the eventual inadequacy of this joint design under heavy aircraft. The joint designs currently authorized for USAF airfields (doweled construction, doweled expansion, and saw-cut contraction joint with aggregate interlock) all have mean load transfer values 5% or more above the design target of 25%.

TABLE 2.2. REPRESENTATIVE CORPS OF ENGINEERS LOAD TRANSFER MEASUREMENTS FOR FULL-SCALE TEST SECTIONS AND IN-SERVICE PAVEMENTS DURING 1942 - 1979 (BASED ON ROLLINGS 1987, 1989)

Type of Joint	Number of Measurements	Load Transfer, %		Coefficient of Variation, %
		Mean	Range	
Doweled Construction Joint	195	30.6	0.0 - 50.0	38.0
Doweled Expansion Joint	15	30.5	15.4 - 42.6	24.4
Contraction Joint with Aggregate Interlock	46	37.2	15.6 - 50.0	19.2
Tied Contraction	6	29.2	23.9 - 34.8	13.4
Doweled Contraction	4	35.1	28.2 - 42.8	17.3
Keyed	61	25.4	5.6 - 49.0	41.4
Tied Key	2	25.8	25.6 - 26.1	-
Butt	8	15.5	5.8 - 24.5	40.9

Notes: Includes load transfer based on direct strain measurements in Table 2.1 plus load transfer estimated from deflections. See Rollings 1987 for methodology of estimating load transfer from measured joint deflection under load.

The Corps of Engineers conducted load transfer measurements with a heavy weight deflectometer at Atlanta, Dallas-Ft. Worth, Denver, and Madison airports in 1992-1993 (Hammons et al. 1995). The overall results of these tests are summarized in Table 2.3. This investigation attempted to assess the impact of other variables on load transfer including: support below the slab, season, and dowel insertion method. The impact of season and base type are apparent in this field data. Like Table 2.2, these data show the doweled contraction joint has lower load transfer than the aggregate interlock contraction joint which is counterintuitive and contrary to the performance data from the Corps' Lockbourne tests. The tied keyed joint is superior to the untied key as also suggested in Table 2.2 and in the Lockbourne joint performance rating given earlier. In general, the mean load transfer in Table 2.3 is lower than 25% design value during the winter. These tests in Table 2.3 had negligible impact on military design philosophy as the tested slab lengths were generally much longer than used in the military which was assumed to lower load transfer values from what would be expected with shorter slabs, and the doweled longitudinal construction joints included data for dowel insertion techniques not allowed in the military. Lessons learned from this current research project show that LT values for FWD loads are expected to be smaller than LT values for larger load areas having smaller contact pressure, or for real multi-wheel gear assemblies. The LT values for say a B-747 gear assembly may be above 25% while the LT value for a small area concentrated FWD load may be less than 20%. The load transfer values in table 2.3 are consistently lower than previous observations due in most part because of the relatively small diameter FWD load plate diameter used to measure load transfer, and also due to increased joint opening sizes present during winter testing.

TABLE 2.3. CORPS OF ENGINEERS LOAD TRANSFER MEASUREMENTS AT CIVIL AIRPORTS (BASED ON HAMMONS ET AL. 1995)

Joint Type	Base	Season	Number of Measure-ments	Load Transfer	
				Mean, %	Coefficient of Variation, %
Doweled Transverse Contraction	stab	winter	58	14.7	36.4
		summer	11	28.1	7.1
	nonstab	winter	11	19.9	28.6
Transverse Contraction	stab	winter	14	21.6	21.1
Doweled Longitudinal Construction	stab	winter	31	18.6	24.8
Tied Longitudinal Construction	stab	winter	12	15.9	30.6
Keyed Longitudinal Construction	stab	winter	9	15.5	37.4
	nonstab	winter	6	23.6	9.8
Tied Keyed Longitudinal Construction	stab	winter	23	20.2	20.4

Notes: stab = stabilized base
nonstab = nonstabilized granular base
Slab lengths varied from 20 to 75 ft with most being reinforced slabs with 50 and 75 ft lengths

The military's policy on load transfer for rigid airfield pavement design has evolved over time. The early expectation that, with accumulating knowledge, one might be able to use higher load transfer design values for doweled joints (unpublished minutes of All-Division Meeting on Doweled Joints, US Army Engineer Ohio River Division Laboratories, September 1958, available at ERDC Technical Library, Vicksburg, MS) never came to fruition as the data failed to support this expectation. Keyed joints proved unreliable under increasingly heavy aircraft and were abandoned for new construction. Data from this study and other past studies has now shown that increasing slab thickness and subgrade stiffness generally results in lower achievable LT values. The importance of construction details was recognized early and this is reflected in very exacting construction specifications for military airfields. A number of dowel construction innovations such as plastic sleeves or machine insertion into plastic slip-formed concrete have not been allowed by the military because of a lack of data showing such innovations will not compromise achievable load transfer values. A number of publications make the point clearly that load transfer is a stochastic variable that changes over time and not a constant (e.g., Rollings 2003, Hammons et al. 1995, Rollings 1987, Barenberg and Smith 1977, Hutchinson 1966), so the long established 25 % load transfer value is best thought of as a "design allowance" rather than a specific single value that is always present in the field.

Allowance for load transfer during design and mandatory provisions for achieving load transfer during construction have been fundamental parts of military airfield rigid pavement design since WWII, and they continue to be so today. While the 25 % load transfer factor used in design by the military and the Federal Aviation Administration is often referred to as an "assumption," the selection of this value represents an engineering estimate based on a variety of measurements during full-scale traffic tests, on experimental pavements, and on in-service pavements. The military data indicates that on the average the joint designs used in current military airfields exceed the design allowance or assumption. Military design aids such as design charts and computer programs routinely include the 25% load transfer in the design aid calculations. When such aids have been used incorrectly to design an airfield pavement that actually does not have joints with load transfer provisions, failure is rapid and dramatic illustrating the structural significance of the load transfer provision (e.g. Rollings, 2001; Rollings and Rollings, 1991). The use of the 25% load transfer design value when coupled with the military's other requirements such as allowable slab length, joint design requirements, and field construction inspection has generally proven effective over the past 50 years as a design tool.

FAA and military design procedures did not evolve independently, but were intertwined from 1940 through the early 1990s with the military essentially establishing methodology and FAA accepting or modifying it to suit their needs. With the more recent establishment of the NAPTF and a program of 3-D FEM, the FAA has been going off in an independent direction separate from the military but basing their philosophy to start with on past military research. The Lockbourne and model tests of the 1940s found Westergaard interior stress was not the critical state but edge stress was. The military funded Westergaard (1948) to help develop his 1948 free-edge equations. These are for single wheel load simulations and this is when the first versions of the B-36 aircraft came out having a large 75,000 lb single wheel gear load. Practicality eventually led to multiple-wheel gears being used on subsequent versions and future large aircraft. The 1948 Westergaard equations do not handle multiple-wheel loading configurations directly. Pickett and Ray (1950) eventually published their well-known multi-wheel influence diagram solution to Westergaard's free-edge formulation. The Corps used these influence diagrams to develop their design curves of this era. Military design of this era used the Westergaard edge stress formulation for stress calculation, made adjustments for load transfer, and used available full scale traffic tests to relate the design factor (calculated stress and flexural strength) to coverages (cycles of stress at a point), which was a fatigue analysis. In the 1960s General Dynamics developed H-51, a computer solution to the Pickett and Ray influence diagrams. The 1970s begins the layered elastic work for airfield pavements (Parker et al. 1979). Inherent in developing the layered elastic analysis for design is the fundamental basis that the layered elastic fatigue algorithms pertain only to pavements using 25% load-transfer capable joint systems. This is because the field fatigue data upon which relation is based all used such joints, and the relations cannot be extrapolated to free-edge conditions. The wars of the 2000s led military to realize layered elastic was not robust enough to handle all of the variations seen in the field so CBR and Westergaard-based design remain in use along with layered elastic. Starting in about 1979, the FAA changed their official design criteria to be based on Westergaard's free-edge stress equation in FAA AC 150/5320-6C (Barenberg and Arntzen 1981) and variations of this approach have been used up to current times, and until arrival of version 6E and the single-slab 3-dimensional FEM structural analysis procedure in FAARFIELD.

2.5 VERTICAL SHEAR STIFFNESS OF A LINEAR JOINT OR CRACK

The most important structural analysis concept regarding how load is transferred across joints is the concept of joint stiffness. The 2-D linear joint stiffness can be represented as discrete springs each having stiffness, *D*, with spacing, *s*, which is the commonly accepted way of representing dowel bars spaced along a joint. Or, line stiffness can be considered more as a continuous linear area elastic spring like the aggregate interlock mechanism, typically referred to as *AGG* or q_0 in past joint studies, uniformly distributed along a joint line.

An extensive literature review revealed no existing methods for directly calculating a value of line-type joint stiffness from FWD load tests. During the literature review stage of this project it became apparent that it was possible to make a closed-form equation for joint stiffness that was a function of only the FWD sensor data from a joint load test. A method of actually measuring joint stiffness was needed in order to accomplish the goals of the study. Therefore, a new way of measuring slab joint structural line stiffness directly from FWD joint load test sensor data was developed. This new method is described in chapter 3. Past methods for estimating joint stiffness in the field ingeniously used estimates of cross section properties, estimated subgrade stiffness at the joint, and the ratio of the unloaded to loaded slab measured deflection values, LTE_δ, along with a structural analysis tool (Skarlatos/Ioannides Equations or FEM analysis) to backcalculate joint stiffness values indirectly. This new method uses a detailed analysis of the geometry of the deflection of the FWD sensors for a joint load test and extracts apparent joint stiffness directly from the deflection geometry without needing a backcalculation routine with an assumed subgrade support value at the joint. This new method allows a closer look than has been previously possible at how ambient temperature variations affect joints, slack and looseness in joints, and at the following generally accepted equation for the most important mechanistic parameter related to load transfer across slab joints, the pavement joint stiffness:

$$k_J = k_{J\text{-}D/s} + k_{J\text{-}AGG} + k_{J\text{-}Base} \text{ , lb/in/in or psi} \quad (4)$$

where,

k_J = Total *measured* line stiffness along the slab joint, lb/in/in, from FWD.
$k_{J\text{-}D/s}$ = Stiffness from point devices (dowels, ties,…) with stiffness, *D*, spacing, *s*.
$k_{J\text{-}AGG}$ = Stiffness contribution from PCC slab crack face aggregate interlock.
$k_{J\text{-}Base}$ = Apparent joint stiffness contribution caused by Elastic Solid base effects.

The structural stiffness of the joint is comprised of three primary components. The first is the amount of vertical shear force transferred through load transfer devices placed across the joints such as dowel bars or tie bars. The second component is the amount of vertical shear force transferred through the joints vertical crack face roughness features, often referred to as aggregate interlock. The third component is related to the amount of "apparent" shear force transferred across the joint caused by elastic solid type base or subbase beneath the concrete slabs. $k_{J\text{-}Base}$ is not really joint stiffness, because joint stiffness is limited to being a part of the concrete slab joint itself. However, the base effect may appear as joint stiffness when trying to quantify stiffness through FWD slab deflections. For example, if two slabs are pulled apart just

far enough such that there is zero contact between slab ends during loading (joint stiffness is zero), some deflection load transfer will still probably be measured during a load test. This is because the subgrade beneath the unloaded slab is pulled down by the adjacent elastic type subgrade deflections caused by the loaded slab. Although some LTE_{δ} is measured, no actual force or load transfer through the joint is present and it is truly free-edge loading. It is difficult to account for this third "base/subbase" component of load transfer across joints. It is also difficult to separate out how much of a total joint stiffness value is caused by dowels versus the aggregate interlock on the crack face. A theoretical discrete vertical "springs" type subgrade support idealization does not have any base/subgrade LTE effects. These base LTE effects only occur when a continuous uncracked elastic solid material behavior is present beneath the joint.

2.6 THE SKARLATOS EXTENSION OF THE WESTERGAARD EQUATIONS

Ioannides et al. (1996) combined dimensional analysis for jointed concrete pavements, and the Skarlatos extension of the Westergaard approach (Skarlatos 1949; Skarlatos and Ioannides, 1998) to develop a closed-form solution for the load transfer (LT) problem, and presented a methodology for use with FWD devices to evaluate load transfer at joints. Figure 2.1 shows the general equations for the closed-form Westergaard/Skarlatos/Ioannides/Hammons method. Figure 2.2 shows the definitions for the parameter f, dimensionless joint stiffness, used in the closed-form solution.

TABLE 1 Closed-Form Solution for the Edge Load Transfer Problem for Square Load, $2\epsilon \times 2\epsilon$, and $\mu = 0.15$ (*14*)

Free Edge Deflection:

$$\Delta_f^* = \frac{\Delta_f\, k\, \ell^2}{P} = \left[0.4314 - 0.3510 \left(\frac{\epsilon}{\ell} \right) + 0.06525 \left(\frac{\epsilon}{\ell} \right)^2 \right]$$

Free Edge Bending Stress:

$$\bar{\sigma}_f^* = \bar{\sigma}^* + \sigma_c^* = \frac{(\bar{\sigma} + \sigma_c)\, h^2}{P}$$

$$\bar{\sigma}^* = \frac{\bar{\sigma}\, h^2}{P} = 1.3945 \left[0.22215 - \log_e \left(\frac{\epsilon}{\ell} \right) \right]$$

$$\sigma_c^* = \frac{\sigma_c\, h^2}{P} = 1.3945 \left[-0.2419 + 0.3822 \left(\frac{\epsilon}{\ell} \right) - 2.1125 \left(\frac{\epsilon}{\ell} \right)^2 + 4.02 \left(\frac{\epsilon}{\ell} \right)^3 \right]$$

Unloaded Side Deflection:

$$\Delta_U^* = \frac{\Delta_U\, k\, \ell^2}{P} = 0.215 \left[\frac{f - 0.6 \log (1 + f)}{f + 0.4} \right] * \left[1 - 0.7 \left(\frac{\epsilon}{\ell} \right) \left\{ 1 + 0.06 \log (1 + f) - 0.01\, f^{0.2} \right\} \right] + \Delta_U^{*\prime}$$

$$\Delta_U^{*\prime} = \frac{1}{2} \left[0.015 + 0.005 \log f \right] \left(\frac{\epsilon}{\ell} \right)^2$$

Unloaded Side Bending Stress:

$$\sigma_U^* = \frac{\sigma_U\, h^2}{P} = 0.54 \left[0.42 + \log (1 + f) + 0.1 \frac{\sqrt{f} - 4.2}{f + 1} \right] * \left[1 - 0.54 \left(\frac{\epsilon}{\ell} \right) \sqrt[4.1]{f + 5.0} \right] + \sigma_U^{*\prime}$$

$$\sigma_U^{*\prime} = 3.75 \log^{-1} \left[0.74 \log f - 1.94 \right] \left(\frac{\epsilon}{\ell} \right)^2 \quad \text{for } f > 10;\ = 0, \text{ otherwise}$$

Note: The unloaded side bending stress should not exceed half the corresponding free edge bending stress.

FIGURE 2.1. THE SKARLATOS/IOANNIDES CLOSED-FORM SOLUTION AS DEVELOPED BY IOANNIDES ET AL. 1996 (REFER TO PAPER FOR DETAILED DESCRIPTION)

$$f = \frac{q_o}{kl} = \frac{AGG}{kl} \qquad \text{for undoweled joints}$$

or

$$f = \frac{D}{skl} \qquad \text{for doweled joints}$$

FIGURE 2.2. DEFINITION OF THE DIMENSIONLESS JOINT STIFFNESS PARAMETER, *f*, FOR DOWELS AND AGGREGATE INTERLOCK TYPE JOINTS (IOANNIDES AND HAMMONS, 1996)

Figure 2.3 shows a key result regarding the behavior of the Skarlatos/Ioannides approach as compared to jointed FEM simulations. Very similar LTE_δ versus dimensionless joint stiffness trends are obtained for any load size area when using FEM jointed finite slabs or when using the infinite slab Skarlatos/Ioannides equations. Figure 2.4 shows how LTE_δ is related to LTE_σ. These trends are significantly affected by load size. Smaller area concentrated loads have smaller LTE_σ than a similar load having a larger area and lower contact pressure. This figure suggests that FWD loads will have smaller LT values than larger area, lower contact pressure aircraft wheels and gears. Similarly, the jointed FEM trend lines generally reveal lower LTE_σ values than the Skarlatos/Ioannides equations. This general trend has been documented by other studies (Bush III and Hall, 1981; Bush III et al., 1989; Guo, 2008)

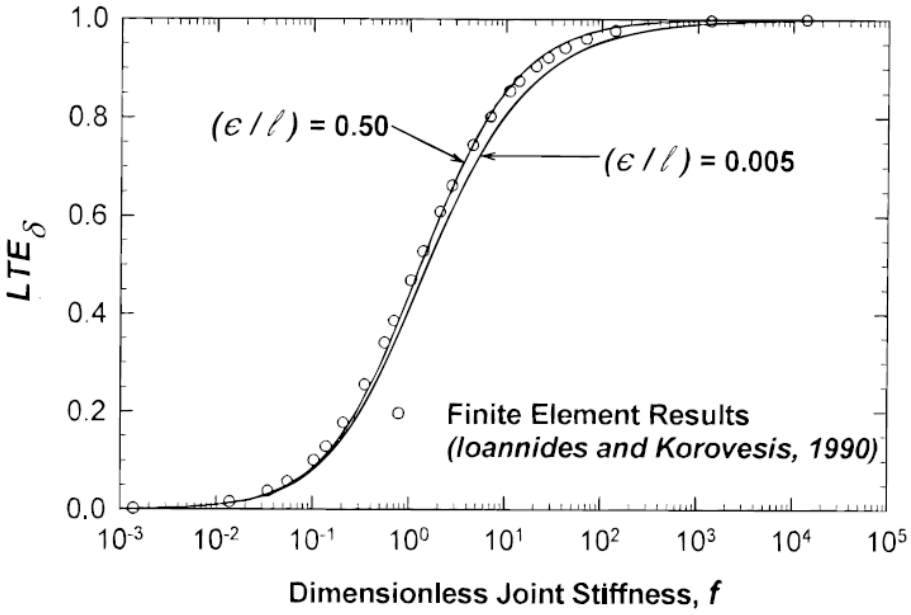

FIGURE 2.3. VARIATION OF LTE_δ WITH DIMENSIONLESS JOINT STIFFNESS AND DIMENSIONLESS LOAD SIZE RATIO (IOANNIDES AND HAMMONS, 1996)

Figure 2.4 also shows perhaps the first measurements of a relation between LTE_δ and LTE_σ. Teller and Sutherland (1936) installed strain gages at a few locations along slab edges and were among the first to recognize that the relation between LTE_δ and LTE_σ was a significantly non-linear relation, and not a one-to-one relation.

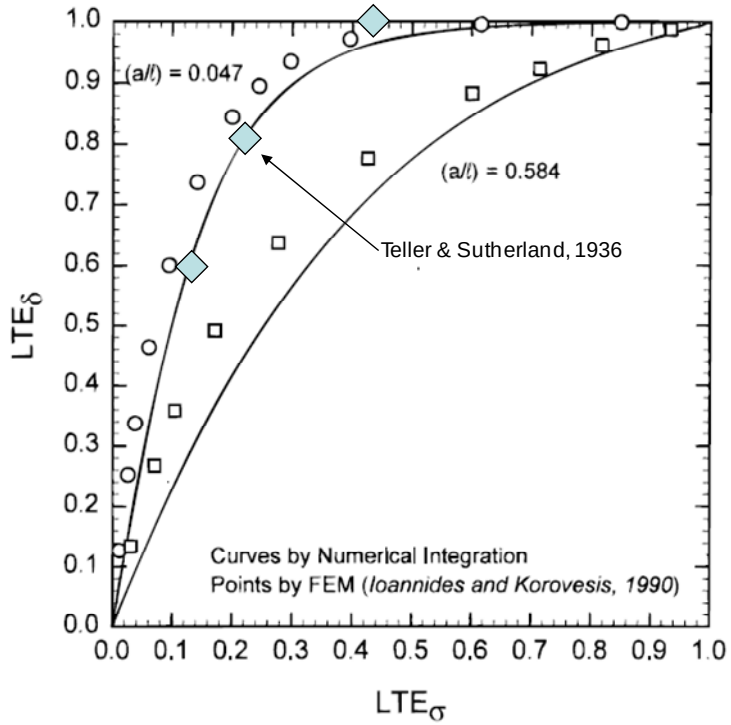

FIGURE 2.4. COMPARISON OF THE SKARLATOS/IOANNIDES TRENDS WITH EARLIER FINITE ELEMENT RESULTS (IOANNIDES AND HAMMONS, 1996) AND PERHAPS THE FIRST THREE STRAIN-GAGE BASED MEASUREMENTS OF THIS KEY PHENOMENON (TELLER AND SUTHERLAND, 1936)

It is important to understand that typical dowel bar systems used in jointed concrete pavements do not offer significant bending moment flexural rigidity at a joint. The presence of dowels at joints will not change the shape of the trends shown above, which are only a function of the (a/ℓ) ratio shown (a = load radius, ℓ = radius of relative stiffness). The presence of dowels will just act to keep joint stiffness and load transfer efficiency at a higher position but on the same trend line. The trend line shapes represent a cross section property, with or without dowels.

New procedures for backcalculating the apparent slab edge support subgrade stiffness for a jointed concrete pavement test site were made possible by the new direct joint stiffness calculation technique for FWD data. Previously, the Skarlatos/Ioannides Edge Stress Equations or FEM results were being used to backcalculate apparent joint stiffness. The new joint stiffness calculation method now allows the Skarlatos/Ioannides Equations or FEM results to be used in a different way: to backcalculate the effective modulus of subgrade reaction along the joint lines, somewhat inverse to what has been done in the past. The previous method used to backcalculate joint stiffness from FWD data (Ioannides and Hammons, 1996) is generally described as follows:

1. Use the FWD device to obtain many joint and mid-slab load tests in a uniform test site.
2. Obtain the LTE_{δ} values for each joint load test.
3. Estimate the modulus of subgrade reaction at the joints by using existing mid-slab FWD basin backcalculation procedures, and using the best possible estimates of slab concrete elastic modulus and thickness.
4. Using the best known guesses for slab thickness, concrete elastic modulus, and modulus of subgrade reaction at joints for the test site, use the Skarlatos/Ioannides Equations and find the *backcalculated joint stiffness* values for each joint load test.
5. If desired, use a complex jointed FEM representation of the pavement cross section, using the assumed subgrade stiffness and develop the site's characteristic joint stiffness versus LTE_{δ} curve. This curve provides the jointed slab's joint stiffness that matches each LTE_{δ} value.

Having to estimate the magnitude of apparent support at the joints is the only weakness of this approach. As shown later, subgrade support stiffness along slab edges was found to almost never be the same as mid slab, and significant measurable loss of support is typically present along slab edges compared to mid-panel areas. The new back calculation procedure for edge support, which will be demonstrated in detail in chapter 3, has the following general steps:

1. Use the FWD to obtain many joint and mid-slab load tests in a uniform test site.
2. Obtain the joint stiffness values as described in chapter 3, and LTE_{δ} values for each joint load test.
3. Make an overall plot of site's characteristic joint stiffness versus LTE_{δ} curve.
4. Perform mid-panel backcalculations to estimate the interior loading modulus of subgrade reaction for the test site, and the slab concrete elastic modulus using best possible estimates for slab thickness.
5. Using the best known guesses for only slab thickness and concrete elastic modulus for the test site, use the Skarlatos/Ioannides Equations and find the backcalculated *Semi-Infinite Slab Edge Modulus of Subgrade Reaction* resulting in a best-fit for the Skarlatos/Ioannides approach to the measured characteristic joint stiffness curve data.
6. Calculate the site *Slab Support Ratio*, equal to the backcalculated Skarlatos/Ioannides edge modulus of subgrade reaction divided by the backcalculated interior loading modulus of subgrade reaction. This ratio gives an index of loss of support at joints relative to mid slab for a site, assuming infinite slab conditions.
7. If desired, fit results from a complex FEM simulation to the stiffness versus LTE_{δ} trend from the site to get a backcalculated *FEM Finite Slab Edge Modulus of Subgrade Reaction* and slab support ratio for the site. Use of FEM matching to the site data is the best way to review thermal variation effects and slab stress for curling related curvature variation and joint uplifts caused by thermal gradients through the slab thickness.

The backcalculated slab edge modulus of subgrade reaction is the effective modulus of subgrade reaction at the joints, and is different than the traditional mid-slab backcalculated modulus of subgrade reaction. These two new slab edge support backcalculation methods in combination with existing subgrade stiffness backcalculation procedures for mid-slab load tests allow a direct comparison of edge support relative to mid slab support at a site, using the *Slab Support Ratio*. Use of this technique shows that in general the full amount of support present under the mid

portion of the slab is generally not present at the joints. Support reduces over time faster at joints than in the mid slab regions. The Slab Support Ratio values ranged from about 0.3 to 0.9 for the project test sites, averaging about 0.45 for typical test sites.

2.7 THE FALLING WEIGHT DEFLECTOMETER

This research relied on a non-destructive on-site evaluation procedure as the basis for the structural evaluation of test sites. No coring or cutting, or other debris generating activities were allowed at the airfield test sites. The on-site testing program is described in chapter 3, but a detailed description of the FWD is presented in this section. Heavy-weight FWD testing devices were used as the primary joint structural behavior evaluation tool. FWD testing was performed using a Dynatest Model 8081 type FWD, as shown in figure 2.5. This device is capable of applying loads in the range of 6,500 to 54,000 lb and recording the resulting pavement surface deflections at several locations at and near the load. The "Heavy-Weight" versions of the FWD were necessary in order to generate enough force to substantially deflect heavy duty airfield pavements enough to measure the deflections accurately.

FIGURE 2.5. THE HEAVY-WEIGHT FWD POSITIONED TO PERFORM A MID-PANEL LOAD TEST

The FWD drops a weight from various drop heights onto a rubber buffer system, which transmits the load to the pavement through a rigid plate of approximately 12 inch diameter. A rubber pad on the bottom of the load plate helps to evenly distribute the applied load over the slab texture. The applied load is measured by a load cell while the deflections at various locations on the pavement surface are measured by high speed velocity transducers. The transducers are oriented along a line attached to a sensor-bar placed on the pavement surface. All operations are computer controlled from the tow vehicle. The applied loads as well as the measured deflections are recorded in the computer. In general, shorter sensor spacing is used for thinner highway type pavement sections, compared to thick airfield pavements. The sensor set-up used for this study consisted of a commonly used seven-sensor line with sensors spaced at 12 inches apart from the center of the load plate, spanning a total distance of 72 inches.

The FWD records the time history responses for each deflection sensor and the load cell. The FWD load test is a rapid pulse type dynamic load test, with the pulse duration designed to simulate a rolling wheel load. Factors such as inertial and material damping in the slab and subgrade, along with shear-wave, compression-wave, and Raleigh-wave propagation effects, are all a part of a typical FWD load test dynamic response. Figure 2.6 shows a typical FWD time history response for a joint load test on a heavy duty runway joint having relatively low load transfer efficiency and joint stiffness. The pulse load has duration of about 25 milli-seconds. For a typical aircraft tire contact patch length of about 1.5 feet, this load pulse duration somewhat simulates a wheel pass-by (zero to maximum to zero load over contact patch) with velocity of about 40 mph. Past research has shown that once wheel velocities exceed about 10 to 20 mph, inertial and material damping effects result in reduced "dynamic" deflections of the pavement compared to static load testing. Therefore, it can be assumed that the deflection values resulting from an FWD test are less than similar magnitude static load test values would be at the same test locations. In turn, backcalculated subgrade support stiffness values from FWD load tests are typically larger than true static load-stiffness values would be. Evidence of this dynamic versus static deflection concept can be observed by looking at the time phase lag between the maximum load cell value (occurs at 15.7 milli-seconds) and the time of the maximum response of the loaded slab deflection sensor (18 milliseconds). It can be observed how the slab bending or impact wave from the FWD impulse load propagates through the sensor array, with sensors further away from the load plate having longer times to peak sensor response value. Peak load was at 15.7 milli-seconds, while peak sensor response at 72 inches from the load was at 25 milli-seconds. It took about 9 milli-seconds for the dynamic shock wave to travel through the sensor array resting on the unloaded slab, or an approximate average horizontal wave velocity of about 670 feet per second.

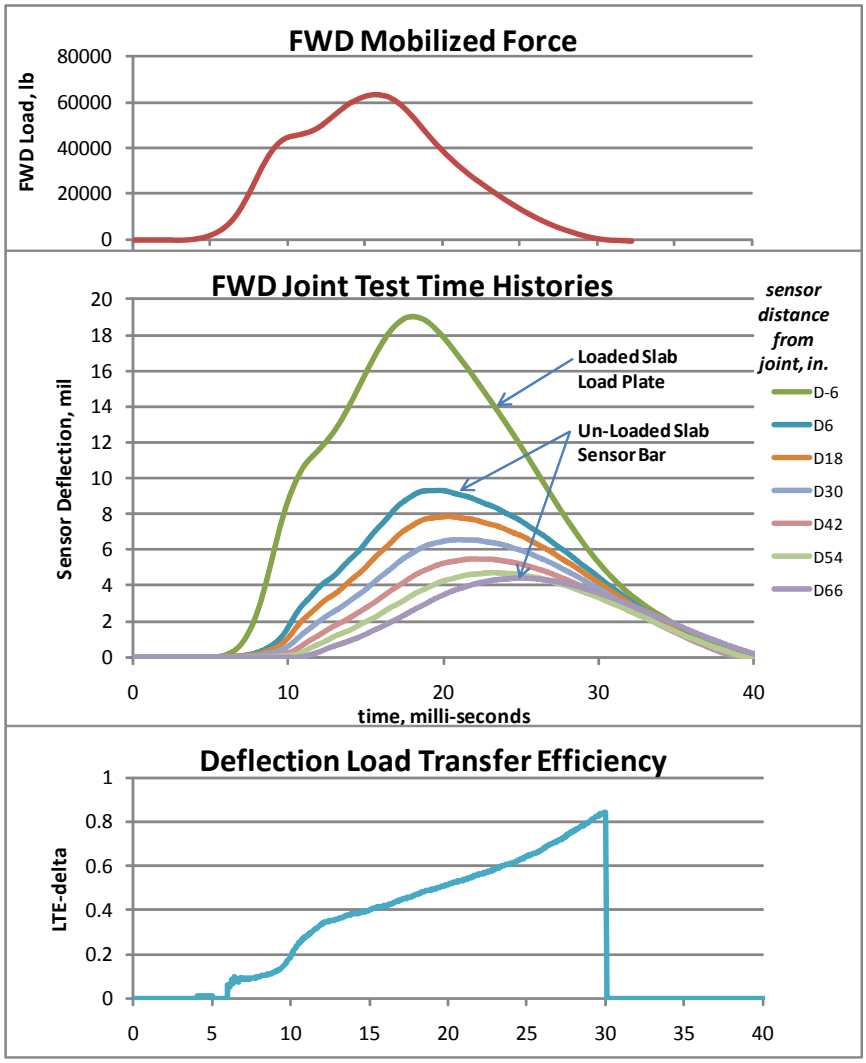

FIGURE 2.6. FWD 20,000 HZ SAMPLING TIME HISTORY DATA FOR THE SEVEN DEFLECTION SENSORS, LOAD CELL AND THE RESULTING LTE_δ RATIO FOR A LOAD TEST PERFORMED ON A LOW STIFFNESS RUNWAY JOINT

For the FWD joint load test, the deflection load transfer efficiency is defined as follows:

$$\text{Load Transfer Efficiency for Deflection } (LTE_\delta) = 100\left(D_6 / D_{-6}\right) \quad (5)$$

Where,

D_{-6} = Loaded slab load plate sensor deflection about 6 inches from joint
D_6 = Unloaded slab sensor deflection at about 6 inches from joint

The time history of LTE_δ for the joint load test is shown in figure 2.6. When looking at the time history of LTE_δ it is obviously a time dependent value that in this case, transitions from a value near 0.10 at the beginning of the test, to a value near 0.85 near the end of the test. Now, how does one select an appropriate single representative value of LTE_δ from such test data that ranges

from nearly zero to 100% over the test duration? This process deserves a clear explanation. Most FWD users do not perform detailed analysis of the time history responses for each load test. Most FWD data analyses use *single representative summary deflection and load values* from the sensors, obtained from each FWD load test time history. These are typically the maximum values from each time history function from the test data regardless of time history phase lag effects. LTE_{δ} has traditionally been calculated using the maximum deflection sensor values for the test, rather than using a fixed point in time as the basis.

Figure 2.7 shows the maximum sensor deflection values for the joint load test described above, and also for a mid-panel load test from the same test slab, for loads of approximately 60,000 lb applied to the 12 inch diameter load plate. The deflected slab shapes assumed for the two cases are shown and are completely different. For an interior mid-panel load test, concrete slab structural continuity is assumed to be present beneath all of the sensors and the slope of the deflected shape is generally assumed to be zero immediately beneath the load plate. This shape is often referred to as the "deflection basin" for mid-panel tests. The assumed deflected shape is significantly different for a joint load test. A structural discontinuity is assumed to be present between the load plate and the first sensor and the deflection slope beneath the load is not assumed to be zero. With a joint load test, the primary goal for this study is to characterize the vertical "*fault*" shaped deflection that develops at a joint during loading. This key measureable parameter is referred to in this report as the *deflection difference* at the joint line adjacent to the load plate. The deflection difference measurement (related to joint stiffness), combined with the total deflections of the sensors (related to subgrade stiffness and slab thickness), characterize the slab joint structural response and define how much load is being transferred across a slab joint during a joint load test. To get an estimate of the deflection difference fault size right at the joint line, the slab slopes near the joint are estimated using the sensor values. These slopes and the sensor deflections must then be used to interpolate the deflection magnitudes assumed present right at the joint line, which is about 6 inches away from the two adjacent deflection sensors on each side of the joint.

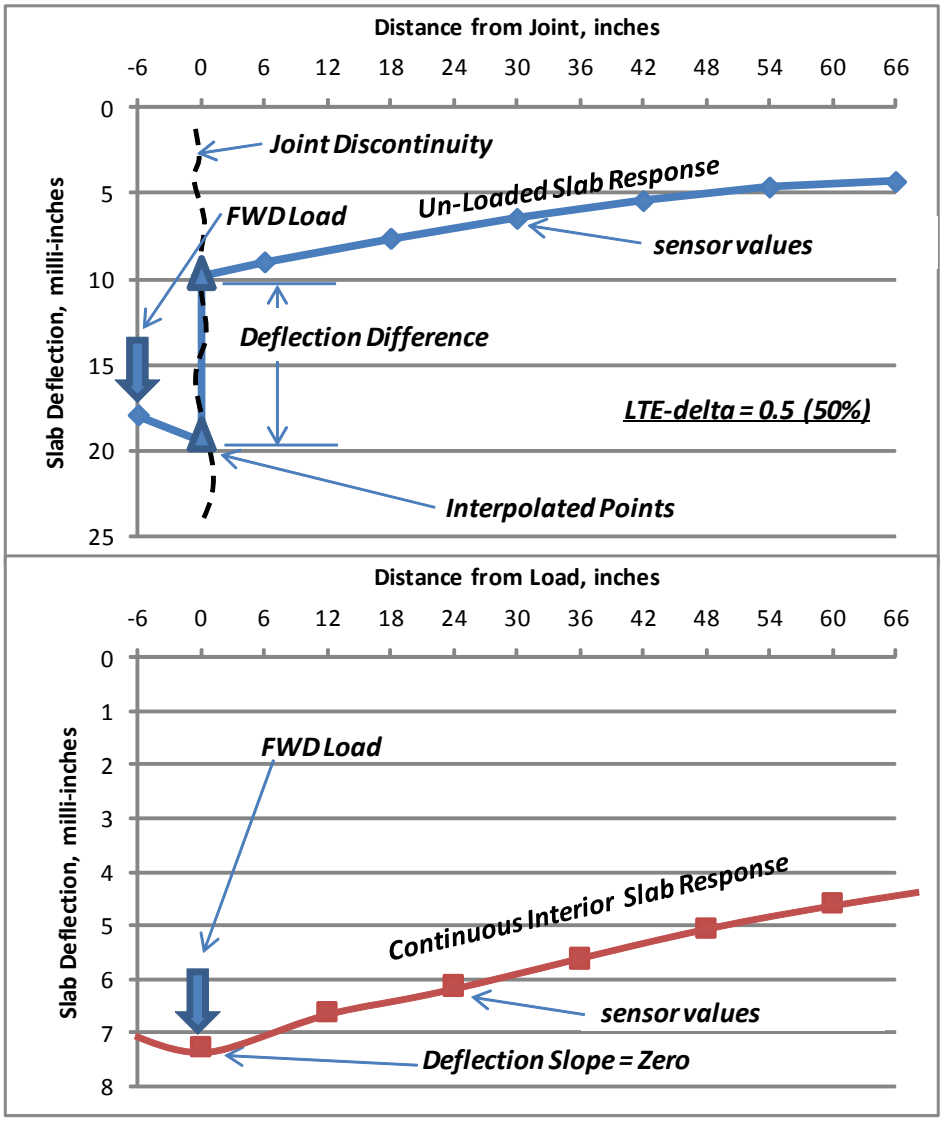

FIGURE 2.7. PLOTS HIGHLIGHTING THE DIFFERENCES IN ASSUMED SLAB DEFLECTION SHAPE FOR MID-PANEL VERSUS JOINT LOADING FWD ANALYSIS

The concept of LTE used for joint analysis is generally not theoretically valid when considering FWD load test data from continuous mid-panel areas with no cracks or faults between sensors. Yet, the LTE calculations can be, and should be, performed on mid-panel FWD load test data and the mid-panel results set an effective upper bound or "uncracked" behavior. This upper limit boundary can be compared to the actual joint tests to decide if an existing joint is functioning as a joint or if it is perhaps not cracked yet, or is in a state of compression lock-up with nearly full concrete slab flexural rigidity mobilized through the crack face. This research has shown that during hot weather, joints that are compressed tightly together can develop significant flexural rigidity and behave the same as structurally continuous mid panel areas.

While the time history data for LTE_{δ} in figure 2.6 ranged from about 10 to 85 percent, the representative deflection load transfer efficiency value assigned to this joint load test is 50

percent. There is a solid rational basis for selecting the 50 percent value. The 50 percent LTE_δ value is the representative single LTE_δ value that is calculated using the maximum sensor deflection values. Figure 2.8 shows the example weak joint load test LTE_δ time history data again along with results from three other FWD load tests: a stronger working joint, a possibly uncracked joint, and a mid-panel test data set from the same test site. The corresponding edge deflection difference time history functions are also shown below the LTE_δ data. The uncracked mid-panel test data reveals immediate LTE_δ mobilization and the slope of the initial mobilization function is steeper than all of the actual joint tests. The possible uncracked joint test data has just a slight zone of reduced slope between LTE_δ values of 0.2 and 0.6, but behaves almost identical to the uncracked mid-panel test data. The behavior of this joint is not significantly different than a mid-panel response, so this joint is characterized as "*possibly uncracked or locked*". The test on the "strong joint" had relatively rapid mobilization of LTE_δ and has a trend shape similar to that of the possibly locked or uncracked joint behavior, just shifted downward on the plot. The shaded area shows the time range for the maximum sensor deflections, and the representative single LTE_δ values shown are representative of this time period. The time at which peak load occurred is also shown in the deflection difference plot. The LTE_δ values calculated at the time of peak load are considerably lower than those calculated based on maximum sensor deflections. The maximum slab edge deflection difference values occur between the time of maximum load and the times of maximum sensor displacements. Theoretically, the maximum force developed across the joint occurs at the point of maximum deflection difference along the joint.

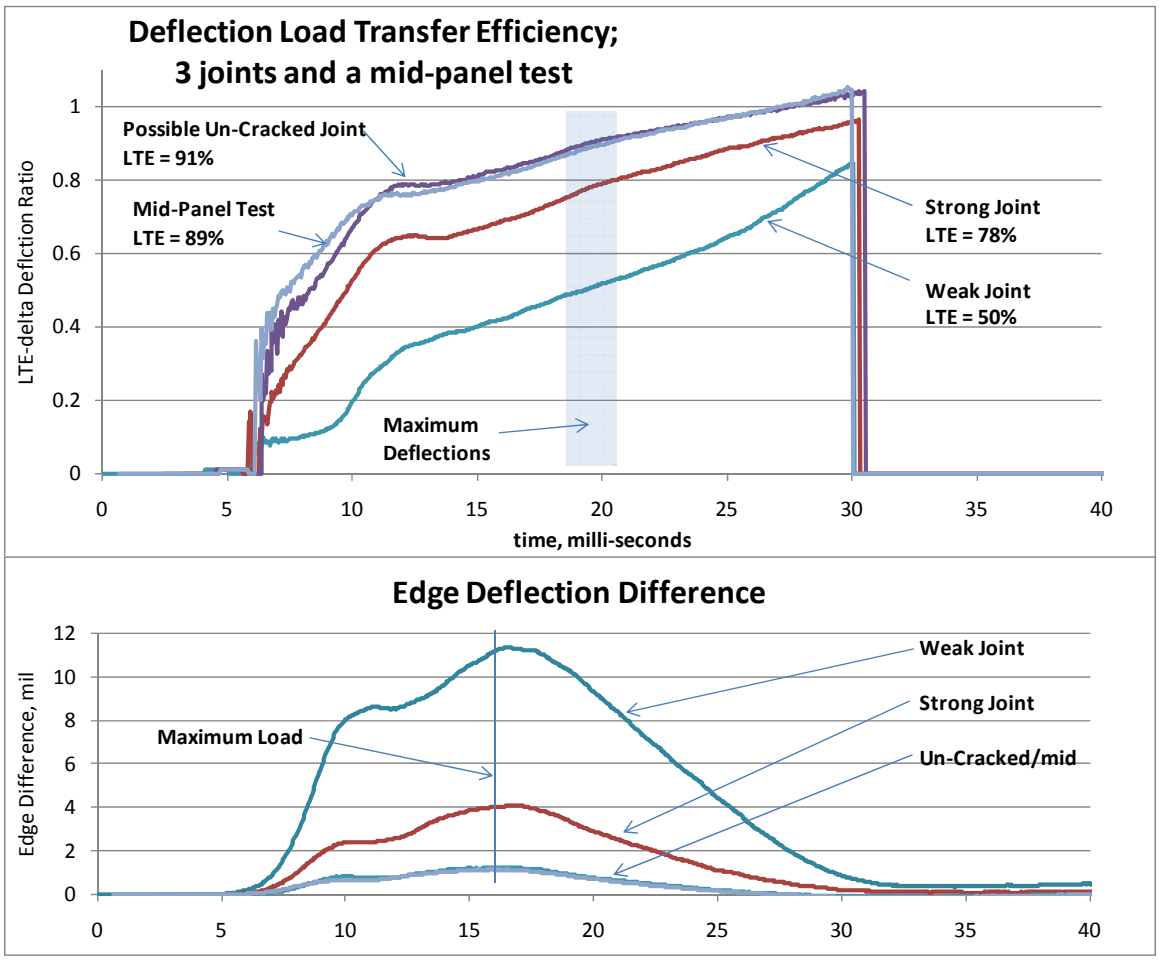

FIGURE 2.8. COMPARISON OF THREE JOINT TESTS, AND ONE MID-PANEL TEST TREATED AS A JOINT TEST, SHOWING TYPICAL TIME HISTORIES FOR LTE_δ AND EDGE DEFLECTION DIFFERENCE MAGNITUDE, SHOWING THE TIMES FOR MAXIMUM LOAD AND SENSOR DEFLECTIONS

As noted previously, the traditional method for calculating LTE_δ from FWD data is to use the maximum sensor deflection values, regardless of when these maximum values occur. There are two other rational procedures that can be used to get an LTE_δ value from a joint load test that are not commonly used in practice. The first other method is to calculate LTE_δ precisely when the load sensor value is at a maximum. This method will give lower magnitudes for LTE_δ and represents a lower bound rational method. Joint deflection difference is not yet fully mobilized at the time of maximum load. The traditional procedure based on maximum sensor deflection values, also completely rational, generates higher LTE_δ values and represents and upper bound calculation. FWD load and joint deflection difference magnitudes are already reducing at the time of maximum slab edge deflections. Perhaps the most logical way to calculate LTE_δ in terms of joint force and stiffness would be to calculate it precisely at the point in time when the joint deflection difference value is at a maximum. This point in time usually occurs between the time to maximum load and the time to maximum edge deflections, and closer to the time of maximum load. This is the point of maximum shear deformation along the joint crack face and

therefore should be the point at which maximum force was mobilized through the joint. Figure 2.9 shows the LTE_δ values from the three different calculation methods for the four load tests described above. The values obtained based on the maximum deflection difference time "snap-shot" are less than those from the traditional maximum deflection method. Nonetheless, it is now again pointed out that the overall magnitude of the dynamic slab edge deflection measured during an FWD load test will probably be less than the true static deflection would be for the FWD test load magnitude. A uniform increase in both the loaded and unloaded slab deflections, to account for the dynamic-to-static effect, while keeping joint deflection difference constant, will result in increasing LTE_δ values, increasing towards the values obtained using the maximum deflections. Therefore, the static-load LTE_δ values are probably greater than those calculated at the time of maximum joint deflection difference during an FWD test.

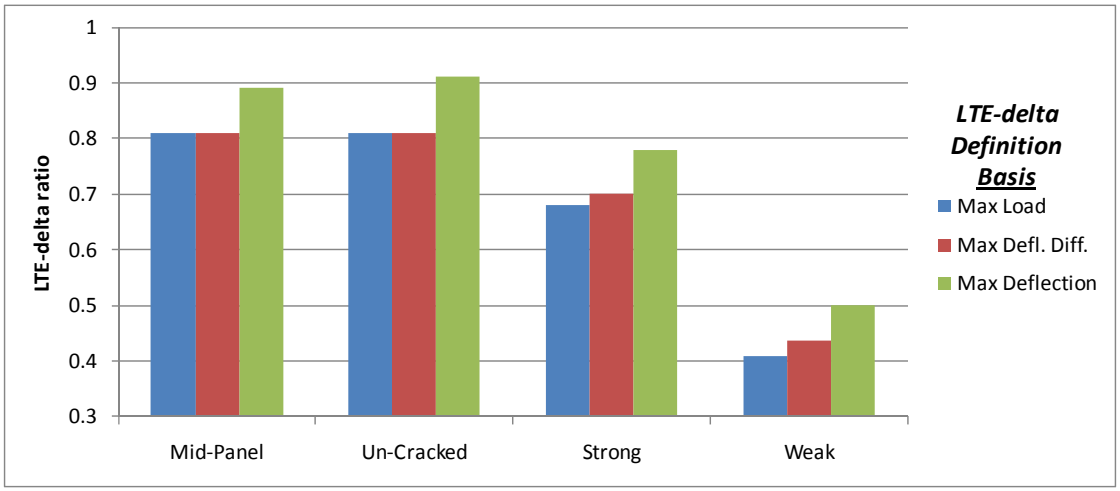

FIGURE 2.9. COMPARISON OF THE THREE RATIONAL METHODS FOR CALCULATING LTE_δ FROM TIME HISTORY DATA FROM THE FWD, WHERE THE TRADITIONAL METHOD IS BASED ON MAXIMUM DEFLECTIONS

Considering the three possible procedures and given the reduced dynamic deflections compared to static, when using the FWD the traditional LTE_δ calculation procedure based on the maximum sensor deflections is considered most representative of truth and is used as the primary basis of analysis and recommendations for this study. Given the dynamic nature of the FWD test discussed above, the traditional method is considered the best estimate of LTE_δ even though it is not calculated at the measured time of maximum joint deflection difference.

As described later in this report, thousands of these FWD pavement joint and mid-panel load tests were performed on in-service pavements for this study. Each daily visit to a test site resulted in approximately 500 to 1500 joint load tests, and 250 to 500 mid slab load tests, using a testing pattern repeated three times: once at about sunrise, once in the late morning and once in the early afternoon.

2.8 SUMMARY OF KEY VARIABLES AFFECTING LOAD TRANSFER

Based on the extensive literature review performed for this project, and considering FWD analysis and available instrumentation data, the following are the key variables related to joint stiffness and load transfer. The variables are divided into two sections. The first section contains the primary variables that control the load transfer value from a mechanistic perspective. The second section includes important secondary variables that cause variation of the primary mechanistic variables. In general, the effective joint stiffness is the key structural analysis parameter that is controlling how much load is transferred across a pavement joint for a given cross section. Most of the factors below affect the value of joint stiffness.

Primary Variables affecting Load Transfer through PCC Slab Joints

1. ***Joint Opening***- This is the primary factor controlling the effective measurable joint stiffness for aggregate interlock joints having no load transfer devices. At temperatures significantly below the casting temperatures for the concrete, the joints will open and lose ability to transfer loads through increasing joint looseness and slack. As pavements age and go through repeated summer thermal expansion cycles, the slabs will physically push or thrust themselves apart over time, causing a progressive opening of some joints. As the joints open, slack and looseness increase resulting in lower LTE and effective measurable joint stiffness.

2. ***Joint Shear Face Roughness***- The size and sharpness of the shape irregularities on the crack that forms through the joint will control how the joint responds to changes in joint opening size. For example a PCC mixture with soft aggregates may tend to crack through aggregates, rather than around aggregates, developing a smoother crack surface, resulting in greater sensitivity of the joint to loss of load transfer capability as a result of small changes in joint opening. The crack faces grind together and interlock in shear to develop joint stiffness. Exhumation of joint faces from older highway joints reveal vertical grooves at the shear contact tips of crack face roughness such as coarse aggregate tips, related to differential deflections at the joints and grinding action. Vertical groove formation causes loss of effective stiffness, and results in greater sensitivity to changes in joint opening and is a primary traffic related aging mechanism.

3. ***Joint Load Transfer Devices***- Devices such as dowels and tie bars placed across joints can resist the loss of load transfer ability during cold weather that results from opening of the joints. Tied joints with deformed bars or steel mesh maintain high when stiffness when the steel holds the crack faces tight, keeping aggregate interlock high. Dowels and tie-bars work in combination with aggregate interlock roughness in the overall total joint stiffness. When the joint opening becomes large enough to eliminate aggregate interlock, the steel reinforcement and its embedment zone support condition (*modulus of dowel-concrete interaction*, often called *K* or *DCI*) are the only joint load transfer mechanism. Dowels can completely lose load transfer ability over time at airfield pavement sites through deterioration of the dowel-concrete interaction zone.

4. ***Slab Thickness***- There is a general trend of increasing joint stiffness for increasing slab thickness as the crack face area increases. Yet, there is also a general trend of lower achievable stress load transfer, LT, between slabs as the slab thickness increases. This is related to the fact that flexural rigidity of slabs increases in proportion with the slab thickness cubed, while the available joint shear area and aggregate interlock stiffness only increase in proportion to slab thickness.

5. ***Slab Curvature***- Changes in slab curvature will not directly affect joint stiffness, but do significantly change the total joint deflections and overall load transfer behavior. The definitions for slab curvature used in this study are those established by the Highway Research Board in the 1940s. Slab curvature caused by thermal gradient related expansion and contraction of the PCC is defined as ***curling***. Slab curvature caused by any other mechanisms such as moisture gradient, curing, construction temperatures, accumulating slab moment creep rotations, base moisture supply… is defined as ***warping***. Curling is well understood and can be accommodated in our current slab analysis software. Warping remains a relative mystery and is one of the largest gaps of knowledge currently existing between real slab behavior and our ability to simulate slab behavior. The primary effect of curvature variation is to cause changes in apparent subgrade stiffness for the slab edges by causing variations in effective subgrade confining pressure and perhaps introducing small air gaps between the slab edges and the subgrade. Curling and warping can also cause residual static tensile and laminar shear stresses to develop in slabs, which will combine with wheel load stress eventually cracking the slabs in fatigue.

6. ***Load Magnitude***- Larger multi-wheel gears mobilize greater stress load transfer percentages than smaller single wheel loads for a given joint stiffness condition. Varying the FWD load magnitude can also affect the LTE value, with LTE generally increasing with FWD load magnitude for "non-locked" joints. This is explained by some slack and/or looseness being present in joints in general.

7. ***Base and Foundation Type***- The test data indicate that bases in general were not behaving like strong uncracked elastic solids. The FWD data reveals joint behavior at most sites to be more like that associated FEM simulations using the dense liquid subgrade. Granular base and subbase systems appear to be more sensitive to changes in apparent stiffness caused by curling. Granular materials can experience great changes in stiffness as a function of effective lateral confining pressure. Curling related slab deflections can cause top-of-base lateral confinement pressures to go from very high during early morning at mid slab when the weight of all up-lifted slab edges is transferred to the mid slab area, to zero at both mid slab and edge locations when slab curling related edge or mid-panel lift-off occurs.

Secondary Variables (Significant Cause Factors for Primary Variables)

1. ***Air Temperature***- Daily and annual changes in air temperature are the primary cause for changes in the joint opening size and the slab curvature changes from curling caused by thermal gradients.

2. ***Annual Precipitation and Humidity***- In general, warping of concrete panels is related to annual precipitation and humidity variations. Flatter slabs and smaller joint openings are associated with higher and more uniform precipitation rates. Research on the warping of highway pavement slabs showed that slabs were generally warped upwards with equivalent warping thermal gradients of about 2 and 3.5 F°/inch thermal gradients for annual precipitation values of about 45 and 10 inches respectively (Byrum, 2000). Annual precipitation may also be related to joint opening sizes where a trend of slightly larger joint openings in drier climates would be expected.

3. ***Slab Length Relative to Thickness***- For the same slab thickness, longer panels will develop larger joint openings and typically have greater curling deformations and residual thermal stresses in response to daily changes in temperature. In the context of slab modeling, the dimensionless ratio of the slab length to the radius of relative stiffness value (L/ℓ) is often used to describe slab geometry. There is a critical slab length for a given radius of relative stiffness. When slab length is about 8.5 times the radius of relative stiffness the mid slab curling stress levels will be a maximum for thermal responses (Westergaard, 1927). Slabs shorter than this will have reduced internal stresses for a given thermal gradient magnitude. Airfield slabs typically use slab dimensions in the range of 3 to 6 times the radius of relative stiffness. Peak curling related vertical joint deflections will occur when slab lengths are about 4 times the radius of relative stiffness. Because airfield slabs are relatively short compared to their thickness, the slabs tend to curl relatively freely while having lower residual curling stress levels. Thermal gradients are expressed more in the form of deflection rather than stress for typical heavy duty airfield pavements using joint spacing less than 20 feet.

4. ***Load Positions/Configuration***- The interaction of typical aircraft multi-tire gear patterns and typical slab dimensions with respect to top of slab versus bottom of slab fatigue crack analysis is complex. This interaction is further complicated and affected by slab curvature from curling and warping. A systematic way of evaluating top of slab stress cracking for multi-gear loading has not yet been fully established. Bottom of slab type cracking under the wheel loads is easier to analyze and better understood.

5. ***Joint Age/Traffic***- Pavement joints will experience progressive loosening and slab edge gap development over time and repeated loads, resulting in a loss of joint and subgrade stiffness. When significant looseness or slack is present, little to no load transfer joint stiffness may be present for smaller loads near the end of service life. Durability distress, if occurring at a site, is almost certainly correlated to more rapid loss of load transfer and the joint face is the first area that will experience durability losses and decay. If durability distress is visible at the surface it almost certainly is worse on the joint face and bottom of slab.

CHAPTER 3. CONCRETE PAVEMENT TEST SITE EVALUATION PROCEDURES

3.1 OVERVIEW

After considering the key factors affecting joint load transfer, the capabilities of the FWD, and other available tools for on-site evaluations, a comprehensive on site testing procedure was developed. The goal was to have a detailed mechanistic evaluation procedure that would capture a site's joint responses three times per day, sampled over the full daily thermal curling cycle. Regarding slab curling, in the few hours just before sunrise, while air temperature is coolest, the top of a concrete slab is generally at its coolest point relative to the bottom of the slab. The thermal contraction of the top surface can cause upward slab curvature to develop, causing joints to lift off of the subgrade. Joint openings reach a local daily maximum during this cooler time period. Conversely, the point when the top of slabs is warmest relative to the bottom occurs in the early afternoon. Downward slab curvature during this time can cause the joints to press into the subgrade and lift the middle portion of slabs off of the subgrade. Joint openings reach a daily minimum during this time period of warmest air temperature. The target times for FWD testing were: Round 1 (slabs curled-upward, just before sunrise), Round 2 (slabs nearly flat, late morning), and Round 3 (slabs curled-downward, just after noon). Several other testing techniques and devices were used and will be described in more detail later. The summary list of on-site testing procedures is as follows:

1. **FWD Testing**- A roughly square "test site" typically six slabs by six slabs in size was used. An FWD test pattern was established and the pattern repeated typically three times, early morning to mid-afternoon. The pattern included mostly joint load tests, but also included mid-panel load tests and corner load tests.
2. **Slab Curvature (Curling and Warping) Measurements**- Analysis of curling and warping was accomplished using an analysis of the variation of slab end slopes. A DIPSTICK slope measurement device was used to obtain slope samples at ends of slabs. These values are used to measure slab curvature changes during the testing window from curling, and to obtain an estimate of the site average locked-in warp curvature value occurring at about 8 AM.
3. **Joint Opening Change Measurements**- deflection measurement devices were epoxy mounted over joints to measure the change in joint opening, or "joint closure" that occurred during the testing window, relative to a zero value taken immediately after installation near sunrise. Actual joint opening widths could not be measured at the sites, but changes in joint openings were measured relatively accurately.
4. **Slab Rotation Measurements**- Two seismic geophones were set at the far edges of slabs during FWD joint load tests in attempt to capture the dynamic uplift of the far slab edges that occurs as a result of slab rotation or tilting under load.
5. **Distress Map**- A distress map was prepared showing types and locations of existing cracks and other distresses to establish an approximate Structural Condition Index value for the test area.

Identifying airfield test sites that qualified as suitable candidates was challenging. The various airfields that allowed testing donated the staff time required to coordinate our efforts and this is greatly appreciated. In general, it was more difficult to access large high traffic airfields, where

extensive security clearance efforts were required. Figure 3.1 shows the general locations of the airfield test sites, along with the approximate locations of the supplemental DIA, NAPTF, and Road test sites evaluated. The border between wet and dry regions shown is approximately 20 inches of annual precipitation. The border between freeze and non-freeze regions is a freezing index value of about 200 ºF-days.

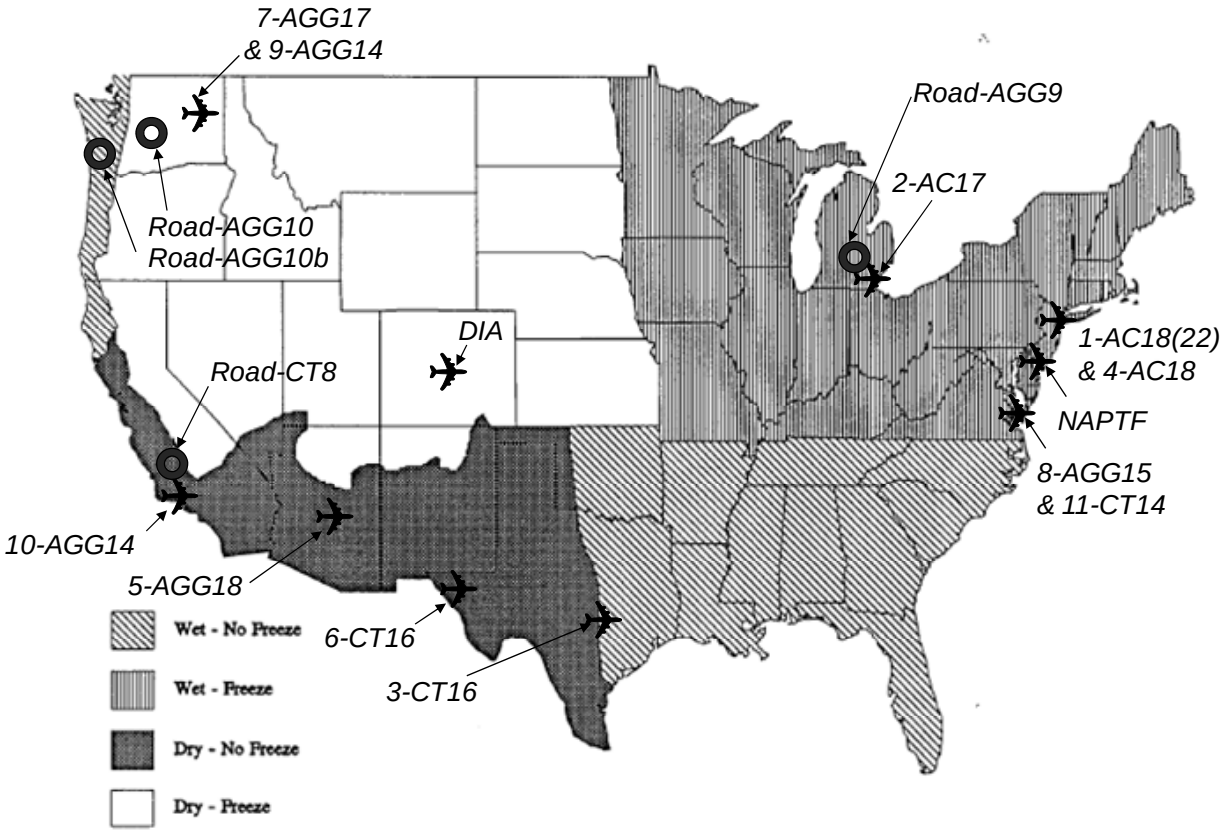

FIGURE 3.1. MAP OF THE USA SHOWING GENERALIZED CLIMATE REGIONS AND TEST SITE LOCATIONS

The NAPTF, DIA, and Road test sites are "*pre-existing data*" test sites. This means the sites had adequate FWD and cross section data to be analyzed in detail, but perhaps are missing other data such as slab curvature or joint opening change data. The new "*full*" test sites are named starting with a number, 1 through 11, listed in order of decreasing mid-panel structural stiffness. The site number is followed by the base type code: AGG, CT, or AC for unbound aggregate base, cement treated base, or asphalt concrete base, respectively. The site base code is followed by a number representing the design concrete slab thickness in inches. In general, coring of the pavement slabs in order to accurately measure slab thickness was not allowed. Therefore, this research relies on the "*design thickness*" as the basis for the assumed slab thickness for all analyses. The design thickness was obtained from construction plans for the test site areas, which were available for all of the full test sites. Figure 3.2 provides a summary of the eleven full test site *design cross sections*.

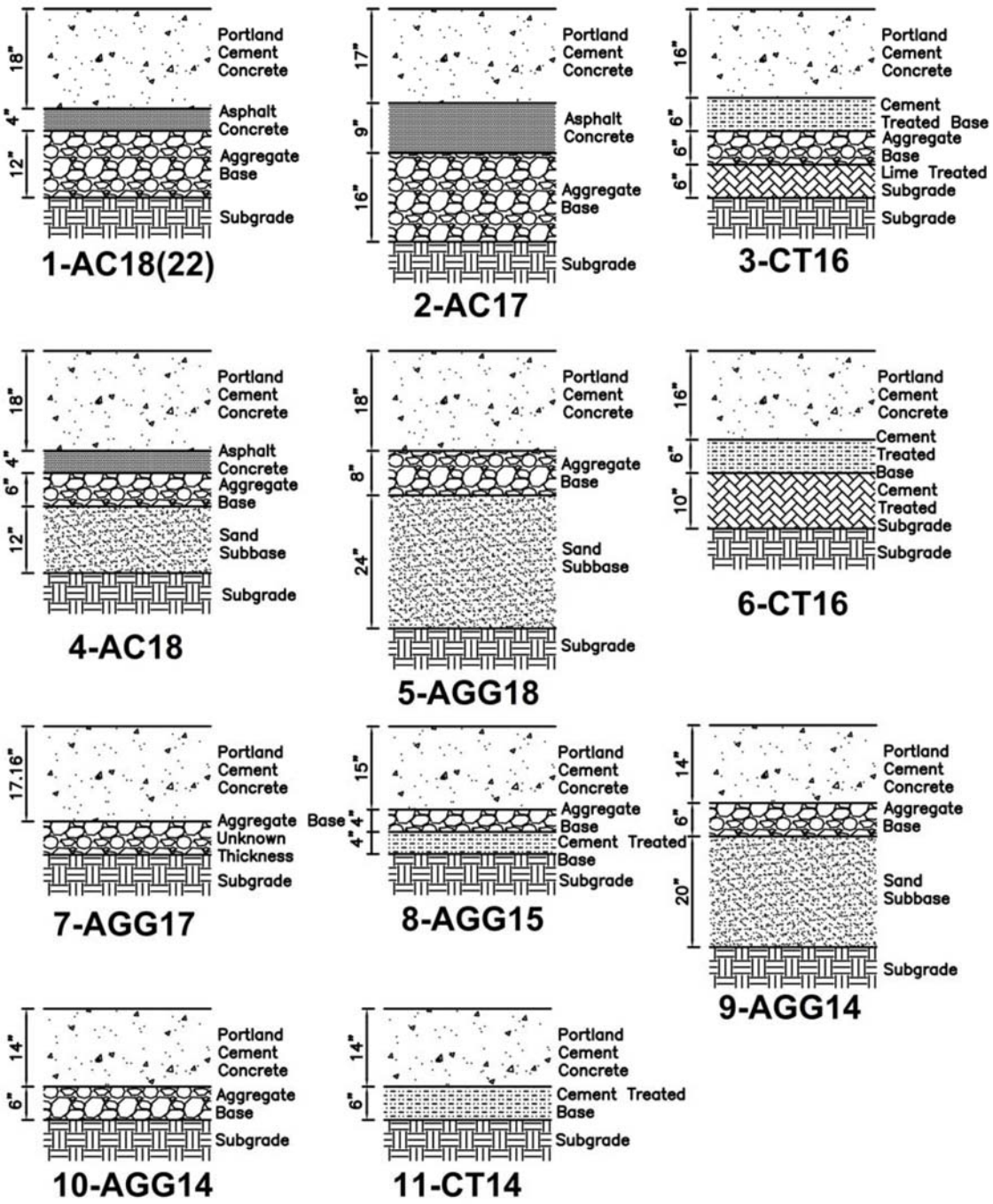

FIGURE 3.2. DESIGN SECTIONS FOR THE ELEVEN AIRFIELD TEST SITES

Figure 3.3 shows the mid-panel FWD load test overall average load versus deflection trends for the design cross sections shown in figure 3.2, and other test sites. In general, a good distribution of pavement cross section mid-panel stiffness was obtained. The deflection equations shown are listed in order of increasing stiffness and represent dynamic FWD deflections, which are slightly less than the static deflections expected for these sections.

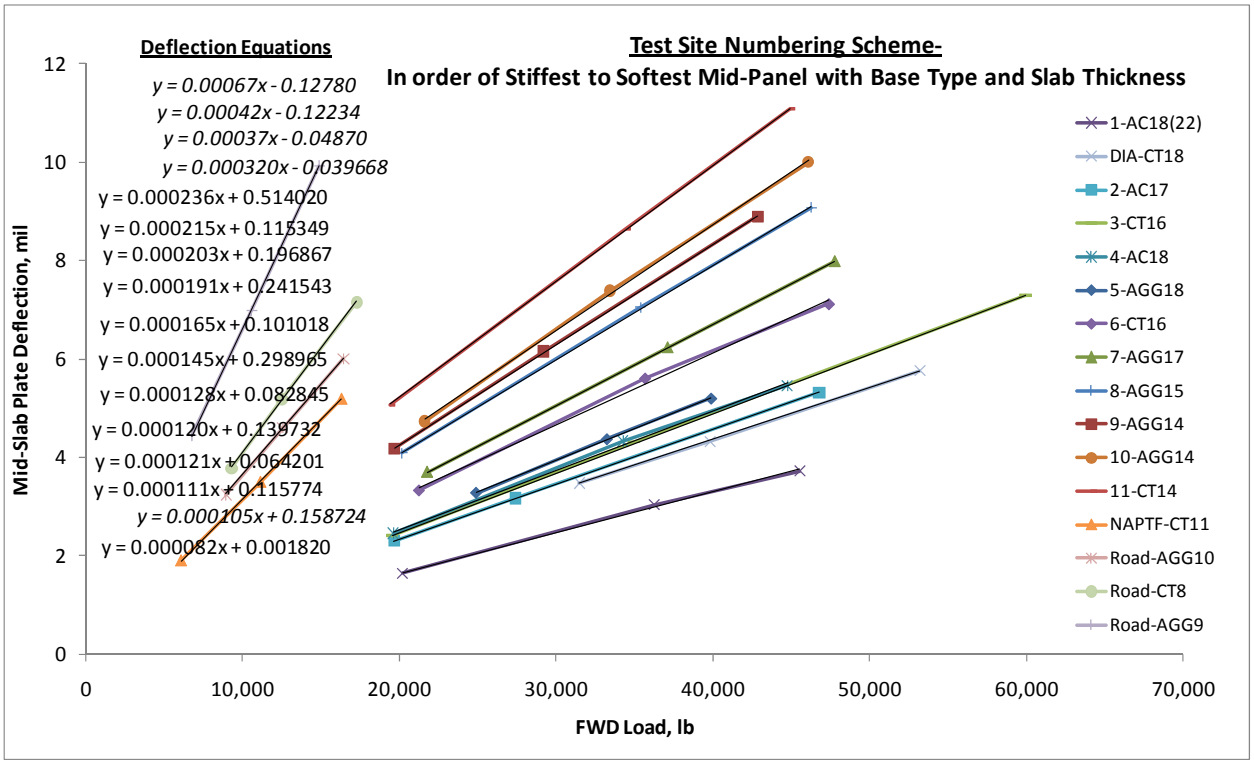

FIGURE 3.3. AVERAGE MID-PANEL LOAD VERSUS DEFLECTION FOR THE TEST SECTIONS, WITH AIRFIELD SITES LISTED IN ORDER OF DECREASING STIFFNESS

Once arriving at a test site, often in the dark just before sunrise, the first part of the evaluation process was to finalize the test patch location and mark and label the slab numbers within the test patch. Figure 3.4 shows a typical test site layout diagram and slab numbering scheme. This site had 25-ft x 25-ft panels and two joint types were identified on the site specific construction plans, "A-Joints and B-Joints". Three cracks were identified to be present in the test patch. The joints in the test patch are assigned a name code, which is the slab number with a N, S, E, or W identifier representing the north south east and west edges of the slab. Mid-panel load tests are assigned an M code, and corner load tests are assigned a C code. These code names are used by the FWD operator to track the locations of each test. The FWD "Test Lanes", Run 1 through Run 12, are shown as lines with FWD vehicle direction of travel arrows. The FWD is pulled along and always tests joints with the sensor bar resting on the unloaded slab. Where double lines are shown, the FWD was run in both directions to gather data regarding joint response symmetry and off-set slack.

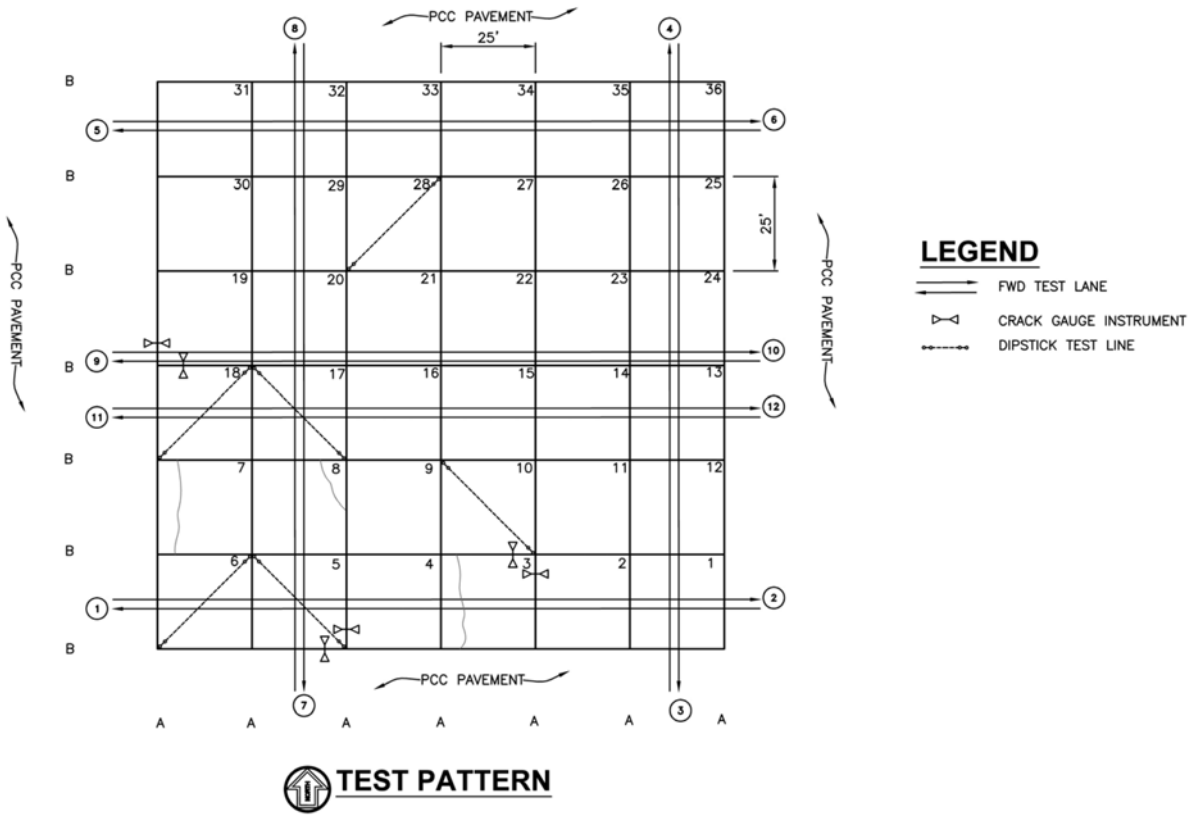

FIGURE 3.4. A TYPICAL TEST SITE LAYOUT DIAGRAM, FROM TEST SITE 4-AC18

At this point, the on-site test procedures and related data analysis will be described in detail. Examples from the test sites are used to demonstrate the procedures and show the type and nature of the resulting data, and how it is used. The detailed summary data and analysis results for the full test sites are provided in Appendix A.

3.2 FWD DATA ANALYSIS PROCEDURE

An FWD testing pattern similar to that shown in figure 3.4 was performed typically three times on the day of testing. At each test location four load tests were performed, using an increasing load magnitude pattern. The first two drop loads were about 20 to 25 kips. The third load ranged from about 30 to 37 kips, and the fourth load ranged from about 40 to 48 kips.

One quality control issue related to joint testing is the issue of how close the FWD load plate must be to the edge of the slab in order to be acceptable as a joint load test. This study pushed the limits of the FWD operator's ability to set the load plate close to the joint. The FWD operator either uses a spotter giving hand signals to get onto the load test spot, or uses an on-board camera showing the load plate and pavement, to make sure the load plate is close to the joint and not overlapping. In general, the edge of the FWD load plate had to be less than about 2 inches from the edge of the slab. This often required 2 to 3 back and forth attempts for

positioning of the vehicle. Overlap of the load plate onto the adjacent slab was strictly not allowed. Mid-panel load tests were visually estimated into position without precise geometric measurement of the mid slab location. The first step of the FWD data analysis is to split the field data into the joint load tests, corner load tests, and mid panel load test data sets. Once the data is split, the site analysis begins with detailed analysis of the mid-panel slab responses.

3.2.1 Step 1 of the Data Analysis- Slab Interior Load Backcalculations

Using the design slab thickness from the construction plans, the ILLI-BACK backcalculation procedure and software (Ioannides, 1989) was used to characterize the mid panel response for a site. This backcalculation procedure is a slab-on-foundation analysis method that backcalculates the apparent subgrade stiffness (dense liquid and elastic solid subgrade idealizations) and slab concrete elastic modulus using the design thickness and FWD deflection basins as input. A key point for this procedure is that the subgrade stiffness value it backcalculates is the "bottom of slab" subgrade stiffness. This stiffness value is representative of the composite foundation system including the natural earth, embankment, subbase materials and base materials. When the resulting backcalculated concrete elastic modulus output value is unusually large, there are two probable explanations: one is that the in-place concrete slab thickness is significantly greater than the design thickness used as input, and the other is that the base materials are acting integrally with the concrete slab, making it appear thicker than it is. In general, most backcalculated elastic modulus values were relatively high, indicating the in-place thickness could have been greater than design plan thickness. Reasonable values for backcalculated concrete elastic modulus were obtained at all but one test site, the stiffest test site evaluated. The backcalculated concrete elastic modulus values for test site 1-AC18(22) were between 9,000,000 and 12,000,000 psi when using the assumed design slab thickness of 18 inches. Real concrete elastic modulus values this high would be unusual. For example, the in-service concrete slab elastic modulus values from the Federal Highway Administration's Long Term Pavement Performance General Pavement Studies 3, 4, and 5 test sections from concrete core samples averaged about 4,600,000 psi for concrete samples between 5 and 40 years old, with elastic modulus values ranging from about 2,000,000 to 7,000,000 psi (Byrum, Kohn and Hansen, 1998). ILLI-BACK can also be used in another way: the input is assumed concrete elastic modulus and FWD loads and deflections, and the output is apparent slab thickness and subgrade stiffness. When a concrete elastic modulus of 5,000,000 psi was used for this stiffest site 1-AC18(22), the backcalculated apparent slab thickness was in the range of 21-24 inches.

The mid-panel deflection basins and loads from a test site were first "normalized" to a common load magnitude. The data was scanned for apparent bad or suspect tests. For example if a mid-panel test has a very low LTE_{δ} value, perhaps there is a mid-panel crack in that slab or sand debris that affected the FWD sensor deflections. Figure 3.5 shows an example of a mid-panel data set, from test site 5-AGG18. This test site was a runway landing zone in the desert southwest climate. The slab panel sizes are 18.75 by 18.75 feet with all joints doweled. Slab surface temperatures measured by the FWD ranged from about 85 °F at the start of testing for Round 1, to about 130 °F at the end of testing for Round 3. This test site showed the largest thermal curling responses of all the full test sites. The slab curvature analysis, described later, showed that the slabs were curling significantly during testing, and this curling affected both

mid-panel and joint responses. Other airfield test sites did not show as much variation in mid-panel response.

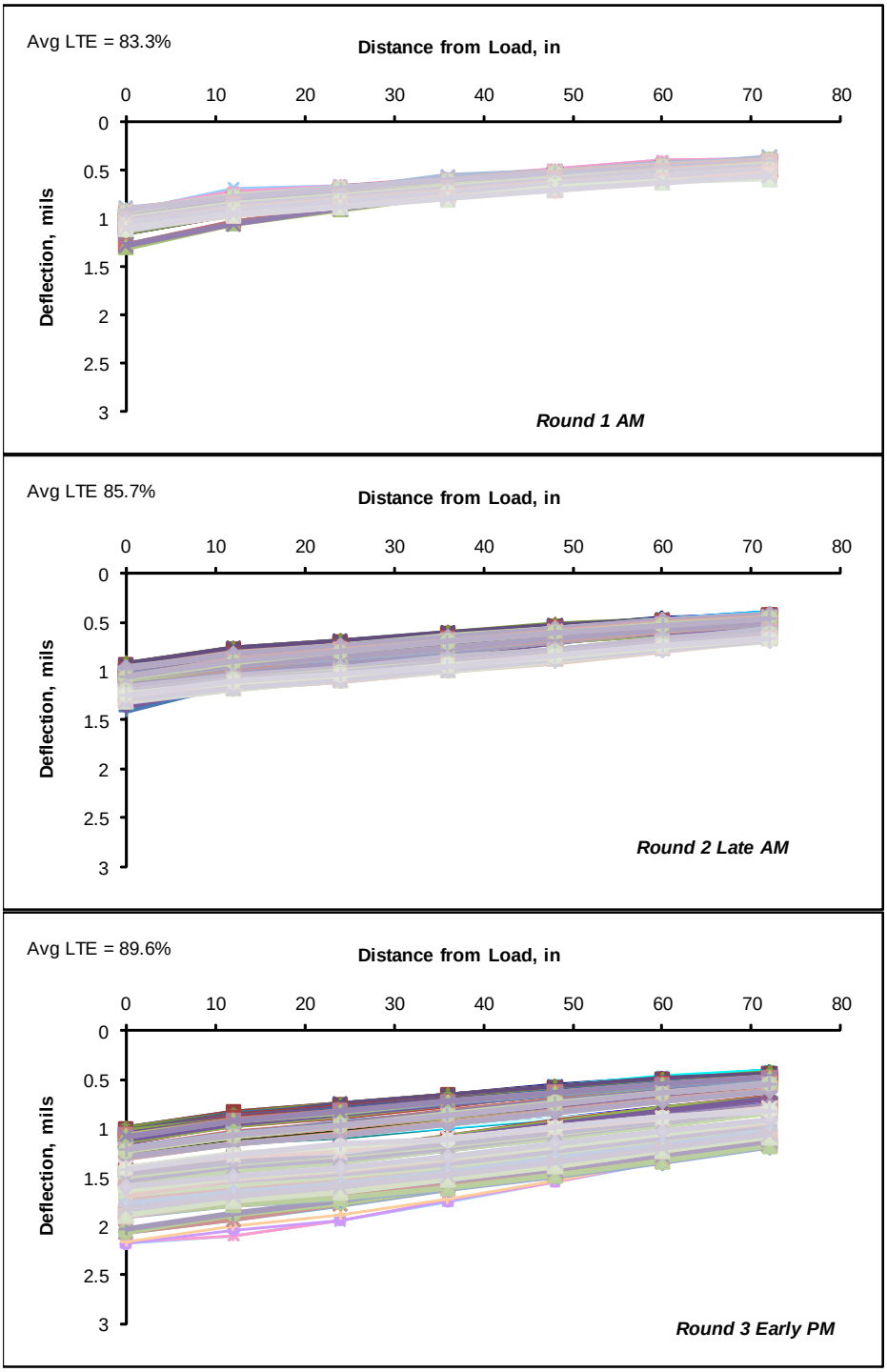

FIGURE 3.5. TOTAL RANGE OF 9-KIP NORMALIZED MID-PANEL DEFLECTION BASINS FROM TEST SITE 5-AGG18, WHICH EXPERIENCED SOME MID-PANEL UP-LIFTING DUE TO AFTERNOON SLAB DOWN-CURL

Figure 3.6 provides the ILLI-BACK summary for the mid-panel FWD data shown in figure 3.5. The backcalculated radius of relative stiffness values are shown for the dense liquid foundation condition. The bar chart shows the coefficient of variation for the normalized sensor deflections. This plot is used as a site variability index, and as a check of FWD data quality. The standard deviations should be similar for all sensors. If one sensor stands out, the sensor may have been loose or bad. For this test site, the early morning standard deviations are low in magnitude compared to other test sites. The Round 2 standard deviations are medium to high, and the Round 3 standard deviations while some mid panel areas experienced uplift were very high relative to the other test sites. This sensor standard deviation pattern reveals that the high variability in mid-panel deflection during Round 3 is probably due to mid-slab uplift occurring in several panels, with variable air gap sizes beneath slabs. Unusual behavior areas are often separated out, such as slab #34 at this site, which experienced large center of panel uplift from curling. The analyst's best estimate of overall representative values for the site to be entered into the final project database are shown, which in this case eliminated slab 34 and Round 3 data from the averaging. It should be noted here that this large apparent subgrade stiffness variation was observed on an unbound aggregate base and subbase system. Unbound granular materials can be susceptible to softening related to loss of lateral confinement pressure. When a mid-panel uplift occurs, the aggregate base material beneath that area essentially has zero confinement pressure at the top surface. If extreme upward curl develops in slabs, completely lifting all joints off of the base material, the slab weight becomes concentrated over the mid slab region. This can create large confining pressures perhaps two to four times the equivalent weight of the concrete slab thickness. At this site, the mid panel confining pressure for the aggregate base materials went from a high value during Round 1, to having low values at several locations during (Round 3) as slabs changed shape from morning up-curl to afternoon down-curl. Some mid-panel areas remained fully seated during Round 3. In general, it was found that some paving lanes at a site could have up-warped slabs, while adjacent paving lanes could be flat or down-warped. This can explain why some mid-panels remain seated and some uplifted during Round 3: varying magnitudes of locked-in up-warp in paving lanes.

Site 5-AGG18 ILLIBACK Summary- Site Averages do not include slab 34M response

	Dense Liquid Subgrade				Elastic Solid Subgrade				Radius of Relative
	k-value	*k* stdev	Slab E_C	E_C Stdev	Subg. E_S	E_S stdev	Slab E_C	E_C Stdev	stiffness (DL subg)
Site Average =	488	59	3.49	0.4	77,380	5,371	2.55	0.18	43.4
Min. Defl. =	791	135	3.21	0.52	112,896	11,200	2.22	0.22	37.7
Max. Defl. =	300	29	2.96	0.27	50,615	2,784	2.22	0.12	47.1
Run 1 avg	671	114	3.10	0.49	98,307	9,973	2.17	0.22	38.9
Run 2 avg	557	75	3.47	0.44	86,173	6,721	2.50	0.2	42.0
Run 3 avg	330	25	3.84	0.27	57,653	2,208	2.91	0.11	49.0
Slab 34M Run1	390	38	3.69	0.34	65,261	3,772	2.76	0.16	46.6
Slab 34M Run2	133	3	4.31	0.09	28,731	455	3.49	0.06	63.4
Slab 34M Run3	86	1	4.01	0.05	20,083	344	3.31	0.06	69.4
Best Guess	**614**		**3.29**		**92240**		**2.34**		**40.4**
	psi/in		*Msi*		*psi*		*Msi*		*inches*

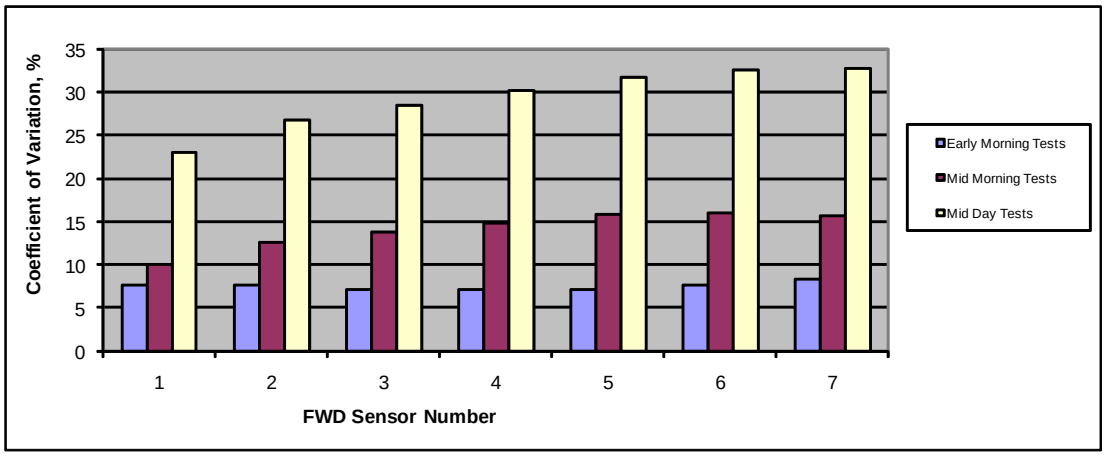

FIGURE 3.6. TYPICAL SUMMARY OF FWD MID-PANEL TESTING (TEST SITE 5-AGG18, 1 MILLION Msi = psi)

At this point it is necessary to introduce the concept of subgrade compliance to curling and warping. Some subgrades and foundation systems appear to have the ability to plastically conform to very slow changes in slab shape caused by curling (24 hour shape changes) and warping (dry to wet cycles cause shape change). At some test sites, curling measurements revealed large curling was occurring, while FWD measurements revealed almost no difference or changes in support at mid panel or joints as a result of slab curling. A site with an apparent great ability to conform to curl and warp was site 2-AC17, where the cross section consisted of 17 inches of concrete over 9 inches of asphalt concrete over unbound aggregate over weak wet clayey subgrade with high groundwater. This type of subgrade probably behaves as a fluid-filled bag with respect to the extremely slow loading rates associated with curling and warping, while behaving stiffer, more un-drained for very high loading rates. These types of subgrades can allow curling shape change to occur without apparently stressing the slabs much and without formations of large voids at slab edges or mid panel. Some sites are clearly not as compliant, like site 5-AGG18 just demonstrated, and each site has some different degree of ability to conform to curling and warping.

3.2.2 Step 2 - Direct Calculation of Joint Stiffness from FWD Deflections

This section describes the new simplified procedure to directly calculate total joint stiffness, k_J, in units of lb/in/in or psi. This calculated joint stiffness has the same units as the Skarlatos/Ioannides q_0 parameter, or the k_{joint} parameter used by Brill (1998), or the G_Z parameter used by Hammons (1998), or the *AGG* parameter used by Ioannides and Hammons, 1996. This procedure starts by estimating two geometric parameters from the joint load test deflection data: the characteristic slab edge response length, L_R, and the approximate edge response angle, ϕ, as shown in figure 3.7. Figure 3.7 shows a joint test from joint number 1-10-D4 contained in the DIA instrumented test site FWD database. Based on the 12-inch sensor spacing FWD configuration with the sensor bar resting on the unloaded slab, these parameters are defined as follows:

$$\textit{Approximate Edge Response Angle, } \phi = \tan^{-1}[(D_6 - D_{66})/60] \quad (6)$$

$$\textit{Characteristic Response Length, } L_R = 66 + D_{66}/\tan(\phi) \quad (7)$$

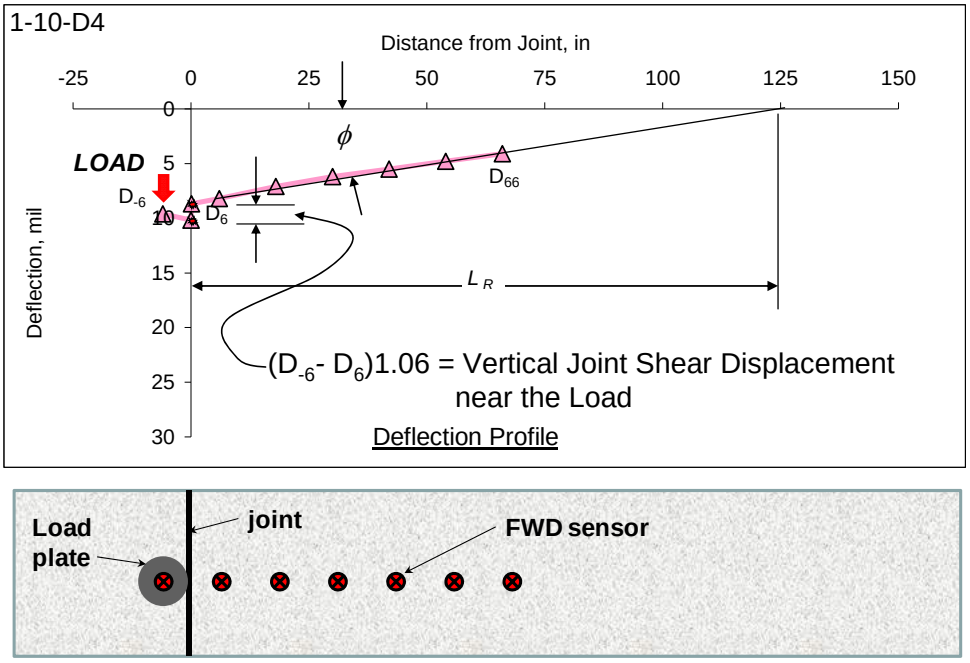

FIGURE 3.7. PLOT SHOWING THE FWD SENSOR MAXIMUM DEFLECTIONS, INTERPOLATED SLAB EDGE DEFLECTIONS, ALONG WITH THE EDGE RESPONSE ANGLE, ϕ, AND RESPONSE LENGTH, L_R, FOR LOAD PLACED AT LOCATION D_{-6}

The 1.06 factor shown reflects that about a 6% increase in the D_6 deflection magnitude was required in order to project the slab deflection shapes from the measured location, out to the joint line six inches away. The same percentage increase is applied to both the D_6 and D_{-6} values, such that the measured LTE_δ ratio is kept the same for the slab deflections that are projected to the joint line. Percentage increase values necessary to project deflections from different sites

ranged from about 5 to 8 percent, generally being higher for thinner slabs with higher deflections. The slope of the response angle line times the distance between the sensor and the slab edge, and divided by the D_6 deflection magnitude can be used as a rational percentage increase magnitude for the D_6 and D_{-6} deflections. Any suitable projection technique can be used.

The characteristic response length, L_R, along with the deflection values interpolated at the joint face are used to develop a linear approximation of the vertical shear displacement that developed along the joint face for a given FWD load test. The deflection response is assumed to be radial symmetric and the response length, L_R, measured perpendicular to the joint is rotated 90 degrees and assumed to also be present parallel with the joint line and in both directions from the load. Figure 3.8 shows the vertical shear displacement estimate for a joint load test. It is the exposed area of the unloaded slab crack face while the loaded slab is deflected downward and after subtracting out the unloaded slab deflections from both sides, i.e. unloaded slab deflection profile serves as a zero reference. The detailed analysis of the load transfer across this vertical joint shear displacement area was the focus of this study.

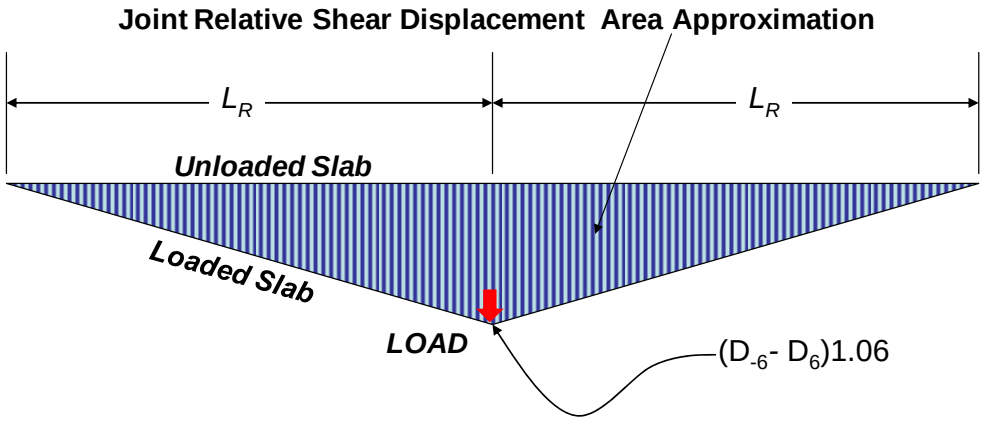

FIGURE 3.8. IMAGE SHOWING THE TOTAL LINEARLY APPROXIMATED JOINT VERTICAL SHEAR DISPLACEMENT PROFILE MOBILIZED ALONG THE JOINT FACE

In the context of joint stiffness, the deflection difference profile along the joint is integrated to obtain the area under the profile, or shear area, and this shear area is multiplied by the joint stiffness constant to obtain the total force mobilized and transferred through the joint. Using the geometry in figure 3.8, the total vertical force transmitted across the joint face shear displacement area is approximated as follows:

$$\textit{Total Joint Vertical Shear Force} = \tfrac{1}{2}\,(2L_R)(D_{-6}-D_6)1.06(k_J) \qquad (8)$$

The unknowns in the above equation are the joint stiffness value, k_J, and the total joint vertical shear force. The total joint shear force is not equal to the FWD load magnitude. Another separate equation is needed that can be solved for the *Total Joint Vertical Shear Force* variable to enable a two equations with two unknowns type of solution for the magnitude of joint stiffness. The LTE_δ and FWD load magnitude can be used to obtain the second equation for the

Total Joint Vertical Shear Force. Figure 3.9 shows the simplified procedure for establishing the second equation for the total joint vertical force used in this method. The key assumption is that the overall subgrade resistance force, R, under each slab is proportional to the loaded slab edge deflection.

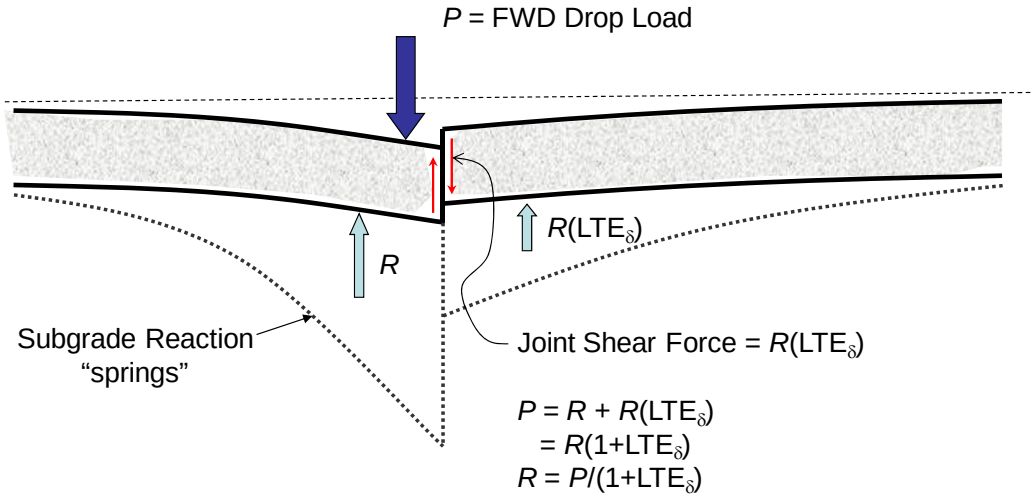

$$\textit{Total Joint Vertical Shear Force} = P(LTE_\delta)/(1+ LTE_\delta)$$

FIGURE 3.9. SIMPLIFIED FORCE DISTRIBUTION DIAGRAM FOR ESTIMATING THE TOTAL MAGNITUDE OF THE JOINT VERTICAL SHEAR FORCE IN THE FWD JOINT STIFFNESS CALCULATION PROCEDURE

To calculate the total joint stiffness, k_J , the two equations for *Total Joint Vertical Shear Force* are set equal to each other and rearranged to solve for joint stiffness magnitude, k_J. The resulting equation to solve for k_J from FWD data using the 12-inch sensor spacing and sensor bar on the unloaded slab is as follows:

$$k_J = P(LTE_\delta)/[(1+LTE_\delta)(D_{-6}-D_6)(1 + i_{\%})\Omega(66+60D_{66}/(D_6-D_{66}))] \quad (9)$$

The $i_{\%}$ factor is the percentage increase factor needed to project the sensor readings out to the joint line. The Ω factor is an unknown function that converts the simplified linearly approximated shear area calculated above into the true shear area, and this function value was set equal to 1.0 for this study. Considerable thought and discussion went into deciding if any such shear area correction constant or function Ω was needed and it was decided that no shear area correction factor was necessary, hence the value of 1.0. Future studies may better quantify the Ω function and more accurately quantify the shear area. The subscript values for the sensor deflections (i.e. D_{-6}, D_6, and D_{66}) indicate the sensor distance, in inches, from the joint line. The equation geometry must be adjusted to match any different FWD sensor configuration used. Divide the k_J value by slab thickness minus saw cut depth and the result is the equivalent unit

shear stiffness, lb/in, per square inch of joint face, which is the concrete material property associated with the k_J index value.

To demonstrate this joint stiffness calculation procedure and also show how combined slab curling and joint opening changes affect typical aggregate interlock joint stiffness behavior, an example using two good-condition, low-fault highway joints is provided. This demonstrated daily range of behavior is large for this highway site. This test site is an interstate freeway in the dry region of central Washington State, LTPP GPS3 site 53-3019. Figure 3.10 shows how two individual aggregate interlock joints behaved. One joint is represented with solid lines and one with dashed lines. The primary physical difference between the two joints is the size of the joint opening between the two slabs. The joint represented by the solid lines has the larger joint opening size and lower load transfer and joint stiffness. The two joints follow very similar "structural behavior" trends and it is obvious that the AM trend is shifted upward and left of the PM trend. This is the effect of slab curling and slight loss of contact for joints during the early morning due to slab up-curl. Overall joint deflections are higher, while slab edge deflection differences may not be during morning upward curling and this will result in higher LTE_δ for a given joint stiffness. Figure 3.11 shows how load magnitude affected apparent joint stiffness, k_J. In general, joint stiffness increases with load magnitude after a certain point where the joint face roughness surfaces begin to contact each other. It is believed that when the line segments in figure 3.11 start to slope upward, the aggregate interlock is starting to significantly engage upon loading. The initial upward sloped lines still intersect the y-axis near a zero value implying zero joint stiffness at zero-load, or right at the point of slack closing. As temperature increases, closing the joint opening, and daytime thermal gradients curl the slab edges closer to the subgrade, the y-intercept values in figure 3.11 start to rise above zero implying there is some compressive contact of the slab ends prior to loading, which results in apparent immediate mobilization of high joint stiffness at very small load levels. PCC slab evaluation staff that have been on freeway concrete pavement sites early in the morning in cooler weather know that this effect can physically be heard at jointed concrete pavement sites with high velocity heavy loads. During testing at site 53-3019, the joints made loud banging noises and vibration as heavy trucks rolled over them in the early morning and this banging vibration was quite perceptible through the feet and legs. This joint banging noise and vibration was no longer noticeable by the time of the afternoon testing, due to the joints nearly compressing shut and the slabs being closer to flat. There was more joint face grinding impact occurring in the early morning prior to joint lock-up in the afternoon, which is occurring for the stiffer of the two joints shown. Notice how the stiffness values for the 17-18 kip loads are decreasing with every FWD drop load. This is probably the result of damage being done to the joint crack face surface by the relatively large FWD loads, causing progressive and rapid loss of joint stiffness. Another possibility is that the horizontal reactions on the crack face during joint loading are progressively pushing the slabs outward laterally with each drop load causing a slight increase in joint opening. When the crack faces do become tight, surprisingly large lateral thrust reactions, which try to push the slabs apart, can develop upon downward loading at the joints (Jensen and Hansen, 2001).

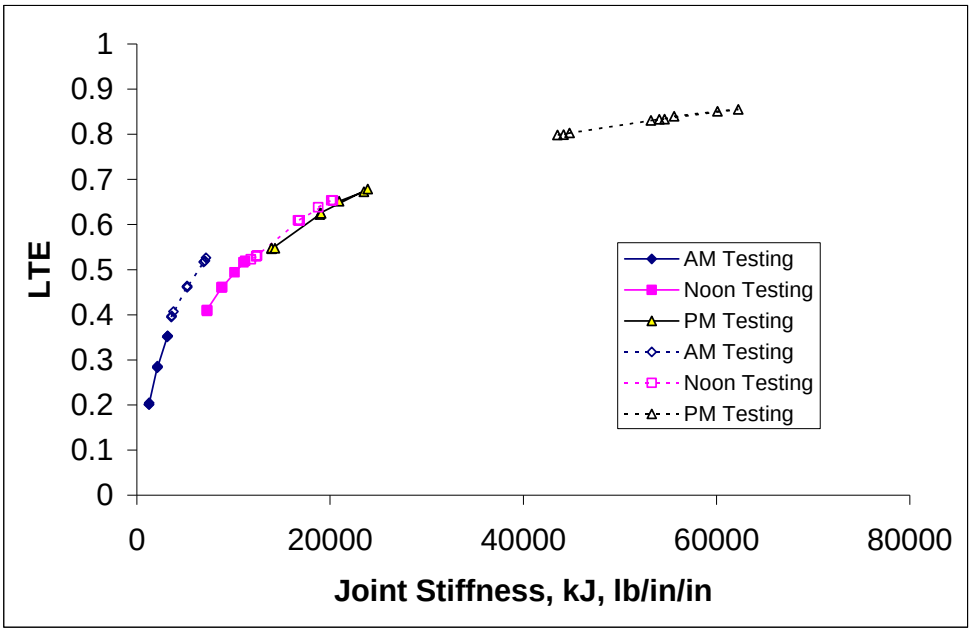

FIGURE 3.10. BEHAVIOR OF TWO GOOD-CONDITION AGGREGATE INTERLOCK JOINTS AT HIGHWAY SITE 53-3019, SHOWING THE EFFECT OF AM JOINT UPLIFT AND JOINT OPENING CHANGE ON LTE_{δ} VERSUS JOINT STIFFNESS TRENDS

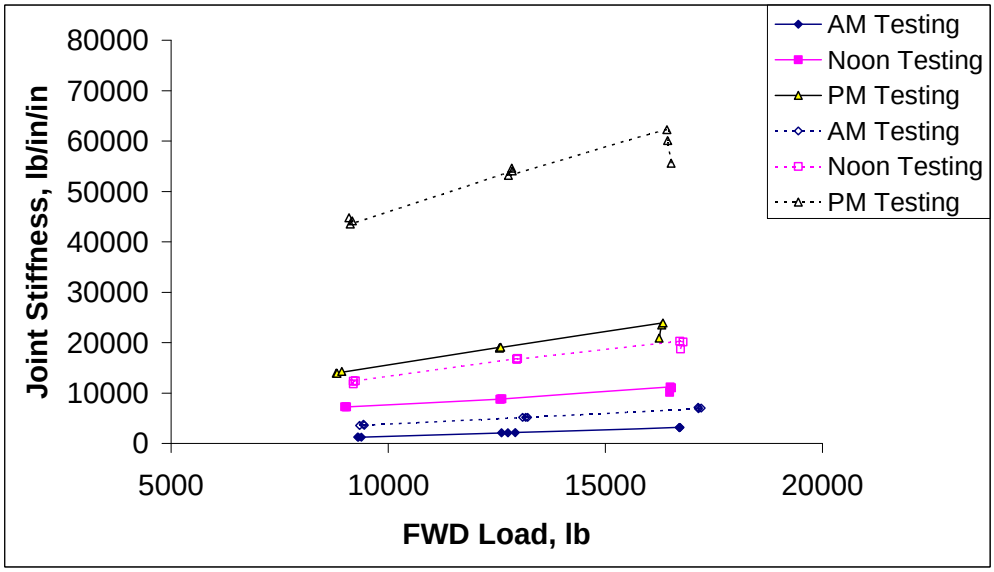

FIGURE 3.11. LOAD VERSUS JOINT STIFFNESS RELATIONS FOR THE TWO JOINTS SHOWN IN FIGURE 3.10 SHOWING HOW INCREASING SLACK OR LOOSENESS IN THE AGGREGATE INTERLOCK RELATED TO INCREASING JOINT OPENING SIZE REDUCES JOINT STIFFNESS

The trend shapes revealed in figure 3.10 are a cross section property. Testing many joints at a site and plotting the LTE_δ versus joint stiffness data reveals the site's characteristic joint stiffness versus LTE_δ response associated with the site's cross section and foundation properties. Plotting the characteristic joint stiffness data reveals information regarding joint type and cross section variability, along with any curling or joint opening effects that may be occurring during the testing window. Figure 3.12 shows the joint stiffness calculation results for the DIA instrumented test site FWD load tests for several joints tested from winter to summer several times over a three year period. The site's characteristic joint structural response curve is quite uniform. Even though these tests were performed on different joint types, on different days over a period of about three years, the joint stiffness versus LTE_δ values tend to fall on the same trend line. The shape of the trend line is a cross section property, almost completely unrelated to joint type or opening size. Variability from the main trend is low at this site indicating a uniform cross section and uniform joint support behavior. The position of each dot on the trend line is related to what joint type, and variation in joint opening size. All low values for LTE_δ in this plot are aggregate interlock joints tested during the winter during cold ambient temperatures, when joint openings would have been relatively large. Their corresponding summer test results are also in this plot and have much higher stiffness and LTE_δ when joints compress closed. The curve for the DIA site appears to intersect the y-axis at an apparent LTE_δ level of about 10-15 percent at a zero joint stiffness value. This is the apparent cement treated base contribution to LTE_δ for open joints with no stiffness or face contact. Figure 3.12 provides the measured characteristic joint structural response curve that outputs from existing FEM codes must be calibrated to reproduce when attempting to simulate joint and slab system response to 12-inch diameter FWD loads at DIA. Curves like this were established for all of the test sites for this study and they represent the primary data source for this research project.

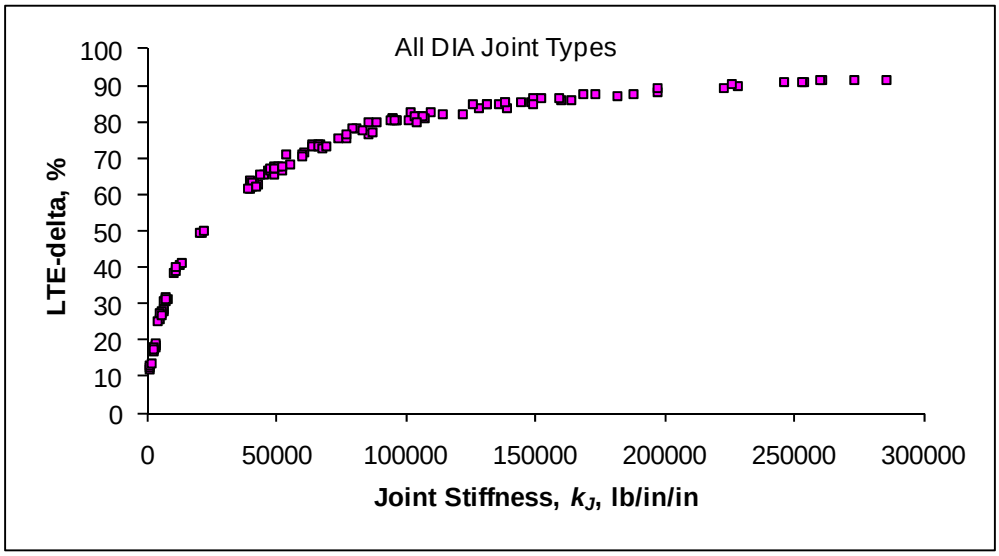

FIGURE 3.12. DIA SITE CHARACTERISTIC STRUCTURAL JOINT STIFFNESS RESPONSE TREND, WHICH IS UNIQUE TO THE DIA PAVEMENT TEST SITE CROSS SECTION AND SUBGRADE PROPERTIES

Not all test sites have such a uniform trend shape as that encountered at the DIA site. When tested, the DIA joints were still relatively young and not much deterioration had developed. If for any reason, variable voids or loss of support are present at a site along joint lines, greater variability is observed in the characteristic joint stiffness data for a site. Larger variability is also observed for increasing upward curling or warping in slabs. Figure 3.13 now returns to the test site 5-AGG18 data and shows the FWD LTE_{δ} versus joint stiffness results from this test site. It was previously demonstrated how this site experienced large curling related mid-panel FWD load test response variations. This test site also revealed the most curling related change in joint stiffness behavior of any airfield test site evaluated. Figure 3.14 shows the temperature measurements from the FWD for the testing window. Almost 50 °F change in concrete surface temperature occurred. This resulted in significant slab curling during testing. In the heat of the afternoon, the joints tended to have higher stiffness, but not necessarily higher LTE_{δ}. This is because of how the structural response trend line shape changes as a result of curling. In the afternoon heat during Round 3 testing the joint behavior tends to become more uniform and follow a lower trend for "flatter slabs" with joints nicely seated into the subgrade and having better support. During Round 1 testing near sunrise, the slab edges are somewhat curled-upward to varying degrees, with larger voids present beneath the slab edges. Jointed FEM simulations reproduce this behavior well, as shown later in Chapter 6. Another interesting point to note is that a joint can have a lower stiffness while having higher LTE_{δ} during upward curling conditions. One could observe a decreasing LTE_{δ} with time of day, even when joint stiffness is increasing during the same test period, due to upward curling related voids at slab edges.

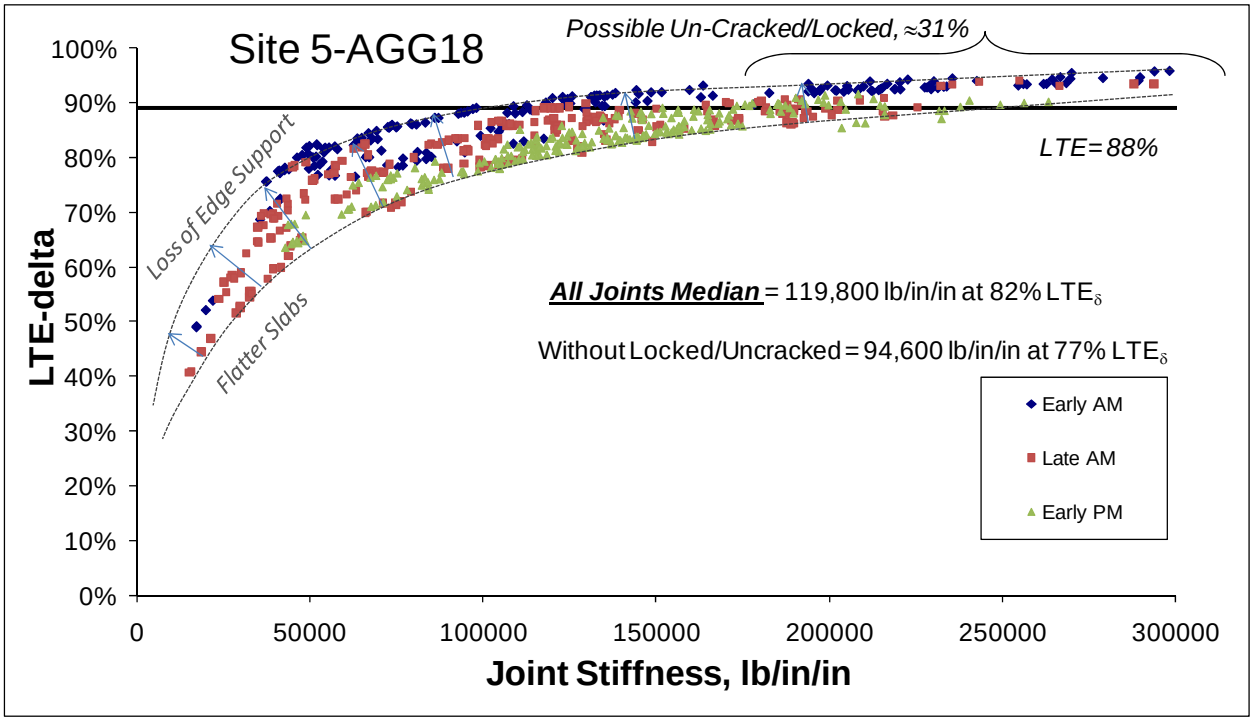

FIGURE 3.13. EXAMPLE OF THE LARGEST CURLING RELATED JOINT STIFFNESS VARIABILITY OBSERVED FOR A HEAVY DUTY RUNWAY

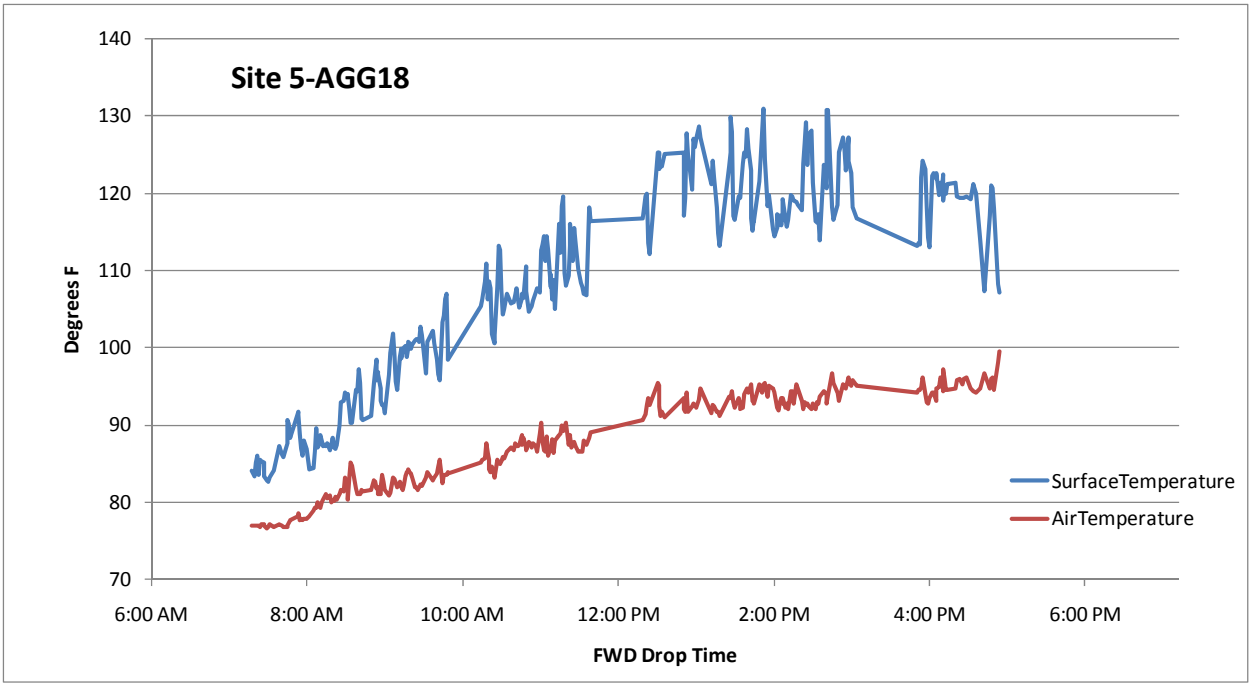

FIGURE 3.14. THE FWD TEMPERATURE SENSOR DATA CORRESPONDING TO THE FWD LOAD TEST RESULTS SHOWN IN FIGURES 3.5, 3.6 AND 3.13

The site just described, which showed the largest amount of slab curl variability in joint response, is in a dry hot climate and resting on unbound granular subgrade that is apparently quite sensitive to curling related changes in confining pressure. As noted previously, some sites appear to have base and subgrade systems that allow curling to occur without changes in support characteristics, essentially conforming to curling shape change. Figure 3.15 shows the computed joint stiffness data from the site 2-AC17, which had weak wet clayey subgrade. Very little change in joint response trend shape occurred for the three Rounds of testing, while measured slab curvature changes were relatively large, similar to site 5-AGG18. The typical trend is still present, where the afternoon data is situated slightly below the morning data, but the difference at this site is very small indicating a high degree of subgrade conformance to curling.

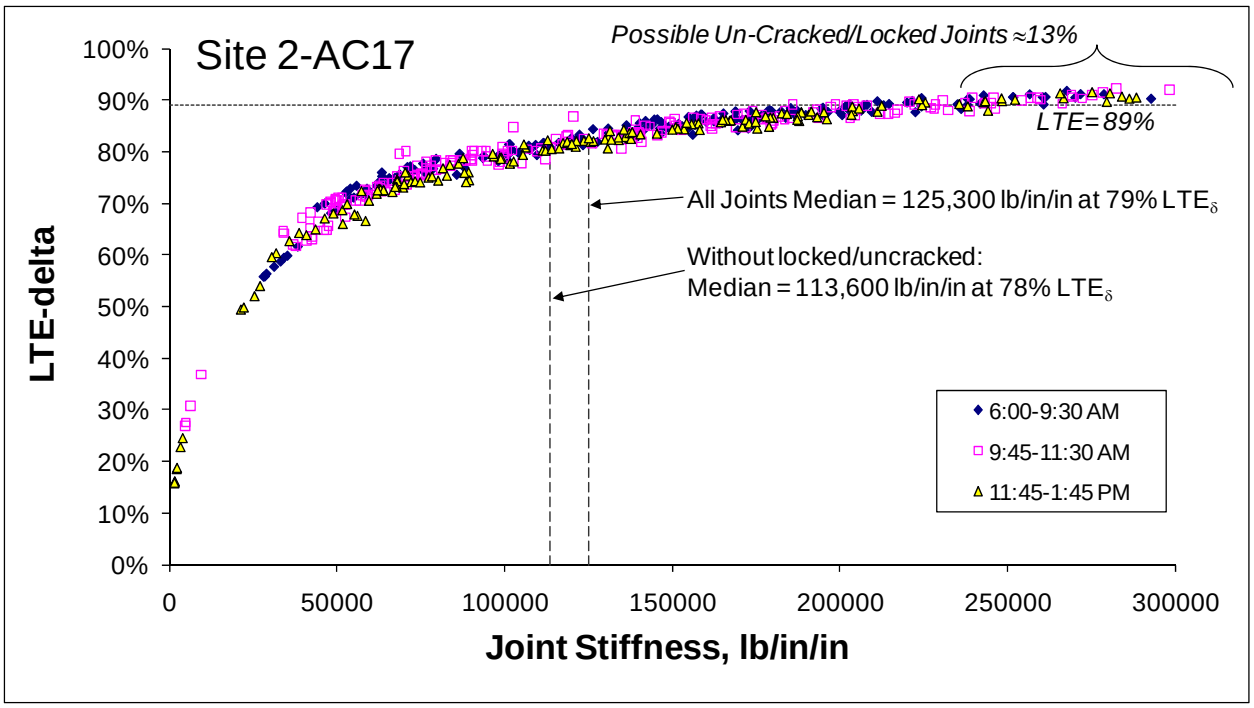

FIGURE 3.15. AN EXAMPLE OF A RELATIVELY UNIFORM JOINT STIFFNESS RESPONSE TREND FOR A HEAVY DUTY RUNWAY ON WEAK CLAYEY SUBGRADE

Once the overall characteristic joint stiffness response trends are obtained from a test site, structural analysis tools, such as jointed FEM codes or the Skarlatos/Ioannides Infinite-Edge equations can be fit to these trend shapes. Once the structural analysis parameters are set such that they reproduce this trend, the FEM or Skarlatos/Ioannides approaches are considered to be calibrated to the site response. This process will be described later. Once established, this overall set of joint stiffness versus LTE_δ data from a test site is strategically broken down by joint types, and time of day effects to establish the in-service LTE_δ and stiffness ranges for various joint details. These data obtained from the test sites are the primary data used as the basis of the recommendations resulting from this research project. In general, prior to establishing a method as described above for calculating joint stiffness directly from the FWD load test data, it was not possible to develop such curves for a test site.

3.2.3 Step 3 - Fitting the Skarlatos/Ioannides Equations to the Characteristic Joint Stiffness Curve

There are two forms of the Skarlatos/Ioannides equations presented by Ioannides and Hammons, 1996 that can be "fit" to the measured joint stiffness versus LTE_δ data. These equations simulate two infinite slabs connected by one infinitely long joint. The first form is referred to here as the "LTE_δ regression for the Skarlatos/Ioannides Solution" and is shown below:

$$LTE_{\delta} = \frac{1}{1 + \log^{-1}\left[\frac{0.214 - 0.183\left(\frac{\varepsilon}{\ell}\right) - \log f}{1.180}\right]} \quad (10)$$

Statistics: $R^2 = 1.0$; $SEE = 0.0070$; $n = 405$.

Where,

$$f = \frac{q_0}{k\ell} = \frac{AGG}{k\ell}$$

k_J = AGG = q_0 = joint stiffness, lb/in/in
ε = wheel load radius, inches
ℓ = pavement radius of relative stiffness, inches
k = modulus of subgrade reaction, psi/in

For each test site, the measured joint stiffness and LTE_{δ} data are set up to solve the following generalized matrix equation:

[Measured LTE_{δ}**] = [Skarlatos/Ioannides** LTE_{δ} **as** f**(site best-fit** $k\ell$**)] + [error]** (11)

In the Skarlatos/Ioannides LTE_{δ} regression formula for a test site, the known variables are: the ε value is set equal to the FWD load plate radius (5.9 inches), the slab thickness value is set as the site design thickness value from the construction plans for the site, the slab concrete elastic modulus value is set to the site best estimate of slab elastic modulus from the mid-panel FWD testing, and the f dimensionless joint stiffness values are set equal to the measured joint stiffness values divided by the overall site average $k\ell_{Skarlatos}$ cluster, where the modulus of subgrade reaction k is unknown. Then, a computer optimization routine is used to find the single best-fit site-wide subgrade k-value that minimizes the size of the L2 norm (sum of squared errors) for the error matrix.

The fitting of the Skarlatos/Ioannides equation to the measured stiffness data will first be demonstrated using the relatively uniformly behaving site 2-AC17. The characteristic joint stiffness versus LTE_{δ} data measured for this site is shown in figure 3.15. This joint stiffness data, the design thickness, the backcalculated slab elastic modulus, and the LTE_{δ} regression of the Skarlatos/Ioannides solution are used in the minimization problem to find the best-fit subgrade k-value at the joints with a model fit as shown in figure 3.16. This is a new rational backcalculation method for apparent slab edge support magnitude for a test site using the general assumptions of: dense liquid foundation, and two semi-infinite slabs with a single infinite joint. It is referred to as the "Backcalculated Skarlatos/Ioannides Infinite Edge Modulus of Subgrade Reaction Value", or $k_{Skarlatos}$. Because the Skarlatos/Ioannides-Westergaard approach assumes infinite slab dimensions along and away from the joint line, the backcalculated $k_{Skarlatos}$ represents a lower bound solution for the support magnitude at joints. It is shown later that when

finite slab dimensions are simulated using FEM codes and similarly matched to the measured joint stiffness curves, a higher backcalculated slab edge support value is generally obtained. This is because the finite slab solutions allow some slab rotation to occur, which increases edge deflections while decreasing edge stresses. So for the same measured deflections at a joint line, the finite slab idealization typically backcalculates a higher subgrade support value.

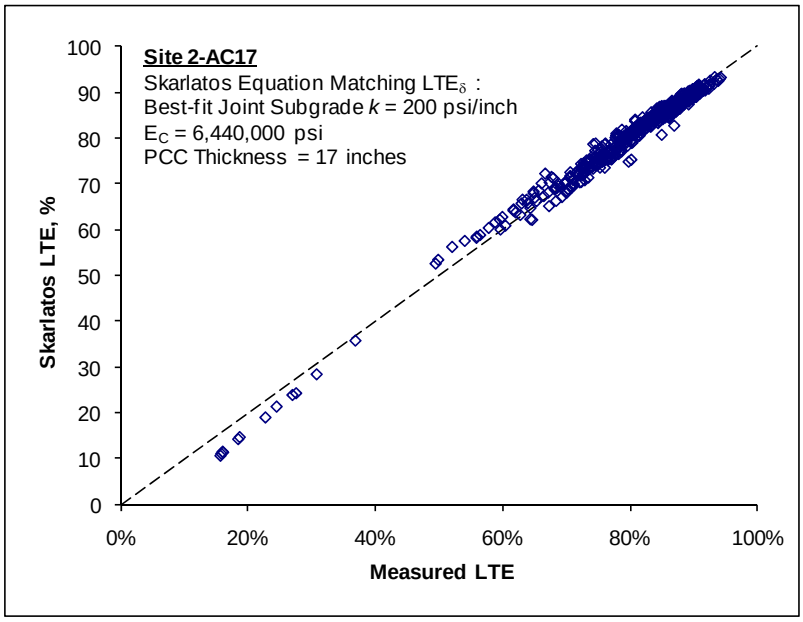

FIGURE 3.16. MEASURED VERSUS SKARLATOS/IOANNIDES LTE_δ VALUES FOR SITE 2-AC17

The Skarlatos/Ioannides solution above is considered the "*calibrated*" Skarlatos/Ioannides LTE_δ joint behavior best-fit formula that best-fits the measured joint stiffness behavior at site 2-AC17. Please note that the method used to calculate joint stiffness values from the site is not related to the Skarlatos/Ioannides equation. The relatively good fit between the measured LTE_δ and the Skarlatos/Ioannides calculated LTE_δ using the measured stiffness data from this new technique is an indication that in-service joint behavior at this test site is very much like Skarlatos estimated it would be.

The overall site 2-AC17 average mid-panel backcalculated subgrade *k*-value from ILLI-BACK was 430 psi/in, while the slab edge *k*-value was 200 psi/in. Therefore, the Skarlatos-Westergaard type *Slab Support Ratio* calculated for site 2-AC17 is 200/430 = 0.47. Calibrated Skarlatos/Ioannides best-fit formulae were established for each test site. The calibration and best-fit process was based on the 12-inch diameter FWD load plate size, which is a key point to note. Once a calibrated best-fit formula is established based on the FWD load plate size, factors such as load radius can be changed in the calibrated best-fit formulae to infer LT trends for various wheel load area sizes.

The Skarlatos/Ioannides solution does not directly consider curling effects. So, if perhaps the measured points were affected by curling, this effect is only visible through how curling affects the backcalculated edge support values for the inherently assumed flat slab. A site with large upward curl lifting the joints off of the subgrade will have a low backcalculated slab edge

$k_{Skarlatos}$ relative to the support value calculated from mid-panel FWD load tests. For example, Skarlatos/Ioannides joint formulae were fit to the three individual FWD Rounds of testing from test site 5-AGG18, to establish the best-fit slab edge $k_{Skarlatos}$ values for the three Rounds. The mid-panel load test modulus of subgrade reaction values were also calculated for the three Rounds of testing. The backcalculated edge and mid-panel *k*-value results are compared in figure 3.17. During the early morning tests, the joints were lifted off the foundation, and the slab self weight became concentrated upon the subgrade situated in the mid-slab areas. The slabs slowly curled as a result of top of slab heating during the testing window. The slab joints deflected downward and became seated on the foundations, while the mid-panel areas of some slabs started to slightly lift off the foundations. The backcalculated edge and mid-slab *k*-values were starting to be similar during the afternoon testing period. During the morning testing, when slab weight was concentrated around the mid-panel regions of the slabs, mid-panel *k*-values were much larger than backcalculated edge *k*-values, due to the slab edges being lifted off the foundations and air gaps being present between the bottom of slab and top of foundation along slab edges. The calculated *Slab Support Ratios* were 0.16, 0.37, and 0.75 for Rounds 1, 2, and 3, respectively. This was the most extreme example of this type of relative subgrade stiffness variation encountered at the heavy duty airfield test sites. Clearly the mid-slab support level can be and is almost always significantly different than the apparent edge support levels. Mid-panel support tends to increase while joint support is decreasing in general due to curling related uplift of portions of the slab. There is almost always some differential permanent deformations along joints that will reduce the effective subgrade stiffness at joints. There is usually some slight upward warp of panels that further reduces subgrade confining pressures and apparent subgrade stiffness along the joint lines. The combination of slight downward permanent deformations of subgrade along joints combined with slight upward warp of panels, causes support at joints to "typically" be significantly less than support available for mid-panel regions of slabs.

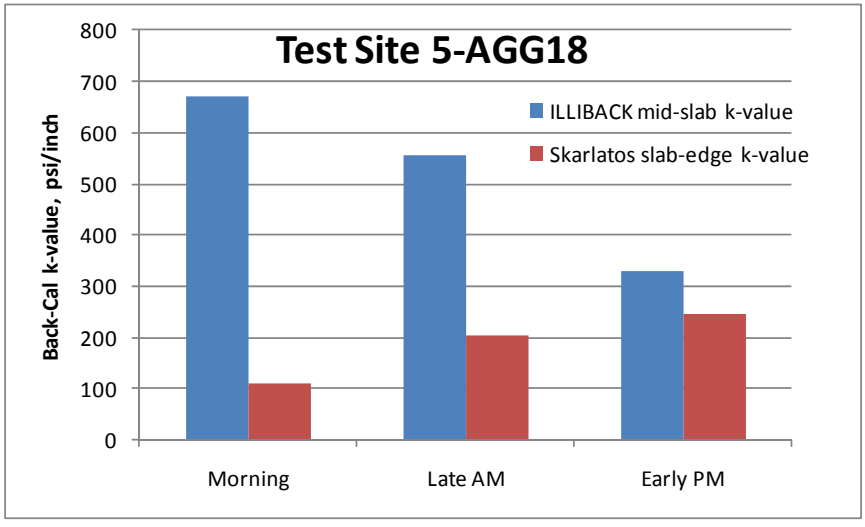

FIGURE 3.17. COMPARISON OF BACKCALCULATED SKARLATOS/IOANNIDES SLAB EDGE AND ILLI-BACK MID-PANEL SUBGRADE *k*-VALUES FOR TEST SITE 5-AGG18, WHICH EXPERIENCED LARGE SLAB SHAPE CHANGES FROM CURLING

The above examples were solved based on the concept of minimizing the errors between the measured LTE_δ and the Skarlatos/Ioannides calculated LTE_δ. Another form of the Skarlatos/Ioannides solution that can be used to backcalculate and apparent slab edge subgrade *k*-value is referred to as the "*log(f)* regression for the Skarlatos/Ioannides solution" as shown below:

$$\log f = \left[0.434829\left(\frac{\epsilon}{l}\right) - 1.23556\right]\log\left(\frac{1}{LTE_\delta} - 1\right) + 0.295205$$

Statistics: $R^2 = 0.995$; $SEE = 0.1661$; $n = 405$. (12)

With this equation form, for each test site, the measured joint stiffness and LTE_δ data is set up to solve the following generalized matrix equation:

[*log*{(FWD Stiffness)/(Site best-fit $k\ell$)}] = [Skarlatos/Ioannides *log(f)*] + [error] (13)

The joint stiffness data, the design slab thickness, the backcalculated slab elastic modulus, and the *log(f)* regression of the Skarlatos/Ioannides solution are used in the minimization problem to find the best-fit $k_{Skarlatos\text{-}II}$ at the joints with model fit as shown in figure 3.18. This *log(f)* fitting approach tends to spread the measured data more evenly into a more uniform distribution, where as the LTE_δ optimization tends to compress the data together at higher LTE_δ values and into a skewed distribution. The backcalculated slab edge *k*-value is typically smaller when using the *log(f)* fitting approach. The residuals pattern tends to be more linear with respect to the line of equality when using the *log(f)* fitting procedure, where as the residuals for the LTE_δ optimization generally somewhat fan out from a common lower value present at higher LTE_δ values. The *log(f)* fitting method tends to match better with the low to medium joint stiffness data at the site, where as the LTE_δ fitting method generally fits better to the higher joint stiffness data from a test site. The LTE_δ fitting approach is the method used extensively in this report.

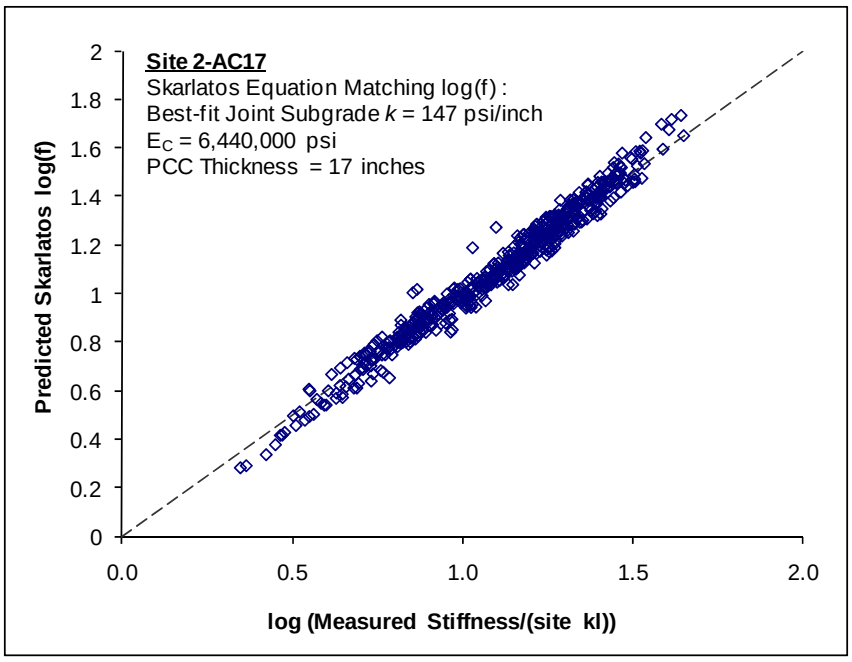

FIGURE 3.18. SKARLATOS/IOANNIDES VERSUS MEASURED JOINT STIFFNESS FOR SITE 2-AC17

Two additional relations, the Crovetti and Zollinger equations, were found to estimate joint stiffness from FWD LTE_δ data. The Crovetti equation is as follows (Crovetti, 1994):

$$LTE_\delta = \frac{100\%}{1+1.2\left(\frac{AGG_{tot}}{k\ell}\right)^{-0.849}} \quad (14)$$

Where,

AGG_{tot} = the total joint stiffness, lb/in/in
k = modulus of subgrade reaction, psi/in
ℓ = radius of relative stiffness, in.

The Zollinger formula is a modified version of the Skarlatos/Ioannides solution presented by Ioannides and Hammons, 1996 and includes an additional R parameter related to how much steel reinforcement is present across the joints or cracks. It is the same as the Skarlatos/Ioannides value when the R value is zero. The Zollinger formula was calibrated to match testing of tightly closed continuously reinforced concrete pavement (CRCP) cracks (Zollinger and Soares, 1999). Zollinger probably recognized that the aggregate interlock, AGG_{tot} value in the Skarlatos/Ioannides regression equation must be limited to feasible upper limit values and this additional separate R parameter was needed to account for the steel and crack-face bending moment transfer effects. This formula form is as follows:

$$LTE_{\delta} = 100\left(1-\left(1-\frac{1}{1+\log^{-1}\left[(0.214-0.183\frac{a}{\ell}-\log(\frac{AGG_{tot}}{k\ell})-R)/1.18\right]}\right)\right) \quad (15)$$

Where,

AGG_{tot} = the total joint stiffness, lb/in/in
k = modulus of subgrade reaction, psi/in
ℓ = radius of relative stiffness, in.
R = residual dowel action factor for CRCP steel = 0.5 for #5 bars, 1.0 for #6 bars, and 1.5 for #7 bars.

Now that joint stiffness can be calculated directly from FWD data, either of these two equations can also be used as a backcalculation tool, with the site measured characteristic joint stiffness versus LTE_{δ} measurements to set up a matrix optimization problem similar to those described above for the Skarlatos/Ioannides equation, and used to find an apparent best-fit subgrade *k*-value for the slab edges. The general trend shape for the Crovetti best-fit formula is subtly different but very close to the trend shape and magnitudes for the Skarlatos/Ioannides solution. This formula should be used with data having similar a/ℓ values used to establish it.

3.2.4 Step 4 - Fitting Finite Element Models to the Characteristic Joint Stiffness Curve

This study primarily used the finite element computer program ILSL2, the second generation of the ILLI-SLAB software, to match with the site response data (Ioannides and Khazanovich, 1998). ILSL2 was relatively easy to use and perform multiple runs with curling simulations. The FEAFAA code with curling simulation ability was also used. This software takes significant technical expert staff hours to use and the total use of FEAFAA was limited. The ILSL2 and FEAFAA codes were set up as 2-slab systems with one joint between the slabs. This allowed a direct comparison of ILSL2 to FEAFAA generated characteristic joint stiffness curves for similar pavement idealizations.

For a given test site, the two-slab FEM representation was established simulating the slab dimensions at the site. The design slab thickness, and the site ILLI-BACK best-fit elastic modulus value were used for the slab properties in the simulation. In general, the mid-panel backcalculated subgrade *k*-value represents an upper bound for subgrade stiffness expected to be present at joints, while the backcalculated Skarlatos/Ioannides Edge subgrade *k*-value represents a lower bound solution for the apparent support at joints. Figure 3.19 shows the characteristic joint stiffness curve measurements from site 2-AC17, along with Skarlatos/Ioannides best-fit formulae and ILSL2 results for these upper and lower bound subgrade *k*-values of 200 and 430 psi/in. The Skarlatos/Ioannides solution with a subgrade *k*-value of 200 psi/in was the "best-fit" Skarlatos/Ioannides formula and runs through the center of the data mass. The Skarlatos/Ioannides solution trend shape is very close to the measured stiffness trend shape. The Skarlatos/Ioannides formula that used a subgrade *k*-value of 430 psi/in is situated well below the measured joint stiffness indicating 430 psi/in is too large. As is typical, the two corresponding

FEM sets of results envelop the measured data as upper and lower bounds. The differences between the Skarlatos/Ioannides formulae and the ILSL2 results for the same subgrade *k*-values shown is related to the assumptions of infinite slab dimensions in the Skalatos model, versus finite slab dimensions in the FEM idealization. The finite slabs enable more of the load to go into the subgrade, and will reveal a higher backcalculated modulus of subgrade reaction than the Skarlatos/Ioannides infinite slab solution for a given sites characteristic joint stiffness curve.

Finding a "best-fit" FEM solution must use a different fitting procedure than is used for fitting a Skarlatos/Ioannides formula to the data. The Skarlatos/Ioannides solution does not directly account for curling or warping. Therefore, it is best to fit a trend line through the center of mass of the data set, a least-square errors type curve-fitting approach. With FEM discretization of this phenomenon, it was found that the flat slab condition (no curling) trend line was always the lowest on the graph and large curling, either downward or upward causes the joint stiffness trend line to shift upward and to the left on the plot. Therefore, when fitting an FEM trend line to the site data, the "flat slab" FEM configuration result is fit to the lower boundary of the data set and any slight lifting upward of the data is explained by curling or any sort of loss of support along the joint line. Any kind of loss of support along the joint line will shift the stiffness trend lines upward and to the left on the plot. So for site 2-AC17, the best-fit ILSL2 slab edge subgrade *k*-value was about 350 to 375 psi/in, compared to the best-fit infinite edge Skarlatos/Ioannides subgrade *k*-value of 200 psi/in, and best-fit mid-panel ILLI-BACK subgrade *k*-value of 430 psi/in. We have found the apparent best-fit subgrade *k*-value resulting in the FEM outputs best reproducing the measured characteristic joint stiffness curve from the test site, while using our best estimates of site slab thickness, elastic modulus, and slab dimensions. The best-fit Skarlatos/Ioannides formula has a subgrade *k*-value of 200 psi/in and goes through the center of mass for the test site data. The best-fit FEM trend line has a subgrade *k*-value of 375 psi/in and hugs the bottom boundary of the test site data. These calibrated response formulae were fit to the measured data based on FWD loading and the FWD load plate size. These calibrated formulae can now be used to infer trends for other load sizes or multi-wheel gears and to calculate apparent load transfer percentages for a wide range of conditions and simulations.

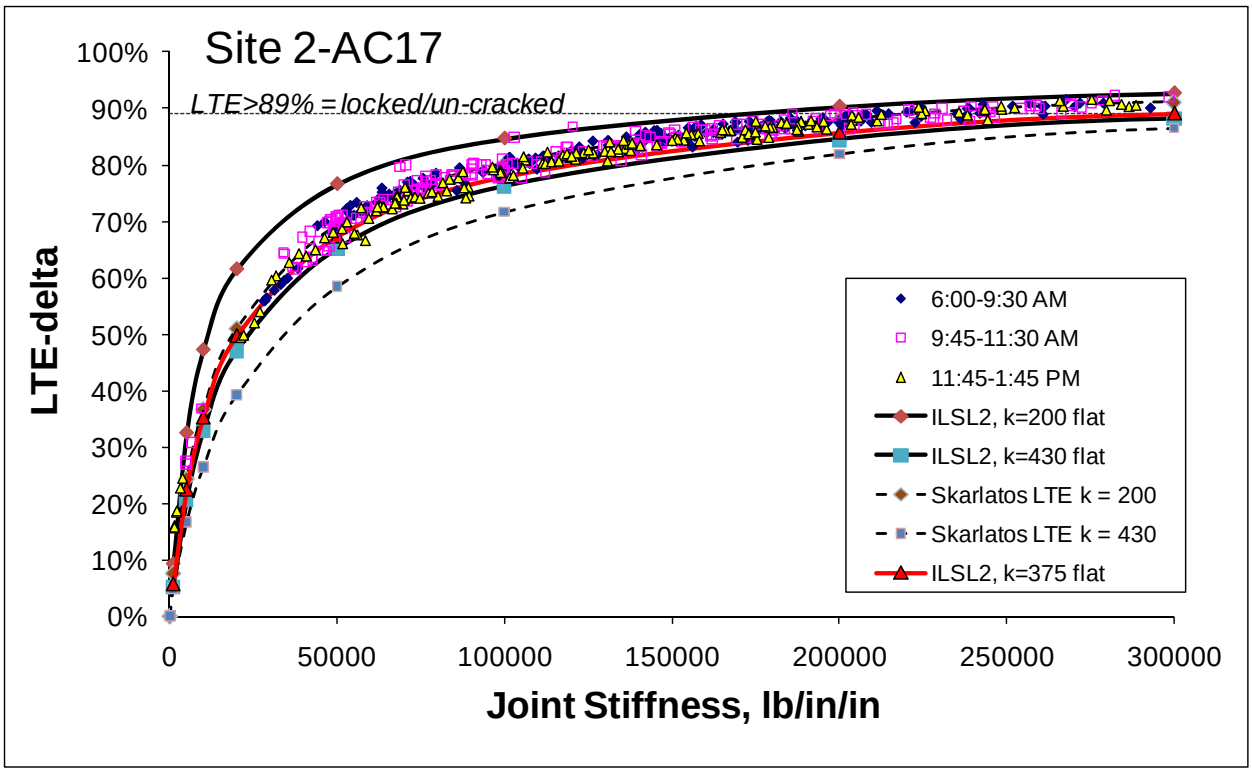

FIGURE 3.19. PLOT SHOWING HOW THE BEST-FIT SKARLATOS/IOANNIDES SLAB EDGE SUBGRADE *k*-VALUE (200 PSI/IN), AND THE ILLI-BACK MID-PANEL SUBGRADE *k*-VALUE (430 PSI/IN) ACT AS UPPER AND LOWER FEM SOLUTION BOUNDARIES, WITH THE APPARENT BEST-FIT ILSL2 FEM SLAB EDGE SUBGRADE *k*-VALUE AT ABOUT 375 PSI/IN

To further show why the FEM "flat slab" analysis is fit to hug the bottom of the measured characteristic joint stiffness data points, figure 3.20 shows the best-fit FEM trend-line to the DIA test site for flat slabs and also for significantly curled-up and curled-down slabs having the same subgrade stiffness. The best-fit FEM subgrade *k*-value for the DIA data set was about 250 psi/in, while the best-fit Skarlatos/Ioannides subgrade *k*-value was about 200 psi/in and the best-fit mid-panel subgrade *k*-value was about 450 psi/in for this cement treated base site having about 18 inch slab thickness. The FEM simulated flat slab joint stiffness trend line, along with the curled slab trend lines for rather large plus and minus 2 °F/in gradients are shown. Note how both of the curled slab trend shapes are situated higher and to the left of the flat slab trend line. This is because joint deflections tend to increase for large upward and downward curling conditions. It is probably intuitive to most readers as to why increased slab edge deflections for upward curled slabs will occur. Nevertheless, why there are increasing slab edge deflections for downward curled slabs may not be so obvious. The explanation is that when large down-curl develops that actually lifts mid-slab regions off of the ground, a phenomenon called "joint knifing" can occur. Exaggerated scale slab deflection plots for this shape give this appearance of the joints knifing into the subgrade, hence the name (see figure 6.2). Because the mid panel region of the slabs is lifted, when joint loading occurs, the joints are initially only supported by the subgrade along the edges of the slab. Less total subgrade area is available to resist wheel loads. Therefore, more deflection locally near the joint is needed to develop the same amount of subgrade resistance

force compared to a flat slab, which is supported over its entire area prior to loading. If load transfer at the joint is weak during this knifing condition, the highest levels of base and subbase shear stresses at joints would be expected to develop during large downward curling.

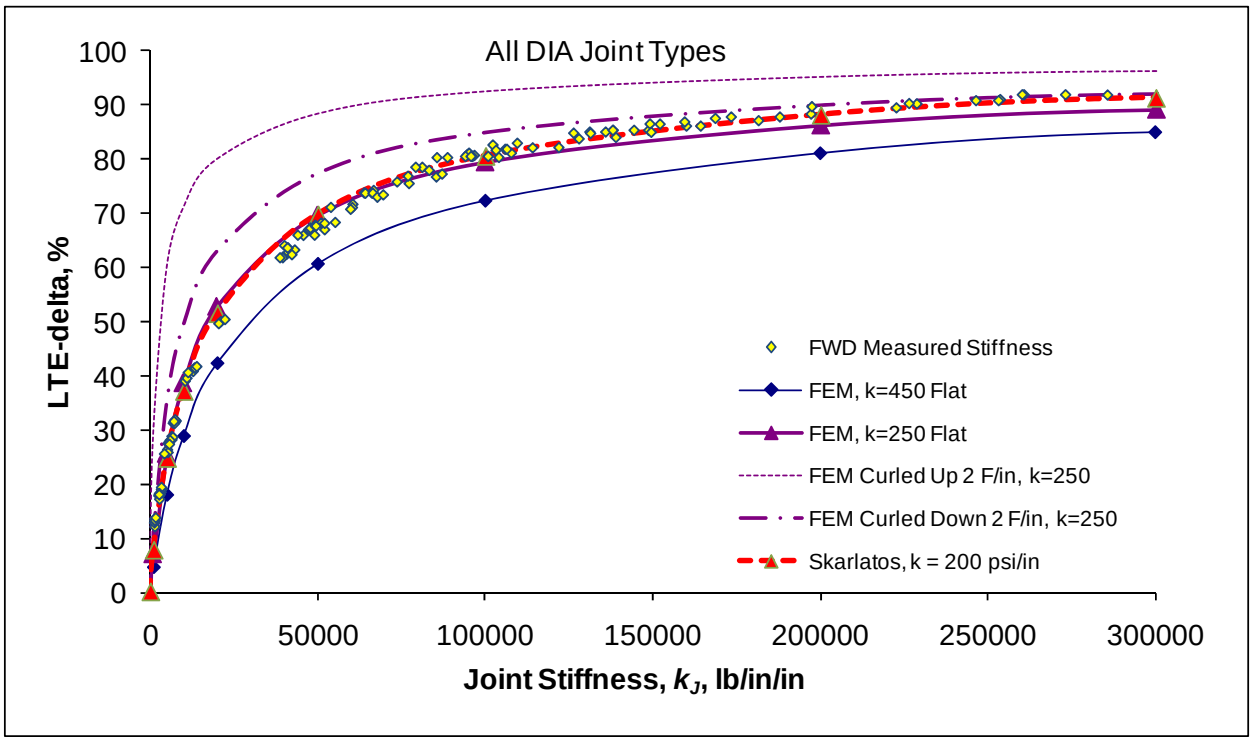

FIGURE 3.20. PLOT SHOWING THE SKARLATOS/IOANNIDES AND ILSL2 FEM TREND-LINES FOR THE DIA CHARACTERISTIC JOINT STIFFNESS CURVE, AND HOW SLAB CURLING AFFECTS FEM GENERATED JOINT STIFFNESS VERSUS LTE_{δ} CURVES

To further expand on this concept of why the flat slab condition appears to be the stiffest overall joint condition, this phenomenon was observed by others studying the DIA data and attempting to develop calibrated FEM simulations of the measured DIA response data (Rufino et al., 2004). Figure 3.21 shows a plot from their FEM formulation calibrated to the DIA test site. It shows how thermal gradient curling simulations were affecting slab edge deflections. The flat zone in the middle of the graph is the response region where no slab edge or mid-panel lift-off is occurring. Self-weight slab sinking deflections are greater than curling deformations within this response zone. This is the region Westergaard made note of in his original manuscripts, stating that his equations were only valid in the solution region where no slab lift-off is occurring (Westergaard, 1927). The zone of increasing slab edge deflections on the right side of the plot is related to the mid-panel uplift and joint knifing phenomenon. The increased slab edge deflections on the left side of the plot are related to the formation of slight air gaps between the slab edges and the foundation. Both extreme up-curl and extreme down-curl represent a loss of support condition for the joint edges of a slab, although from entirely different mechanisms. Now back to figure 3.20, the effect of this increasing slab edge deflections for large positive or

negative gradients, shows up in the joint stiffness trend lines as trends being higher and to the left of the flat slab condition for both large up-curl and large down-curl. Higher and to the left means loss of joint edge support. There is an intermediate range of gradients centered about a flat condition associated with full slab support with relatively constant slab edge deflection regardless of gradient. The characteristic joint stiffness line will remain close to the flat slab position for effective thermal gradients within this zone of full support. Outside of the full support zones, the characteristic joint stiffness lines go up and to the left.

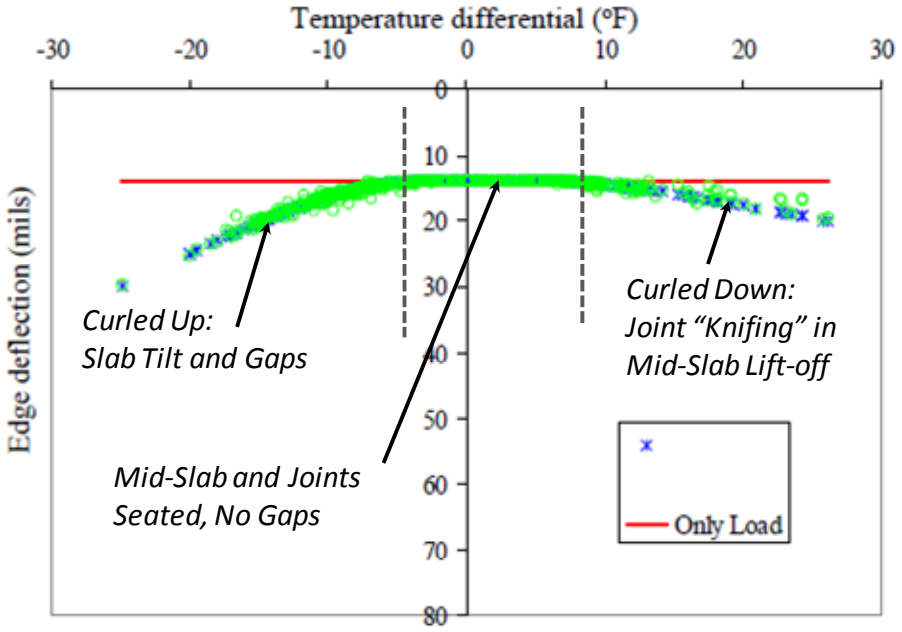

FIGURE 3.21. CALIBRATED DIA FEM DATA FROM RUFINO, ROESLER AND BARENBERG 2004, WITH ADDITIONAL COMMENTARY OVERLAID SHOWING THE MIDDLE RANGE OF FULL SUPPORT, THE EFFECTS OF EXTREME UP-CURL (LEFT) AND DOWN-CURL (RIGHT) ON SLAB EDGE DEFLECTIONS

The calibrated FEM simulations can be used to review the effects of curling on slab edge bending stress for a site. Rufino et al. (2004) also showed how slab curling affected slab edge bending stress estimates from their calibrated DIA FEM analysis, and showed a key point also encountered in this study. Figure 3.22 shows a plot of stress calculations showing how varying the thermal gradient in the FEM analysis affects: residual curling stress (T), load stress without curling (L), combined load and curling stress (L+T), and then a key parameter referred to as {(L+T)-T}, which is the combined stress analysis minus the thermal only residual stress analysis. This key value represents the slab edge strain change that was related only to the load, and is plotted as a function of thermal gradient. The curled-downward joint knifing condition results in the highest edge strain, while the curled-up scenario results in lower calculated edge strain for a given load magnitude. This is because when slabs are curled upwards, with joints lifted off the foundation, some initial load energy is dissipated while the slab rotates and until the joint seats itself on the subgrade. The remaining load energy is then expended in pressing the slab edge into the subgrade, which causes a reaction on the bottom of the slab and eventually some bending

stress. If one does not know a slab is curled and embedded strain gages are present, this change in stress related to load plus curl, minus residual {(L+T)-T} strain is what is being measured if the residual strain, T, is not accounted for in some rigorous way, and assumed to be zero. Another key point is that the thinner highway slab considered on the right side of the plot had only a small zone of reduced edge strain during smaller morning curling, and then edge strains increased as up-curl became larger. The same basic trend would also occur for the thicker airport slab trends if larger gradients or longer slabs had been considered.

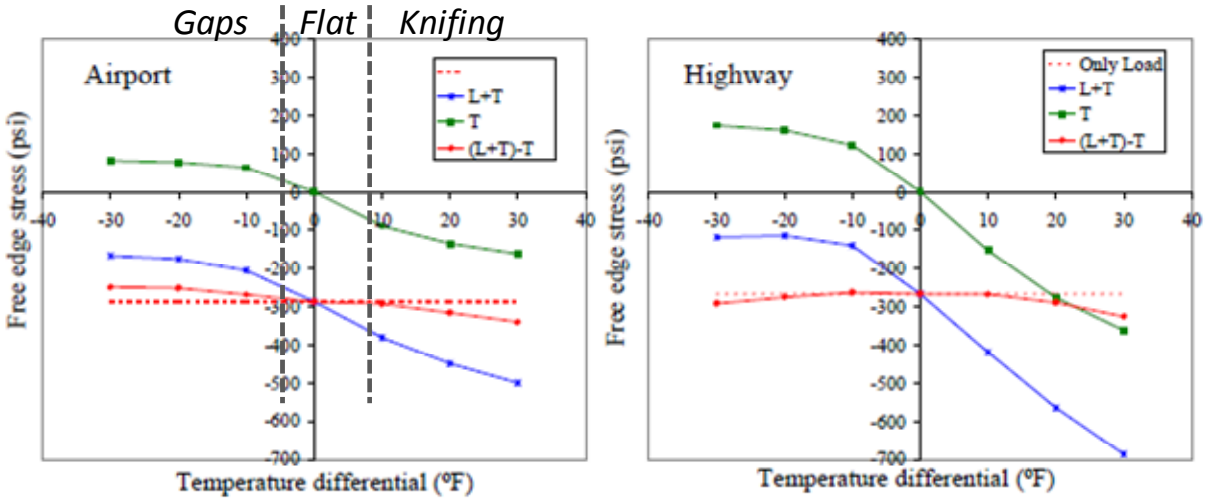

FIGURE 3.22. A KEY PLOT FROM RUFINO, ROESLER AND BARENBERG 2004 SHOWING THE DIFFERENCE BETWEEN THE COMBINED STRESS (L+T) AND THE CHANGE IN STRESS {(L+T)-T} CONCEPTS, AND HOW THE CHANGE IN STRESS IS HIGHER FOR THE DOWN CURLED JOINT KNIFING RANGE OF BEHAVIOR

If the FAA modifies the version 6E FAARFIELD thickness design procedure to consider curling in the slab stress analysis for design, a decision must be made as to whether to use the *Combined Stress* = (L+T) calculations, or the *Change In Stress/Strain* = {(L+T)-T} calculations as the basis of thickness design. The current Version 6E FAARFIELD design procedure uses the *Load Only* dashed line in the damage algorithm as the basis of the thickness design procedure. A future algorithm that considers curling and uses a *Combined Stress* concept would use the (L+T) stress values in the damage algorithm as the basis of design. A future algorithm that incorporates curling but uses load-only strain, or *Change In Stress* concept would use the {(L+T)-T} stress values in the damage algorithm as the basis of design. It is a fact that the residual tension level (T) is important with respect to pavement damage because when slab dimensions increase, the time to appearance of mid-panel cracks decreases significantly as residual tension is greater for longer slabs. The residual tension clearly affects fatigue life for a given load magnitude. If slabs become short enough, however, perhaps it will be found that the residual stress contribution from curling becomes small enough to be disregarded in a fatigue type damage algorithm, allowing the use of the {(L+T)-T} function as the basis of design. Notice how the middle zone of the {(L+T)-T} function is relatively flat and about the same magnitude as the load-only function. If it can be justified that total stress analysis is not required, then it in turn can be justified that in most cases, the load only stress values are "close enough" to the {(L+T)-T} stress values to be

used as a basis of design and that one need not consider residual curling stresses in the thickness design damage algorithm. Taking this concept much further is beyond the scope of this study but it is a very important concept.

Our independent analysis of DIA data using another calibrated FEM analysis revealed a similar {(L+T)-T} trend with lower edge stress change for curled-up conditions. Figure 3.23 shows the calculated edge strain magnitudes for flat-slab and ±2 °F/in gradient simulations for the calibrated DIA FEM analysis and simulating a B747 four wheel landing gear. The data in figure 3.22 was representing one single joint stiffness value for varying gradients. The similar data in figure 3.23 is now shown as a function of joint stiffness, for three different gradients, zero and ±2 °F/in. The load-related edge strain here is defined as the {(L+T)-T} edge stress level divided by the simulated concrete elastic modulus value.

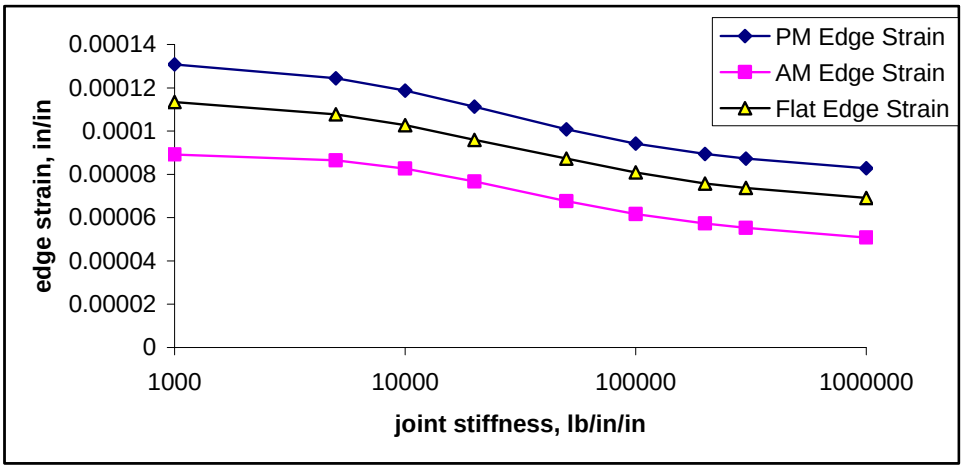

FIGURE 3.23. PLOT SHOWING ILSL2 FEM ESTIMATED CHANGE IN EDGE STRAIN MAGNITUDES (EQUAL TO {(L+T)-T} VALUE DIVIDED BY CONCRETE ELASTIC MODULUS) FOR THE B747 GEAR AND THE DIA CALIBRATED FEM APPROACH

Figure 3.24 shows a key finding from this study: a comparison of change in edge stress/strain {(L+T)-T} calculations for the Load Transfer (LT) magnitude, versus combined stress based LT magnitudes for the DIA data and simulating a B747 four wheel landing gear. The strain based LT calculations are similar for the typical working range for joints (between about 10,000 and 200,000 lb/in/in), while the combined stress based LT curves have a wider range of variation. Over this working range of joint stiffness, the strain based LT values ranged from about 15 to 35 percent. The overall site average DIA joint stiffness value was about 80,000 lb/in/in. The FEM results suggest that if one were to have measured the strain based LT value beneath this gear assembly assuming the residual strain was zero, the joint LT would have been about 27-28% for all curling cases. The curves in figure 3.24 represent the design LT functions for the DIA test site and the B747 gear configuration. These are the kind of simulations that can be done once a calibrated FEM model is established. More findings from FEM analysis is the focus of Chapter 6 of this report.

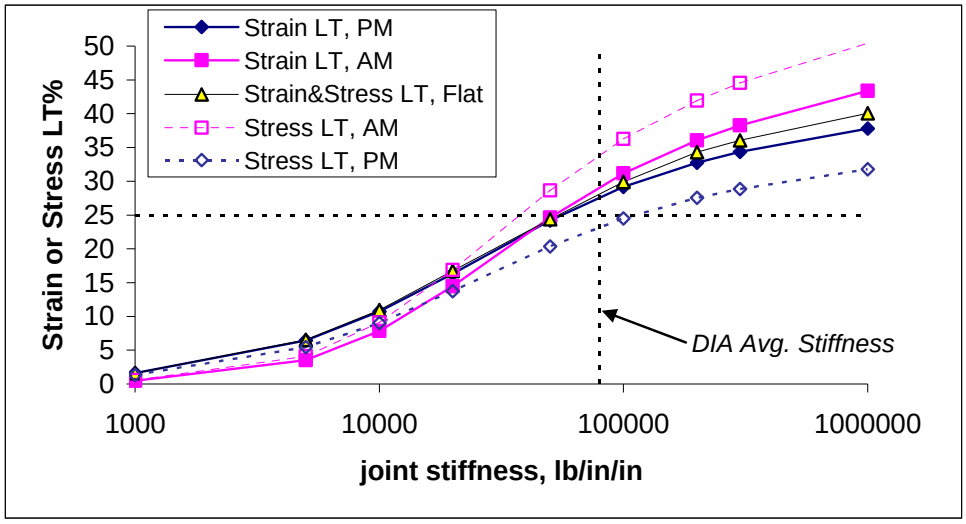

FIGURE 3.24. COMPARISON OF STRAIN AND STRESS BASED LT FUNCTIONS FROM THE TWO-SLAB ILSL2 FEM MODEL CALIBRATED TO DIA BEHAVIOR, FOR THE B747 GEAR ASSEMBLY

3.2.5 Step 5 - Slab Edge Gap and Joint Looseness Evaluations

Index values for slab edge gaps and joint looseness were obtained from the test sites. Figure 3.25 shows how the *Edge Gap* and *Joint Looseness* values are calculated for each joint load test location. Each of these index values takes into account the non-linear load versus deflection response or joint deflection difference response for the FWD load test on a joint. The Edge Gap index is the apparent y-intercept (zero load) value for the FWD load versus loaded slab edge deflection trend line. The Joint Looseness index is the apparent y-intercept (zero load) value for the joint slab edge deflection difference trend line. These index values are generally correlated to each other because they both increase with age, but they are also separate effects. In some cases, for example, relatively large slab edge gaps caused by upward warping were present while no significant joint looseness was measured. Estimates of these values were obtained for every FWD joint test location and site summary statistics established. The load plate deflection plot compares slab edge responses to mid-slab responses. A significant number of joint load tests appear similar to the mid-slab load test responses. These joint load tests indicate possible un-cracked or thermally locked joints.

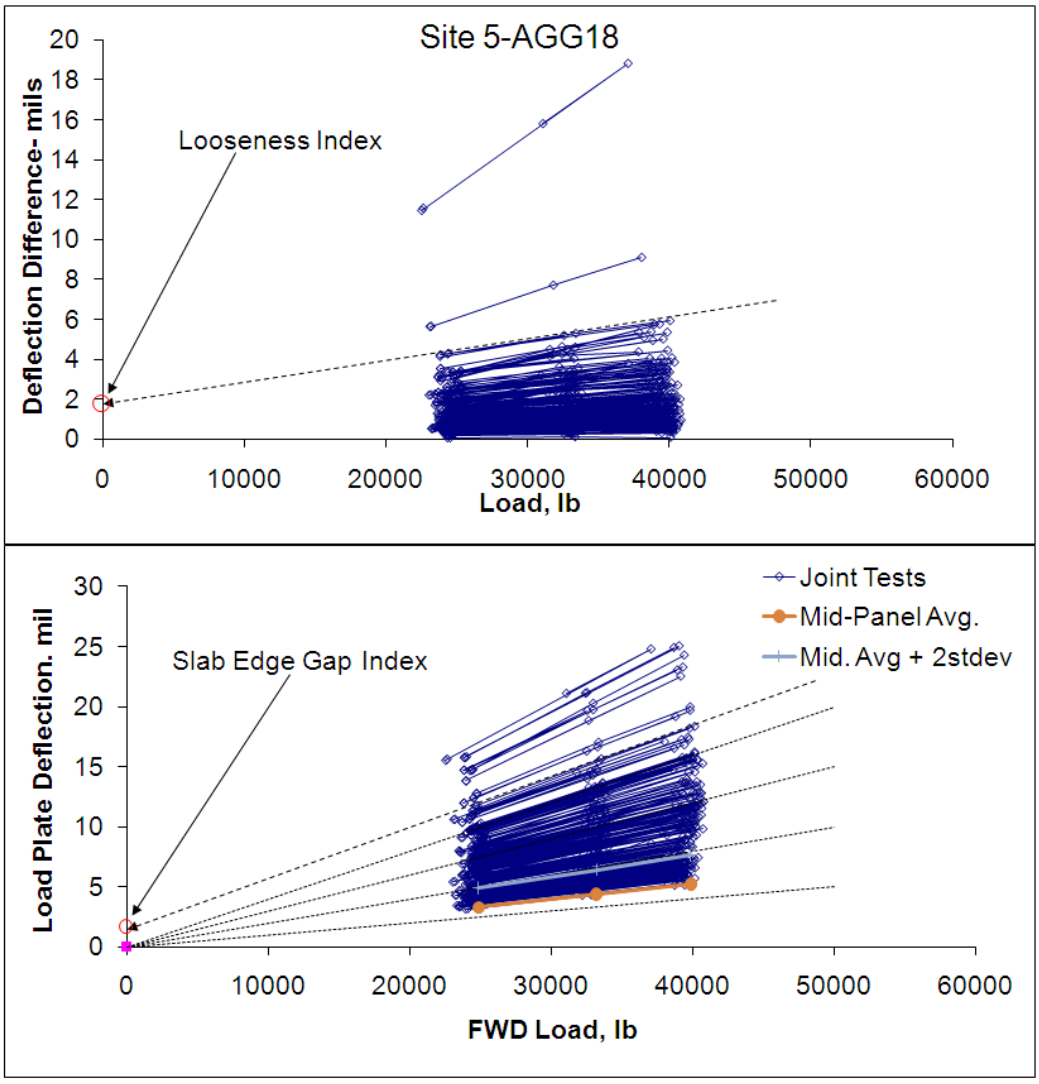

FIGURE 3.25. SITE DATA PLOTS FOR THE LOADED SLAB EDGE DEFLECTION, AND FOR JOINT DEFLECTION DIFFERENCE, VERSUS FWD LOAD MAGNITUDE FOR SITE 5-AGG18, SHOWING HOW THE SLAB EDGE GAP AND JOINT LOOSENESS Y-INTERCEPT VALUES ARE CALCULATED

Table 3.1 shows the overall site summary data for slab edge gap and looseness index values for the data shown in figure 3.25. In general, when measuring these values, one is attempting in most cases to measure something that is very close to zero in magnitude, and there are both positive and negative values in the distributions of estimates. When attempting to measure something that may have a zero magnitude, it is more important to know the magnitude of the standard error of the mean value. For example, the overall site 5-AGG18 average edge gap index size has a mean value of 0.29 mils, a standard deviation of 0.44 mils and was based on a total of 216 joint location based estimates from 864 FWD joint load tests, four per location at different load magnitudes. The standard error of the mean value estimation is the standard deviation of the distribution divided by the square root of the number of values in the distribution and is equal to 0.03 mils, about 10% of the calculated edge gap value, which indicates a

reasonable precision. There is power in numbers here, because a large number of samples were obtained, the mean value is reasonably accurate. Similar standard deviation, and therefore precision of the mean value estimates occur for both the edge gap and looseness index values. A key point regarding the edge gap data in table 3.1 for site 5-AGG18, is how the apparent edge gap had shrunk to a zero size during afternoon testing and was about 0.5 mil during morning testing while slabs were curled-up. An edge gap of 0.5 mils may appear to be small. Yet, the site overall average unloaded slab edge deflection for 25,000 lb FWD loads was only about 5 mils. Therefore the edge gap size was about 10% of the sites average unloaded slab edge deflection at this load level. Although both of these phenomenon and index values are barely measurable for these heavy duty airfield concrete slabs, magnitudes of just a few tenths of a mil in size can represent a significant percentage of the unloaded slab deflections occurring under typical wheel loads. Many samples are needed of such a variable phenomenon in order to obtain a reasonable estimate for mean value.

TABLE 3.1. SITE 5-AGG18 SUMMARY EDGE GAP (A) AND LOOSENESS (B) INDEX VALUES

(A). SLAB EDGE GAPS, MILS

	All	AM	Mid	PM
Avg	0.29	0.48	0.35	0.03
Min	-1.04	-1.04	-0.78	-0.59
Max	1.58	1.58	1.47	0.49
Stdev	0.44	0.48	0.47	0.19

(B). JOINT LOOSENESS, MILS

	All	AM	Mid	PM
Avg	0.09	0.02	0.21	0.04
Min	-2.65	-2.65	-1.50	-0.56
Max	1.66	1.66	1.53	0.38
Stdev	0.43	0.56	0.43	0.18

Table 3.1 and other data from site 5-AGG18 demonstrated how slab edge gaps can vary by time of day and affect joint behavior. All joints at site 5-AGG18 are doweled joints with little to no looseness. Figure 3.26 demonstrates the joint looseness calculations on an aggregate interlock joint from DIA that was tested at three different temperatures typical of winter to spring conditions. This joint reveals large looseness in the winter, but near zero looseness in spring as a result of joint closure and face lock-up. The measurable joint looseness during the winter condition had an intercept value of about 3.2 mils. This intercept value represents a significant 80 to 120 percent of the unloaded slab edge deflections that were occurring during the FWD load tests during winter. During winter, joint opening was large and this measurable looseness is mostly related to joint opening size. During summer testing, the joint had almost completely closed. There is not much discussion in past literature relating concepts of looseness to aggregate interlock joints. Most discussion of looseness has been around doweled joints. It is however this looseness concept that is the primary cause of variations in load transfer over time of year for aggregate interlock joints. All aggregate interlock surfaces will experience increasing measurable looseness as the crack faces are pulled further and further apart.

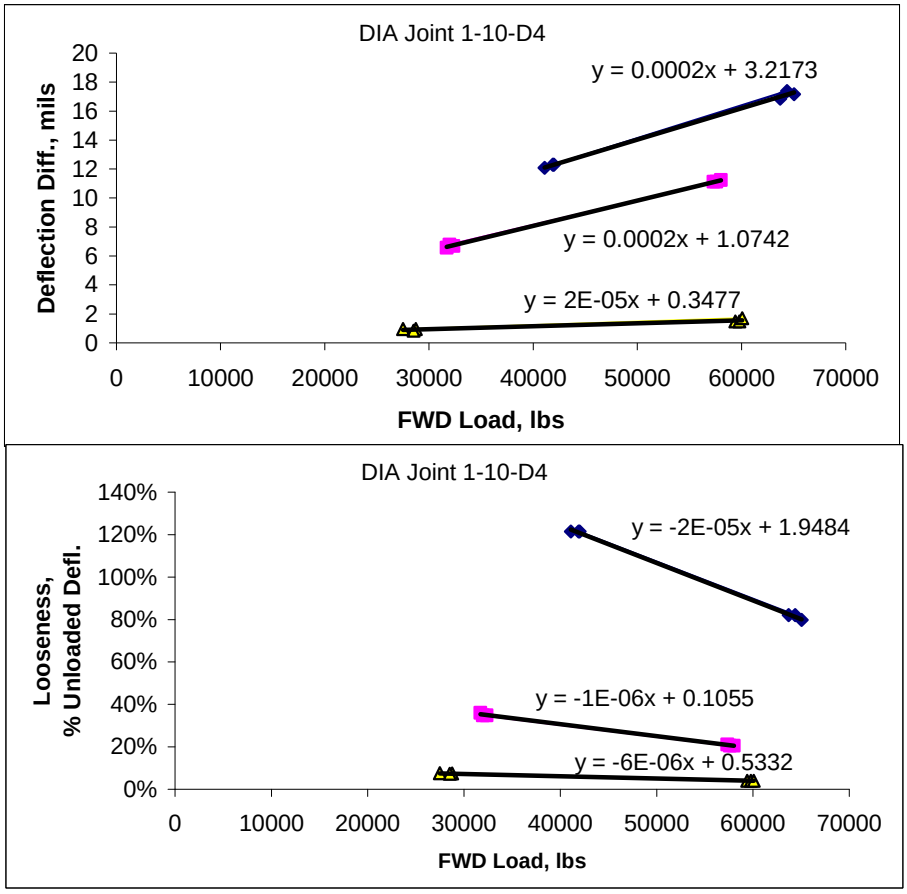

FIGURE 3.26. LOOSENESS INDEX VALUES FOR AN AGGREGATE INTERLOCK JOINT AT DIA TESTED AT 10, 18, AND 73 °F AND SHOWING HOW LOOSENESS DEVELOPS AS A RESULT OF INCREASING JOINT OPENING

The joint deflection difference trends shown in figure 3.26 are the basic measured trend shapes that calibrated FEM analysis results must be able to emulate for aggregate interlock joints if attempting to simulate the effects of progressive joint opening and looseness on the key parameter of *joint deflection difference*. Figure 3.27 shows the calculated joint stiffness trends for the looseness example joint from DIA discussed above. The cold weather tests revealed almost no joint stiffness, indicating the joint faces were not contacting each other to a significant extent. By the time the air temperature had reached 73 °F, the joint faces had apparently closed, which is indicated by a large y-axis intercept value of about 88,000 lb/in/in. All of these stiffness values are included in the plot in figure 3.12, showing the characteristic site joint stiffness curve for DIA. The concrete slabs simply see this joint stiffness variation as changes in spring stiffness at the edges of the slabs, and joint behavior varies along the site characteristic joint stiffness trend, which is more a function of the slab and subgrade cross section properties and has almost nothing to do with joint type, presence of dowels or not, joint details, etc. The seasonal variation of joint behavior observed at DIA and other test sites will be discussed in more detail later.

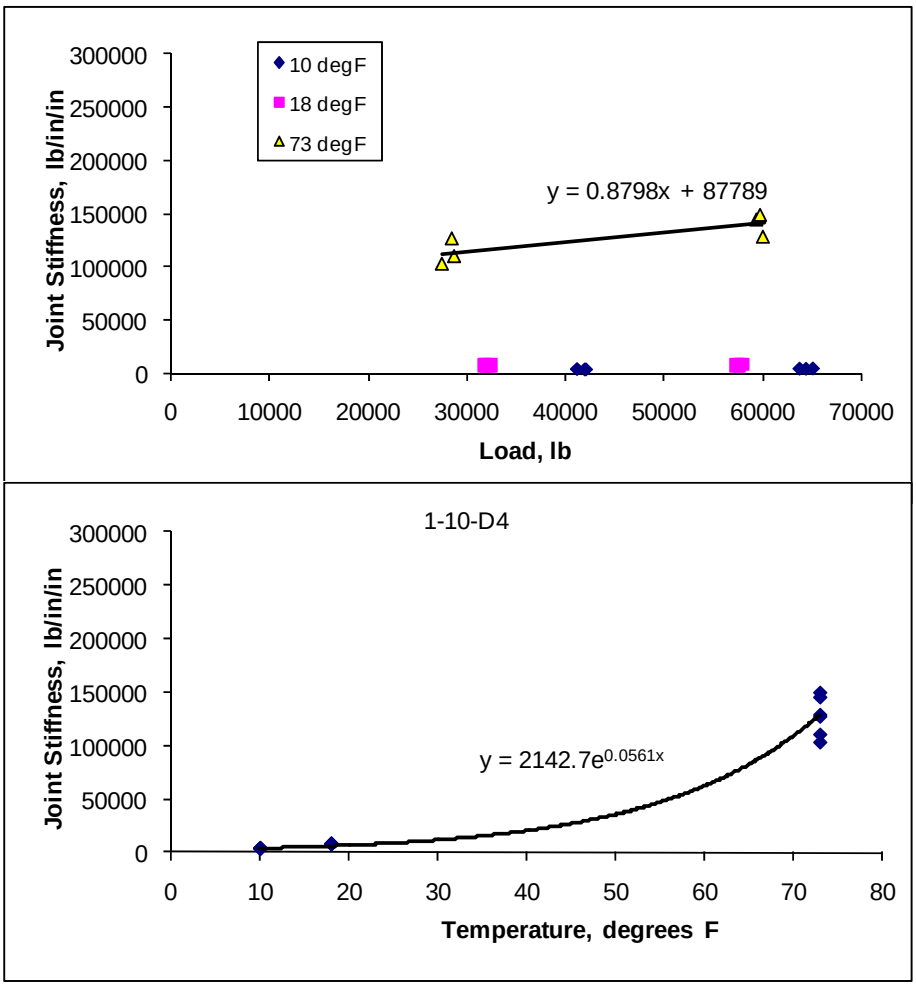

FIGURE 3.27. JOINT STIFFNESS TRENDS FOR THE JOINT DATA SHOWN IN FIGURE 3.26

3.2.6 Step 6 - Site Average Load versus Deflection Trends

To represent the overall average condition at the time of testing for each site, the average trends for joint edge deflections were established to be used in the test site final database. The deflection equations for mid-panel load versus deflection site averages were provided in figure 3.3 and were used as the basis for the test site numbering scheme, listed in order of stiffest to softest mid-panel structural response. In addition to those mid-panel site average response trends, similar structural response deflection equations were established for the loaded slab and unloaded slab edge responses for each test site. These are the site average measured deflection trends that would be matched to calibrated FEM analyses or backcalculation procedures. Figure 3.28 shows an example of the site average edge deflections, for site 5-AGG18. The sum of the two edge deflection lines has in the past often been considered to be equal to an equivalent free-edge deflection for a test site. If significant upward warp or curl is present, however, the sum of edge deflections can be as much as 30 to 40% larger than the equivalent free edge deflection. The joint line deflection difference between the two-slab edge deflection lines is the key joint load transfer parameter related to joint stiffness. The deflection difference combined with the

overall deflection magnitudes provides the sites overall average LTE_{δ} behavior reflecting its age, past traffic, and condition. Deflection difference is related to joint properties and must be considered entirely separately from total edge deflections, which are more related to subgrade stiffness and slab thickness.

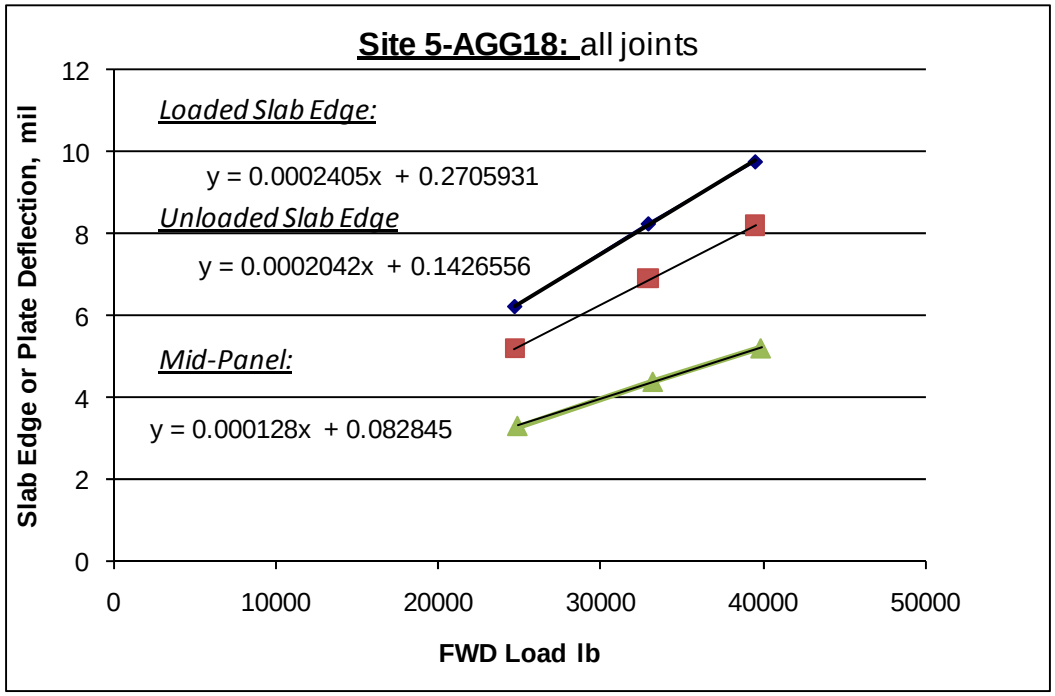

FIGURE 3.28. SITE AVERAGES FOR LOADED AND UNLOADED SLAB EDGE DEFLECTIONS

3.2.7 Step 7 - Evaluate Load versus Joint Stiffness

Summary plots of load versus calculated joint stiffness were obtained for all test sites. The expected trend was revealed where most doweled joints, and compressed/locked joints tend to have relatively constant stiffness over a range of FWD load magnitude. Only the looser and more open aggregate interlock joints and deteriorated doweled joints exhibited a trend of increasing joint stiffness with load. Figure 3.29 shows a summary plot of the observed load versus stiffness trends for site 5-AGG18. Each line segment represents a joint location. All joints at this site are doweled. As expected most of the trend lines are nearly flat. Figure 3.11 showed how a loose aggregate interlock joint had linearly increasing load versus stiffness trend. This is because as load increases, the looseness becomes a progressively smaller and smaller percentage of the total deflections, and the *perceived* joint stiffness using this method of measurement increases. This has the effect of creating an observed non-linear joint stiffness function, similar to that described by Guo et al. (1993). In figure 3.29, there is a slight visible horizontal gap in the data situated at about 80,000 lb/in/in joint stiffness. This is a real break between joint types at this site. The longitudinal formed doweled construction joints all had low stiffness at this desert site, probably due somewhat to lack of confinement by "other slabs". Because the runway is only six slabs wide, with asphalt shoulders, the slabs can more easily progressively push apart each summer during the warmest weather in the transverse direction. They do not push back together each winter, so they progressively push themselves apart causing

progressively greater joint openings along longitudinal joint lines. The transverse doweled sawed contraction joints all had very high stiffness at this site, being compressed together and confined by many "other slabs" in the longitudinal direction of the runway. Testing at this site was located in the skidded touch-down area of this runway, such that there were several hundred feet of slabs in each direction acting to confine these slabs in their original as-built positions and keep transverse joint openings smaller. This longitudinal versus transverse trend was observed at multiple test sites. Longitudinal joints do have lower measured stiffness and lower stiffness values for design are clearly justified. This general confinement effect was also well documented in the 17-year joint opening size study included in the Michigan Road Test (Finney and Oehler 1959).

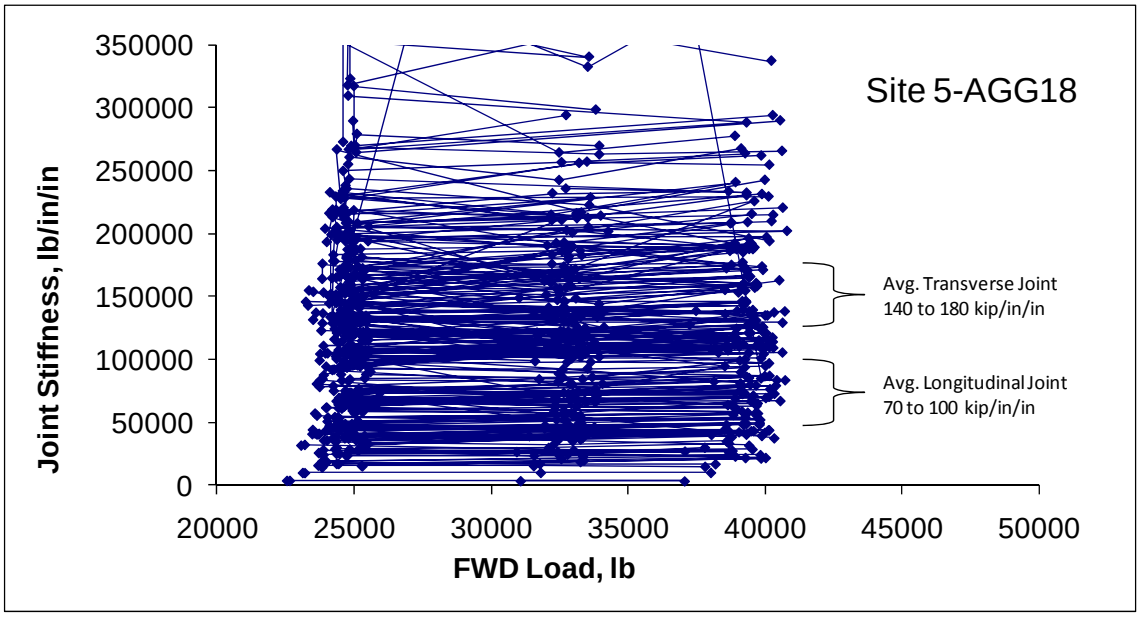

FIGURE 3.29. TYPICAL PLOT OF JOINT STIFFNESS VERSUS FWD LOAD MAGNITUDE FOR ALL OF THE JOINT LOAD TESTS FROM A TEST SITE

Overall site average load versus joint stiffness trends were established for each site as shown in figure 3.30. Both the median and mean values are calculated when considering a site "average" value. Median value is better for use with the characteristic joint stiffness curve shapes being observed. Because joint stiffness values are somewhat asymptotic towards infinity at LTE_{δ} = 90-100%, frequency distributions of joint stiffness values from a test site tend to be skewed. Mean and median values will differ significantly for skewed distributions, but will be about the same for relatively normal or uniform distributions. The median joint stiffness from a test site is almost always smaller than the average joint stiffness from a test site. The ranges of stiffness values shown in figure 3.29 for transverse and longitudinal joints present the site median value (lower value) and average value (higher value) for the joint stiffness distributions for each joint type.

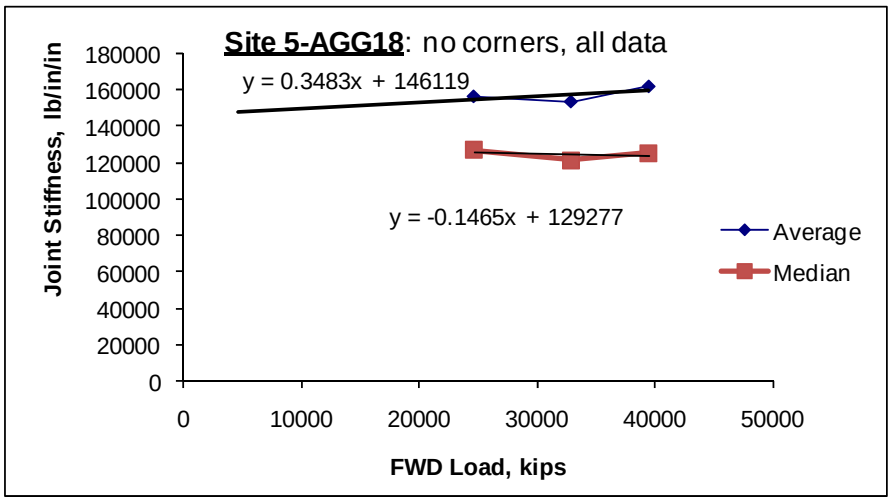

3.30. TYPICAL SITE AVERAGE AND MEAN JOINT STIFFNESS VERSUS LOAD TRENDS

3.2.8 Step 8 - Load Work versus Slab Strain Energy Analysis

The next step in the analysis process was to calculate a load work index, along with a slab system strain energy index for each FWD drop. Figure 3.31 shows the work to energy ratio plots for the DIA site, the test site 2-AC17, and the test site 5-AGG18. These values are defined as follows:

$$\text{Load Related Work, } \boldsymbol{Work} = P(\delta_L - gap) \tag{16}$$

$$\text{Slab Edge Displacement Energy, } \boldsymbol{Energy} = \tfrac{1}{2}(k_{slab})[(\delta_L - gap)^2 + (\delta_U - gap)^2] \tag{17}$$

Where,

P = FWD Drop Load, lb
δ_L = the loaded slab edge deflection, mil
δ_U= the unloaded slab edge deflection, mil
gap = loaded slab edge gap, mil
k_{slab} = stiffness of the loaded slab edge, load versus deflection trend, lb/mil

This work to energy ratio is an index of how much of the load energy passes through to the subgrade. When LTE_δ is high, the apparently recoverable slab strain energy is about the same magnitude as the load work energy. When LTE_δ is low, the load work energy is about double of the slab strain energy. This index is a good way of looking at joint performance, alternative to LTE_δ data, or stiffness data, but it tends to reveal more about the low stiffness behavior of the joints and this index has physical meaning. This plot also reveals how well the higher stiffness joints are supported. When the joints become seated into the subgrade, the slab edge strain energies decrease and the edge stiffness increases significantly, resulting in higher work to energy ratio values. When slabs are curled upwards with joints lifted, this index indicates that significantly less energy passes through to the subgrade, and more is locked into slab rotation and edge strain energy. Test site 2-AC17 had relatively good joint support. Test site 5-AGG18

is the site that experienced large curling and joint uplift and poor support during the early morning, but had fully seated good joint support in the mid day period. The data from this site displays the full range of poor to good edge support, from morning to afternoon as a result of curling. The DIA site has slight up-warp with voids at joints and shows apparent lower joint support.

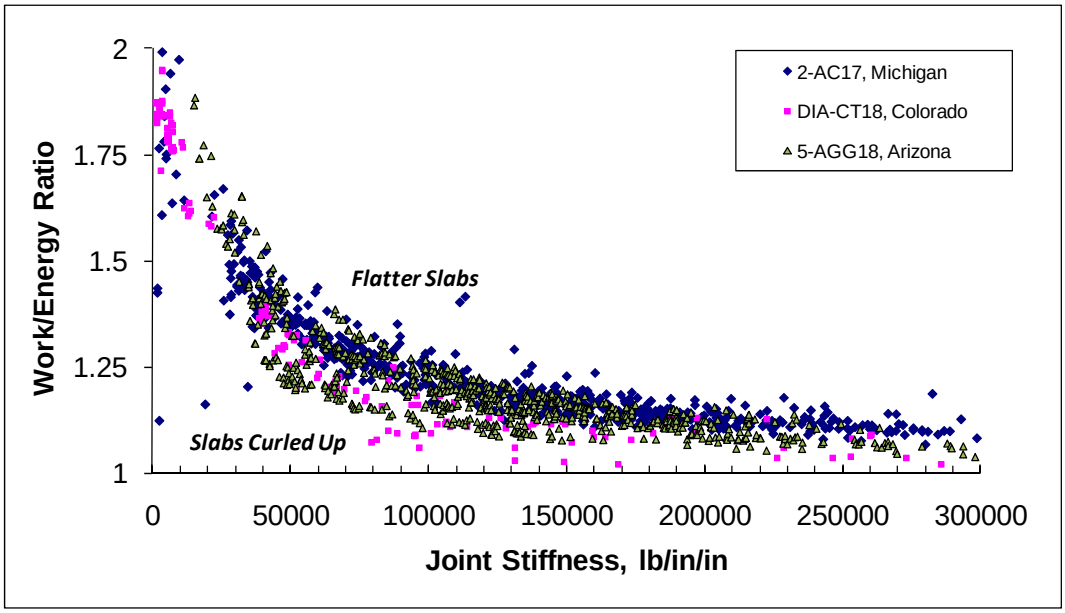

FIGURE 3.31. PLOTS OF THE LOAD RELATED WORK DIVIDED BY THE SLAB STRAIN ENERGY FOR THREE SITES

3.4 DIPSTICK SLAB CURLING AND WARPING ANALYSIS PROCEDURE

Slab shape changes were quantified at the sites using the FACE corporation DIPSTICK hand-held slope measurement device. This device is considered an ASTM Class A profiling device and provides an accurate way to measure slope and slab shapes. For this study, the slab curling and warping were evaluated using a method of analyzing the variation of slab end slopes (Byrum, 2009). Five separate readings of slab slope are taken at each corner of a test slab and oriented along a diagonal line across the slab from corner to corner as shown in figure 3.32. An average of 8 or 9 slabs per site were evaluated typically 4 times per day during the site evaluation. The first time the readings are taken, the DIPSTICK circular feet locations are precisely outlined onto the pavement surface with a marker such that slope measurements can be repeated. Repeat slope measurements at different times of day are taken at exactly the same spots as previous slope measurements. This is key to success with this method so as to accurately measure changes in slab curvature caused by curling. Figure 3.33 shows the calculation procedure for determining the average slab curvature for a slab using slab end slope values and the standard mean value theorem integral from calculus applied to the slab curvature function. The average of the five slope samples from each slab corner are used for the calculations. These average end slope values are plugged directly into the curvature mean value theorem integral solution. Although there may be considerable variation in the magnitudes of average slab curvature from slab to slab at a test site, the *changes* in average slab curvature in

individual slabs caused by curling at different times throughout a day will be relatively uniform at the site and are measured quite accurately with this technique. In general it is not necessary to measure any of the slab shape between the end slope regions in order to quantify slab shape change from curling accurately. Average slab curvature from warping is a separate issue, different than the change in slab curvature from curling, and warp must be considered differently in terms of statistics. Moreover, warp causes the same kind of slab shape (curvature) to develop. It is difficult to tell how much of a site's total slab curvature is from warp versus curl without actually measuring thermal gradients in the slabs.

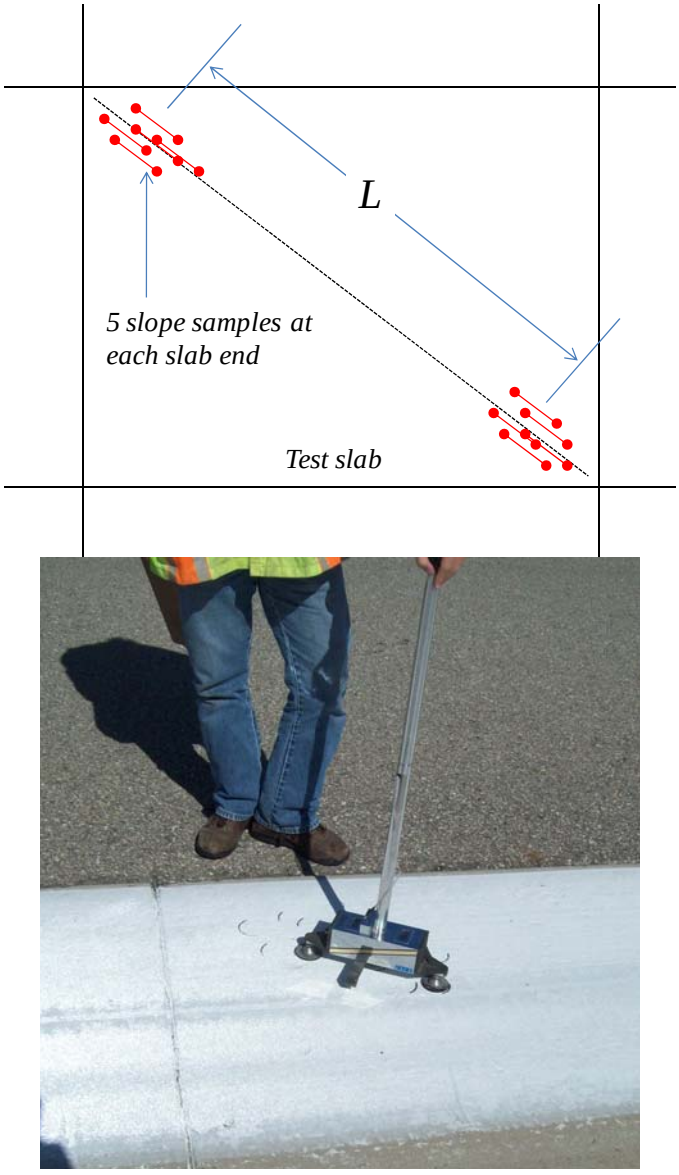

FIGURE 3.32. PHOTO IMAGE OF THE DIPSTICK AND THE SAMPLING PATTERN USED FOR THE SLAB END SLOPE CURLING ANALYSIS PROCEDURE

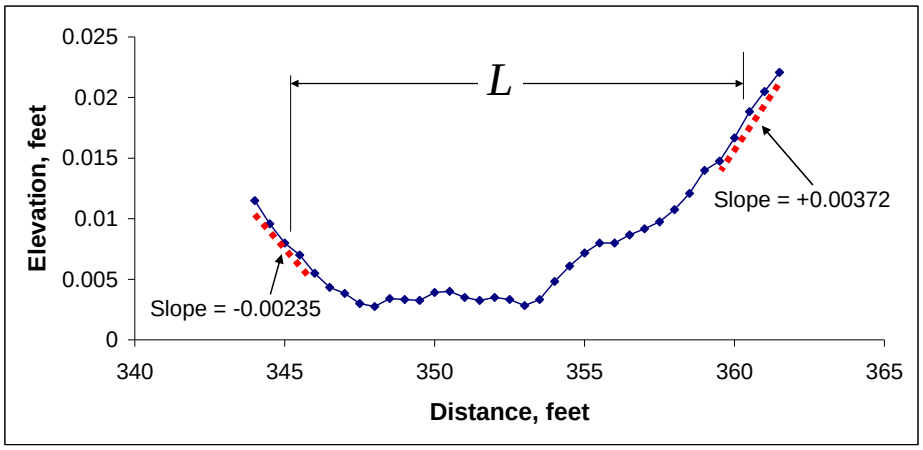

$$\kappa_{mean} = \frac{\int_0^L z''(x)dx}{L} = \frac{z'(L) - z'(0)}{L} \tag{18}$$

FIGURE 3.33. THE MEASUREMENTS AND REQUIRED EQUATION FOR CALCULATING MEAN VALUE OF SLAB CURVATURE FROM SLAB END SLOPE MEASUREMENTS FROM A TEST SLAB

The Central Limit Theorem and Standard Error of the Mean concepts from statistics are key concepts for understanding the measuring of slab curling and warp. Measuring curling and warp involves the challenging task of attempting to measure a value of zero. Curling theoretically causes slab curvature to vary around the zero value. Warping can become extreme both in the upward or downward direction and also varies around the zero value. It is difficult to actually measure or verify zero slab curvature, or perfectly flat with no curling or warping. The central limit theorem states that for any large population having finite standard deviation, the mean of sample size, *n*, approaches the true mean of the population as *n* becomes large. When attempting to measure a value of zero it is more important to quantify the standard error of the mean value, for the attempted measurement of zero. That way one can answer the question: zero plus or minus how much? The standard error for the average slab curvature determination is obtained based on the following formula:

$$\textit{Standard Error for the Average Curvature Estimate} = \frac{\sigma_\kappa}{\sqrt{n}} \tag{19}$$

Where,

σ_κ= Standard deviation of the slab curvature estimates frequency distribution.
n = Number of estimates in the frequency distribution.

Figure 3.34 shows the results for the analysis of the variation of curvature for test slabs from site 5-AGG18. There is considerable variation in the overall average value of curvature, or apparent warp in each slab. The magnitude of slab curvature present at just after sunrise, when the effective thermal gradient becomes zero, is the approximate locked-in warp value. Slab surface texture and finishing can affect the measurement of the warp value so many slabs need to be measured to get a good estimate of average warp present at a test site. Nonetheless, the change in curvature measured in each slab will be nearly identical, and this change in curvature is the curling effect. Fewer slab samples are needed to get a good estimate of curling, as compared to warp. To demonstrate the precision of the estimate for the curling related change in curvature at site 5-AGG18, the average curvature change from the seven slabs was about 0.000111 ft^{-1} and the standard error for this mean value is estimated as: the standard deviation of the curvature change values (0.000012 ft^{-1}) divided by the square root of seven, or approximately 0.0000045 ft^{-1}. The standard error is about 4% of the magnitude of and typical range of curling related slab curvature change, which can be as high as 0.0001 to 0.0002 ft^{-1} change from morning to afternoon on thermally active days. Therefore, the measured average is a good estimate of true mean value of the curling related change in slab curvature with seven slabs as its basis.

The overall 8 AM approximate average slab curvature from the seven slabs was about 0.00013 ft^{-1}, with a positive value meaning upward curvature or joints lifted. This is the approximate locked-in warp magnitude at the test site. The time of 8 AM, right after sunrise, is the approximate time when the effective linear portion of the thermal gradient through the slab becomes zero. This site has a significant upward curvature near this time, which is expected given it is in the desert. This apparent locked-in warp of about 0.00013 ft^{-1} is a typical locked-in warp value, about the same value as encountered in typical highway slabs in this type of climate (Byrum, 2000). The standard error for the average slab curvature calculation is approximately equal to 0.000287 divided by the square root of seven, which is about 0.0001 ft^{-1}. Slab warp curvatures typically are within the range of about +0.0005 to -0.0004 ft^{-1}. Therefore the standard error is about 13% of the possible range of warping. Figure 3.35 provides an example of how the number of slabs used for the warp sample affects the warp estimate standard error. For this study an average of 8 or 9 slabs per site were used, which should be considered a minimum number of slabs for measuring curling related changes in slab curvature. When using the DIPSTICK slab end slope approach, use a minimum of 7 slabs for fine texture and flat finishing, 11 slabs for medium texture and poor to average finishing, and 15 slabs for coarse textures and rough finishing when your project objective is primarily to measure the change in slab shape from slab curling. A fair to poor estimate of warp will be obtained using this number of samples. If in addition it is desired to obtain a good estimate of slab warp at a site, a minimum of 15 slabs for finer textures and smooth finish, or 30 slabs for coarser textures and rougher finish, should be used in the slab end slope calculations for a test site. Avoid placing DIPSTICK feet on any sign of edge slump, patching or spalling. Broom-clean the slab within the slope sampling areas to further reduce the standard error of estimates.

In general, it was not the goal of this study to precisely measure locked-in warp at the test sites, but it was a project goal to precisely measure curling and this was accomplished while obtaining a reasonable estimate for warp. It would have taken an additional DIPSTICK staff on site, or use

of a rapid travel profiler to obtain enough slab end slope readings to get a really good estimate of overall warp at these test sites. In a past study performed by the author (Byrum, 2000), 500-ft long highway samples were used to obtain warp estimates. A typical set of highway slab curvature data, taken along the wheel paths, is also shown in figure 3.34. The standard error of the warp estimate for the highway site is about 0.00021 divided by the square root of 33 = 0.000037 ft^{-1}. This standard error magnitude is about one third of standard error for the site 5-AGG18 and is about 4% of the potential range of warping related curvatures in slabs, which can be much larger than curling related curvatures. The overall range of individual slab curvature values for the highway site compared to site 5-AGG18 is about the same, being about 0.0008 to 0.0009 ft^{-1}. Standard deviation was slightly higher for the airfield site. The highway site was severely up-warped, while the airfield site was just slightly up-warped. These slab end slope based curvature statistics were obtained for all of the full test sites.

	500-ft Highway GPS3 55-3009	***Site 5-AGG18*** ≈ 8AM average	AM-PM Change
average curvature, 1/ft	0.000547	0.000126	0.000111
min. curvature	0.000203	-0.000362	0.000089
max. curvature	0.001077	0.000555	0.000124
st. dev. of curvature	0.00021	0.000287	0.000012
number of slabs	33	7	7

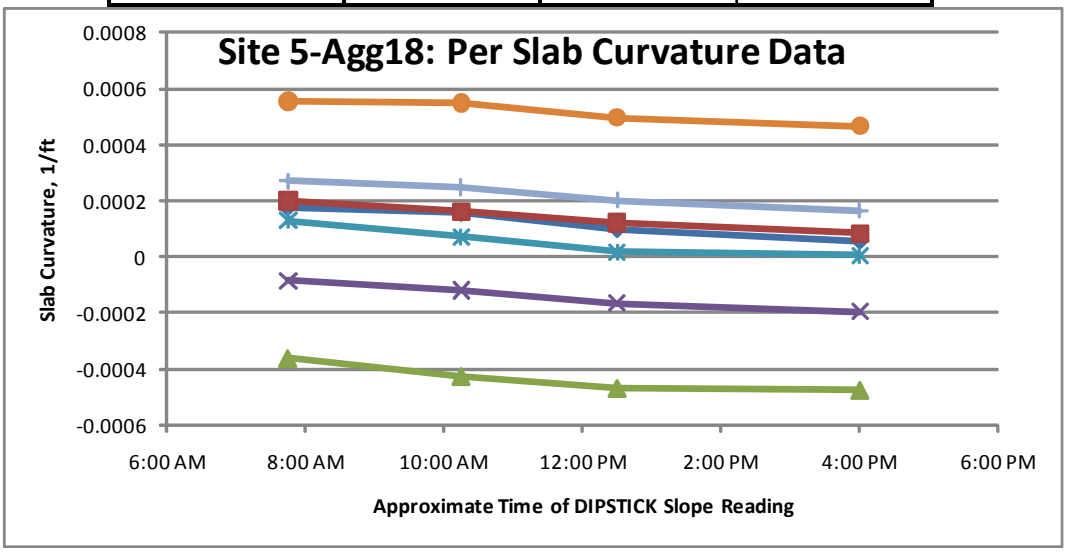

FIGURE 3.34. TYPICAL RESULTS OF DIPSTICK SLAB END SLOPE CURLING AND WARP ANALYSIS, FOR SITE 5-AGG18

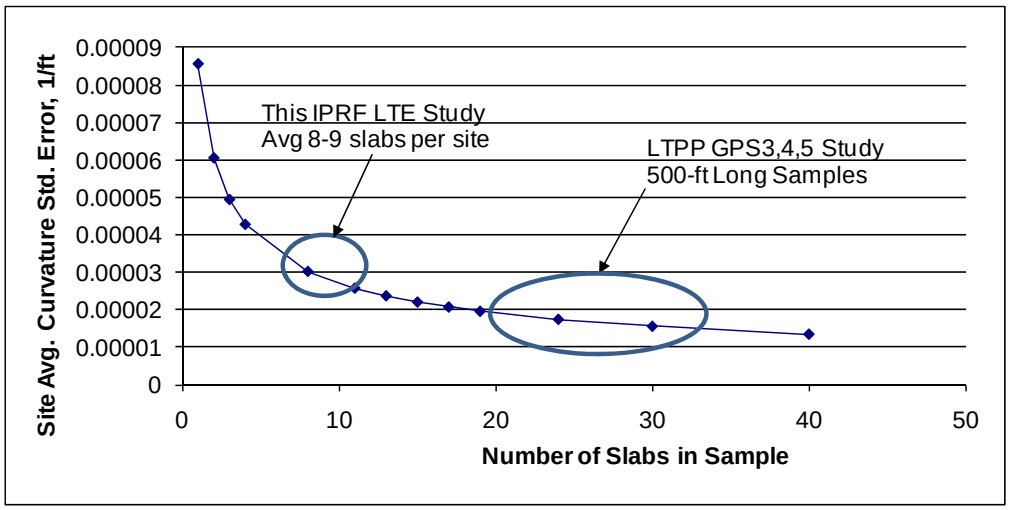

FIGURE 3.35. PLOT SHOWING HOW THE STANDARD ERROR OF THE MEAN VALUE FOR AVERAGE SLAB WARP CURVATURE DECREASES AS NUMBER OF MEDIUM TEXTURED 17.5-FT TEST SLABS USED FOR THE ESTIMATE INCREASES

Once the estimates of slab curvature are obtained, FEM analyses or the Westergaard slab curling approach (Westergaard, 1927) can be used to backcalculate the apparent thermal gradients that were occurring at the site, and the related residual curling stress. Fitting of the Westergaard curling equations to measured curvature changes is now demonstrated. Fitting of FEM models to curling data is described in Chapter 6. For any site estimate of average slab curvature, it represents the overall combination of all curvature causing effects, $\kappa_{total,}$ along a continuous slab of length L combined into one overall number as shown below:

$$Average\ Slab\ Curvature = \frac{\int_0^L \kappa_{total}(x)dx}{L} \tag{20}$$

In the context of the Westergaard slab curling shape function for the infinite strip considered, slope is always zero at the mid-slab position. This fact and given the system symmetry, the overall site average curvature can be related to one-half of the Westergaard infinite strip shape function in the following way:

$$Average\ Slab\ Curvature = \frac{\int_0^{L/2} \kappa_{Westergaard}(x)dx}{L/2} \tag{21}$$

$$= \frac{\int_0^{L/2} z''_{Westergaard}(x)dx}{L/2} \tag{22}$$

$$= \frac{[-z'_{Westergaard}(0)]}{L/2} \tag{23}$$

The change in curvature parameters (curling) can also be simulated in the same way. All that needs to be done is to adjust the parameters entering the Westergaard equation until the end slopes from the theoretical solution with the same slab length give the same average curvature values obtained from the test site slab end slope measurements.

An infinite number of possible solutions of the Westergaard equation exist for a given average curvature, varying primarily as a function of the assumed subgrade stiffness, and thermal gradient magnitude, but also with the slab elastic modulus, poisson's ratio, thermal expansion coefficient and thickness. The problem in general is very sensitive to assumed subgrade *k*-value. Westergaard warned that the equations he developed are not valid for analysis on stiff subgrades where slab corner uplift off of the subgrade would occur, because full slab edge to subgrade contact is assumed in the derivations. This is why Westergaard only reported data for *k*-values less than 100 psi/in. A more sophisticated FEM type approach is needed to simulate air gaps between the slab and the foundation caused by curling, warping or loss of edge support. An example of the solution for a Westergaard fit for the 8 AM average slab curvature condition at site 5-AGG18 and assuming a subgrade *k*-value of 300 psi/in is shown in figure 3.36. For this analysis, the Westergaard slab length was set as the distance between the DIPSTICK sampling areas at the slab corners. The symmetrical "infinite strip" idealization was used for the fit. A generic optimizer is used to vary the equivalent thermal gradient until the Westergaard solution's deflected shape average slab curvature matches the measured value from the test site.

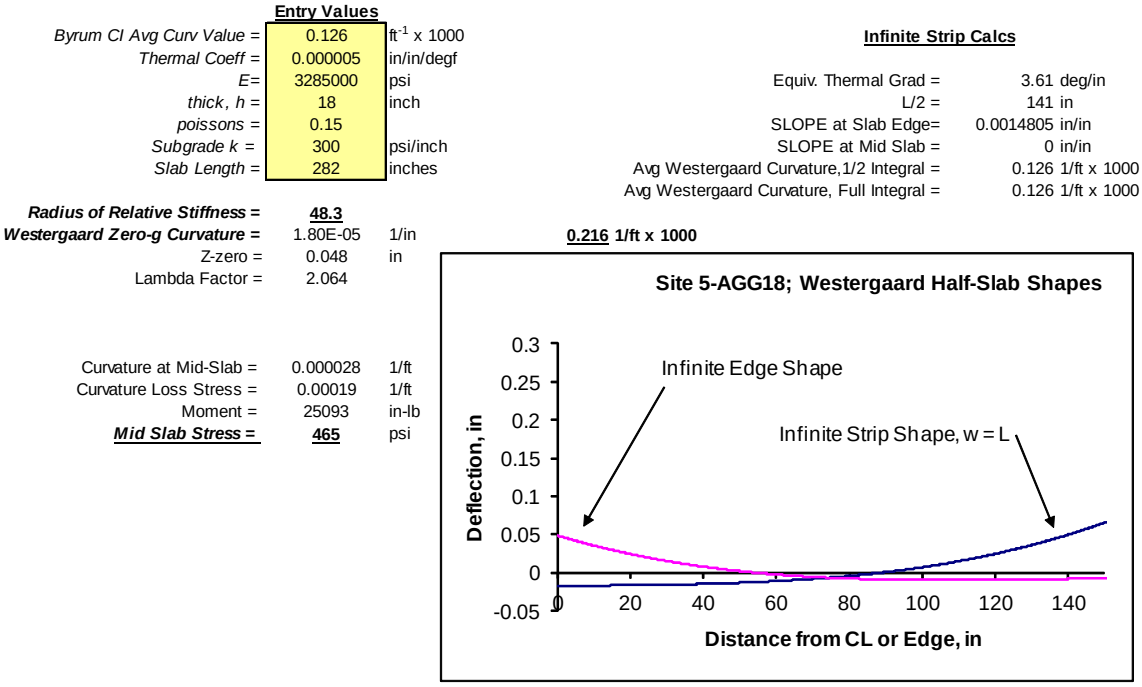

FIGURE 3.36. AN EXAMPLE OF HOW TO FIT THE WESTERGAARD, 1927 CURLING SOLUTION TO DIPSTICK BASED MEASUREMENTS OF AVERAGE SLAB CURVATURE REPRESENTING THE 8 AM SITE AVERAGE CURVATURE AT TEST SITE 5-AGG18 (REFER TO THE ORIGINAL PAPER FOR CURLING EQUATION DETAILS)

Figure 3.37 shows the backcalculated Westergaard curling solutions for the site 5-AGG18 used in previous examples. The solution is expressed as the set of lines, and as a function of the assumed "warping response subgrade *k*-value". The analysis allows estimation of a zero-restraint curvature value for a given thermal gradient, which is the magnitude of curvature that would develop in the slab if it were floating in zero gravity, or floating on a fluid-filled bag, and exposed to a gradient. With this idealization, no edge stress develops from unrestrained curling in zero gravity. Accordingly, the Westergaard slab is rested on a subgrade and the thermal gradient is varied until the average curvature of the deflected Westergaard shape function matches the average curvature measured at the site and for varying *k*-values. The loss in curvature (or anti-curvature) at mid-slab, which develops after resting the curved slab on the earth, can be converted into an estimate of curling stress magnitude at mid-slab. Figure 3.17 provided the backcalculated subgrade stiffness values for site 5-AGG18. During the afternoon testing the average of the edge and mid-slab subgrade *k*-values were between about 250 and 325 psi/in. From the Westergaard curling fit for site 5-AGG18 and assuming a subgrade value of 300 psi/in was present, the plots in figure 3.37 are showing that for a measured average curvature value of 0.000126 ft^{-1}, the slab would need to have a constant curvature of about 0.00022 ft^{-1} in zero gravity or a *k*=0 condition. Once the slab was rested on the *k*=300 psi/in subgrade, the anti-curvature that occurs at mid slab results in an estimated 460 psi bending stress level. For the *k*-value of 300 psi/in example, an unrealistic equivalent thermal gradient of 3.6 F°/in, cooler on top, through an ideal flat slab (over 65 F° temperature difference top to bottom) would be needed to

curl an ideal Westergaard "flat" slab into the same average curvature condition as was present at full test site 5-AGG18 at about 8-AM, when the curling gradient would be expected to be about zero, or flat.

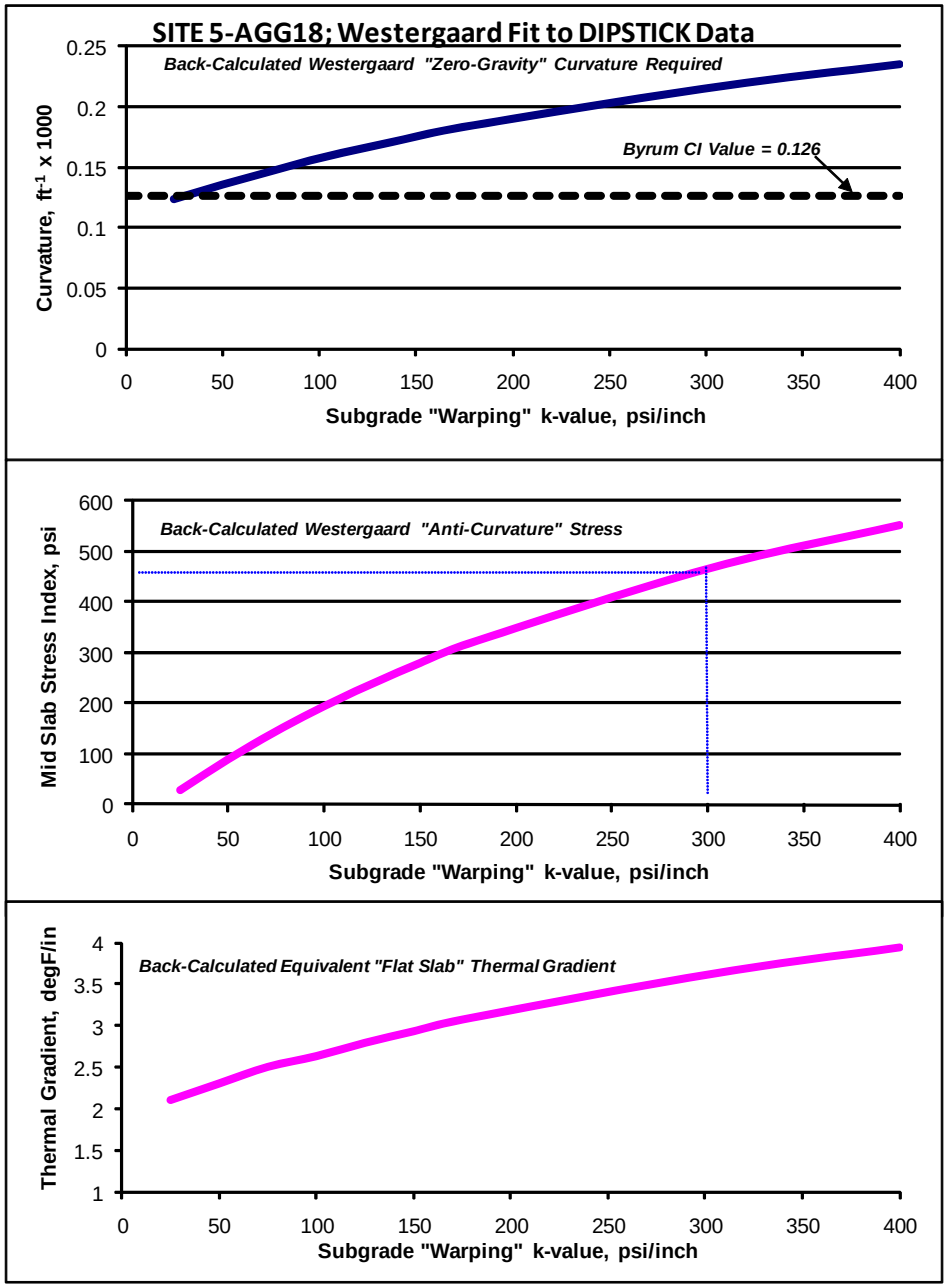

FIGURE 3.37. WESTERGAARD BEST-FIT CURLING SOLUTIONS FOR THE 8 AM AVERAGE SLAB CURVATURE ESTIMATES (LOCKED-IN WARP) FOR TEST SITE 5-AGG18

The measured temperature data for test site 5-AGG18 was provided in figure 3.14. Looking at the data, it would be almost impossible to have had a thermal gradient change at this site greater than about 50/18 = 2.7 °F/in with air and pavement temperature ranging between about 80 and

130 °F during testing. The change in curvature data from the site can be used to estimate the change in thermal gradient that occurred at a test site using the Westergaard edge curling solution. As shown in figure 3.34, the change in curvature measured at the site was about the same magnitude as the average curvature measured at 8 AM. So, for example purposes, the plots in figures 3.36 and 3.37 also represent the amount of thermal gradient change that occurred at site 5-AGG18 during testing. In a zero-gravity or fluid-filled bag support condition, the Westergaard solution indicates that about 2 °F gradient change could have caused the observed curvature change at the site. For a subgrade *k*-value of 300 psi/in assumption, the solution shows that a 3.6 °F/in gradient would have been necessary to cause the observed curvature change. This is much larger than probably did occur at the site. If one assumes or had measured a gradient of 2.5 °F/in through the slabs, the Westergaard solution reveals that a "warping *k*-value" of about 70 psi/in would have been present. This apparent low value ties back into the concept of subgrade compliance to curling and warping. Because the effective subgrade loading rates from curling and warping are very slow, plasticity effects may result in significant subgrade relaxation or compliance to the desired curled or warped slab shape. This compliance effect is why some highway panels have experienced extreme warp, but can remain uncracked after millions of wheel passes (Byrum, 2009). These slabs become highly warped without developing considerable residual stress, to levels that would be reproduced, for example, by the Westergaard curling solution used here. The idealized subgrade behavior here is fluid filled bag, where no change in support or residual curling stress develops as a result of totally unrestrained curl or warp shape changes. Based on this study, it appears appropriate to apply a reduction factor to the range of expected thermal gradients at a site to account for subgrade compliance effects, while acknowledging that slab edges will lose support from warp and permanent foundation deformation over time.

The following general relation would be used to match results from the FEAFAA code, or similar FEM computer program with curling analysis capabilities to the measured average curvature. For a given subgrade stiffness and slab properties combination, the thermal gradient in the FEM software would be varied until the resulting FEM average curvature, or changes in curvature, matches the curvature measured at the site using the DIPSTICK. To do this, the slope values near the ends of slabs quantified in the FEM discretization are matched to the measured site average curvature using the equations below.

$$Average\ Curvature = \frac{\int_0^L z''_{FEAFAA}(x)dx}{L} \qquad (24)$$

$$= \frac{[z'_{FEAFAA}(L) - z'_{FEAFAA}(0)]}{L} \qquad (25)$$

This procedure is demonstrated in more detail in Chapter 6. The use of this Westergaard fitting technique on many sites has revealed that significant subgrade compliance to curling must be occurring at most sites. The example site 5-AGG18 described above is the one full airfield test site for this study that exhibited the least amount of apparent subgrade compliance. Yet the

Westergaard fit approach still indicates a large amount of subgrade compliance is probably occurring at this site.

3.5 JOINT OPENING CHANGE MEASUREMENTS

Upon first arrival at the test site in the early morning, the joint opening sizes are about as large as they will be during the testing window. Shortly after arrival, brackets were epoxy mounted to each side of several joints in order to support digital deflection indicators having a 0.0001-inch resolution. These devices measured the change in joint opening, or "joint closure" that occurs from morning to afternoon during the site visit. Figure 3.38 shows a typical device set-up.

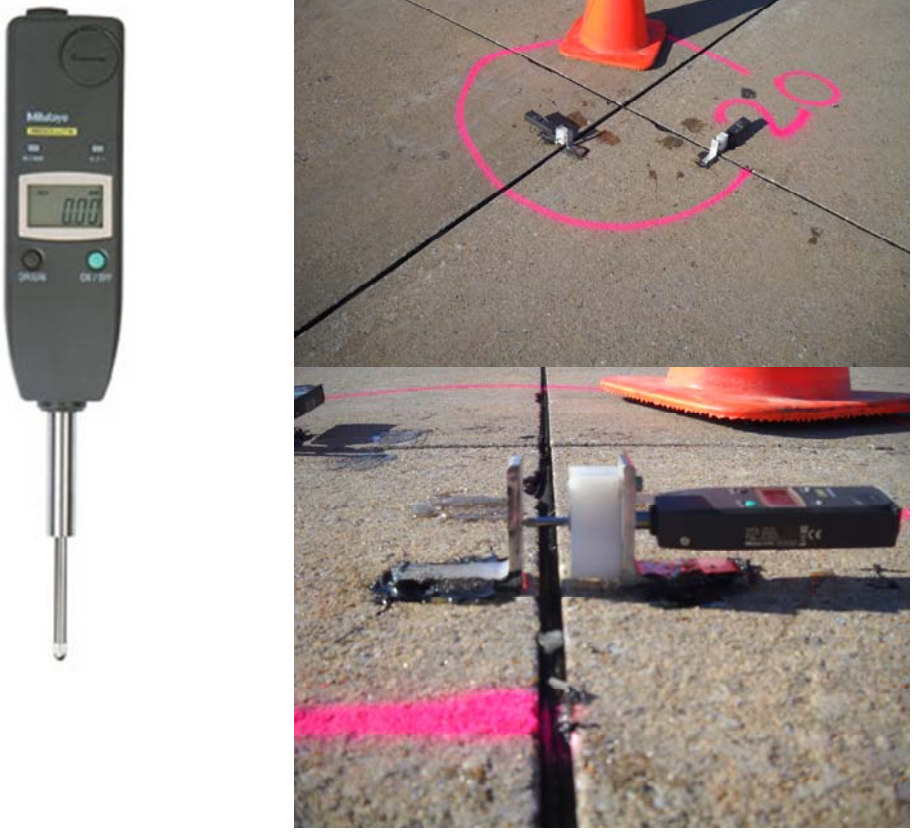

FIGURE 3.38. MITUTOYO DIGITAL INDICATORS USED TO MEASURE THE CHANGES IN JOINT OPENING SIZE

Figure 3.39 shows a typical plot of joint closure measured at test site 10-AGG14, which experienced large thermal changes during testing. Figure 3.40 shows the FWD temperature measurements from the same time period for comparison. The concrete slab surface temperature at the site ranged from about 76 to 120 °F while the joint closure followed a trend having the same shape as the slab surface temperature trend. Measured opening changes averaged about 27 mil, resulting in a joint closure rate of about 0.63 mil per °F. This test site also experienced the

largest measured curling slab shape variation of all test sites, about 0.00013 ft^{-1} curvature change during testing.

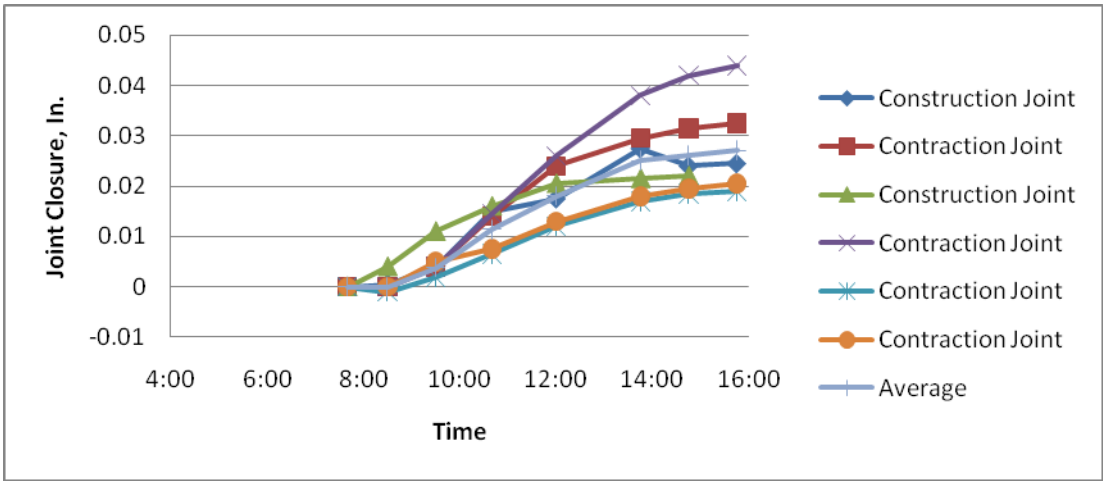

FIGURE 3.39. TYPICAL SET OF JOINT CLOSURE MEASUREMENTS, FROM SITE 10-AGG14 ON A HOT SUMMER DAY IN A DRY MILD CLIMATE REGION

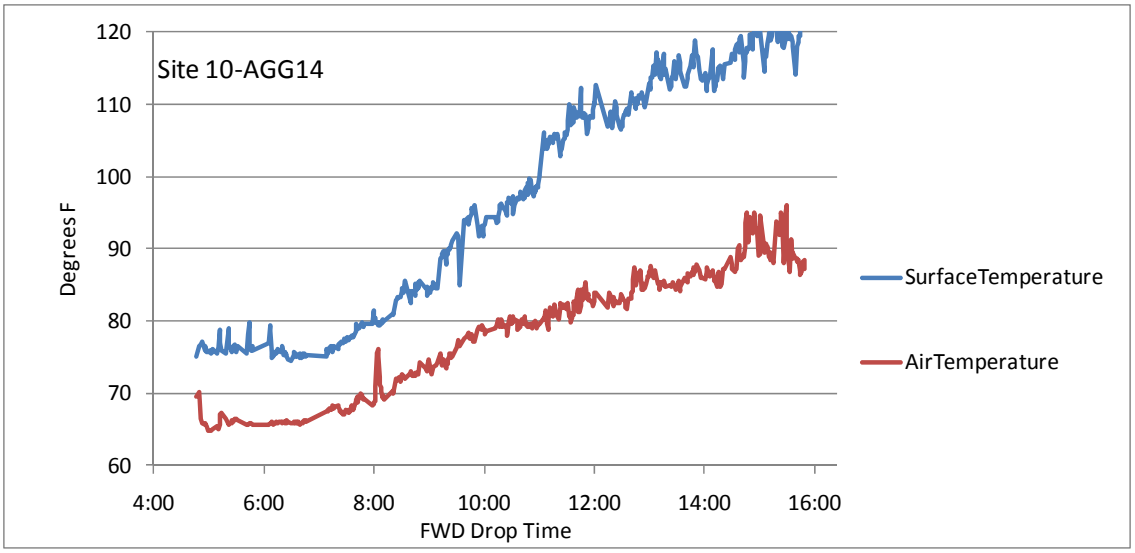

FIGURE 3.40. THE FWD TEMPERATURE MEASUREMENTS CORRESPONDING TO THE JOINT CLOSURE MEASUREMENTS SHOWN IN FIGURE 3.39

3.6 SLAB ROTATION GEOPHONE ACCELERATION MEASUREMENTS

The test routine also included measuring slab rotations during FWD testing. Slab rotation was measured by utilizing two Nomis Mini SUPERGRAPH Seismographs. The seismographs are portable and measure frequency response with a seismic velocity range of 0 to 10 inches per

second. The seismic velocity is then converted to deflection estimates using computer software that integrates the measured velocity data. The seismographs are similar to the velocity transducers used by the FWD to measure deflections.

FIGURE 3.41. REMOTE SEISMOGRAPHS USED TO EVALUATE SLAB ROTATION AND LTE_{δ} AT THE FAR ENDS OF SLABS OPPOSITE OF THE FWD LOAD LOCATION

One seismograph was placed on each side of the far joint of the joint load test. Figures 3.42 and 3.43 illustrate the test setup configuration. The seismographs were manually triggered during the FWD drop sequence to only record the deflection of the largest FWD load (about 40 to 50 kips).

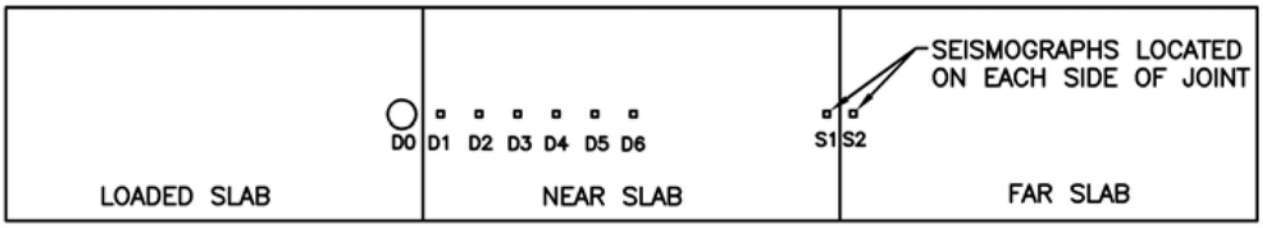

FIGURE 3.42. SLAB ROTATION TEST SEISMOGRAPH CONFIGURATION

FIGURE 3.43. SLAB ROCKING TEST IN PROGRESS.

Table 3.2 shows the average deflections for the slabs tested for rotations. A "Rocking Ratio" was calculated using the following formula:

$$Rocking\ Ratio = \frac{Average\ Deflection\ measured\ by\ Seismograph\ at\ S1\ or\ S2}{Average\ Deflection\ measured\ by\ FWD\ at\ D1} \quad (26)$$

The rocking ratio values range from a low of about 7% for test site 11-CT14, which had unusually large downward warping and thinner longer slabs, to a high of about 25% for test site 1-AC18(22) tested during winter, which had short thick slabs and worn/open joints.

TABLE 3.2. SLAB ROTATION TEST RESULTS

Site	Date	Average Deflection by FWD at D1 (mils)*	Average Deflection by Seismograph at S1 (mils)	Average Deflection by Seismograph at S2 (mils)	Rocking Ratio S1/D1	Rocking Ratio S2/D1
1-AC18(22)	12/15/09	3.47	0.84	0.86	0.24	0.25
1-AC18(22)	7/20/10	3.87	0.75	0.83	0.19	0.22
2-AC17	9/28/09	6.54	0.55	-	0.08	-
3-CT16	6/1/10	9.41	1.36	1.27	0.14	0.14
4-AC18	12/14/09	6.63	0.68	0.68	0.10	0.10
4-AC18	7/21/10	7.60	0.67	0.65	0.09	0.09
7-AGG17	12/7/10	7.85	0.70	0.68	0.09	0.09
8-AGG15	12/11/09	10.53	1.96	1.89	0.19	0.18
10-AGG14	8/25/10	10.66	1.43	1.38	0.13	0.13
11-CT14	12/10/09	9.63	0.65	0.66	0.07	0.07

*Deflection measured was during the approximate 45 kip drop with exception to 3-CT16 which was measured during a 60 kip drop.

3.7. DISTRESS SURVEY AND CONDITION RATING

While on site, a visual condition survey was performed to document the distress types, locations, and severity throughout the test area. The major distress observed, if present, is indicated on the test pattern maps included in Appendix A. Using the distress maps and photographs, the distress was coded per the USACE Concrete Surfaced Airfields PCI Field Manual. The collected data was then imported into the PAVER software and the PCI and SCI was estimated. The estimated PCI and SCI values are indicated on the test site summary sheets and summarized in table 3.3.

TABLE 3.3. TEST SITE VISUAL CONDITION SUMMARY

Test Site	Est. Construction Date	Est. PCI	Est. SCI
1-AC18(22)	2000	97	97
2-AC17	1993	73	78
3-CT16	1997	100	100
4-AC18	2002	79	79
5-AGG18	1996	91	100
6-CT16	2001	94	94
7-AGG17	1994	78	78
8-AGG15	1998	94	95
9-AGG14	1998	92	92
10-AGG14	1991	96	98
11-CT14	1982	52	54

CHAPTER 4. SUMMARY OF OBSERVED JOINT AND SLAB BEHAVIOR

This chapter presents an overall summary of the range of joint and pavement system behaviors observed at the test sites as viewed through the on-site mechanistic behavior evaluation procedures. Appendix A of this report contains the summary database and the detailed analysis results for each test site. The data contained in the Appendix is extensive and can be used to calibrate FEM analyses attempting to simulate the observed behaviors at individual sites.

4.1 OVERALL RANGE OF JOINT STIFFNESS ENCOUNTERED

Figure 4.1 shows the overall plot of the joint stiffness versus LTE_δ data obtained for this study. Joint stiffness values higher than 250,000 lb/in/in are eliminated from view as values above this are generally from joints that are not cracked. LTE_δ values less than 30% are not shown in order to better show the general trends. It is important to understand that the LTE_δ values shown for each joint stiffness value represent the trends associated with the 5.91 inch radius FWD load plate. Different LTE_δ versus stiffness trends are expected for different load area sizes. Each site has a considerable range of LTE_δ and joint stiffness values that follow the general Skarlatos/Ioannides-like trend shape. This large range is primarily related to typical significant variations in joint opening sizes at any given site. Although this plot is far too cluttered to see any individual site well, there is a strong basic trend in this data related to pavement cross section. The thinner 8-11 inch thick slabs occupy the upper left portion of the plot while the heavy duty 17-22 inch thick slabs occupy the lower right portion of the plot. Individual plots for each test site are provided in the appendix.

This plot alone can be used as a quick guide to estimate a joint stiffness value that corresponds to an FWD LTE_δ measurement at a site. At a joint stiffness value of about 50,000 lb/in/in, an 18-22 inch thick slab was revealing an LTE_δ of about 63%, while a 9-10 inch slab has an LTE_δ of about 85%. The apparent "lock-up" joint stiffness values (at LTE_δ of about 86 to 90%) are about 100,000 and 250,000 lb/in/in for the 9-10, and 18-22 inch thick slab thickness. For this study LTE_δ calculations were performed on all mid-panel drops to estimate where the threshold of locked/uncracked LTE_δ was. The overall average mid-panel LTE_δ ranged from about 86 to 90%. Joint LTE_δ above these levels indicate "possible locked or uncracked" joint behavior. Two methods for reproducing this data set have been developed: a simplified approach for establishing the basic joint stiffness versus LTE_δ trend shape, and a more comprehensive joint behavior simulation that accounts for many factors such as joint spacing, average slab temperature, load transfer devices, and traffic. These investigations will be described later in chapter 5.

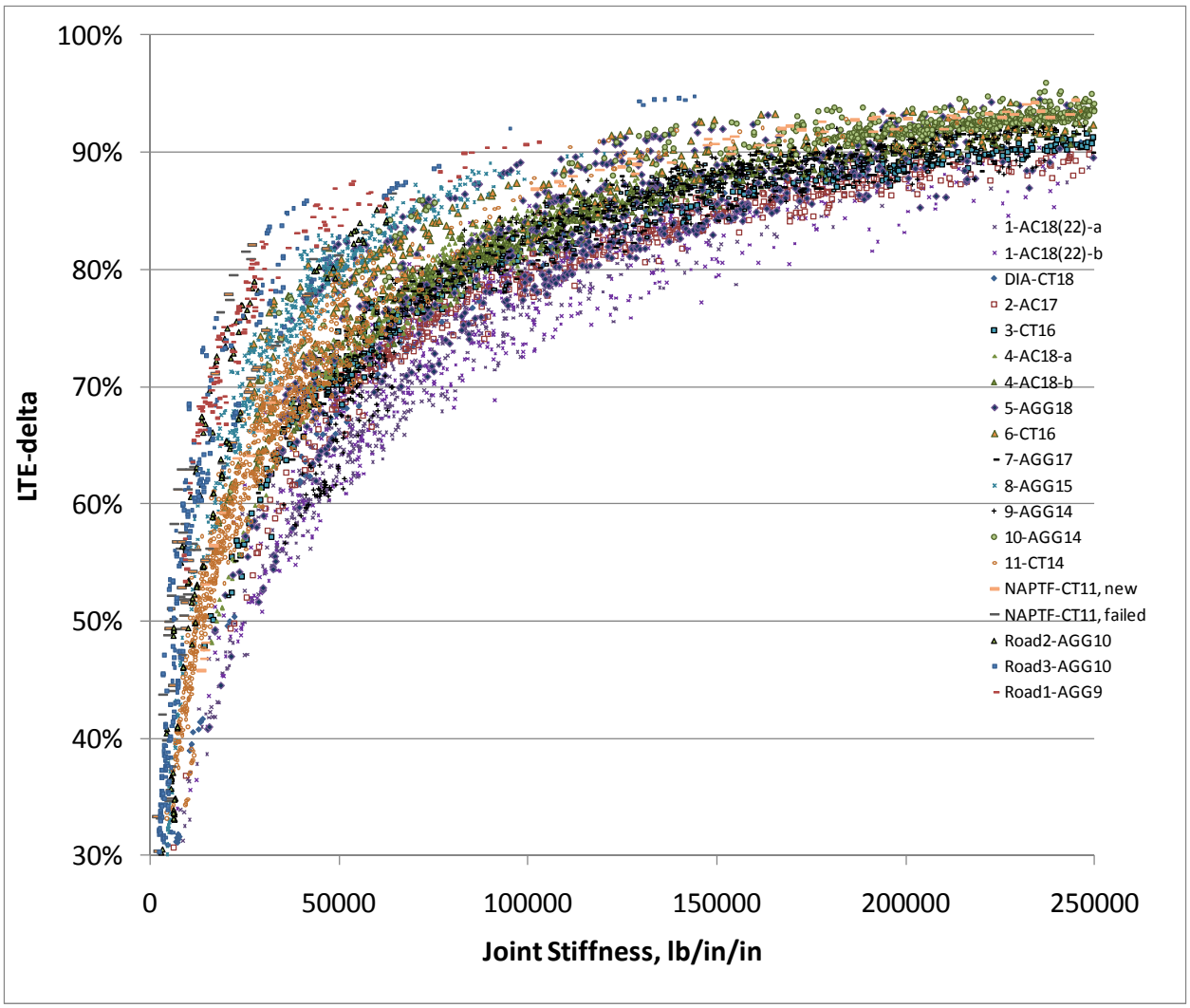

FIGURE 4.1. THE JOINT STIFFNESS DATA FROM THIS STUDY (K_J<250 KIP/IN/IN, LTE_δ > 30%, 5.91 INCH RADIUS FWD LOAD PLATE) SHOWING HOW EACH TEST SITE HAS A WIDE RANGE OF LTE_δ AND JOINT STIFFNESS, BUT FOLLOWS THE SKARLATOS/IOANNIDES-TYPE TREND SHAPE

As described in Chapter 3, best-fit Skarlatos/Ioannides-type formulae were fit to each test site. This Skarlatos-Westergaard edge solution as modified/solved by Ioannides and Hammons (1996) essentially allowed all of the test sites to be "non-dimensionalized" and presented on the same dimensionless joint stiffness characterization scheme. Figure 4.2 shows how all of the test site dimensionless joint stiffness measurements fit the Skarlatos/Ioannides solution trend shape. To obtain this plot, each joint stiffness measurement from a test site was divided by the site's single best-fit $k\ell$ cluster for the Skarlatos/Ioannides LTE_δ regression fit to the joint stiffness measurements. The observed variation around the Skarlatos/Ioannides function value is due primarily to cross section variations and slab curling variations. Actual joint behavior is very "Skarlatos-like" but one slight noticeable trend difference is related to apparent elastic solid base effects. This appears as the real measurements wanting to approach a y-intercept value above zero. Apparent base effects ranged from about 0 to 15% LTE_δ for the test sites. This is the LTE_δ

range that an FWD will probably measure when the joints are completely separated with zero joint stiffness. Although some apparent LTE_δ is measured at zero joint stiffness when elastic solid base action is present, there is no load transferred through the joint and it is free-edge loading. The Skarlatos/Ioannides solution shape is clearly a very good way of mathematically mapping the FWD-based joint stiffness values into design philosophies and approaches. The FWD joint stiffness calculation technique is not related to the Skarlatos/Ioannides solution and the joint stiffness calculations represent a completely independent check of the suitability of the Skarlatos/Ioannides solution shape in general. In this study, the Skarlatos/Ioannides solution is used more as a regression algorithm form, and as the basis of the reproduction formulae for the measured joint stiffness data. Various calibration factors are applied to the equation such that the original measurements can be reproduced using the design type information from the test sites. The Skarlatos/Ioannides solution is essentially a near-perfect regression equation form to use to simulate the FWD-based joint stiffness data. This logarithmic s-curve is otherwise a difficult shape to simulate with typical polynomials, exponentials and power functions.

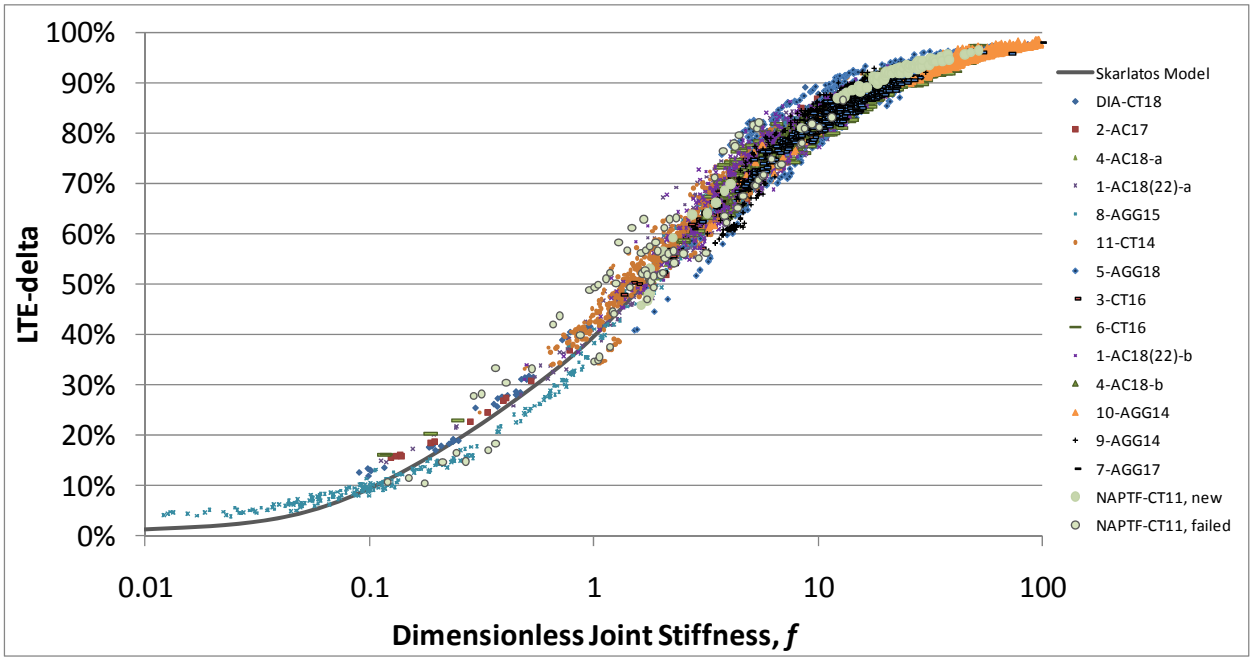

FIGURE 4.2. THE JOINT STIFFNESS MEASUREMENTS DIVIDED BY THEIR SITE BEST-FIT SKARLATOS/IOANNIDES EDGE SUPPORT $K\ell$ CLUSTER, SHOWING HOW SITES DEVIATE FROM AN OVERALL AVERAGE SITE $K\ell$ ASSUMPTION DUE TO CROSS SECTION VARIABILITY, CURLING EFFECTS, AND LOSS OF EDGE SUPPORT

Figure 4.3 provides the summary of the average joint response length, L_R, values from the test sites. The response length value can be used with the joint dowel/tie bar spacing and type information for a refined estimate of dowel bearing stresses and shear forces. Thinner slabs and pavements with loss of support at edges had shorter response lengths in the 100-120 inch range. This implies that for a 20-ft by 20-ft panel, slab edge deflections were just reaching a zero value near the mid-slab position or slab corners when assuming a radial symmetric deformation pattern

around the edge load. Response length values for the thicker slabs were between 140 and 200 inches. These longer values imply that edge loading on a 20-ft by 20-ft panel would cause slab edge deformation to extend beyond the slab corners and into adjacent slabs and joints. So for thinner 20-ft by 20-ft slabs, edge loading response appears to be almost confined to two-slabs and one joint, where as for the thicker 20-ft by 20-ft slabs, edge loading will have a larger area response, extending into several adjacent slabs and joints.

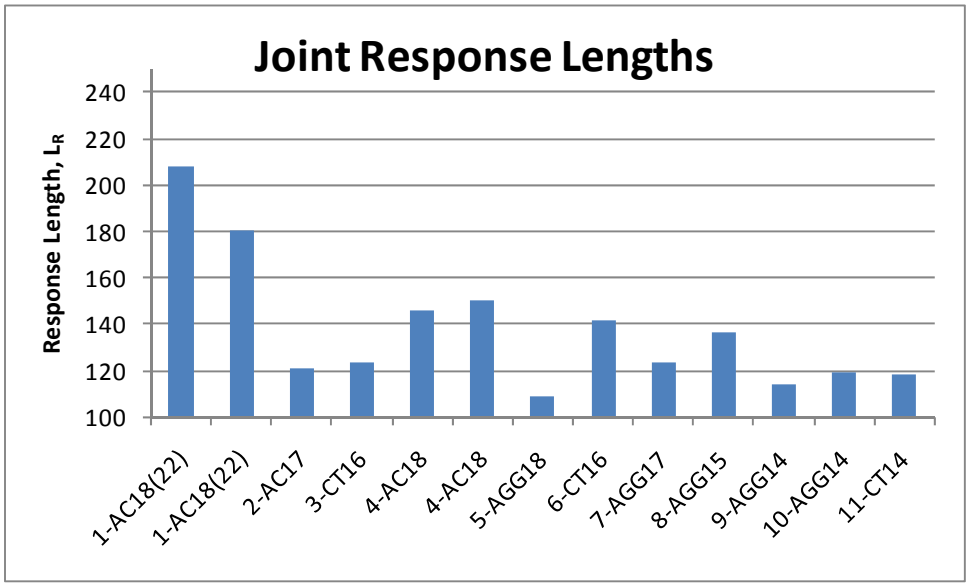

FIGURE 4.3. SUMMARY OF THE AVERAGE CHARACTERISTIC JOINT RESPONSE LENGTH, L_R, VALUES FROM THE TEST SITES

4.2 ANALYSIS OF CURLING AND WARPING CURVATURES AT TEST SITES

Figure 4.4 shows slab curvature data from the full airfield test sites superimposed with the overall site average slab curvature estimates from the FHWA LTPP GPS3 right wheel path profiles from 500-ft long jointed concrete pavement highway test sites. With the exception of test site 11-CT14, the airfield test sites fall within the more typical range and on the same general trend as those measured from highway data (Byrum, 2000; Byrum, 2009). The thin black solid line is the best-fit trend line to the entire FHWA LTPP GPS3 slab curvature data set considered as one test site. Over North America, the average GPS3 highway slab experienced about 0.00008 ft^{-1} curvature change from about 7 AM to 1 PM. This is slightly less than the curling experienced at site 05-AGG18 described in detail in chapter 3.

Figure 4.5 shows the site average slab curvature change from curling for the test sites. The overall average measured slab curvature change from the heavy duty airfield site visits was about 0.000035 ft^{-1} for this cluster of airfield pavements, less than half of that for the average highway slab. A few highway test sites were warped downwards (joints down) as much as site 11-CT14, but this test site can be considered down-warped in an unusual way. It is safe to say that on average, and similar to highway slabs, the airfield test sites have a slight locked in up-warp, where the slab curvature in the afternoon when slabs are warmer on top than bottom, is closer to "flat" and not actually curled downward. The typical curling curvature from thermal gradients

present in the afternoon is about the same magnitude, but in the opposite direction as the locked in up-warp magnitude that is typical in slabs. Yet, large variation in warp can exist. Based on past experience, slab curvature values less than about ± 0.00025 ft^{-1} are generally not visible to the eye. But slab curvature larger than this starts to become visible and can be easily displayed with a tight string-line stretched from corner to corner across a slab for the up-warped shape. For example site 2-AC17 had significant measured average up-warp, and had one full paving lane where every slab was visibly up-warped and snow plows were obviously hitting the corners of the slabs and dragging along slab edges and deep saw-cut tines texture causing abrasion and low severity spalling debris. This site having relatively large up-warp matched observations in the FHWA LTPP data that most cases of large locked-in warp were encountered on clayey subgrades and were attributed to the subgrade compliance effect and accumulation of curvature creep. Site 2-AC17 was constructed on wet clayey subgrade with relatively high groundwater levels probably within 5-10 feet of the bottom of the slabs, the apparent ideal conditions to develop some slab warp. Site 2-AC17-b shows somewhat of an atypical slab curvature trend. Prior to this site visit heavy rains occurred with humidity staying high until just after the start of testing. During testing, an extreme dry front moved over the site dropping the relative humidity from about 100% down to a low 45% with high winds. It appears that the slab surface drying related to this rather extreme windy dry air mass caused progressive and relatively rapid up-warp to occur, which was apparently stronger than the expected down-curl tendency from increasing air temperature. The detailed climate data for this site is included in Appendix A. The site with the highest measured curling was site 10-AGG14, which was cut into short 12.5-ft by 12.5-ft panels and these short panels easily curl more (i.e. curvature change), while having lower edge curling deflections and residual curling stress levels.

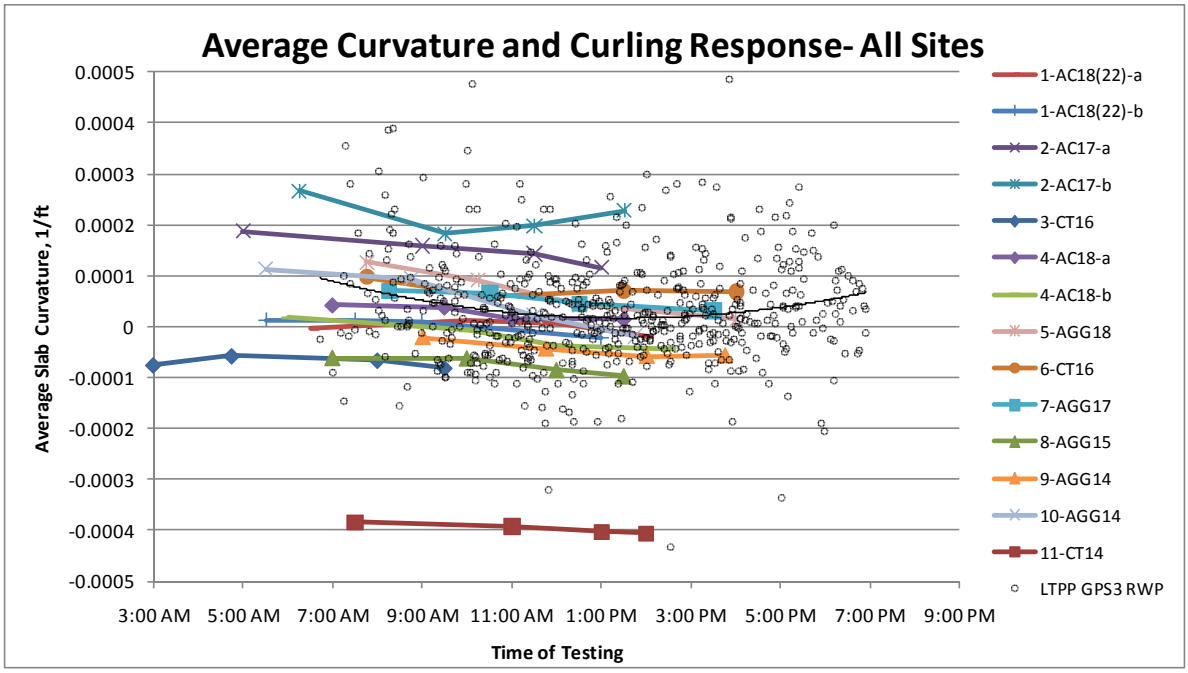

FIGURE 4.4. THE MEASURED SLAB CURVATURE TRENDS FOR THE FULL TEST SITES AS COMPARED THE RIGHT WHEEL PATH CURVATURE MEASUREMENTS FROM THE FHWA LTPP GPS3 HIGHWAY PAVEMENT TEST SITES

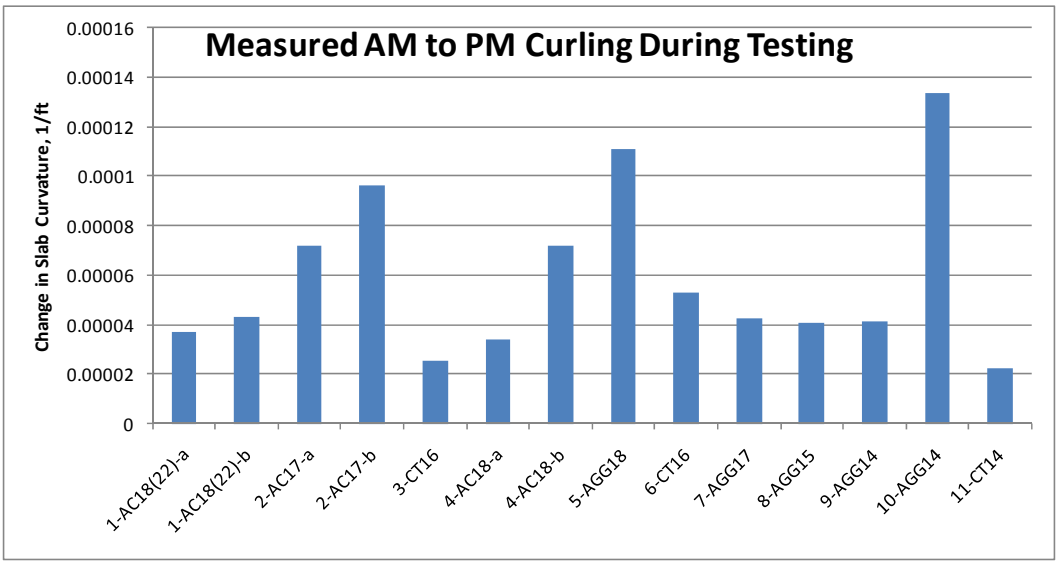

FIGURE 4.5. THE SITE AVERAGE CHANGE IN SLAB CURVATURE FROM CURLING MEASURED USING SLAB END SLOPE MEASUREMENTS

4.3. COMPARSION OF MID-PANEL AND EDGE SUBGRADE SUPPORT VALUES

The new joint stiffness calculation procedure has allowed the Skarlatos/Ioannides joint solution to be used to backcalculate an apparent slab edge subgrade *k*-value using the same basic Westergaard type slab and foundation idealization as the ILLI-BACK procedure uses for mid-panel backcalculation procedures. This allows a direct comparison of slab edge versus mid-panel support at a test site using the Westergaard basis. Figure 4.6 shows the summary results for the backcalculated subgrade *k*-values and slab support ratio values for the test sites. In general, the slab support ratio values average between about 0.4 and 0.5 for most sites. Two values near 0.9 were encountered, sites 9-AGG14 and 11-CT14. Site 9-AGG14 was tested during below freezing conditions and required snow removal in order to test. This site was probably in a frozen joint and foundation condition during testing. Site 11-CT14 was found to have extreme down-warp in panels and was also tested in freezing conditions. Site 5-AGG18 had locked-in up-warp and an apparent large sensitivity to curling. This site had the lowest average slab support ratio near 0.3. The values shown are the average values for the sites. Sites with curling-compliant subgrades have just a slight change in slab support ratio during the day, while sites with non-compliant foundations can experience large variation in apparent slab support ratio during a daily curling cycle.

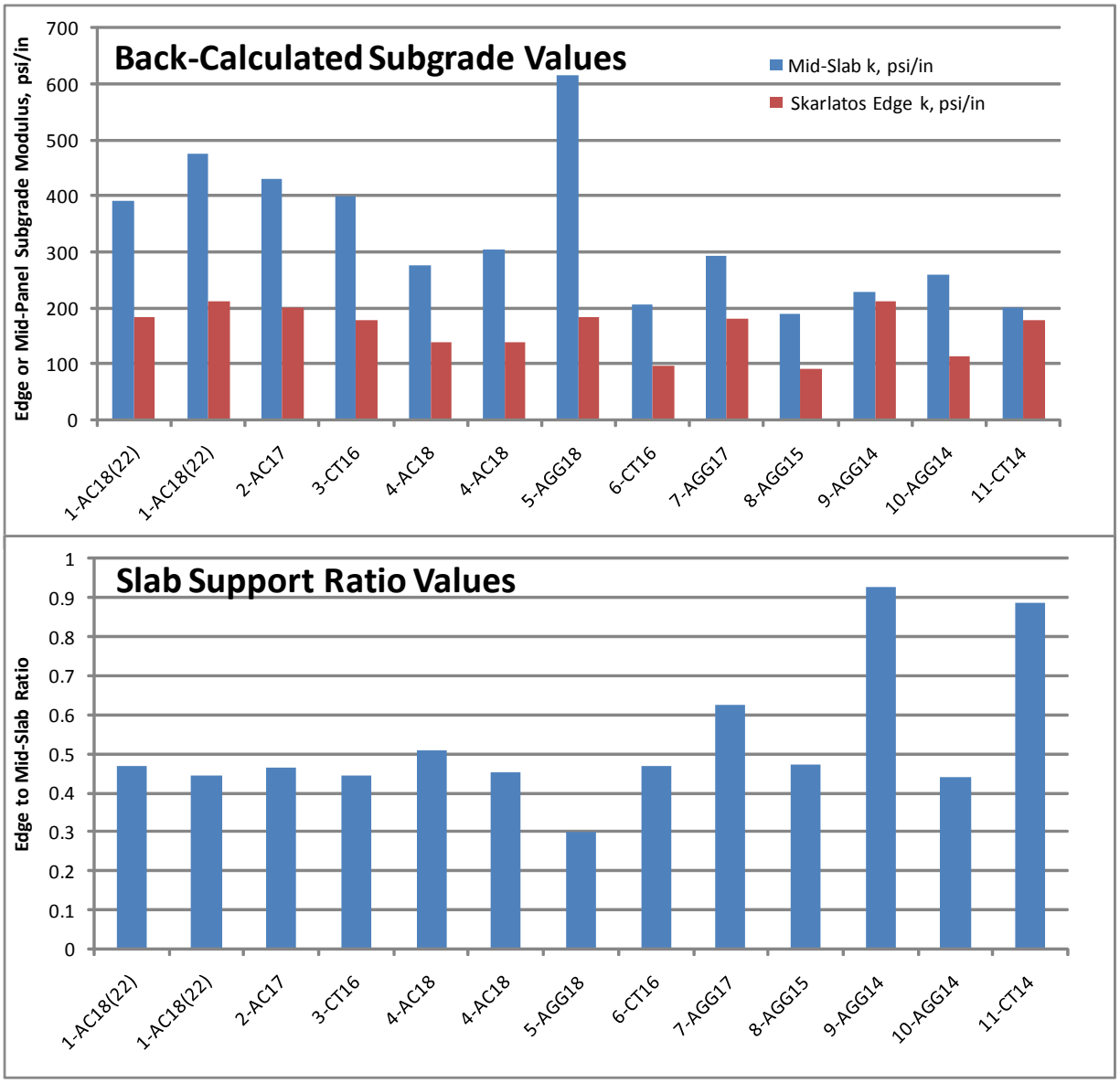

FIGURE 4.6. SUMMARY OF BACKCALCULATED MID-PANEL AND SLAB EDGE MODULUS OF SUBGRADE REACTION VALUES AND THE SITE SLAB SUPPORT RATIO VALUES

Figure 4.7 compares slab support ratio values to another slab support index: the ratio of the estimated free edge deflection to the mid-panel deflection. The approximate free edge deflection is calculated as the sum of the loaded and unloaded slab edge deflections. If one were to calculate this ratio for structurally continuous mid-panel load test data, the slab support ratio would be greater than 1.0, while the free-edge to mid-panel deflection ratio would be right at 2.0. Site 9-AGG14 is right near this condition and was estimated to be frozen when tested. The joint load test data in most cases appeared no different than the mid-panel load test data from this test site. Test site 9-AGG14 can be considered "frozen or uncracked". Site 8-AGG15 had an unusual foundation system and had larger edge deflections relative to mid-panel. This test site was in a de-icing pad area and the foundation consisted of an upper porous stone collection

system overlying a cement treated layer. It is judged that frequent applications of de-icing fluids may have enhanced base damage and loss of support for this test site. Loading rates are slow to static in this area. Large slab edge air gaps related to loss of support at joints have developed. Site 5-AGG18 also had a high edge deflection relative to mid-slab and this site was in the dry desert and also had apparent large slab edge gaps and loss of support. So, for real pavements, the free-edge to mid-slab deflection ratio from FWD testing should range from about 2 for an uncracked new condition, to near 4 for large loss of support conditions.

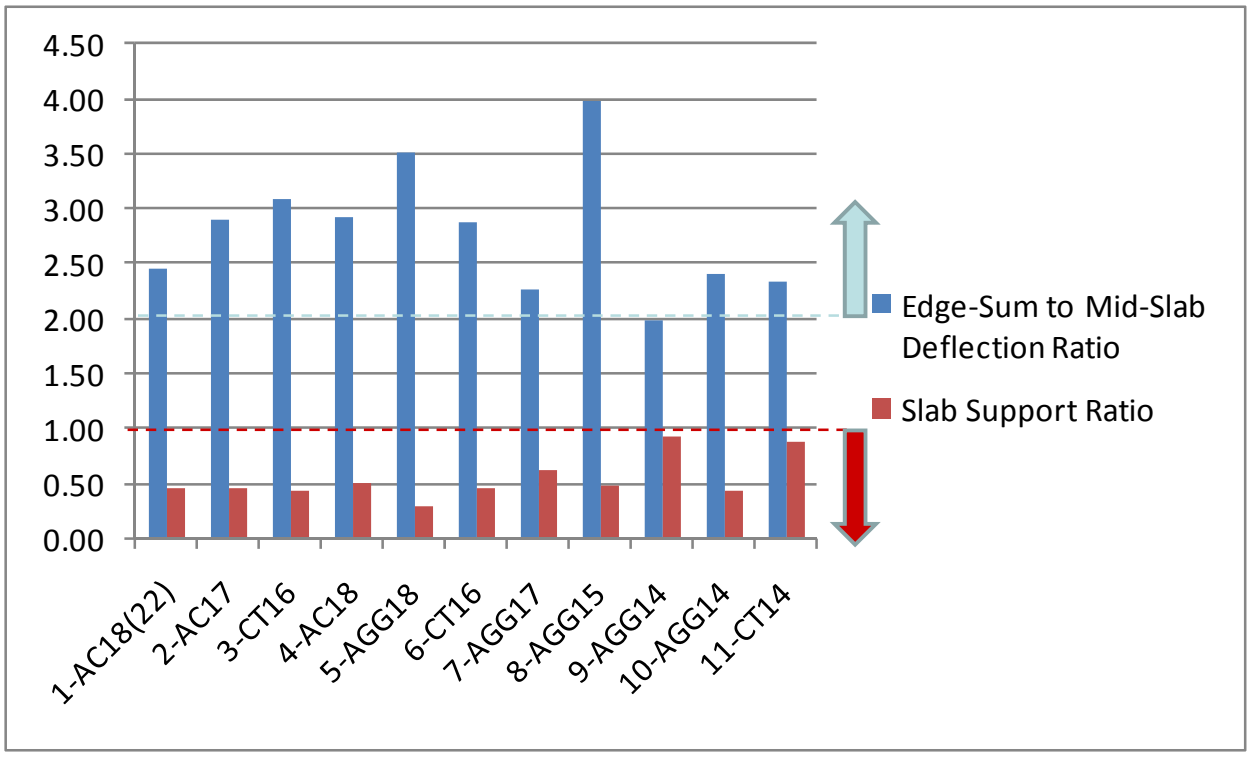

FIGURE 4.7. COMPARISON OF TWO SLAB EDGE LOSS OF SUPPORT INDEX VALUES FOR THE TEST SITES, WHERE SLAB SUPPORT RATIO = 1, AND EDGE-SUM TO MID-SLAB RATIO = 2 INDICATES LOCKED/UNCRACKED CONDITIONS

Figure 4.8 provides a summary of the test site average backcalculated PCC elastic modulus values from ILLI-BACK established using the design slab thickness as the basis of calculations. When using the design slab thickness, the backcalculated elastic modulus can give an indication of the in-place thickness and an indication of possible slab to base bonding and composite bending. If a backcalculated elastic modulus is unusually high, either slab thickness is higher than assumed, or there is significant interaction and bonding of the base to the slab making the slab appear thicker than it is. Test site 1-AC18(22) had a design thickness of 18 inches but ILLI-BACK analyses indicate the slab is probably significantly thicker than 18 inches, probably closer to 22 inches in thickness. Test sites 3-CT16 and 6-CT16 are situated in the desert southwest and it is doubtful that such high modulus concrete, as shown, was used in this climate region. It is believed that there was significant composite action with cement treated base for mid-panel FWD tests at these sites. Sites 5-AGG18 and 10-AGG14 are also in the mild southwest climate and had a lower backcalculated concrete elastic modulus, more typical of concretes used in non-

freeze mild to hot climates. Typically, the higher elastic modulus concrete mixtures are found in deep freeze regions, or in wetter climate areas not subject to warp and where good aggregates are readily available.

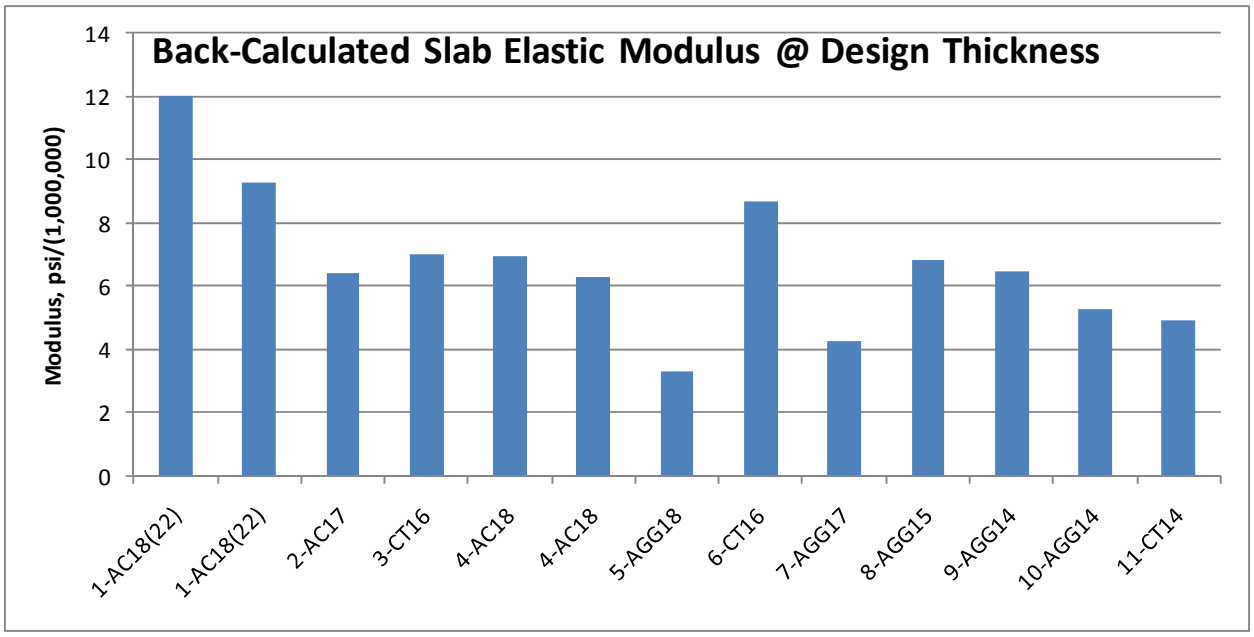

FIGURE 4.8. THE ILLI-BACK CONCRETE SLAB ELASTIC MODULUS VALUES FROM THE TEST SITES OBTAINED WHEN USING THE DESIGN PLANS PCC THICKNESS VALUES

4.4 SEASONAL AND DAILY VARIATIONS IN LOAD TRANSFER

Data from the Denver International Airport instrumented test site provides a basis for thorough understanding of seasonal variation of joint behavior. Joints at DIA were tested over a wide range of temperatures during the year and can be compared to extensive embedded instrumentation that was installed. Figure 4.9 shows LTE_δ versus slab surface temperature for a few select joints from DIA and key joint performance parameters used for the remainder of this research report. Aggregate interlock joints tend to follow a generally linear trend for LTE_δ versus temperature. A given test site will have its own unique average aggregate interlock slope $d(LTE_\delta)/dT$, which is a function primarily of slab length, concrete thermal coefficient, and subgrade drag effects. At DIA, the apparent values of the LTE_δ derivative with respect to temperature range from about 0.9 to 1.3 loss in LTE_δ percentage per drop in average slab temperature in degrees Fahrenheit. There is an apparent joint lock-up temperature, T_{Lock}, and an apparent joint release temperature, $T_{Release}$, for aggregate interlock joints. The doweled joints, which are also designed to open and close, are essentially undergoing the same amount of joint opening as aggregate interlock (dummy) joints, but the steel reinforcement keeps LTE_δ high, through the dowel-concrete interaction. The tied joints at DIA, designed to remain nearly closed at all times essentially remained closed and retained nearly full aggregate interlock magnitude over all temperatures. Figure 4.10 shows DIA data from Rufino et al. (2004) with some additional definitions and commentary added. This plot shows the measured joint opening changes that corresponded to the changes in LTE_δ shown in figure 4.9. This data allows a

relatively precise estimate of the derivative of joint opening size with respect to temperature for DIA, dO/dT, of about 1 mil per degree Fahrenheit. Dividing the $d(LTE_\delta)/dT$ derivative by the joint opening derivative dO/dT reveals the apparent loss of LTE_δ rates with respect to joint opening size, $d(LTE_\delta)/dO$ of about 0.9 to 1.3% LTE_δ loss per 1 mil joint opening increase for DIA aggregate interlock joints. This $d(LTE_\delta)/dO$ is a fundamental property of the joint aggregate interlock face roughness and durability. More rough faces with strong aggregates will have lower loss rates. Smooth faces like construction joints will have more rapid or even sudden loss. The Michigan Road Test joint opening size model, established using over seventeen years of joint opening measurements on slabs lengths ranging from 12 to 100 feet, reproduces very well the DIA joint opening behavior. This model can be turned into one unique function for dO/dT as a function of slab length (Finney and Oehler, 1958). Later in this report, this linear $d(LTE_\delta)/dT$ concept is combined with the Michigan Road Test joint opening size model for $d(LTE_\delta)/dO$, the calibrated Skarlatos/Ioannides joint stiffness curves, and the FAA doweled joint stiffness equation to develop a comprehensive joint behavior simulation methodology. This methodology can determine joint stiffness as a function of slab temperature for a given pavement design scenario. The input to the joint behavior model consists of typical design parameters and the output consists of the temperature related variation in joint stiffness and LTE_δ at the site for doweled and aggregate interlock contraction joints. The output from the joint model can then be used as input to FEM discretizations in order to evaluate load transfer effects. The joint stiffness prediction methodology is presented in Chapter 5 of this report.

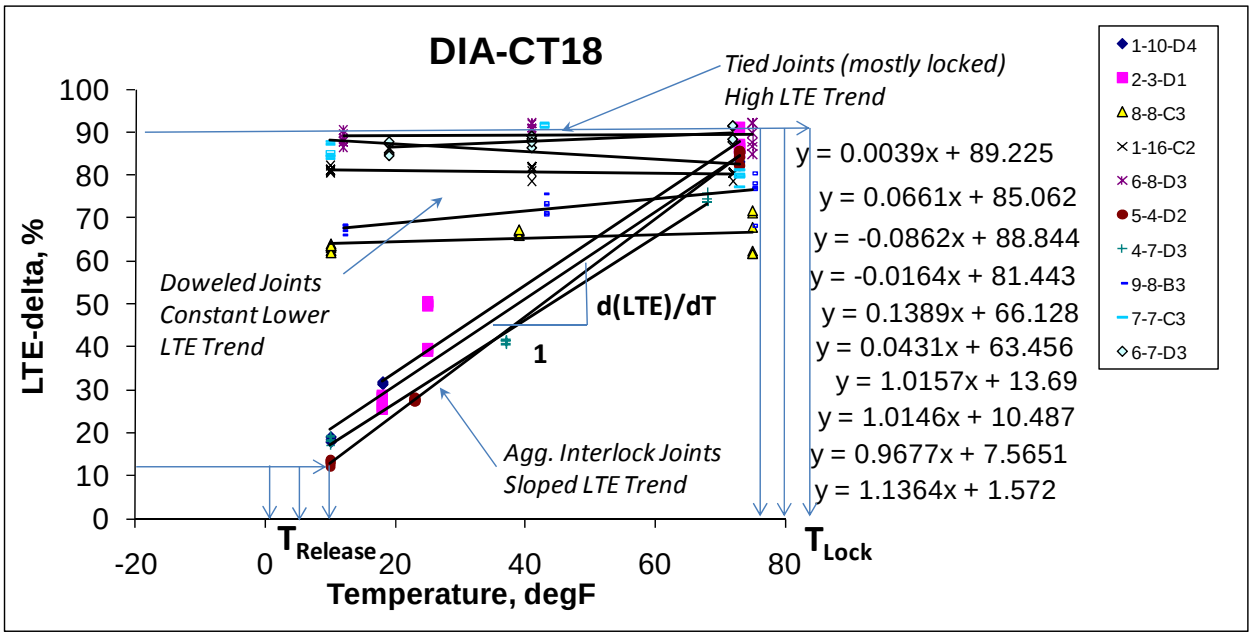

FIGURE 4.9. JOINT LOAD TEST DATA FROM DIA SHOWING THE KEY VARIABLES DEFINING AGGREGATE INTERLOCK BEHAVIOR AT A SITE; T_{Lock}, $T_{Release}$, AND $d(LTE_\delta)/dT$

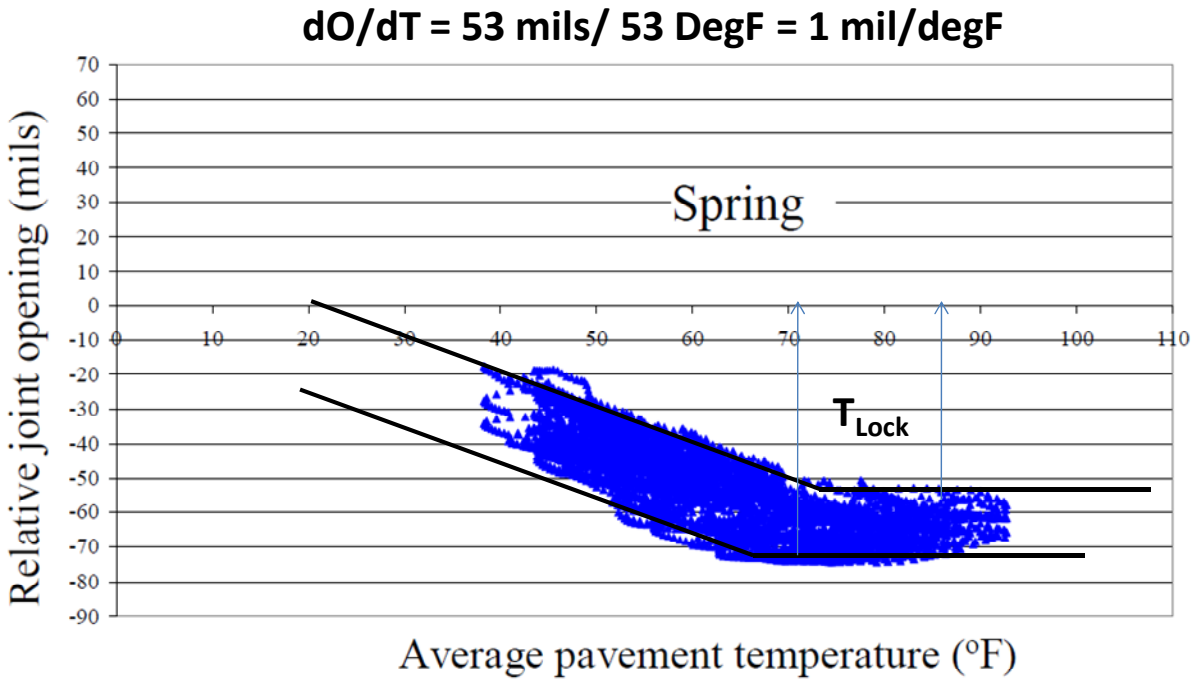

FIGURE 4.10. DATA FROM RUFINO ET AL. 2004, WITH ADDITIONAL COMMENTARY SHOWING THE APPARENT *d*O/*d*T AND THE RANGE OF PROBABLE JOINT LOCK-UP TEMPERATURES FOR THE DIA DUMMY JOINTS

The annual variations in joint behavior at DIA are as described in figures 4.9 and 4.10, while the overall pavement system response follows a very tight joint stiffness versus LTE_{δ} structural behavior trend as shown in figure 4.11. The changes in LTE_{δ} during the year simply cause the data points to move back and forth on the same general cross-section behavior trend line for LTE_{δ} versus joint stiffness. Sites with compliant foundations will have a uniform LTE_{δ} versus joint stiffness trend, while non-compliant foundation sites will have variations in the LTE_{δ} versus stiffness data trends related to curling loss of support at edges. Sites with more variable thickness and foundation support will also have greater variability in the measured joint stiffness data.

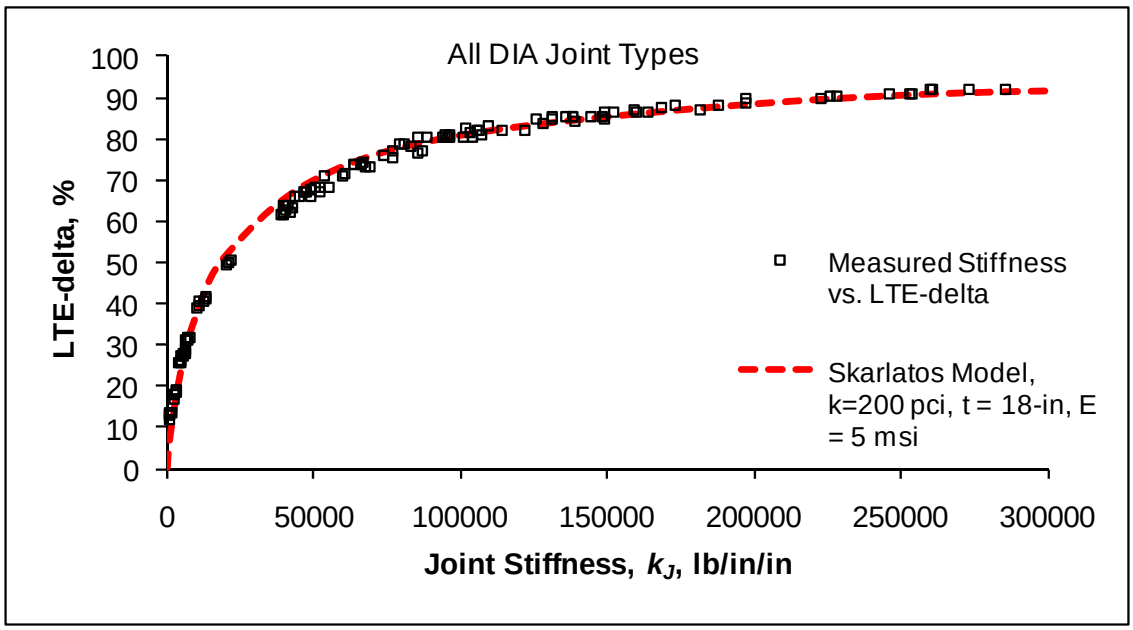

FIGURE 4.11. OVERALL DIA CHARACTERISTIC JOINT STIFFNESS RESPONSE TREND FOR THE DATA SHOWN IN FIGURE 4.9

Figures 4.12-4.14 show some examples of data from highway sites showing $d(\text{LTE}_\delta)/dT$ and dO/dT obtained from aggregate interlock joints. Test site 16-3023 showed about 60% LTE_δ change over a temperature change of about 18 degrees, or just over 3 LTE_δ percentage point loss per °F. Test site 48-4142 reveals a dO/dT value of 0.0359 mm/°C, which equals about 0.78 mils/°F, about 80% of the DIA rate. The plot for Site 53-3019 shows how joint stiffness and LTE_δ can vary for two aggregate interlock joints in good condition. LTE_δ ranged from about 20-50% during mid-morning tests, and about 55 to 85% during the afternoon tests, with the differences in the two joints being differences in joint opening sizes.

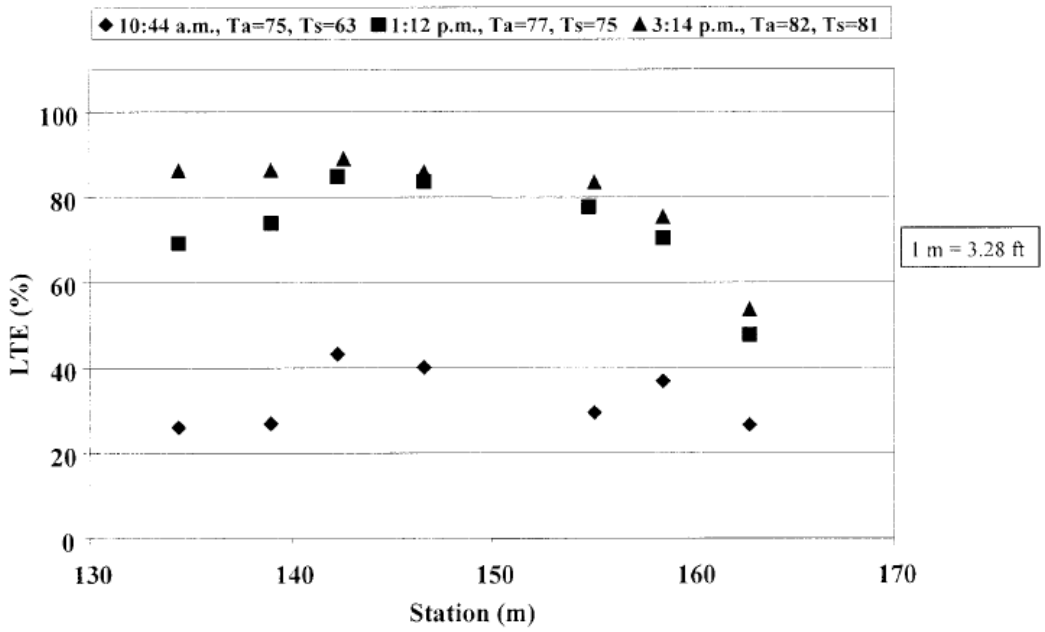

Figure 57. Daily variation in calculated leave LTE, section 163023 (October 1992).

FIGURE 4.12. DATA FROM LTPP SITE 16-3203 SHOWING HOW TEMPERATURE AFFECTS LTE_{δ} FOR AGGREGATE INTERLOCK JOINTS (KHAZANOVICH AND GOTLIF, 2003)

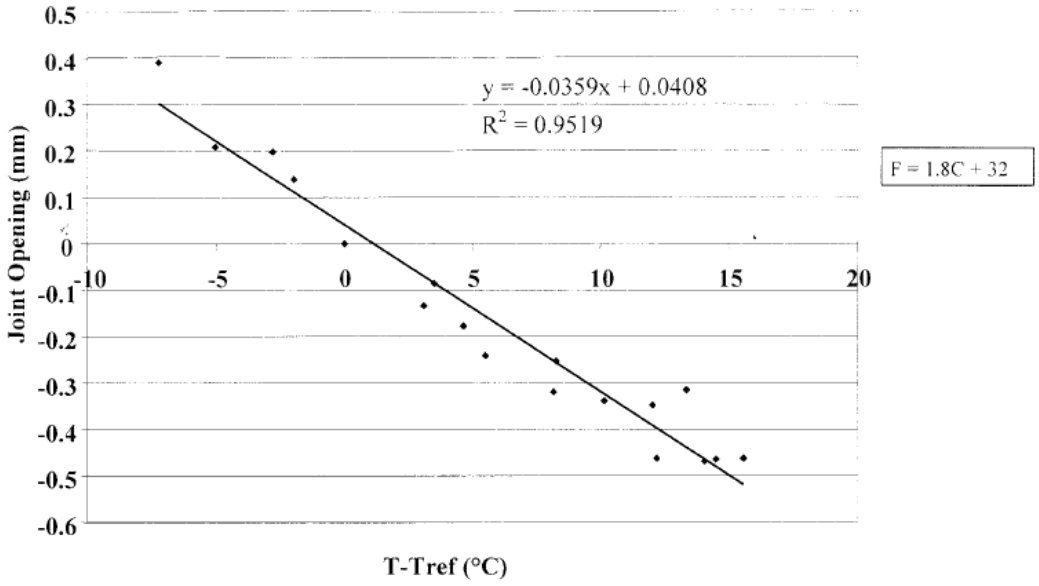

Figure 86. Change in joint opening versus change in PCC temperature, section 484142.

FIGURE 4.13. DATA FROM LTPP TEST SITE 48-4142 SHOWING HOW JOINT OPENING IS TYPICALLY A LINEAR FUNCTION OF AVERAGE SLAB TEMPERATURE (KHAZANOVICH AND GOTLIF, 2003)

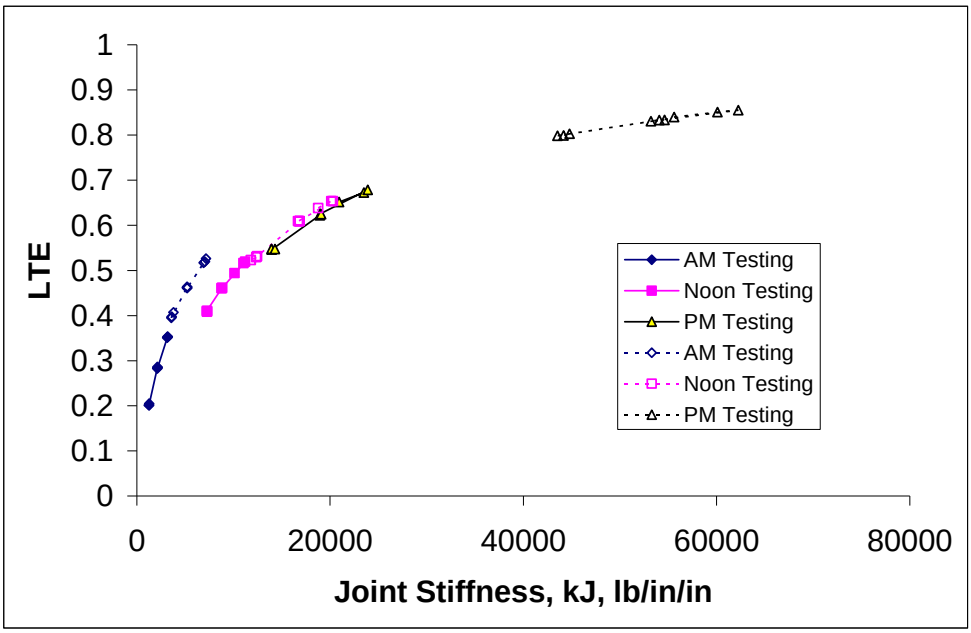

FIGURE 4.14. DATA FROM TEST SITE ROAD-AGG10 (LTPP SITE 53-3019) SHOWING HOW COMBINED SLAB CURLING AND JOINT OPENING CHANGES AFFECT LTE_{δ} AND JOINT STIFFNESS FOR AGGREGATE INTERLOCK JOINTS (JOINT A = SOLID LINES, JOINT B = DASHED LINES)

Figure 4.15 demonstrates the largest daily variation in pavement system behavior encountered at an airfield test site. Figure 4.16 shows the slab curvature variation associated with the joint behavior variations in figure 4.15. As discussed in Chapter 3, this site experienced over 50 °F temperature variation during testing and Westergaard curling backcalculation analysis revealed that about a 2.5 °F/inch gradient change at this site would explain the amount of curvature variation measured. The looser joints had LTE_{δ} near 40% in the mid-morning and increasing to near 65% in mid afternoon. Joint stiffness values for these looser joints were about 20,000 and 50,000 for the morning and afternoon testing, respectively. An interesting observation in this plot is that some joints experience a relatively constant or slightly decreasing LTE_{δ}, while at the same time experiencing increasing joint stiffness, from morning to afternoon. This is because for the same joint deflection difference magnitude (which controls load transfer), a soft subgrade (higher overall edge deflections) reveals higher LTE_{δ} than a hard subgrade (lower overall deflections). This is because a given slab edge deflection difference size is a smaller fraction of total displacements for the soft subgrade. This data indicates the slabs were still contracting during Round 2 testing (decreasing joint stiffness), but that the slabs were slightly flatter during Round 2 testing. There is a cluster of data points visible on the left of the plot that has LTE_{δ} values of about 80, 70, and then 78%, while joint stiffness values went from about 55,000, to 45,000, and then to 110,000 during the three Rounds respectively. The high morning LTE_{δ} was due to large slab upward warp and higher overall edge deflections and low apparent edge support. This site showed enough curling variation to where it was decided to fit three Skarlatos/Ioannides curves to the data: one for each Round of FWD testing. Figure 4.17 shows

the back calculated modulus of subgrade reaction values for the three Rounds of testing for mid-panel and slab edge. Slab edge support had changed significantly from morning to afternoon, and some of the mid-slab areas had clearly lifted off the foundation somewhat during afternoon testing.

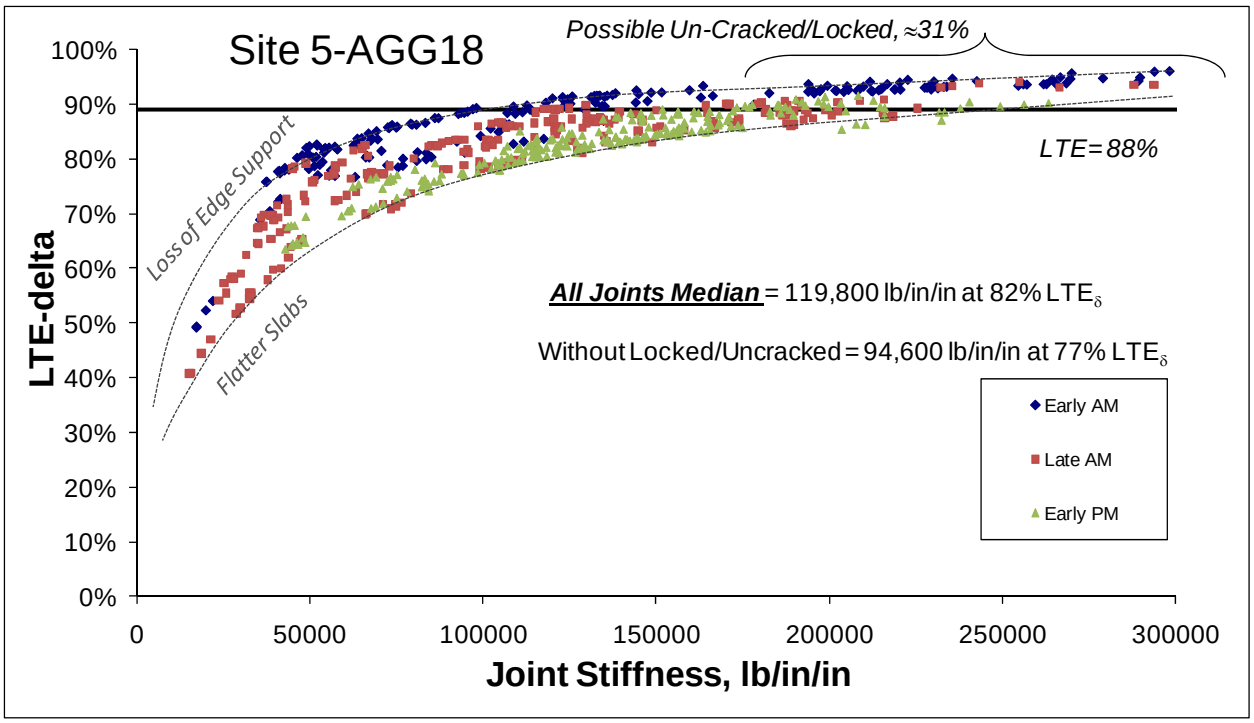

FIGURE 4.15. THE LARGEST CURLING RELATED JOINT STIFFNESS BEHAVIOR CHANGES ENCOUNTERED FOR A HEAVY DUTY AIRFIELD

	500-ft Highway GPS3 55-3009	*Site 5-AGG18* ≈ 8AM average	AM-PM Change
average curvature, 1/ft	0.000547	0.000126	0.000111
min. curvature	0.000203	-0.000362	0.000089
max. curvature	0.001077	0.000555	0.000124
st. dev. of curvature	0.00021	0.000287	0.000012
number of slabs	33	7	7

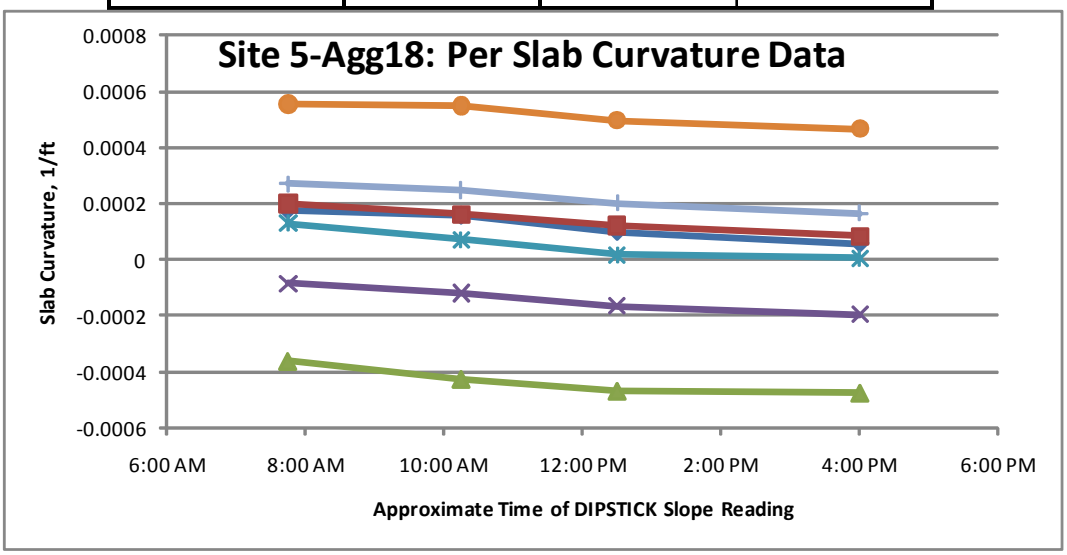

FIGURE 4.16. SLAB CURLING CURVATURE CHANGE MEASUREMENTS THAT ARE DIRECTLY RELATED TO THE JOINT BEHAVIOR CHANGES SHOWN IN FIGURE 4.15

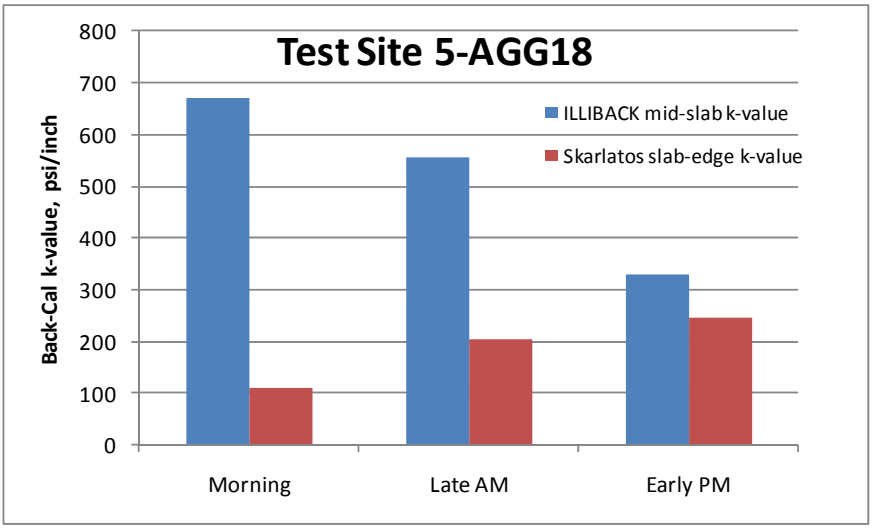

FIGURE 4.17. SKARLATOS/IOANNIDES-EDGE AND ILLI-BACK BACKCALCULATED MODULUS OF SUBGRADE REACTIONS VALUES FOR THE THREE ROUNDS OF FWD TESTING SHOWN IN FIGURE 4.15

Figure 4.18 shows the joint data from test site 5-AGG18 further broken down to individual joint types and by Round of testing to evaluate time of day effects on joint load test response. This

test site is in a heavy duty runway landing zone area. The transverse doweled joints are saw-cut joints and are confined from both directions by hundreds of feet of additional concrete panels. The runway is only 6 panels wide so the longitudinal joints are not nearly as "confined" as the transverse joints. The longitudinal joints have a flat smooth construction joint face and it appears that this face began to lock-up during the Round 3 testing, but during Round 1 and Round 2, this face may have been disengaged, with all observed joint stiffness possibly being mobilized through the dowels. The transverse saw-cut joints with dowels appear to have had some mobilization of aggregate interlock in the morning, with increasing aggregate interlock as the temperatures rose. The slab corner tests showed the most sensitivity to time of day as the thermal expansion and contraction is occurring in two dimensions at the corners and is magnified. During the Round 3 testing, the corners appeared stiffer than the construction joints.

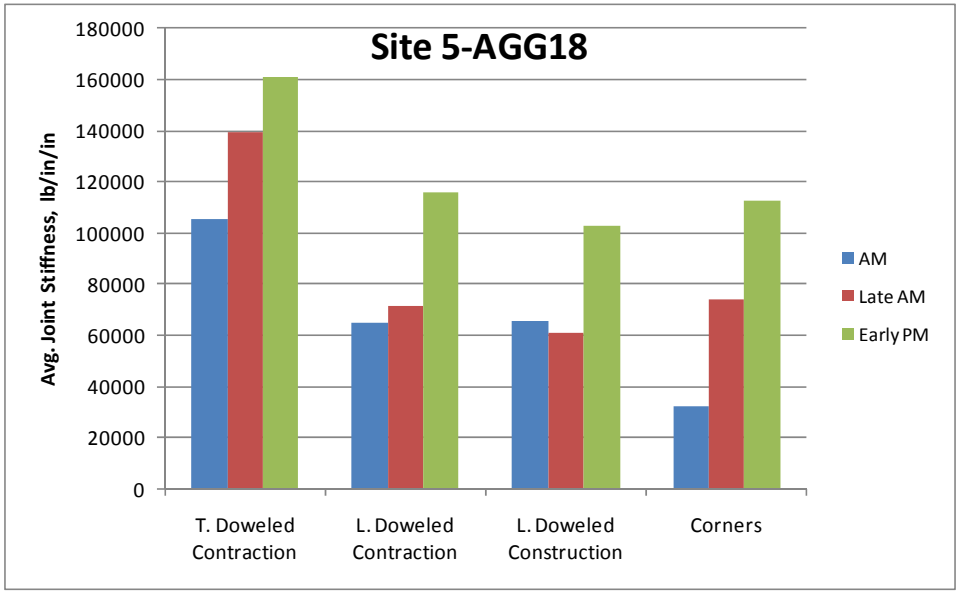

FIGURE 4.18. BEHAVIOR OF INDIVIDUAL JOINT TYPES AT SITE 5-AGG18 FOR THE THREE ROUNDS OF TESTING

Two of the full test sites were visited twice. Figures 4.19 and 4.20 show the winter and summer summary results for test site 1-AC18(22). During winter, there was a steady increase in joint stiffness during testing indicating about 25,000 lb/in/in of aggregate interlock had mobilized in addition to the stiffness level that was present during early morning testing. It is unclear as to how much of the early morning, roughly 60,000 lb/in/in joint stiffness is from dowels versus aggregate interlock. Corner stiffness remained low indicating that aggregate interlock was only just starting to mobilize, if any, at the corners. Both joint types had reached about 90,000 lb/in/in stiffness during the afternoon testing. The summer testing revealed that as a result of continued joint closure and mobilization of aggregate interlock, stiffness had risen to about 120,000 lb/in/in for the contraction joints, but had stayed at about 90,000-100,000 lb/in/in for the construction joints. This is an indication that the available aggregate interlock on the construction joint face was limited compared to that available on the saw-cut cracked face. During summer testing, the corners had enhanced thermal expansion outward in two directions, and appeared as stiff, or stiffer than the joints, whereas during winter the corners were far softer than the joints.

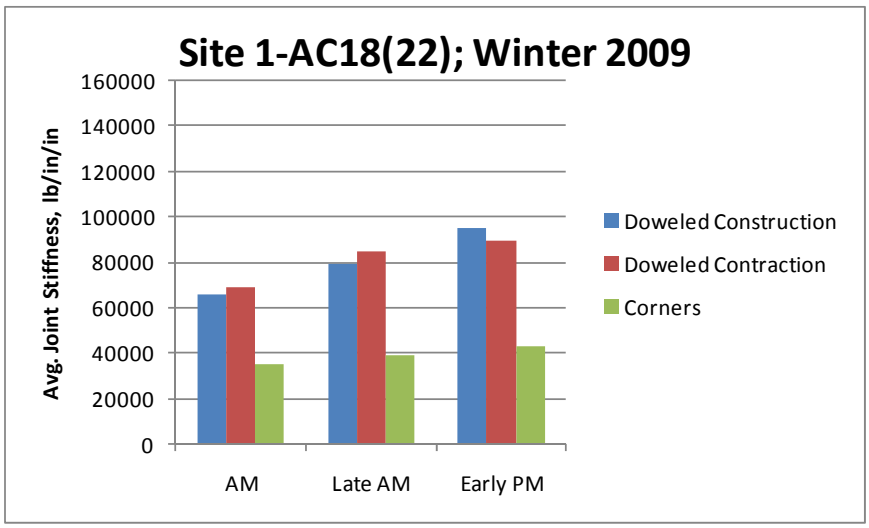

FIGURE 4.19. BREAKDOWN OF JOINT STIFFNESS BY JOINT TYPE AND ROUND OF TESTING FOR SITE 1-AC18(22) FOR WINTER OF 2009

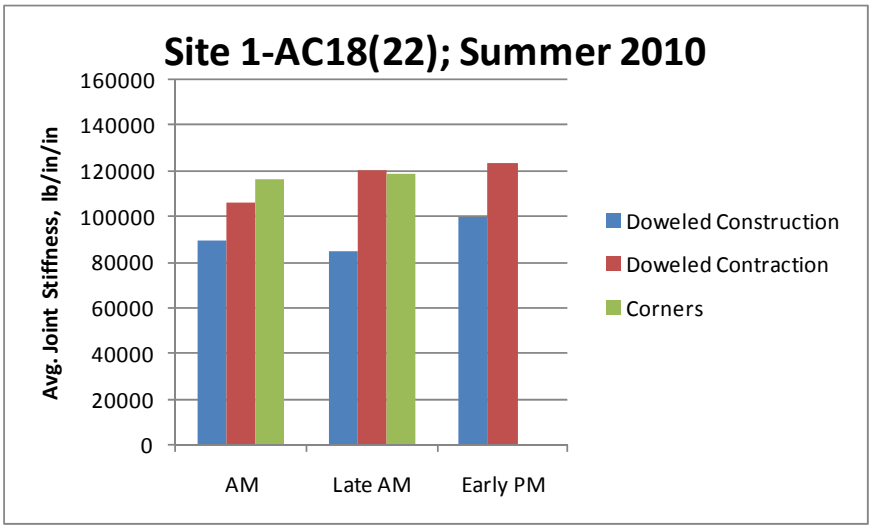

FIGURE 4.20. BREAKDOWN OF JOINT STIFFNESS BY JOINT TYPE AND ROUND OF TESTING FOR SITE 1-AC18(22) FOR SUMMER OF 2010

Figures 4.21 and 4.22 show the winter and summer testing results for site 4-AC18. During winter, the joints retained a relatively constant stiffness during testing and it is believed the joints were substantially open and the stiffness observed is almost entirely from the dowels and dowel concrete interaction. During summer testing, the corners had become just as stiff as the joints indicating full aggregate interlock stiffness mobilization, and a thermally compressed or locked condition had been reached in many cases. It appears that aggregate interlock had contributed an additional 20,000 to 40,000 lb/in/in to the doweled contraction joint stiffness, and an additional 60,000 to 80,000 lb/in/in to the doweled construction joint stiffness. The stiffness of all joints and corners were peaking near 140,000 lb/in/in joint stiffness.

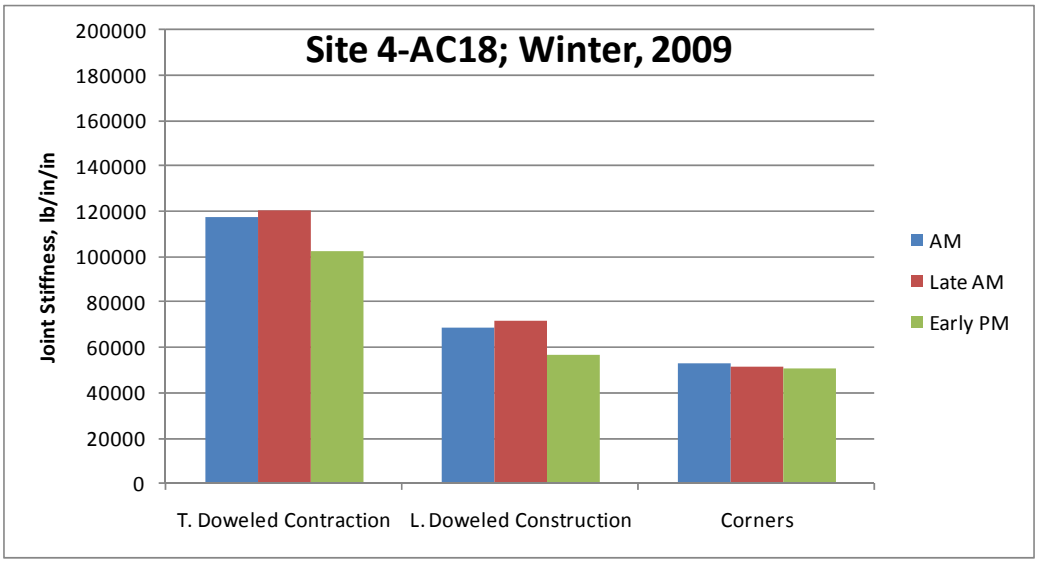

FIGURE 4.21. BREAKDOWN OF JOINT STIFFNESS BY JOINT TYPE AND ROUND OF TESTING FOR SITE 4-AC18 FOR WINTER OF 2009

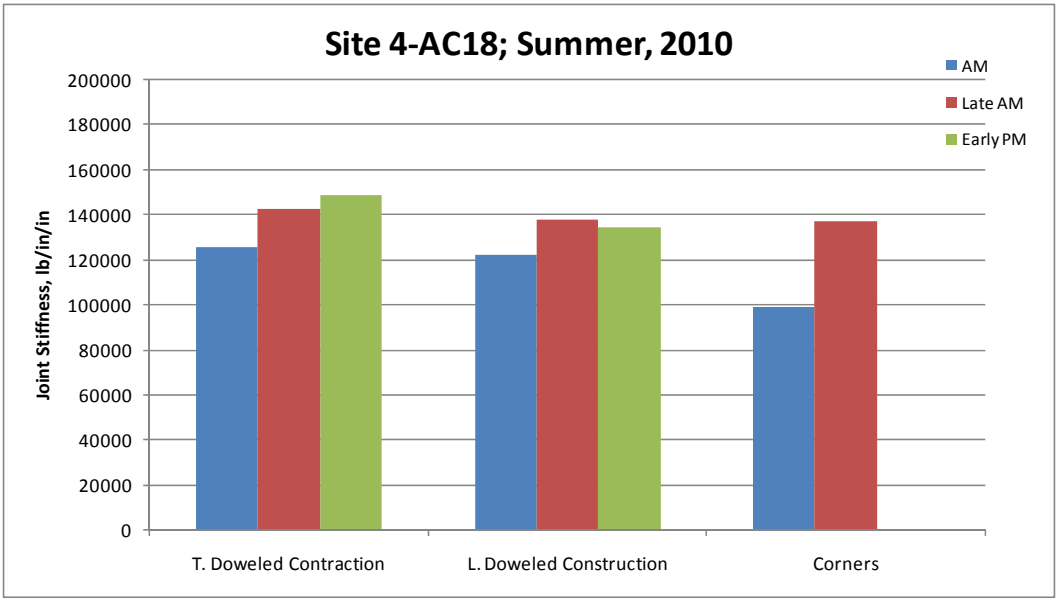

FIGURE 4.22. BREAKDOWN OF JOINT STIFFNESS BY JOINT TYPE AND ROUND OF TESTING FOR SITE 4-AC18 FOR SUMMER OF 2010

4.5 BACKCALCULATED MODULUS OF DOWEL-CONCRETE INTERACTION

Figure 4.23 shows an example of the doweled joint data analysis procedure developed for this project. For each doweled or tied joint type at a test site, the statistics for the joint parameters are accumulated and compared to the joint load transfer device design information from the construction plans. The data shown is the statistical breakdown for the transverse doweled

contraction joints shown in figure 4.21. The FAA typical doweled joint stiffness equation is matched to the design plan information and the modulus of dowel-concrete interaction, often referred to as *K* or DCI, is varied until the calculated doweled joint stiffness matches the median measured joint stiffness value. The best-fit dowel-concrete interaction factor for this joint type's median stiffness value, assuming aggregate interlock is zero, is 1,279,760 psi. The value of 0.1 inch joint opening was assumed for all joint backcalculations. Considerable changes in joint opening assumptions do not change the resulting backcalculated values much for the doweled joint stiffness equation shown. The value of 0.1 inches, or 100 mils is relatively large and represents an open joint condition where aggregate interlock would be significantly reduced. It was not considered necessary to vary this parameter.

4-AC18 Winter 2009; Doweled Contraction Joints- including locked/un-cracked

	LR	LTE	Avg Stiffness	
avg	148	84%	113380	% possibly un-cracked, LTE>89% = 7%
Median	147	84%	103252	***Sawed, 2" dowels at 15"***
min	129	63%	31628	
max	194	96%	596011	Steel Area/ft = 2.513274
stdev	7	4%	50372	reinf. ratio = 1.16%

Without locked/un-cracked joints

	LR	LTE	Avg Stiffness	
avg	148	83%	109027	% possibly un-cracked, LTE>89% = 5%
Median	147	83%	101613	
min	131	63%	31628	
max	194	95%	377526	Probable Agg Interlock = 0 to 100000
stdev	7	4%	41025	

$$k = \frac{1}{s\left(\frac{\varpi}{0.9 G_d A_d} + \frac{\varpi^3}{12 E_d I_d} + \frac{2+\beta\varpi}{2\beta^3 E_d I_d}\right)}$$

s is the dowel bar spacing =	15	in
ϖ is the joint opening =	0.1	in
d is the dowel diameter =	2	in
A_d is the dowel cross-sectional area =	3.14	sq in
E_d =	29000000	psi
G_d =	11153846	psi
I_d =	0.785	in^4
Back-Calculated Dowel-Concrete Interaction modulus, K=	1279760	psi

$$\beta = \sqrt[4]{\frac{Kd}{4 E_d I_d}} = 0.409$$

Doweled Joint Stiffness = **101613** lb/in/in (27)

FIGURE 4.23. EXAMPLE OF THE DETAILED DOWELED JOINT ANALYSIS FORMAT DEVELOPED FOR THIS STUDY, SHOWING THE MEASURED DATA, THE DESIGN PLAN INFORMATION, TYPE OF JOINT, AND THE BACKCALCULATED DOWELED JOINT PARAMETERS

Figure 4.24 shows the median and minimum joint stiffness values for the doweled joints from the test sites. Sites 3-CT16, 5-AGG18, 6-CT16, and 10-AGG14 were tested during hot conditions. The transverse doweled contraction joints at these test sites were significantly stiffer than doweled construction joints. Some of this difference is related to effective aggregate interlock

being higher on a cracked face versus a smooth construction joint face. Some of this difference is like due to better dowel-concrete interaction for sawed contraction joints versus construction joints. Sites 3, 5 and 6 are on runways and the transverse joints are confined by hundreds of feet of slabs in either direction, while the construction joints are not significantly confined as the runway is only on average 6 to 12 slabs wide. The transverse joints in the interior portion of the runway tend to lock up tightly during hot weather, while the longitudinal joints are more able to spread apart over time and remain looser and become looser more quickly.

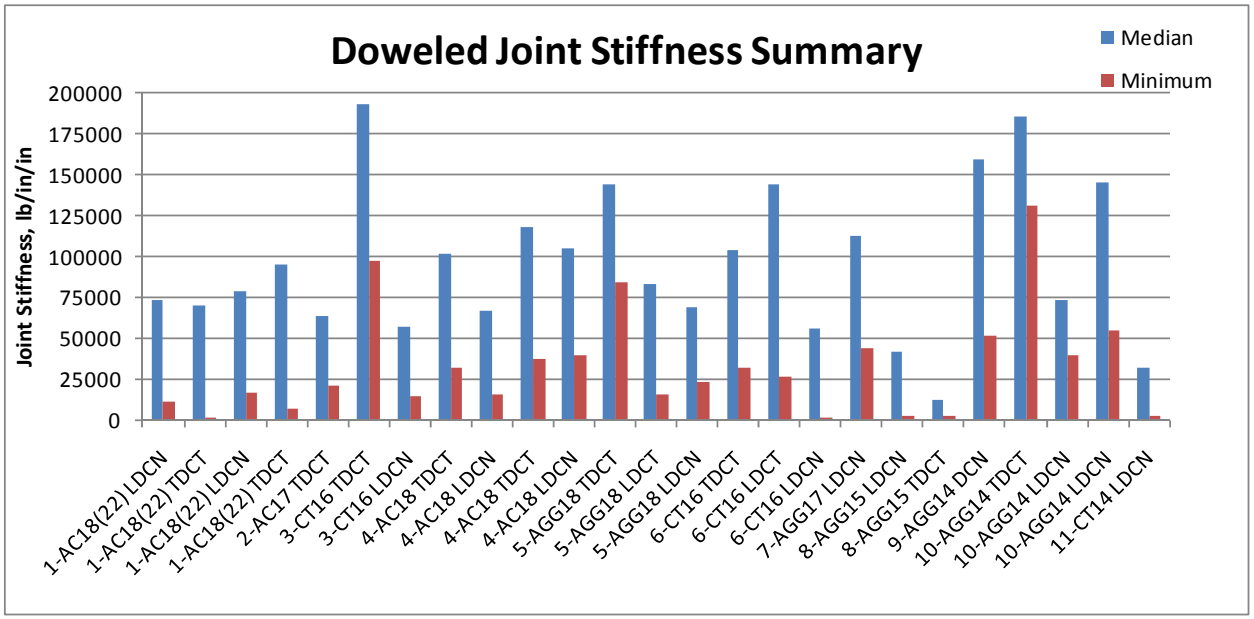

FIGURE 4.24. MEDIAN AND MINIMUM JOINT STIFFNESS VALUES FOR THE DOWELED JOINTS FROM THE TEST SITES (L=LONGITUDINAL, T=TRANSVERSE, CN=CONSTRUCTION, CT=CONTRACTION)

Figure 4.25 provides the backcalculated dowel-concrete interaction factors for both the median joint stiffness and the minimum joint stiffness values for each joint type. For this analysis, possible aggregate interlock that was present was completely ignored, so the values shown represent upper-limit values matching 100% of the calculated total joint stiffness. Some aggregate interlock was probably present at some of the test sites but it is difficult to estimate how much of the total joint stiffness is from dowels versus aggregate interlock at any point in time. The magnitude of aggregate interlock and joint opening is continuously changing over time. The overall test group average dowel-concrete interaction coefficient, *K*, matching the site average joint stiffness values was 3,100,000 psi. The overall test group average dowel-concrete interaction *K* value matching the minimum joint stiffness values for the various joint types was about 810,000 psi. Test site 9-AGG14, which was deemed to be either completely frozen or uncracked was omitted from these calculations as unusually high dowel-concrete *K* values resulted from backcalculations from this site. Similarly, the doweled transverse contraction joints from site 10-AGG14 were omitted as these joints were clearly in a thermally locked condition with very high aggregate interlock present, and unusually high dowel-concrete *K* values were backcalculated.

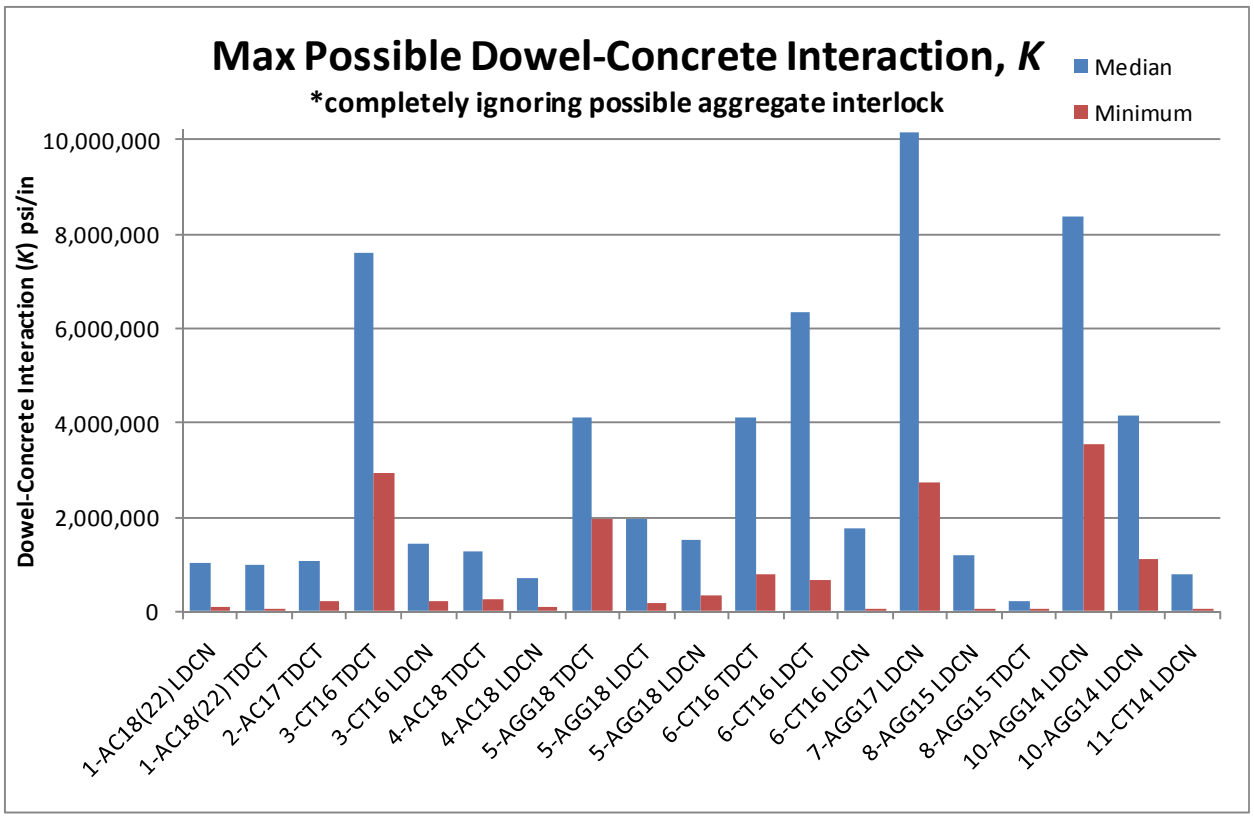

FIGURE 4.25. SUMMARY OF APPARENT MAXIMUM POSSIBLE MODULUS OF DOWEL-CONCRETE INTERACTION VALUES FOR THE MEDIAN AND MINIMUM JOINT STIFFNESS VALUES FROM FIGURE 4.24

4.6 JOINT LOOSENESS AND SLAB EDGE GAPS

The slab edge gap behavior is demonstrated here with the most extreme example encountered: site Road-AGG10 (GPS3 site 53-3019). Figure 4.26 shows the load versus deflection trend lines for the morning testing and the afternoon testing of the same joints at the test site. The apparent y-intercept (deflection intercept) at zero load is the *Slab Edge Gap* size. During early morning testing, edge gaps were between 9 and 23 mils, and edge gaps reduced to between 1 and 3 mils by the time of mid afternoon testing. This change in edge gap is related to slab curling.

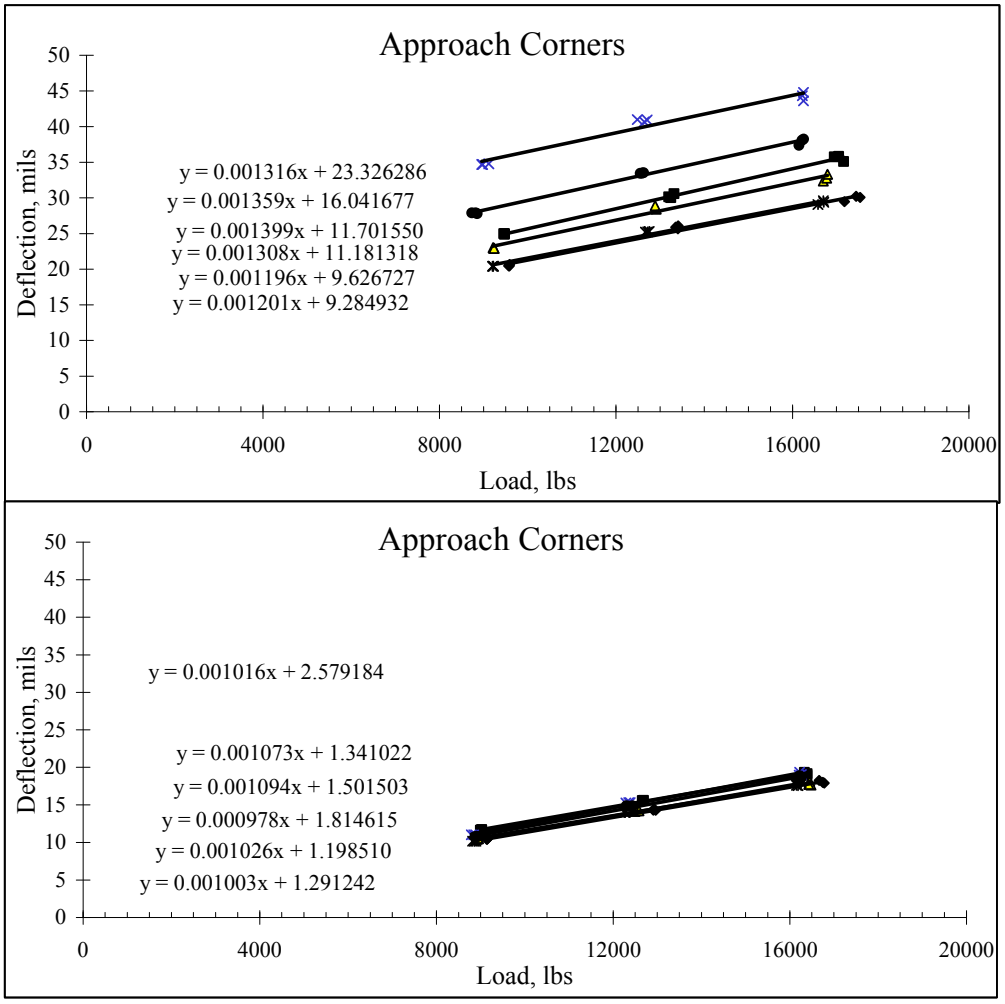

FIGURE 4.26. SITE ROAD-AGG10 EARLY MORNING (TOP) VERSUS MID-AFTERNOON (BOTTOM) LOAD VERSUS DEFLECTION TRENDS FOR FWD JOINT LOAD TRANSFER TESTS ON THE TRAFFIC APPROACH SIDES OF JOINTS

Figures 4.27-4.29 show a looseness analysis using DIA FWD data. Figure 4.27 shows the looseness index applied to an aggregate interlock joint. The top plot is the deflection difference plot, with the y-intercept looseness values shown in the equations. The lower plot shows the magnitude of the apparent joint looseness presented as percentage of the unloaded slab deflection during the FWD joint test. This joint, 1-10-D4, had about the loosest behavior encountered at DIA, with about 3.2 mils of apparent looseness during cold weather testing at 10 °F. This 3.2 mil looseness was about 80 to 120% of the unloaded slab deflection for loads ranging from about 65,000 to 40,000 lb, respectively. The apparent joint looseness decreases significantly as slab temperature increases, closing the joint opening and allowing the aggregate interlock shear surface to compress together. During warm weather, the apparent looseness of the joint is only about 4 to 7% of the unloaded slab deflection.

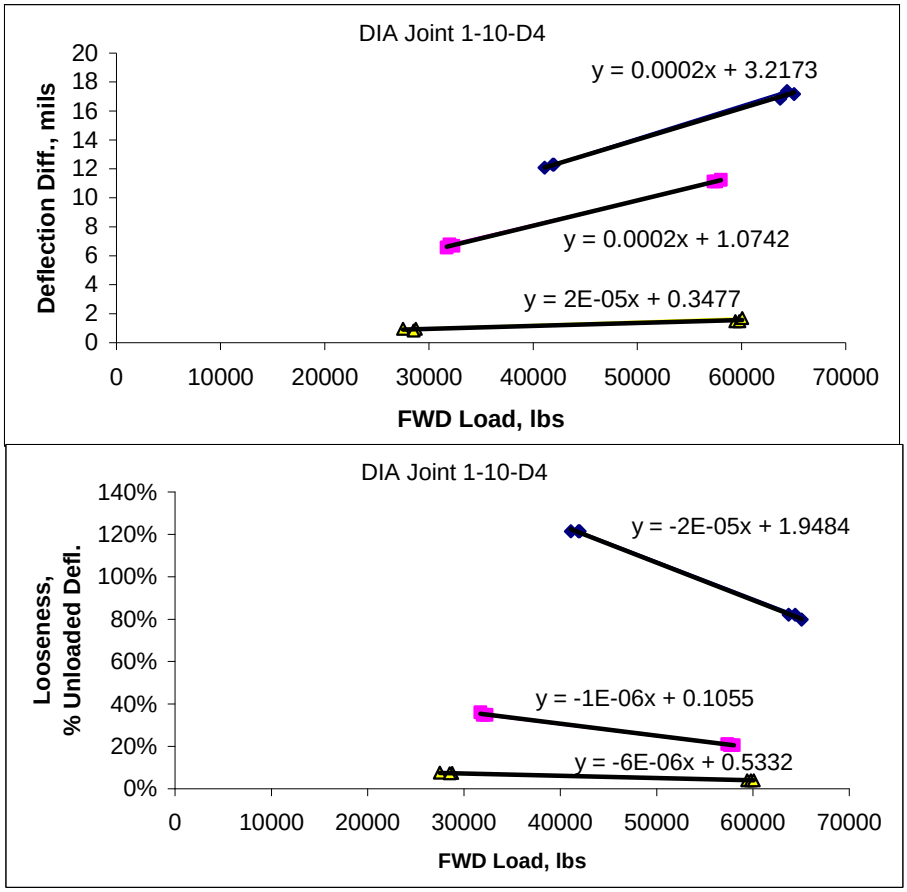

FIGURE 4.27. JOINT LOOSENESS EVALUATION FROM FWD DATA FOR A SITE DIA-CT18 AGGREGATE INTERLOCK TYPE JOINT AT THREE DIFFERENT TEMPERATURES

Figure 4.28 shows one of the stiffest tied joints encountered at the site DIA-CT18. The deformed tie-bars prevent the joint from opening during cooler weather. The apparent looseness values are small and are constant across a wide range of temperatures. Looseness at this joint represents about 3 to 8% of the overall deflection of the unloaded slab for the load magnitudes shown.

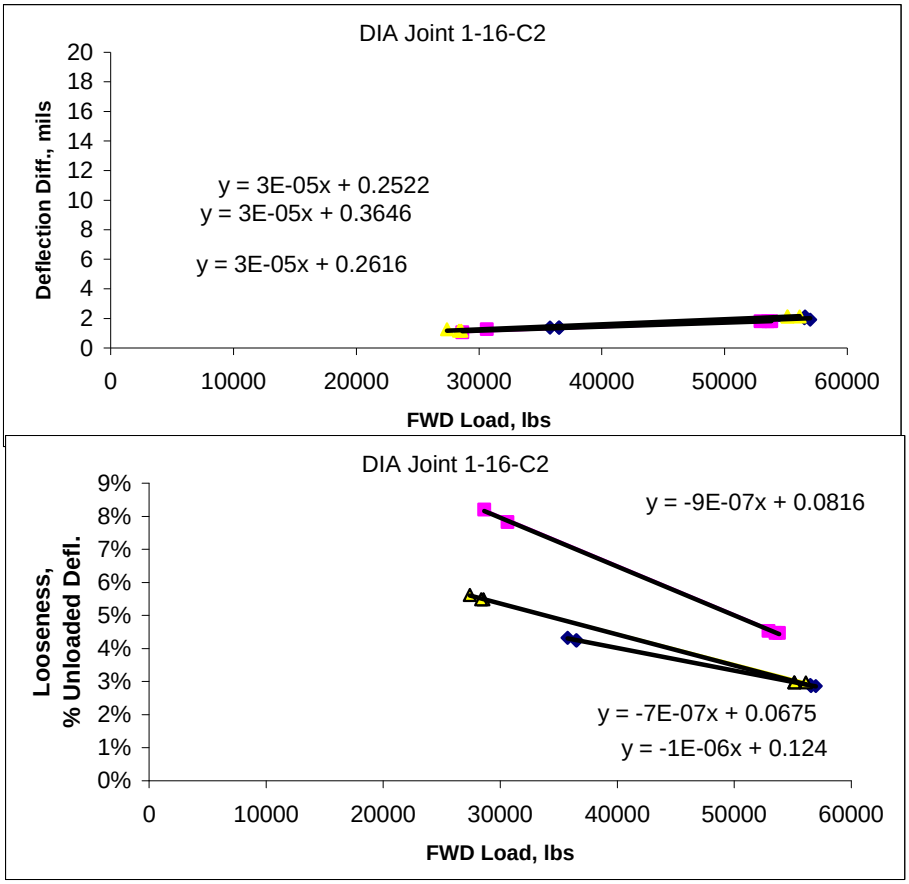

FIGURE 4.28. JOINT LOOSENESS EVALUATION FROM FWD DATA FOR A SITE DIA-CT18 TIED DEFORMED BAR HINGE JOINT AT THREE DIFFERENT TEMPERATURES

Figure 4.29 shows plots from two immediately adjacent corner FWD tests from site DIA-CT18. The joint along one edge was a hinge type joint, and the joint along the other edge was an aggregate interlock (dummy) joint. The trend for corner looseness is generally between the two extremes of trends for the individual joint types meeting at the corner, as previously shown in figures 4.27 and 4.28.

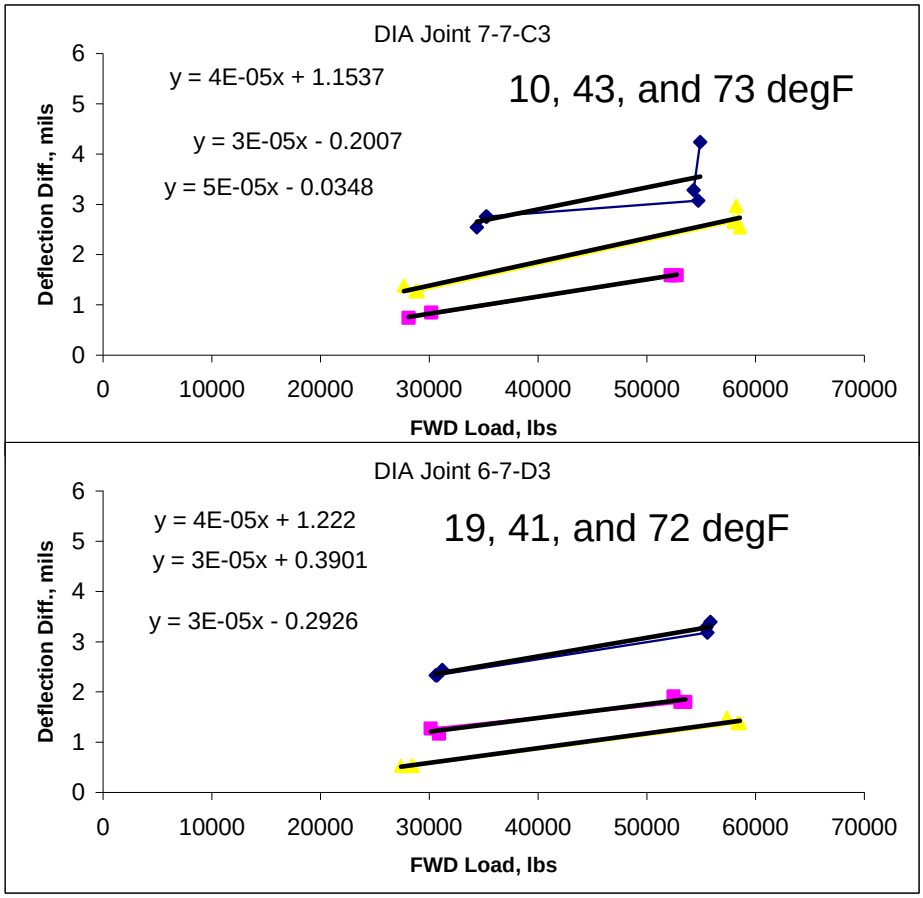

FIGURE 4.29. LOOSENESS EVALUATION OF ADJACENT CORNER LOAD TESTS WHERE ONE JOINT IS A TIED JOINT AND THE OTHER IS AN AGGREGATE INTERLOCK JOINT

Figure 4.30 shows joint looseness evaluation for the highway test site 53-3019. This looseness analysis is for a good condition freeway pavement aggregate interlock joint, which had large morning slab edge gaps as shown in figure 4.26. The data are from three test times in one day, once right after sunrise, again near noon, and then near the thermal maximum in the mid-afternoon. The y-intercept looseness values are about the same for the approach side slab (top plot) and the leave side slab (bottom plot). The approach side deflection difference slope is highly load dependent, while the leave side deflection difference trends are not load dependent. This is because the leave side slab hardly moved at all during approach side loading. The early morning loading of the approach slab is a nearly free-edge load response. The looseness magnitudes are about the same for both sides indicating the joint opening change is affecting each side about the same. The LTE_{δ} values for the approach side are 10, 22, and 33% for the morning, noon, and afternoon tests. The LTE_{δ} values for the leave side are about 60, 70 and 75% for the morning, noon, and afternoon tests. For both cases, however, the deflection difference y-intercept values, looseness values, are about the same. In the heat of the afternoon, almost no looseness is present, while in the early morning, about 10 mils of apparent looseness is measured.

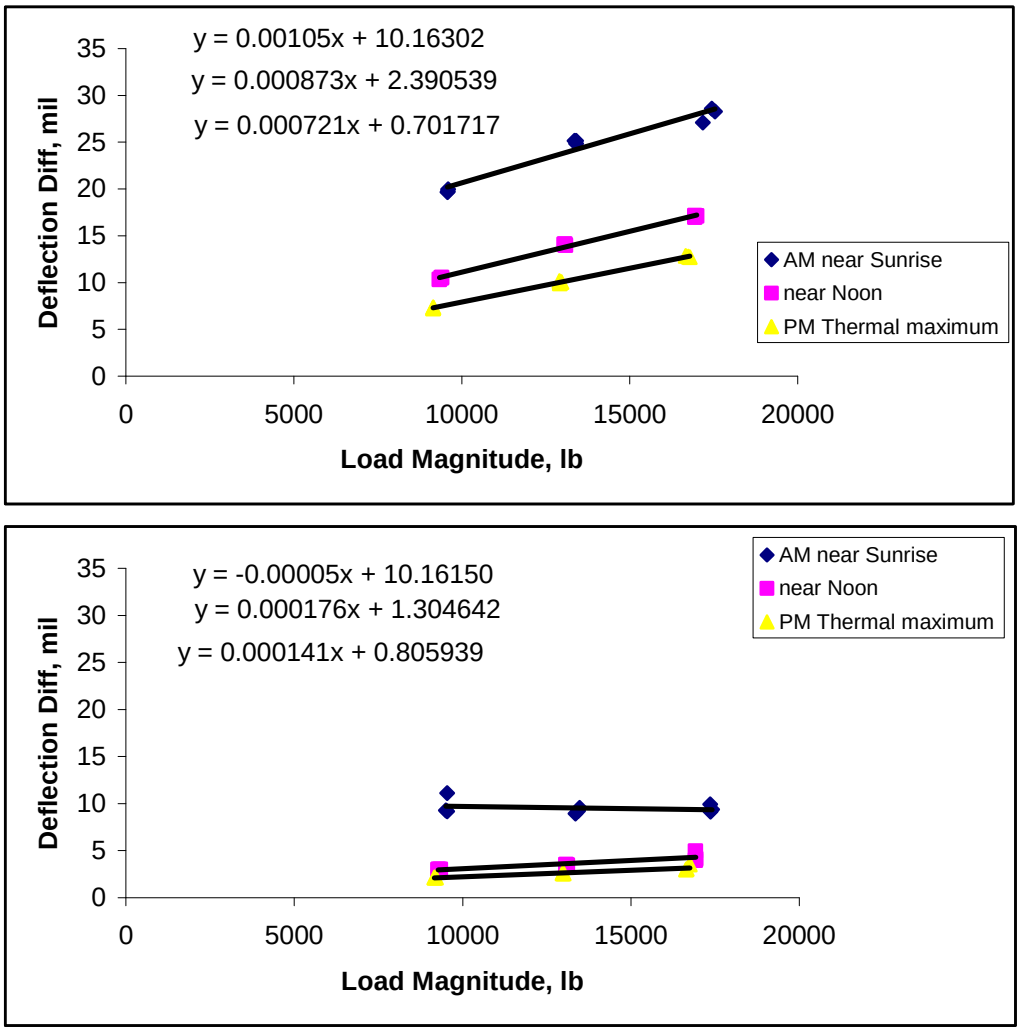

FIGURE 4.30. PLOT SHOWING JOINT LOOSENESS FOR AN AGGREGATE INTERLOCK HIGHWAY JOINT THAT HAS LOW FAULTING SHOWING HOW TIME OF DAY AFFECTS SLAB EDGE DEFLECTION DIFFERENCE TRENDS FOR TYPICAL APPROACH SIDE (TOP) AND LEAVE SIDE (BOTTOM) LOADING OF THE JOINT (GPS3 SITE 53-3019)

Figure 4.31 shows the morning looseness data from figure 4.30 plotted as percentage of the unloaded slab deflection magnitude. At the 10,000 lb load level, the joint looseness is about 100% of the unloaded slab deflection for leave slab loading, but is about 600% of the unloaded slab deflection when the load is applied on the approach side of the joint, as the unloaded leave slab hardly moves. The leave side of this good condition low-fault highway joint has about the same looseness behavior as the relatively new DIA aggregate interlock (dummy) joint in very cold conditions, in terms of relative behaviors, where the apparent looseness magnitude is about equal to the unloaded slab deflection magnitude. The approach slab loading has large apparent looseness and low LTE_{δ} and joint stiffness due to the off-set slack caused by small joint faulting and differential settlement.

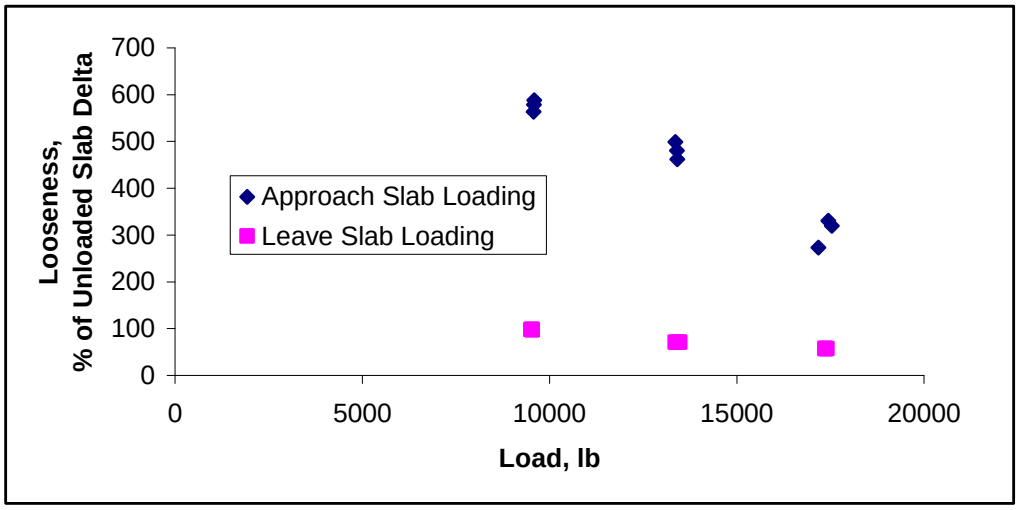

FIGURE 4.31. JOINT LOOSENESS EXPRESSED AS PERCENTAGE OF UNLOADED SLAB DEFORMATION FOR THE EARLY MORNING TESTING (GPS3 SITE 53-3019)

The previous examples demonstrate some rather extreme ranges of looseness and edge gaps that can be encountered on a slab by slab basis. Figures 4.32 and 4.33 provide the joint looseness and slab edge gap summaries for the full airfield test sites. The values shown represent the site averages based on hundreds of joint load tests. In general, there were typically a few joints at a test site that had large looseness or edge gaps. In general, negative values for the zero-load intercept values for edge gaps and looseness indicate a load versus deflection softening response, while positive values indicate a load hardening response was observed for the range of FWD loads used at the test site. Negative values are essentially zero values and are associated with good slab edge support conditions and/or locked-joint conditions. Sites 7 and 9 were tested in freezing conditions and displayed large negative slab edge gaps and looseness. Sites in dry regions (sites 3, 5, 6, 10) generally had locked-in up-warp resulting in positive slab edge gaps in the morning that decreased with time of day as curling flattened the slabs.

Figure 4.33 presents the looseness and slab edge gap data as percentage of unloaded slab deflection and shows only positive values. Site 8 was the de-icing pad test site that experienced large loss of support along slab edges. This site also developed large joint looseness representing a significant site-wide average of 15 to 30% of the unloaded slab deflection for a 35-kip FWD load. Sites 2 and 11 are older test sites that have developed site-wide joint looseness equal to about 5 to 10% of typical 35-kip FWD test unloaded slab deflections at the sites. Based on the test data it is safe to assume that at the end of life, FWD type deflection difference looseness will represent 5 to 10% of the unloaded slab deflection occurring under a 35-kip FWD load for typical airfield pavements, with some joints at the site having significantly higher values.

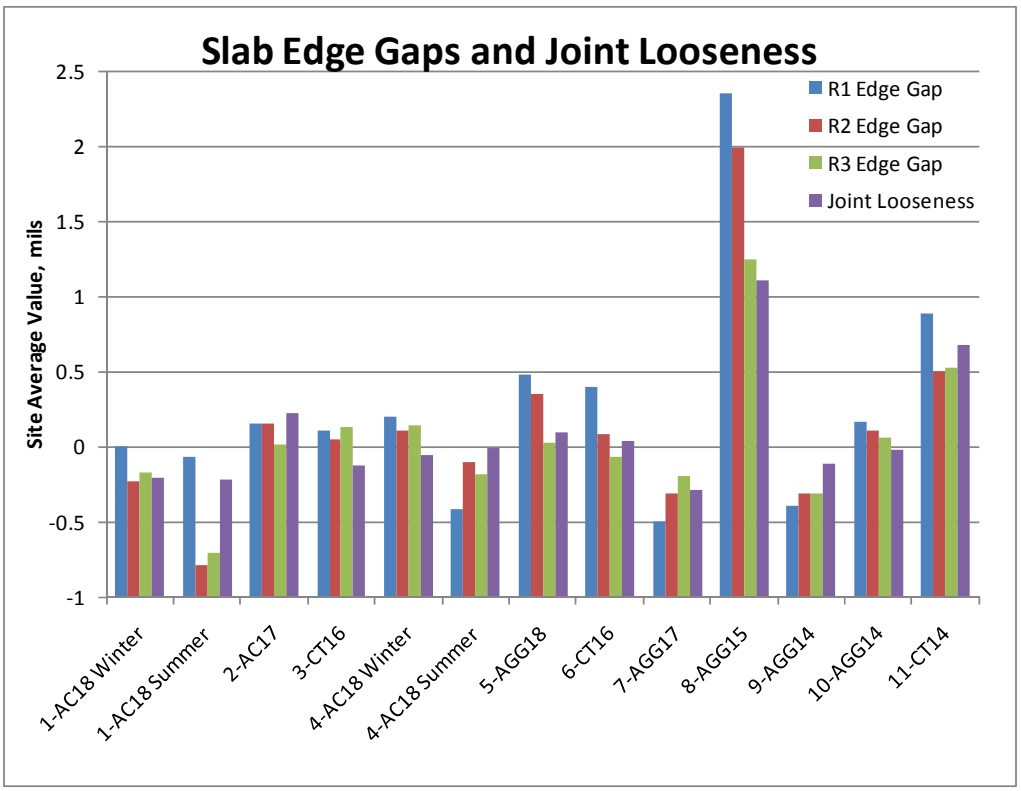

FIGURE 4.32. SUMMARY OF OVERALL SITE AVERAGE SLAB EDGE GAP AND JOINT LOOSENESS INDEX VALUES FROM THE FULL TEST SITES

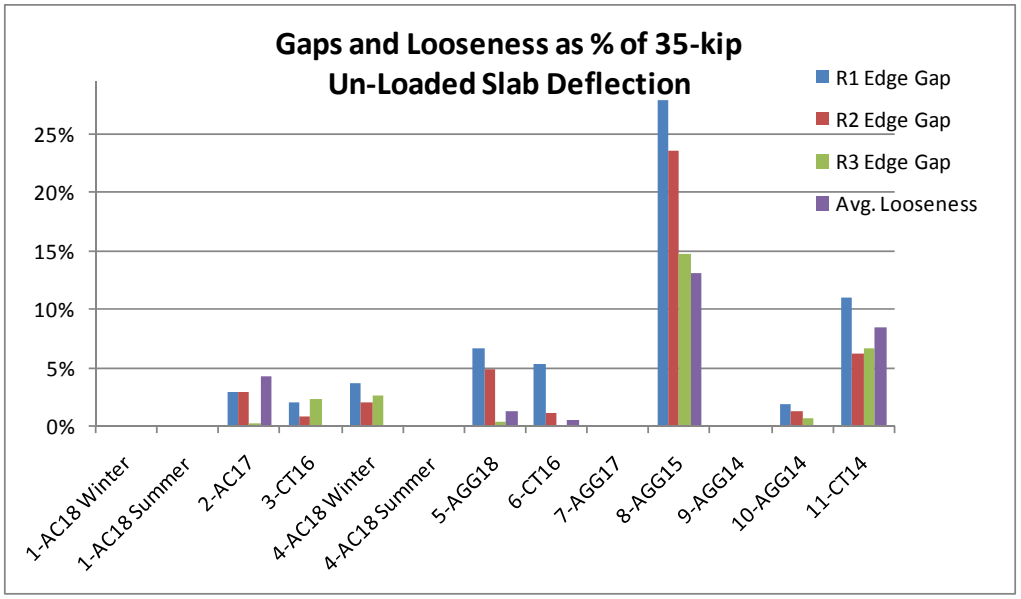

FIGURE 4.33. SLAB EDGE GAPS AND LOOSENESS PLOTTED AS PERCENTAGE OF THE UNLOADED SLAB EDGE DEFLECTION FOR A 35-KIP FWD LOAD, AND SHOWING ONLY POSITIVE VALUES

4.7 TRAFFIC AND DIFFERENTIAL SETTLEMENT EFFECTS

Traffic and differential settlement of slabs tends to cause the same effect on joint behavior. Traffic can cause differential settlement at a joint, and once the differential settlement forces initiate, wear patterns on the crack face surfaces will be different and an offset slack will develop in the joint. Figure 4.34 shows the general behavior related to differential settlements at a joint that has a significant opening. This off-set slack can be visible in FWD data while only a tiny vertical fault has developed. The slab end that has lost more support tends to drop relative to the slab that has better support. This causes the settling slab crack face to drop down and essentially rest on the higher slab's crack face roughness features. When a load is placed on the high slab edge, there is an initial offset slack in the joint and the loaded slab must drop significantly before it re-engages the low slab aggregate interlock. LTE_{δ} values for loading on the high slab (often referred to as the "approach slab to the joint" for freeway traffic) are typically low compared to loading on the low slab due to this offset slack phenomenon. The phenomenon is very visible in faulted highway joints. It is also occurring to a significant degree in airfield pavements. For example, it will be shown later in this section that the NAPTF CC-2 Test Strip pavements had as much as 40% LTE_{δ} difference for loading on one side versus the other for FWD joint tests performed after applying accelerated heavy loading to the test pavement. This offset slack develops early, before faulting gets large.

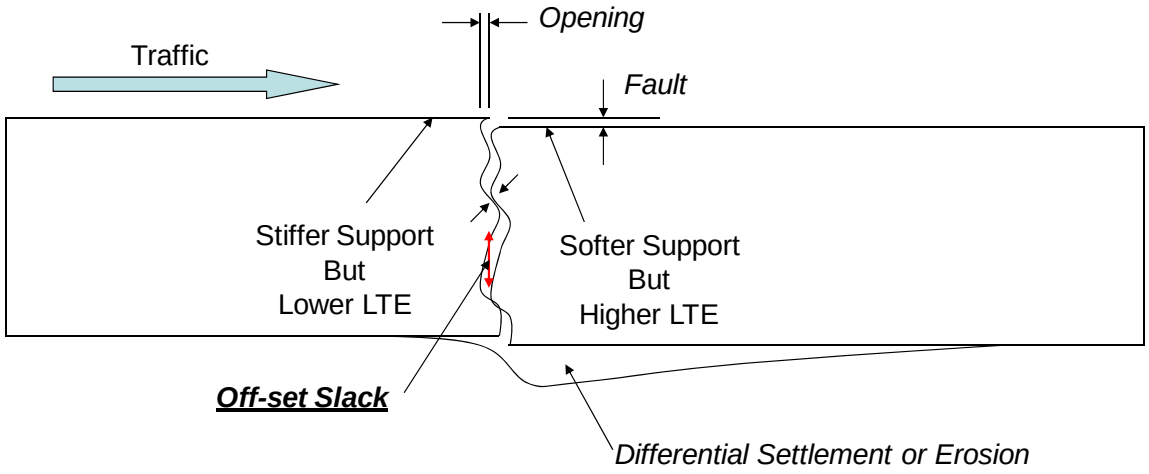

FIGURE 4.34. THE GENERAL EFFECT DIFFERENTIAL SUPPORT RESULTING FROM SETTLEMENT OR TRAFFIC HAS ON THE AGGREGATE INTERLOCK COMPONENT OF JOINT STIFFNESS, AND THE CONCEPT OF OFF-SET SLACK

As a part of past research into joint behavior, a simple way of estimating the offset slack using FWD joint load tests performed on both sides of a joint has been developed (Byrum, Hansen, and Kohn, 1998). Figures 4.35 and 4.36 show data from Prozzi et al. (1993) with the general equation for estimating the magnitude of offset slack overlaid above their data. Figure 4.35

shows deflection influence (history) functions for stationary points situated on the approach and leave slab edges as a vehicle rolled over a joint that has significant off-set slack. Clearly the LTE_{δ} values for the approach loading were near 0%, while the leave side loading had LTE_{δ} between about 50 and 60%. Approach slab edge deflections are not as large as the true off-set slack magnitude when approach LTE_{δ} is near zero. Figure 4.36 shows the LTE_{δ} versus temperature relationship for the test joint from Prozzi et al. (1993). A generally linear loss in LTE versus temperature drop was encountered that is similar for both leave and approach slabs, but there is an apparent shift in the lock-up and release temperatures for the leave side versus approach side for the test joint.

(28)

$$Offset = \delta_{approach}(LTE_{Leave} - LTE_{approach})$$

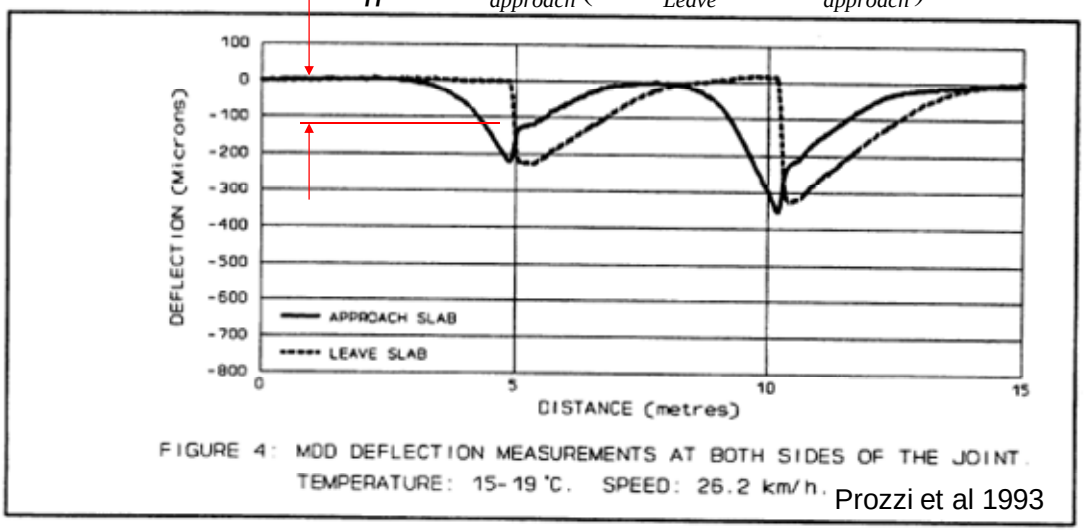

FIGURE 4.35. DATA FROM PROZZI ET AL. WITH THE METHOD FOR ESTIMATING THE MAGNITUDE OF OFF-SET SLACK OVER-LAID ONTO THEIR DATA

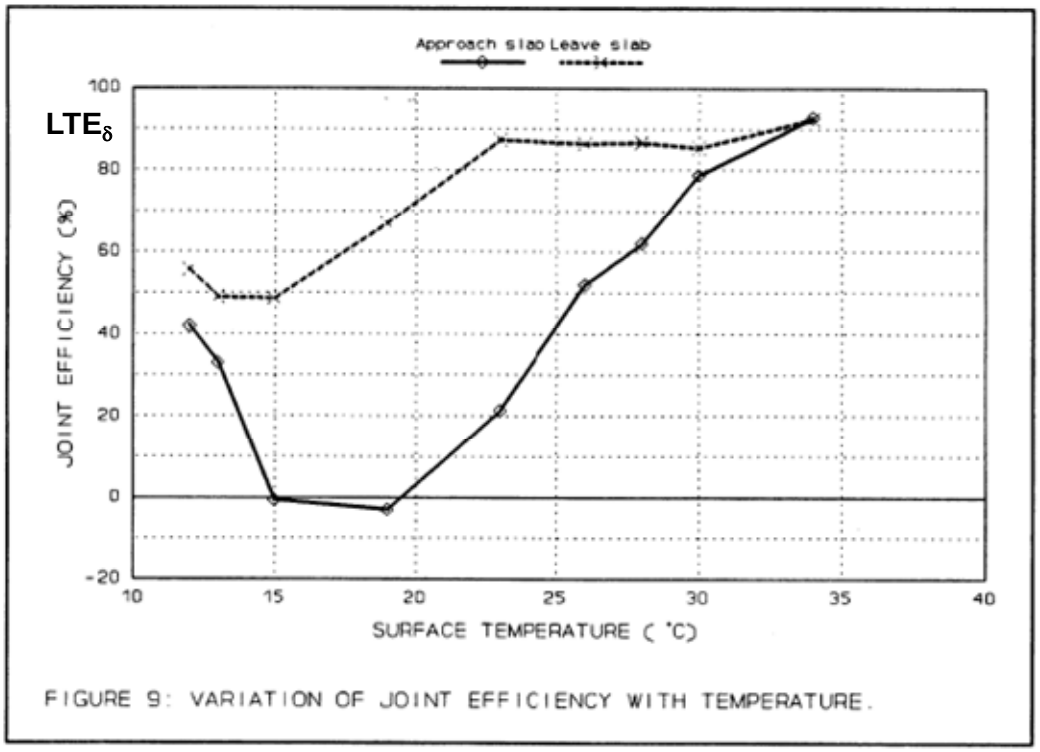

Prozzi et al 1993

FIGURE 4.36. DIFFERENCES IN LTE_{δ} BEHAVIOR FOR THE HIGH AND LOW SIDES OF A HIGHWAY JOINT HAVING SIGNIFICANT OFF-SET SLACK

Figures 4.37-4.40 demonstrate how site Road-AGG10 (53-3019) joint stiffness calculations and Skarlatos/Ioannides best-fit edge support equations fit to an aggregate interlock joint site having small faults but significant off-set slack. It will be shown that a small amount of faulting can have large effects on LTE_{δ} and joint stiffness. This road section is a 9.9-inch thick slab with 11.5-ft joint spacing that had very low faulting over its life. Measured PCC split tensile strength was about 579 psi, and PCC elastic modulus was about 5,827,000 psi with hard high quality aggregates used. Figure 4.37 shows the estimated average fault size versus time trend at the site. This site had small faulting less than 1 mm average size, after an estimated 8 Million Equivalent Single Axle Loads at 17 years old (Byrum, 2010). The FWD testing was performed at approximately 12 years after construction.

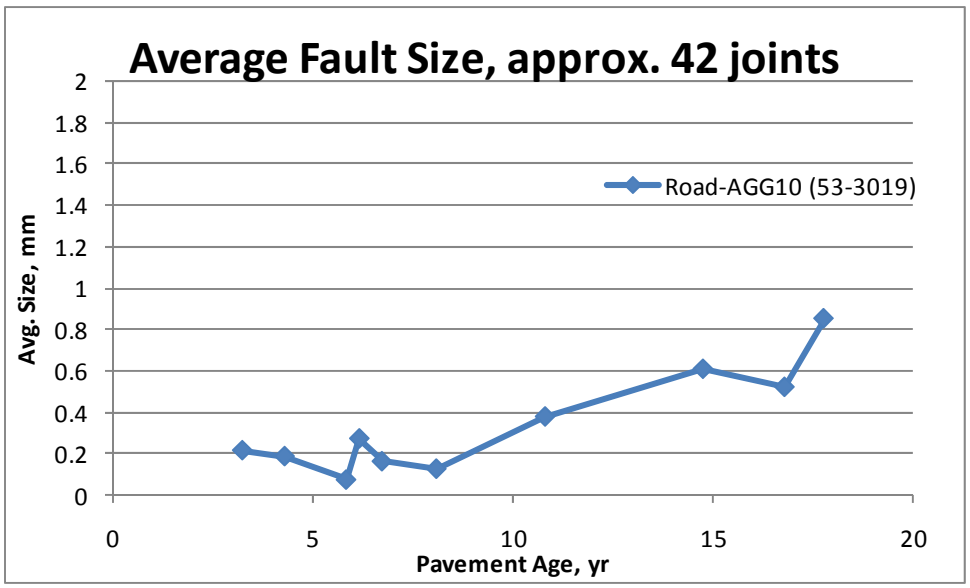

FIGURE 4.37. AVERAGE FAULT SIZE TREND VERSUS PAVEMENT AGE, FOR EXAMPLE TEST SITE ROAD-AGG10 (1 INCH = 25.4 mm)

Even though faulting was very low at this site, the off-set slack effect is large. Figure 4.38 reveals very low joint stiffness and LTE_{δ} for the approach slab loading. Figure 4.39 shows a zoomed in view of the approach slab joint stiffness data revealing small base load transfer effects. The corresponding joint stiffness and LTE_{δ} values for the leave side loading are much higher as shown in figure 4.40. Applying the Skarlatos/Ioannides solution to the approach and leave slab FWD joint stiffness data revealed similar apparent edge support with slightly lower values for the leave slab support. Slab support ratio values are shown in figure 4.41 for the 3 Rounds of FWD testing. The approach slab had a Slab Support Ratio near 1.0 for the PM testing, where the Skarlatos/Ioannides Slab Edge support backcalculated subgrade *k*-value was the same as the overall average ILLI-BACK mid-panel backcalculated subgrade *k*-value. Upward curling during the morning caused the apparent slab support ratio value to drop to about 0.3. This curling related range of apparent slab support ratio variation is slightly smaller than was observed at heavy duty runway site 5-AGG18, which experienced large curling effects. Figure 4.42 shows the calculated off-set slack magnitudes. Off-set slack calculated using the method described in figure 4.35 was about 18 mil in the early morning, and about 8 mil in the afternoon for a roughly 17,000 lb FWD load. The average fault size at 12 years old was about 0.4 mm, or about 16 mil, generally matching the average fault size measurements.

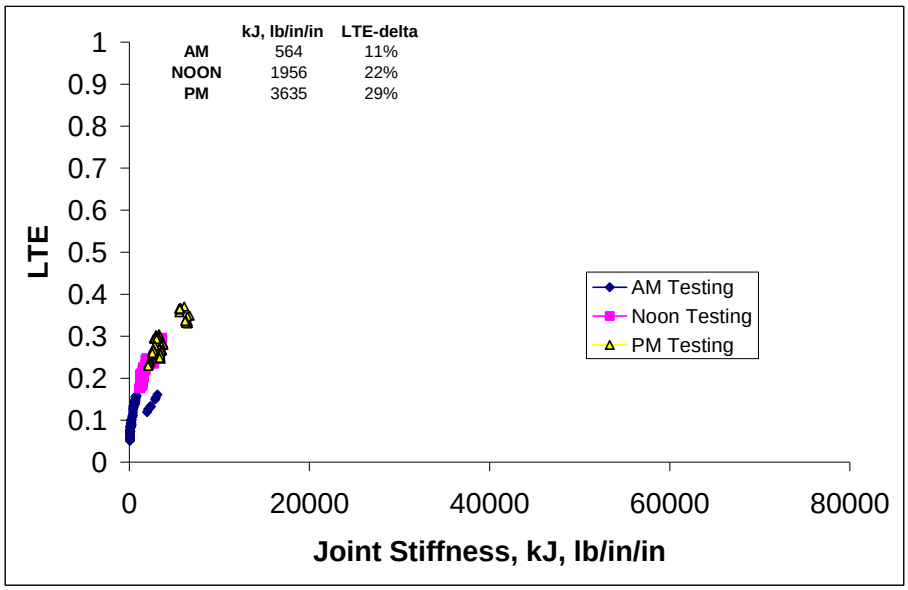

FIGURE 4.38. APPROACH SLAB LOADING JOINT STIFFNESS BEHAVIOR TRENDS FOR SITE 53-3019

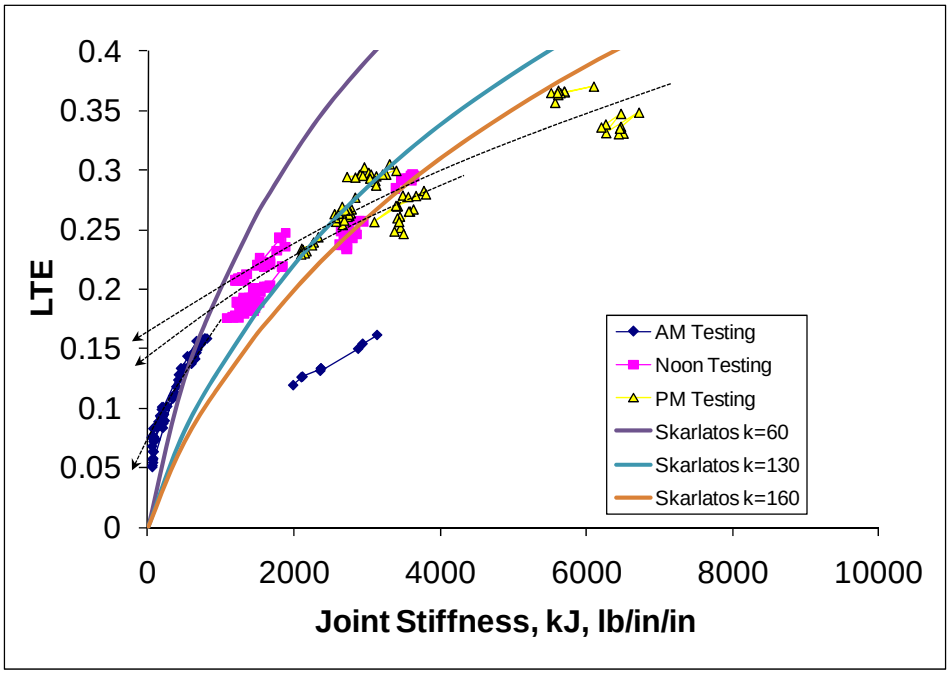

FIGURE 4.39. ZOOMED IN VIEW OF THE APPROACH SLAB DATA SHOWN IN FIGURE 4.38, SHOWING SOME APPARENT ELASTIC SOLID BASE COMPONENT OF LTE_{δ} OF 5 TO 15%

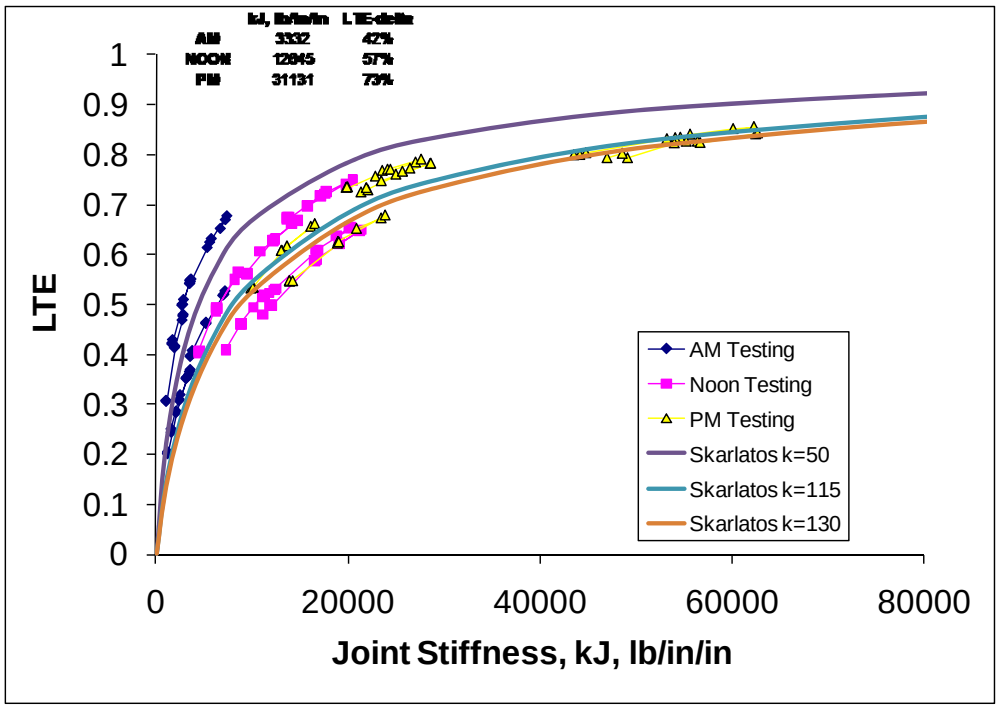

FIGURE 4.40. LEAVE SLAB LOADING JOINT STIFFNESS BEHAVIOR TRENDS FOR SITE 53-3019, SHOWING THE EFFECT OF INCREASING JOINT OPENING AND MORNING CURL RELATED JOINT UPLIFT ON LTE TRENDS, WITH MUCH HIGHER JOINT STIFFNESS MOBILIZED THAN APPROACH SLAB LOADING

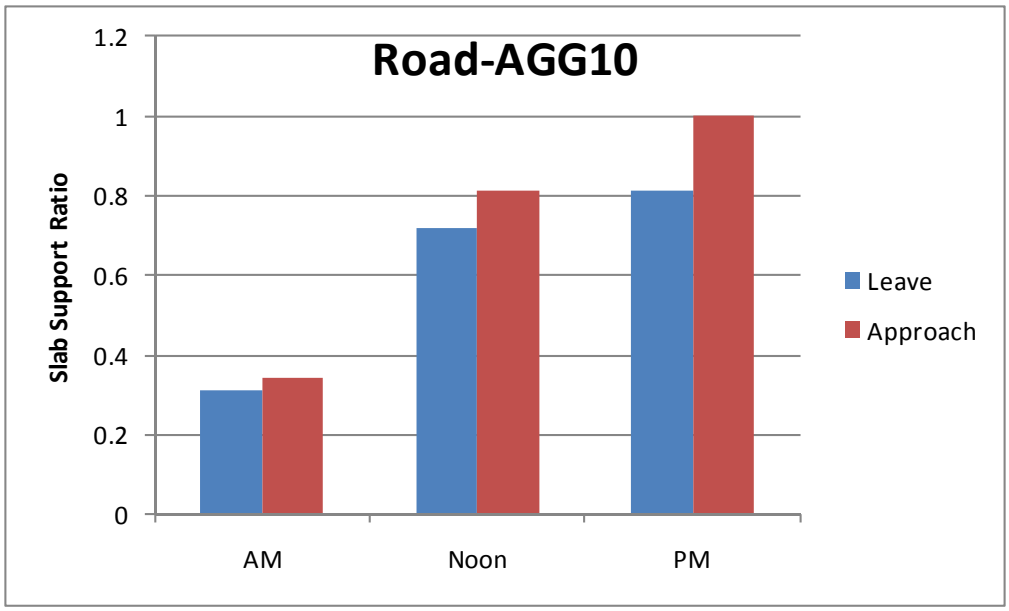

FIGURE 4.41. APPARENT SLAB SUPPORT RATIO VALUES FOR TEST SITE ROAD-AGG10 (AVERAGE ILLI-BACK MID-PANEL REACTION *K*-VALUE WAS 160 PSI/IN)

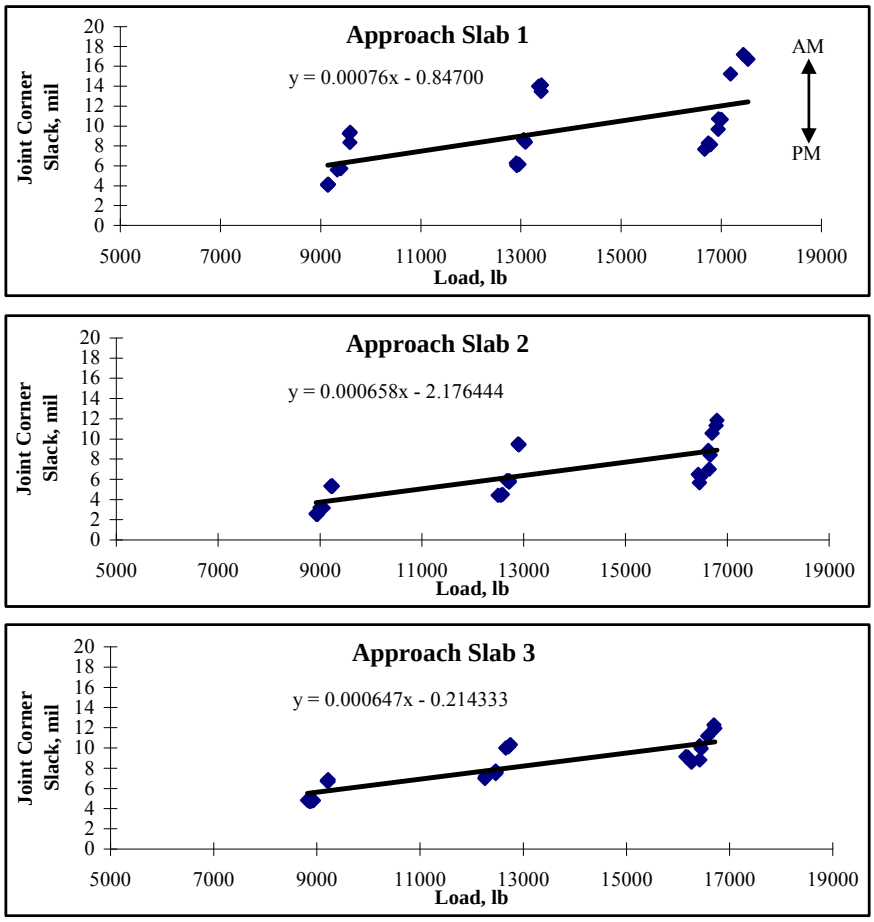

FIGURE 4.42. ESTIMATES OF OFF-SET SLACK MAGNITUDES ASSOCIATED WITH GOOD CONDITION AGGREGATE INTERLOCK HIGHWAY SLAB JOINTS

Case Study- Evaluation of the NAPTF FWD data for the CC-2 Test Strip

FWD testing was performed on the CC-2 test strip at the NAPTF site and the data was available at the NAPTF web site. This case study demonstrates pure traffic effects on joint stiffness and deterioration. The test strip was designed to compare two different PCC mixtures (Ricalde and McQueen 2004). Slabs were 11 inches thick and were either 15-ft by 15-ft or 20-ft by 20-ft in dimension. What was considered unusual rapid top of slab type corner cracking of the original CC-1 concrete panels in the first CC-1 experiment at the NAPTF site inspired this CC-2 Test Strip study. To reduce chances of upward warp and non-representative extreme desert climate type behavior of the CC-2 slabs, the slabs were frequently watered to simulate natural surface moistening from rainfall, and intensive curing methods were used. One half of the site used the same PCC mixture that had been used for the original CC-1 studies and these slabs were called the "S Slabs". The other half of the site was constructed using a special dense graded aggregate

PCC mixture designed to reduce slab warp, and were called the "C Slabs". FWD testing was performed at the site before and after the accelerated traffic tests. The applied traffic consisted of a 4-wheel gear assembly with 55,000 lb per wheel, 220,000 total load. This loading is relatively severe for an 11-inch thick slab, and the slabs had all cracked into several pieces after only a few hundred or thousand load applications. At this site, it appears in general that the slabs likely were deemed as failed due to cracking before the joints had worn out substantially. For sites that have relatively thicker slabs designed at a lower working stress level for substantially more allowable repetitions, the joints may develop more looseness and loss of load transfer ability before the slabs have reached such a cracked condition.

The FWD methodology developed for this study was applied to the before and after traffic FWD data from the CC-2 test strip. Table 4.1 shows the summary results for the ILLI-BACK analysis for the before-traffic conditions and using the design PCC thickness value of 11 inches. The estimated bottom-of-slab modulus of subgrade reaction was about 200 psi/in. The backcalculated effective elastic solid subgrade elastic modulus was 32,556 psi. The backcalculated effective slab elastic modulus was 7.8 million psi, which is relatively high. This is an indication that the slab was placed thicker than 11 inches on average, and/or, the slab was effectively bonded to the cement treated base during mid-panel load tests resulting in a higher effective slab thickness for mid-panel bending response, with some composite base-slab bending action. Overall average mid-panel responses were nearly the same for the C and S slabs for the "new-condition" testing performed before the accelerated loading of the slabs. The design thickness of 11 inches and the backcalculated concrete slab elastic modulus are used as input into the Skarlatos/Ioannides edge response solution to backcalculate the apparent slab edge support modulus of subgrade reaction for the CC-2 slabs, before and after accelerated loading. The edge support is compared to the mid-panel support using the Slab Support Ratio concept.

TABLE 4.1. SUMMARY OF ILLI-BACK FOR NAPTF-CC2 TEST STRIP, NEW CONDITION

	AREA	LK	LE	K	ES	EDL	COV	EES	COV
Mean	***52***	***46***	***32***	***198***	***32556***	***7.8***	***6.9***	***5.8***	***2.8***
Median	52	45	31	203	32441.5	7.95	6.4	5.8	2.2
Min	48	39	26	77	17312	3.6	2.4	2.6	0.7
Max	60	67	49	305	46547	13.3	25.7	10.9	21.3
stdev	2.11	4.67	3.77	49	7609	2.55	2.96	2.02	2.49
std err	0.22	0.49	0.39	5	793	0.27		0.21	

The overall joint testing responses for before and after the accelerated traffic testing are shown in figure 4.43. The summary joint stiffness and LTE_{δ} data is provided in figure 4.44. For the new slab testing, many of the joints had not fully cracked. Only three locations had a noticeable crack present, the joints between slabs C1-C2, C4-C5, and S4-S5, and loss of load transfer was also evident at the construction joint at the edge of slab S1. The test data reveals that the FWD loading was responsible for the initial crack release at joint location C1-C2. For the FWD testing of the new slabs, significant differences caused by offset slack were observed for joint stiffness and LTE_{δ} for testing of the joints on the approach or leave sides. The data from both the approach and leave side testing does fall on the same general LTE_{δ} versus joint stiffness trend line indicating this effect may be real and loss of stiffness may occur for loading on one side of a

joint first, prior to being detectable for loading of the other side. The only loss of load transfer detected in the initial testing was along the transverse joint line between slabs 4 and 5, which was the transition joint between the 20-ft by 20-ft slabs and the 15-ft by 15-ft slabs. These joints immediately dropped to stiffness values of about 20,000 to 30,000 lb/in/in. These were aggregate interlock joints, which indicates that significant crack opening size developed early along this joint line. This observation highlights a key behavior for new jointed concrete pavements. The first joints to form at a site will probably have greater joint opening sizes and corresponding lower LTE_{δ} and joint stiffness. The S-slabs appeared to have experienced greater traffic-related loss of support than the C-slabs relative to the apparent initial stiffness conditions. Ricalde and McQueen (2004) reported that the S-slabs in general had consistently higher joint deflections than the C-slabs, matching the data in figure 4.43.

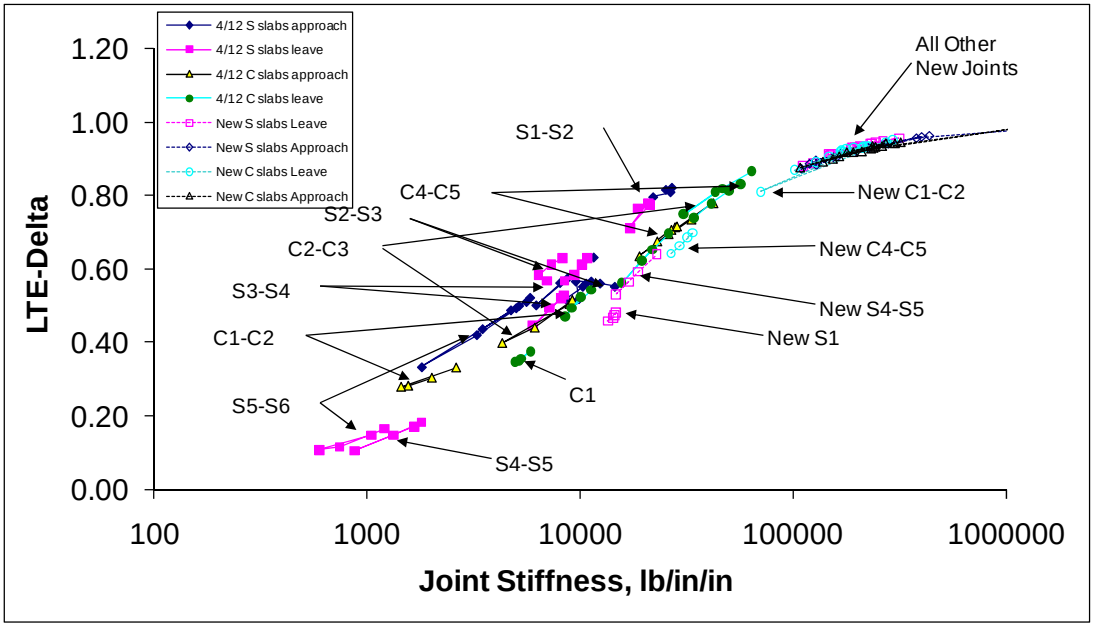

FIGURE 4.43. JOINT STIFFNESS ANALYSIS RESULTS FOR THE FWD TESTING AT THE CC-2 TEST STRIP AT THE NAPTF SITE FOR BEFORE AND AFTER THE ACCELERATED TRAFFIC TESTING IN YEAR 2002, HIGHLIGHTING DIFFERENCES IN APPROACH AND LEAVE LTE_{δ} AND JOINT STIFFNESS WITH ARROWS

	Test/Load Point	Avg. Joint Stiffness	Joint Stiff. Stdev	Avg LTE-delta	LTE-d stdev
End of Test 4/12/2002	S slabs, Approach	10761	7387	0.57	0.13
	S slabs, Leave	7710	6382	0.46	0.24
	C slabs Approach	16428	13357	0.54	0.18
	C slabs, Leave	25534	19143	0.62	0.18
New 1/22/2002	S slabs, Approach	357890	540063	0.92	0.03
	S slabs, Leave	135192	96471	0.79	0.20
	C slabs, Approach	275922	244701	0.93	0.03
	C slabs, Leave	155461	82421	0.87	0.11

FIGURE 4.44. SUMMARY DATA FOR THE LTE_{δ} AND JOINT STIFFNESS ESTIMATES FOR THE BEFORE AND AFTER TRAFFIC TESTING OF THE NAPTF CC-2 TEST STRIP

Figure 4.45 shows Skarlatos/Ioannides best-fit curves to the before and after traffic NAPTF joint stiffness calculations. The apparent loss of support from before to after the accelerated traffic testing for the C and S slabs is shown conceptually as a drift upward and left in the plot over time. The S and C slabs were constructed using about 6 inches of econocrete stabilized base over about 8.4 inches of aggregate, over the low resistance subgrade, LRS, which was a high plasticity clay with CBR estimates of 4 to 5%. Using the ILLI-BACK backcalculated PCC elastic modulus of 7.8 million psi, and design PCC thickness of 11 inches, the best-fit Skarlatos/Ioannides edge curve indicates an effective modulus of subgrade reaction of about 180 psi/in along the joint edges for the FWD testing of new joints prior to loading. Most of the new joints were functioning in the locked or uncracked range of LTE_{δ} above about 85%. The accelerated load tests resulted in loss of LTE_{δ} and loss of apparent subgrade support along slab edges. The loss of support estimated by the Skarlatos/Ioannides trend lines would indicate the effect was similar to reducing the slab edge subgrade *k*-value to about 105 psi/in for the C-slabs, and about 70 psi/in for the S-slabs. The loss of support consists of two primary effects: permanent downward deformation of the foundation at slab edges relative to mid-panel, and accumulating upward warp deflection of slab edges.

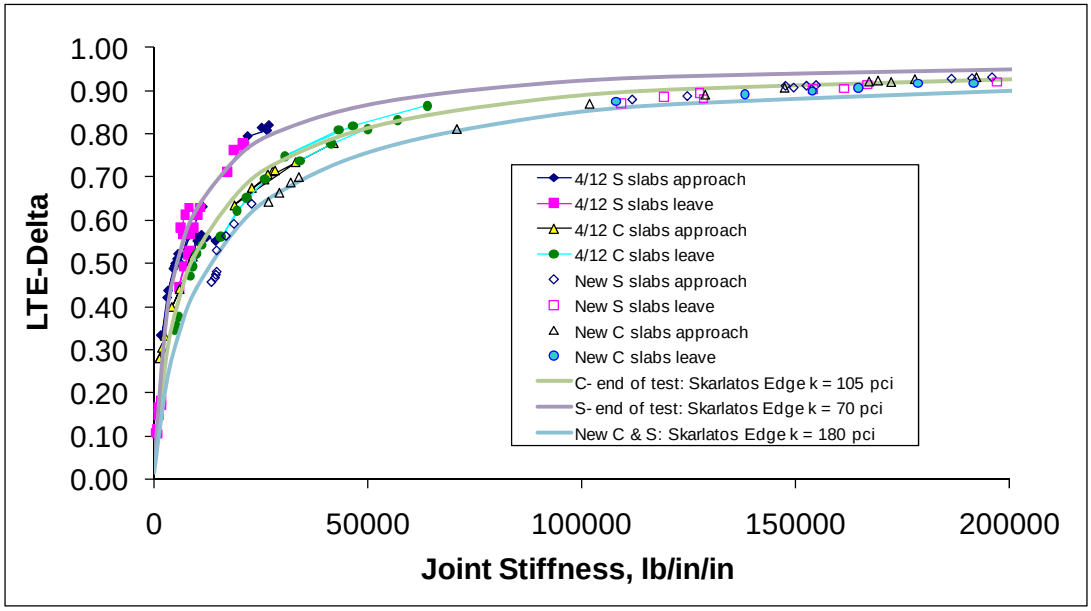

FIGURE 4.45. A PLOT SHOWING THE NAPTF JOINT STIFFNESS MEASUREMENTS BEFORE AND AFTER LOADING TO FAILURE, ALONG WITH THE SKARLATOS/IOANNIDES BEST-FIT CURVES TO THE INITIAL AND FINAL CONDITIONS FOR THE NAPTF CC2 TEST SLABS

Figure 4.46 shows the slab support ratio values obtained from before and after traffic FWD data. The slab support ratio is the Skarlatos/Ioannides slab edge subgrade *k*-value divided by the ILLI-BACK mid-panel subgrade modulus *k*-value. The slab support ratio for the new joints was about 0.9, which is unusually high and reflects that most joints were uncracked when tested before traffic. The slab support ratio for the S-slabs dropped to about 0.35 at the end of testing. The

slab support ratio for the C-slabs was at about 0.5 at the end of testing and this value is similar to slab support ratios encountered for older slabs in-service at airfields, having good joint conditions. The C-slabs are calculated to have experienced less loss of support at joints compared to the S-slabs, which was the intent of the special concrete mixture used for the C-slabs. Re-analysis of the CC-2 data using this the FWD evaluation techniques developed in this study shows that the C-mixture appears to have worked in terms of maintaining better edge support.

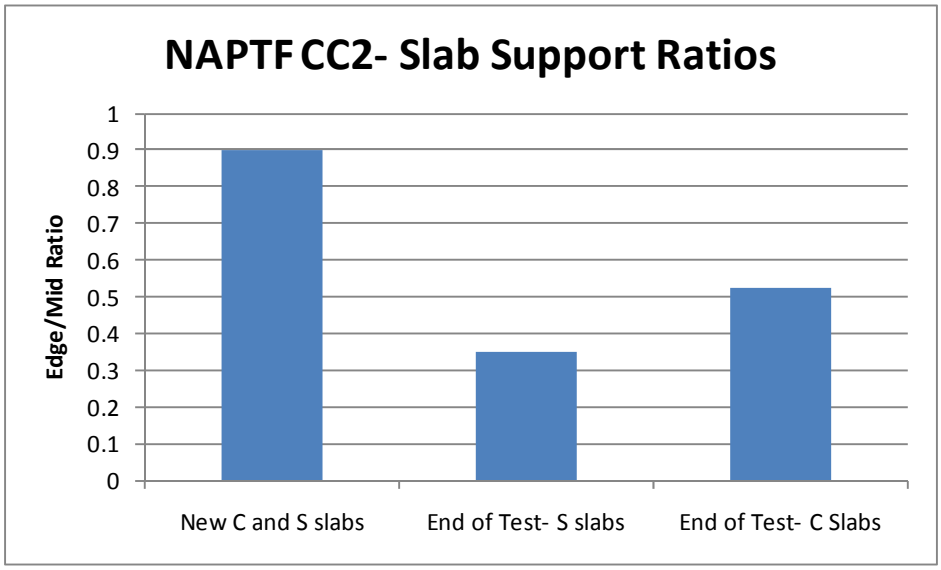

FIGURE 4.46. SLAB SUPPORT RATIOS FOR BEFORE AND AFTER ACCELERATED LOAD TESTING OF THE NAPTF CC2 TEST STRIP SLABS

Figure 4.47 shows how the characteristic joint response length values changed for the S and C slabs. Before the traffic testing, all slabs had similar responses. Both the C and S slabs had about a 120 inch joint response length before accelerated loading. The S slabs showed more degradation in joint response length as a result of the accelerated loading, compared to the C slabs.

Slab Group	Response Length, L, in	L, stdev
S slabs 4/12/02	92	22
C slabs 4/12/02	117	36
S slabs 1/22/02	120	21
C slabs 1/22/02	120	12

FIGURE 4.47. AVERAGE CHARACTERISTIC RESPONSE LENGTHS FOR THE TWO-SLAB GROUPS

Figure 4.48 shows the joint looseness evaluation for before and after traffic for the CC-2 Test Strip. The looseness values are relatively small, but did grow from less than 5% of the unloaded slab deflection before traffic, to about 10 to 20% of the unloaded slab deflection after the traffic had occurred. Where the deflection difference values were essentially near zero for any load, it

is an indication that the crack at the joint had not fully formed. Only two joint locations shown in the top plot in figure 4.48 (S4-S5 and C4-C5) appear to have been cracked initially and had significant openings. This looseness is the result of the initial crack opening for the aggregate interlock joints.

Test Time/ Load Point	Avg. looseness	16-kip, % un-loaded defl.	Max	Stdev
New Approach	0.09	2%	0.22	0.087
New Leave	0.14	4%	0.51	0.172
End of Test Approach	0.87	13%	2.87	0.853
End of Test Leave	1.44	21%	5.85	1.909

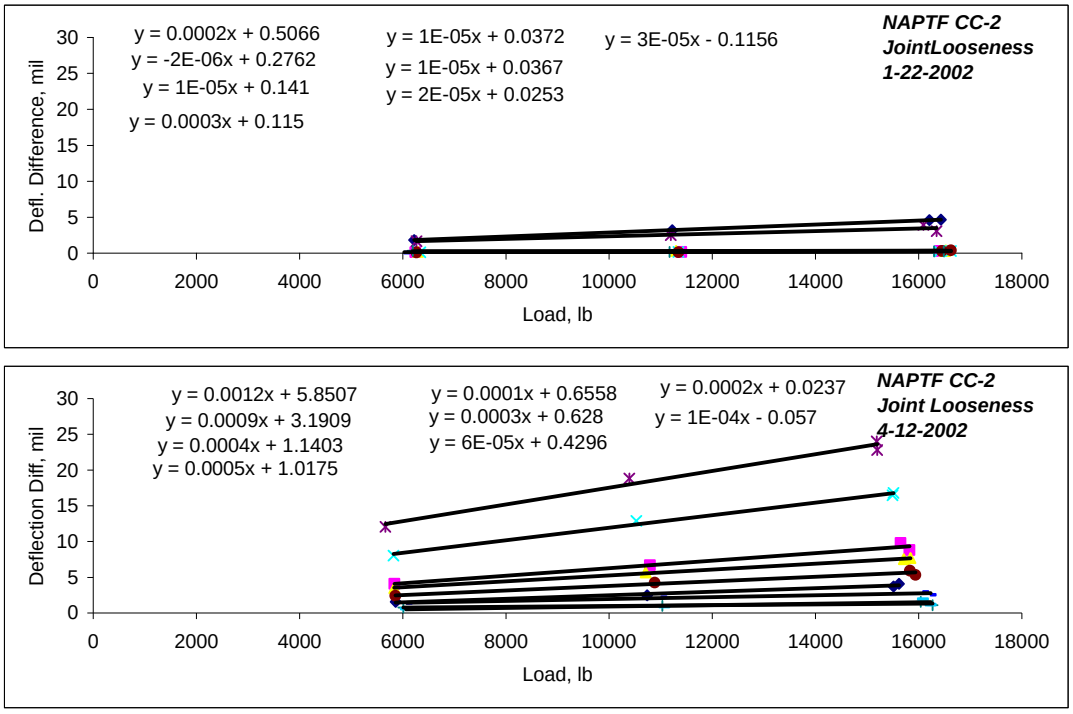

FIGURE 4.48. FWD JOINT LOOSENESS DATA FOR BEFORE (TOP) AND AFTER (BOTTOM) ACCELERATED LOADING AT THE NAPTF CC-2 TEST STRIP SITE

CHAPTER 5. MODELING THE OBSERVED JOINT STIFFNESS BEHAVIOR

This chapter presents methods to predict the joint stiffness behavior for a given pavement design. Numerical methods are developed that can reproduce the observed joint stiffness behaviors described in chapters 3 and 4. These tools can be used to develop estimates of joint stiffness for various designs, which in turn can be used in FEM analysis to obtain estimates of joint load transfer (LT) for various designs. The characteristic joint stiffness data is the key data set used to calibrate an FEM simulation to a site's measured joint response. There are two joint behavior simulation approaches developed from this study. A simplified approach allows an estimate of the characteristic joint response curve for a design using as little as slab thickness as the required input. This simplified method is the same as the joint stiffness backcalculation method introduced by Ioannides and Hammons (1996) but is refined based on the data from this study to include a slab support ratio concept and practical upper limits for joint stiffness values for locked/uncracked joints. A second comprehensive calibrated joint simulation tool is also developed, which can estimate joint behavior as a function of factors such as joint opening size, slab temperature, slab length, materials variations, traffic, for both doweled and aggregate interlock joints.

5.1 ESTABLISHING THE CHARACTERISTIC JOINT STIFFNESS CURVE

The simplified approach can use as little as slab thickness as a basis for estimating a characteristic joint response curve to match to FWD data or use as a basis of design. To establish the prediction methodology, various Skarlatos/Ioannides edge response curves were fit to the project joint stiffness versus LTE_{δ} data set. The slab thickness values in the Skarlatos/Ioannides curves were varied over the range of 7 to 22 inches. The concrete elastic modulus is set at 5 million psi for all curves. The slab edge subgrade *k*-values were then varied in the Skarlatos/Ioannides solutions until the set of Skarlatos/Ioannides curves were reproducing the general thickness related trend in the data, while accounting for some apparent loss of support at edges that was present at the in-service pavement test sites to varying degrees. Figure 5.1 shows the three resulting Skarlatos/Ioannides control curves for the simplified approach. The range of subgrade *k*-values shown are the "empirically adjusted" modulus of subgrade *k*-values considering the typical *Slab Support Ratio* values observed for in-service pavements. As described around figure 4.6, typical average in-service measured *Slab Support Ratio* values range between about 0.4 and 0.5. Therefore, the slab edge *k*-values shown of 120, 180, and 240 psi/in represent equivalent mid-panel *k*-values of roughly double those values. These values can be considered empirically calibrated edge support *k*-values that force the Skarlatos/Ioannides Equation developed by Ioannides and Hammons (1996) to fit the measured data, while assuming a constant slab elastic modulus of 5 million psi. As described in chapter 3, these Skarlatos/Ioannides infinite-edge support values are probably lower than the real edge support values, as the infinite slab edge idealization requires lower edge support input than jointed FEM discretizations do for the same slab edge deflection magnitude. The curves for the assumed *k*-values shown represent newer conditions, before substantial loss of support develops along edges and they may appear as shifted slightly lower and right of the aged field measurements. Loss of support at edges from permanent downward foundation deformation, or permanent upward warp of slabs appears as reducing slab edge *k*-values in the Skarlatos/Ioannides solution, without much change in mid-panel response. The banded zone highlighted around an LTE_{δ} value of 90% is the

zone where the joint stiffness trends become relatively asymptotic with respect to LTE_{δ}. Slab bending moment is being transmitted across joint faces for high LTE_{δ} values above this transition zone and the concept of linear joint stiffness as the explanation for load transfer becomes invalid.

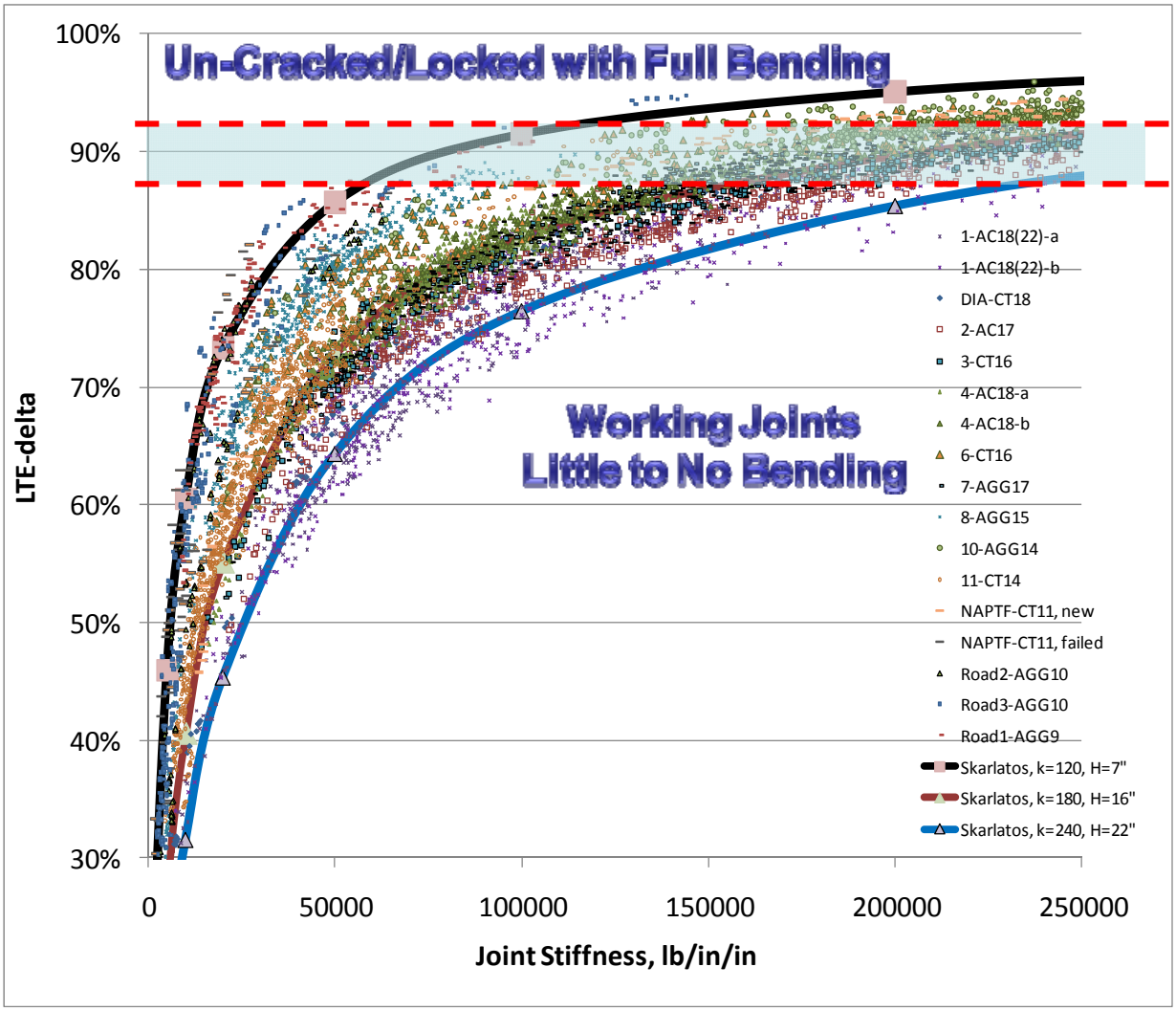

FIGURE 5.1. THE THREE SKARLATOS/IOANNIDES CURVES USED IN THE SIMPLIFIED APPROACH FOR ESTIMATING A SITE CHARACTERISTIC JOINT STIFFNESS CURVE, AND THE TRANSITION ZONE BETWEEN LOCKED/UNCRACKED BEHAVIOR AND OPEN JOINT BEHAVIOR

The simplified approach reflects the general trends shown in figure 5.2 as the basis of the Skarlatos/Ioannides solution fits. There was a general trend in the data of higher mid-panel and slab edge subgrade support values for increasing slab thickness. This may be related to the fact that thicker slabs are heavier and provide greater confining pressures for subgrades. A 20-inch thick slab develops double the subgrade confining pressure that a 10-inch thick slab develops. This trend may also reflect that thicker base and subbase layers are generally used for thicker slabs resulting in stiffer conditions for thicker slabs. Typical test sites had slab support ratio

values just below 0.5. The two sites having high slab support ratio values were either frozen or had unusually large down-warp. The one site having a low slab support ratio was the site having unusually large curling response and significant upward warp. It should be assumed that after the joints have cracked open, the overall average slab support ratio will be about 0.5 when using the Skarlatos/Ioannides slab edge model, and this value will probably drop over time.

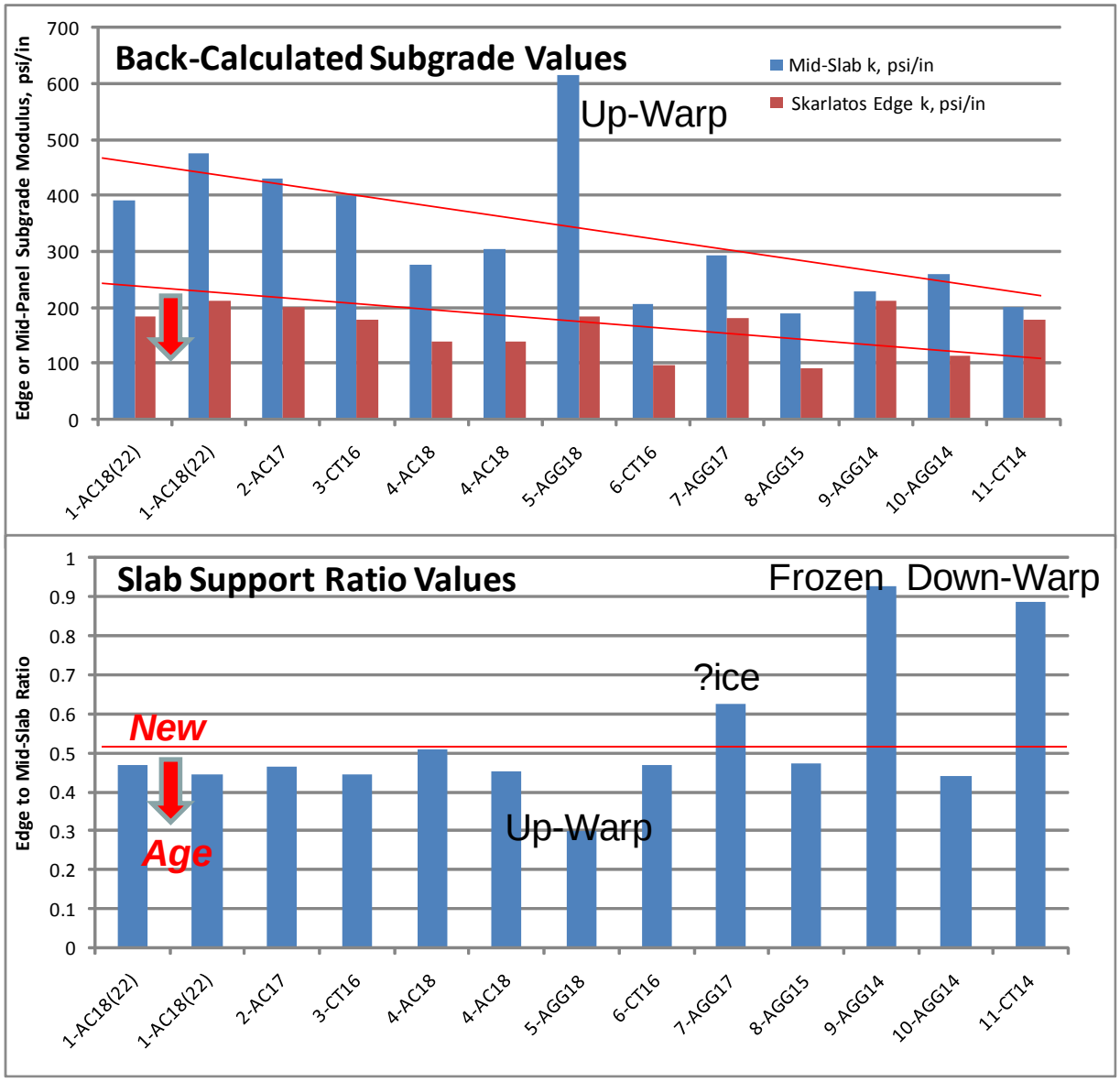

FIGURE 5.2. THE GENERAL TRENDS RESULTING IN THE RECOMMENDATIONS FOR THE SIMPLIFIED APPROACH SKARLATOS/IOANNIDES TREND SHAPES

The Skarlatos/Ioannides LTE_{δ} versus *log(f)* regression formula is used to establish the characteristic joint stiffness versus LTE_{δ} curve for a site. The Skarlatos/Ioannides edge solution regression form used is as follows:

$$LTE_{\delta} = \frac{1}{1 + \log^{-1}\left[\dfrac{0.214 - 0.183\left(\dfrac{\varepsilon}{\ell}\right) - \log f}{1.180}\right]} \quad (29)$$

Statistics: $R^2 = 1.0$; $SEE = 0.0070$; $n = 405$.

Where,

$$f = \frac{q_0}{k\ell} = \frac{\text{AGG}}{k\ell}$$

k_J = AGG = q_0 = joint stiffness, lb/in/in
ε = wheel load radius, inches
ℓ = pavement radius of relative stiffness, inches
k = modulus of subgrade reaction, psi/in

The recommended calibrated slab edge *k*-values for the three curves in figure 5.1 and to be used in the simplified approach, when only an estimate of slab thickness is available, are shown in figure 5.3. Use of this trend line will simulate newer pavement conditions and slightly higher slab support ratio values than observed at the in-service test sites. Aging and loss of support will reduce effective slab support ratios.

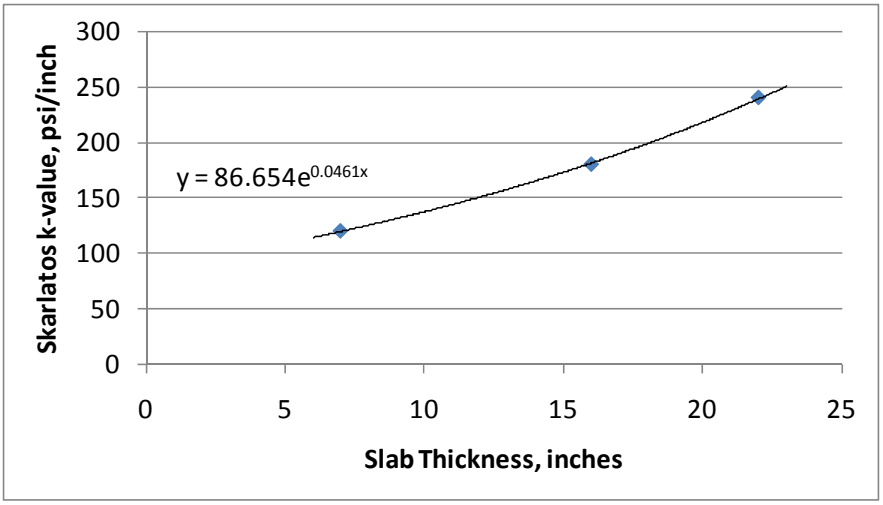

FIGURE 5.3. THE CALIBRATED SKARLATOS/IOANNIDES SOLUTION SUBGRADE *K*-VALUES FOR ESTABLISHING THE CHARACTERISTIC JOINT STIFFNESS CURVE FOR A SITE FOR EARLY-LIFE CONDITIONS AND USING ONLY SLAB THICKNESS AS INPUT

To use the simplified approach with a pre-existing data set of LTE_δ values from a test site of known thickness, the inverted form of the Skarlatos/Ioannides edge response solution shown below can be used, along with the recommended slab edge *k*-values shown in figure 5.3, to convert all FWD LTE_δ values into estimated joint stiffness values. If the ILLI-BACK mid-panel modulus of subgrade reaction *k*-value and slab elastic modulus averages are available from a pre-existing FWD data set, a refined estimate of the characteristic joint stiffness curve can be obtained by using 0.45 times the ILLI-BACK mid-panel modulus of subgrade reaction value along with the ILLI-BACK concrete slab elastic modulus value and best estimate of slab thickness as the input to the Skarlatos/Ioannides edge response solution. This general procedure is the same as the joint stiffness backcalculation routine developed by Ioannides et al. 1996 with one key refinement. The refinement is the use of a reduced Skarlatos/Ioannides slab edge *k*-value accounting for the slab support ratio values calculated from the test sites. Use of this overall average 0.45 reduction factor for edge support was required to force the Skarlatos/Ioannides solution joint stiffness estimates to match the calculated joint stiffness values from the FWD, and as related to the ILLI-BACK backcalculated mid-panel modulus of subgrade reaction. The 0.45 is approximately the average slab support ratio for the full airfield test sites evaluated and shown in figure 4.6. The actual ratio may vary from about 0.2 for large loss of support, to 0.9 for uncracked/frozen/locked joint conditions with good edge support.

$$\log f = \left[0.434829\left(\frac{\epsilon}{l}\right) - 1.23556\right]\log\left(\frac{1}{LTE_\delta} - 1\right) + 0.295205$$

Statistics: $R^2 = 0.995$; $SEE = 0.1661$; $n = 405$. (30)

Another recommended control for joint stiffness evaluation is quantification of the apparent upper boundary of total joint stiffness that is related to a joint being either not fully cracked or being compressed tightly closed, behaving uncracked and near the asymptote for the joint stiffness curve. In this study, the LTE_δ calculations were performed on joints and on mid-panel FWD load test data. The LTE_δ analysis of mid-panel data sets an upper boundary. Joint load tests that look like mid-panel load tests must be considered to be possibly locked or uncracked. When short slab lengths are used, the chances of having joints that never crack is relatively high and apparent uncracked joints were common at airfield sites. Because the typical trend shape for joint stiffness versus LTE_δ becomes asymptotic at high LTE_δ values, stiffness estimates for possible locked or uncracked joints are extremely high relative to the range encountered for functioning joints that do not have large bending moment transfer occurring. When bending moment is mobilized through a joint that is locked or compressed shut, it makes the theoretical linear joint stiffness appear very high, but in reality line stiffness is now no longer the only load transfer mechanism at work. It is very important to remove these extremely high calculated stiffness values from the statistics so as not to skew the frequency distributions of joint stiffness values dramatically. It is more important to summarize the statistics for the joints that are performing below this threshold and to report the percentage of possibly locked/uncracked joints above this threshold. The overall site average LTE_δ values for mid-panel load tests ranged from about 86 to 90%, generally being lower for stiffer foundations and flatter slabs. Also, FWD

testing on hot days tended to reveal lower LTE_{δ} for mid-panel tests, and lower backcalculated concrete elastic modulus values. Figure 5.4 presents the recommended upper limits for joint stiffness for joint designs. This data was established by evaluating the shapes of predicted LTE_{δ} versus joint stiffness curves and values present near the joint lock-up condition occurring at high LTE_{δ} values. It should be assumed that shortly after construction, a significant percentage of joints will rapidly fall just below the "new working joint" threshold line. The first joints to open will probably have larger joint openings and corresponding lower joint stiffness for the full life of the pavement.

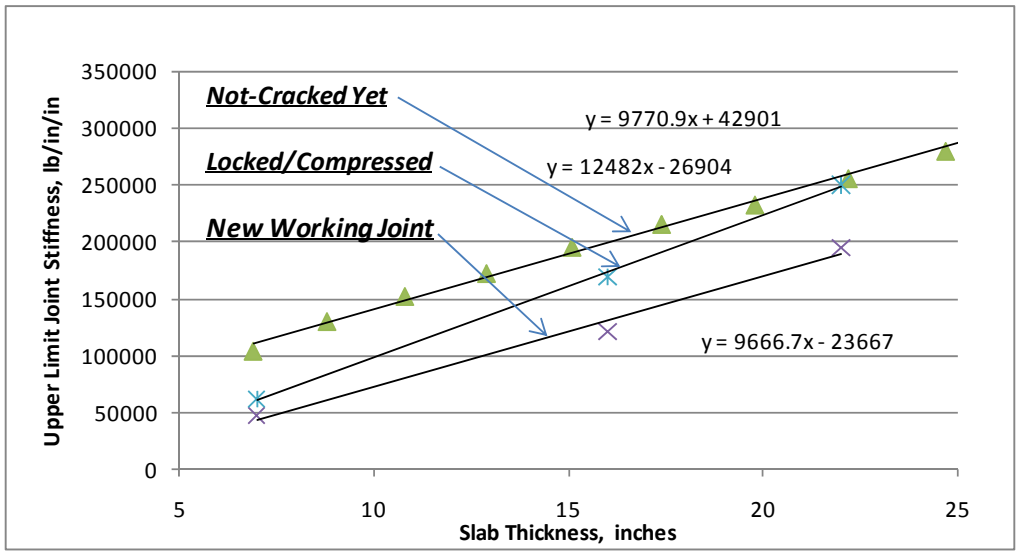

FIGURE 5.4. RECOMMENDED UPPER LIMITS FOR TOTAL JOINT STIFFNESS

In summary, the simplified approach allows an existing FWD data set of measured LTE_{δ} values to be used with the site slab thickness to estimate the sites characteristic joint response curve and distribution of apparent joint stiffness values, and apparent locked and uncracked thresholds. Or it can be used as a design scheme related to joint stiffness asumptions in a structural analysis routine. For joint stiffness values above the upper limit recommendations for locked or uncracked joints, joint line stiffness is no longer the primary load transfer mechanism. This method is a "simplified calibrated" version of the procedure developed by Ioannides et al. 1996 with the calibrations being the reduced slab edge support *k*-value of 0.4 to 0.5 times the mid-panel ILLI-BACK value, and the upper limit cut-off recommendations. The simplified form only needs slab thickness to generate a characteristic joint stiffness curve and the threshold values for a conceptual pavement design. If more detailed information from a test site such as slab thickness, elastic modulus, and mid-panel FWD ILLI-BACK results are available, using the Skarlatos/Ioannides curve with a slab edge *k*-value of about 0.45 times the mid-slab backcalculated subgrade *k*-value will give a better estimate of the site characteristic joint stiffness versus LTE_{δ} curve, without actually calculating the joint stiffness values directly.

5.2 THE DETAILED CALIBRATED JOINT BEHAVIOR MODEL

The characteristic joint stiffnes versus LTE_δ curve for a given pavement cross section is primarily a function of the thickness and stiffness of the pavement layers and is not much affected by joint types or other design parameters. Climate related joint opening changes will cause the LTE_δ of aggregate interlock joints to vary considerably causing the joint stiffness magnitude to drift back and forth along nearly the full shape of the characteristic joint response curve from summer to winter. Adding dowels will keep LTE_δ higher during winter, resulting in less movement back and forth along the characteristic joint stiffness curve. A more comprehensive joint simulation approach was needed to demonstrate the temperature and aging effects observed at the test sites.

Figures 5.5 and 5.6 show data from site DIA-CT18 that provide the control basis for the detailed comprehensive joint behavior model aggregate interlock loss rate as a function of temperature (Rufino, et al., 2004). Past research has shown the LTE_δ tends to have a relatively linear rate of change with respect to average slab temperature with slope $d(LTE_\delta)/dT$. The loss rate is related primarily to slab length and roughness/tortuosity of the crack face aggregate interlock surface. A rough crack face or a short slab will have a flatter LTE_δ versus temperature slope, while a smooth face or long slab will have a very steep slope, or sudden release with slab thermal contraction. Age and traffic effects will essentially grind joint faces smoother causing a flattening of the temperature response slope for a given joint. The T_{Lock} temperature is the point at which the joint face completely compresses shut and full joint stiffness is mobilized. Additional thermal joint compression beyond the lock point can result in the joint behaving as if it was not cracked, behaving just as a mid-panel load test would, with bending moment being transferred through the joint face. In general, if the compression pre-load strain at the joint face is equal to or greater than the tensile strain at the bottom of slab during loading, then no bending moment reduction occurs along the crack line. The bottom of the joint must physically open in order for joint deflections to increase beyond those of a mid-panel load. Continued slab shrinkage with age, and grinding of the joint face will cause an increase in the T_{Lock} temperature. The $T_{Release}$ temperature is the point at which the joint faces no longer have shear contact during joint deflections. The comprehensive joint behavior model yields the T_{Lock} and $T_{Release}$ temperatures and the LTE_δ loss rate slope for a given aggregate interlock joint design and uses a "calibrated" FAA doweled joint stiffness equation combined with the aggregate interlock algorithm to simulate dowel effects. The Skarlatos/Ioannides edge best-fit curves previously described are then matched to the linear LTE_δ versus temperature trends established for a joint design to estimate joint stiffness trends as a function of slab temperature. These joint stiffness versus slab temperature trends can then be used in any sort of advanced analysis tools such as FEAFAA or ILSL2 as a basis of design and analysis to establish load transfer, LT as a function of slab temperature.

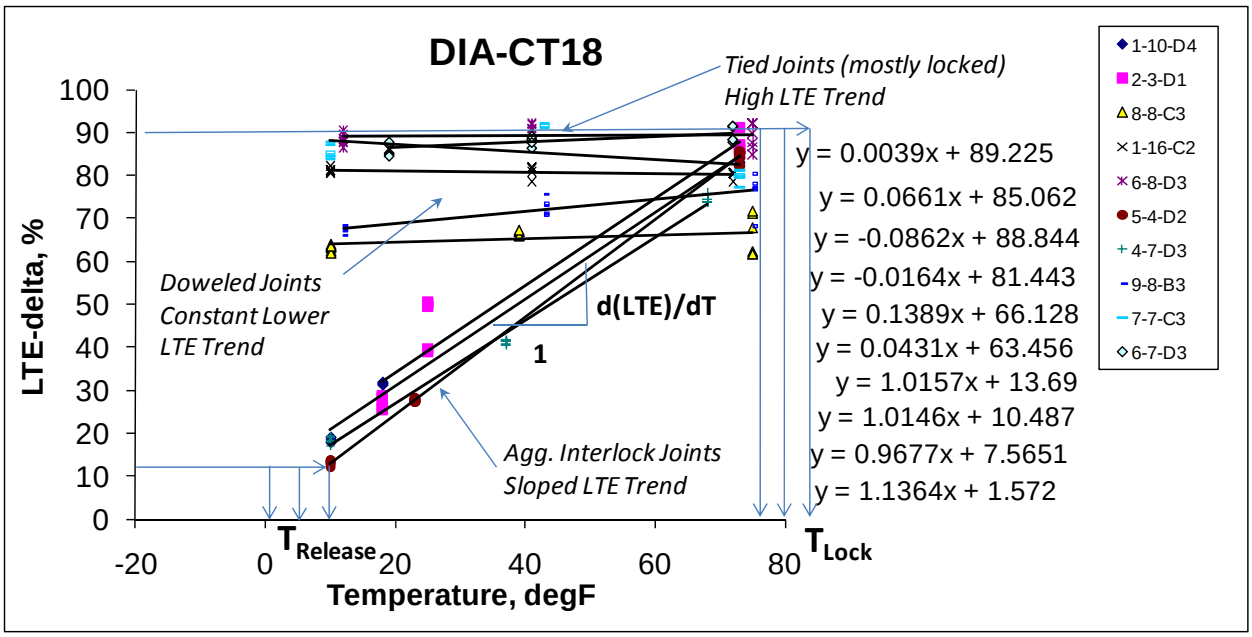

FIGURE 5.5. THE LINEAR TEMPERATURE VERSUS LTE_{δ} RELATION USED AS THE BASIS FOR ESTIMATION OF THE AGGREGATE INTERLOCK COMPONENT OF JOINT STIFFNESS FOR A JOINT DESIGN, WITH THE CONCEPTS OF T_{Lock} , $T_{Release}$ AND LTE_{δ} LOSS RATE SLOPE $d(LTE_{\delta})/dT$

The DIA aggregate interlock joints described in figure 5.5 were also instrumented with joint opening measurement gages (Rufino et al. 2004). Figure 5.6 shows DIA aggregate interlock joint opening size data for one of the joints shown in figure 5.5. Combining these two plots allows a very precise estimate of the apparent loss in LTE_{δ} as a function of joint opening for aggregate interlock joints at the DIA test site. This LTE_{δ} loss rate as a function of joint opening size is a key aggregate interlock joint behavior parameter.

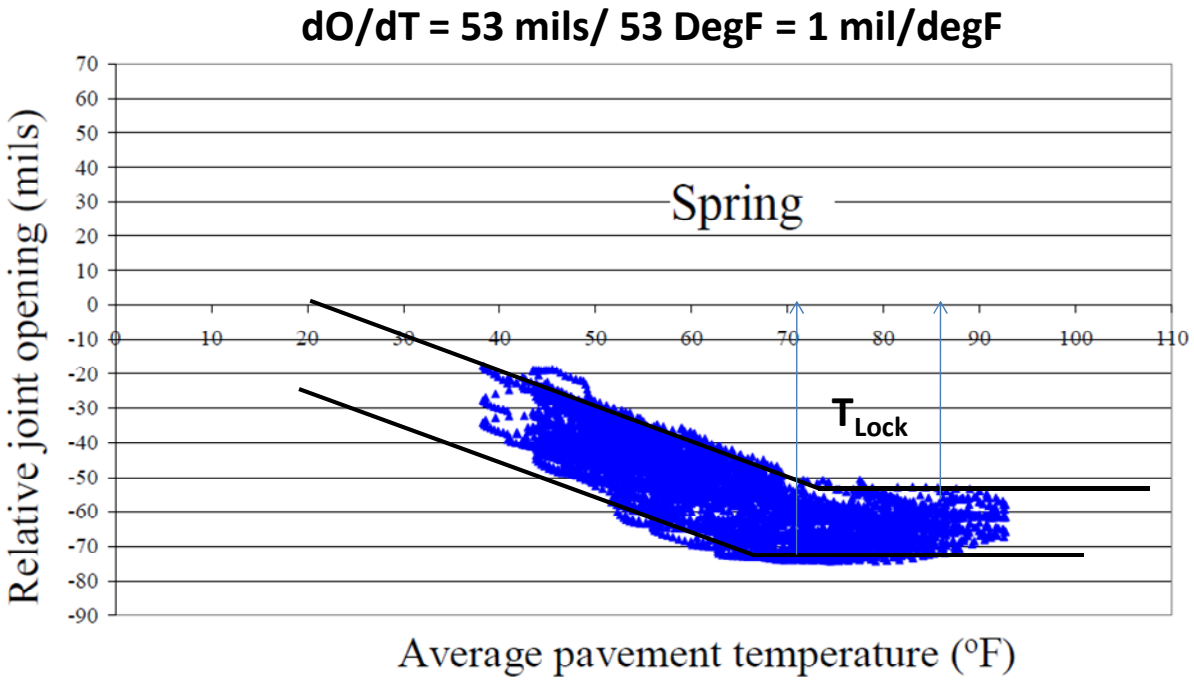

FIGURE 5.6. MEASUREMENTS OF JOINT OPENING (RUFINO ET AL., 2004) FOR ONE OF THE AGGREGATE INTERLOCK JOINTS SHOWN IN FIGURE 5.4, ALONG WITH DATA OVERLAID SHOWING THE RATE OF JOINT OPENING CHANGE, dO/dT

The generally constant $d(LTE_\delta)/dT$ slope can be divided by the generally constant dO/dT slope to get the variable $d(LTE_\delta)/dO$. This is a key parameter, $d(LTE_\delta)/dO$, for the DIA aggregate interlock joints and represents a precise measurement of loss in LTE_δ with respect to change in joint opening size. At DIA, the aggregate interlock joints experienced approximately 0.9 to 1.3 percentage point loss in LTE_δ for each 1 mil increase in joint opening. For purposes of this research, a loss rate of 1.3 LTE_δ percentage for each 1 mil of joint opening is considered an average typical loss rate for normal sawed joint natural crack face conditions. The dO/dT parameter is related to slab length. Short slabs have small dO/dT and long slabs have large dO/dT. If, for example, longer slabs had been used at DIA, the $d(LTE_\delta)/dT$ slope in figure 5.5 would be steeper because joints would open faster. In addition, the lock-up temperature would probably be higher for longer slabs due to higher initial-shrinkage related joint opening size. A pre-existing algorithm for joint opening size estimation was needed to develop a comprehensive joint behavior model.

The Michigan Department of Transportation (MDOT) performed an extensive joint opening size study in the mid 1900s. Caliper pins were cast into many joints and monitored over a 17 year period. Figure 5.7 presents their final joint opening estimation algorithm. This algorithm can be used to calculate a dO/dT for any given slab length for the range of temperatures evaluated, and turned into a unique line for dO/dT as a function of slab length. The MDOT algorithm is unique to the subgrade drag and concrete thermal expansion coefficients that were present at the test sites used for the study. This unique line is presented in figure 5.8 and compared to the joint opening model contained in the Mechanistic Empirical Pavement Design Guide (MEPDG) for

highway pavement thickness designs (Khazanovich and Gotliff, 2003). Relative to the MEPDG curve, the MDOT trend shape is assuming that smaller friction coefficients would be present for shorter slabs on a given foundation, where as the MEPDG curve assumes constant level of mobilized base-to-slab friction regardless of slab length. Now compare the measured *d*O/*d*T from DIA in figure 5.6 to the calculated *d*O/*d*T from the MDOT and MEPDG joint opening algorithms for a 20-ft slab length. Both algorithms adequately reproduce the *d*O/*d*T measured at DIA. In the context of the MEPDG lines, the MDOT algorithm is assuming a friction factor ranging from about 0.6 for 10-ft slabs to about 0.85 for 30-ft slabs. It would be expected that shorter slabs would not mobilize as much base friction as longer slabs because the amount of thermal movement increases as a function of distance from mid-slab and the middle portions of the slabs do not move. Plotted in this way, the MEPDG curve backcalculates apparent slab to base friction factors of about 0.75 to 0.95 for the DIA *d*O/*d*T values between about 0.9 and 1.3 mil/°F encountered on a treated base. These values are higher than those recommended in MEPDG for use on treated bases (0.65). The MDOT joint opening algorithm has been incorporated into the new comprehensive joint stiffness simulation approach. Simlar to the MEPDG concept, the MDOT trend line can be rotated about the origin slightly to account for apparent higher or lower concrete coefficient of thermal expansion and/or base friction effects.

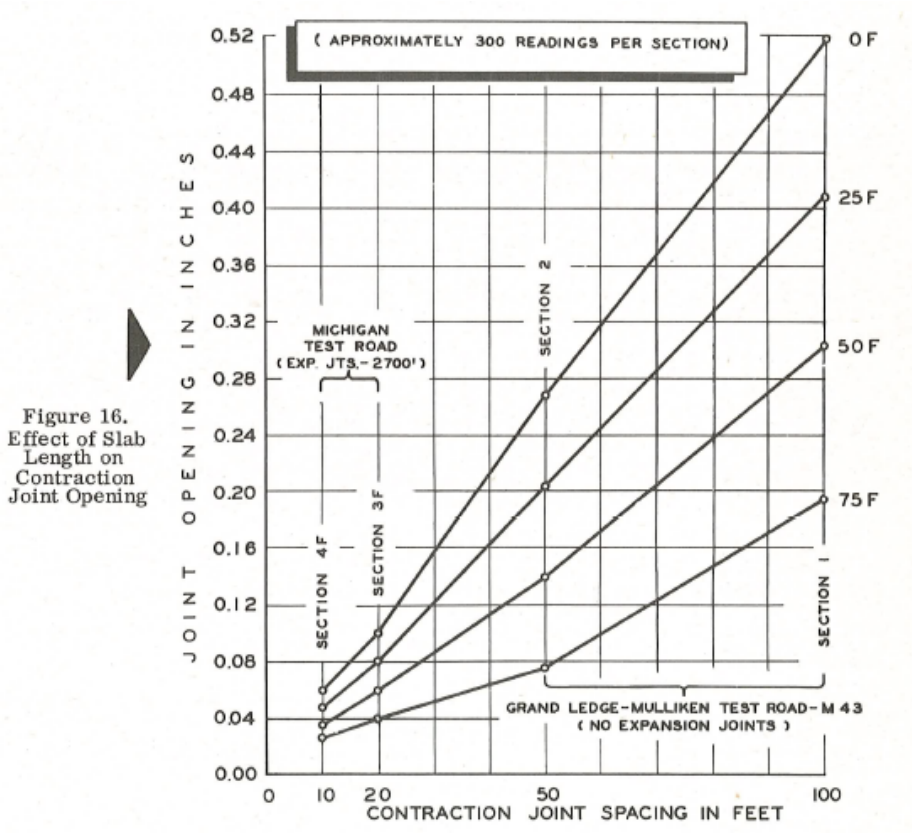

Figure 16. Effect of Slab Length on Contraction Joint Opening

(Finney and Oehler 1959).

FIGURE 5.7. THE MDOT JOINT OPENING ALGORITHM

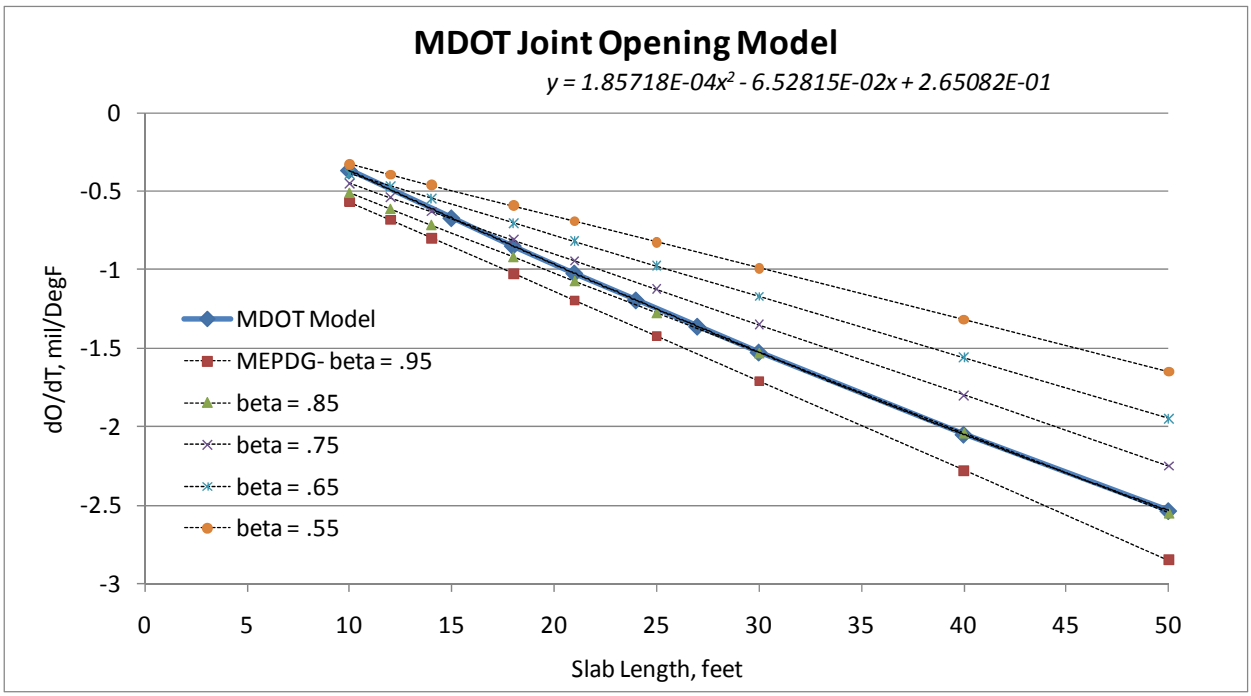

FIGURE 5.8. THE UNIQUE *d*O/*d*T FUNCTION FROM THE MDOT JOINT OPENING ALGORITHM, AS COMPARED TO THE MEPDG ALGORITHM FOR VARYING SLAB TO BASE FRICTION COEFFICIENTS (BETA VALUES)

The following expression suitably yields the absolute joint opening size trends plotted by MDOT researchers in figure 5.7, as a function of slab length and temperature.

$$\textbf{Joint Opening} = A(\text{slab length})^2 + B(\text{slab length}) + C$$

where,

$A = 7.42165E\text{-}10x^2 + 1.11501E\text{-}07x + 3.31260E\text{-}07$

$B = -1.12539E\text{-}07x^2 - 5.40276E\text{-}05x + 5.06279E\text{-}03$

$C = 2.05231E\text{-}06x^2 + 5.98515E\text{-}05x + 9.24817E\text{-}03$

X = temperature, deg F (31)

*slab length in feet

*joint opening in inches

The detailed measurements at DIA form the model's assumed basis for typical $d(LTE_\delta)/dO$ for aggregate interlock, and the 17 years of measurements by MDOT form the basis of the model's assumed dO/dT as a function of slab length. These two expressions are divided to obtain $d(LTE_\delta)/dT$ for a joint design. The model allows dO/dT to be adjusted proportionally for varying coefficients of thermal expansion, about a typical mean of 0.00005 in/in/°F. The model allows $d(LTE_\delta)/dO$ to be adjusted slightly about the mean value based on a concrete toughness and durability factors ranging from 1 to 10. Figure 5.9 shows the joint behavior presentation scheme used for the final comprehensive joint behavior model. Figure 5.10 shows the required input for the model. These figures represent the calibrated DIA joint behavior curves. The input

data is used to set the T_{Lock} and $T_{Release}$ temperatures and LTE_{δ} temperature loss slope for a given joint design. Both a "new condition" and "end-of-life condition" state are simulated. The new condition simulation in this example matches closely the measured data from DIA, which was obtained when the pavement was relatively young. The LTE_{δ} versus temperature trends used as control points are then converted to joint stiffness versus temperature trends using the calibrated Skarlatos/Ioannides edge formulae. The following form of the Skarlatos/Ioannides edge solution (Ioaniddes et al. 1996) is used to convert LTE_{δ} versus temperature estimates into joint stiffness versus temperature estimates:

$$\log f = \left[0.434829\left(\frac{\epsilon}{l}\right) - 1.23556\right]\log\left(\frac{1}{LTE_{\delta}} - 1\right) + 0.295205$$

Statistics: $R^2 = 0.995$; $SEE = 0.1661$; $n = 405$. (32)

The solid lines in the lower plot in figure 5.9 represent aggregate interlock joints, while the dashed lines represent doweled joint behavior. In cold temperatures, doweled joint stiffness is controlled by the dowel component of total stiffness, while the aggregate interlock component drops to zero for fully open joints. The dowel component of total joint stiffness is computed using the following formula, which is also used in the FEAFAA FEM software:

$$k_{J-D/s} = \frac{1}{s\left(\frac{\varpi}{0.9G_dA_d} + \frac{\varpi^3}{12E_dI_d} + \frac{2+\beta\varpi}{2\beta^3E_dI_d}\right)} \quad (33)$$

Where: s is the dowel bar spacing, ω is the joint opening, A_d is the dowel cross-sectional area, and E_d, G_d, and I_d are the Young's modulus, shear modulus and moment of inertia of the dowel bar, respectively, d is the bar diameter, and K is the mysterious "Modulus of Dowel-Concrete Interaction" between the bar and the concrete. The variable β is defined as:

$$\beta = \sqrt[4]{\frac{Kd}{4E_dI_d}} \quad (34)$$

In general, E_d = 29 million psi for steel dowels. The modulus of dowel-concrete interaction K used to simulate new conditions in the comprehensive joint model starts out at a value equal to 5 million psi or the elastic modulus of the concrete, whichever is greater. The K value assumed for the aged end-of-life condition simulation reflects the dowel-concrete interaction backcalculation results from this study. The dowel-concrete interaction factor is reduced based on the traffic and durability factors in the formula input. Higher traffic and low durability factors result in more loss of dowel-concrete interaction modulus, down to low levels similar to those backcalculated for old worn joints. It is not known at this point precisely how these aging trends develop as a

function of time, only that the measurements revealed that significant losses are occurring. Many in-service doweled joints had low backcalculated modulus of dowel support values of 1 million psi or less.

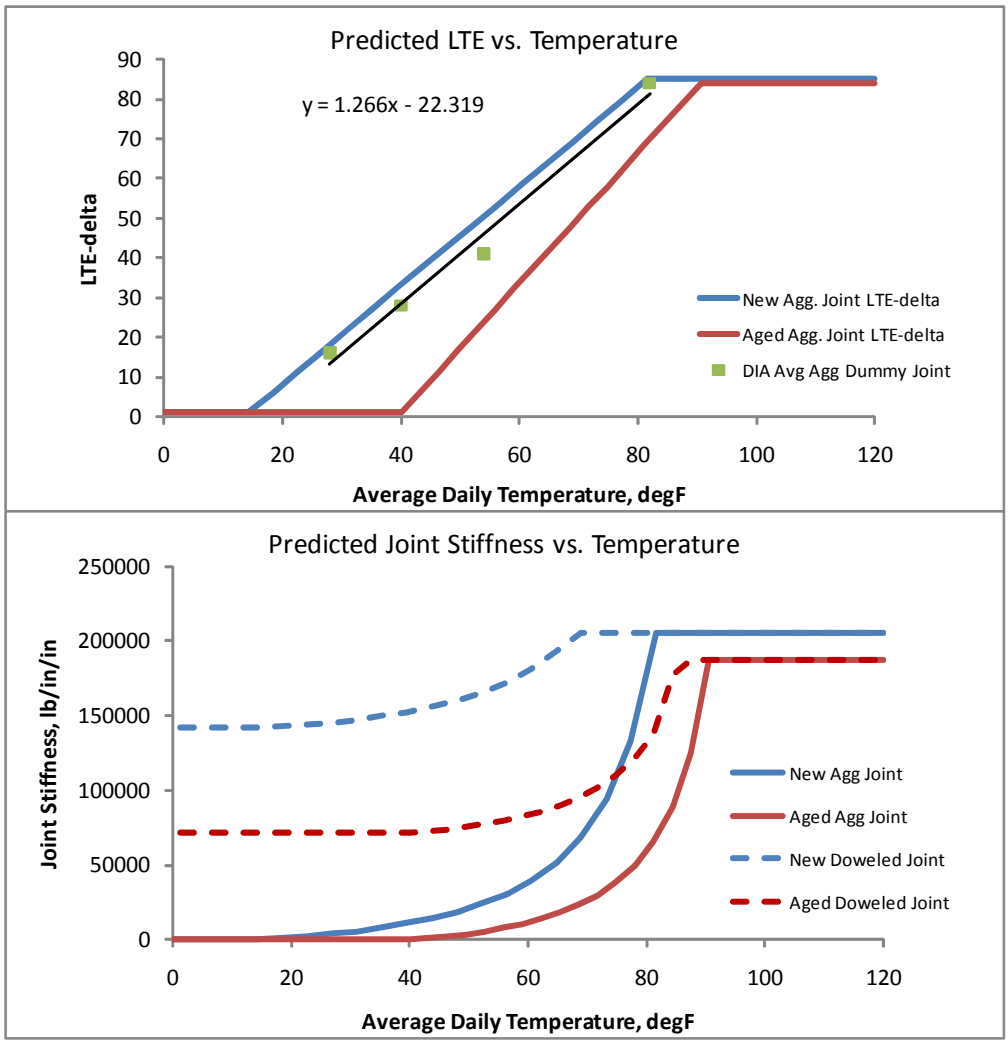

FIGURE 5.9. THE COMPREHENSIVE JOINT MODEL PREDICTS LTE_{δ} AS A FUNCTION OF SLAB TEMPERATURE AND THEN USES THE CALIBRATED SKARLATOS/IOANNIDES EDGE SOLUTION AND THE FAA DOWELED JOINT FORMULA TO ESTABLISH JOINT STIFFNESS VERSUS TEMPERATURE FOR DOWELED AND AGGREGATE INTERLOCK JOINT DESIGNS

INPUT PARAMETERS		
Traffic Factor (1=low, 2= med, 3=high) =	2	
Slab Thickness, inches =	18	
Slab Elastic Modulus, psi =	5000000	
Mid-Panel FWD Subgrade k. psi/in =	450	
Slab Length, ft =	20	
Avg. Slab Temp 1st 5-days, degF =	65	
Annual Precip, inches =	28	
Shrinkage Factor, 1 = low to 10 = high	5	
Crack Toughness, 1 = low to 10 = high	5	
Thermal Coefficient, in/in/degF =	0.000005	
Summer Max. Daily Avg Temp =	75	
Winter Min. Daily Avg Temp =	25	
Daily Change in Avg. Slab Temp =	5	
Dowel diameter, inches =	1.5	
Dowel Spacing, inches =	18	
Initial Dowel DCI =	5,000,000	
Final Dowel DCI =	2,000,000	
	Avg Temp	**LTE**
Age = 0 Lock-up Temp, degF =	81.6	85
Age = 0 Release Temp, degF =	14.2	1
End-of-Life Lock-up Temp, degF =	90.6	84
End-of-Life Release Temp, degF =	40.1	1
New Joints		
mils to release =	65.1	
MDOT Model dO/dT =	-0.00097	
Temp Diff to Release =	-67.4	
Old Worn Joints		
mils to release	48.8	
MDOT Model dO/dT =	-0.00097	
Temp Diff to Release =	-50.5	

FIGURE 5.10. THE INPUT REQUIRED FOR THE COMPREHENSIVE JOINT BEHAVIOR MODEL, WHERE SHADED VALUES ARE USER INPUTS AND THE NON-SHADED VALUES ARE CALCULATED CONTROL POINTS FOR THE BEHAVIOR SIMULATION

There are some arbitrary miscellaneous relations used in the detailed joint behavior model that allow sensitivity analysis for certain variables within known ranges. For example, the following relations are used to estimate the joint lock-up temperatures:

New Condition: $T_{Lock\text{-}1} = T_{Ref} + 15(f_{sh}/5) + 0.08(\text{Slab Length, feet}),\ °F$ (35)

End-of-Life Condition: $T_{Lock\text{-}20} = T_{Lock\text{-}1} + 5 + 2(f_{trf})$, °F (36)

Where,

T_{Ref} = Estimated average slab temperature present during the first five days after casting, °F
f_{sh} = Shrinkage sensitivity factor, which can be varied, and a value of 5 was set to match DIA behavior and is considered average behavior.
f_{trf} = Traffic rate factor, where values of 1-3 represent the apparent aging loss rates associated with airfield traffic as observed in this study, and higher rates simulate more grinding losses for the crack faces.

The exact relations between these variables and how the lock-up temperature is related to the casting temperature are not known but these relations at least allow sensitivity studies within known ranges of behavior. The above arbitrary relations assume that the lock-up temperature will be about 15 to 20 °F above the average slab temperature present for the first few days after construction, for new and old conditions respectively, and then allow some variations of those values based on known shrinkage and traffic related loss effects. Some additional insights into these behaviors can be obtained through the study of the MEPDG and South African CNC-Pave joint algorithms, where shrinkage has been considered more explicitly in the joint behavior simulations.

Once the joint lock-up temperatures are estimated for a given pavement design, the temperature change required to reach a fully open joint condition, or release temperature ($T_{Release}$) is estimated. This is accomplished first by estimating the dO/dT rate for the design as follows:

$$dO/dT = [(0.000000185717)L^2\text{-}(0.0000652815)L\text{+}(0.000265082)]*(\alpha_c)/0.000005, \text{ in/°F} \quad (37)$$

where,

dO/dT = Joint opening rate, in/°F
L = Slab length, feet.
α_c = The coefficient of thermal expansion of the concrete slab, in/in/°F

The estimated total joint opening required to go from locked to fully released/open states is then estimated using the LTE_δ values at lock-up and release and using the overall average $dLTE_\delta/dO$ values measured at DIA as follows:

New Condition, mils to release =

$$[(\text{Lock } LTE_\delta) - (\text{Release } LTE_\delta)]/1.3 \quad (38)$$

End-of-Life, mils to release =

$$[(\text{Lock } LTE_\delta) - (\text{Release } LTE_\delta) - 5f_{trf} - 10(5\text{-}f_{toughness})]/1.3 \quad (39)$$

The value of 1.3 is the measured value of $d\text{LTE}_\delta/d\text{O}$ obtained from embedded joint opening sensors and temperature measurements at DIA for aggregate interlock contraction joints. For estimation purposes, this relatively precise DIA measured value is considered a mean value of LTE_δ loss with respect to joint opening size for saw-cut type aggregate interlock joint faces. The mils-to-release values are then divided by the $d\text{O}/d\text{T}$ values to get the estimates of the temperature change magnitudes required to transition from locked to fully released conditions. These temperature change values are then subtracted from the T_{Lock} values to get the $T_{Release}$ values for new and old conditions.

As shown earlier, the dowel-concrete interaction modulus value obviously deteriorates over time, but the rate in which it deteriorates over time is not known. The model relation will set the DCI value equal to the concrete elastic modulus for new conditions, and will drop the DCI value to as low as 0.1 times the concrete elastic modulus at the end of life for higher traffic factors. DCI values as low as this were observed at the test sites. The final end-of-life value for the dowel concrete interaction modulus value is the maximum of the following two expressions:

1. Absolute Lower Limit DCI = $(E_c)/10$, psi/in (40)
2. $\text{DCI} = E_c - 700{,}000(f_{trf}) - 10{,}000{,}000/(f_{toughness})$, psi/in

Where,

DCI = Modulus of dowel concrete interaction, psi/in

$f_{toughness}$ = A sensitivity parameter varying between 1 and 10 and representing the fact that durability of aggregate interlock and dowel-to-concrete interaction surfaces will vary based on aggregate types used, actual service level dowel bearing stresses, and overall concrete strength.

E_c = The concrete slab elastic modulus value, psi

In order to show apparent daily and seasonal characteristic LTE_δ versus joint stiffness trends for a given pavement design section and joint spacing, the model plots LTE_δ as a function of an assumed annual average slab temperature profile and assumed daily variation in slab average temperature. A simple sine-wave yearly temperature simulation is used here for demonstration purposes, but any temperature profile shape can be used. The average annual daily air temperature profiles for all test sites are provided in Appendix A. Figures 5.11 and 5.12 show the simulated temperature profile data, and the DIA estimated aggregate interlock joint LTE_δ versus slab temperature functions for new and old joint conditions over a simulated 1-yr thermal cycle.

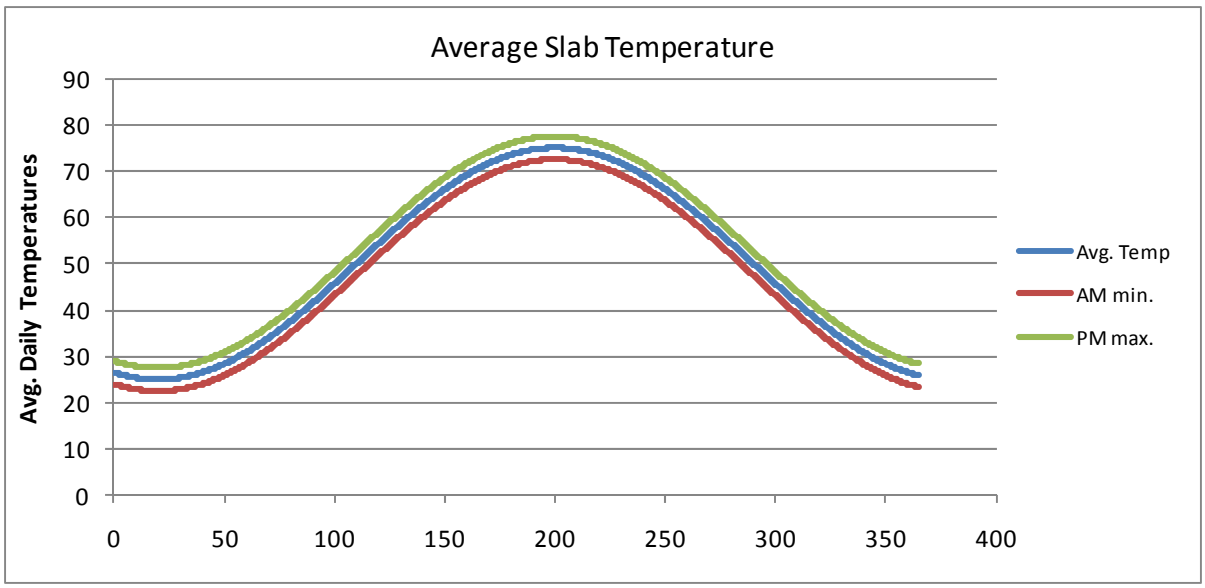

FIGURE 5.11. A SIMULATED 365-DAY SINE-WAVE AVERAGE SLAB TEMPERATURE PROFILE USED IN THE DETAILED JOINT BEHAVIOR MODEL EXAMPLE PROBLEM

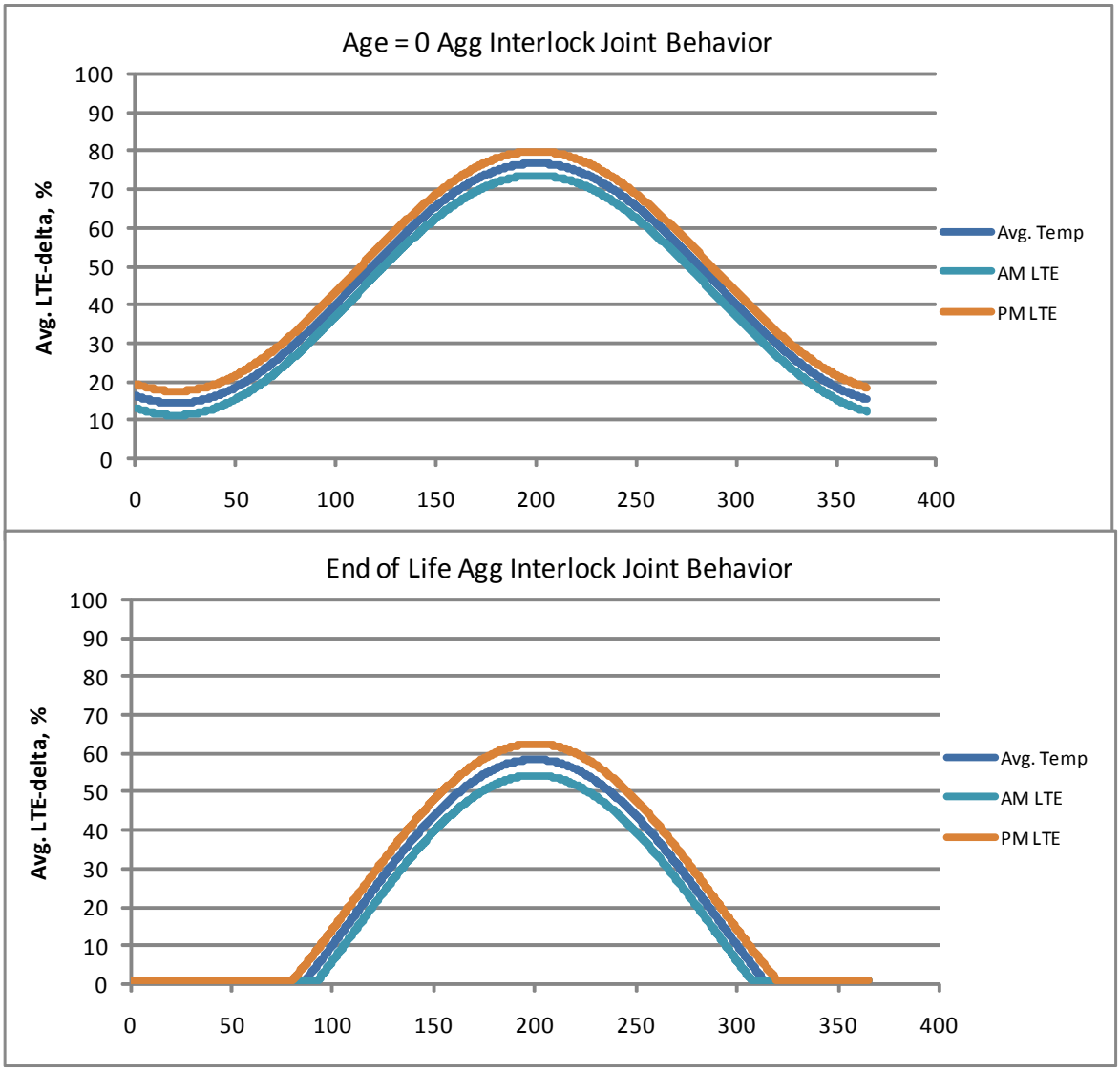

FIGURE 5.12. THE LTE_{δ} TRENDS ESTIMATED FOR BEGINNING AND END OF LIFE FOR THE AGGREGATE INTERLOCK JOINTS IN THE CALIBRATED DIA JOINT MODEL FOR SIMULATED 1-YEAR PERIODS

The calibrated Skarlatos/Ioannides edge formulae are used to convert LTE_{δ} versus slab temperature functions into joint stiffness versus slab temperature functions, which are presented for the 365 day thermal cycle. Figure 5.13 represents a simulated annual variation of joint stiffness values for doweled and aggregate interlock joints for a temperature range similar to that at DIA. The new-condition joint results are considered to be a precise estimate of how joint stiffness varies at DIA based on close matches to the measured data from that site in many respects. The end-of-life joint simulation includes projections of how those joints will deteriorate over time. Notice the "flat-top" for the doweled joint stiffness data. This reflects the recommended upper cut-off for total joint stiffness. Based on the DIA slab thickness and joint designs 200,000 lb/in/in is considered the upper cut-off stiffness for a joint with aggregate

interlock closed just at the point of thermal compression lock-up and initiation of significant bending moment transfer through the crack face. Apparent stiffness will continue over the flat top in reflection of the data below it, but the joint should be considered locked/uncracked to where its behavior will not be noticeably different than a mid-panel load test. This flat top represents an upper-limit stiffness recommended for design considerations. It should be assumed that shortly after construction a significant percentage of joints will open substantially and be functioning below this upper cut-off stiffness level. Joint openings appear as a probability distribution around a mean value, with some joints opening much more than others. This explains why there is large variation in joint stiffness measured at all of the test sites, as the joint stiffness is strongly related to joint opening size. The duration of the flat top is the warm summer period when these joints are likely to be locked most of the time. The simulated continuing slab shrinkage, loss of dowel support, and joint face grinding from traffic reduce LTE_{δ} and stiffness over time, with the calculated effects shown in the lower plot.

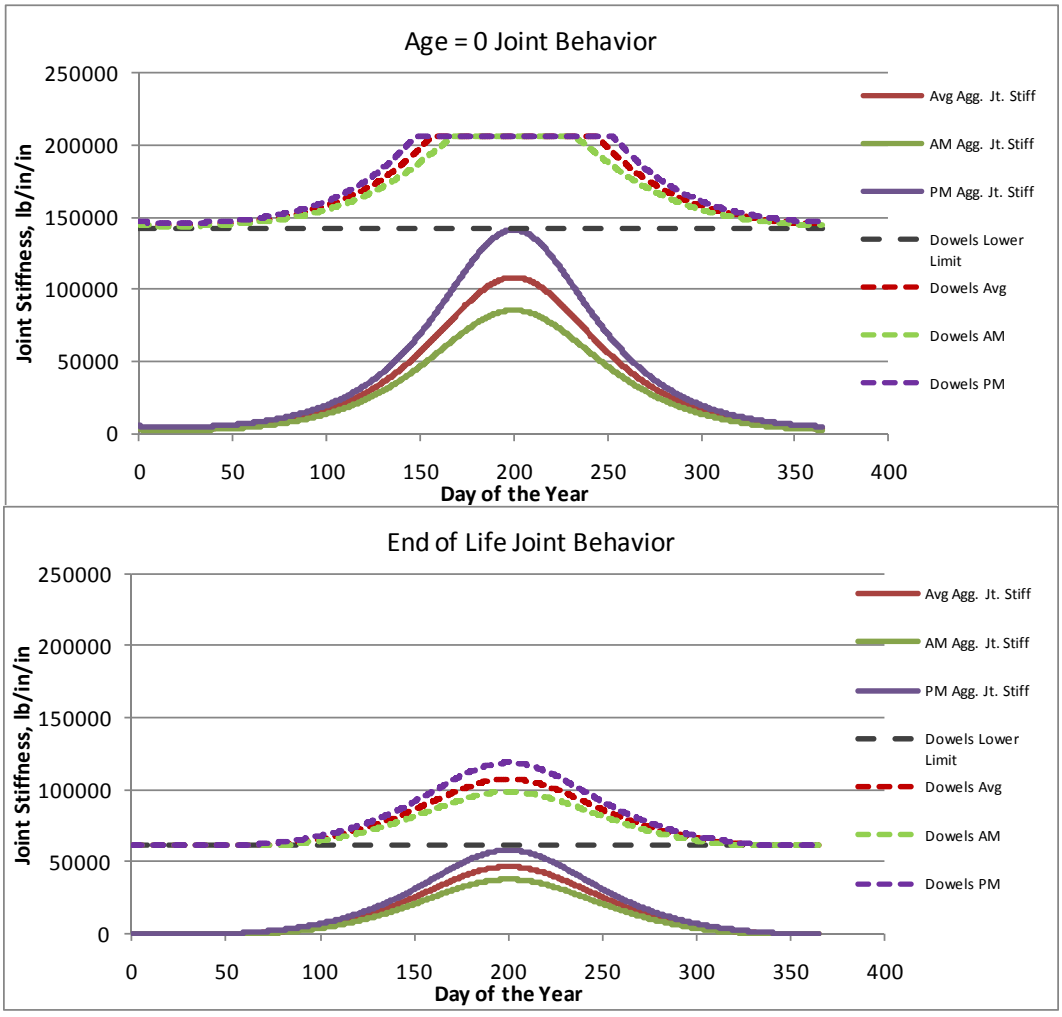

FIGURE 5.13. ESTIMATES OF JOINT STIFFNESS VERSUS TIME OF YEAR FOR DOWELED AND AGGREGATE INTERLOCK CONTRACTION JOINTS USING THE COMPREHENSIVE JOINT BEHAVIOR MODEL

5.3. EXAMPLES AND SENSITIVITY STUDIES

To demonstrate how to use the joint behavior simulations as design tools, figure 5.14 shows joint stiffness measurements from site 2-AC17, along with the simplified model predicted behavior for the site. This airfield had been using a standard 17-inch slab thickness with a standard foundation layering scheme for runways and taxiways at the facility for quite some time, and subgrade is relatively uniform across the site. FWD testing reveals similar mid-panel FWD responses from several jointed concrete pavement areas at this facility. ILLI-BACK mid-panel *k*-values typically are about 400 psi/in at this facility for the standard cross section with concrete elastic modulus values between about 5 and 6 million psi. To estimate the characteristic joint stiffness curve for the standard section, a slab support ratio of 0.5 is assumed (newer conditions) and a slab edge subgrade *k*-value of 200 psi/in is to be used in the Skarlatos/Ioannides solution to estimate the site response for 12-inch diameter FWD loads. This estimate is shown as the thick line in the plot. The three upper limit threshold values (uncracked, locked, working) are shown representing the zone where the joint is closing and substantial bending moment is beginning to transfer through the joint face. If thickness alone were used to get a Skarlatos/Ioannides slab edge *k*-value from figure 5.3, the slab edge value used would be 190 psi/in, along with a default value for elastic modulus of 5,000,000 resulting in approximately the same trend line. The thick line is what would be calculated for Site 2-AC17 without visiting the site and with little site knowledge other than estimated design slab thickness. The fact that the actual measurements are close to the predicted trend-line reflects how well this simplified method using the Skarlatos/Ioannides trend shape confirms the FWD measured joint stiffness versus LTE_{δ} response at the site.

Once the engineer has the estimated characteristic joint stiffness trend line, any previous LTE_{δ} measurements from the standard section can be converted into backcalculated joint stiffness estimates using the Skarlatos/Ioannides edge formula for the site, similar to the Ioannides and Hammons (1996) procedure. Nevertheless, only the direct measurements of joint stiffness versus LTE_{δ} will reveal loss of support and curling effects. This simplified approach places all backcalculated joint stiffness values on the same Skarlatos/Ioannides solution trend line, where as curling can appear as a change in apparent Skarlatos/Ioannides slab edge modulus of subgrade reaction.

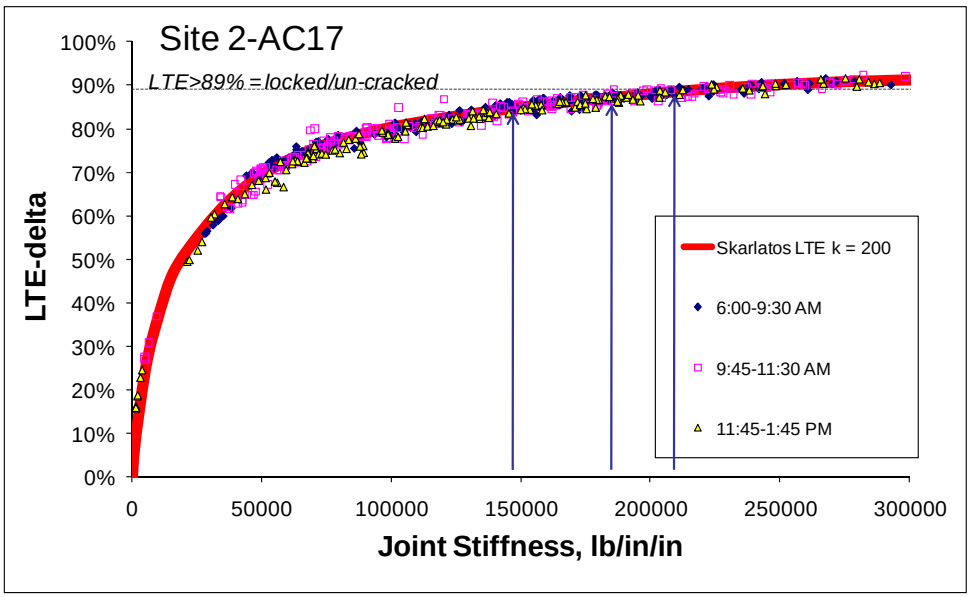

FIGURE 5.14. EXAMPLE APPLICATION OF THE SIMPLIFIED MODEL FOR DEVELOPING A CHARACTERISTIC JOINT STIFFNESS CURVE FOR SITE 2-AC17 DESIGN DATA, AS COMPARED TO THE ACTUAL FWD JOINT STIFFNESS VERSUS LTE_{δ} MEASUREMENTS FROM THE TEST SITE

The characteristic joint stiffness line in figure 5.14 represents the FWD 12-inch diameter load plate response that would probably be observed at the site. The simplified method allows this curve to be established without testing, and used as part of a design analysis for a site.

To further estimate how joints will behave at this site, the detailed joint model is established using the site 2-AC17 design parameters. The behavior determinations are shown in figures 5.15 and 5.16. The details for joint types and slab dimensions for site 2-AC17 are included in Appendix A. The slabs at this site were cast at 25-ft by 25-ft and then intermediate longitudinal saw cuts were placed resulting in 12.5-ft by 25-ft slab dimensions. The transverse joints alternated between doweled and tied-hinge joint details such that joint opening behavior for the doweled transverse joints may have been better associated with 50-ft long panels. All longitudinal joints at this site were tied joints using #6 deformed steel bars. The FWD data indicates that about 23% of the intermediate saw-cut longitudinal joints appeared as uncracked after almost 18 years of service for the 12.5-ft spacing. The average slab temperature during FWD testing probably ranged between about 50 and 55 °F, corresponding approximately to simulated day 275 of a typical year, shown on the x-axis of the example figures. Figure 5.17 shows the actual average joint stiffness values from the site, which can be compared to estimates in figures 5.15 and 5.16 for day 275. The transverse doweled contraction joints are shown to have joint stiffness of about 90,000 to 110,000 lb/in/in with only a small amount from aggregate interlock. The directly calculated values average between about 70,000 to 80,000 lb/in/in indicating slightly more loss in dowel-concrete interaction modulus.

Figure 5.16 shows the simulated behavior for the tied longitudinal joints having 12.5-ft spacing. The estimated range of joint stiffness is between about 120,000 and 160,000 lb/in/in near day

275. The steel tie-bar component of stiffness is estimated to be about 50,000 lb/in/in. Therefore, the remaining 70,000 to 110,000 lb/in/in joint stiffness is attributed to aggregate interlock. The overall average tie-bar joint stiffness values ranged from about 110,000 to 150,000 lb/in/in, reproduced well by the detailed joint behavior model.

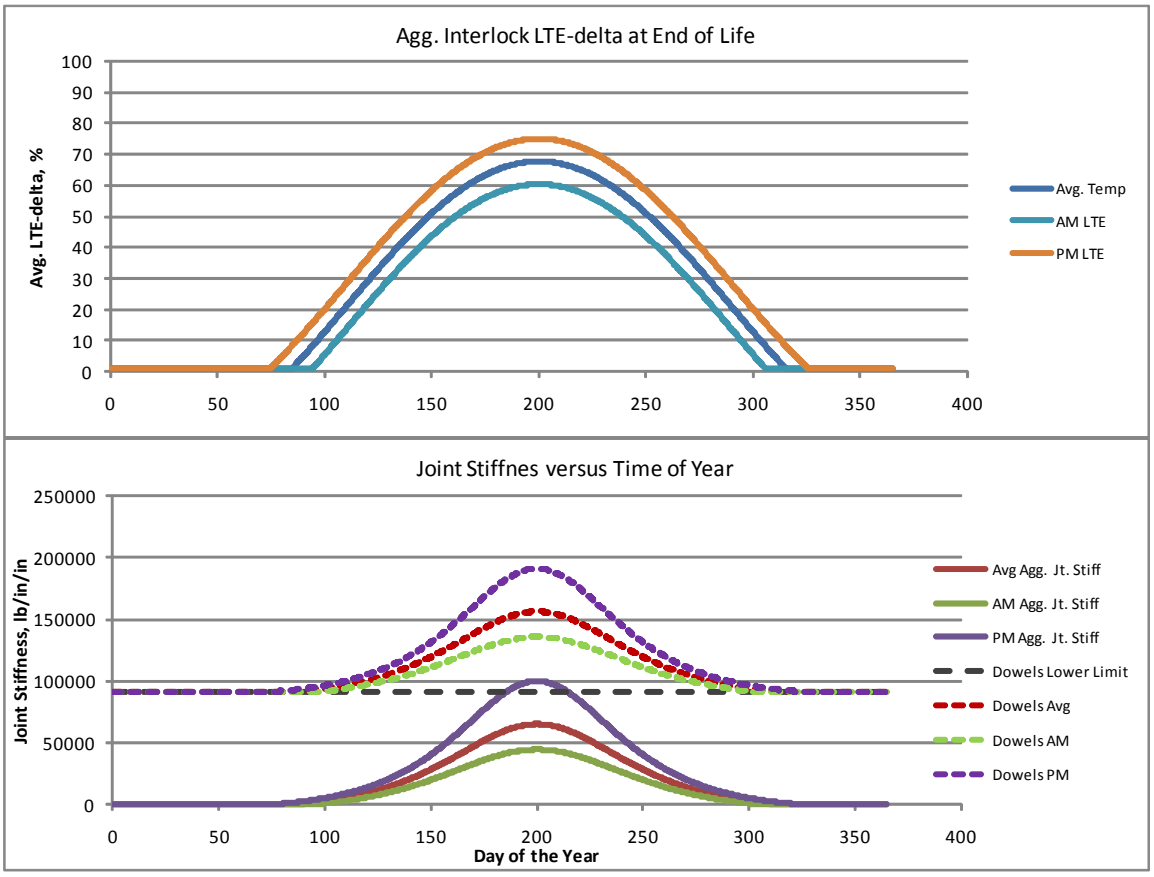

FIGURE 5.15. THE SIMULATED JOINT BEHAVIOR FOR THE SITE 2-AC17 DOWELED TRANSVERSE JOINTS FOR A 25-FT SLAB DIMENSION

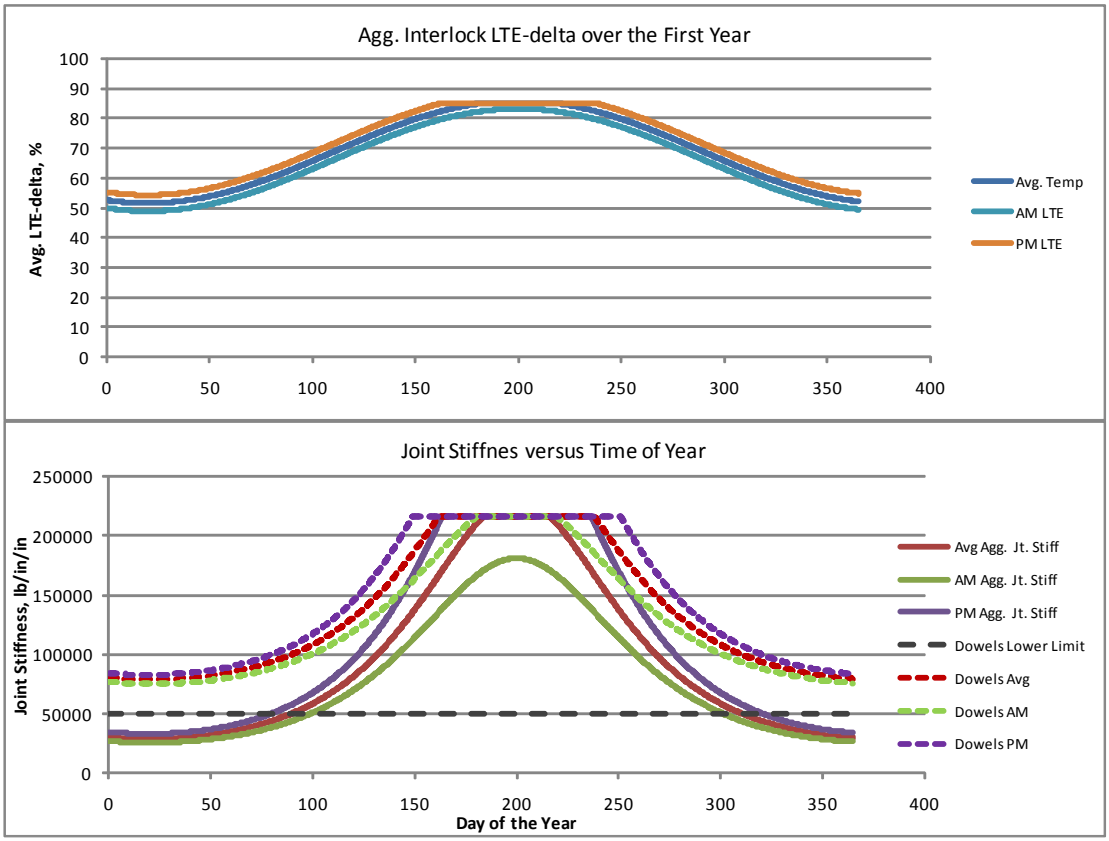

FIGURE 5.16. THE SIMULATED JOINT BEHAVIOR FOR THE SITE 2-AC17 TIE-BAR LONGITUDINAL CONSTRUCTION JOINTS FOR 12.5-FT SLAB DIMENSIONS

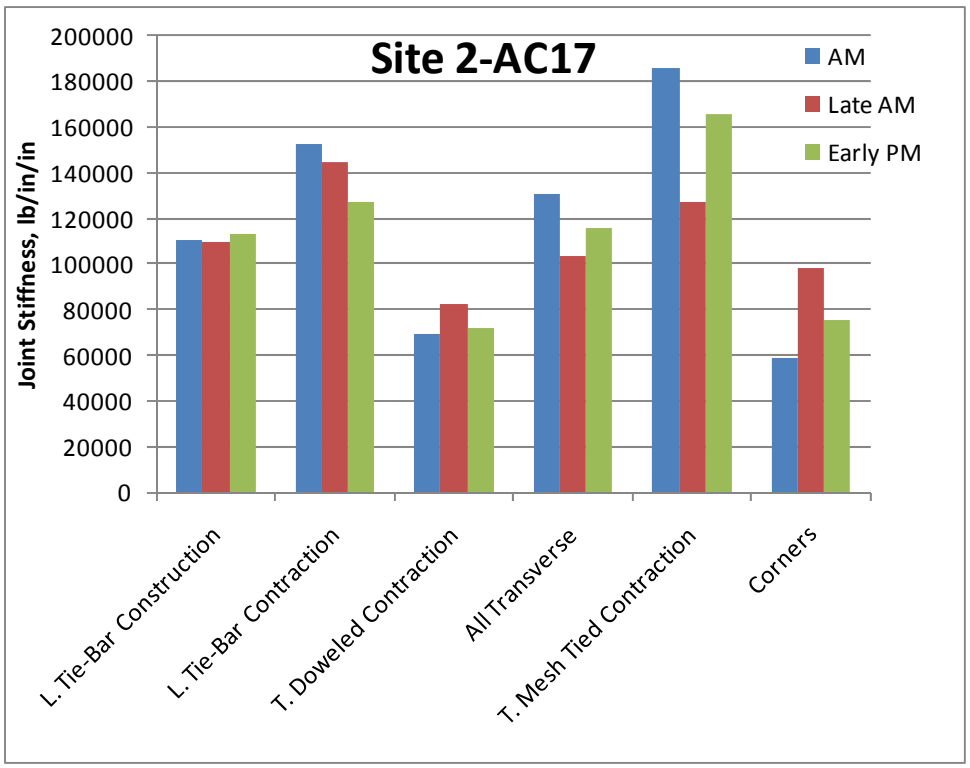

FIGURE 5.17. ACTUAL MEASURED JOINT STIFFNESS VALUES TO COMPARE TO ESTIMATES GENERATED IN FIGURES 5.15 AND 5.16 FOR DAY 275

The design engineer can make reasonable predictions of site 2-AC17 joint behavior using the simplified and comprehensive joint behavior models. The next step in the process would be to use the joint stiffness estimates in a structural analysis procedure to estimate how Load Transfer, LT, will vary as a function of average slab temperature for the joint designs. Figures 5.18 and 5.19 show the approximate B747 gear LT values that correspond to the joint behavior model results shown in figure 5.15 and 5.16. Aggregate interlock joints were not used at this site. The lower plot in figure 5.18 presents the estimated B747 LT values for the transverse doweled contraction joints. The multiple curves in each plot simulate 20 years of aging, with higher curves representing newer pavement. Estimated LT values range between about 0.35 for new conditions, to about 0.28 for aged conditions for the doweled joints. As shown in figure 5.19, the estimated LT values range between about 0.35 for new conditions, to about 0.23 for aged conditions for the tied joints using 12.5-ft spacing. Notice how the aggregate interlock component of the tie-bar joints at 12.5-ft spacing does not drop to a zero value during cold weather like the 25-ft joint spacing arrangement. The doweled joint behavior simulation assumes the joints are free to open and close. The tie-bar joints generally will not be free to open and close. Tied joints would maintain "summer-like" joint opening and behavior conditions even during cold weather, with LT values staying above about 0.27. Note that one joint at this site had apparently fractured steel and was behaving as an aggregate interlock joint. This was a longitudinal joint located 12.5 feet from the outer edge of the runway, right at a taxiway turnout location. This study has revealed that in general, the outer longitudinal joints for runways and taxiways are perhaps the most susceptible to loss of joint load transfer because of less lateral confinement resulting in a tendency for larger joint openings, and some enhanced curling effects.

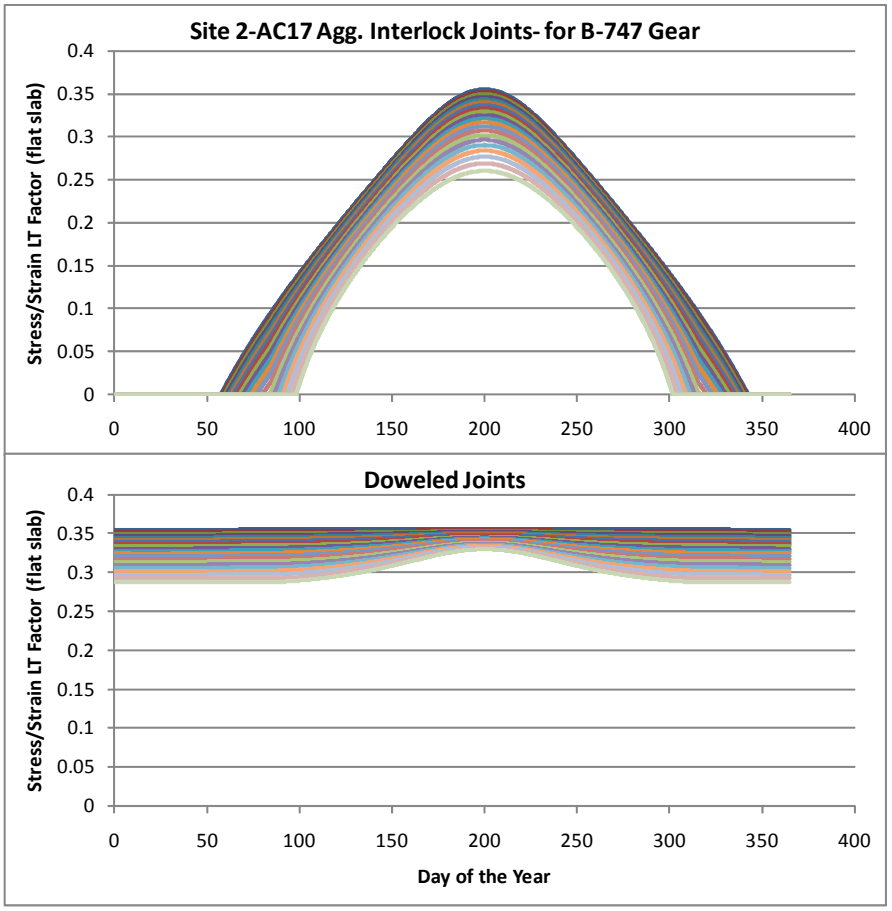

FIGURE 5.18. APPROXIMATE 25-FT JOINT SPACING DOWELED JOINT LT VALUES FOR A B747 FOUR WHEEL GEAR AS A FUNCTION OF DAY OF THE YEAR FOR SITE 2-AC17 AVERAGE WEATHER CONDITIONS

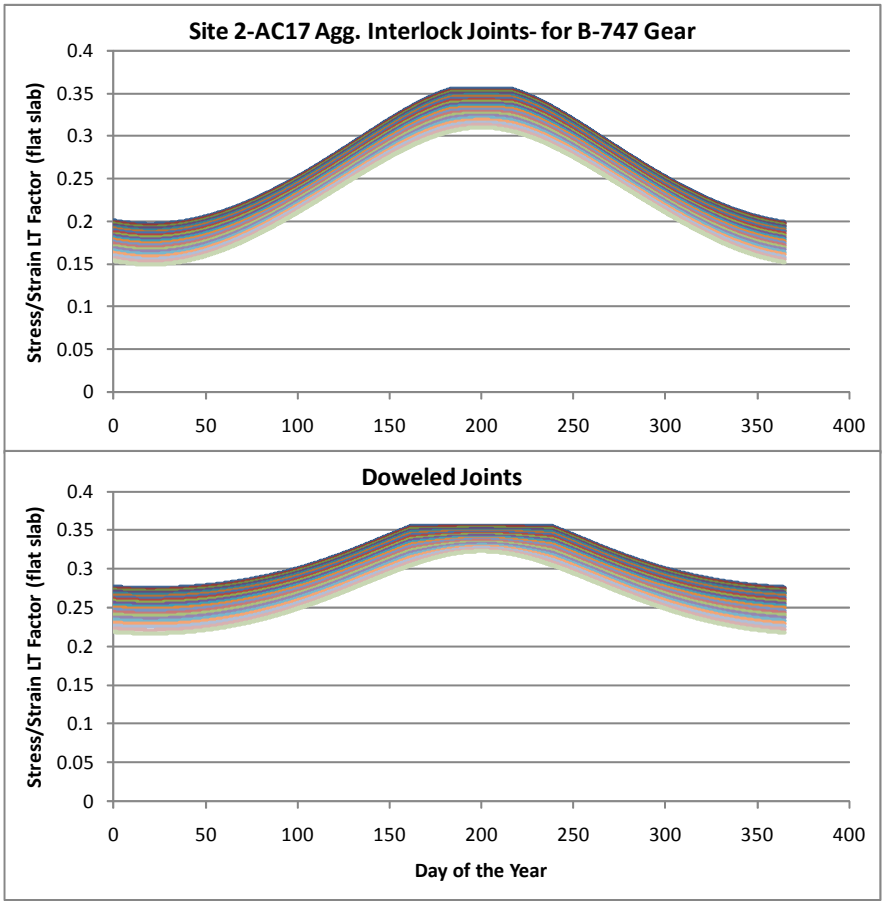

FIGURE 5.19. APPROXIMATE 12.5-FT JOINT SPACING TIE-BAR CONSTRUCTION JOINT LT VALUES FOR A B747 FOUR WHEEL GEAR AS A FUNCTION OF DAY OF THE YEAR FOR SITE 2-AC17 AVERAGE TEMPERATURE RANGE

This site 2-AC17 case study reveals that the joint behavior simulations are quite sensitive to the joint spacing variable. To demonstrate the joint spacing sensitivity, figure 5.20 shows the effect of varying joint spacing from 10 to 30 feet on aggregate interlock joint stiffness for the site 2-AC17 parameters. This plot simulates how aggregate interlock joints would behave in a cooler northern USA climate, as a function of slab length and assuming spring or fall northern construction temperatures. The model indicates that for joint spacing of about 16 to 17 feet, the aggregate interlock and LT will drop to zero during cold weather for just a few days during the coldest of weather. For a joint spacing of 30 feet, the aggregate interlock joints have an estimated zero stiffness and LT for about 165 of the cooler days of the year. For a 10-ft joint spacing, aggregate interlock stiffness is predicted to remain effective at about 30,000 lb/in/in during the coldest winter days.

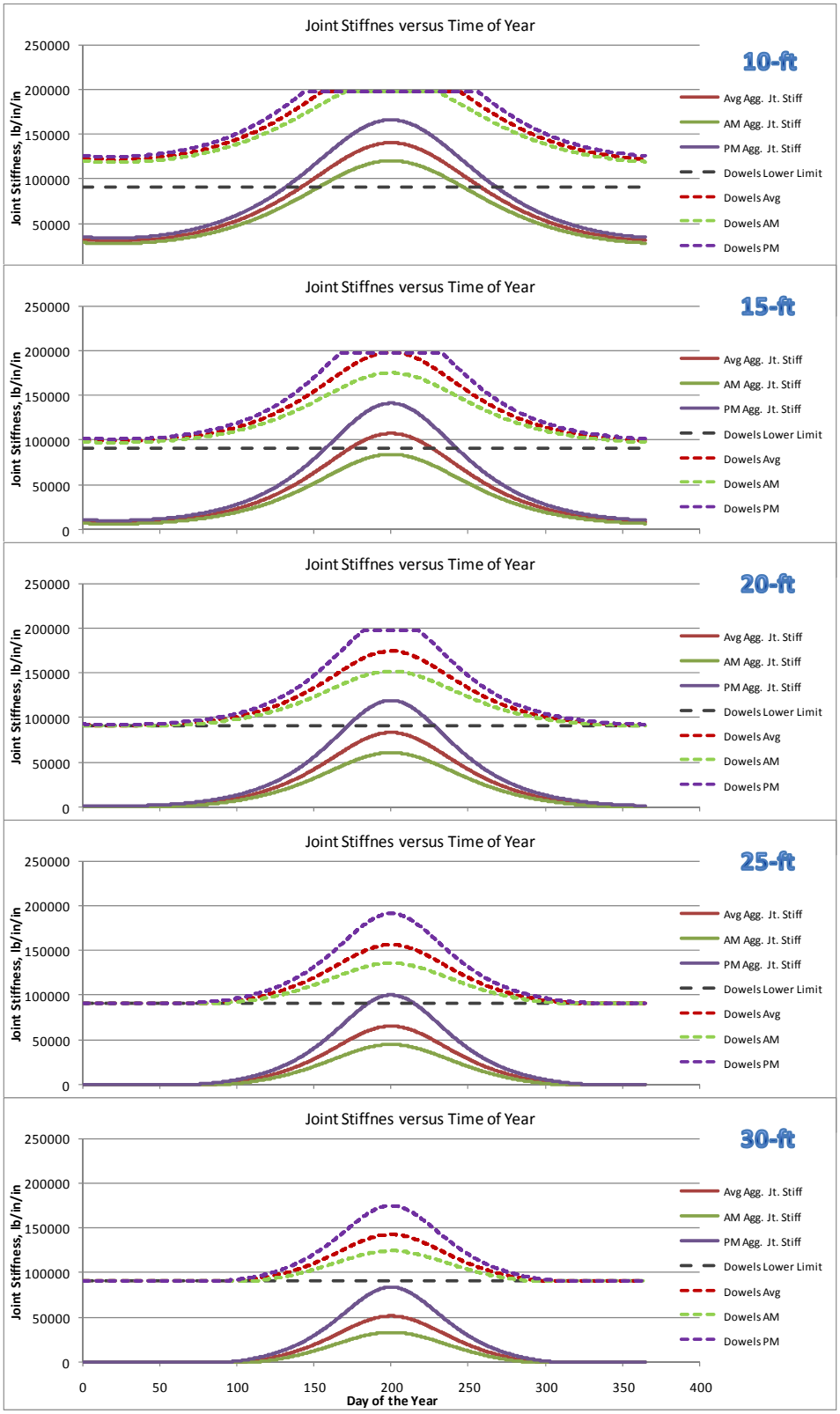

FIGURE 5.20. THE EFFECT OF VARYING JOINT SPACING ON JOINT STIFFNESS ESTIMATES FOR NORTHERN CLIMATE AND 2-AC17 CROSS SECTION DATA

CHAPTER 6. COMPARING TEST SITE DATA TO FEM ANALYSIS RESULTS

The data obtained from the test sites and the resulting calibrated joint stiffness algorithms have established the joint design input for FEM analysis using linear spring type joint stiffness representation. The calibrated joint stiffness input takes into account the effects of typical loss of support along slab edges and looseness of aggregate interlock and dowels on overall joint stiffness levels. The method for fitting FEM results to characteristic joint stiffness curve was briefly described in chapter 3 and some examples of how the FEM results are used were provided. This chapter describes in more detail the use of calibrated FEM algorithms to analyze apparent stress load transfer in slabs, multi-wheel gear effects, and the effects of curling and warp in slabs.

6.1 SIMULATING JOINT BEHAVIOR AND CURLING WITH CALIBRATED FEM MODELS

FEM models matching FWD data sets from four of the test site were developed using the ILSL2 FEM computer program (Ioannides and Khazanovich, 1998). A two-slab one-joint system sitting on a Winkler foundation was used. The geometry and loads were set symmetrical about a system centerline such that FEM discretization symmetry could be leveraged to reduce mesh size and allow a finer mesh surrounding the wheel loads. The calibrated FEM algorithm for site DIA-CT18 will now be used to demonstrate fundamental slab and joint load transfer behaviors of interest to this study. The DIA FEM simulation parameters used are as follows:

- Slab dimension: 20 by 18.75 ft.
- Slab thickness: 18 in.
- Load: 40-kip FWD, 12-in diameter load area, $a/\ell \approx 0.11$
- Temperature gradient: flat (zero), and curled-up and down by 2 ºF/in.
- Concrete modulus: 5,000,000 psi
- Subgrade *k*-value: 250 and 450 psi/in
- Joint stiffness: 0, 1, 5, 10, 20, 50, 100, 200, 200, and 1000 kip/in/in

Figure 6.1 shows the FWD-based DIA joint stiffness data, along with the Skarlatos/Ioannides infinite slab edge solution ($k_{Skarlatos}$ = 200 psi/in), and ILSL2 2-slab discretization (k_{ILSL2} = 250 psi/in) matching the measured joint stiffness data. These trends look very similar. The slight shape differences and significantly different subgrade values are because the Skarlatos/Ioannides infinite edge model does not allow any slab rotation, while the ILSL2 discretization does allow slab rotation. For the same slab thickness and subgrade stiffness, the ILSL2 discretization will result in higher overall edge deflections than the Skarlatos/Ioannides edge solutions. The FEM 2-slab system needed a k_{ILSL2} = 250 psi/in to have about the same overall slab edge deflections and characteristic joint stiffness versus LTE_δ curve as the infinite slab system with a $k_{Skarlatos}$ = 200 psi/in.

The FEM generated characteristic joint stiffness curves for both upward and downward thermal curling gradients of 2 °F/in are provided with the flat slab curve, for the k_{ILSL2} = 250 psi/in. The flat-slab joint stiffness curve for k_{ILSL2}= 450 psi/in is also shown. The 450 psi/in is the site average ILLI-BACK mid-panel backcalculated modulus of subgrade reaction. The statement

that the ILSL2 discretization having a k_{ILSL2}= 250 is a "better fit" than the one for k_{ILSL2}= 450 is inherently assuming that the slabs were not in a state of large up-warp with joints lifted off the ground when tested with the FWD and that the measured characteristic joint stiffness trend represents relatively well seated joints without large loss of edge support. If the joints were relatively seated during afternoon FWD testing, then the "flat slab" FEM trend line will fit to the lower boundary of the measured characteristic joint stiffness data points, which in this case is the k_{ILSL2} = 250 psi/in curve. If large up-warp was present in panels and major loss of support was present at joints during all FWD testing, one could argue that a k_{ILSL2} of greater than 250 psi/in and up to the mid-panel 450 psi/in was present under the joints but that the site perhaps had large voids present beneath all slab edges such that the "effective" k_{ILSL2} for the combined air gap and 450 psi/in subgrade was only 250 psi/in. FWD testing reveals the DIA joint stiffness data to have low scatter, which is in general indication that relatively uniform joint support/behavior was present during testing. Fitting the flat-slab FEM curve to the bottom of the data set reveals the maximum possible "effective" subgrade *k*-value for the joints corresponding to a nearly-flat slab assumption. For this study, it was assumed that the afternoon testing did occur during nearly-flat slab conditions, so the flat slab FEM responses were matched to the bottom of the data sets to find this apparent maximum possible flat slab full support subgrade *k*-value = 250 psi/in. With the FEM, it would be time consuming to rigorously find the numerical best-fit subgrade *k*-value, unlike the Skarlatos/Ioannides closed-form solution true best-fit approach, which is easily determined from a matrix equation minimization problem. For this study, the apparent best-fit FEM algorithms noted were typically visually selected from a small number of runs performed using 25 to 100 psi subgrade stiffness increments, and the visually closest curve selected and considered good enough for analysis purposes. The actual calculated DIA data points are slightly higher than the simulation shape for high LTE, and slightly lower than the simulation shape for lower LTE. This general trend implies that the slab edge subgrade response was experiencing a load hardening response, behaving softer than 250 psi/in for smaller edge deflections (high LTE) and stiffer than 250 psi/in for larger edge deflections.

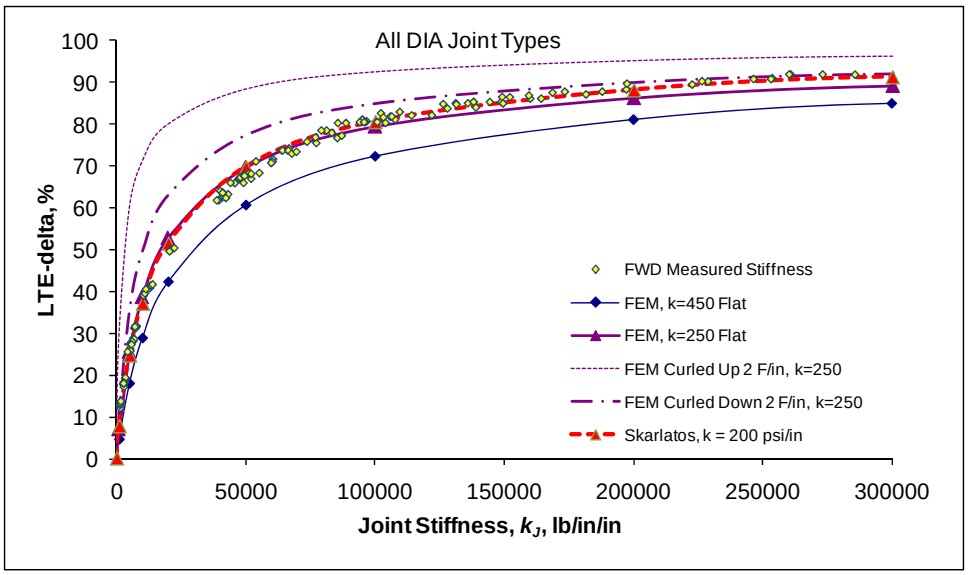

FIGURE 6.1. A PLOT SHOWING THE BEST-FIT SKARLATOS/IOANNIDES AND ILSL2 FEM RESULTS FOR THE DIA CHARACTERISTIC JOINT STIFFNESS CURVE, AND HOW SLAB CURLING AFFECTS FEM GENERATED JOINT STIFFNESS VERSUS LTE_δ CURVES

The analysis of stresses and deflections for any FEM model starts with establishing the flat slab self weight sinking magnitude and stress distribution. Flat-slab self weight stresses will be small, but self weight downward deflection into the subgrade is significant and must be considered. Thinner slabs will not deflect downward due to self-weight as much and will lose support at edges sooner during morning upward curling. In general, all calculated load and curling deflections must be corrected to account for the initial self weight downward deflection.

The FEM slab deflections due to curling-only were denoted as δ_T and these deflections are equal for both slabs in the model and symmetrical about the joint. Deflections at the loaded and unloaded slab edges due to an edge loading and without any curling (flat-slab conditions) were denoted as $\delta_{L(L)}$ and $\delta_{U(L)}$, respectively, where the (L) designation means "load-only". Deflections for the loaded and the unloaded slabs for the combined load and curling (L+T) analyses were denoted as $\delta_{L(L+T)}$ and $\delta_{U(L+T)}$, respectively. Similar definitions apply for the stresses generated by FEM models for σ_T, $\sigma_{L(L)}$ and $\sigma_{U(L)}$, and $\sigma_{L(L+T)}$ and $\sigma_{U(L+T)}$.

As shown in chapter 3 and by other past research (Rufino et al. 2004), the combined load plus temperature curling response (L+T) does not simply equal the sum of the load only (L) plus temperature only (T) responses. Load related edge stress change {(L+T)-T} does not equal load-only stress L, and the difference quantifies the effects of air gaps between the slab and subgrade caused by curling. There is a complex interaction with loading and curling when any sort of slab edge gap or mid-panel air gap forms in the FEM idealization as a result of curling.

When using FEM analysis and simulating loads plus curling, it is the percentage stress reduction in the loaded slab caused by the joint, as compared to a free-edge stress condition, that is the key index of Load Transfer, LT. In the past, the measured strain in the unloaded slab was often

assumed to be equal in magnitude to the reduction in strain in the loaded slab. This research has shown that this is not true when significant upward or downward slab curvature from curling is present. The percentage stress reduction in the loaded slab must be directly obtained from the jointed FEM loaded slab stresses as follows:

% Reduction in Loaded Slab Free-Edge Stress, LT =

$$[\sigma_{L(L+T)}\ (\textit{free-edge},\ k_J=0) - \sigma_{L(L+T)}\ (k_J>0)]/\ [\ \sigma_{L(L+T)}\ (\textit{free edge},\ k_J=0)] \qquad (41)$$

Where, $\sigma_{L(L+T)}$ is the calculated stress in the loaded side slab from the jointed FEM analysis for the combined curling and load scenario for varying joint stiffness values, compared to the free edge stress. i.e. joint stiffness = zero. The jointed FEM analysis should be performed for a zero stiffness value in order to obtain free edge stress and deflection values.

Figures 6.2-6.4 show the FEM analysis results for curled-down analysis for a 2 °F/in thermal gradient and for a nearly-free-edge condition low stiffness joint, like a nearly open aggregate interlock joint. The afternoon curled-down condition is the critical design stress condition for traditional bottom of slab cracking analysis for slab edge loads. Self-weight sinking has been subtracted out of these plots, and the top of subgrade is at approximately -0.0056 inches (– 5.6 mils). Prior to loading, the curled-down slab is supported by only a narrow zone of subgrade around the perimeter of the slab, while the entire mid-slab region is lifted up to 55 mil above the subgrade. This plot shows the "joint knifing" effect discussed earlier associated with curled-down slabs, where the exaggerated plot scale reveals this appearance. Base and subgrade stress beneath the joint will be at a maximum during this condition. One interesting finding is that load-related joint edge deflections and strains for the curled-down shape are greater than those for the flat slab condition. When mid-panel uplift is present, this perimeter-only support condition does represent a loss of support condition for joints. The 40-kip FWD edge load simulation does not fully push the mid-slab area down into contact with the subgrade. This "knifing" condition probably accelerates stabilized base cracking and causes permanent deformations along joint lines as a result of occasional extreme down-curl conditions. Figure 6.3 shows the traditional load related bottom of slab edge stress and related stress profile for the 40-kip FWD load at the joint. The combined curling plus load edge stress for a joint condition similar to a winter aggregate interlock (dummy) joint at DIA is estimated at about 530 psi. For the curled-down condition, the residual curling edge stress and the load related edge stress are combining effects. Figure 6.4 shows the mid-panel stress and related top of slab stress profile along a line through the load center and perpendicular to the loaded edge. For the curled-down shape, the edge loading acts to reduce the residual thermal tensile stress maximum at mid-slab, as these effects counteract each other along this dimension. It is generally accepted that the critical stress location for edge loading of flat to curled-downward short slabs will be at the mid-slab edge load location and at the bottom edge of the slab. Residual stress from downward curling of 2 °F/in, a feasible event in more extreme climates, could cause load plus curl (L+T) edge stress to rise from about 400 psi for a flat slab, to about 530 psi for a curled-down slab, for 40-kip FWD edge loads.

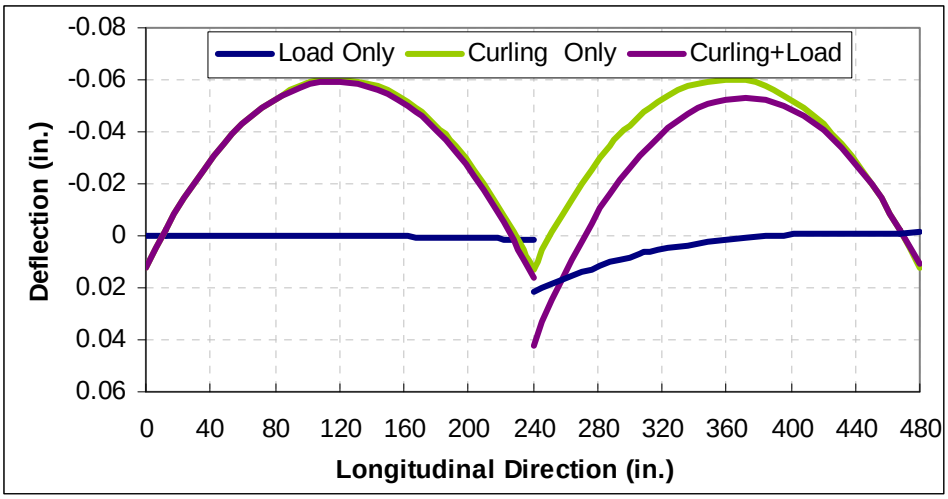

FIGURE 6.2. THE CALIBRATED DIA FEM ALGORITHM EDGE-LOAD DEFLECTION PROFILES ALONG SLAB CENTERLINE SHOWING THE "JOINT KNIFING" DEFLECTED SHAPE (40-kip FWD, curled-down 2 ºF/in, k_J=1,000 lb/in/in, load at 246 inches)

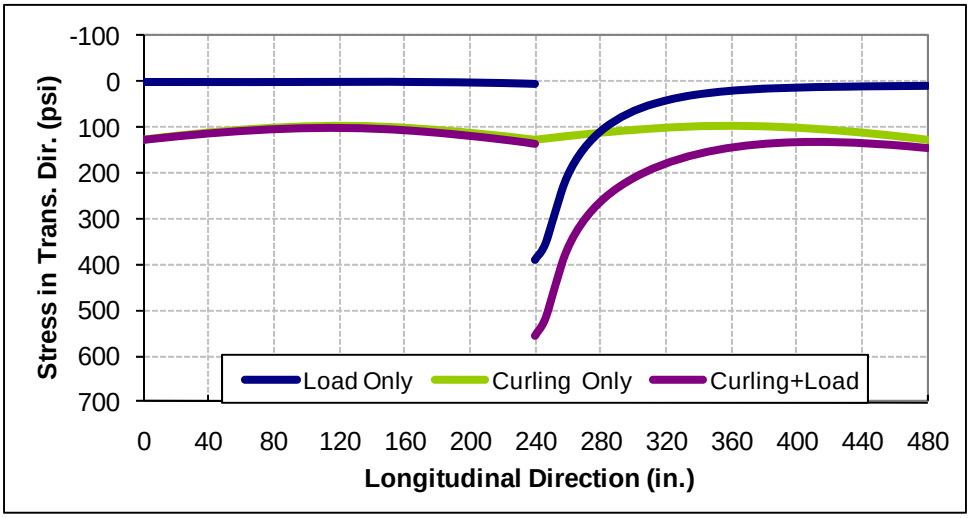

FIGURE 6.3. THE CALIBRATED DIA FEM ALGORITHM EDGE STRESS AND RELATED STRESS PROFILES ALONG SLAB CENTERLINE (40-kip FWD, curled-down 2 ºF/in, k_J =1,000 lb/in/in, load at 246 inches)

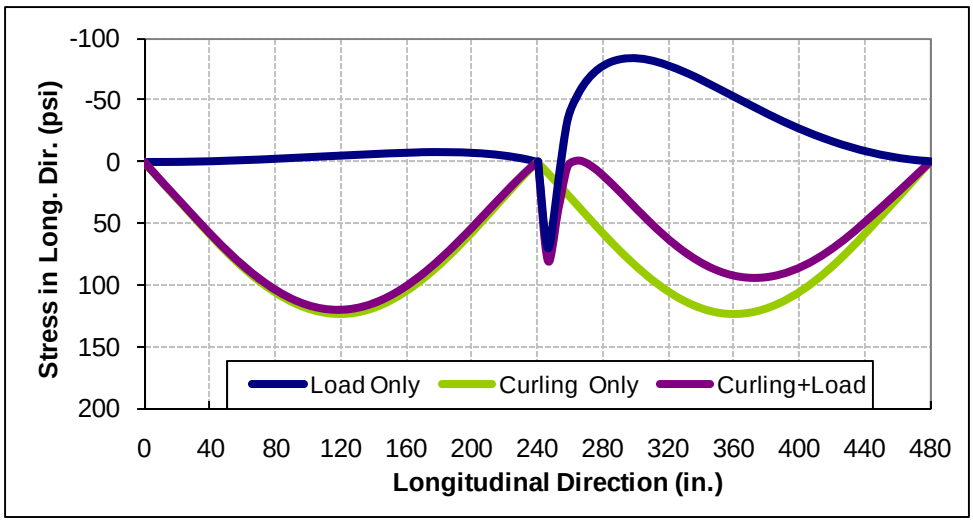

FIGURE 6.4. THE CALIBRATED DIA FEM ALGORITHM MID-PANEL STRESS AND RELATED STRESS PROFILES ALONG SLAB CENTERLINE (40-kip FWD, curled-down 2 ºF/in, k_J =1,000 lb/in/in, load at 246 inches)

Figures 6.5-6.7 show the ILSL2 FEM analysis results for curled-up analysis for a 2 °F/in thermal gradient and for a nearly-free-edge condition, like an open aggregate interlock joint. The top of subgrade is again at approximately -0.0056 inches (– 5.6 mils), i.e. self weight sinking. Prior to loading, the slab is supported by only the middle roughly 75% of the slab length, while the joints are lifted up to 35 mils above the subgrade. This data shows how large upward curling or warping conditions result in the slabs behaving like cup-shaped structures with rounded bottoms resting on the subgrade. Notice how the center of support shifted left significantly when the load was placed on the simulated slab edge as the cup-shaped slab rotated towards the load. The 40-kip FWD load did fully push the slab edge down into the subgrade, but by only a few mils. At the far edge of the slab, slab rotation related uplift was estimated to be about 20 mils. Figure 6.6 shows the traditional load related bottom of slab edge stress and related stress profiles for the 40-kip FWD load at the joint. The combined upward curling plus load total edge stress for the loose open joint is reduced to about 280 psi compared to 400 psi for the flat slab. For the curled-up condition, the residual curling edge stress and the load related edge stress are counteracting effects. Figure 6.7 shows the maximum mid-panel stress location and related stress profile along a line through the slab center. For the curled-up shape, the edge loading combines with the residual thermal stress, and the point of maximum top of slab stress shifts from mid-slab towards the loaded edge somewhat. Note that the bottom of slab edge stress is at about 280 psi, while the top of slab stress at mid-panel is at about 220 psi. For a rolling wheel load, there are two top of slab load peaks for each passing of one wheel, one for each joint crossing. For edge loading there is one load peak, under the wheel load. From a fatigue damage perspective to estimate the relative damage for top of slab versus bottom of slab cracking for the slab, one would compare two mid-slab top tension peaks at 220 psi with residual stress at 140 psi, against one bottom of slab edge stress peak at 280 psi with a residual stress level at negative 70 psi. The stress range is much greater for edge loading and stress goes from negative to positive to negative. Please note: if slab length was longer, or if there were a larger thermal gradient, residual tension at mid-slab would increase significantly, eventually to the point of exceeding the bottom edge stress for edge

loading. Also, the Iwama non-linear curling gradient thermal stress correction factor concept would suggest that: when using linear temperature gradient stress idealizations, calculated stress magnitudes on top of slabs should be increased by about 30%, while bottom of slab edge stresses could be reduced by about 30% to account for the typical non-linear temperature gradient profiles encountered in slabs (Nishizawa, 2010). These adjustments are related to the typical magnitudes of the stresses caused by the self-equilibrating non-linear component of typical temperature profiles measured through the thickness of outdoor slabs, which are typically non-linear with respect to depth in the concrete slab.

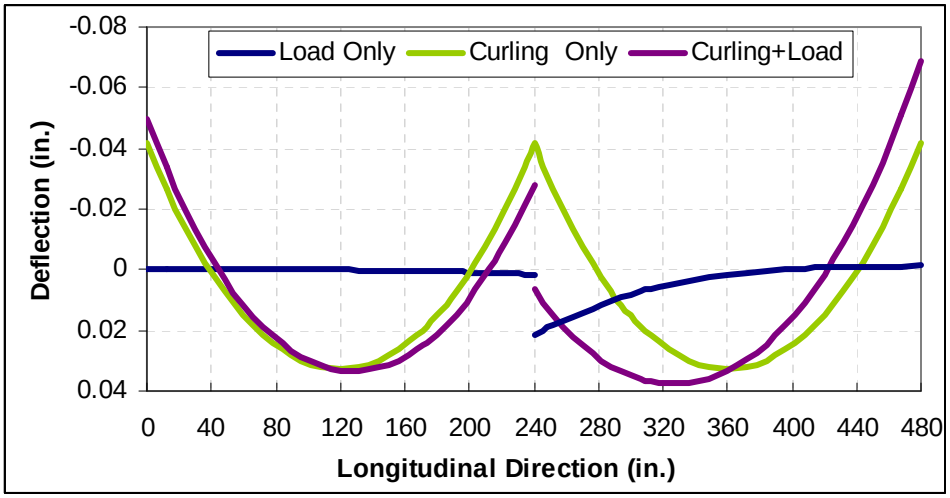

FIGURE 6.5. THE CALIBRATED DIA FEM ALGORITHM EDGE-LOAD DEFLECTION PROFILES ALONG SLAB CENTERLINE FOR UPWARD CURLING AND LOAD (40-kip FWD, curled-up 2 ºF/in, k_J =1,000 lb/in/in)

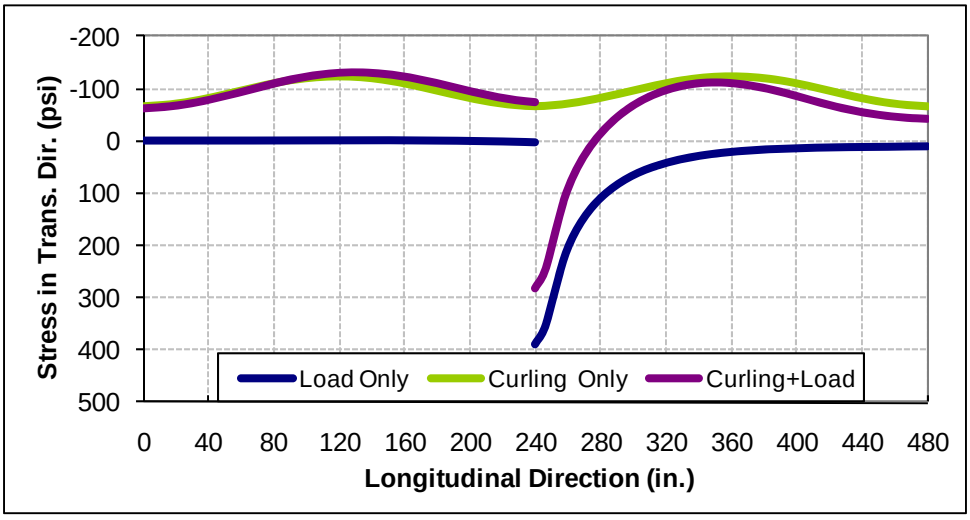

FIGURE 6.6. THE CALIBRATED DIA FEM ALGORITHM EDGE STRESSES AND RELATED STRESS PROFILES ALONG SLAB CENTERLINE (40-kip FWD, curled-up 2 ºF/in, k_J =1,000 lb/in/in)

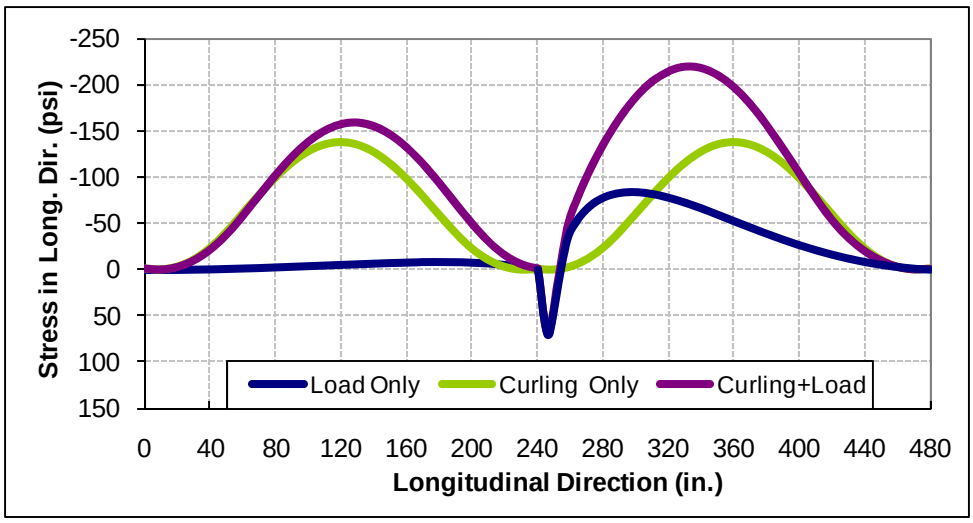

FIGURE 6.7. THE CALIBRATED DIA FEM ALGORITHM TOP OF SLAB CRACK MID-PANEL STRESS AND RELATED STRESS PROFILES ALONG SLAB CENTERLINE (40-kip FWD, curled-up 2 ºF/in, k_J =1,000 lb/in/in)

The multiple FEM runs for varying joint stiffness are used to obtain the key Load Transfer, LT, versus joint stiffness curves from the calibrated FEM analyses for a range of load sizes and gear configurations. Figure 6.8 shows the LT functions for 40-kip FWD load simulations for the calibrated DIA algorithm. Results are shown for the combined stress (L+T) analysis, and for the change in stress {(L+T)-T} analysis. The most correct interpretations of LT are the "*% Reduction*" curves. With these curves, the free-edge stress reference magnitude includes curling stress. The "*Unloaded Slab*" curves were established using the stress magnitudes in the unloaded slab subtracted from the free edge stress reference. These lines also include residual curling stress in the free-edge stress reference magnitude. Because the change in stress in the unloaded slab is not equal to the change in stress in the loaded slab when significant slab curvature from curling is present, these trend lines based on unloaded slab data are not valid. Yet, they do have similar magnitude to the correct percent reduction LT curves. The third set of curves take residual curling stress out of the free-edge stress reference value used to calculate LT. These are called *loaded slab total stress* LT curves. These are the curves that bring the effects from curling into a totally flat slab analysis reference frame, such as the 30x30-ft single-slab FEM idealization without curling analysis in the Version 6E FAARFIELD software, or to the Westergaard free edge stress solution. The total stress curves are an abstract concept and do not represent the actual physical percentage stress reduction caused by the joint at a point in time. The total stress LT curves force the residual curling stress into the LT value magnitude by always using the flat-slab free edge stress as the reference magnitude.

Notice how the upward curling % Reduction LT curves have negative LT for low joint stiffness values. The FEM algorithm reveals that a 40-kip FWD free edge load has slightly less bending stress than occurs when a joint with just a slight stiffness is present. There is initially a 6 to 7% increase in loaded-slab stress (negative LT) as the joint shear force just begins to act. The joints are initially lifted off the subgrade. As a small amount of joint stiffness mobilizes, it at first actually prevents the loaded slab from deflecting through the air-space gap and mobilizing as

much uniform subgrade resistance along the edge, and instead mobilizes line resistance along the edge of the slab. A joint stiffness of at least 10,000 to 20,000 lb/in/in was necessary to provide just enough joint load transfer to overcome this effect and bring LT back to zero, meaning the edge stress at k_J = 10-20 kip/in/in equals the free edge stress. This negative LT effect diminishes for heavier multi-wheel gears. The total stress curves intersect the y-axis at large values for near-zero joint stiffness. This reflects that the combined curl plus load free-edge stress levels at bottom of slab edge for curled-up and curled-down conditions were about 30% less, and 45% greater than the flat-slab free-edge stress, respectively. During afternoon down-curl, even for very stiff locked/uncracked joints, the bottom of loaded slab tension stress reduction caused by the joint is smaller than the added residual tension stress caused by curling, hence negative "flat-free-edge" LT. Combined load plus downward curling bottom of slab edge stress values ranged between about 115 to 145% of the flat slab free-edge stress value for closed to open joints. Combined load plus upward curling bottom of slab edge stress values ranged between about 35 to 70% of the flat slab free-edge stress value for closed to open joints. As noted previously, the range of thermal gradients shown ± 2°F/in represents large gradients and most sites will experience less than this amount on average per day.

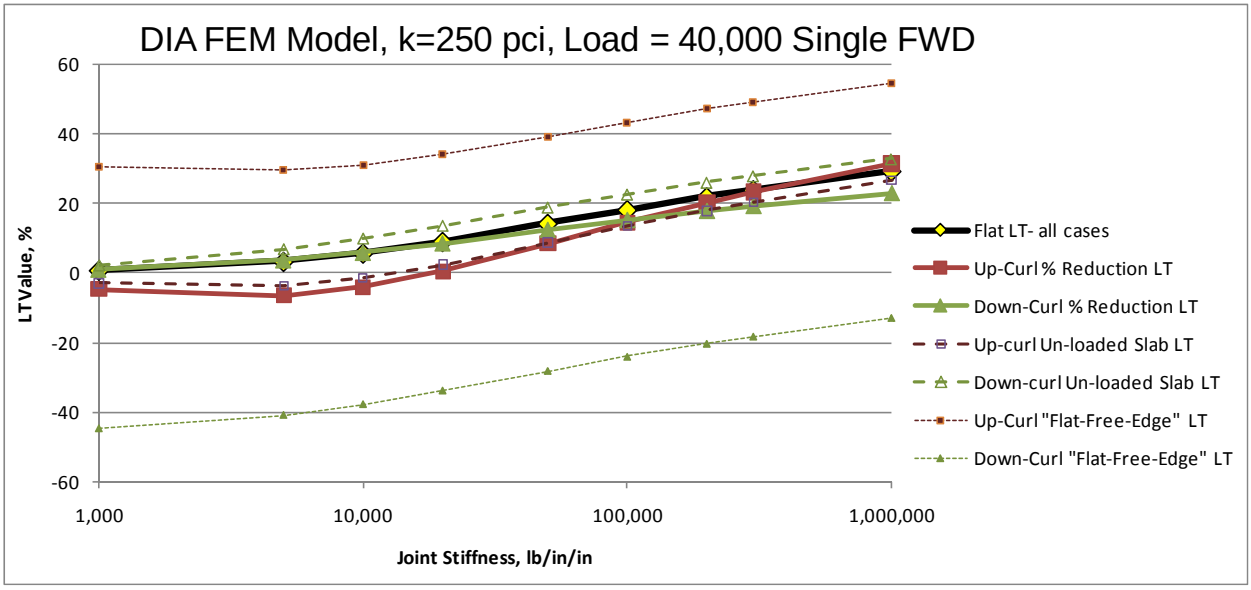

FIGURE 6.8. EFFECTIVE 40-KIP FWD EDGE-LOADING, BOTTOM OF SLAB TENSILE STRESS LT TRENDS OBTAINED FROM AN FEM ALGORITHM CALIBRATED TO THE DIA CHARACTERISTIC LTE_{δ} VERSUS JOINT STIFFNESS CURVE (FLAT SLAB FREE EDGE STRESS = 360 psi)

The above analyses were for simulated 40-kip FWD loads and 12-inch diameter load plate size. Different LT curves will be obtained for different load areas or for multi-wheel gears. To demonstrate, the single wheel responses for simulated FWD loads above are now compared to a four wheel gear assembly arranged like a Boeing 747-400 landing gear. The 40-kip FWD load results in about 280 psi applied contact pressure on the 12 inch diameter load simulation. The B747 gear is based on a 200 psi contact pressure applied over larger footprints and total weight of about 210-kip as shown in figure 6.9.

Basic information for the Boeing 747-400 gear

Gross Weight (lbs):	873,000
% GW on Main Gears:	95%
No. Main Gears:	4
Wheels on main Gear:	4
Tire Pressure (psi):	200

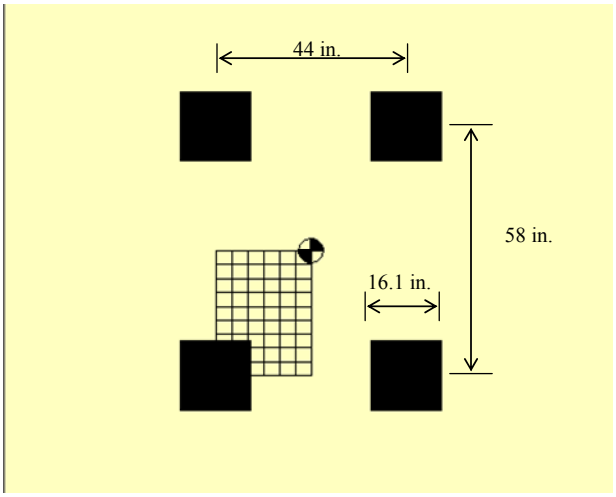

- Individual wheel load on the main gear = (873000*95%)/4/4 = 51834.4 lbs
- Footprint side length (square footprint) = sqrt (51834.4/200) = 16.1 in.

FIGURE 6.9. B747 GEAR SIMULATION USED IN THE 2-SLAB JOINTED FEM ANALYSES

The simulated B747 gear loads have a lower effective average contact pressure, but overall wheel load magnitude is about 30% larger than the simulated FWD loads. The four-wheel gear was rested at the edge of the joint and centered as shown below in figure 6.10. This figure shows how large a typical B747 landing gear is relative to the 18.75-ft by 20-ft slab dimensions used at DIA.

Position of a Dual-Tandem Gear

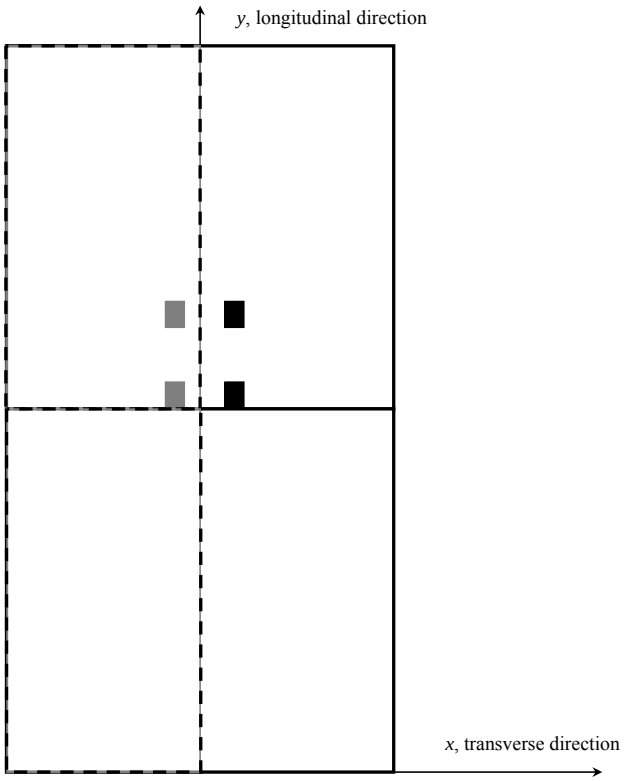

FIGURE 6.10. B747 GEAR POSITION FOR THE 2-SLAB FEM ALGORITHM, CENTERED ALONG THE JOINT EDGE, AND NOTING THE SYMMETRY CENTERLINE (DASHED LINE) FOR THE FEM MESH

Figure 6.11 shows the LT curves calculated for the B747 gear simulation for the combined stress (L+T) analysis, and for the change in stress {(L+T)-T} analysis. Notice how the upward curling curves no longer have negative LT for low joint stiffness values. This is because the 210-kip B747 gear is much heavier than the 40-kip FWD load. The total stress curves still intersect the y-axis at large values for near-zero joint stiffness. This reflects that the combined curl plus load free-edge stress levels at bottom of slab edge for curled-up and curled-down conditions were about 35% less, and 35% greater than the flat-slab free-edge stress, respectively. Regarding the downward curling simulation, at a joint stiffness of about 200,000 lb/in/in, the bottom of slab tension stress reduction caused by the joint is equal to the opposing residual slab tension stress increase caused by curling hence the total stress LT curve reaches zero. Combined load plus downward curling bottom of slab edge stress values ranged between about 95 to 135% of the flat slab free-edge stress value for closed to open joints. Combined load plus upward curling bottom of slab edge stress values ranged between about 35 to 65% of the flat slab free-edge stress value for closed to open joints.

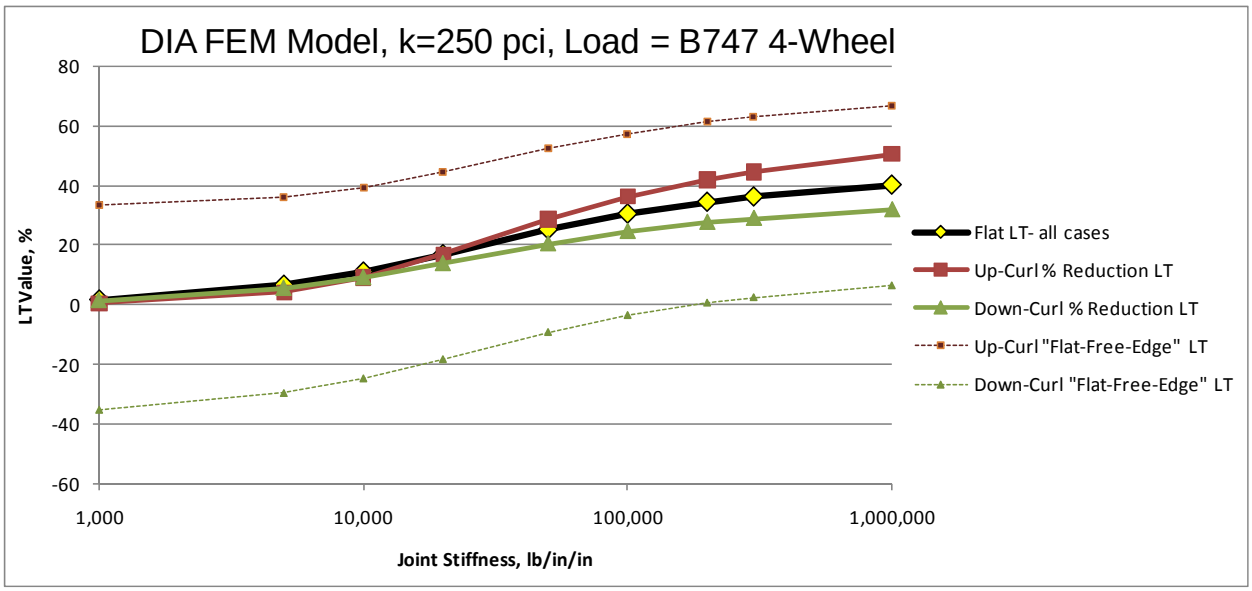

FIGURE 6.11. B747 GEAR EDGE-LOADING BOTTOM OF SLAB TENSILE STRESS LT TRENDS OBTAINED FROM THE CALIBRATED DIA FEM ALGORITHM (FLAT SLAB FREE EDGE STRESS = 542 psi)

Figure 6.12 shows the resulting FEM generated percentage stress reduction true LT curves for the 210-kip B747 gear assembly compared to the 40-kip FWD load. The down-curl and flat slab trend shapes are similar and are shifted higher for the B747 gear compared to the FWD load. The curled-up trend shapes are different and vary more. A key point to note is that during morning up-curl conditions, bottom of slab edge total stresses from loads and curling are at their lowest levels due to opposing locked in residual compressive stress form curling. The most critical LT curves are the curled-down curves, where load and curl cause combining tension at the bottom of slab edge beneath the load. The LT value is lowest and bottom of slab cracking edge stress is highest during the curled-down condition for both load types.

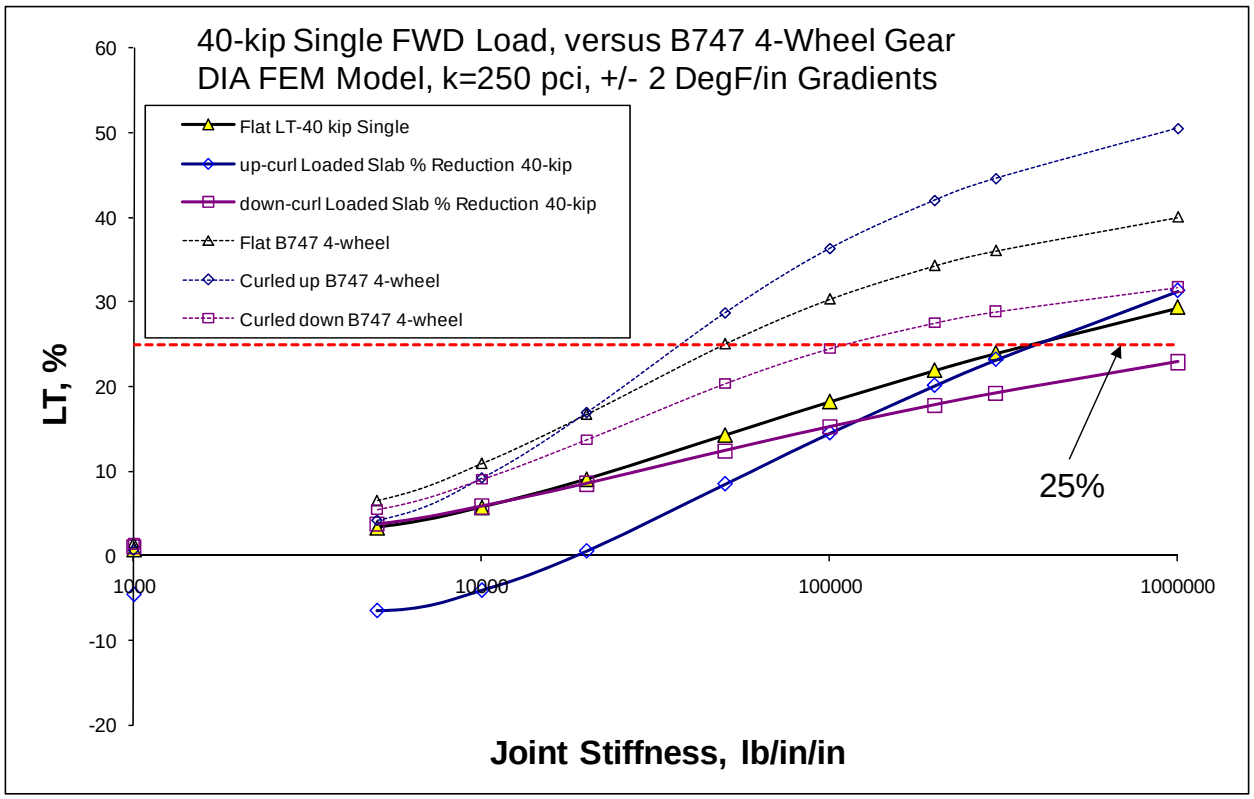

FIGURE 6.12. COMPARISON OF TRUE LT CURVES FOR THE FWD LOAD AND B747 4-WHEEL GEAR SHOWING HOW THE LARGER GEAR ACHIEVES HIGHER LT THAN THE SMALL CONCENTRATED SINGLE LOAD

Figure 6.13 shows summary edge stress data for the 40-kip FWD load and B747 gear, for the flat and curled up and down 2 F°/inch gradients for the DIA calibrated FEM algorithm and 80,000 lb/in/in joint stiffness level. This is about the average joint stiffness calculated from DIA FWD data. These values are compared to the Westergaard free-edge stress values obtained from the late 1980s FAA Westergaard equation used in Version 6D of the FAA pavement thickness design guides. The FEM algorithm and the Westergaard equation both produce adjusted edge stress level near 390 psi for the flat condition for the B747 gear assembly. LT-adjusted edge stress is shown to rise to near 570 psi for large daytime curling. The 75% of Westergaard edge stress value of 392 psi is what traditionally would have been used as the basis of design for a B747 gear for all times of day and all days of the year. In reality, the edge stress level caused by combined curling and B747 gear load for the DIA pavement design probably ranges from about 300 to 500 psi for the average DIA joint stiffness of about 80,000 lb/in/in. During cold winter conditions at DIA, open aggregate interlock (dummy) joints with joint stiffness near zero are expected to have B747 gear load related edge stress values ranging from about 550 to 650 psi for flat to curled-down conditions.

AM Free-edge Stress =	238	psi	Adj. AM Tension =	210	psi
AM LT =	11.8	%	Adj. Flat Tension =	300	psi
Flat Free-edge Stress =	360	psi	Adj. PM Tension =	451	psi
Flat LT =	16.8	%			
PM Free-edge Stress =	526	psi	Westergaard Edge =	451	psi
PM LT =	14.3	%	75% =	338	psi

40,000 lb Single FWD Load @ 280 psi

AM Free-edge Stress =	362	psi	Adj. AM Tension =	241	psi
AM LT =	34%	%	Adj. Flat Tension =	390	psi
Flat Free-edge Stress =	542	psi	Adj. PM Tension =	571	psi
Flat LT =	28%	%			
PM Free-edge Stress =	743	psi	Westergaard Edge =	523	psi
PM LT =	23%	%	75% =	392	psi

B747 Gear, 4@ 51,834 lb, @ 200 psi

FIGURE 6.13. EDGE STRESS AND LT MAGNITUDES FOR THE TWO LOAD CONFIGURATIONS, AND COMPARED TO THE WESTERGAARD-MODIFIED STRESSES FOR THE DIA CONDITIONS

In summary, regarding classical bottom of slab tensile stress at the edge loading location, figure 6.14 shows how the current FAA design philosophy relates to what a detailed FEM analysis implies is really happening at the edge stress location. The overall 75% design allowance attempts to average out the daily and seasonal stress variations caused by curling, warping and joint opening size variations. Over a 24 hour period, most classical edge stress damage is probably occurring during warm on top thermal gradient conditions. Relative pavement damage curves are shown and are calculated using the relatively simple late 1980s FAA pavement damage formula. When the edge stress calculated using the average DIA joint stiffness of 80,000 lb/in/in, is compared to cold winter free edge stress, the magnitude of the peak for the free edge fatigue damage function shown is about 10 times the size of the peak for the 80,000 lb/in/in average joint stiffness. Existing pavement damage formulae are sensitive to edge stress magnitude. During the cold of winter, the DIA aggregate interlock joints are near free edge conditions and slabs are accumulating much more damage. At the same time, day time thermal gradients are typically smaller during winter while the joints are in a more susceptible condition. If the Iwama reduction factor to account for the non-linear gradient effect (Nishizawa, 2009) were applied to the FEM edge stress values above, the calculated edge stress magnitude during afternoon conditions would be reduced significantly.

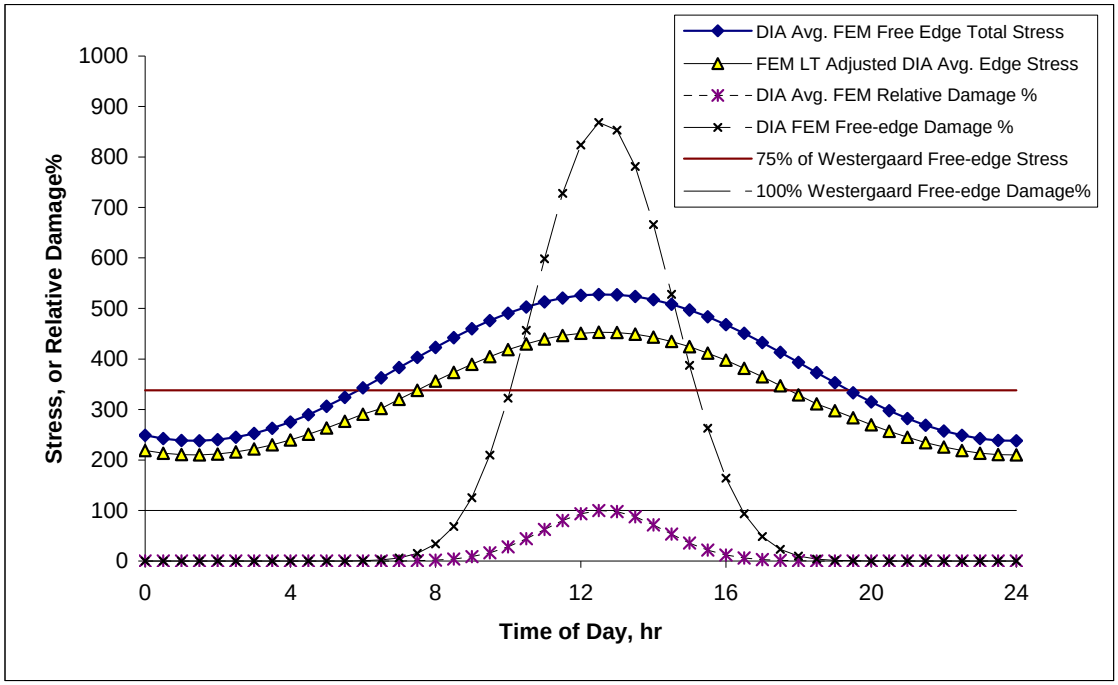

FIGURE 6.14. GENERAL IMAGE OF VERSION 6D AND 6E DESIGN PHILOSOPHY (TAKING AN OVERALL DAILY AVERAGE = LINES), COMPARED TO CURRENT FEM SIMULATION OF HOURLY EDGE STRESS VARIATIONS, AND THE RELATIVE SHAPES OF FEM SLAB EDGE DAMAGE FUNCTIONS FOR FREE-EDGE VERSUS AVERAGE DIA JOINT STIFFNESS CASES (DIA AVG. k_J = 80,000 lb/in/in)

An important issue regarding damage formulae for concrete pavements is whether the damage is more related to the combined stress magnitudes (L+T) or more related to the magnitude of strain reversals, i.e. stress differences from peak to trough, or {(L+T)-T}. Figure 6.15 shows the FEM estimated edge strain (loaded slab change in stress divided by concrete elastic modulus) for the 40-kip FWD and 210-kip B747 gear simulations. The FEM algorithm indicates that more load-related strain is occurring along the edge during the afternoon curled-down gradient condition. The joint loss of support related to the narrow-perimeter-support condition and joint knifing associated with large down-curl has a more severe effect on load-related edge strain than the loss of support associated with up-curl. This is because when slabs are curled upwards, with joints lifted off the foundation, some initial load energy is dissipated while the slab rotates and until the joint seats itself on the subgrade, the remaining load energy then presses the slab edge into the subgrade, which causes a reaction on the bottom of the slab and eventually some bending stress.

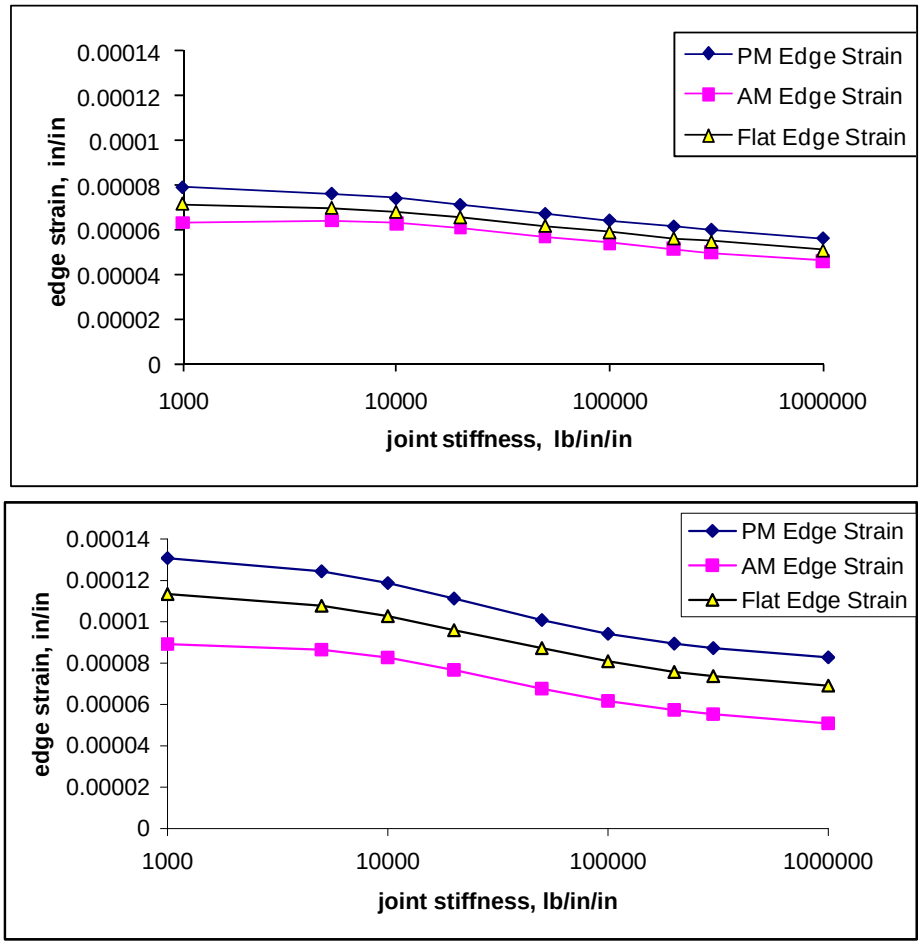

FIGURE 6.15. PLOT SHOWING ESTIMATED LOAD RELATED {(L+T)-T} EDGE STRAIN MAGNITUDES FOR THE 40-KIP FWD LOAD (TOP PLOT) AND 210-KIP B747 GEAR (BOTTOM PLOT) FROM THE DIA CALIBRATED FEM ALGORITHM

The concept of LT can also be applied to estimated {(L+T)-T} strain magnitudes resulting from FEM algorithms. This simulated strain LT analysis probably best simulates how LT has been historically measured. Figure 6.16 shows a comparison of load-strain versus combined-stress FEM LT curves for the 40-kip FWD and 210-kip B747 gear loads. In general, LT calculations based on strain reductions are similar for flat and curled-down shapes, and there are greater differences in combined stress LT calculations related to slab curling. The load-strain LT is associated with the {(L+T)-T} curves, while the combined stress LT calculations are based on the (L+T) curves. In general, if residual curling stress is assumed to be insignificant the {(L+T)-T} load transfer LT curves can be used as a basis of design. Alternately, if residual curling stress is considered significant and being addressed directly in the concrete slab material damage formula, the (L+T) curves for LT would be used as a basis of design.

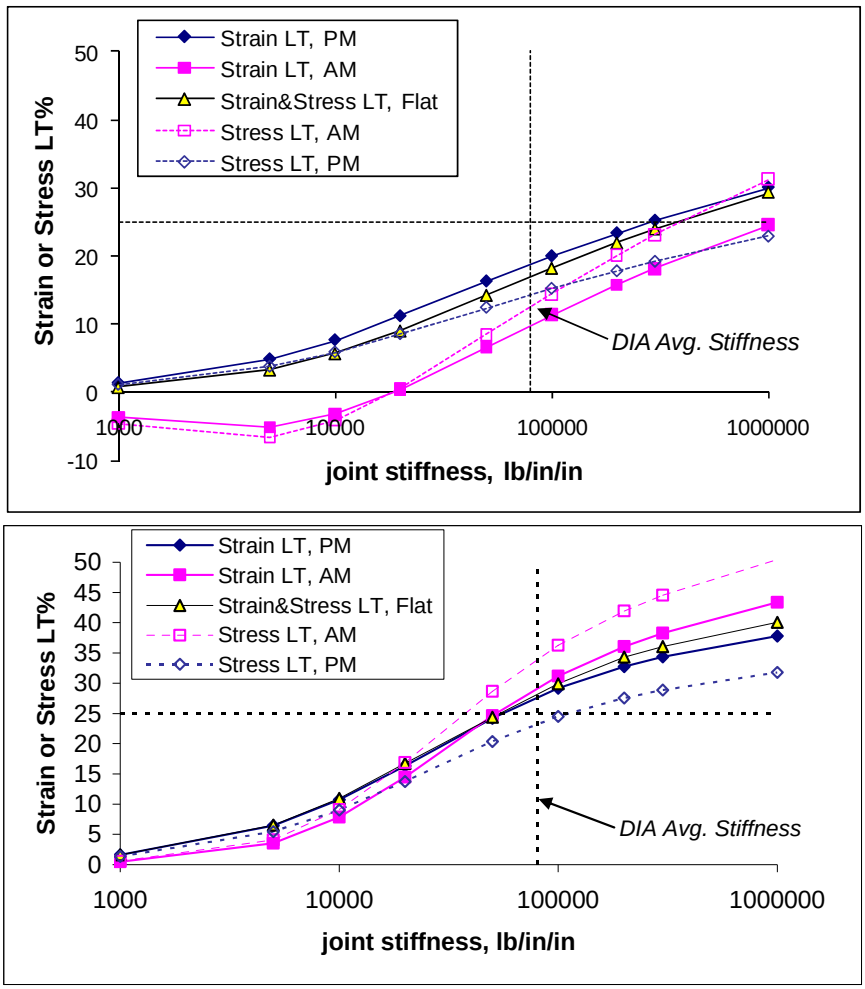

FIGURE 6.16. COMPARISON OF LOAD-RELATED EDGE STRAIN {(L+T)-T} AND COMBINED STRESS (L+T) BASED LT FUNCTIONS FROM THE 2-SLAB FEM ALGORITHM CALIBRATED TO DIA BEHAVIOR, FOR THE 40-KIP FWD LOAD (TOP) AND 210-KIP B747 GEAR (BOTTOM)

6.2 THE EFFECTS OF SLAB CURLING ON EDGE STRESS LT VALUES

This section demonstrates how to match the DIPSTICK slab curling data along with the measured joint stiffness versus LTE_{δ} data to FEM algorithm responses estimated for curling using the data from site 5-AGG18. This test site showed the most curling related effects on joint load transfer of all airfield test sites. Additional discussion regarding how curling at this test site affected joint and mid-panel behavior was provided in chapter 3 around figures 5, 6, 13, 14, 17, 34, 36, and 37. Figure 6.17 shows the calculated joint stiffness versus LTE_{δ} data along with the FEM algorithm estimated characteristic joint stiffness curves for 0, 1, 2, and 3 °F/in thermal gradient magnitudes. The flat slab condition FEM algorithm hugs the lower boundary of the measured data set, and increasing upward curling explains the observed changes in the joint stiffness responses at the site. Based on the range of measured behavior at the site, the apparent

joint support changes caused by curling are about equal to the effects calculated for a 1.5 to 1.8 °F/in thermal gradient in the FEM algorithm. The variation appears to be closer to 1.5 °F/in for higher stiffness values, and closer to 1.8 °F/in for lower stiffness values.

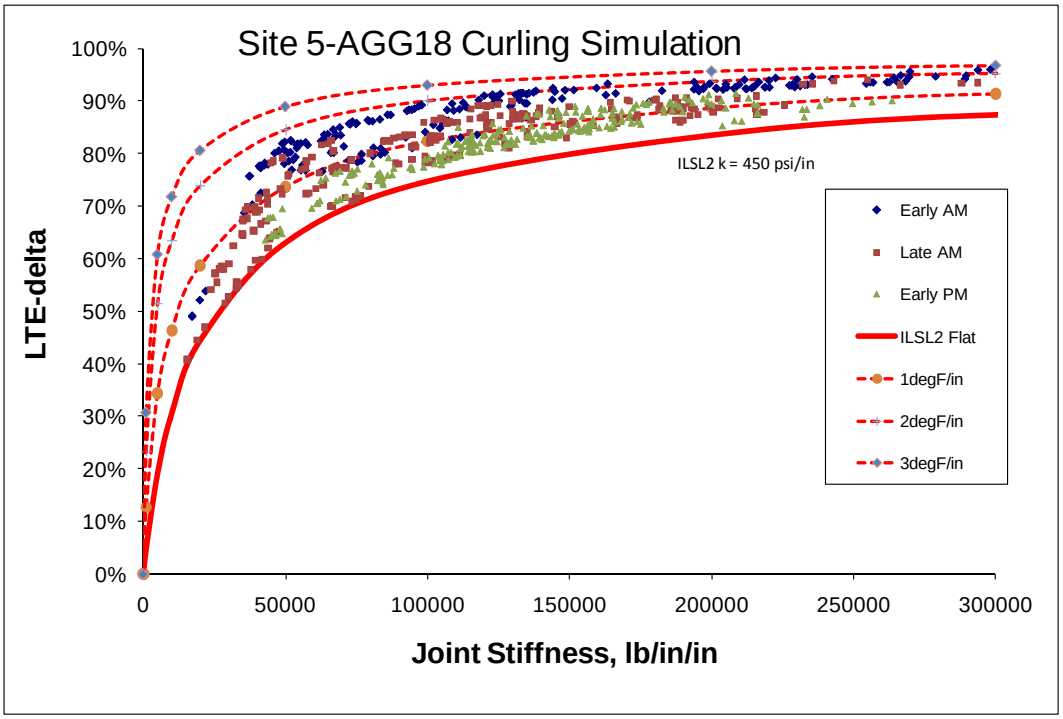

FIGURE 6.17. COMPARISON OF FWD JOINT STIFFNESS VERSUS LTE_{δ} MEASUREMENTS FOR THREE TIMES OF THE DAY, TO FEM ALGORITHM CURLING SIMULATIONS FOR THE CALIBRATED ILSL2 FEM ALGORITHM FOR SITE 5-AGG18

Figure 6.18 shows the FEM generated LT versus joint stiffness curves from the calibrated algorithm for site 5-AGG18, along with the range and average values of joint stiffness for the three Rounds of FWD testing. These curves are for the 12-inch diameter FWD load plate simulations. Average values of LT ranged from about 14 to 20%. Any given joint at the site may be expected to have varying LT over a 24 hour period in a rotating pattern similar to that shown. The variation in measured joint stiffness is relatively high at all sites because the variability in joint opening sizes is significant. Therefore, the functional joint stiffness range at the test sites varies considerably. Some joints had LT values varying between 5 and 10%, while others had LT varying between about 23 and 27% for the FWD sized loads.

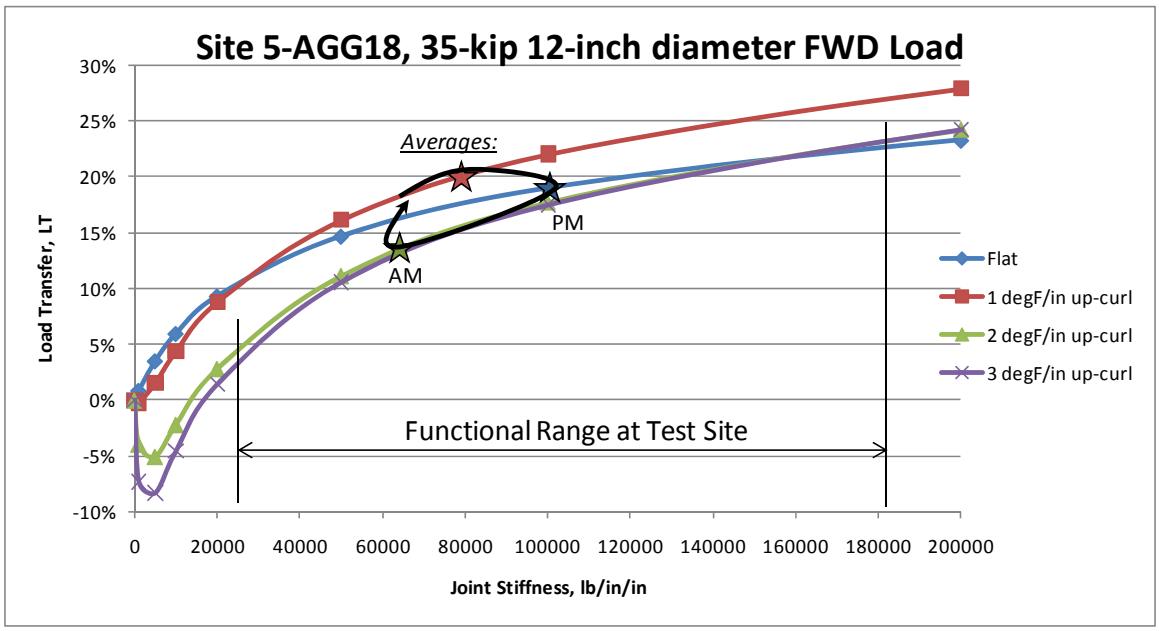

FIGURE 6.18. FEM GENERATED LT FUNCTIONS FOR 35-KIP, 12-INCH DIAMETER FWD LOADS PRESENTED FOR INCREASING THERMAL GRADIENTS

The DIPSTICK measured slab curling data from site 5-AGG18 was presented in figures 3.34 and 4.16. The measured slab curvature data is now compared to the FEM algorithm calculated slab curvature in figure 6.19. The slab end slope sampling and mean value integral for curvature was applied in the same way to the resulting FEM slab shapes to obtain average slab curvature values for different thermal gradients. The measured temperature data from test site 5-AGG18 was provided in figure 3.14. Looking at the data, it would be almost impossible to have an overall thermal gradient at this site greater than about 50/18 = 2.7 °F/in with air and pavement temperature ranging between about 80 and 130 °F during testing. For the measured curling curvature change of 0.00011 ft^{-1}, the FEM algorithm indicates a linear thermal gradient of about 2.1 °F/in would be required to develop this magnitude of curvature, a reasonable value. This is just slightly larger than the Westergaard (1927) curling solution zero-gravity curvature gradient matching this shape change, described in figure 3.37. Assuming the average value of slab curvature measured at about 8 AM represents the locked-in warp equivalent for the site, the equivalent magnitude of thermal gradient locked in as warp is shown by the FEM discretization to be about 2.4 °F/in in the upward direction. The measured joint stiffness response trends in figure 6.17 imply an effective thermal gradient effect on edge support of less than about 1.5 to 1.8 °F/in thermal gradient range. Site 5-AGG18 was the one test site having apparently the least compliant foundation to curling deformations. A relatively high percentage of the measured thermal gradient curling slab shape change did show up in the joint response data. As discussed previously, some sites experienced very little apparent change in slab edge support while at the same time experiencing significant slab curvature changes from curling. These sites have softer more compliant foundations, acting more like fluid filled bags beneath the slabs. An ideal fluid filled bag foundation would allow curling to occur without having significant change in slab edge support. The apparent degree of compliance can be calculated using a plot like that shown in figure 6.19. The degree of foundation compliance can be estimated by obtaining the apparent

percentage reduction in measured thermal curling gradient viewed in the joint response data, as compared to that measured in slab shape changes. For example, using the above data for site 5-AGG18, the degree of compliance is about (2.1-1.7)/2.1, about 20%. This means that the combination of slab self-weight sinking and foundation creep compliance reduce the apparent thermal gradient effects on joints to about 80% of measured thermal gradients. Test site 2-AC17, overlying relative weak wet clayey subgrade, revealed almost no change in FWD slab edge support response, while experiencing almost the same amount of measured slab shape change as site 5-AGG18. This site was about 80 to 90% compliant, to the point where the edge support remains very close to that of a "flat slab" even during relatively large slab curvature changes. Residual curling stress in the slabs would be higher and significant for site 5-AGG18 with low compliance. Residual curling stress would be low, near zero for site 2-AC17 having high compliance. Slabs at site 2-AC17 are essentially supported by a material with behavior close to a fluid filled bag with respect to very slow loading rates associated with curling and warping.

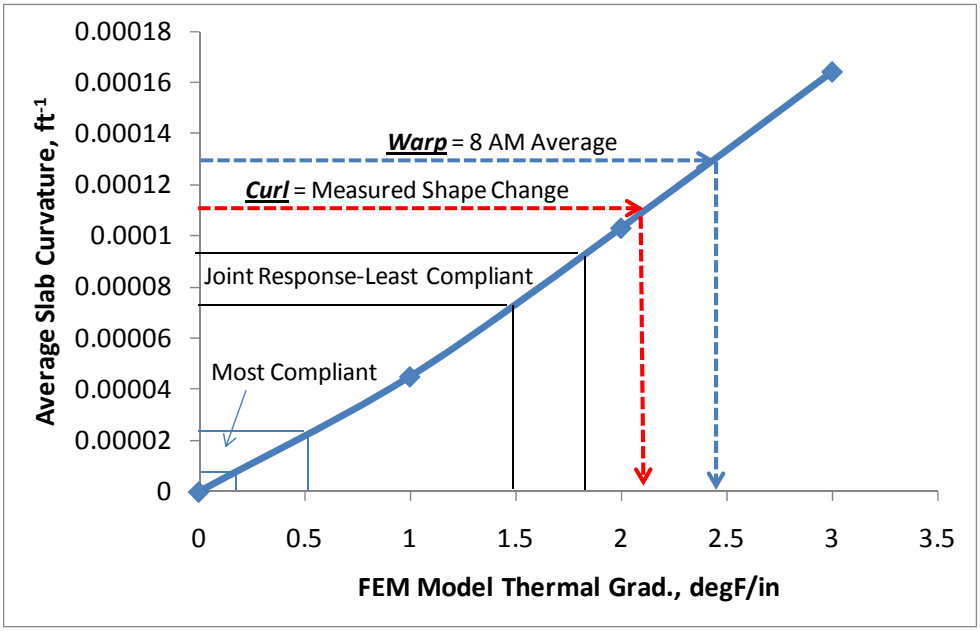

FIGURE 6.19. COMPARISON OF DIPSTICK MEASURED SLAB CURVATURE DATA TO FEM CALCULATED SLAB CURVATURE DATA FOR SITE 5-AGG18

6.3 COMPARISON OF ILSL2 TO FEAFAA

The primary difference between the ILSL2 and FEAFAA FEM codes is the foundation idealizations as shown in figure 6.20. ILSL2 used the dense liquid (bed of springs) foundation idealization and FEAFAA used a layered elastic solid foundation idealization. ILSL2 uses a two dimensional plate representing the slab, while FEAFAA uses three dimensional solid elements for the slab. Both models use the linear spring constant (lb/in/in) representation for joint stiffness.

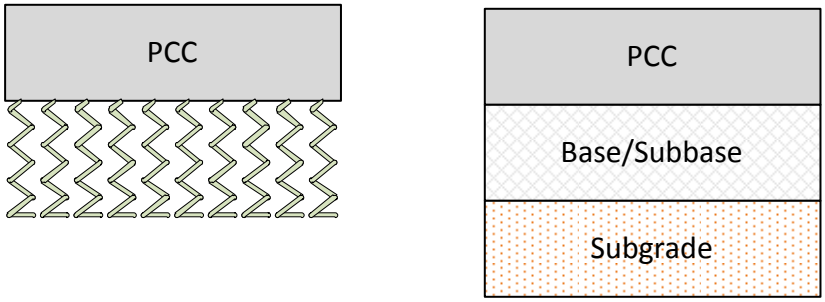

FIGURE 6.20. DIFFERENCES IN FOUNDATION IDEALIZATIONS FOR ILSL2 (BED OF SPRINGS, OR DENSE LIQUID) AND FEAFAA (LAYERED ELASTIC SOLID MATERIALS)

The FEAFAA software converts dense liquid modulus of subgrade reaction *k*-values (psi/in) to equivalent subgrade elastic modulus, E_S, values (psi) using the following equation.

$$E_S = 26 \cdot k^{1.284} \tag{42}$$

As part of this study, attempts were made to establish identical models in ILSL2 and FEAFAA for comparisons. The FEAFAA simulations for this study assumed the base and subgrade layers to have the same elastic modulus to simulate a single layer or uniform foundation like ILSL2. For dense liquid subgrade *k*-values of 200 psi/in and 430 psi/in, the converted elastic moduli are 23,415 psi and 62,567 psi, respectively using the above equation. ILLI-BACK was used for analysis of the FWD mid-panel load test data from the test sites. This software backcalculates the dense liquid and elastic solid subgrade parameters. The backcalculation results from the test sites allow an independent check of the equation shown above. Figure 6.21 shows this comparison. Each data point shown represents the overall site average based on hundreds of mid-panel load tests. Most of the test sites ended up slightly above the FAA equation trend, with only one site (5-AGG18) being below. The best-fit power function for the test site data, similar to the FAA equation form, is provided. This relation represents apparent equivalencies for top-of-base foundation stiffness.

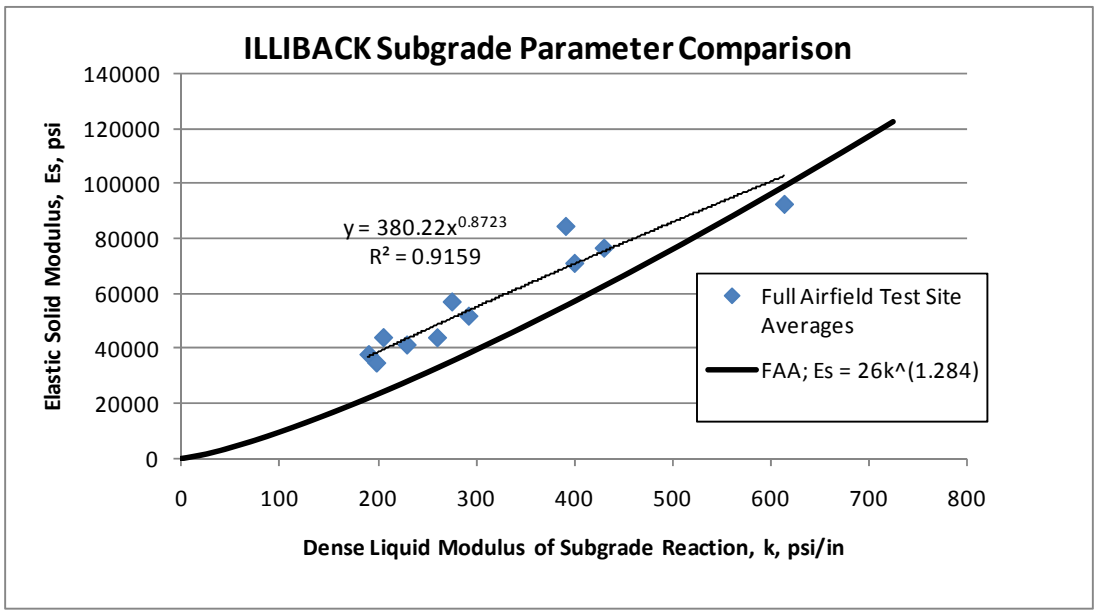

FIGURE 6.21. A COMPARISON OF THE k TO E_S CONVERSION EQUATION FROM FEAFAA TO THE OVERALL TEST SITE AVERAGE TOP-OF-BASE VALUES OBTAINED USING ILLI-BACK

In order to compare the output from FEAFAA to ILSL2, two-slab arrangements having nearly identical cross sections were established in both software packages, simulating site 2-AC17. The characteristic joint stiffness curves generated from the two FEM discretizations are shown in figure 6.22 overlying the calculated joint stiffness data. The upper and lower limit subgrade stiffness values of 200 and 430 psi/in determined from Skarlatos/Ioannides-Edge and ILLI-BACK mid-panel analyses were used to develop the FEM curves. As discussed previously, the Skarlatos/Ioannides and ILLI-BACK k-values of 200 and 430 psi/in tend to act as upper and lower boundary solutions for the ILSL2 FEM results relative to the FWD-based joint stiffness data. The FEAFAA generated joint stiffness curves do not match the FWD trend as well as the ILSL2 curves. This is due primarily to the elastic solid base and subgrade idealization in FEAFAA. The best-fit FEAFAA curve is approximately the k=200 psi/in equivalent (E_S = 23,415 psi) curve.

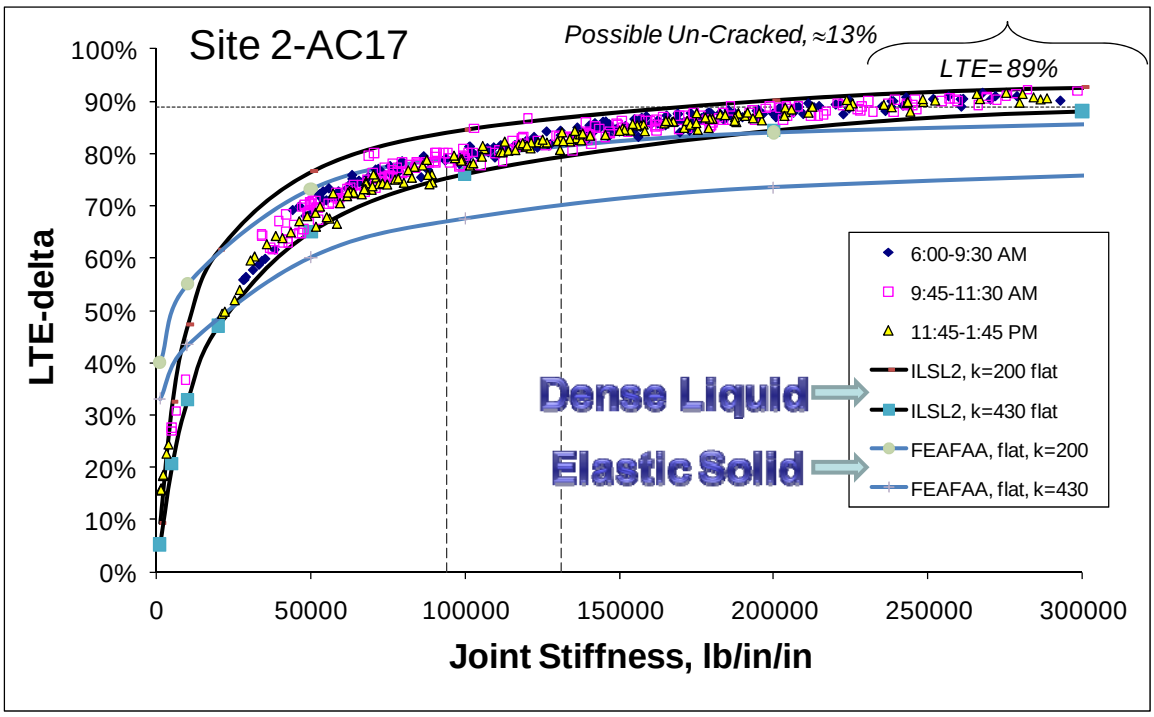

FIGURE 6.22. COMPARISON OF CHARACTERISTICS JOINT STIFFNESS CURVES GENERATED FROM FEAFAA AND ILSL2 AND SIMULATING SITE 2-AC17 SITE CONDITIONS

Figure 6.23 shows the same data plotted using a logarithmic scale for joint stiffness. The logarithmic scale highlights the low stiffness joint behavior more, but diminishes the important asymptote effect visible when using the linear scale for joint stiffness. This plot highlights the differences between reality (FWD-based joint stiffness) and the ideal extremes from the two computer codes. The FEAFAA software yields higher LTE_{δ} values for low joint stiffness due entirely to the elastic solid base effects. The ILSL2 program has no elastic solid base effect, and the real test sites tend to show just a small amount of apparent elastic solid base effect. It is believed that once a joint becomes deteriorated and has low stiffness, the base shearing action associated with the low stiffness joint will quickly diminish the elastic solid base behavior by developing localized cracking and crushing beneath the joint, making it behave more like a cracked base ideal linear shear spring on a dense liquid foundation. In the high joint stiffness range, the FEAFAA software yields lower LTE_{δ} than was calculated for the site, or calculated by ILSL2. It is believed that typical slight up-lift warping and permanent downward deformation voids increase overall joint deflections, increasing LTE_{δ} values and making the joint behavior appear more like the linear spring on a dense liquid foundation.

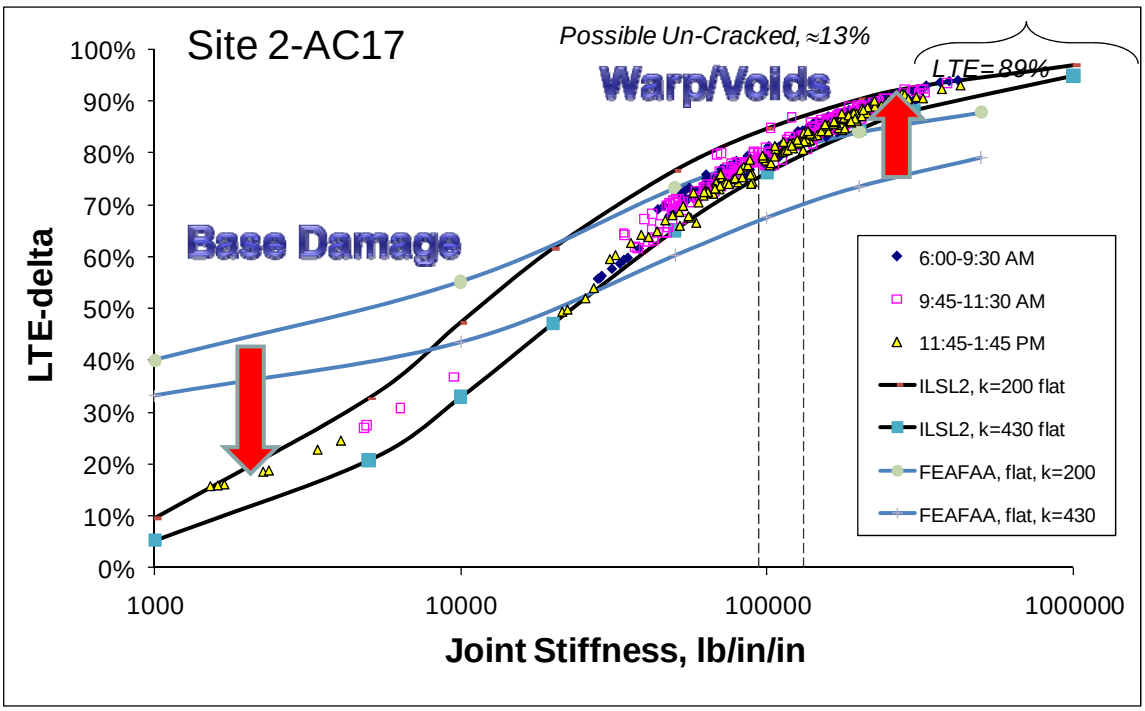

FIGURE 6.23. A PLOT HIGHLIGHTING THE APPARENT KEY FACTORS CAUSING DEVIATION FROM THE FEAFAA ELASTIC SOLID SUPPORT ASSUMPTIONS

Figure 6.24 shows the combined stress (L+T) percentage reduction LT curves, and figure 6.25 shows the load-strain {(L+T)-T} curves for LT generated from FEAFAA and ILSL2 for site 2-AC17, for the flat conditions and the upward and downward curling conditions. The LT values generated from FEAFAA are generally lower than LT values generated from ILSL2. The trends generated are similar in shape, but curling has greater effect on FEAFAA results than ILSL2 results. The apparent negative LT trend, or increase in edge stress above free edge stress levels for low joint stiffness, is greater for the FEAFAA software than for the ILSL2 program. Importantly, both codes indicate that the lowest amount of LT will occur during the curled-down edge loading condition, when edge load stress values are also at their greatest magnitude. The strain LT estimates are more similar than stress LT calculations for the two codes. Another key trend is: there is decreasing achievable LT as subgrade stiffness increases. This means oddly that as more effort is spent to create a stiffer foundation, less joint load transfer will be realized. This is a strain compatibility concept. When the subgrade is softer, the joints deflect more and mobilize force more effectively.

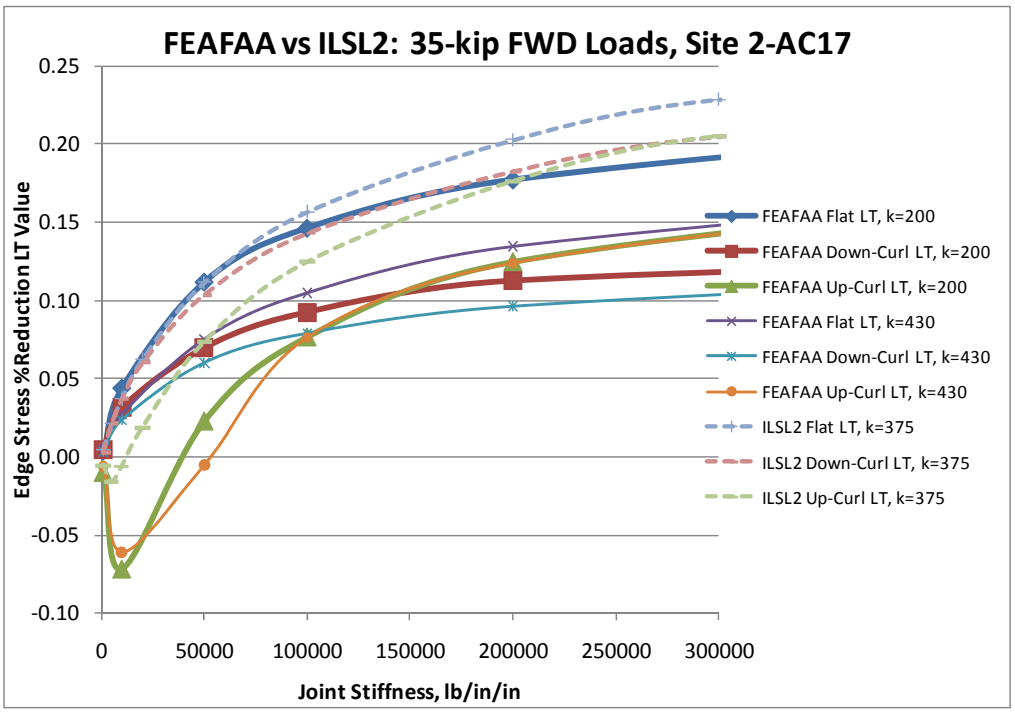

FIGURE 6.24. COMPARISON OF (L+T) EDGE STRESS LT FUNCTIONS GENERATED FROM FEAFAA AND ILSL2, FOR 35-KIP FWD LOADS, AND FOR FLAT UPWARD AND DOWNWARD CURLING CONDITIONS

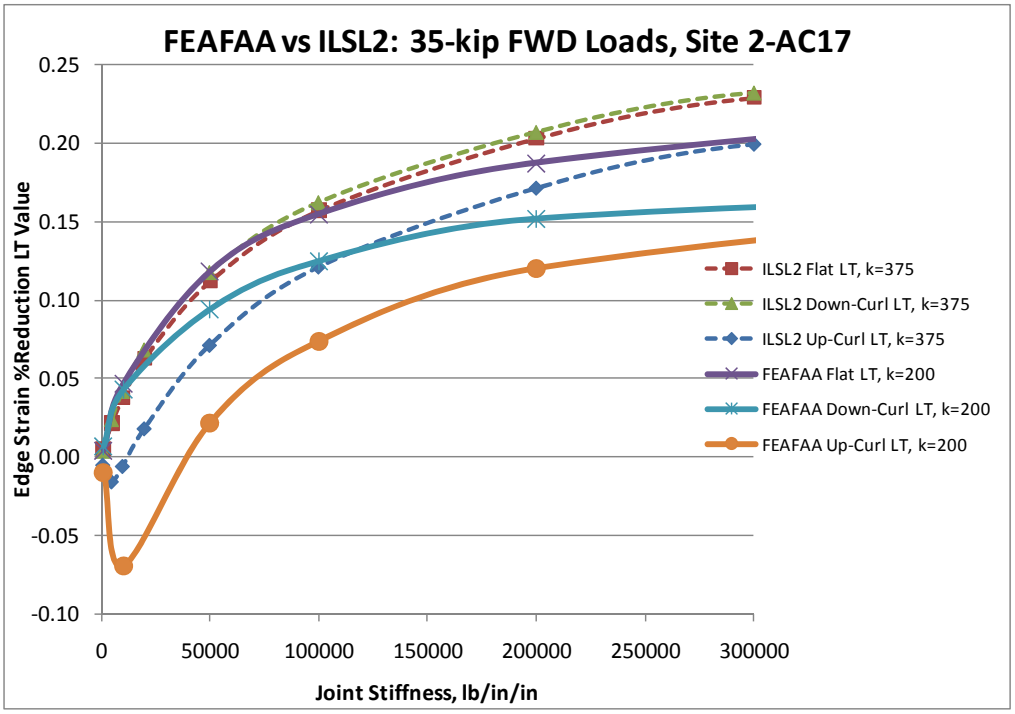

FIGURE 6.25. COMPARISON OF {(L+T)-T} LOAD RELATED EDGE STRAIN LT FUNCTIONS FROM FEAFAA AND ILSL2 FOR 35-KIP FWD LOADS

6.4. SUMMARY OF BOTTOM OF SLAB STRESS LT FROM FEM ANALYSIS

This section summarizes the LT variations observed for the traditional edge loading bottom of slab stress analyses using a range of simulated loading and the calibrated FEM algorithms. In addition to the 12-inch diameter FWD load and the B747 four-wheel gear load simulations previously described: 30-kip, 60-kip, and 90-kip single wheel loads at 200 psi were also simulated with the ILSL2 FEM software to study load area size affects. The B737 two-wheel gear as shown in figure 6.26 was also simulated.

Boeing 737-900ER

Gross Weight (lbs): 188,200
%GW on Main Gears: 95.00
No. Main Gears: 2
Wheels on Main Gear: 2
Tire Pressure (psi): 200.0

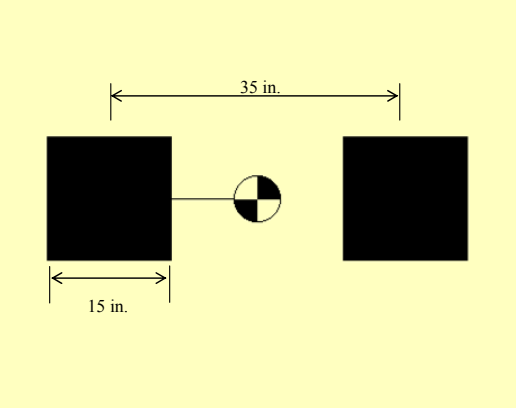

- Individual wheel load on the main gear = (188200*95%)/2/2 = 44697.5 lbs
- Footprint side length (square footprint) = sqrt (44697.5/200) = 14.95 in.≈ 15.0 in.

FIGURE 6.26. B737 GEAR SIMULATED IN THE FEM ANALYSES

The single-wheel loads and gear combinations evaluated represent a considerable range of load magnitudes spanning what would probably have been encountered on these airfield test sites. To demonstrate the range of LT values calculated using the FEM, summary LT versus joint stiffness plots are presented in figures 6.27 through 6.30 for four of the test sites. The plots show the FEM generated LT functions for the various load types and broken down by simulated thermal gradient magnitude (0, -2, and +2 °F/in) for flat, curled-down, and curled-up conditions. The ± 2 °F/inch gradients simulated are relatively large and represent the extreme outer boundary of probable variation that will be observed at an airfield site. If the site subgrade is compliant to curl and warp, the joint LT values will stay near the flat slab zero gradient values. If the subgrade is not very compliant, LT values could vary about the flat slab values to some extent between the ranges shown. If large up-warp develops at a site, the LT trends may shift and range between the flat slab and up-curled LT values shown, with the concrete slabs never experiencing

a true down-curled slab shape joint support condition. The opposite condition of large down-warp can also develop.

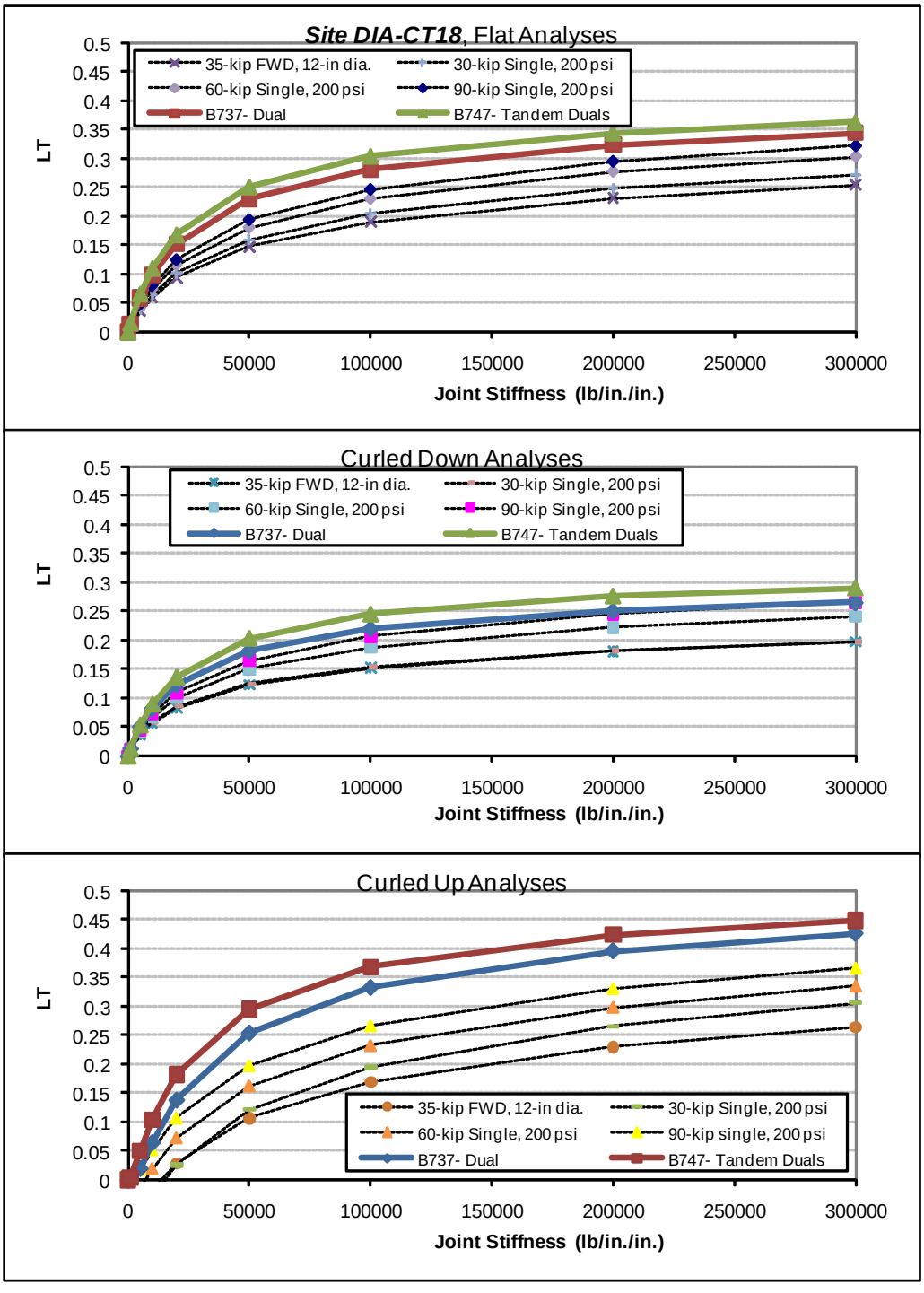

FIGURE 6.27. SUMMARY OF LT FUNCTIONS FOR VARIOUS LOAD TYPES FOR THE CALIBRATED ILSL2 FEM ALGORITHM FOR SITE DIA-CT18 (k=250 psi/in, E_C =5,000,000 psi, Slab Length = 18.75 feet)

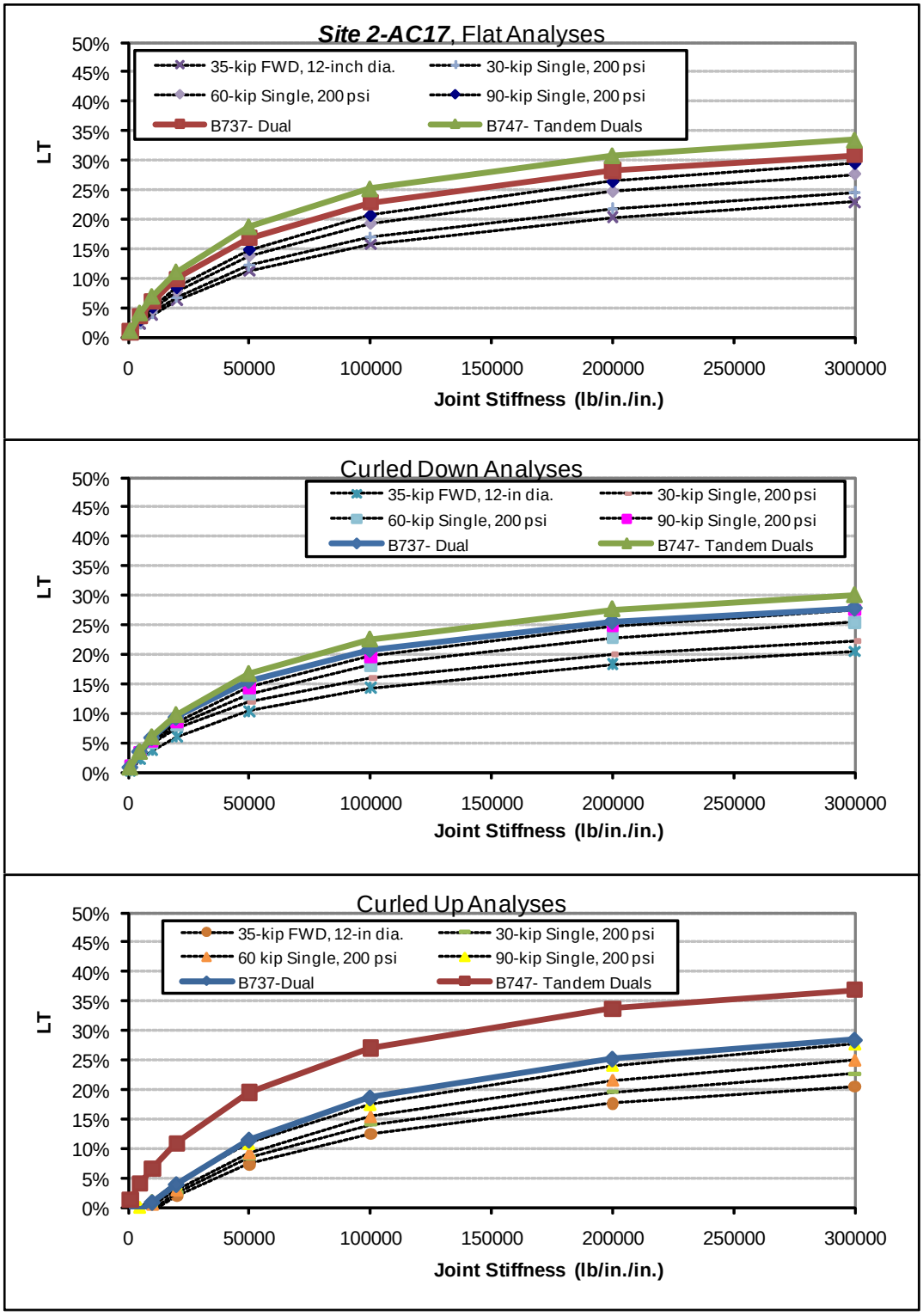

FIGURE 6.28. SUMMARY OF LT FUNCTIONS FOR VARIOUS LOAD TYPES FOR THE CALIBRATED ILSL2 FEM ALGORITHM FOR SITE 2-AC17 (k=375 psi/in, E_C =6,440,000 psi, Slab Length = 12.5 feet)

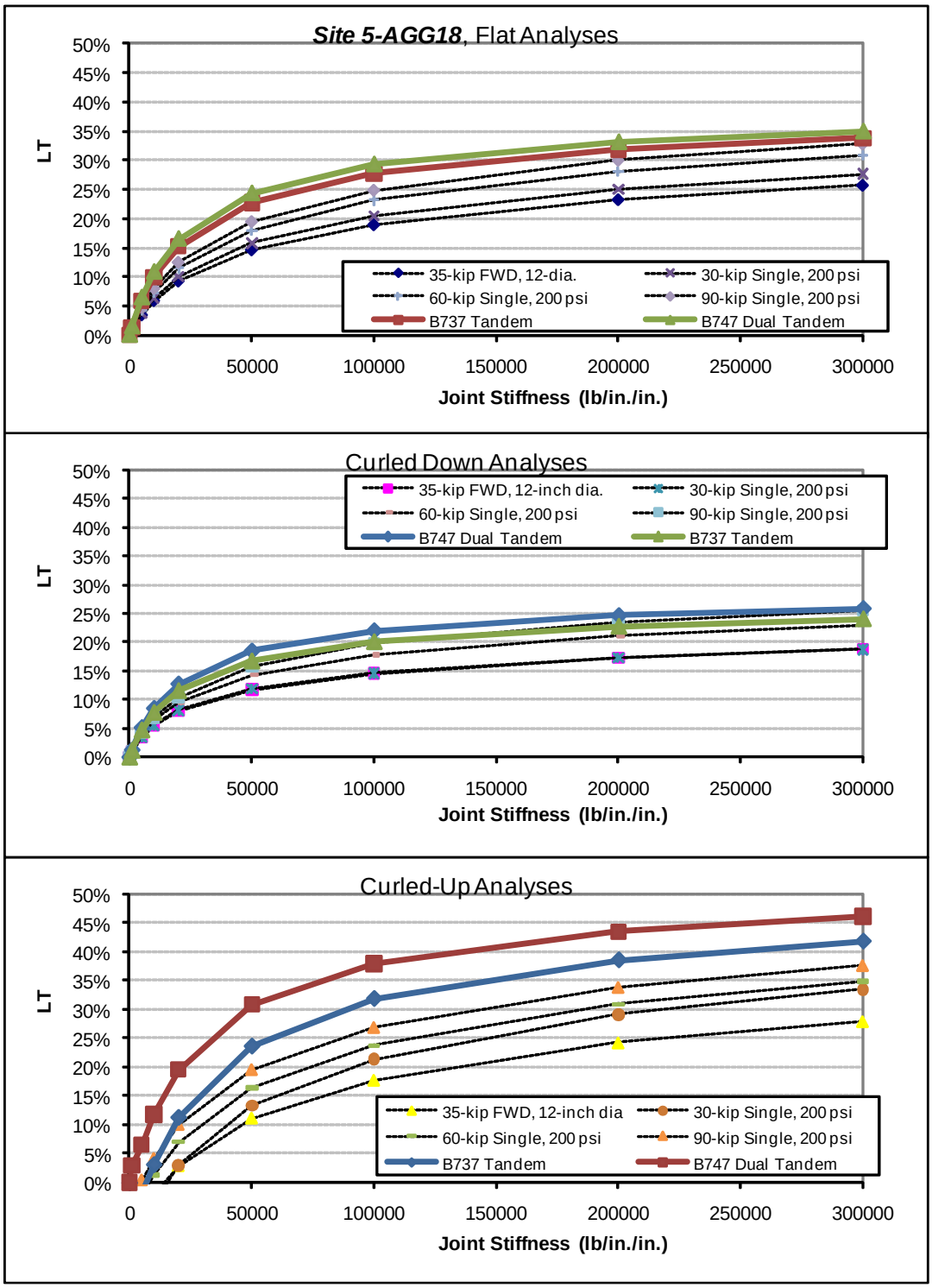

FIGURE 6.29. SUMMARY OF LT FUNCTIONS FOR VARIOUS LOAD TYPES FOR THE CALIBRATED ILSL2 FEM ALGORITHM FOR SITE 5-AGG18 (k=450 psi/in, E_C =3,290,000 psi, Slab Length = 18.75 feet)

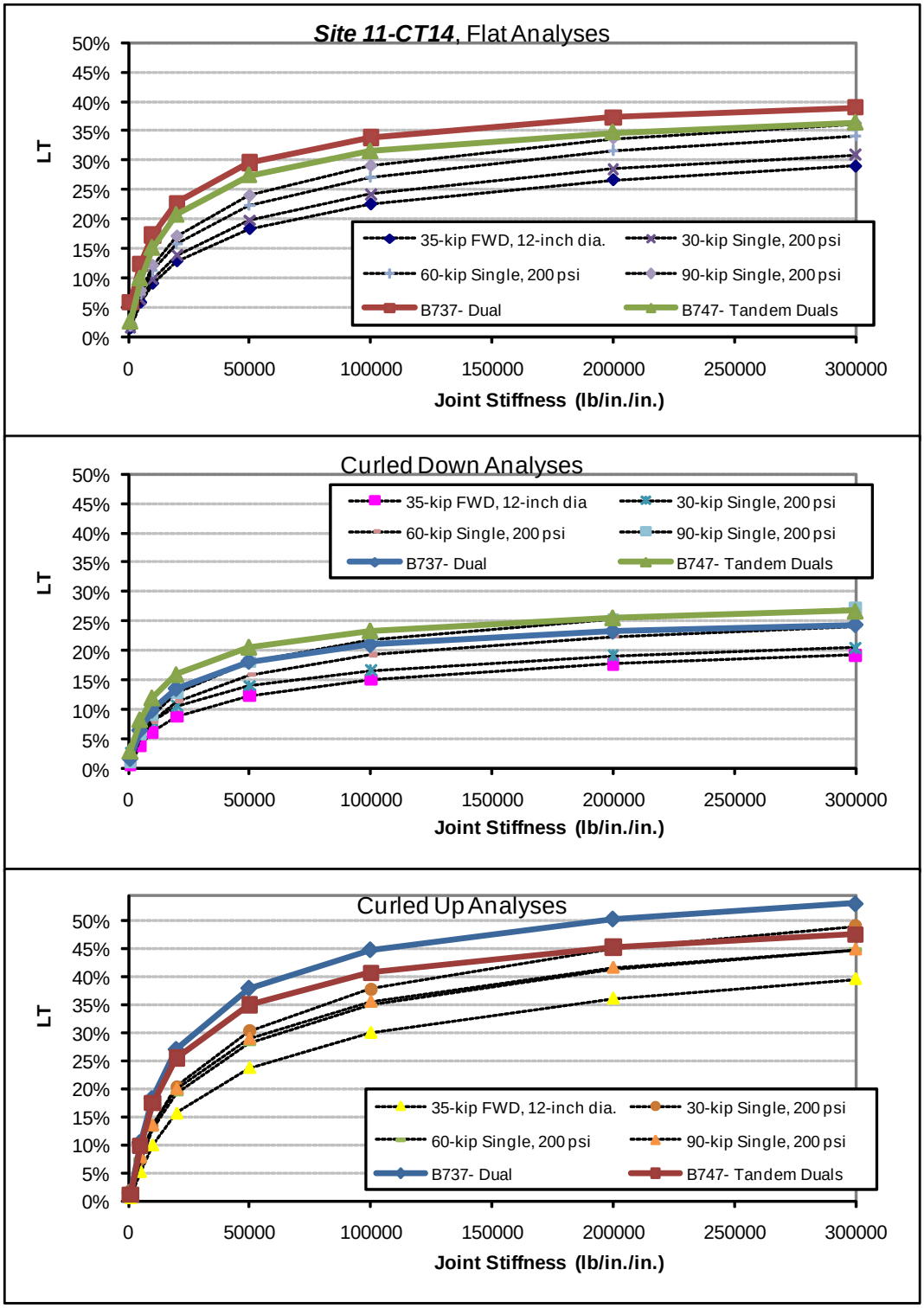

FIGURE 6.30. SUMMARY OF LT FUNCTIONS FOR VARIOUS LOAD TYPES FOR THE CALIBRATED ILSL2 FEM ALGORITHM FOR SITE 11-CT14 (k=200 psi/in, E_C =4,900,000 psi, Slab Length = 25 feet)

The DIA test site and site 5-AGG18 have similar slab dimensions and thickness, and the resulting LT curves are similar for these test sites. These test sites use common joint spacing that is generally conforming to current joint spacing requirements in FAA AC 150/5320-6E. These two test sites are considered to have designs closest to airfield concrete pavement designs that will be constructed in the near future. Test site 2-AC17 was simulated as 12.5-ft by 25-ft slabs, with the loads placed on the shorter 12.5-ft slab dimension. Loading of this short slab dimension resulted in significantly lower LT values. Test site 11-CT14 used 25-ft by 25-ft slab dimensions with a smaller 14-inch thickness, and this test site had higher LT values. There is a trend of decreasing LT values achievable for shorter slab dimensions for a given joint stiffness. This trend is however, compensated for by a general trend of increasing joint stiffness values for decreasing slab lengths as discussed in Chapter 5. Although less LT is achievable for shorter slabs, LT values will tend to stay up higher on the LT curves during winter conditions as a result of smaller changes in joint openings and higher aggregate interlock stiffness.

Many staff-hours were required to develop all of the FEM algorithms and simulations to obtain the four summary LT plots. As is evident, there are many factors affecting the actual LT value that will be present at any point in time, and there is large variation by load type and thermal gradient conditions. In attempt to summarize all of the above FEM LT curves into one simple rapid calculation algorithm, all of the solution values and inputs were combined into a statistical database and non-linear regressions algorithms developed to reproduce the LT curves. The shapes of the FEM generated LT curves are somewhat difficult to reproduce, having asymptote values and curvature shape that varies for each curve. The Skarlatos/Ioannides solution trend shape again becomes a valuable tool for reproducing joint behavior, and is used here in a regression formula for yielding the LT values calculated from jointed FEM algorithms. The regression formula form used is as follows:

$$\textbf{\textit{Estimated LT}} = \boldsymbol{A} + \boldsymbol{B}(\textit{Skarlatos Guess}) + \boldsymbol{C}(\textit{log(f)}) + \mathrm{Y}(\textit{GearLoad}/k_J)^{\mathrm{Z}} + \mathrm{AA}(\textit{Slab Length, ft})^{\mathrm{BB}} \quad (43)$$

Where,

$\boldsymbol{A}$, $\boldsymbol{B}$, and $\boldsymbol{C}$ are functions of site parameters as follows:

$$\boldsymbol{A} = [8\text{-}\mathrm{A}(\textit{linear }^{\circ}\mathrm{F}\ \textit{grad.})^{\mathrm{B}} + \mathrm{C}(k\ell)^{\mathrm{D}} + \mathrm{E}(\textit{PCC thickness})^{\mathrm{F}} + \mathrm{G}(L/\ell)^{\mathrm{H}}]/1200 \quad (44)$$

$$\boldsymbol{B} = [\mathrm{I}(\textit{linear }^{\circ}\mathrm{F}\ \textit{grad.})^{\mathrm{J}} + \mathrm{K}(k\ell)^{\mathrm{L}} + \mathrm{M}(\textit{PCC thickness})^{\mathrm{N}} + \mathrm{O}(L/\ell)^{\mathrm{P}}]/16 \quad (45)$$

$$\boldsymbol{C} = [\mathrm{Q}(\textit{linear }^{\circ}\mathrm{F}\ \textit{grad.})^{\mathrm{R}} + \mathrm{S}(k\ell)^{\mathrm{T}} + \mathrm{U}(\textit{PCC thickness})^{\mathrm{V}} + \mathrm{W}(L/\ell)^{\mathrm{X}}]/900 \quad (46)$$

The values of A-Z, AA and BB are regression parameters as shown in table 6.1. The regression parameters were determined for four cases: All Simulated Load Cases Results, Single-Wheel Results, B737 2-Wheel Gear Results, and B747 4-Wheel Gear Results. In general, the FEM solutions matrix and results database used to establish these LT regression algorithms is not well distributed with respect to site design parameters and can be considered sparse. The resulting LT regression algorithms do very well at reproducing the results for the four calibrated FEM discretizations. It is conceded, however, that the regression formulae are not good at estimating results for other input data combinations significantly outside of or even significantly between

the four FEM discretization input data sets used as the basis of the algorithms. The four cases do represent a full range of designs that may be used. Therefore, the relatively accurate estimates for the four simulated sites using the exact specific inputs considered can be used themselves as the basis of design for "similar" designs varying around the input properties for these four calibrated FEM algorithms. This type of scheme is recommended below.

TABLE 6.1. REGRESSION CONSTANTS FOR THE LT ESTIMATION ALGORITHMS

Cluster	*applies to…*	*Constant*	All Loads	Singles	B747	B737
A - offset value	Temp. Gradient	A	0.966681796	2.010800429	2.399133923	5.744261648
		B	3.390636044	2.886760877	1.993329976	2.162334201
	(kl) cluster	C	-0.00834416	38.73463132	38.73463132	19.50890305
		D	5.876320748	-3.58540112	-3.58540112	1.336330642
	slab thickness	E	983.9071667	119.0977461	19.96506614	0.720350462
		F	-0.66320084	-1.353289728	-1.711758257	0.310986525
	Dimensionless L/l	G	-3.28966E-10	-3.28966E-10	-3.138087592	-6.464099496
		H	15.03195137	14.6552733	1.774411362	1.98446523
B - Skarlatos Function slope modifier	Temp. Gradient	I	1.347565336	1.543474492	2.241021439	4.144421967
		J	1.675905435	1.516230234	1.142712152	1.012790111
	(kl) cluster	K	9.803738002	9.412224106	9.412224106	-72.73637538
		L	-0.047138031	-2.717280257	-2.717280257	-0.076134108
	slab thickness	M	0.00899559	5.291265068	2.925803489	0.22608396
		N	6.05251905	1.610659701	1.977189615	5.7866128
	Dimensionless L/l	O	-1.11483E-05	-0.000209115	9.928250446	101.007214
		P	7.529123279	4.484523239	-1.173741458	-0.24449032
C - Log(f) multiplier	Temp. Gradient	Q	-0.210342557	-0.448477345	2.128246828	60.11203443
		R	3.56830862	2.903552691	-0.640041598	-0.125750868
	(kl) cluster	S	-7.190889669	0.087320106	-0.251784854	-91.63802868
		T	-6.727220759	2.729995335	2.729995335	0.433746573
	slab thickness	U	264.9227379	102.2090106	22.5970748	0.253718411
		V	-5.176277331	-2.795975905	0.427380529	-0.014277744
	Dimensionless L/l	W	26.22045376	-88.92916981	-12.29228592	10.77469223
		X	0.78140125	-0.436496408	-1.208725311	1.46891082
Load and Slab Size	Total Load/kJ	Y	0.521796179	0.02481453	0	0
		Z	-0.054589053	0.326658114	0	0
	Slab Length	AA	-4.12915E-09	-4.12915E-09	0	-3.24076E-05
		BB	4.385012188	4.823933347	0	1.570012061

The *Skarlatos Guess* parameter is the Skarlatos/Ioannides estimated LT (Ioannides et al., 1996) versus joint stiffness curve for the FEM simulated pavement cross section and using a wheel load radius size equal to that of the single wheel sizes simulated in the FEM discretizations. For the B737 and B747 simulations, the initial *Skarlatos Guess* LT curve is established using the magnitude and size of one of the single wheels in the multi-wheel gear analysis. The regression algorithm essentially takes a first guess at the FEM generated LT curve using the Skarlatos/Ioannides LT curve for a given design case and using the wheel load radius for one of a gears individual wheels. It then modifies the *Skarlatos Guess* using the various parameters shown above, to yield the FEM LT for the same design scenario simulation and considering curling variations. The ***A*** function shifts the *Skarlatos Guess* curve up and down along the y-axis. The ***B*** function changes the slope of the *Skarlatos Guess* curve. The ***C*** function is multiplied by the joint stiffness so is also a slope modifier. The *Skarlatos Guess* function is also modified by non-linear functions of the gear load and the slab length.

Figures 6.31-6.34 show the LT regression best-fit results showing the r-square values range from about 0.95 (all load cases) to 0.98 (B747 gear only) with generally linear residual trends. The estimate errors are small for the sites DIA-CT18 and 5-AGG18 as these two sites represent the "middle region" of the regression analysis data. These sites have 18.75-ft to 20-ft joint spacing. The other two sites 2-AC17 and 11-CT14 have 12.5-ft and 25-ft loaded slab edge lengths and represent outer boundaries for the data set. Estimation errors are larger for these outer boundary sites. Estimation errors are smaller for the flat-slab simulations, which also represent a middle region for the regression space.

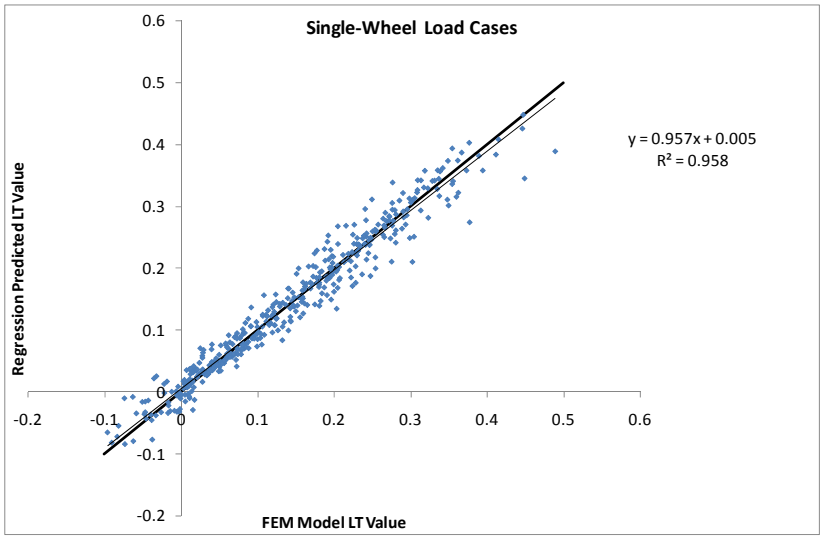

FIGURE 6.31. THE SINGLE WHEEL LOADS FEM LT REGRESSION MODEL ACCURACY SUMMARY

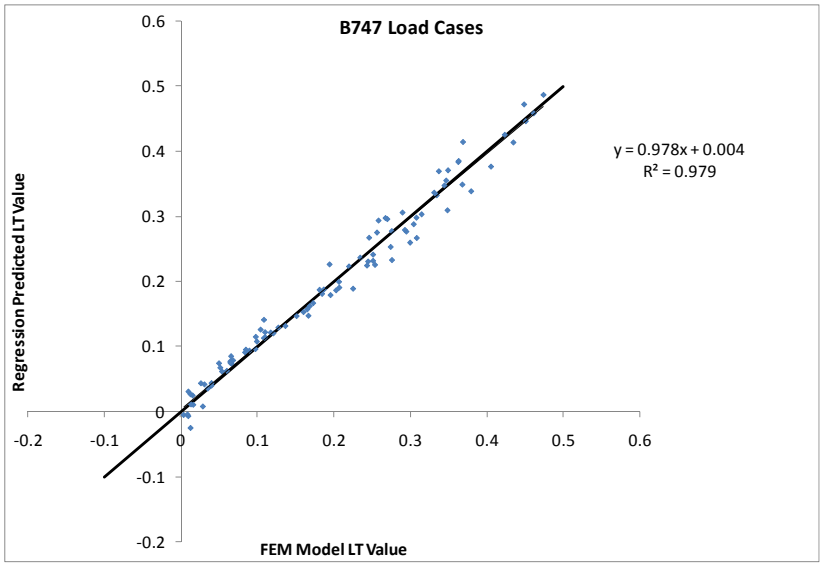

FIGURE 6.32. THE B747 4-WHEEL GEAR FEM LT REGRESSION MODEL ACCURACY SUMMARY

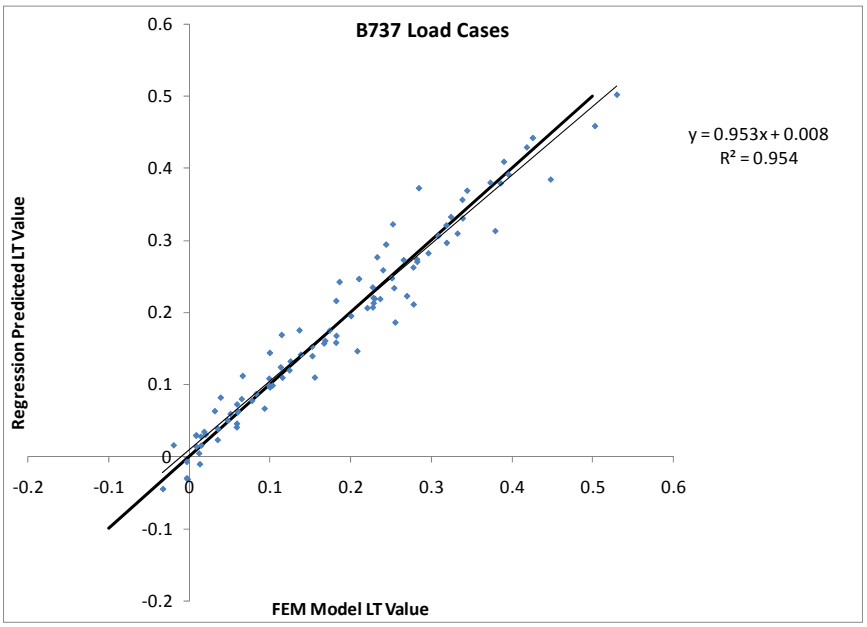

FIGURE 6.33. THE B737 2-WHEEL GEAR FEM LT REGRESSION MODEL ACCURACY SUMMARY

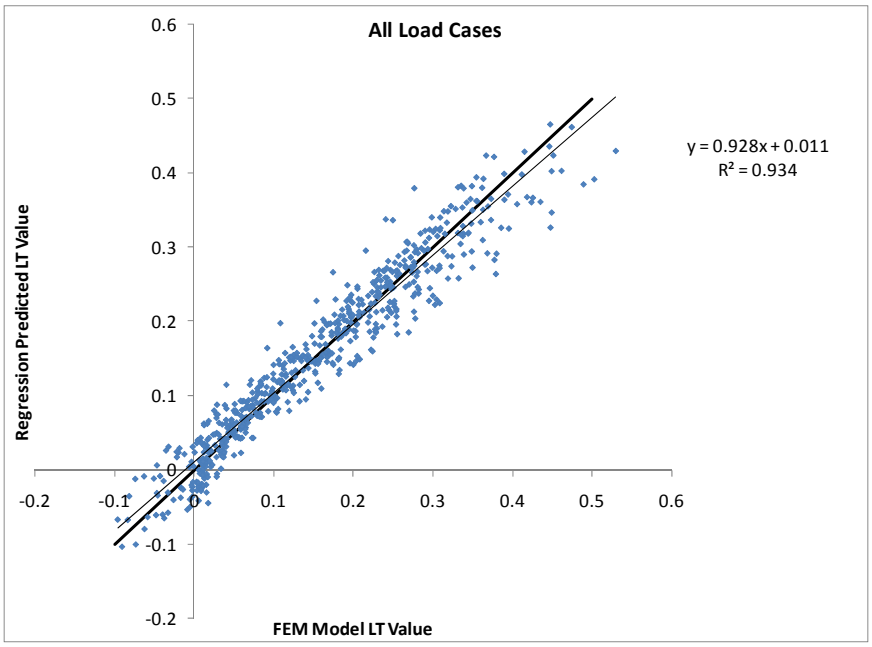

FIGURE 6.34. THE ALL-LOADS FEM LT REGRESSION MODEL ACCURACY SUMMARY

To demonstrate the overall LT versus joint stiffness curve shapes generated by the FEM LT regression analysis, figure 6.35 shows the test site DIA-CT18 FEM model LT versus joint stiffness results again, and now with the regression simulations overlaid on top of the FEM analysis results, shown as heavy dashed lines. The regression model in general produces the LT values well and is a suitable rapid closed-form estimation of many FEM analyses that can be easily programmed into design procedures.

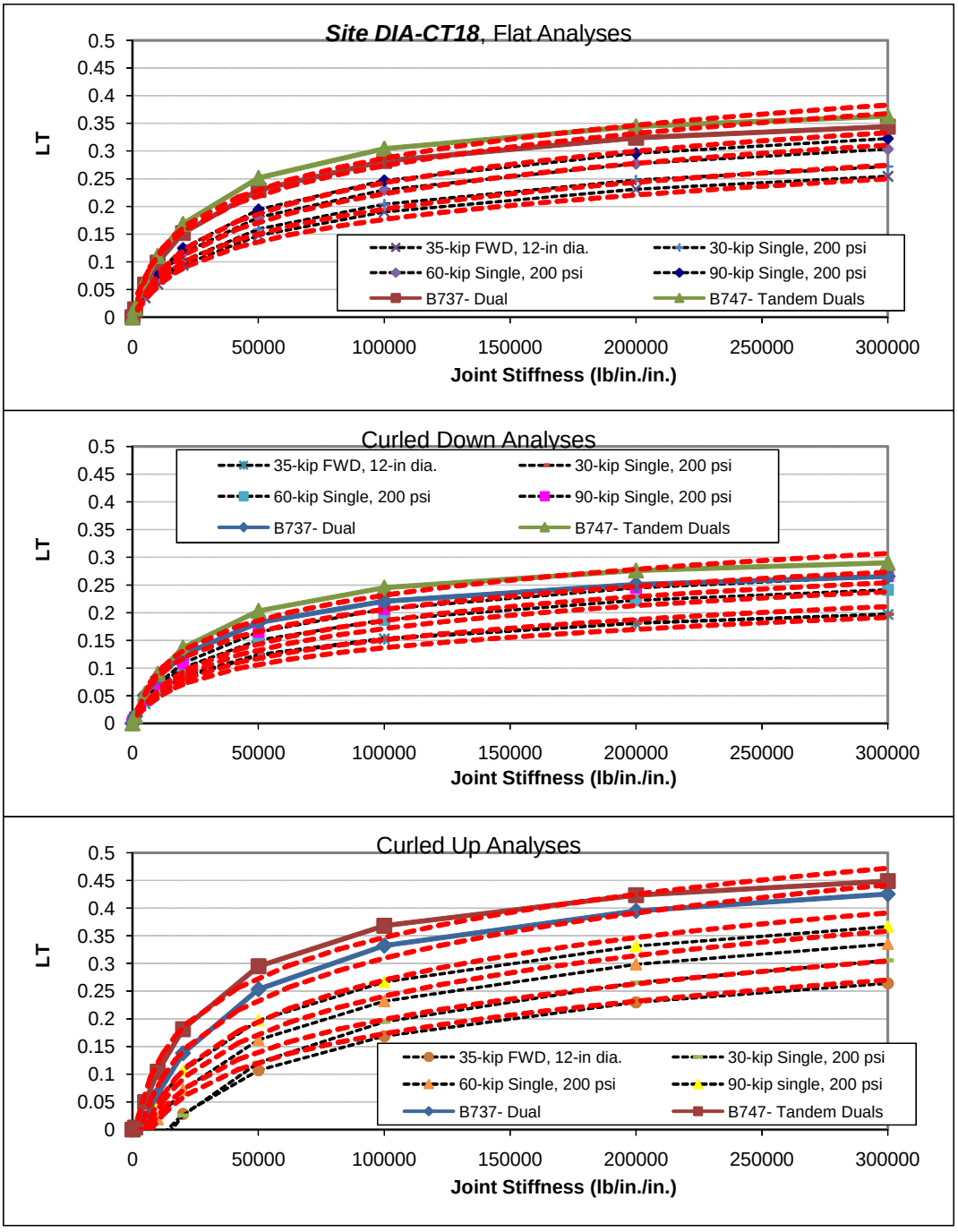

FIGURE 6.35. THE FEM LT VALUES CALCULATED FOR SITE DIA-CT18 AND SHOWING THE LT REGRESSION MODEL ESTIMATES (HEAVY DASHED LINES) FOR THE FEM RESULTS

Table 6.2 provides the required *base-curve* input parameters to be used with the above regression models. As noted, these models are not recommended for interpolating design cases that use input parameters significantly outside of or between those used in the four FEM idealizations used to conduct the regression analysis. The accurate output from these regressions using the

precise input matching each calibrated FEM idealization can be scaled later using the dimensionless joint stiffness concept. In any case, the initial solutions extracted from the regression analysis should use input parameters closely matching those used in the initial FEM simulations. The parameters used for the site DIA-CT18 simulation are representative of typical heavy duty airfield pavements having lower stiffness clayey foundations with higher stiffness slab concrete. An example would be a higher strength frost resistant northern climate type PCC slab overlying weak clayey subgrade. The site DIA-CT18 input parameters should be used for all analyses where the expected ILLI-BACK (or similar procedure) mid-panel modulus of subgrade reaction from FWD testing would be between 250 and 450 psi/in. The parameters used for the site 5-AGG18 simulation are representative of typical heavy duty airfield pavements having relatively hard foundations and having softer slab concrete. An example would be dense sand and gravel subgrade with a warm mild climate where softer concrete is typically found. The site 5-AGG18 input parameters should be used for all analyses where the expected mid-panel modulus of subgrade reaction from FWD testing would be between 450 and 700 psi/in. The curves generated from sites DIA-CT18 and 5-AGG18 are the best estimates of true LT for site designs using 18 to 20-ft joint spacing. These two sets of input parameters are recommended for establishing base-curves for all designs having joint spacing between 16 and 22 feet. The parameters from site 11-CT14 represent longer 25-ft by 25-ft slabs and have higher LT values. These base-curves should be used for all sites having joint spacing greater than 22 feet. The input values from test site 2-AC17 were established using an FEM slab edge length of 12.5 feet for the loaded edge. These LT curves should be used for all designs having a proposed joint spacing of less than 16 feet.

TABLE 6.2. REQUIRED REGRESSION MODEL INPUTS TO ESTABLISH BASE-CURVES FOR LT VALUES

	Site DIA-CT18	*Site 5-AGG18*	*Site 2-AC17*	*Site 11-CT14*
Input Parameter	**ILLIBACK Subgrade < 450 psi/in Joint Spacing = 16 to 22 feet**	**ILLIBACK Subgrade > 450 psi/in Joint Spacing = 16 to 22 feet**	**Short Joints, Stiff Subgrade Joint Spacing < 16 feet**	**Thin Slabs, Weaker Subgrade Joint Spacing > 22 feet**
PCC thickness, in. =	18	18	17	14
PCC Elastic Modulus, psi =	5,000,000	3,285,000	6,440,000	4,900,000
Joint Spacing, feet =	18.75	18.75	12.5	25
Subgrade k, psi/in =	250	460	375	200
Joint Stiffness, lb/in/in =	2,000 to 300,000	2,000 to 300,000	2,000 to 300,000	2,000 to 300,000
Thermal gradient, degF/in =	-2 to +2	-2 to +2	-2 to +2	-2 to +2
Single Wheel Load Radius, in. =	5.9 to 11.5	5.9 to 11.5	5.9 to 11.5	5.9 to 11.5
Single Wheel Gear Load, lb =	30,000 to 90,000	30,000 to 90,000	30,000 to 90,000	30,000 to 90,000
All 4-Wheel Gears: Total Load, lb =	207,336	207,336	207,336	207,336
4-Wheel; Single Wheel Radius, in. =	9.1	9.1	9.1	9.1
All 2-Wheel Gears: Total Load, lb =	89,394	89,394	89,394	89,394
2-Wheel; Single Wheel Radius, in. =	8.4	8.4	8.4	8.4

NOTE: Limit the simulated single-wheel tire contact pressures to the range of 175 to 225 psi

Once the base-curves for LT are established for a range of designs using the same input as was used in one of the calibrated FEM algorithms, the accurate base-curves can have the x-axis (joint stiffness values) scaled as a function of slab thickness, using the concept of dimensionless joint stiffness. As shown in figures 4.1 and 4.2, the measured joint stiffness data was all unified into a common behavior when joint stiffness values were converted into log of dimensionless joint stiffness, *log(f)* values. The regression model generates the base-curve LT as a function of joint stiffness magnitude and using the required values for slab thickness shown above. Once the LT values are calculated, the original input joint stiffness values can then be scaled to represent minor changes in slab thickness values for use in a design evaluation or iteration scheme. The original regression model input joint stiffness values for the base-curves are turned into *log(f)*

values. Then, using a new radius of relative stiffness value for a different slab thickness, while holding all else constant, calculate the "adjusted" joint stiffness input values having the same *log(f)* values, where *log(f)* = log[$k_J/(k\ell)$], to be plotted with the original LT output values. This *log(f)* scaling of only the x-axis joint stiffness values will not change the fundamental relation between *log(f)* and LT as determined from the FEM models and LT regression models, but will allow the LT versus joint stiffness curves to be scaled for slab thickness in a stable and suitable way.

In summary, the bottom of slab edge stress LT versus joint stiffness problem, as viewed through the FWD device and matched FEM results, has been approximated herein and simplified into a scheme that uses three basic closed-form type regression curves as the basis (for single-wheels, 2-wheel gears, and 4-wheel gears). The regression curves should not be used for sensitivity studies for the LT parameter. Instead, the regression lines are used to reproduce what is called a fixed base-curve for LT versus joint stiffness that will apply to a range of design conditions. The base-curve is established using the exact same calibrated FEM input parameters used as the basis of the regression analyses, as shown in Table 6.2. The base-curve is considered to represent the behavior of a range of design conditions similar to the calibrated FEM algorithm used to establish the base curves. After obtaining the base-curve from the regression analysis, the joint stiffness values for the base-curve can be scaled proportionally to match the initial base-curve *log(f)* values to simulate change in slab thickness for a given design scenario. In reality, both horizontal and slight vertical changes in LT trend lines will result from changes in slab thickness while holding all other parameters constant. The *log(f)* scaling of the base-curve x-axis joint stiffness values only, changes the trends horizontally, but not vertically. This horizontal scaling is suitable for minor variation in slab thickness, such as those typical of thickness design calculation iteration ranges, but may become invalid for larger changes in thickness. The regression curves can be used to perform sensitivity studies for some parameters. For example, the temperature gradient effect extracted by the regression curves appears stable over the full range from -2 to +2 °F/in. Nonetheless, because the FEM results matrix is sparse and not well distributed for all key design parameters, some strange and invalid trends can be observed for simulated cases too far from actual FEM discretization conditions evaluated for some input parameters. A much more comprehensive and intentionally designed FEM solutions matrix would have to be used to establish a comprehensive single regression model that performed well over the probable ranges of all key design variables and load types. The described method is simple and a sufficient approximation until this type of study is performed and a more thorough and stable regression model developed. The two 18.75-ft joint spacing models are considered most representative of current design practice and are the recommended base curves for use as a basis of design for typical 18 to 20-ft joint spacing designs. The two sets of base curves (for softer and harder foundations) are then adjusted to account for slab thickness using *log(f)* scaling of the initial joint stiffness values used as input to the regression model. For now, all aircraft gears having greater than two wheels and having interior slab wheel loads should use the B747 LT curves as the basis of design. All 2-wheel gears should use the B737 curves as the basis of design.

In chapter 5, methods were established to determine joint stiffness as a function of average slab temperature. The previous sections of this chapter 6 described how to establish LT as a function of joint stiffness for various load types using simple regression equations. Now these simple site

specific LT versus joint stiffness regression models can be linked back to the site specific joint stiffness versus slab temperature joint behavior model output to establish a pavement design-specific set of LT versus average slab temperature curves for single-wheels, 2-wheel gears, and 4-wheel gears. If desired, climatic formulations can be used to estimate a frequency distribution of slab temperature for a design year, and algorithms or trend-lines from this study used to turn this into a frequency distribution of LT values for a given design year. If desired, the LT distribution can be turned into a distribution of slab edge stress occurring over a given year for various loads and times of day. The combination of the closed-form joint behavior simulations and the closed-form LT calculation formulae allows the simulation of slab edge damage to be taken down to the hour by hour level if desired. These estimated actual edge stress values can be turned into "weighted damage" or "accumulated damage" values using the damage formula that will be associated with the final pavement thickness designs, and the distribution of loads as a function of slab temperature. The concept of an overall "weighted LT value" for a given joint design is presented at the end of this chapter. An overall weighted value is a single equivalent value of LT that would be used for a given joint type in a pavement design and considering annual temperature variations and the concrete damage formula.

6.5. TOP OF SLAB CRACKING STRESS LT ANALYSIS

The following example demonstrates the top of slab stress analysis procedure used to evaluate top of slab (top-down) cracking stress. This analysis shows how during the early morning when upward curling is present, the maximum design stress for B747 loading on an airfield runway pavement can be in the unloaded slab adjacent to the gear assembly, and at the top of the slab near the mid-panel location. Figure 6.36 shows the stress calculations for a B747 gear load resting on the site 5-AGG18 calibrated ILSL2 FEM simulation. Both the top of slab and bottom of slab design cracking stress profiles are shown. The stress profiles for both plots are at the same physical locations, but the top of slab stresses are oriented perpendicular to the joint line, 90 degrees rotated from the bottom of slab cracking stress direction, which is parallel to joint line. The thermal gradient simulated for the (L+T) analysis is an upward curling gradient of 2°F/in. The residual stress (T) and load-only (L) stress profiles are also shown. The (L+T) plots represent the design stress levels during large upward curling condition. The joint stiffness is set at 100,000 lb/in/in for these plots, a common value for runway joints. The traditional bottom of slab (L+T) edge stress value right near one of the B747 wheels is shown to be about 180 psi. The top of slab bending stress in the unloaded slab caused only by combined curling stress and joint load transfer forces is the highest stress, the controlling design stress during morning up-curling, and is about 230 psi. The presence of the two interior wheels for the four-wheel B747 gear actually reduces the top-of-slab tension in the loaded slab, to levels below stress levels in the unloaded slab. Because the B747 gear induces large downward deflections of the loaded slab, the joint load transfer into the unloaded slab is large and acts as a pure edge load, maximizing the moment arm distance relative to mid-slab stress development, which couples with top of slab cracking thermal stress.

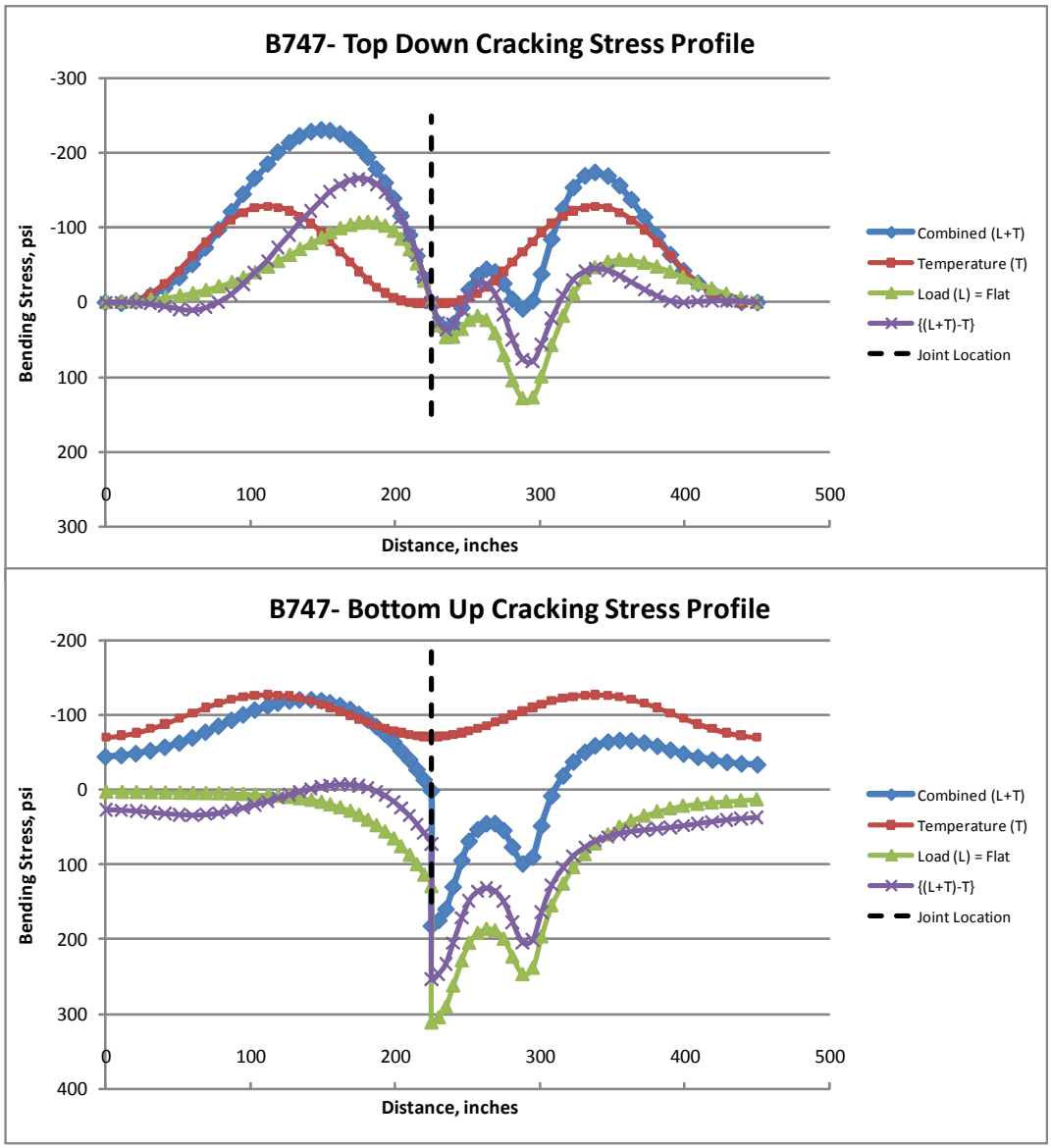

FIGURE 6.36. THE DESIGN STRESS CALCULATIONS FOR MORNING UPWARD CURLING OF 2°F/in FOR THE TOP OF SLAB AND BOTTOM OF SLAB CRACKING MODES FOR A B747 GEAR LOAD AND USING THE SITE 5-AGG18 CALIBRATED FEM SIMULATION (k_J = 100,000 lb/in/in)

The stress profiles for flat slab analysis are also shown in the plots in figure 6.36 (triangle symbols). For flat slab conditions, the traditional bottom of slab edge stress is about 305 psi, while the top of slab cracking stress generated in the unloaded slab is only about 100 psi. Comparing the flat slab stress analysis (L) results to the {(L+T)-T} stress profiles reveals how differences in slab shape from curling affect how load stress is distributed in the slab. The lower plot reveals that during upward curling, local edge stress is reduced while bending stress is increased at the far edges of slabs in the cantilever overhang portions of the slabs that are lifted off of the foundations from slab rotation and curling effects. The stress transferred to the

uplifted cantilever slab masses reduced the slab stresses beneath the wheels. This shifting of stress from one area to another is a conservation of energy concept, where for upward curling, some load energy is initially dissipated in order to rotate the slab and cause the upward curled slab edge to come in contact with the foundation. The remaining reduced load energy then causes a slab edge bending response. For the top of slab stress profiles, the curled shape results in very little stress being transferred to the outer edges of slabs away from the joints and bending stress becomes more concentrated in the interior two thirds of the slabs near the joints. The outer edges are uplifted and have no subgrade contact pressure.

Figure 6.37 shows the loaded and unloaded slab top of slab cracking stress summary plots for the four calibrated FEM algorithms. The unloaded slab stress at a joint stiffness = zero is the residual curling stress near mid-slab. Notice how the residual thermal stress values for the 25-ft long slabs range from about 230 to 260 psi while the values for the 20-ft slab length range vary from about 120 to 130 psi. This is about a 50% reduction in curling stress calculated for just a 20% reduction in slab length. The loaded slab stress values are the peak top of slab stress and are located somewhere between mid slab position and the load. For single wheel loads and the 2-wheel B737 gear, the loaded slab stress is always higher than the unloaded slab stress. Surprisingly, for the 4-wheel gear having two interior slab wheel loads, the unloaded slab stress is higher than the loaded slab stress for three of the four FEM algorithms. The site 11-CT14 algorithm did not show this trend as it has longer thinner slabs and the interior wheel load effect from the 4-wheel gear is diminished. The design top of slab cracking stresses were reduced by almost 50% in all load cases for the 18.75-ft to 20-ft joint spacing, as compared to the 25-ft joint spacing. This indicates a rather extreme sensitivity to joint spacing for the top of slab stress effect. For thick airfield slabs, if joint spacing is less than 20 feet, the apparent top of slab cracking stress from the FEM analysis will be less than about 200 to 250 psi for fully loaded B737 and B747 gears for good condition joints. At a 25-ft joint spacing, the design top of slab cracking stress is estimated at about 360 to 430 psi for fully loaded B737 and B747 gears. As discussed previously, the Iwama correction factor may suggest that the top of slab cracking stresses obtained from linear thermal gradient simulations may need to be increased by about 30% to account for some stress magnification caused by the typical non-linear thermal temperature versus depth profile shape (Nishizawa, 2010).

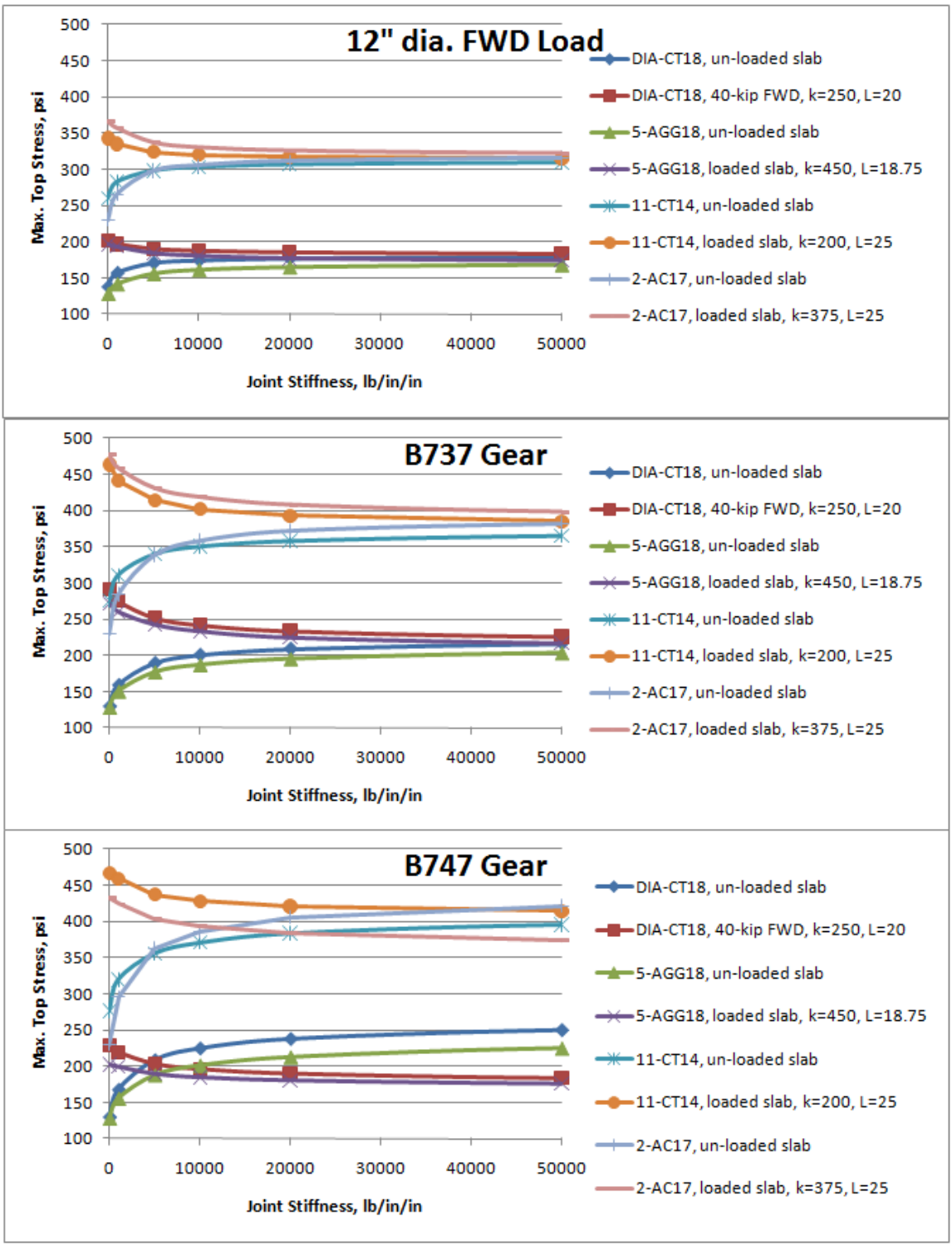

FIGURE 6.37. COMPARISON OF TOP OF SLAB CRACKING STRESSES FOR FWD LOAD, AND B737 AND B747 GEARS FOR THE CALIBRATED FEM ALGORITHMS (thermal gradient = curled-up 2 °F/in)

Figure 6.38 shows the percentage reduction in loaded slab top of slab cracking stress (LT) caused by joint load transfer for the four calibrated FEM algorithms and the different load simulations and for a 2 °F/in upward curling linear temperature gradient. Top of slab cracking stress LT values are in all cases less than 25%. Top of slab stress LT values for the FWD sized loads were small between about 8 and 12% and are mobilized at small joint stiffness values. The highest top of slab stress LT values were for the B737 gear, which has two wheels both right on the joint line. LT values for the B747 4-wheel gear, which has two-slab interior loads, were lower than 2-wheel B737 gear LT values. Figure 6.39 summarizes the unloaded slab top of slab stress caused only by joint load transfer, for relatively stiff joints and plotted as percentage increase in the residual stress value. Site 11-CT14 had thin slabs and showed less change in stress. The greater variation for DIA algorithm may be because it has a softer subgrade than the similar algorithms for sites 2-AC17 and 5-AGG18.

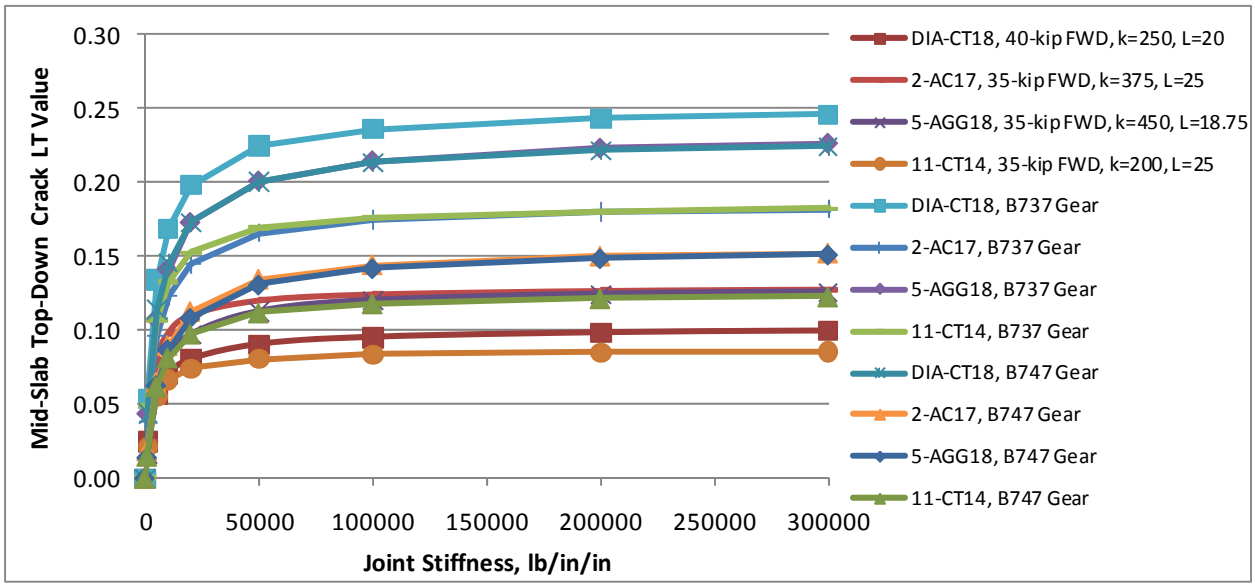

FIGURE 6.38. TOP OF SLAB CRACKING STRESS LT FUNCTIONS FOR THE LOADED SLAB, FROM CALIBRATED FEM ALGORITHMS AND USING A SIMULATED UPWARD CURLING GRADIENT OF 2 °F/in

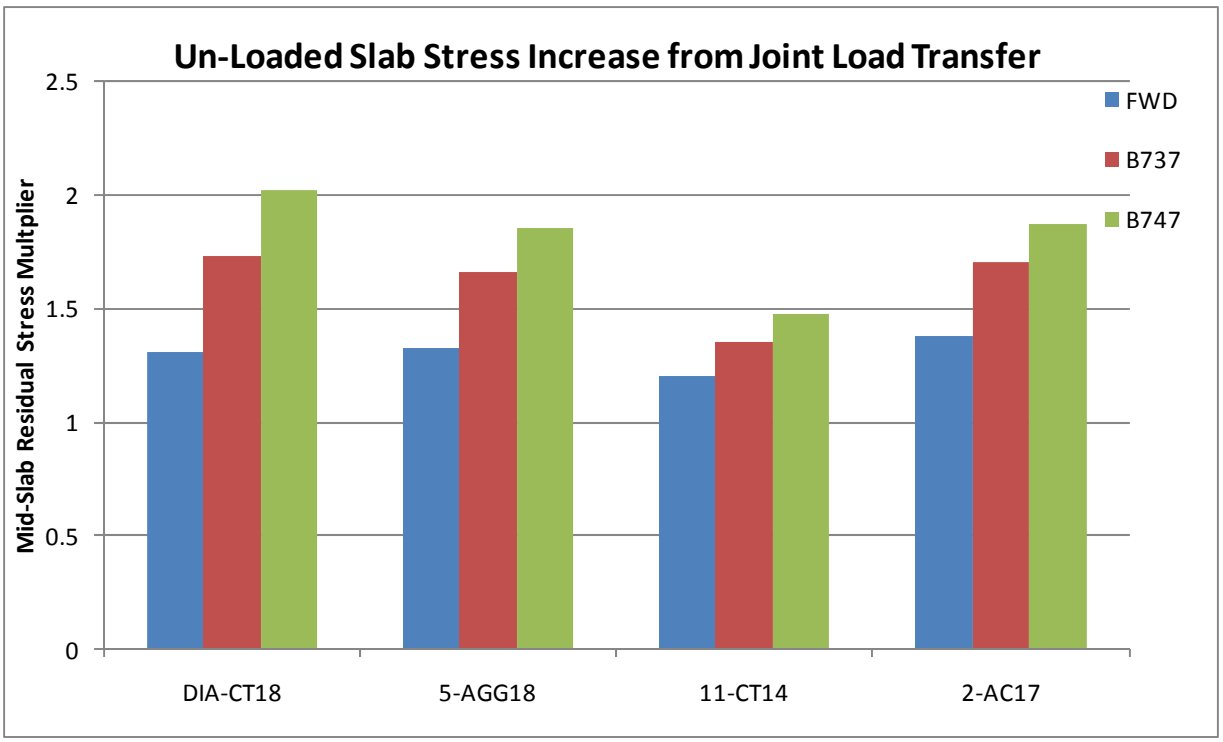

FIGURE 6.39. THE MAGNIFICATION OF THERMAL RESIDUAL STRESS NEAR MID-SLAB IN THE UNLOADED SLAB THAT IS CAUSED ONLY BY JOINT LOAD TRANSFER, FOR THE B747 GEAR, AND SIMULATED UPWARD CURLING GRADIENT OF 2 °F/in

Figure 6.40 shows how increasing thermal gradients affected design top of slab cracking stresses and LT values for one of the calibrated FEM algorithms, site 5-AGG18. As shown previously, the bottom of slab edge stress for the flat slab condition was just over 300 psi. Even at an extreme simulated 3 °F/in upward curling gradient, the top of slab stress is only about 260 psi for these simulated 18.75-ft by 18.75-ft panels. Top of slab cracking stress LT values for the flat slab condition rapidly rise to levels well above 25%. In contrast, the top of slab cracking stress LT values are anticipated to drop rapidly as upward curling develops in the slabs. Figure 6.41 summarizes the data in terms of how much stress increase was observed in the unloaded slab, and also in terms of percentage increase over residual stress levels in the unloaded slab. The stress increase in the unloaded slab caused only by joint load transfer was relatively constant for the four gradients modeled.

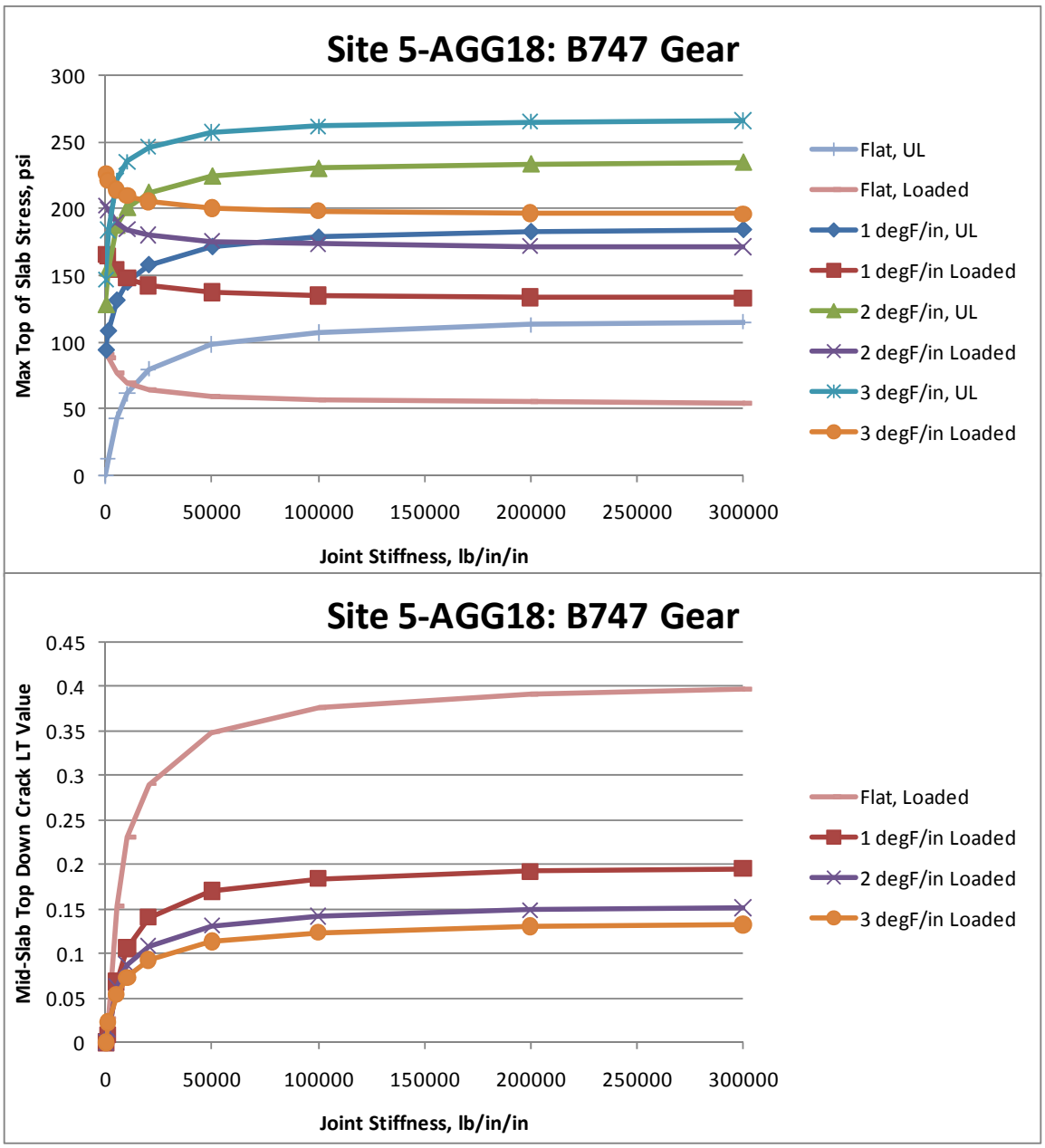

FIGURE 6.40. THE EFFECT OF INCREASING THERMAL GRADIENT ON THE TOP OF SLAB STRESSES AND THE LOADED-SLAB LT FUNCTIONS FOR THE B747 GEAR AND USING THE CALIBRATED FEM ALGORITHM FOR SITE 5-AGG18

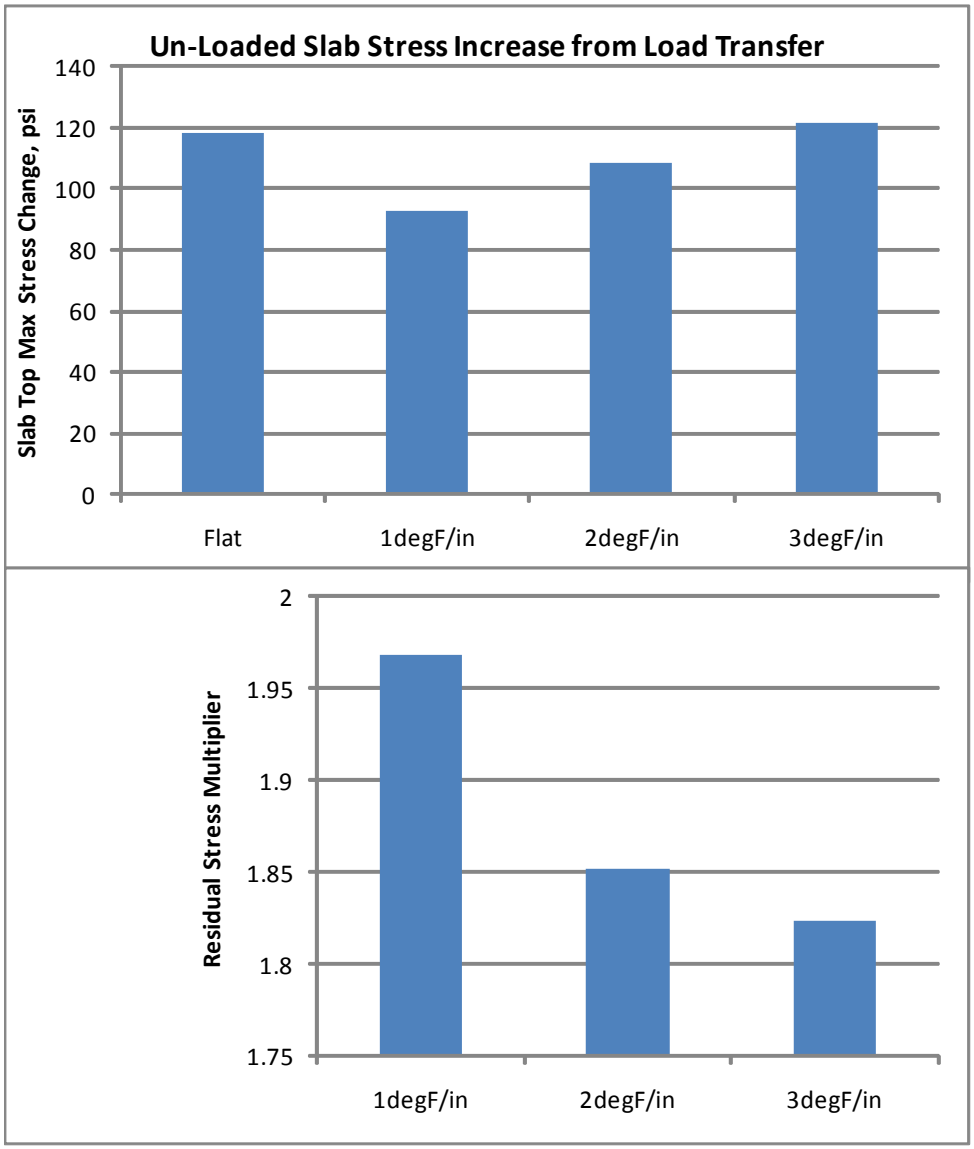

FIGURE 6.41. SUMMARY OF TOP OF SLAB STRESS TRANSFERRED INTO THE UNLOADED SLAB AND RESIDUAL STRESS MULTIPLIERS FOR INCREASING THERMAL GRADIENTS FOR THE SITE 5-AGG18 CALIBRATED FEM ALGORITHM

Top of slab cracking is not a design failure mode checked in current FAA design procedures. Therefore, top of slab cracking stress LT regression curves were not established. These type of simplified curves are achievable but the Skarlatos/Ioannides function would not be as good of a "first guess" function for use with the top of slab cracking stress LT trends as it was for the bottom up cracking trends, which were a good match to the Skarlatos/Ioannides shape. This analysis has revealed an almost 50% reduction in top of slab stress for 20-ft slabs as compared to 25-ft slabs. When using slab lengths less than 20 feet, top of slab stress in thicker airfield slabs will probably be less than 200 to 250 psi for B747 gears for most days of the year.

The condition of top of slab corner breaking was also not evaluated in detail as part of this study. Nevertheless, extensive FWD corner testing was performed and that data can one day be used to help calibrate an extensive corner breaking analysis simulation. The FWD tests showed that corners do expand outward and lock-up during high temperatures, but also tended to lose apparent joint stiffness more rapidly with loss of slab temperature as compared to slab edges, perhaps due to enhanced three dimensional thermal expansion and contraction effects at corners. All curling actions and loss of support effects, such as upward curling lift-off magnitudes, are also magnified at corners. The variations observed at corners will be similar to but greater than those presented in this report for slab edges.

6.6. RECOMMENDED RANGES OF LT COEFFICIENTS FOR DESIGNS

This section attempts to bring the research observations and algorithms together into a scheme that is useful in the context of the current FAARFIELD single-slab FEM code, which does not use temperature gradient curling simulations. The effect of the LT variations on pavement thickness design is highly dependent on the type of material damage formula being used as the basis of thickness design calculations. The FAARFIELD single-slab FEM code places a gear load on the slab edge considered and calculates a slab free edge stress for use in design. The traditional 25% edge stress reduction LT value is then applied to the free edge stress values for all load cases. These "75% of free edge stress" values are then entered into the current FAA pavement damage formula (Brill, 2010) and the damage caused by each load is estimated and accumulated. Slab thickness is adjusted until the accumulated damage is just less than 100% for the proposed amount and type of traffic at the facility. After reviewing the damage formula form it was apparent that relative-damage functions could be generated from the damage formula for a wide range of loads and LT values. The damage formula was set up to represent typical base and subgrade stiffness conditions and 18-inch thick slabs, conditions similar to those used to develop the LT functions recommended for designs in the previous sections of this chapter. Four ratios of free edge stress to modulus of rupture were used (3/7, 4/7, 5/7, and 6/7) and then a range of LT values were applied to the free-edge stresses. The number of passes to failure was determined for each simulated LT-adjusted stress value and the relative damages plotted as shown in figure 6.42 for the 700 psi flexural strength assumption. The relative damage functions can be reproduced using a series of fourth order polynomials. The coefficients (A-D) for the four polynomials shown can be further parameterized as a series of third order polynomials as shown in figure 6.43. This nested polynomial parameterization allows a relative damage versus LT function to be determined for any free edge stress magnitude around the range of 3/7 to 6/7 times the flexural strength.

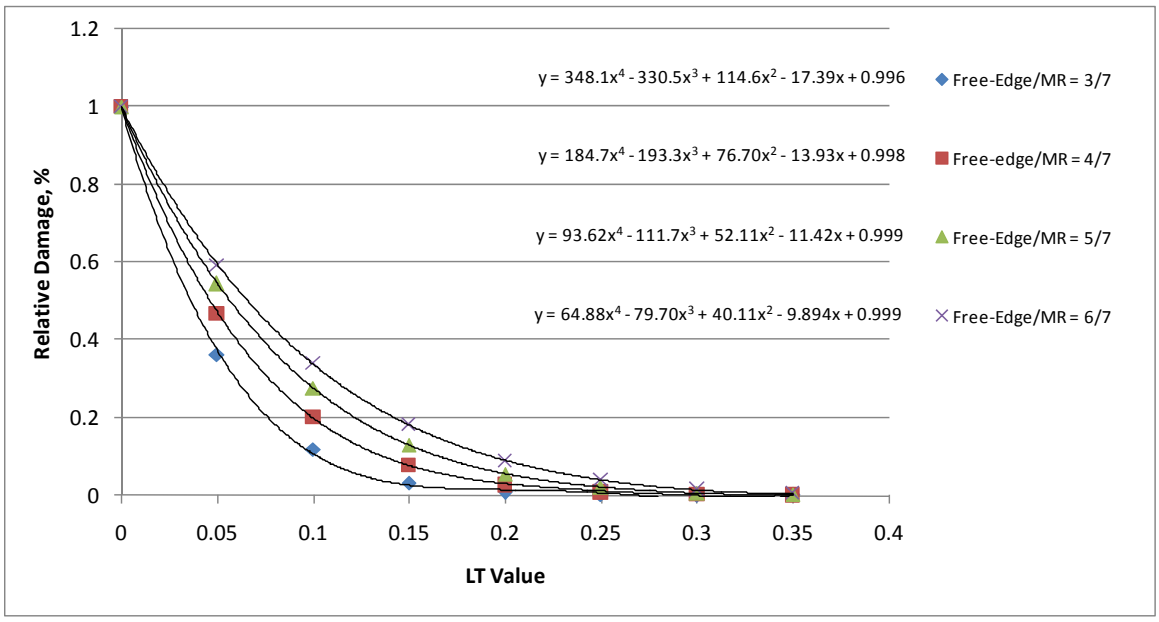

FIGURE 6.42. RELATIVE DAMAGE FUNCTIONS EXTRACTED FROM THE VERSION 6E PAVEMENT DAMAGE FORMULA FOR FLEXURAL STRENGTH = 700 PSI AND USING BASE AND SUBGRADE CONDITIONS SIMILAR TO THOSE USED FOR SITES DIA-CT18 AND 5-AGG18

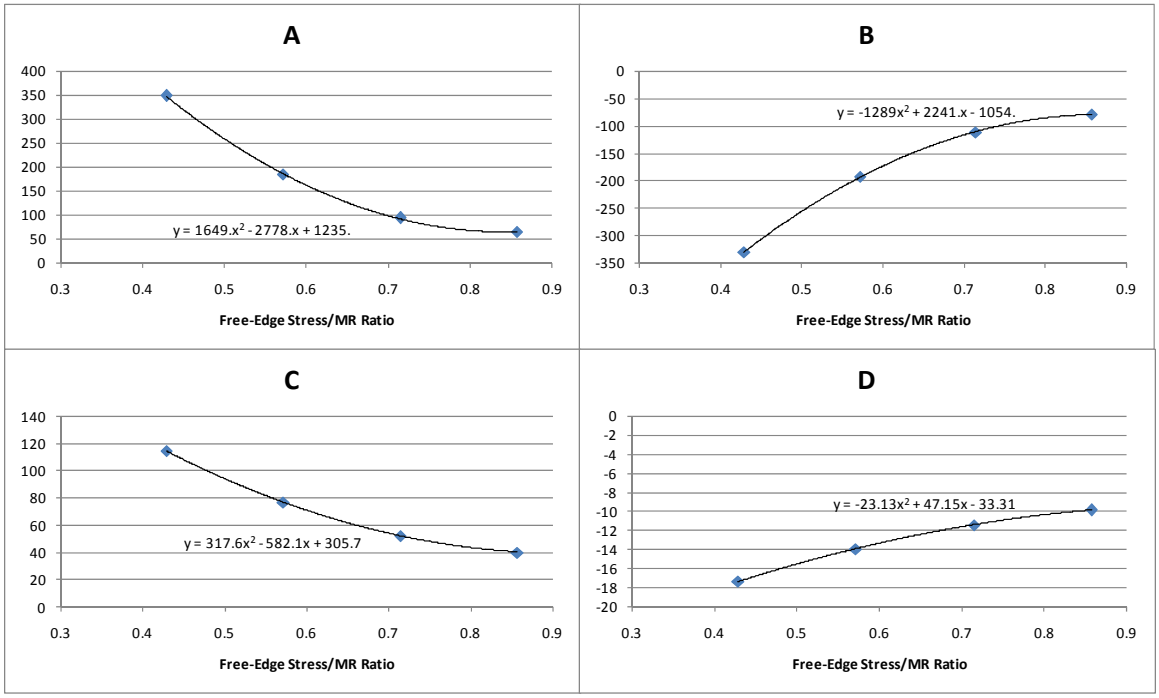

FIGURE 6.43. THIRD ORDER POLYNOMIALS FOR DETERMINING THE FOURTH ORDER RELATIVE DAMAGE FUNCTION POLYNOMIAL COEFFICIENTS TO BE USED FOR CONDITIONS BETWEEN THOSE SHOWN IN FIGURE 6.42

In general, each site will have a frequency distribution of LT values for each joint design that is primarily a function of the average slab temperature, and also whether or not dowels or ties are used across the joint. Take for example an average aggregate interlock joint in a relatively extreme northern mid-west climate that will have LT values ranging from 0.00 during winter, to fully locked = 0.35 in the summer. As visible in the relative damage functions in figure 6.42, the amount of relative pavement damage occurring for each load during winter is tens to hundreds of times greater than the damage occurring during summer when LT is near 0.35. If one assumes that the frequency distribution of LT values over the year is shaped like a uniform distribution between 0.0 and 0.35, then the weighted LT value considering the relative damages is the x-axis centroid for the relative damage function, or the relative damage functions x-axis area moment arm about the origin.

Figure 6.44 provides a set of lines representing the weighted LT functions calculated assuming a uniform distribution of LT values within the ranges shown. The lowest line on the plot represents the weighted LT value that would be used for the aggregate interlock joint when LT varies between 0.0 and 0.35 with a uniform distribution of LT values. The weighted LT value would range from about 0.05 to 0.08 for increasing free edge stress magnitudes. For a doweled joint at the same site and having LT ranging from 0.20 to 0.35 during the year, a weighted LT value of 0.23 to 0.25 would apply. The y-intercept values and slopes for this set of lines can be parameterized suitably into continuous functions using fourth order polynomials as shown in figure 6.45. In general, Chapter 5 described how to estimate joint stiffness versus slab temperature for a given joint design. The first part of this Chapter 6 described how to turn this data into LT values versus slab temperature for a given joint design. Figure 6.45 shows the most-simple form of the final answer to the fundamental question: what value of LT is appropriate for doweled versus tied versus aggregate interlock joints as a basis of design in FAARFIELD. This most simple form requires only an estimate of the winter and summer joint stiffness and LT values for a joint type and then is assuming a uniform distribution of LT values between winter and summer minimum and maximum values and is based on the current FAA pavement damage formula.

The weighted LT regression curve in figure 6.45 can be easily programmed into any design routine. The line solutions for weighted LT are numerically stable and can be interpolated for any stress level between 0.0 and 1.0 times the flexural strength. It is noted, however, that the 4^{th} order polynomial representations for the relative damage curves in figure 6.42 are becoming hyper-sensitive for ratios of free-edge stress to flexural strength values below 3/7. It is recommended that for ratios less than 3/7, the curve for the 3/7 ratio be used.

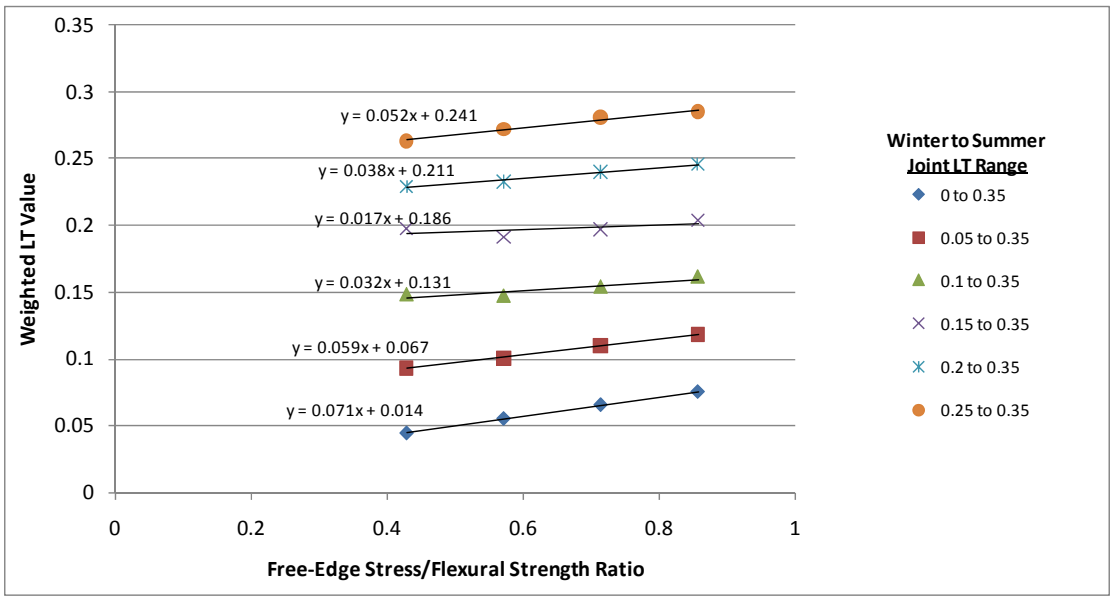

FIGURE 6.44. THE SIMPLIFIED WEIGHTED LT VALUES TO BE USED WHEN ASSUMING A UNIFORM DISTRIBUTION OF LT VALUES BETWEEN THE WINTER AND SUMMER LT VALUES SHOWN

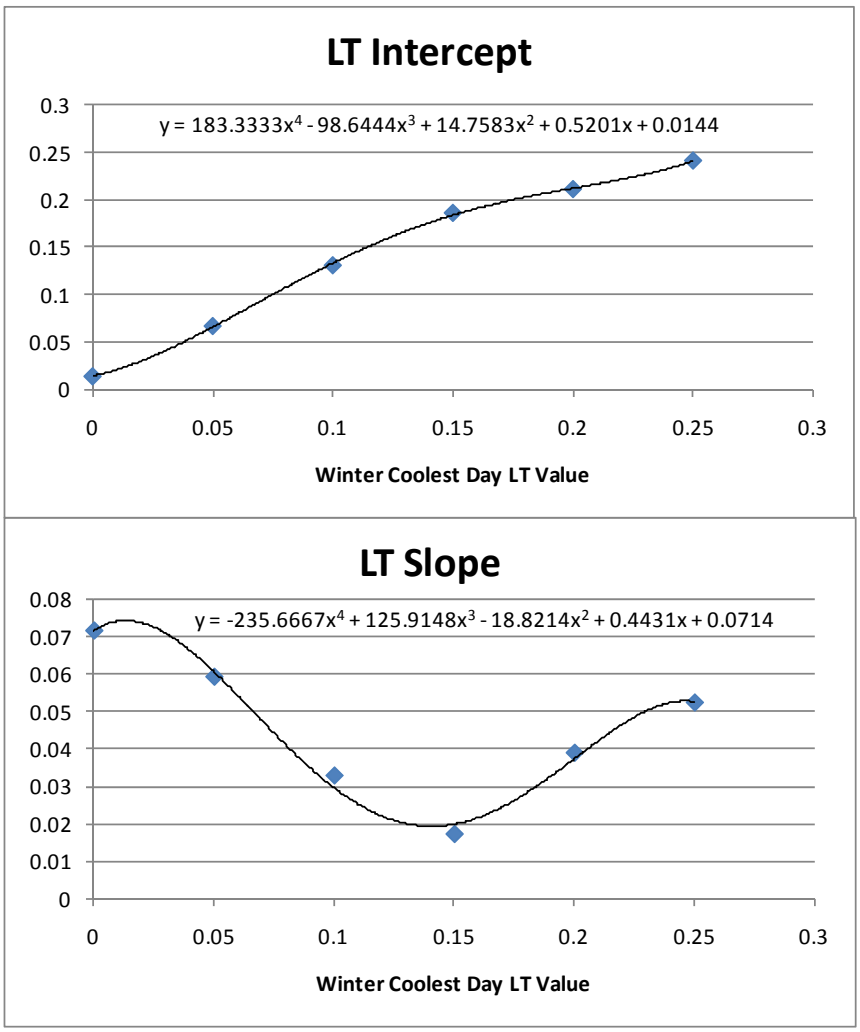

FIGURE 6.45. POLYNOMIALS FOR ESTIMATING THE LT INTERCEPT AND SLOPE VALUES FOR THE SET OF LINES DESCRIBED IN FIGURE 6.44 AND TO BE USED TO ESTABLISH THE WEIGHTED LT VALUES

Figure 6.46 links the FEM model generated LT curves to the comprehensive joint behavior model to predict LT as a function of average slab temperature for the calibrated DIA joint and FEM models. The corresponding LTE_{δ} and joint stiffness versus temperature trends were shown in figure 5.9. These plots can be used as a guide to estimate the winter LT values for a given site for thicker airfield pavements having joint spacing between about 16 and 22 feet. The plots show the new and projected older joint LT conditions for doweled and aggregate interlock joints. This plot reveals a key finding. The LT versus average slab temperature prediction is nearly a linear trend for the aggregate interlock component of joint stiffness. LT versus temperature can be suitably approximated using a line between the T_{Lock} and $T_{Release}$ temperatures, with LT = 0.0 at release and LT equal to the upper limit value associated with the upper limit joint stiffness for a given pavement cross section and load configuration at the T_{Lock} temperature, or about 0.35 at joint thermal lock-up. In general, the joint stiffness versus average slab temperature trends have significant upward curvature, while the joint stiffness versus LT trends have significant

downward curvature. When these two relations are combined, the LT versus average slab temperature trend that results is nearly linear for the aggregate interlock.

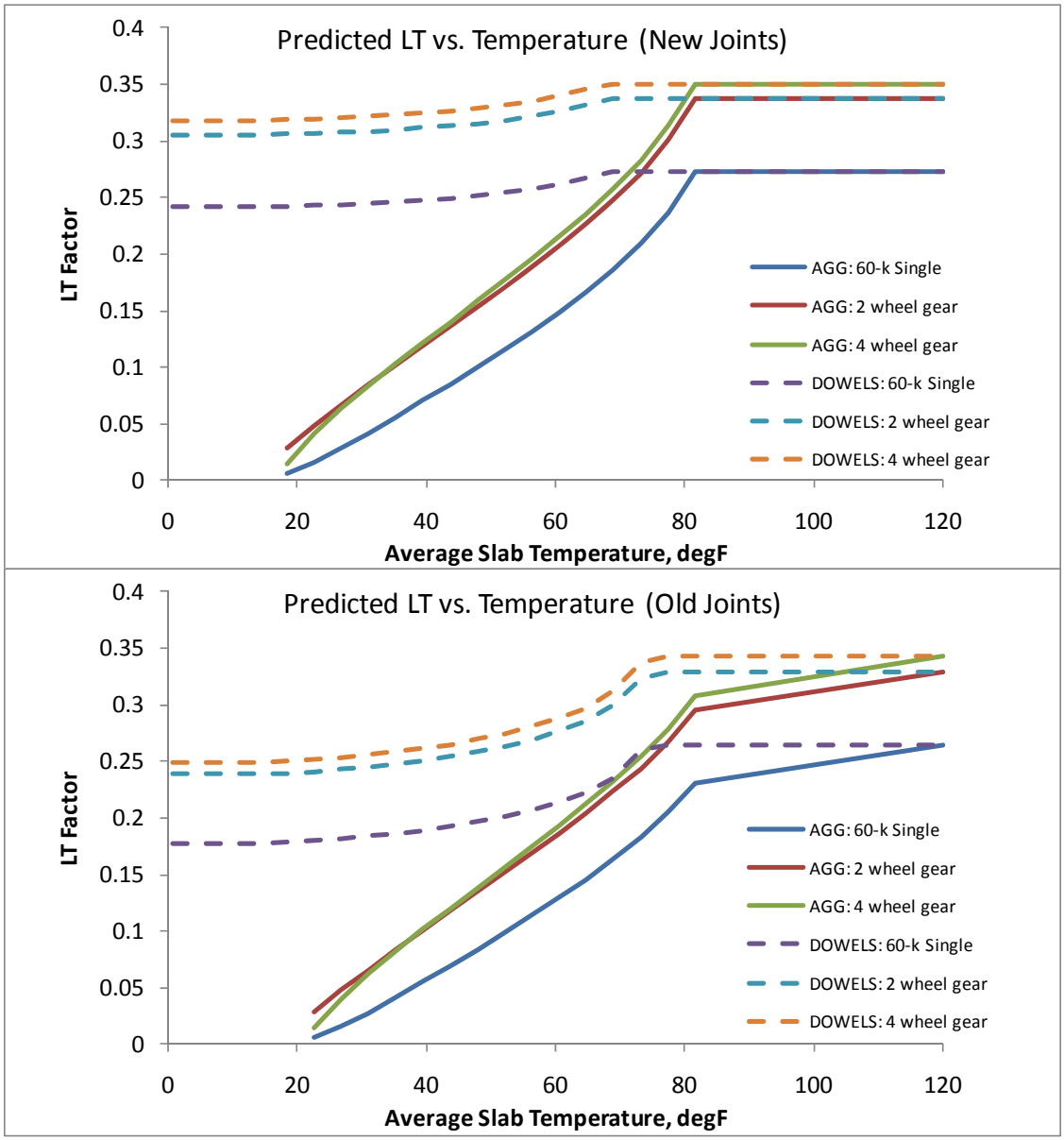

FIGURE 6.46. PLOTS TO BE USED FOR PREDICTING THE WINTER LT VALUES, GENERATED BY COMBINING THE FEM LT MODELS AND THE COMPREHENSIVE JOINT BEHAVIOR MODEL

The following example demonstrates how to combine all of the models developed from this study to obtain the best possible estimate of weighted LT for a given pavement design and load scenario. Figure 6.47 shows measured average slab temperature data from DIA along with predicted temperatures from the integrated climate model (Rufino et al., 2004). The detailed LT prediction process starts with this type of site pavement temperature data and includes the following steps:

1. Establish an estimated frequency distribution of the average slab temperature data for a given year for the design site as shown in figure 6.48. Average slab temperatures will vary less than average air temperatures.
2. Use the comprehensive joint stiffness behavior model from Chapter 5 to convert the x-axis temperature data from figure 6.48 into joint stiffness values as shown in figure 6.49. This plot provides the frequency distribution of average joint stiffness values for a year for the doweled and aggregate interlock joint designs used at the DIA site.
3. Use the LT regression models developed to reproduce FEM generated LT versus joint stiffness functions and convert the x-axis joint stiffness values into LT values for various wheel loads and gears, as shown in figure 6.50 for a B737 gear assembly.
4. Multiply the LT frequency distribution by the relative damage weighting function from figure 6.42 to obtain the damage weighted LT frequency distributions for the different joint designs as shown in figure 6.51.
5. Establish the weighted LT function's x-axis centroid values. This value is the best guess single weighted annual LT values considering the best estimates of slab temperature variation at a site.

This example assumed a compliant softer subgrade and used the flat slab LT curves and did not simulate curling variations in LT. This is the type of "average-daily-value" analysis that would be used, for example, when annual temperatures are being accounted for, while curling variations are not being accounted for. This is the type of LT estimation process that is considered most appropriate for use with the current FAARFIELD single slab model that does not simulate curling variations.

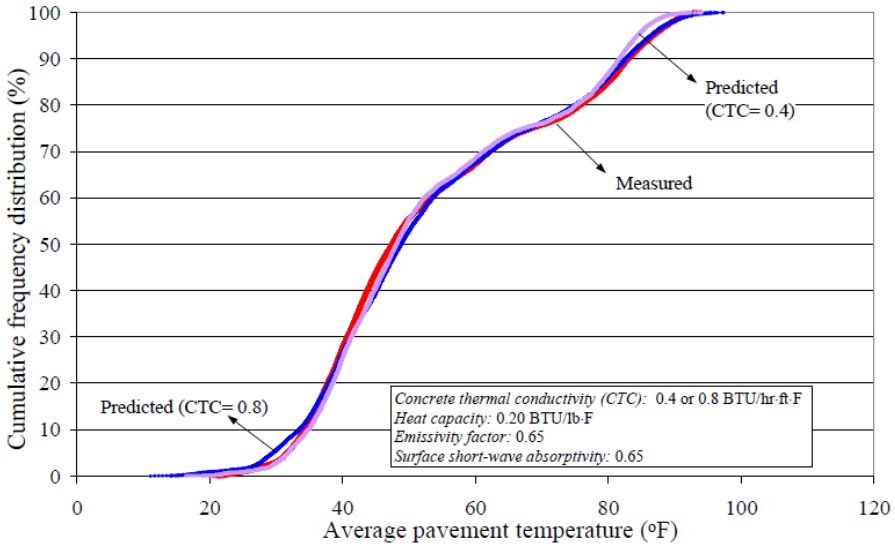

FIGURE 6.47. DIA AIRPORT MEASURED VERSUS PREDICTED AVERAGE SLAB TEMPERATURE DATA FROM RUFINO, ROESLER AND BARENBERG, 2004

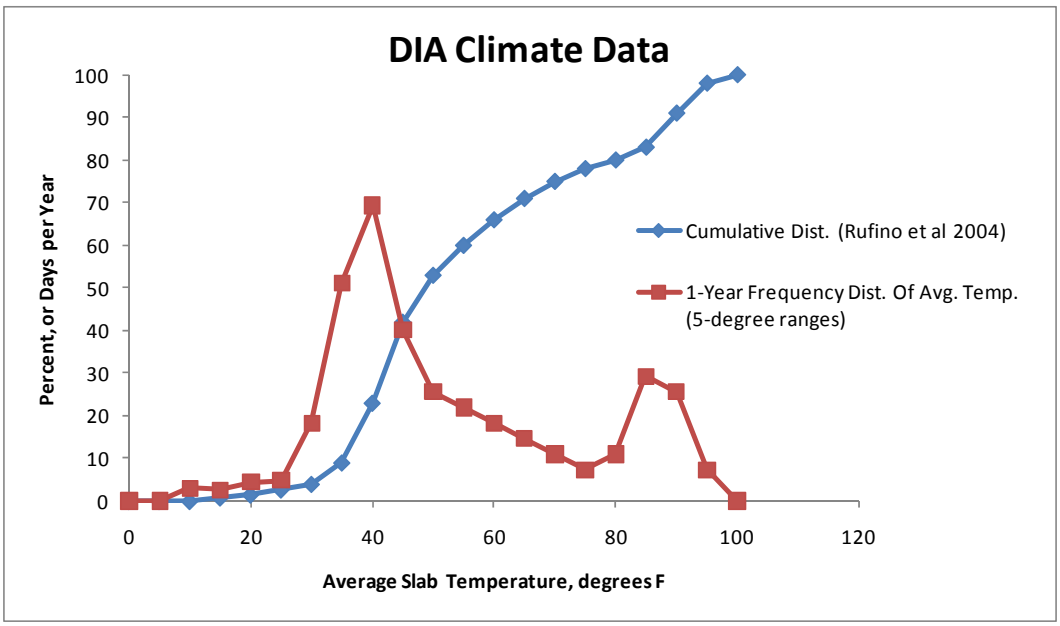

FIGURE 6.48. THE ANNUAL FREQUENCY DISTRIBUTION OF AVERAGE SLAB TEMPERATURE FOR THE DIA SITE

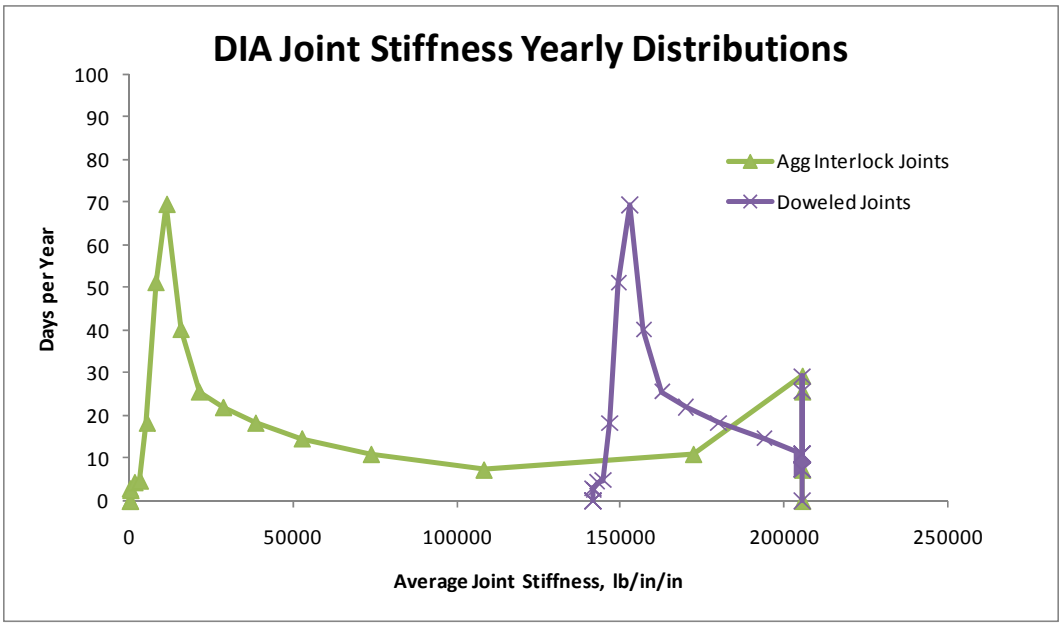

FIGURE 6.49. ANNUAL FREQUENCY DISTRIBUTIONS OF JOINT STIFFNESS AT DIA

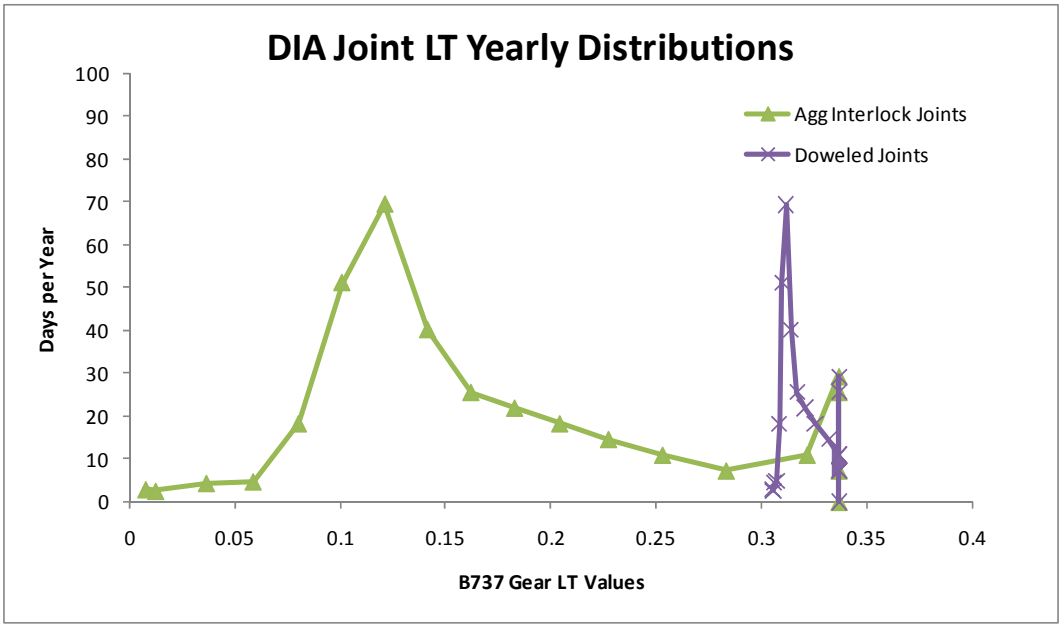

FIGURE 6.50. THE FREQUENCY DISTRIBUTION OF LT VALUES AT DIA

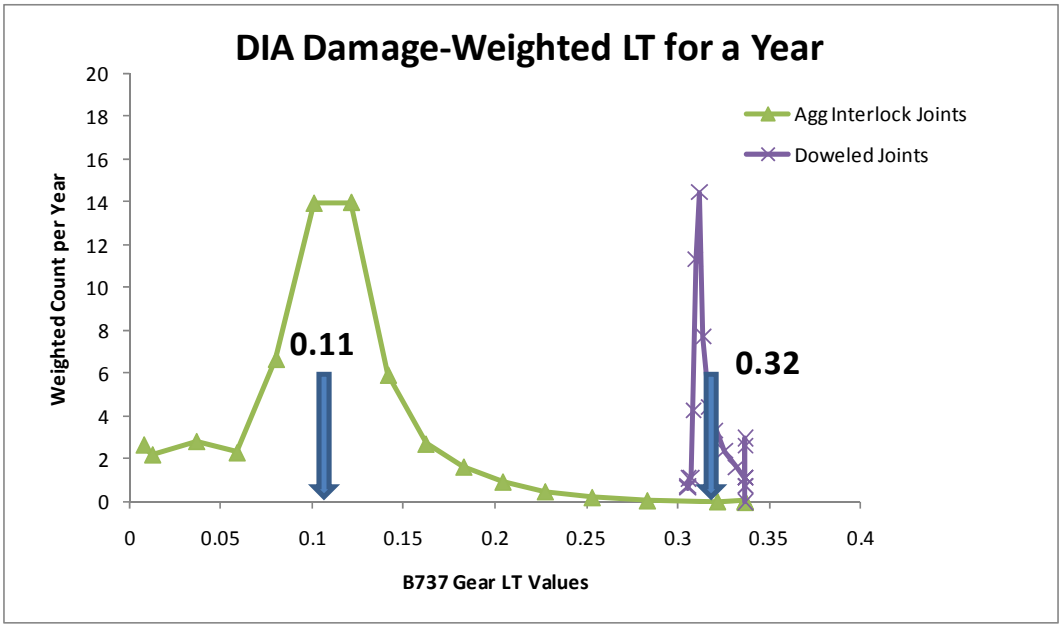

FIGURE 6.51. DAMAGE-WEIGHTED LT FREQUENCY DISTRIBUTIONS AT DIA AND OVERALL WEIGHTED LT VALUES

Comparing the results in figure 6.51 to the simplified weighted LT values in figure 6.44 reveals similar results. If one were to select the simplified trend for DIA for aggregate interlock joints having winter to summer LT range of 0.05 to 0.35, which generally matches the actual LT frequency distribution range as shown in figure 6.50, the predicted weighted LT values would be about 0.09 to 0.12, as compared to 0.11 obtained using an actual temperature frequency

distribution estimate. This comparison should give confidence in using the simplified winter to summer LT range as the basis of design.

As can be observed, the relatively accurate frequency distribution for LT values is not a uniform distribution. Because of the nature of the damage function, these weighted LT value trends are dominated by how the pavement system will behave in cooler weather. As shown in figure 6.48, the frequency distribution of temperatures has two primary peaks and these peaks represent the winter and summer equilibriums at a site (solstices). Spring and fall are times of maximum rates of change and there are fewer days per year in these intermediate temperature ranges. Slab temperature frequency distributions for Denver, Colorado are dominated more by the winter equilibrium conditions as a result of being situated well north of the equator.

As demonstrated previously, it is difficult to predict the winter LT value for a given design site. The winter LT prediction is perhaps most sensitive to the joint spacing selected for design. Figure 6.52 provides a guide for estimating the effective thermal range for the aggregate interlock component of joint stiffness. The upper plot provides a relatively accurate prediction of the temperature range from T_{Lock} to $T_{Release}$ as a function of slab length. This upper plot is obtained from the DIA-calibrated comprehensive joint behavior model. The lower plot uses the temperature range data to estimate the site average $T_{Release}$ temperature for the aggregate interlock component of joint stiffness for varying estimated average slab temperatures shortly after construction. The lower plot arbitrarily assumed the T_{Lock} temperature is about 20 °F higher than the average slab temperature present during the few days after construction. The values in the plots are representative of newer joint conditions. Aging will reduce aggregate interlock thermal range and increase the release temperatures. Changing from a 25-ft joint spacing to a 20-ft joint spacing is estimated to lower the $T_{Release}$ temperature for aggregate interlock by about 20 °F. To estimate if the winter LT will be zero for aggregate interlock at a site, compare the estimated release temperature for the proposed joint spacing, slab curing and early life temperatures to the typical average winter temperatures at the site.

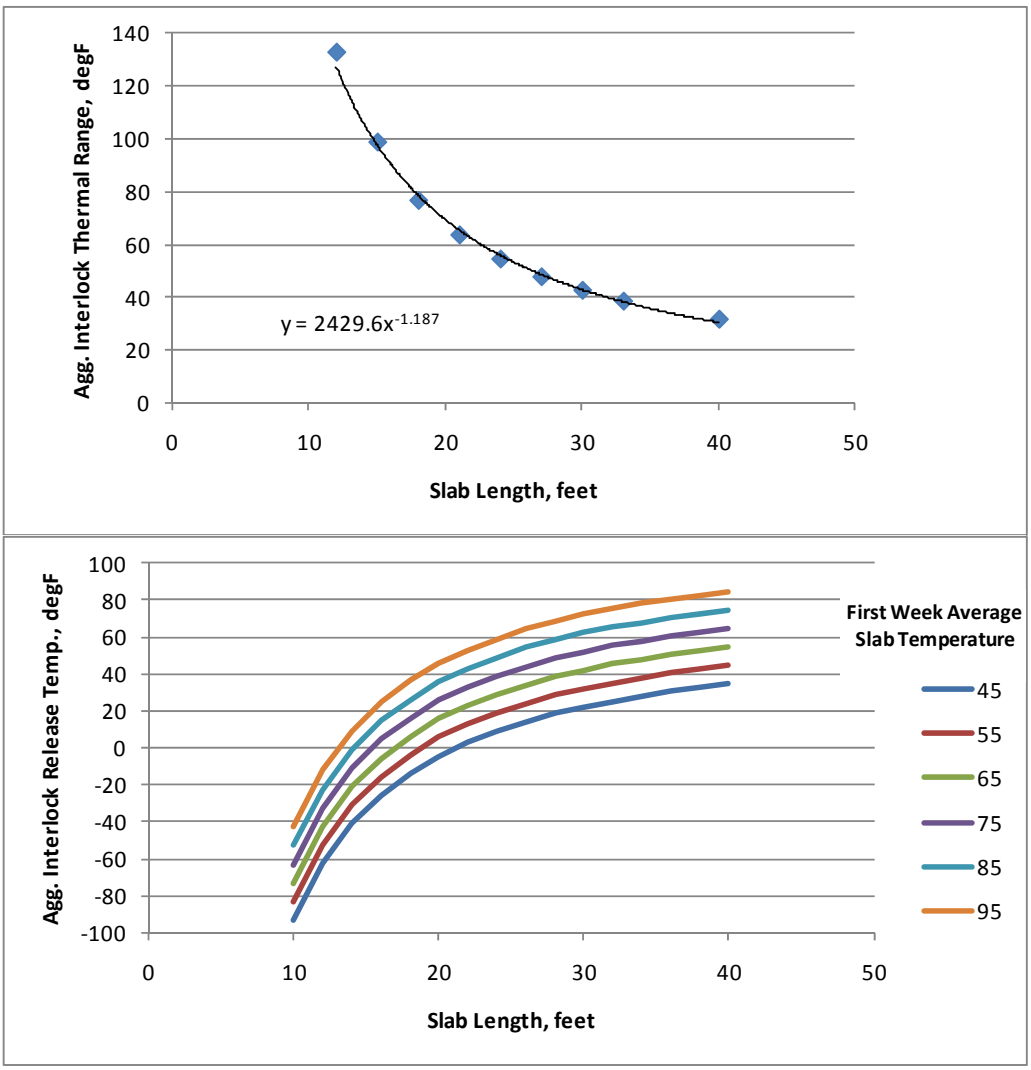

FIGURE 6.52. THE SENSITIVITY OF MEASURED DIA AGGREGATE INTERLOCK THERMAL RANGE ($T_{Lock} - T_{Release}$) TO SLAB LENGTH AND EARLY LIFE AVERAGE SLAB TEMPERATURES AFTER PLACEMENT

Addition of dowel bars can keep LT values high during the winter. Testing of doweled joints has revealed that the modulus of dowel-concrete interaction can deteriorate significantly over time and from repeated traffic. Doweled joints must be properly designed considering dowel-to-concrete bearing stresses and loads on individual dowels. If the dowel-concrete interaction support zone is over-stressed dowels will lose support more rapidly over time. This study used the typical FAA doweled joint stiffness equation and performed backcalculations of apparent modulus of dowel-concrete interaction factors for doweled joint designs. In general, use the FAA doweled joint stiffness model along with the following recommendations to develop joint stiffness estimates for doweled joint designs:

- Limit the assumed modulus of dowel-concrete interaction for new joints to 5,000,000 psi/in.

- The average modulus of dowel-concrete interaction during the service life will likely be about 3,000,000 psi/in, with considerable variation likely.
- In heavy traffic areas the effective modulus of dowel-concrete interaction will likely drop to levels below 1,000,000 psi/in near the end of the service life.
- Set the *D/s* dowel component of joint stiffness determined from the FAA doweled joint stiffness model to be just less than the upper limit total joint stiffness values for locked joints shown in figure 5.4 for a given design slab thickness.
- Aggregate interlock can be assumed to be present and vary with temperature in doweled contraction joints.

Tied contraction joints are generally designed to remain closed with nearly full aggregate interlock. The joint stiffness and corresponding LT values for new working joints shown in figure 5.4 can be assumed to be present at all times of the year for properly designed tied joints. However, a line of tied joints may cause greater joint openings to develop for joint lines adjacent to the tied joint lines. Excessive amounts of tied joints can result in slab cracking. Random cracks will likely behave similar to aggregate interlock joints but possibly with poor spalling performance as the pavement ages. Tied joints must be used with care and in strategic locations. Doweled and/or aggregate interlock joints are needed to allow and control thermal expansion and contraction and joint opening sizes.

Construction joints were perhaps the most variable and least predictable type of joint. Further study is needed to better quantify construction joint stiffness and LT. In general aggregate interlock should be ignored for flat-faced construction joint designs and all joint resistance attributed to the dowel bars or tie-bars. As an interim guide until better data is available, the modulus of dowel concrete interaction factors recommended above for doweled contraction joints should be multiplied by 75% for use with doweled construction joint designs. In general, it will likely be either the plain aggregate interlock joints or the doweled construction joints that will be the weakest joints with lowest load transfer ability at an airfield test site.

CHAPTER 7. SUMMARY AND CONCLUSIONS

This research project set out to address a long list of key questions regarding concrete airfield pavement joint load transfer behavior and history. This list of questions was presented in the beginning of this report and is now revisited. Brief summary answers are provided below for each question.

- *What is the genesis of the assumption that a partial load transfer of the load at a joint reduces flexural stress by 25%?*

  Answer: Detailed pavement analysis began to be used in the early and mid 1990s as a result of rapidly increasing demand for aircraft and increasing sizes of aircrafts, WWII and other factors. The first tools to arrive for pavement slab analysis could not consider multiple slabs with joint effects in mathematical simulations. Only free-edge stress prediction equations were available (Westergaard, 1926). The 25% factor was a result of extensive research studies designed to calibrate the available free-edge stress model by Westergaard to field measurements of bending strain at real pavement joints. It was recognized early that LT was a dynamic stochastic variable and would vary considerably. The 25% factor is a design allowance factor and is not to be considered a real value present at all times in the field.

- *What were the variables examined that resulted in the adoption of the 25% value?*

  Answer: Test sites were established and strain gages installed in slab edges adjacent to joints. The test sites had varying slab thickness and foundation materials. Various load sizes and different types of joints were evaluated.

- *What variables used in the development of the current 25% assumption are valid and applicable to pavement design as it exists today?*

  Answer: All of the variables originally reviewed are still applicable today.

- *How sensitive are the pavement thickness design protocols being used to the assumed load transfer variables?*

  Answer: The sensitivity is closely related to the pavement damage model used for thickness design calculations. One way to view this sensitivity is through the relative damage functions provided in figure 6.42. For example, for LT values of 0.25 and 0.20, the relative damage factors are about 0.02 and 0.05, respectively. This means that less than 40 percent of the allowable traffic would be available for a design using 0.2 as the LT factor compared to an LT factor of 0.25.

- *Do the minimum design requirements dictate the thickness requirement?*

  Answer: When using the current FAA pavement damage model, the selection of the load transfer coefficient will dictate the required design thickness.

- *Is it feasible to dictate the use of a "short duration" period of low load transfer for the design?*

  Answer: It does appear feasible to develop such a design scheme. However, this research has shown that the LT factor for aggregate interlock joints will vary with a

nearly linear trend with respect to slab temperature. LT values will range from zero (for open joints) to about 0.35 (for joints tightly closed). For sites having longer slab lengths greater than 20 feet, it may be necessary to assign a short duration period of zero LT for aggregate interlock joints during the colder portions of winter in cold northern climates, as demonstrated in figure 5.20. For properly designed doweled and tied joints it does not appear necessary to use a period of low load transfer. The concept of the damage weighted annual effective LT is a better way of addressing seasonal variations in LT.

- *Under what conditions is there a difference in load transfer efficiency for a doweled, tied, and plain contraction joint?*

  Answer: The primary condition for which there are significant differences is cold weather when slabs contract and joint openings become large. The three joint types above all have fundamentally different behaviors. Tied joints are designed to remain tightly closed retaining high aggregate interlock stiffness and high LT during cold weather. In a properly designed tied joint, load transfer is mobilized primarily through aggregate interlock. LT values will remain high for tied joints during all slab temperatures provided the tie steel does not yield or break. Doweled joints are designed to open and close, and during winter all load transfer will be through the dowels. Dowel effectiveness will be dependent on how well the dowels are supported in the slabs. Aggregate interlock joints can completely lose all load transfer ability during cold weather.

- *On a contraction joint, does the depth of saw cut impact the value of load transfer efficiency?*

  Answer: Although this was not directly studied, it is clear that the answer is yes. The amount of aggregate interlock joint stiffness available will depend on the amount of joint crack face area that develops shear contact during joint deflections. However, it is more important to provide adequate saw cut depth to promote cracking of fresh concrete at the desired joint locations. Deeper saw cuts will result in less aggregate interlock joint stiffness being available and will also result in higher load related shear stresses on the aggregate interlock surfaces that do remain after saw cutting.

- *Is there an ambient environment regime where load transfer efficiency is nearly constant?*

  Answer: There are two ambient temperature regimes where joint stiffness and load transfer are nearly constant, very cold temperatures (joints fully open) and very hot temperatures (joints fully closed). When joints become fully closed, the upper limit joint stiffness trend lines provided in figure 5.4 should be considered to be present for all temperatures above the joint lock-up temperature.

- *Is there an ambient temperature environment when load transfer efficiency has a minimum value?*

  Answer: Yes it is during very cold weather. When joints become fully open during cold weather, aggregate interlock joints will have a constant zero LT value for longer slab lengths and higher paving temperatures (see figures 5.20 and 6.46). Doweled joints can also lose all aggregate interlock during cold weather and the load transfer will be constant and related to the dowel support quality.

- *Can ambient environment be a design variable? If so, what are the conditions that must be satisfied before a reasonable value for load transfer can be assigned?*

  Answer: Yes, ambient temperatures expected at a design site should be a design consideration. This research has shown that slab temperature is one of the most important parameters regarding load transfer. The calibrated joint stiffness versus slab temperature models and the FEM LT versus joint stiffness curves developed for this study were necessary in order to be able to obtain reasonable estimates for load transfer coefficients for designs as a function of ambient temperature variations.

- *What are the variables that affect the quantitative value of load transfer efficiency and are those variables equally significant?*

  Answer: Perhaps the most significant factor affecting load transfer is the choice of whether or not to use load transfer devices. If the design site will experience cold weather with temperatures well below the concrete casting temperatures, joint openings will likely be large during cold weather. If joint openings are expected to be large at a site (i.e., very cold winters), then load transfer devices are more desired. The two most important variables are slab length and ambient temperature variations and these appear to be roughly equally significant. These variables are followed by factors such as the concrete coefficient of thermal expansion. A high thermal expansion coefficient indicates a greater chance of larger joint openings during cold weather. Downward slab curling can cause an increase in slab bending stress while at the same time causing a decrease in the LT factor.

- *If not equally significant, what variables can be ignored for the purpose of assigning a value for load transfer?*

  Answer: This study revealed that base type has relatively small effect on load transfer and may be ignored. There is just slight evidence that joints over cement treated bases may experience larger slab edge gaps during upward curling.

- *Is there a simple technique that can be employed to determine when aircraft gear configuration will significantly influence the quantitative value of load transfer efficiency?*

  Answer: Yes. Although it was not demonstrated in this summary report, the full report for this study provides simple regression formulae that can predict LT values for single wheel loads, two-wheel gears and four-wheel gears as a function of joint stiffness values for use in pavement analysis. Figure 7.6 demonstrates these curves showing how wheel load area size and gear type affected LT values.

- *Is there sensitivity in the thickness computation that is a result of the interaction between gear configuration, slab curling, slab warping, slab size and load transfer for a given set of variables?*

  Answer: Yes. Figures 6.27-6.30 demonstrate the sensitivity of LT to variations in joint stiffness and curling magnitudes for four different pavement designs. Figure 7.1 shows simplified example that demonstrates the thickness design sensitivity to the LT value assumed. For the example, free edge stress values were calculated for a 60-kip 200 psi wheel load simulation for varying slab thickness values. Then varying LT values were

applied to the free edge stress values to develop the curves on the plot. For this example, assume the FAA pavement damage model indicates that the LT-adjusted edge stress must be limited to 450 psi in order to support the number of effective aircraft coverages proposed for the example design. If the traditional LT factor of 0.25 is applied to the free edge stress, the required slab thickness is about 15.1 inches. If the site design used all doweled joints with effective damage weighted LT values of 0.3, the required slab thickness would be about 14.6 inches. If the design were to use primarily aggregate interlock contraction joints and had a damage weighted LT value of about 0.05 (northern climate with cold winters and warm summer construction), the required slab thickness would be about 17.6 inches. Each type of gear at a design site will have a different value of effective limiting LT-adjusted edge stress that is related to the traffic mix and the number of coverages anticipated at the design site. Each type of gear will have a set of LT-adjusted stress curves as shown below.

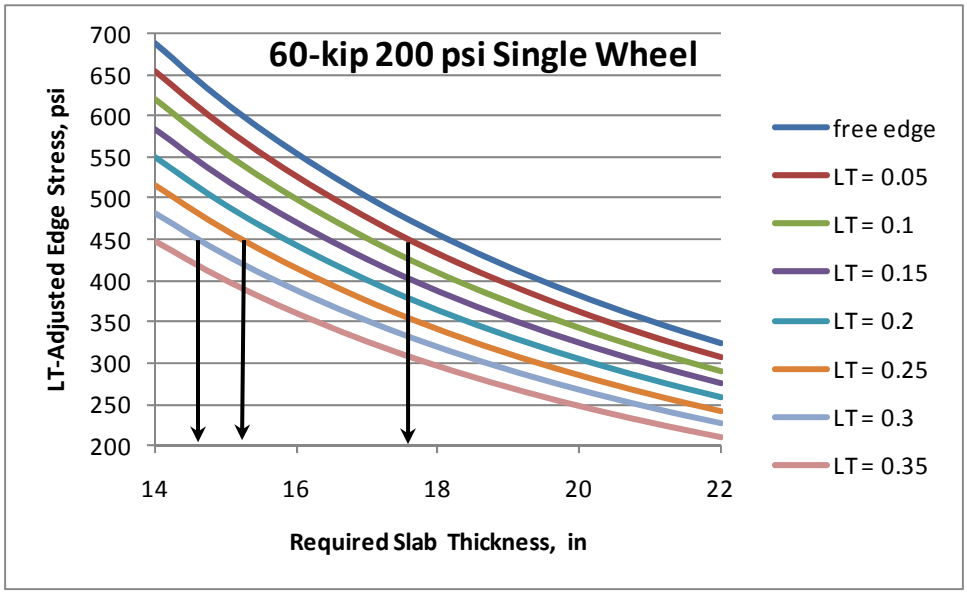

FIGURE 7.1. THE SENSITIVITY OF REQUIRED PAVEMENT SLAB THICKNESS VERSUS ASSUMED LT VALUE FOR THE EXAMPLE ALLOWABLE SLAB EDGE STRESS OF 450 PSI

- *What metric is best used to define and model joint load transfer when data are collected using a Falling Weight Deflectometer (FWD)?*

  Answer: The FWD device is designed to quantify slab deflections and therefore the deflection based load transfer efficiency (LTE_δ) is the best index to obtain with the FWD device. Although not presented in this summary report, part of this research project included reviewing time history data for dynamic FWD joint load tests. Three different ways of calculating load transfer efficiency were evaluated: LTE_δ calculated at the time of maximum load, LTE_δ calculated at the time of maximum joint deflection difference, and LTE_δ calculated using the maximum displacement values obtained from each FWD

sensor (the traditional method). It was determined that the best index is the LTE_{δ} determined using the traditional method using the maximum sensor displacements.

- *When using the FWD is it necessary to correct for slab bending?*

  Answer: Past research has proposed a bending correction factor for use with FWD joint load tests (Khazanovich and Gotliff, 2003). This bending correction factor adjusts the LTE_{δ} measured from FWD deflections taken at 6-inches from the joint line to account for slab bending deflections occurring in the small zone on 6 inches on either side of the joint. This past research has been primarily based on thinner roadway slab evaluations. Because airfield slabs are relatively thick and typically have relative dense edge subgrade support, it is not considered necessary to use this type of bending correction factor for thick heavy duty airfield pavement FWD evaluations. This slab bending correction is more important for thinner concrete slabs.

- *What dynamic loading is required to evaluate load transfer efficiency?*

  Answer: This is the one question on the list that remains relatively untested. A special load testing device would be needed to evaluate different loading rate effects on load transfer efficiency. The FWD device is a stationary dynamic load pulse type load test. This dynamic pulse can be considered to be somewhat like a rolling wheel load. When considering the typical load pulse duration for the FWD it is similar to the load pulse duration that would be generated by an aircraft wheel moving at about 40 mph. Therefore, it is safe to assume that the deflections measured using the FWD load test are smaller than deflections that would be measured for a static load test of the same magnitude. In order to develop a longer duration load pulse, the FWD device would have to be modified to use a softer rubber buffer system for the FWD drop weight impact, along with a heavier drop weight. A device capable of using variable loading rates and heavy loads was not readily available for this study.

The researchers of the past studied load transfer and assigned the single 0.25 LT factor to all joints. Although the research behind this design allowance is sound, this 0.25 factor is clearly too large for aggregate interlock joints or for older worn doweled joints for pavement sites subject to cold weather.

Table 7.1 provides what is considered to be revised overall average LT allowances for designs and considering the results and observations from this study. It represents a step forward in understanding and away from past use of a global single value for all joint types. The table presents single representative LT design allowances for different joint types and broken down into three categories related to temperatures expected at the site. The category of *Southern USA or Mild Climate* is defined as sites where paving temperatures are likely to be below the average temperature for the pavement during the service life and joint openings will likely remain relatively small retaining significant aggregate interlock during winter (Examples: California/Oregon Coast, Hawaii, Florida). The category of *Middle USA Variable Climates* is defined as sites where paving temperatures are likely to be about at or just below the average temperature for the pavement during service life and joint openings will vary more and be open larger during winter, but without fully opening and reaching a zero joint stiffness condition (North Carolina, Georgia and Tennessee). The category of *Northern USA* is defined as sites

where paving temperatures are likely to be above the average temperature for the pavement during service life and joint openings will likely be larger and more variable with joints having a zero joint stiffness condition during the winter (Minnesota, Michigan, and Wisconsin). As demonstrated in figure 7.15, the weighted LT values for aggregate interlock and doweled joints at DIA were 0.11 and 0.32, respectively. DIA would be right near the border of the Northern USA category.

TABLE 7.1. SIMPLIFIED LT VALUES CONSIDERING THERMAL EFFECTS AND JOINT TYPES

Joint Type	Southern USA or or Mild Climate	Middle USA Variable Climates	Northern USA
Aggregate Interlock Joint	0.2	0.15	0.1
Doweled Contraction Joint	0.3	0.3	0.25
Doweled Construction Joint	0.25	0.25	0.2
Fully Tied Joint	0.3	0.3	0.3

The magnitude of joint stiffness is the primary input variable for modern pavement FEM analyses that controls how much load is transferred from slab to slab and the overall load transfer, LT, value for a joint. In real pavement systems, the joint opening size, the roughness and stiffness of the crack face contact, and the amount and type of load transfer devices (dowels, tie bars) present across the joint control how load is transferred from slab to slab through the joint. During the literature review phase of the project, it was realized that there were no pre-existing methods for computing joint stiffness directly from joint deflection measurements. At the same time, it was realized that some way of directly calculating joint stiffness was required in order to accomplish the objectives of this research project. Therefore, considerable effort was put forth to develop a method for direct calculation of joint stiffness using non-destructive FWD data from joint load tests. This was the first major accomplishment of this study.

The development of the new method for direct calculation of joint stiffness allowed new methods for backcalculating the modulus of subgrade reaction along joint lines using the Skarlatos/Ioannides solution or FEM results calibrated to match a sites characteristic LTE_{δ} versus joint stiffness response. This was the second major accomplishment for this study. This accomplishment allows a direct comparison of mid-slab support to slab edge support using the *Slab Support Ratio* concept.

A detailed on-site non-destructive mechanistic evaluation procedure was developed for this study. The testing started typically before sunrise and extended to early afternoon and was designed to measure a site's typical thermal curling response and how this curling affected joint response. The evaluation procedure was performed thirteen times at eleven heavy duty airfield test sites. Additional test sites such as DIA, NAPTF, and LTPP GPS3 highway sites were also evaluated at multiple times of day and used for this study. The establishment of the FWD joint stiffness database was the third major accomplishment of this study. The field evaluations showed that the Skarlatos-type average *Slab Support Ratio* value was about 0.45 for typical in-service airfield pavements. Curling can cause apparent *Slab Support Ratio* to range from about 0.25 to 0.75 from morning to afternoon for sites experiencing large curling shape change.

Curling and warp trends measured at the airfield sites generally match trends previously measured at highway sites. Slab edge gaps and joint looseness were estimated and results show that the magnitude of joint looseness that will develop near the end of service life can be assumed to be about 5 to 10% of the unloaded slab edge deformation for a typical 40-kip FWD load. The field evaluations allowed many backcalculations of apparent dowel-concrete interaction modulus values for in-service doweled joints. The average modulus of dowel-concrete interaction backcalculated for the study was just over 3,000,000 psi.

The extensive joint behavior measurements are used to establish comprehensive joint stiffness behavior simulation tools for jointed concrete pavements. This was the fourth major accomplishment of this study. These joint stiffness simulation algorithms use the derivative concepts of $dLTE_{\delta}/dT$ and dO/dT, along with the MDOT joint opening size calculation formula to develop a useful tool for estimating joint stiffness of aggregate interlock joints as a function of average slab temperature and pavement design parameters. For doweled joints, the stiffness determination equation commonly used by FAA for joint designs is used to establish the component of joint stiffness added by load transfer devices. The joint models use typical pavement design parameters as input and the output is a joint stiffness versus slab temperature curve for a given pavement and joint design. The joint stiffness model simulations can demonstrate how joint stiffness will vary with slab temperature, by joint type, slab length and other parameters. The joint behavior model can also simulate aging by reducing factors such as the modulus of dowel-concrete interaction for doweled joints, or $dLTE_{\delta}/dO$ for aggregate interlock.

Finite element method (FEM) models were calibrated to reproduce the measured joint responses for four test sites. Using these calibrated FEM algorithms, Load Transfer (LT) curves were developed for various wheel load sizes, 2-wheel gears and 4-wheel gears, as a function of joint stiffness and as a function of FEM curling temperature gradients. The summary LT versus joint stiffness plots demonstrate the full range of LT values expected at commercial airfields. Regression models are provided that can reproduce the FEM generated LT functions, for use as a basis of design. These LT versus joint stiffness curves can be combined with the joint stiffness versus temperature curves generated from the joint behavior model to obtain LT estimates as a function of average slab temperature for a design. The analysis has shown that the relation between LT and slab temperature is nearly linear. The FEM results are also used to show how slab curling affects joint behavior. The effect of joints on top of slab stresses and LT curves is demonstrated. The development of the calibrated FEM algorithms and regression models to reproduce the FEM LT trends was the fifth major accomplishment of this study.

The pavement damage formula contained in the version 6E FAARFIELD pavement thickness design code is combined with the joint stiffness versus temperature data from the comprehensive joint behavior model, and the LT versus joint stiffness data from calibrated FEM algorithms to develop the concept of a “damage weighted LT value” for a given joint design. Because of the nature of the version 6E pavement damage formula, and because LT values drop as joint opening size increases, the weighted LT value is dominated by how the joints will behave during cold weather. Simplified recommendations are provided for selecting a representative single value of LT for a given joint design. This was the underlying primary objective for this research project and represents the sixth major accomplishment of this study.

In general, aggregate interlock joints having no load transfer devices have a nearly linear relation between LTE_{δ} and average slab temperature. The slope of this linear relation is most related to slab length. In extreme climates and for long slabs, aggregate interlock joints will probably range from fully closed/locked during summer to fully open with zero LT during the coldest days of winter. As slab lengths become shorter and climate milder, the lower winter LT values may be above zero. Adding load transfer devices will keep the winter LT values high provided the joints are properly designed. If the dowel-concrete interaction modulus zone surrounding the dowel bars is over-stressed or becomes deteriorated, the dowels may become ineffective and the joint will lose load transfer ability over time. Dowels may lose support completely such that the joint behaves as an aggregate interlock joint. Tied joints using deformed steel bars essentially are designed to remain closed and keep aggregate interlock stiffness at levels more associated with summer joint opening sizes. A properly functioning tied joint is developing total joint stiffness more from aggregate interlock than it is from the tie steel. The aggregate interlock component of construction joint smooth faces has smaller magnitude than naturally cracked faces. It is generally recommended that only the dowel component of total joint stiffness be used for construction joint designs. It should be assumed that initial dowel-concrete interaction modulus values will be lower for construction joints, and that the dowel-concrete interaction modulus will deteriorate faster for construction joints. This study has clearly shown that smooth-face longitudinal doweled construction joints should use lower design joint stiffness and LT than transverse naturally cracked doweled joints across the paving lanes. Many more side-by-side comparisons, as demonstrated herein, will be required before these differences can be accurately quantified. Regarding joint design philosophy, it is recommended that the dowel component of total joint stiffness not be set too high. The dowel component of total joint stiffness should be designed to be less than the "locked" upper limit total joint stiffness values recommended from this study and presented in Chapter 5. This way the dowels will be slightly softer than the crack face aggregate interlock when fully engaged. It is believed that if the dowel springs are slightly softer than the max aggregate interlock spring, the joint will better engage both effects. There may be an un-desirable stress concentration effect if the dowel stiffness is significantly larger than the upper limit aggregate interlock stiffness associated with a fully tight compressed crack face.

Based on this study, it is recommended that FWD evaluations for sites be focused on testing during the cooler periods of the year, but wet frozen foundation conditions should be avoided. It should be attempted to occasionally obtain data below freezing in good conditions but this data should be obtained in the fall cycle before the foundation becomes frozen solid. FWD testing of joints during the warm summer months will reveal more locked joints and reveal less critical information.

Pavements built in cooler weather will generally have higher load transfer values than those built in warmer weather, but paving temperature is not necessarily a controllable design value. It appears that cool weather paving would result in higher LT over the year by shifting the $dLTE_{\delta}/dT$ trend line between T_{Lock} and $T_{Release}$ to be lower on the temperature scale, meaning higher LTE_{δ} for a given average slab temperature for cooler paving temperatures. The relation between the paving temperatures and the T_{Lock} and $T_{Release}$ temperatures for aggregate interlock joints deserves extensive future study. Even if pure aggregate interlock joints are not being

constructed much in the future, this mechanism is still occurring with the doweled joints and should be studied independently. It will be easier to quantify this effect by evaluating pure aggregate interlock joints without having to attempt to mathematically separate out dowel effects. It is difficult to precisely determine how much of a total joint stiffness measurement is from dowels versus aggregate interlock unless the temperature versus LTE_{δ} trend for the aggregate interlock component for that joint is available and the temperature at the time of testing is available.

Appendix A provides the summary database and the summary data from the eleven heavy duty airfield full test sites. This database provides the data necessary to calibrate an advanced jointed multi-slab structural analysis tool to the field measurements and design cross section properties from the test sites. Appendix B is a separate report and is the literature review document developed during the first years of this study.

In general, this study has demonstrated how a properly designed non-destructive mechanistic evaluation procedure can be used to quantify a site's key mechanistic responses. These fundamental mechanistic responses are common to most all design procedures and evaluation schemes. In this study, these fundamental mechanistic responses were compared specifically to the FAA airfield pavement design concepts: the LT value and the version 6E pavement damage formula. The result is a suitable closed-form approximation of the Load Transfer, LT design problem in the context of the version 6E damage formula.

BIBLIOGRAPHY

Advisory Circular AC 150/5320-6D (1995), with four official changes. Federal Aviation Administration.

Advisory Circular AC 150/5320-6E (2010). Federal Aviation Administration.

Ahlvin, R. G. (1991). "Origin of Developments for Structural Design of Pavements", Technical Report GL-91-1, USAE Waterways Experiment Station, Vicksburg, MS.

Ahlvin, R. G. et al. (1971). "Multiple-Wheel, Heavy Gear Load Pavement Tests", Technical Report No. S-71-1, 5 volumes, USAE Waterways Experiment Station, Vicksburg, MS.

Armaghani J.M., Lybas J.M., Tia M., Ruth B.E., (1986). "Concrete Pavement Joint Stiffness Evaluation". *Transportation Research Record 1099*, TRB.

Barenberg E. J. and R. E. Smith. (1979). "Longitudinal Joint Systems in Slip-Formed Rigid Pavements, Vol. I: Literature Survey and Field Inspection" Report No. FAA-RD-79-4-I, Federal Aviation Administration, Washington, D.C.

Barenberg, E.J. Arntzen, D.M. (1981). "Design of Airport Pavement as Affected by Load Transfer and Support Conditions". Proceedings of the Second International Conference on Concrete Pavements. Purdue University.

Barker W.R. (1981). "Introduction to a Rigid Pavement Design Procedure". Proceedings of the Second International Conference on Concrete Pavements. Purdue University.

Bradbury, R.D. (1938). "Reinforced Concrete Pavements", Wire Reinforcement Institute, Washington, DC.

Brill, D.R. (1998). "Development of Advanced Computational Models for Airport Pavement Design". DOT/FAA/AR-97/47. US DOT Office of Aviation Research.

Brill, D.R. (2010). "Calibration of FAARFIELD Rigid Pavement Design Procedure". DOT/FAA/AR-09/57. Office of Research and Technology Development, Washington, DC 20591.

Bush III, A.J. Hall, J.W. (1981). "Experience with Nondestructive Structural Evaluation of Airport Pavements". Proceedings of the Second International Conference on Concrete Pavements. Purdue University.

Bush III, A.J., Alexander, D.R., Hall, J.W. (1985). "Nondestructive Airfield Rigid Pavement Evaluation". Proceedings of the Third International Conference on Concrete Pavements. Purdue University.

Bush III, A.J., Brown, W.R., Bailey, C.E. (1989). "An Evaluation Procedure for Rigid Airfield Pavements". Proceedings of the Fourth International Conference on Concrete Pavements. Purdue University.

Byrum, C.R., Hansen W., Kohn S.D. (1997) "The Effects of Strength and Other Properties on the Performance of PCC Pavements". Proceedings of the Sixth International Conference on Concrete Pavements Design and Materials for High Performance. Purdue University, Nov. 18-21, 1997.

Byrum, C.R. (2009) "Measuring Curvature in Concrete Slabs and Connecting the Data to Slab Modeling Theory". *Transportation Research Record 2094*, Transportation Research Board, National Academy Press, Washington DC.

Byrum, C.R. (2000). "A High Speed Profiler Based Slab Curvature Index for Jointed Concrete Pavement Curling and Warping Analyses". Ph.D. Dissertation, University of Michigan, 2001.

Byrum, C.R. (2001). "The Effect of Locked-in Curvature on Pavement Performance". Published in a book titled, "Long-Term Pavement Performance: Making Something of It". Edited by R.G. Hicks and J. B. Sorenson. American Society of Civil Engineers, 2001.

Crovetti, J.A. (1994). "Design and Evaluation of Jointed Concrete Pavement Systems Incorporating Open-Graded Permeable Bases". PhD Dissertation, University of Illinois at Urbana-Champaign

Department of Defense. (2001). "Pavement Design for Airfields" UFC 3-260-02, Washington, DC.

Fine, Lenore and Remington (1972). "The US Army in WWII: The Corps of Engineers: Construction in the United States", Office of the Chief of Military History, US Army, Washington, D.C.

Finney, E., Oehler, L. (1959). "Final Report- Design Project Michigan Test Road". Michigan State Highway Department Report No. 302, Project No 39 F-7(2).

Gillespie, T. D. et al. (1993). "Effects of Heavy-Vehicle Characteristics on Pavement Response and Performance". NCHRP Report 353, TRB National Research Council. Washington D. C.

Grau, R. W. (1972). "Strengthening of Keyed Longitudinal Construction Joints in Rigid Pavements" Miscellaneous Paper S-72-43. US Army Engineer Waterways Experiment Station, Vicksburg, MS.

Guo, H., Larson, R.M., Snyder, M.B. (1993). "A Non-Linear Mechanistic Model for Dowel Looseness in PCC Pavements". Proceedings of the Fifth International Conference on Concrete Pavements. Purdue University.

Hammons, M., D. Pittman, and D. Mathews. (1995). "Effectiveness of Load Transfer Devices"

DOT/FAA/AR-95/80, Federal Aviation Administration, Washington, D.C.

Hammons, M. I (1998). "Advanced Pavement Design: Finite Element Modeling for Rigid Pavement Joints, Report II: Model Development". DOT/FAA/AR-97/7. US DOT Office of Aviation Research.

Hansen, W. et al. (1996). "The Effect of Higher Strength and Associated Concrete Properties on Pavement Performance (Interim Report)". FHWA DTFH61-95-R-00108.

Hutchinson, R. L. and P. Vedros (1977). "Performance of Heavy-Load Portland Cement Concrete (Rigid) Airfield Pavements" Proceedings of the 1st International Conference on Concrete Pavements, Purdue University, West Lafayette, IN.

Hutchinson, R. L. (1966). "Basis for Rigid Pavement Design for Military Airfields", Miscellaneous Paper No. 5-7, USAE Ohio River Division Laboratory, Cincinnati, OH.

Ioannides, A. M. and M. I. Hammons. (1996). "Westergaard-Type Solution for Edge Load Transfer Problem" *Transportation Research Record 1525*, Transportation Research Board, Washington, D.C.

Ioannides, A.M. and Khazanovich, L., "Nonlinear Temperature Effects on Multi-Layered Concrete Pavements," *Journal of Transportation Engineering*, ASCE, 124, 2, (Mar./Apr., 1998): 128-136.

Jensen, E.A., Hansen, W. (2001). "Mechanism of Load Transfer Crack Width Relation in JPCP: Influence of Coarse Aggregate Properties". Proceedings of the Seventh International Conference on Concrete Pavements. Purdue University.

Jun, D.X., Ming, H.X., Jun, Z.J., (1997). "The Loss of Load Transfer Capacity at Joints of Airfield Concrete Pavements Under Repetitive Loads". Proceedings of the Sixth International Conference on Concrete Pavements. Purdue University.

Kawa, I. et al. (2002) "Implementation of Rigid Pavement Thickness Design for New Pavements" Proceedings of the 2002 Airport Technology Transfer Conference. Federal Aviation Administration. May, 2002.

Kazuyuki, K., Nakagawa, S., Nishizawa, T., Kasahara, A. (1993). "Evaluation Method for Joint Load Transfer Efficiency in Concrete Pavements". Proceedings of the Fifth International Conference on Concrete Pavements. Purdue University.

Khazanovich L. Gotlif, A. (2003) "Evaluation of Joint and Crack Load Transfer- Final Report". FHWA-RD-02-088. National Technical Information Services, 2003.

Kohn, S.D. (1985). "Evaluation of the FAA Design Procedure for High Traffic Volume Rigid Pavements". Proceedings of the Third International Conference on Concrete Pavements. Purdue University.

Kohn, S.D., Gemayel, C.A., Alexander, D.R. Tons, E. (1989). "Development of a Thickness Design Procedure for Stabilized Layers under Rigid Airfield Pavements". Proceedings of the Fourth International Conference on Concrete Pavements. Purdue University.

Marsey, W., Dong, M. (2004) "Profile Measurements of Portland Cement Concrete Test Slab at the National Airport Test Facility". Proceedings of the 2004 FAA Worldwide Airport Technology Transfer Conference.

Mellinger, F. and P. Carlton. (1955). "Application of Models to Design Studies of Concrete Airfield Pavements" Proceedings of the 34th Annual Meeting, Highway Research Board, Washington, D.C.

Nishizawa, T., Koyanagawa, M., Takeuchi, Y., Kimura, M. (2001). "Study on Mechanical Behavior of Dowel Bar in Transverse Joint of Concrete Pavement". Proceedings of the Seventh International Conference on Concrete Pavements. Purdue University.

Nishizawa, T., Fukuda, T., Matsuno, S., (1989). "A Refined Model of Doweled Joints for Concrete Pavement using FEM Analysis". Proceedings of the Fourth International Conference on Concrete Pavements. Purdue University.

Nishizawa, T., Ozeki, T., Katoh, K., Matsui, K., (2009). "FEM Analysis of Thermal Stresses in Thick Airfield Concrete Slabs". Proceedings of the 88th Annual Meeting of the Transportation Research Board, pre-print CD ROM. The National Academies.

Owusu-Antwi, EB., Meyer, A.H., Hudson, W.R., (1989). "Preliminary Evaluation of Procedures for the Assessment of Load Transfer Across Joints and Cracks in Rigid Pavements using the Falling Weight Deflectometer". Proceedings of the Fourth International Conference on Concrete Pavements. Purdue University.

Parker Jr., F., Barker, W., Gunkel, R., Odom, E. (1979) Development of a Structural Design Procedure for Rigid Airport Pavements. FAA-RD-77-81. U.S.D.O.T. 1979.

Pringle, T. (1950). "Structural Design of Joints for Airport Pavements" American Concrete Institute Title No. 46-59

Prozzi, J., Balmaceda, P., De Beer, M. (1993). "Nondestructive Tests Procedure for Field Evaluation of Transverse Joints in Concrete Pavements". Proceedings of the Fifth International Conference on Concrete Pavements. Purdue University.

Ricalde, L (2007). Analysis of HWD Data from CC2 Traffic Tests at the National Airport Pavement Test Facility. Proceedings of the 2007 FAA Worldwide Airport Technology Transfer Conference.

Roesler, J.R., Hiller, J.E., Littleton, P.C. (2005). "Large Scale Airfield Concrete Slab Fatigue Tests". Proceedings of the Eighth International Conference on Concrete Pavements. Purdue University.

Roesler, J., Evangelista, F., Domingues, M. (2007). "Effect of gear positions on airfield rigid pavement critical stress locations". Proceedings of the 2007 FAA Worldwide Airport Technology Transfer Conference. Atlantic City, NJ. 2007.

Rollings, R. S. (2003). "Evolution of Airfield Design Philosophies" *Proceedings*, XXII World Road Congress, Permanent International Association of Road Congresses, Durban, South Africa.

Rollings, R. S. (2001). "Concrete Pavement Design: Its More than a Thickness Design Chart" Proceedings, 7th International Conference on Concrete Pavements, Orlando, Florida.

Rollings, R. S. and D. W. Pittman. (1992). "Application of Field Instrumentation and Performance Monitoring of Rigid Pavements,"ASCE *Journal of Transportation Engineering*, Vol. 118, No. 3.

Rollings, R. S. and M. P. Rollings. (1991). "Pavement Failures: Oversights, Omissions, and Wishful Thinking," ASCE *Journal of Performance of Constructed Facilities*, Vol. 5, No. 4.

Rollings, R. S. (1987). "Design of Rigid Overlays for Airfield Pavements," doctoral dissertation, University of Maryland, (UMI Dissertation Information Services, No. 8808598).

Rollings, R. S. (1989). "Developments in the Corps of Engineers Rigid Airfield Pavement Design," Proceedings, 4th International Conference on Concrete Pavements, Purdue University, West Lafayette, IN.

Rollings, R. S. (1981). "Corps of Engineers Design Procedures for Rigid Airfield Pavements," Proceedings, 2nd International Conference on Concrete Pavements, Purdue University, West Lafayette, IN.

Rufino, D.M., Roesler, J. Berenberg, E., Tutumuler, E. (2001). "Analysis of Pavement Responses to Aircraft and Environmental Loading at Denver International Airport". Proceedings of the Seventh International Conference on Concrete Pavements. Purdue University.

Rufino, D.M. (2003). "Mechanistic Analysis of In-Service Airfield Concrete Pavement Responses". PhD Dissertation, University of Illinois at Urbana-Champaign.

Rufino, D.M., Roesler, J. Berenberg, E (2004). "Mechanistic Analysis of Pavement Responses From Denver International Airport". FAA Center of Excellence for Airport Technology. C.O.E. Report No. 26.

Rufino, D., Roesler, J. (2004) "Effect of pavement temperature on concrete pavement joint responses" Proceedings of the 2004 FAA Worldwide Airport Technology Transfer Conference. Atlantic City, NJ. 2004.

Sale, J.P. (1977). “Rigid Pavement Design for Airfields”. Proceedings of the First International Conference on Concrete Pavements. Purdue University.

Sale, J. P. and R. L. Hutchinson. (1959). “Design of Rigid Pavement Design Criteria for Military Airfields” *Journal of the Air Transport Division*, Vol. 85, No. 3, ASCE.

Skarlatos, M.S. and Ioannides A.M. (1998). "The Theory of Concrete Pavement Joints" Proceedings, Fourth International Workshop on design theories and their verification of concrete slabs for pavements and railroads, 10-11 September, Bussaco, Portugal, pp. 187-208.

Skarlatos, M. S. (1949). “Deflections and Stresses in Concrete Pavements of Airfields with Continuous Elastic Joints” Report AD 628501, US Army Engineer Ohio River Division Laboratories.

Strauss, P.J., Perrie, B.D., du Plessis, L., Rossmann, D. (2005). “Load Transfer through Aggregate Interlock: Crack Width, Aggregate Type, and Performance”. Proceedings of the Eighth International Conference on Concrete Pavements. Purdue University.

Tabatabaie, A.M. et al (1979). “Longitudinal Joint Systems in Slip-Formed Rigid Pavements, Vol. II: Analysis of Load Transfer Systems for Concrete Pavements” Report No. FAA-RD-79-4-I, Federal Aviation Administration, Washington, D.C.

Teller, L.W., Sutherland E.C. (1936). “The Structural Design of Concrete Pavements Part 2- Observed Effects of Variations in Temperature and Moisture on Size Shape and Stress Resistance of Concrete Pavements”. *Public Roads* Journal of Highway Research, USDA Vol 16., No. 9.

Teller, L.W., Sutherland E.C. (1936). “The Structural Design of Concrete Pavements Part 3- A Study of Concrete Pavement Cross Sections”. *Public Roads* Journal of Highway Research, USDA Vol 16., No. 10.

Teller, L.W., Sutherland E.C. (1936). “The Structural Design of Concrete Pavements Part 4- A Study of the Structural Action of Several Types of Transverse and Longitudinal Joint Designs”. *Public Roads* Journal of Highway Research, USDA Vol 17., No. 7 and No. 8

Teller, L.W., Cashell, H.D. (1958). “Performance of Dowelled Joints under Repetitive Loading”. *Public Roads*, Volume 30, No. 1. US Department of Commerce.

US Army Corps of Engineers. (1950a). “Lockbourne No. 2 - Experimental Mat,” Rigid Pavement Laboratory.

US Army Corps of Engineers. (1950b). “Lockbourne No. 2 - Modification, Multiple-Wheel Study,” Rigid Pavement Laboratory.

US Army Corps of Engineers. (1946). "Lockbourne No. 1 Test Track, Final Report," Rigid Pavement Laboratory.

Van Breemen, W., Finney, E. (1950). "Design and Construction of Joints in Concrete Pavements". *American Concrete Institute* Title No. 46-59.

Westergaard, H. M., (1948). "New Formulas for Stresses in Concrete Pavements of Airfields," *Transactions*, ASCE, Vol. 113, pp. 425-444.

Westergaard, H.M. (1927). "Analysis of Stresses in Concrete Roads Caused by Temperature". *Public Roads* Journal of Highway Research, USDA Vol 8., No. 3.

Westergaard, H.M. (1926). "Stresses in Concrete Pavements Computed by Theoretical Analysis". *Public Roads* Journal of Highway Research, USDA, Vol. 7., No. 2.

Zollinger, D.G., Soares, J. (1999) "Performance of Continuously Reinforced Concrete Pavements: Volume VII: Summary". FHWA-RD-98-102. Federal Highway Administration.

APPENDIX A:
SUMMARY OF DATA FROM THE FULL TEST SITES

This appendix provides the compilation of test results and analyses for the full test sites. Figure A.1 shows the general locations of the test sites. Figure A.2 provides a summary of the design cross sections. Tables A.1 through A.11 summarize key site features and analysis results and provide representative values for each test site. After the tables, the full testing and analysis results summaries for each test site are provided. The data for each test site starts with a design cross section summary page taken from the construction plans for the test patch area. This is followed by a weather summary sheet and general description of site topography and subgrade, and then all of the site data. Some commentary is provided where necessary. The following data is generally included for each test site:

- Cross section data
- Weather/subgrade summary
- Temperatures encountered during testing
- Slab curling and warp data
- Mid-panel back-calculation results
- Characteristic joint stiffness curve
- Best-fit Skarlatos LTE-delta model
- Best-fit Skarlatos log(f) model
- Site average load versus deflection functions; mid-panel and edges
- Summary statistics for each joint type at the site
- Average load versus joint stiffness trend at the site
- Slab edge gap and joint looseness data
- Load work to slab strain energy ratio versus stiffness plot

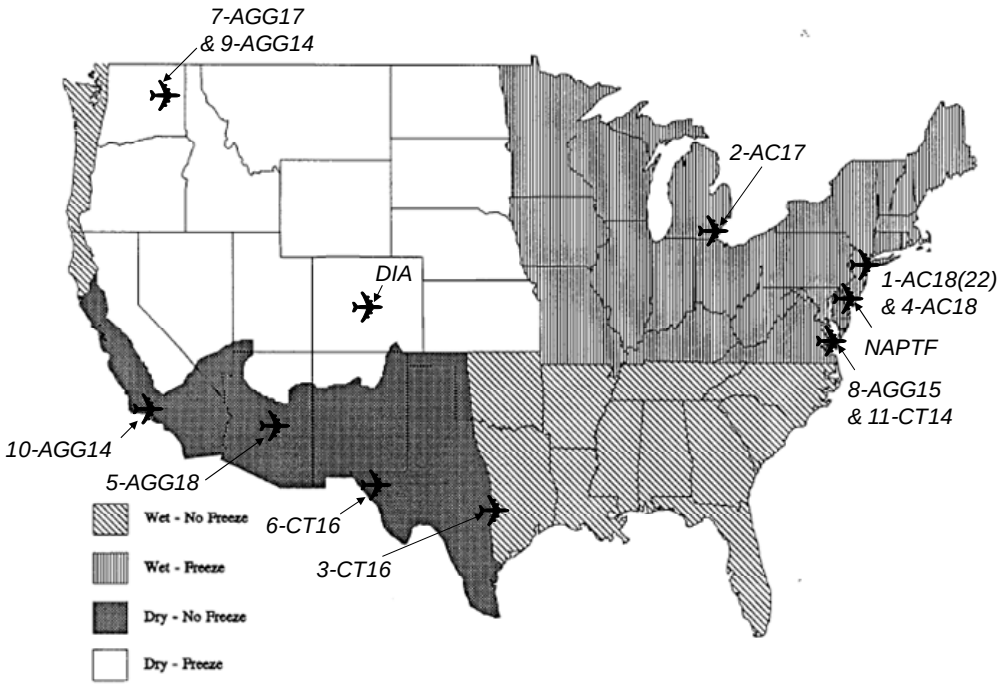

FIGURE A.1. MAP OF THE USA SHOWING GENERALIZED CLIMATE REGIONS AND TEST SITE LOCATIONS

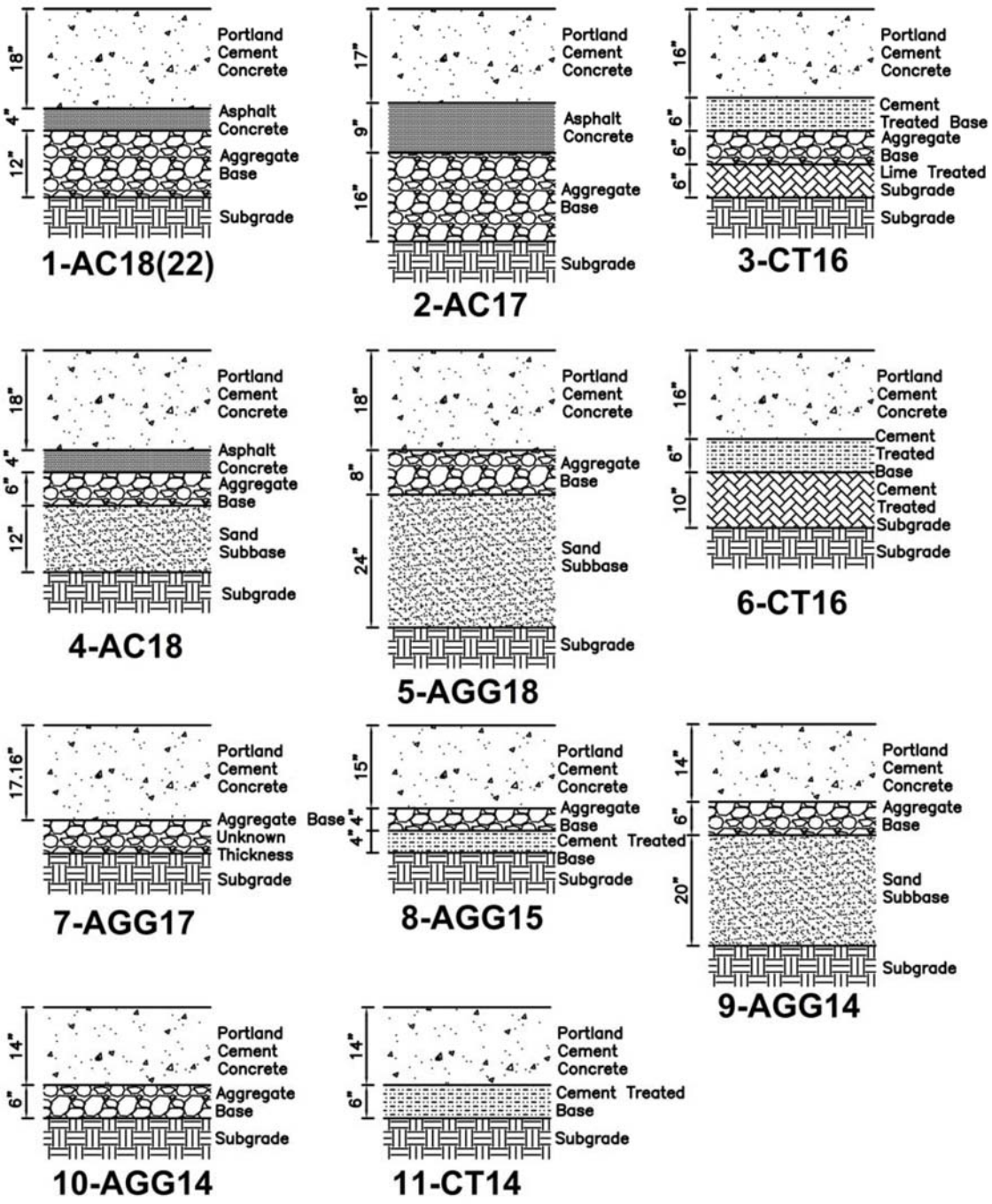

FIGURE A.2. CROSS SECTION IMAGES FOR THE ELEVEN FULL TEST SITES

TABLE A.1. GENERAL INFORMATION FOR THE FULL TEST SITES

Section ID	Date Tested	Climate	Use	Est. Construction Year
1-AC18(22)	7/20/10 & 12/15/09	Wet/Freeeze	Taxiway	2000
2-AC17	9/30/2009	Wet/Freeeze	Runway	1993
3-CT16	6/1/2010	Wet/No Freeze	Runway	1997
4-AC18	7/21/10 & 12/14/09	Wet/Freeeze	Apron	2002
5-AGG18	9/23/2010	Dry/ No Freeze	Runway	1996
6-CT16	9/21/2010	Dry/ No Freeze	Apron	2001
7-AGG17	12/7/2010	Dry/Freeze	Apron	1994
8-AGG15	12/11/2009	Wet/Freeeze	Apron	1998
9-AGG14	12/6/2010	Dry/Freeze	Apron	1998
10-AGG14	8/25/2010	Dry/ No Freeze	Apron	1991
11-CT14	12/10/2009	Wet/Freeeze	Apron	1982

TABLE A.2. SLAB DIMENSION SUMMARY FOR THE FULL TEST SITES

Section ID	Paved Width	Transverse Joint Spacing	Longitudinal Joint Spacing	Effective Slab Dimensions	Slab Thickness
1-AC18(22)	20'	18'	N/A	20'x18'	18"
2-AC17	25'	25'	12.5'	12.5'x25'	17"
3-CT16	25'	25'	N/A	25'x25'	16" P501
4-AC18	25'	25'	N/A	25'x25'	18"
5-AGG18	37.5'	18.75'	18.75'	18.75'x18.75'	18" P501
6-CT16	25'	16.67'	12.5'	16.67'x12.5'	16" P501
7-AGG17	18.75'	20'	N/A	20'x18.75'	17.16"
8-AGG15	20'	20'	N/A	20'x20'	15"
9-AGG14	18.5'	20.67'	N/A	20.67" x 18.5'	14"
10-AGG14	25'	12.5'	15'	15'x12.5'	14" P501
11-CT14	25'	25'	N/A	25'x25'	14"

TABLE A.3. SLAB, BASE AND SUBBASE SUMMARY FOR THE FULL TEST SITES

Section ID	Est. Coarse Aggregate Type	Steel Mesh	Base	Subbase
1-AC18(22)	Basalt	Yes	4" AC	12" Aggregate Base
2-AC17	Limestone	Yes	9" AC	16" Crushed Aggregate
3-CT16	--	No	6" P304 CTB	6" P200 Aggregate Base, 6" P155 Lime stabilzed with bit cure coat
4-AC18	Basalt	Yes	4" AC	6" Aggregate Base 12" Sand
5-AGG18	Round River Gravel	No	8" P209 Aggregate Base	24" P152 Sand
6-CT16	--	No	6" P304 CTB	10" P301 Cement Soil Subbase
7-AGG17	Basalt	No	Aggregate Base-unknown"	none
8-AGG15	Limestone	No	4" Crushed Aggregate	4" CTB
9-AGG14	Basalt	No	6" Aggregate Base	20" Select Non Frost Susceptible Subbase
10-AGG14	--	No	6" Aggregate Base	None
11-CT14	Limestone	No	6" CTB	None

TABLE A.4. TRANSVERSE JOINT SUMMARY DATA FOR THE FULL TEST SITES.

Section ID	Transverse Joints						
	Bar Diameter, in.	Bar Spacing, in.	Bar Length, in.	Bar Type	Joint Width, in.	Sawcut Depth, in.	Sealant Type
1-AC18(22)	2	18	24	Smooth, one side greased	0.5		Preformed
2-AC17	1.5	12	20	Smooth			Preformed
3-CT16	1.375	15	20	Smooth	0.5		Poured Rubber
4-AC18	2	15	24	Smooth, one side greased	0.5	4.5	Preformed Elastomeric
5-AGG18	1.5	15	20	Smooth, one side painted and oiled	0.375	6	Preformed
6-CT16	1.25	15	20	Smooth, one side painted and greased	0.5	4	Preformed
7-AGG17	--	--	--	--	0.5		Preformed
8-AGG15	1.25	15	20	Smooth, one side greased and painted	0.5	3.75	Silicone
9-AGG14	--	--	--	--	0.5		Preformed
10-AGG14	1.5	15	20	Smooth, one side greased	0.5	3.5	Poured Rubber
11-CT14	--	--	--	--	0.5	4	Preformed

TABLE A.5. SUMMARY DATA FOR LONGITUDINAL CONTRACTION JOINTS

Section ID	Longitudinal Contraction Joints						
	Bar Diameter, in.	Bar Spacing, in.	Bar Length, in.	Bar Type	Joint Width, in.	Sawcut Depth, in.	Sealant Type
1-AC18(22)	--	--	--	--	--	--	--
2-AC17	0.75	20	42	Deformed			Poured Rubber
3-CT16	--	--	--	--	--	--	--
4-AC18	--	--	--	--	--	--	--
5-AGG18	1.5	15	20	Smooth, one side painted and oiled	0.375	6	Preformed
6-CT16	1.25	15	20	Smooth, one side painted and greased	0.5	4	Preformed
7-AGG17	--	--	--	--	--	--	--
8-AGG15	--	--	--	--	--	--	--
9-AGG14	--	--	--	--	--	--	--
10-AGG14	0.625	30	30	Deformed	0.5	3.5	Poured Rubber
11-CT14	--	--	--	--	--	--	--

TABLE A.6. SUMMARY DATA FOR LONGITUDINAL CONSTRUCTION JOINTS

Section ID	Longitudinal Construction Joints						
	Bar Diameter, in.	Bar Spacing, in.	Bar Length, in.	Bar Type	Joint Width, in.	Sawcut Depth, in.	Sealant Type
1-AC18(22)	2	18	24	Smooth, one side greased with key way	0.5		Preformed
2-AC17	0.75	20	42	Deformed			Poured Rubber
3-CT16	1.375	15	20	Smooth	0.5		Poured Rubber
4-AC18	2	15	24	Smooth, drilled and epoxied with one side greased	0.5	2	Preformed Elastomeric
5-AGG18	1.5	15	20	Smooth, one side painted and oiled	0.375	1.25	Preformed
6-CT16	1.25	15	20	Smooth, one side painted and greased	0.5		Preformed
7-AGG17	1	18	20	Smooth, one side oiled	0.5		Preformed
8-AGG15	1.25	15	20	Smooth, one side greased and painted	0.5	1.25	Silicone
9-AGG14	1	18	20	Smooth, one side oiled	0.5		Preformed
10-AGG14	1.5	15	20	Smooth, drilled and epoxied, threaded, one side greased	0.5		Poured Rubber
11-CT14	1.25	15	20	Smooth, one side oiled and painted	0.5	1.875	Preformed

TABLE A.7. SITE AVERAGE JOINT STIFFNESS AND LTE-DELTA RESPONSES

Stiffness Summary

SITE ID	Jt Response LR, inches	Site Avg. LTE-delta	Site Avg Joint Stiffness, lb/in/in	Site Median Joint Stiffness, lb/in/in	% possible uncr/locked	# Jt. Tests
1-AC18(22)	208.2	69.6%	73883	64533	1.1%	940
1-AC18(22)	180.6	75.5%	129653	90325	11.2%	642
2-AC17	121.4	79.0%	131327	125257	13.4%	659
3-CT16	124.0	80.6%	135575	108616	28.9%	495
4-AC18	145.7	79.0%	84400	79845	3.9%	820
4-AC18	150.7	85.1%	140354	114373	17.8%	551
5-AGG18	109.1	82.2%	146393	119835	41.9%	864
6-CT16	141.7	84.7%	149484	128394	15.5%	412
7-AGG17	123.5	85.1%	159403	145725	18.3%	676
8-AGG15	136.3	58.8%	28256	24578	0.0%	839
9-AGG14	114.4	83.8%	155762	152845	14.8%	488
10-AGG14	119.3	93.7%	337380	267051	89.8%	1383
11-CT14	118.5	62.7%	31364	29783	0.5%	860

TABLE A.8. SUMMARY OF SKARLATOS-EDGE AND ILLIBACK MID-PANEL BACK-CALCULATION DATA

	Skarlatos Edge Back-Cal Data		ILLIBACK Mid Panel Back-Cal Data				
SITE ID	Site Avg Skarlatos ks, LTE-d fit, psi/in	Site Avg Skarlatos ks, *kl* fit, psi/in	Site Avg. DL ks, psi/in	Site Avg DL Ec, Msi	Site Avg Es subg, psi	Site Avg Es Ec, Msi	Edge-to-Mid Slab Support Ratio
1-AC18(22)	183	135	391	12	84203	9.7	0.47
1-AC18(22)	211	151	475	9.25	92794	7.24	0.44
2-AC17	200	147	430	6.44	76295	4.91	0.47
3-CT16	177	126	400	7.01	70742	5.34	0.44
4-AC18	140	111	275	6.96	56700	5.52	0.51
4-AC18	138	97	305	6.27	60178	4.93	0.45
5-AGG18	184	130	614	3.285	92240	2.34	0.30
6-CT16	96	72	205	8.69	43712	6.98	0.47
7-AGG17	182	127	292	4.26	51501	3.25	0.62
8-AGG15	90	65	190	6.8	37500	5.35	0.47
9-AGG14	213	139	229	6.46	41030	4.96	0.93
10-AGG14	114	76	260	5.29	43636	3.95	0.44
11-CT14	177	131	200	4.9	35000	3.7	0.89

TABLE A.9. SUMMARY OF MID-PANEL LOAD TEST DATA

	Mid-Panel Load Data			9-kip normalized avg mid-slab basin						
SITE ID	ILLIBACK/Plan PCC Thickness, inches	Mid-Panel Sensor COV	Mid-Panel LTE-delta Avg.	*mils* D0	D12	D24	D36	D48	D60	D72
1-AC18(22)	18	13.33	89	0.716	0.648	0.612	0.580	0.541	0.510	0.477
1-AC18(22)	18	16.16	91	0.734	0.642	0.600	0.569	0.529	0.504	0.467
2-AC17	17	6.78	89	1.043	0.914	0.838	0.763	0.680	0.599	0.526
3-CT16	16	6.47	89	1.100	0.979	0.899	0.812	0.728	0.659	0.602
4-AC18	18	8.27	89	1.123	1.005	0.956	0.901	0.837	0.774	0.709
4-AC18	18	9.24	90	1.119	1.001	0.940	0.879	0.811	0.747	0.681
5-AGG18	18	17	86	1.167	1.009	0.917	0.816	0.719	0.627	0.549
6-CT16	16	20.84	93	1.398	1.305	1.228	1.145	1.034	0.948	0.872
7-AGG17	17	9.102	90	1.517	1.367	1.260	1.150	1.015	0.890	0.768
8-AGG15	15	7.99	91	1.802	1.657	1.551	1.424	1.292	1.163	1.037
9-AGG14	14	13.34	92	1.879	1.733	1.597	1.443	1.263	1.092	0.920
10-AGG14	14	12.66	91	1.969	1.803	1.641	1.454	1.270	1.094	0.947
11-CT14	14	15.02	89	2.301	2.072	1.909	1.713	1.525	1.338	1.160

TABLE A.10. SITE AVERAGE DEFLECTION EQUATIONS FOR SLAB EDGES AND MID-PANEL

	Site Average Linear Deflection Equations						Mid-Slab Power-Functions	
Site Number	Mid-Panel Stffness, lb/mil	Mid-Panel y-intercept	Loaded Slab Edge, lb/mil	Loaded Slab y-intercept	Un-Loaded Edge, lb/mil	Un-Loaded Slab y-intercept	Mid-slab Initial Mod, lb/mil	Load Exponent
1-AC18(22)	12195	0.00	7952	-0.20	12658	0.07	13514	1.011
2-AC17	9009	0.12	5556	0.22	6849	-0.07	6211	0.967
3-CT16	8264	0.06	4762	0.10	6293	0.23	6211	0.975
4-AC18	8333	0.14	5076	0.18	6494	0.22	7353	0.990
5-AGG18	7813	0.08	4158	0.27	4897	0.14	6329	0.982
6-CT16	6897	0.30	3759	-0.82	4717	-0.42	3984	0.954
7-AGG17	6061	0.10	4658	-0.29	5734	-0.01	4878	0.981
8-AGG15	5236	0.24	2075	1.75	4149	0.52	3401	0.962
9-AGG14	4926	0.20	4246	-0.36	5160	-0.23	3497	0.970
10-AGG14	4651	0.12	3757	0.17	4014	0.17	4149	0.991
11-CT14	4237	0.51	2899	0.43	4367	-0.02	1916	0.930

TABLE A.11. SITE AVERAGE 35-KIP FWD RESPONSE AND LOSS-OF-SUPPORT VALUES

	Avg 35-kip FWD Load Response			Avg Loss-of-Support Indices	
Site Number	Mid-Panel defl, mils	Loaded Edge defl, mils	Un-Loaded Edge defl, mils	Edge sum to Mid slab Deflection Ratio	ISM type FWD Stiffness Ratio
1-AC18(22)	2.87	4.40	2.77	2.45	1.45
2-AC17	4.00	6.30	5.11	2.89	1.53
3-CT16	4.30	7.35	5.56	3.08	1.64
4-AC18	4.34	6.90	5.39	2.92	1.55
5-AGG18	4.56	8.42	7.15	3.50	1.77
6-CT16	5.37	9.31	7.42	2.88	1.73
7-AGG17	5.88	7.51	6.10	2.27	1.23
8-AGG15	6.93	16.87	8.44	3.98	2.38
9-AGG14	7.30	8.24	6.78	1.98	1.09
10-AGG14	7.64	9.32	8.72	2.41	1.17
11-CT14	8.77	12.08	8.02	2.34	1.38

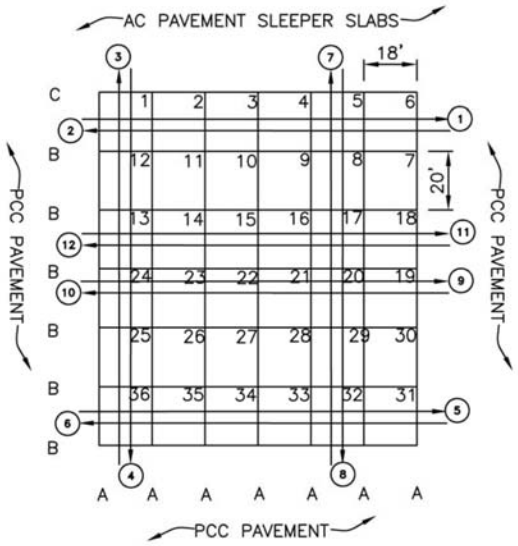

TEST PATTERN

LEGEND

(2) FWD TEST LANE NUMBER

A CONTRACTION JOINT: 2" DIA. SMOOTH DOWEL BAR, 24" LONG, 18" SPACING, ONE SIDE GREASED.

B CONSTRUCTION JOINT: 2" DIA. SMOOTH DOWEL BAR, 24" LONG, 18" SPACING, ONE SIDE GREASED, WITH KEY WAY.

C THICKENED EDGE JOINT SLEEPER SLAB JOINT: SLAB THICKNESS INCREASED TO 24", NO. 5 DEFORMED TIE BAR, 30" LONG, 30" SPACING.

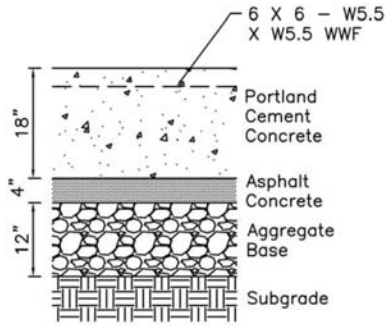

1-AC18(22)

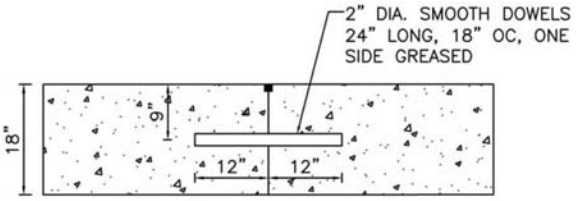

CONTRACTION JOINT - A

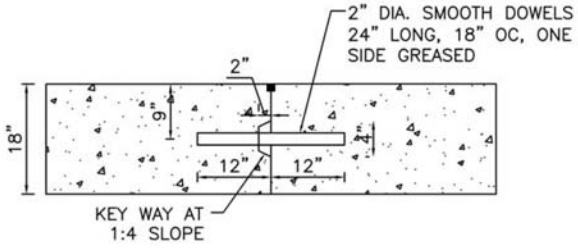

LONGITUDINAL CONSTRUCTION JOINT - B

TEST SITE 1-AC18(22)

1-AC18(22)

Site Description: The site is located on east coast of the United States. Elevations of the site, as indicated by USGS maps, are approximately 10 to 20 feet above sea level. The airport is surrounded by a rivers on three sides. Based on topographic information and observations, the site appears to be constructed on 5 to 10 feet of fill, overlying natural soils. The typical natural subgrade soils as indicated by USDA soil maps is gravelly sand over loamy sand. The estimated PCI and SCI of the site is 97 and 97, respectively. The primary distress observed included low severity joint spall.

Site Weather: The site is located in a wet/freeze climate zone. The below figures indicate the average temperature, average precipitation, average number of days above 90 degrees Fahrenheit, and average number of days below 32 degrees Fahrenheit.

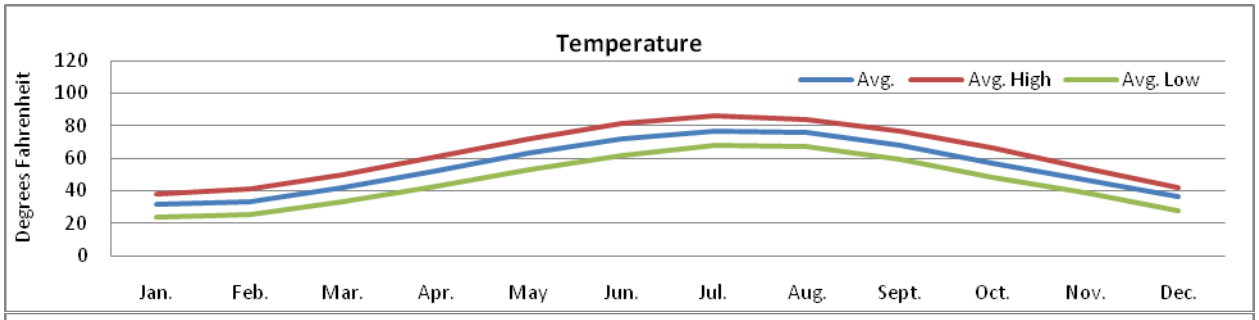

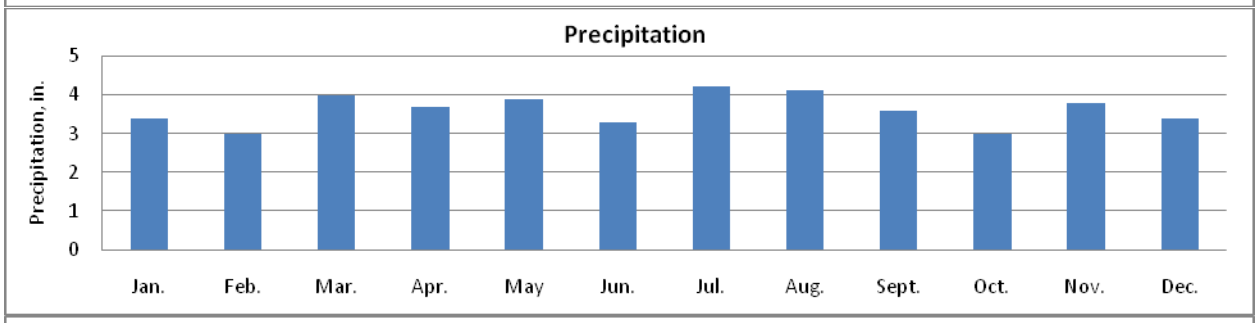

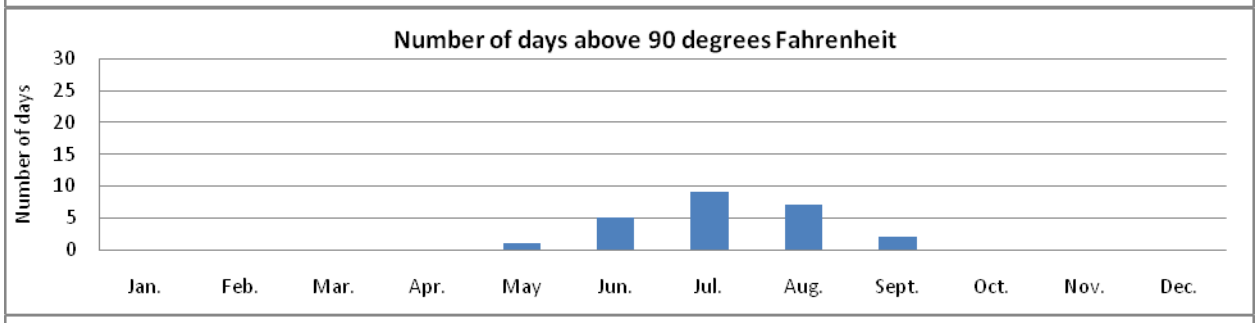

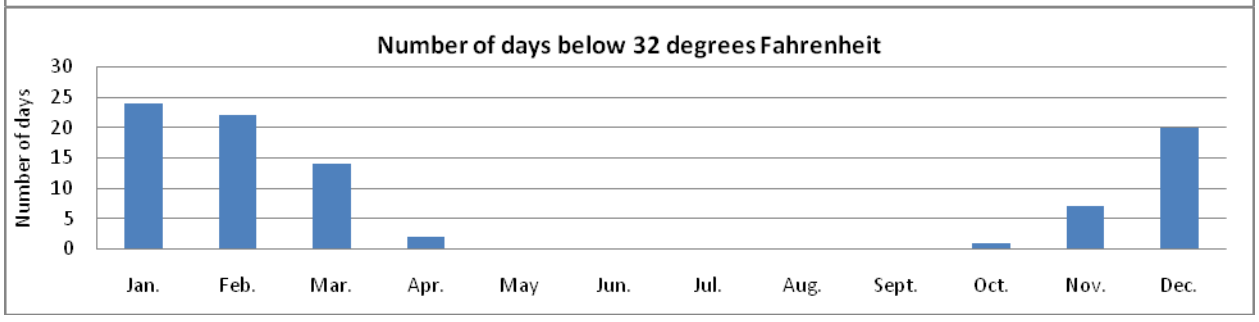

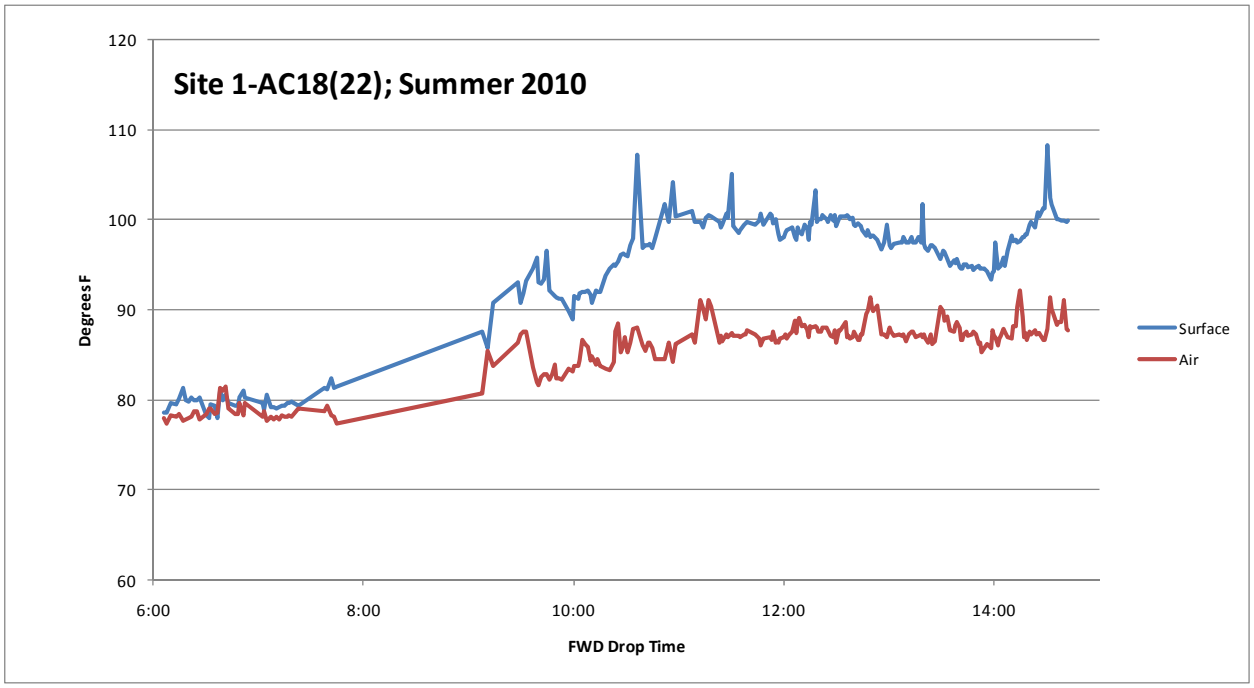

	Highway GPS3 55-3009	*Site 1-AC18(22) Winter 2009* 8AM average	AM-PM Change
average curvature, ft^{-1}	0.000547	0.000004	0.000037
min. curvature	0.000203	-0.000519	0.000011
max. curvature	0.001077	0.000369	0.000088
st. dev. of curvature	0.00021	0.000328	0.000025
number of slabs	33	8	8

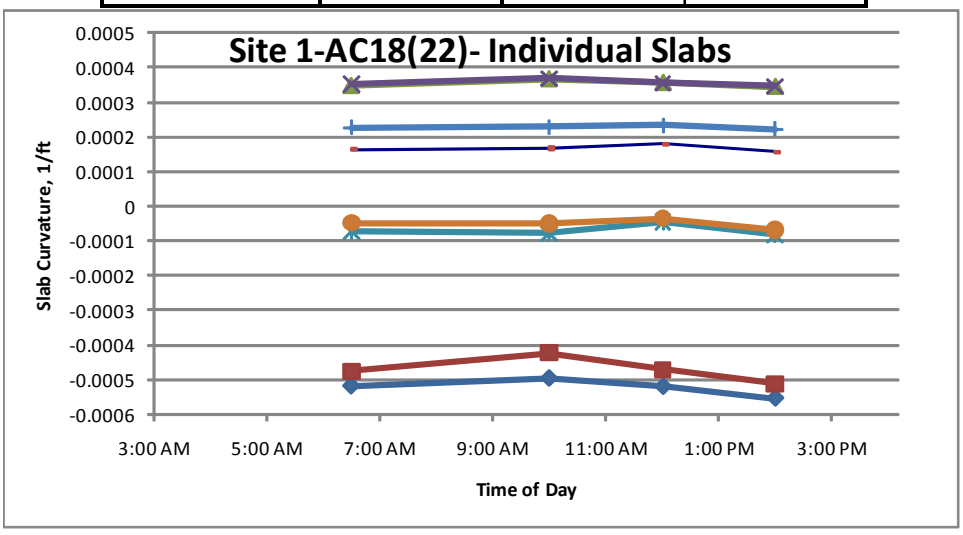

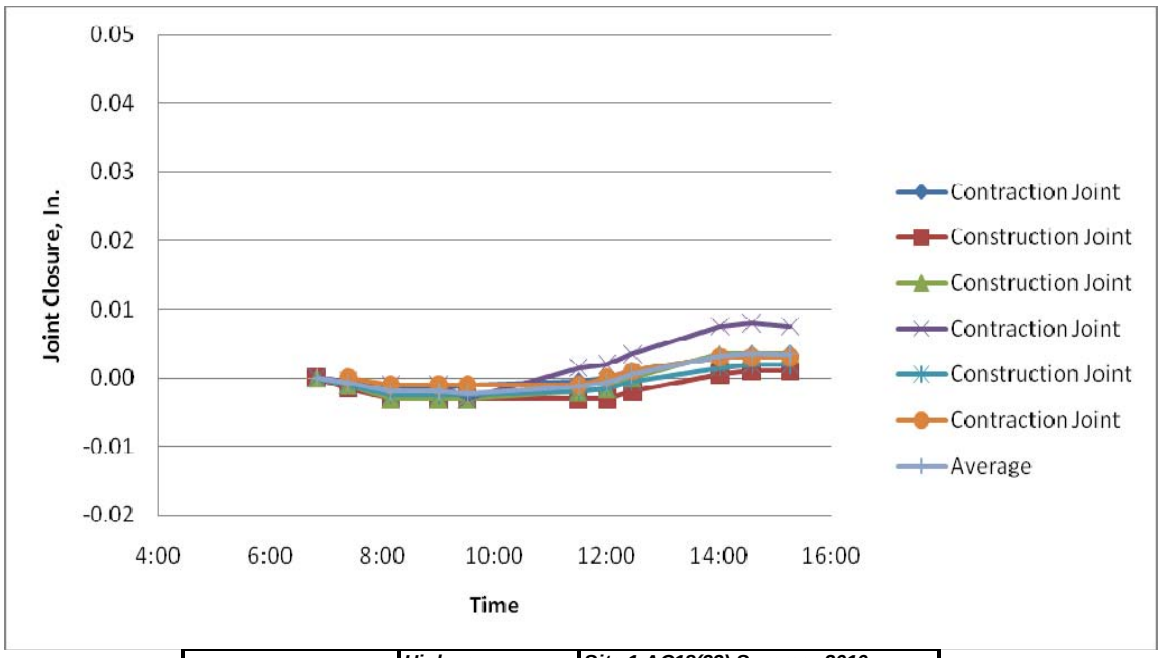

	Highway GPS3 55-3009	*Site 1-AC18(22) Summer 2010* 8AM average	AM-PM Change
average curvature, ft^{-1}	0.000547	0.000013	0.000043
min. curvature	0.000203	-0.000536	0.000025
max. curvature	0.001077	0.000379	0.000052
st. dev. of curvature	0.00021	0.000329	0.000009
number of slabs	33	7	7

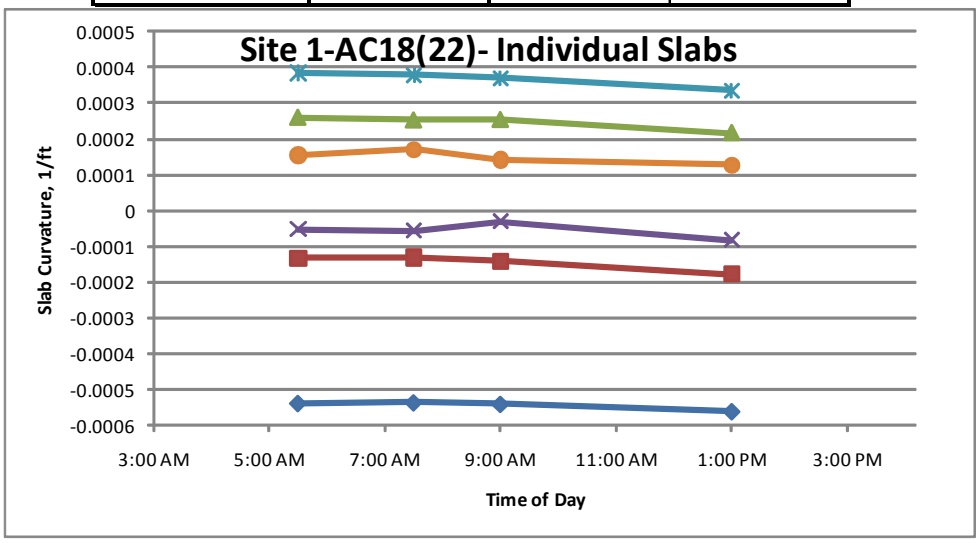

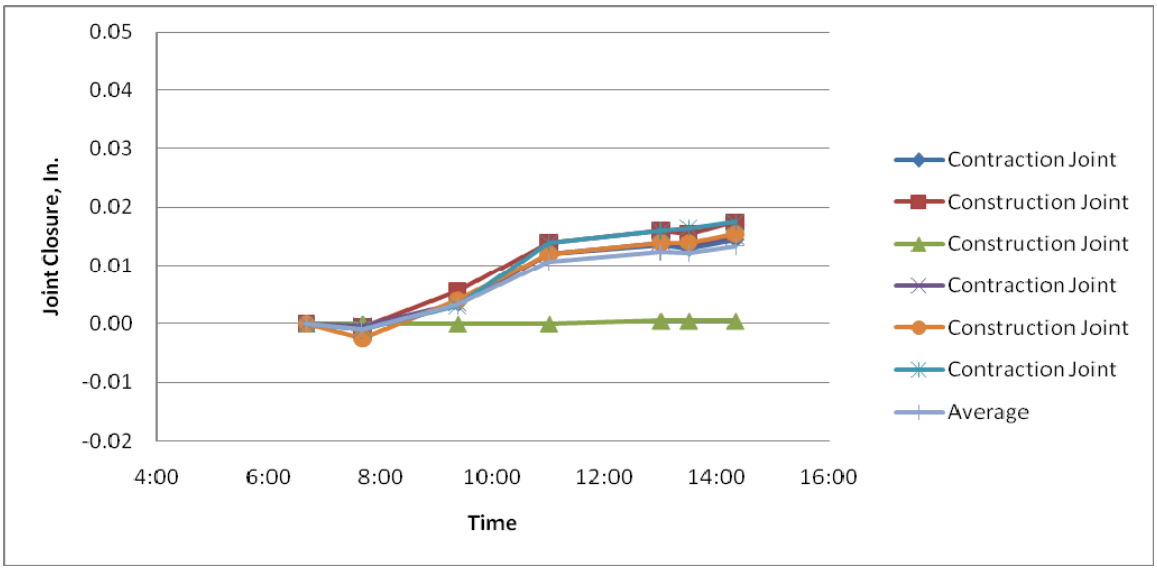

Site 1-AC18(22), Winter 2009- ILLIBACK Summary

	Dense Liquid				*Elastic Solid*				*Radius*
	***k*-value**	***k* stdev**	**Slab E_C**	**E_C Stdev**	**Subg. *E***	***E* stdev**	**Slab E_C**	**E_C Stdev**	***l*-values**
Site Average =	391	34	12.00	1	84,203	5,267	9.70	0.6	62.500141
Site Min. =	609	72	13.30	1.45	122,205	10,730	10.47	0.92	57.403512
Site Max =	352	39	8.12	0.86	71,269	6,070	6.40	0.55	58.194671
AM Average =	387	36	12.54	1.1	84,312	5,844	10.13	0.7	
Mid Average =	381	30	13.59	1	84,591	4,729	11.05	0.62	
PM Average =	404	36	10.27	0.85	83,538	5,194	8.15	0.51	
Best Guess	**391**		**12.00**		**84203**		**9.70**		**62.50**
	psi/in		*Msi*		*psi*		*Msi*		*inches*

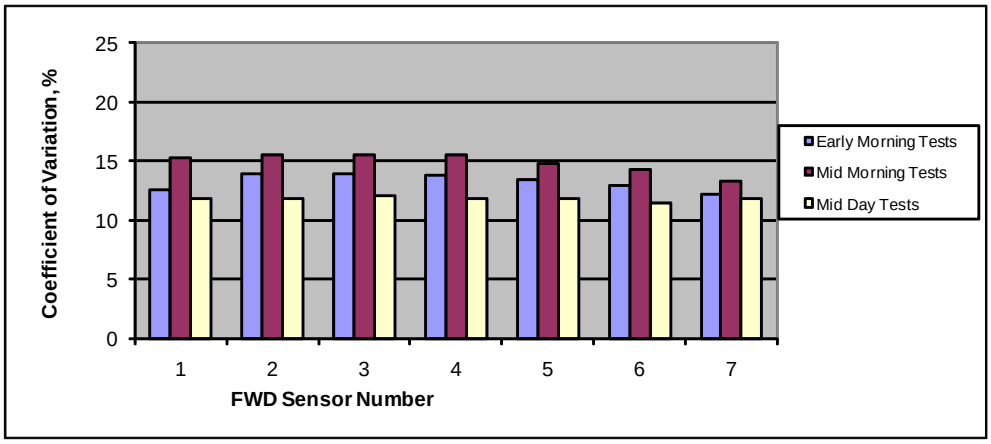

Site 1-AC18(22), Summer 2010- ILLIBACK Summary

	Dense Liquid				*Elastic Solid*				*Radius*
	***k*-value**	***k* stdev**	**Slab E_C**	**E_C Stdev**	**Subg. *E***	***E* stdev**	**Slab E_C**	**E_C Stdev**	**I-VALUES**
Site Average =	***475***	***58***	***9.25***	***1.05***	***92,794***	***8,401***	***7.24***	***0.66***	55.8
Site Min. =	511	41	23.60	1.91	119,222	7,925	19.48	1.29	69.2
Site Max =	342	42	7.22	0.83	68,234	6,360	5.67	0.53	56.9
AM1	458	52	10.33	1.1	92,510	7,892	8.12	0.69	57.9
AM2	476	61	8.67	1.03	91,596	8,687	6.75	0.64	54.9
PM3	495	63	8.78	1.04	94,764	8,926	6.83	0.64	54.5
Best Guess	**475**		**9.25**		**92794**		**7.24**		**55.8**
	psi/in		*Msi*		*psi*		*Msi*		*inches*

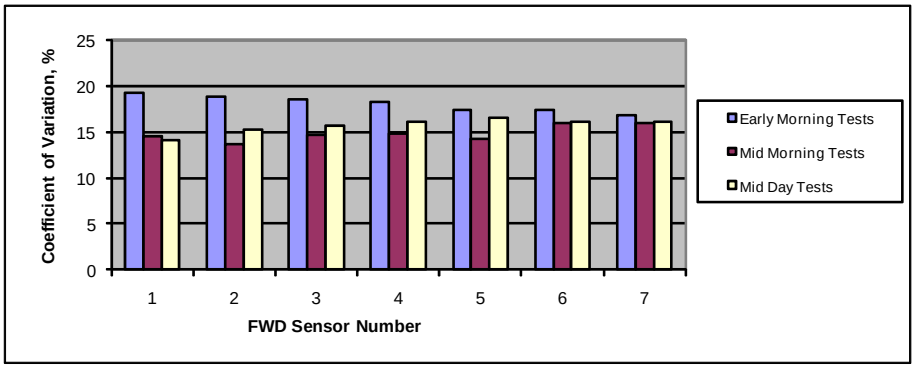

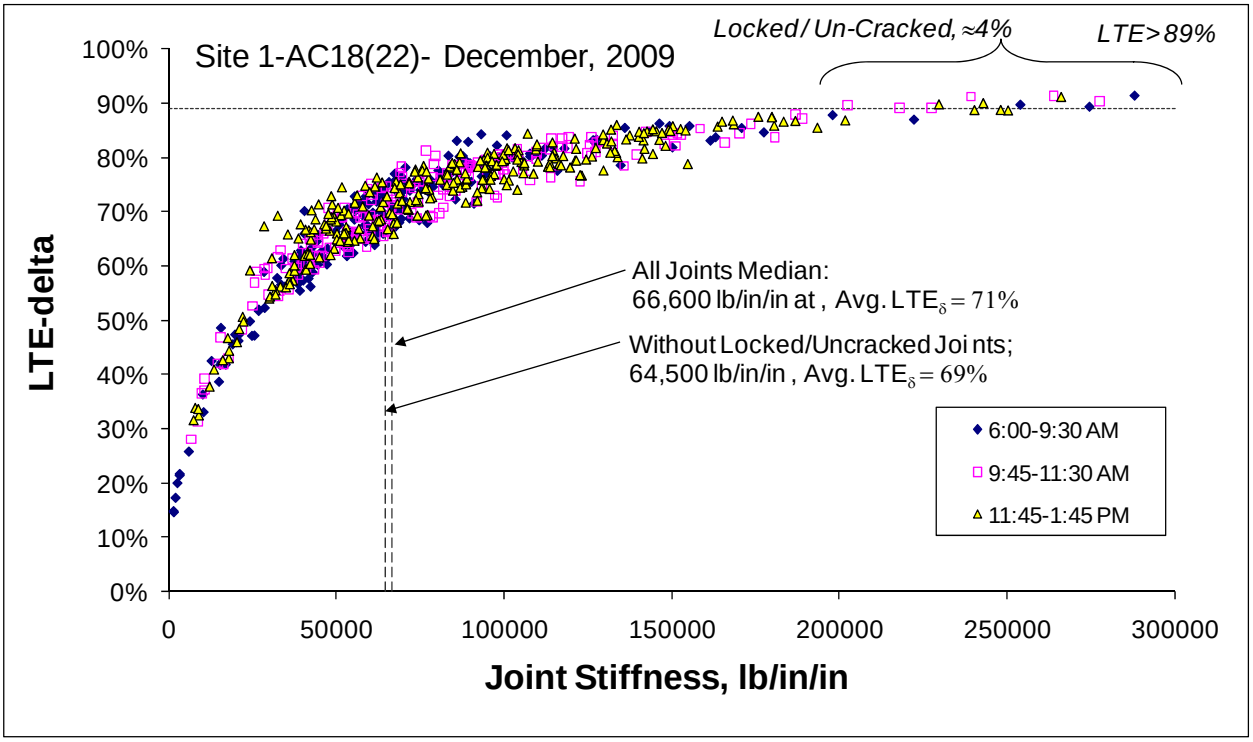

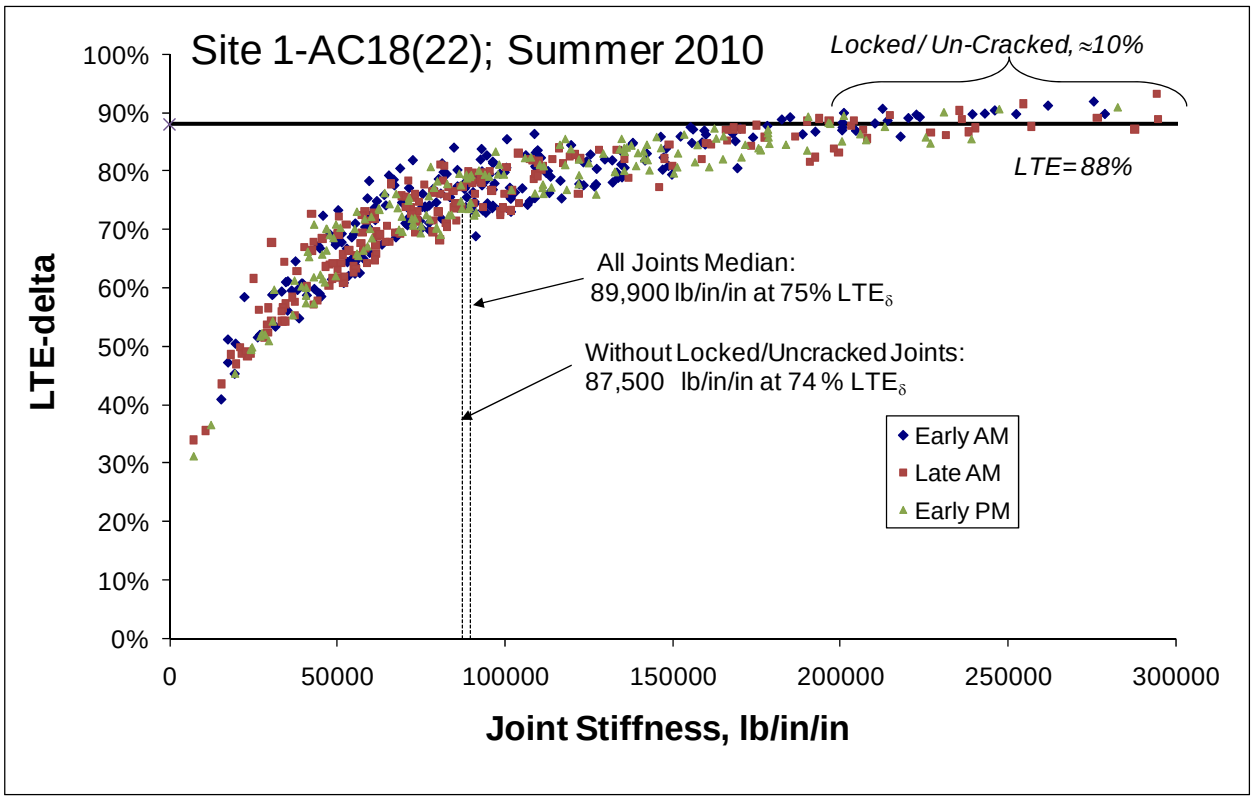
Site 1-AC18(22); Summer 2010
Locked / Un-Cracked, ≈10%
LTE=88%
All Joints Median:
89,900 lb/in/in at 75% LTE$_\delta$
Without Locked/Uncracked Joints:
87,500 lb/in/in at 74 % LTE$_\delta$
Early AM
Late AM
Early PM
LTE-delta
Joint Stiffness, lb/in/in
100%
90%
80%
70%
60%
50%
40%
30%
20%
10%
0%
0
50000
100000
150000
200000
250000
300000

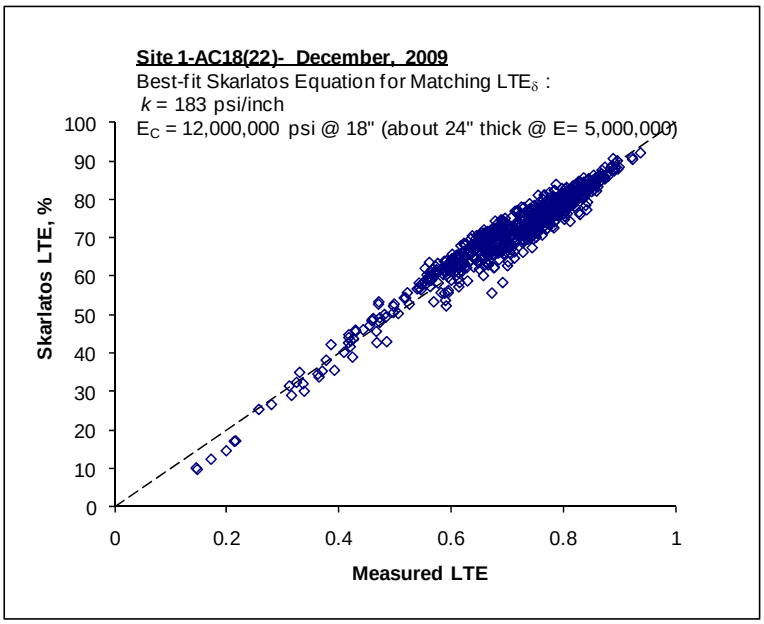
Site 1-AC18(22)- December, 2009
Best-fit Skarlatos Equation for Matching LTE$_\delta$:
k = 183 psi/inch
E$_C$ = 12,000,000 psi @ 18" (about 24" thick @ E= 5,000,000)
Skarlatos LTE, %
Measured LTE
100
90
80
70
60
50
40
30
20
10
0
0
0.2
0.4
0.6
0.8
1

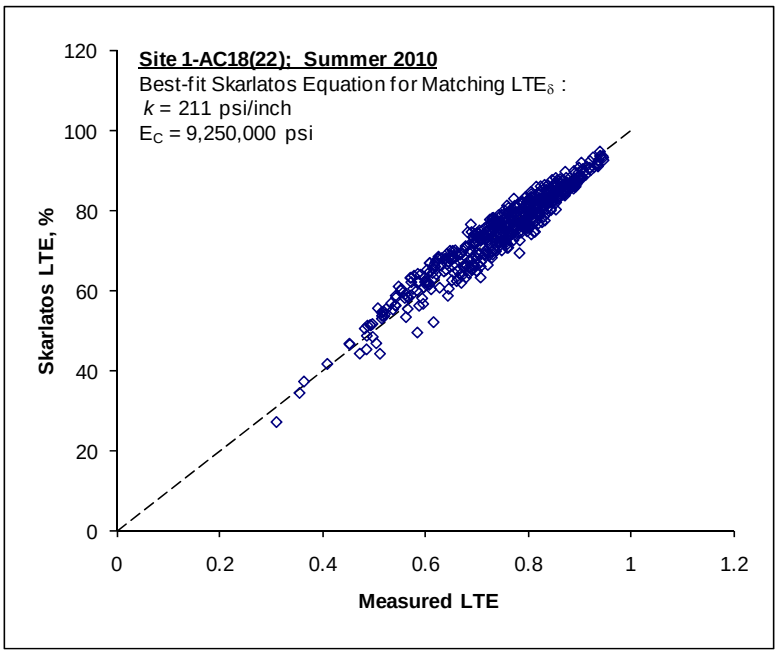
Site 1-AC18(22); Summer 2010
Best-fit Skarlatos Equation for Matching LTEδ :
k = 211 psi/inch
EC = 9,250,000 psi
Skarlatos LTE, %
Measured LTE
120
100
80
60
40
20
0
0
0.2
0.4
0.6
0.8
1
1.2

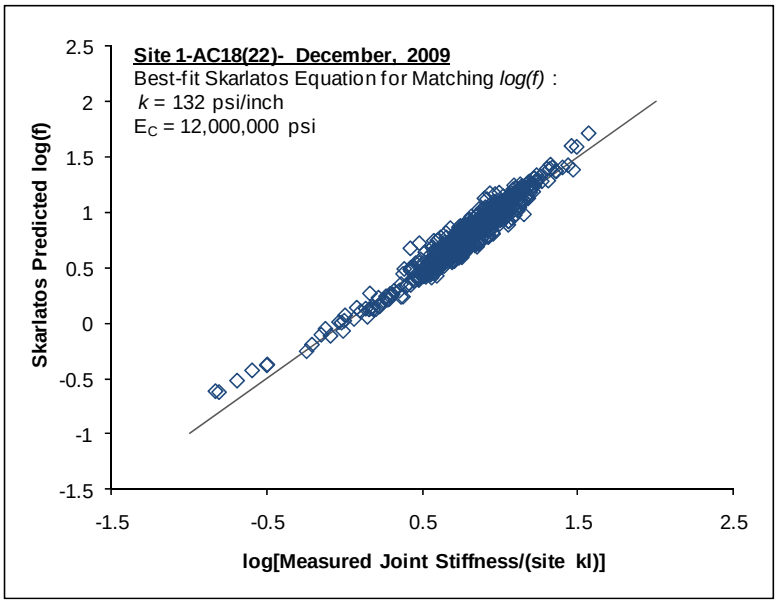
Site 1-AC18(22)- December, 2009
Best-fit Skarlatos Equation for Matching log(f) :
k = 132 psi/inch
EC = 12,000,000 psi
Skarlatos Predicted log(f)
log[Measured Joint Stiffness/(site kl)]
2.5
2
1.5
1
0.5
0
-0.5
-1
-1.5
-1.5
-0.5
0.5
1.5
2.5

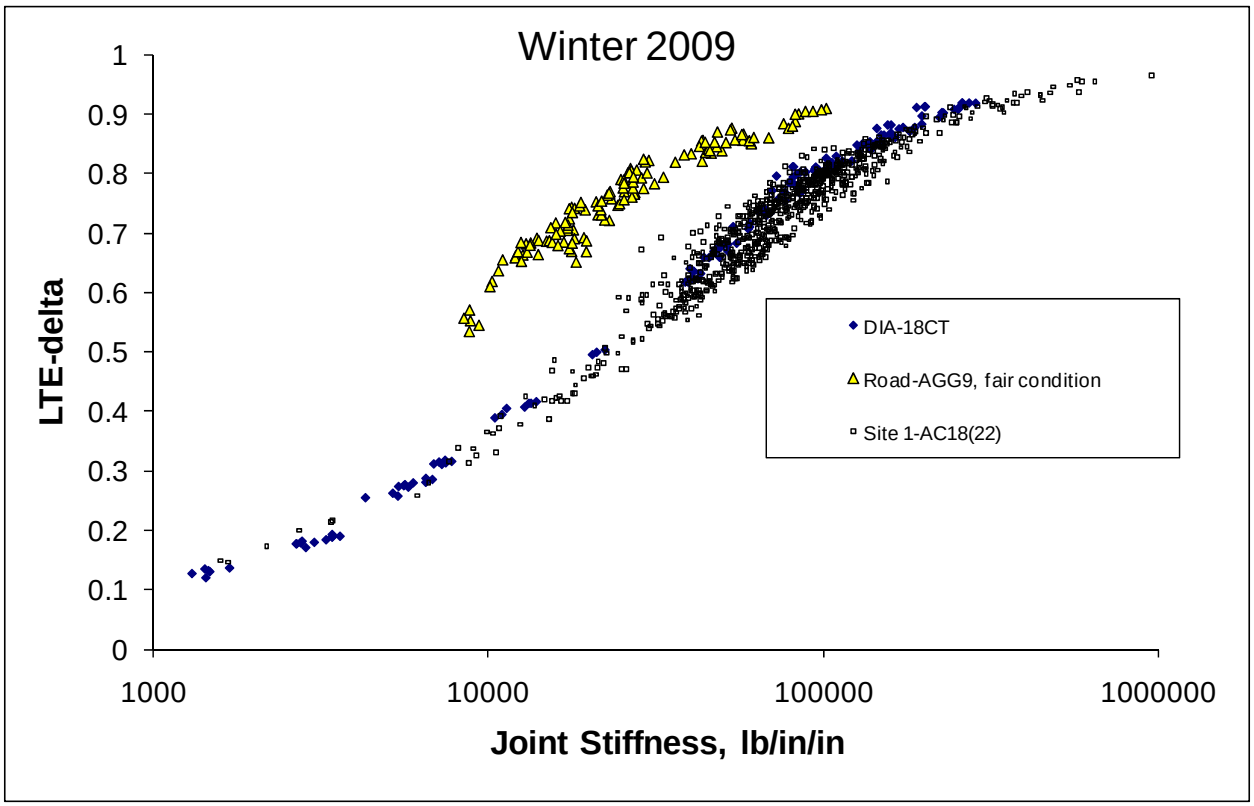
Winter 2009
LTE-delta
Joint Stiffness, lb/in/in
1
0.9
0.8
0.7
0.6
0.5
0.4
0.3
0.2
0.1
0
1000
10000
100000
1000000
DIA-18CT
Road-AGG9, fair condition
Site 1-AC18(22)

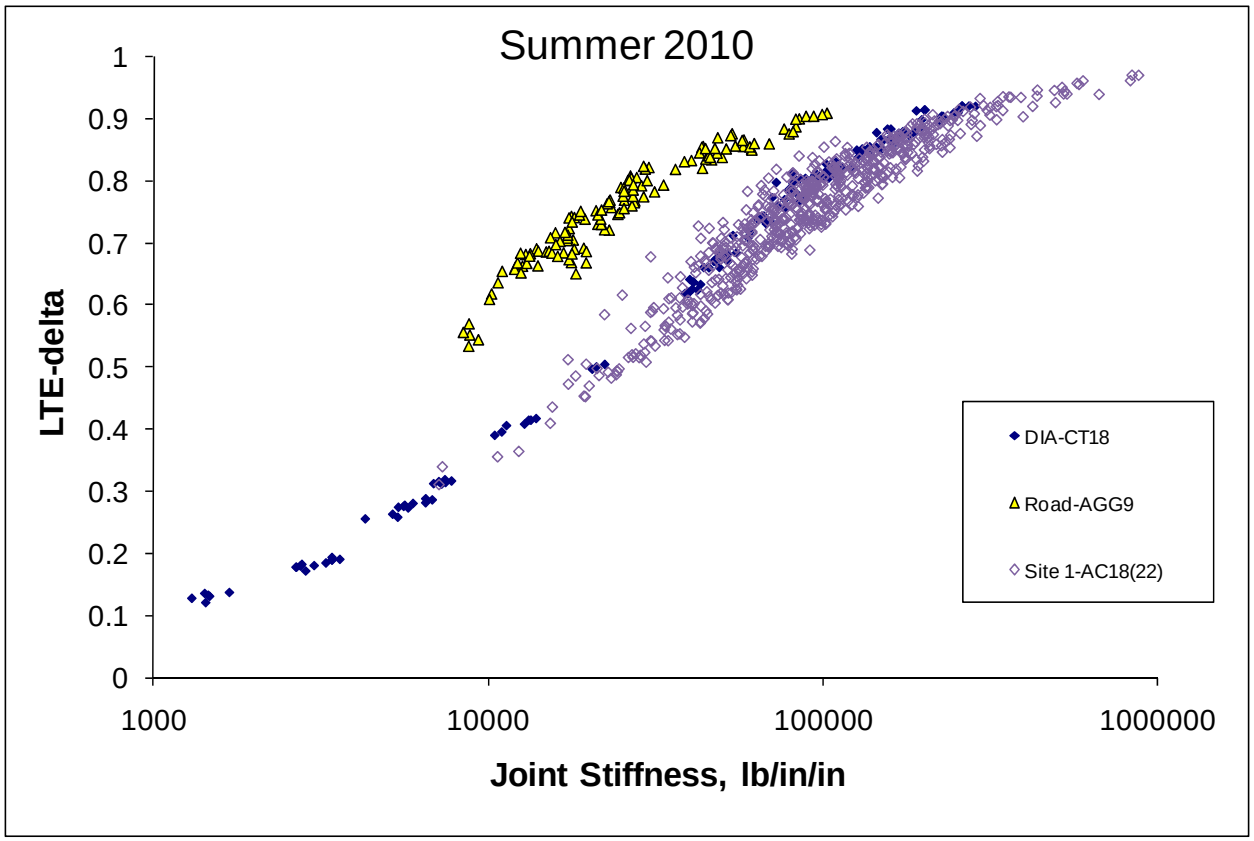
Summer 2010
LTE-delta
Joint Stiffness, lb/in/in
1
0.9
0.8
0.7
0.6
0.5
0.4
0.3
0.2
0.1
0
1000
10000
100000
1000000
DIA-CT18
Road-AGG9
Site 1-AC18(22)

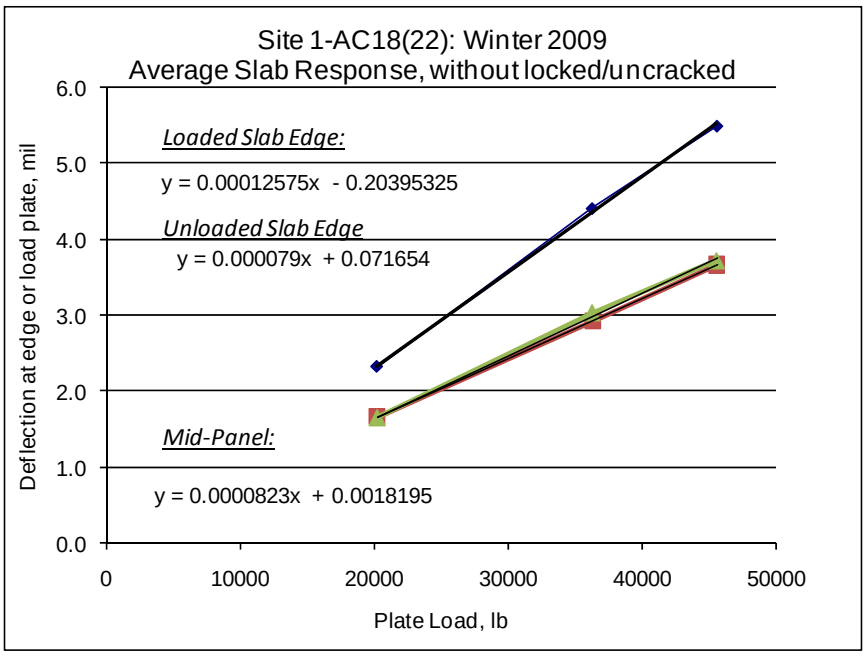
Site 1-AC18(22): Winter 2009
Average Slab Response, without locked/uncracked
Loaded Slab Edge:
y = 0.00012575x - 0.20395325
Unloaded Slab Edge
y = 0.000079x + 0.071654
Mid-Panel:
y = 0.0000823x + 0.0018195
Deflection at edge or load plate, mil
Plate Load, lb
0.0
1.0
2.0
3.0
4.0
5.0
6.0
0
10000
20000
30000
40000
50000

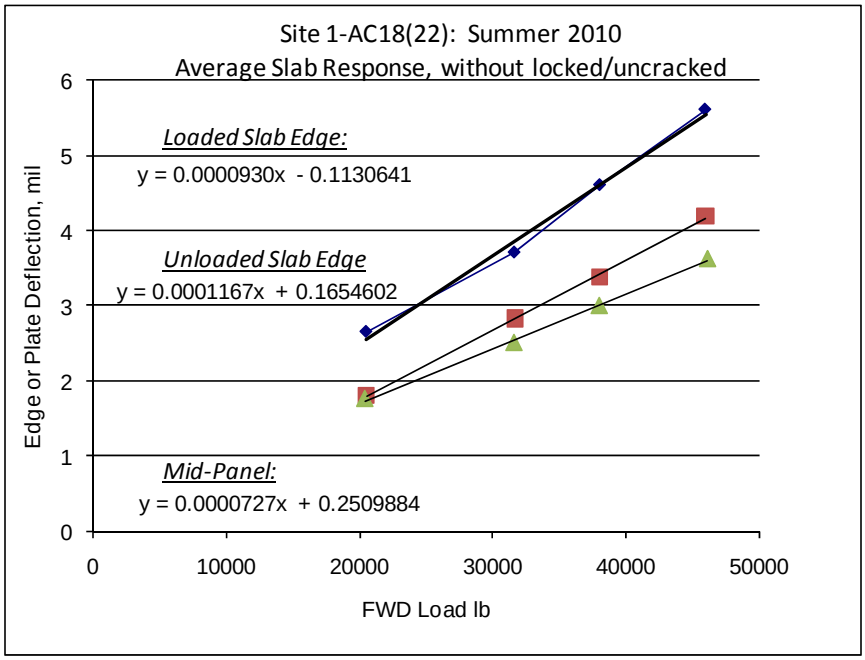
Site 1-AC18(22): Summer 2010
Average Slab Response, without locked/uncracked
Loaded Slab Edge:
y = 0.0000930x - 0.1130641
Unloaded Slab Edge
y = 0.0001167x + 0.1654602
Mid-Panel:
y = 0.0000727x + 0.2509884
Edge or Plate Deflection, mil
FWD Load lb
0
1
2
3
4
5
6
0
10000
20000
30000
40000
50000

Winter 2009

****Site 1-AC18(22) Doweled Construction Joints, with un-cracked, locked…**

	LR, in.	LTE	Jt. Stiffness, lb/in/in
avg	219	73.2%	157058
median	212	74%	77598
min	122	39%	10858
max	456	99%	4695435
stdev	48.3	11%	446306

Possible Un-cracked, LTE>89% = 8.6%

Formed, 2" dowels at 18", with keyway

Steel Area/ft = 2.09 sq. inches

reinf. ratio = 0.97%

****Without un-cracked, locked…..**

	LR, in.	LTE	Jt. Stiffness, lb/in/in
avg	220	71.4%	79209
median	213	73%	73080
min	122	39%	10858
max	456	90%	344910
stdev	49.7	10%	40078

Possible Un-cracked, LTE>89% = 0.8%

Probable Agg Interlock = 0 to 70000

$$k = \frac{1}{s\left(\frac{\varpi}{0.9 G_d A_d} + \frac{\varpi^3}{12 E_d I_d} + \frac{2 + \beta\varpi}{2\beta^3 E_d I_d}\right)}$$

s is the dowel bar spacing =	18	in
w is the joint opening =	0.1	in
Dowel Diameter =	2	in
Ad is the dowel cross-sectional area =	3.14	sq in
Ed =	29000000	psi
Gd =	11153846	psi
Id =	0.785	in^4
Back-Calculated Dowel-Concrete Interaction modulus, DCI =	1049270	psi

$$\beta = \sqrt[4]{\frac{Kd}{4 E_d I_d}} = 0.390$$

Doweled Joint Stiffness = **73080** lb/in/in

Summer 2010

****Site 1-AC18(22) Doweled Construction Joints, with un-cracked, locked...**

	LR	LTE	Avg Stiffness	
avg	188	73%	103564	
min	142	45%	17304	
max	321	96%	638951	
stdev	26	11%	85228	Steel Area/ft = 2.094395
Median	183	74%	81435	reinf. ratio = 0.970%

% possibly un-cracked, LTE>88% = 10%

Formed, 2" dowels at 18", with keyway

****Without un-cracked, locked.....**

	LR	LTE	Avg Stiffness
avg	188	72%	91306
min	142	45%	17304
max	321	95%	490855
stdev	27	11%	63574
Median	185	74%	78890

% possibly un-cracked, LTE>86% = 5%

Probable Agg Interlock >5000 to 75000

$$k = \frac{1}{s\left(\frac{\varpi}{0.9G_d A_d} + \frac{\varpi^3}{12E_d I_d} + \frac{2+\beta\varpi}{2\beta^3 E_d I_d}\right)}$$

s is the dowel bar spacing =	18	in
w is the joint opening =	0.1	in
Dowel Diameter =	2	in
Ad is the dowel cross-sectional area =	3.14	sq in
Ed =	29000000	psi
Gd =	11153846	psi
Id =	0.785	in^4
Back-Calculated Dowel-Concrete Interaction modulus, DCI =	1163248	psi

$$\beta = \sqrt[4]{\frac{Kd}{4E_d I_d}} = 0.400$$

Doweled Joint Stiffness = **78890** lb/in/in

Winter 2009

****Site 1-AC18(22) Doweled Contraction Joints, with un-cracked, locked…**

	LR, in.	LTE	Jt. Stiffness, lb/in/in
avg	206	71.7%	99300
median	202	74%	71939
min	143	15%	1585
max	328	99%	2866024
stdev	24.7	13%	150602

Possible Un-cracked, LTE>89% = 4.4%

Sawed 2" dowels at 18"

Steel Area/ft = 2.09 sq. inches

reinf. ratio = 0.970%

****Without un-cracked, locked…..**

	LR, in.	LTE	Jt. Stiffness, lb/in/in
avg	206	71.0%	82218
median	202	74%	70245
min	143	15%	1585
max	328	92%	339152
stdev	24.8	13%	50161

Possible Un-cracked, LTE>89% = 3.9%

Probable Agg Interlock = 0 to 70000

$$k = \frac{1}{s\left(\frac{\varpi}{0.9G_d A_d} + \frac{\varpi^3}{12E_d I_d} + \frac{2+\beta\varpi}{2\beta^3 E_d I_d}\right)}$$

s is the dowel bar spacing =	18	in
w is the joint opening =	0.1	in
Dowel Diameter =	2	in
Ad is the dowel cross-sectional area =	3.14	sq in
Ed =	29000000	psi
Gd =	11153846	psi
Id =	0.785	in^4
Back-Calculated Dowel-Concrete Interaction modulus, DCI =	994798	psi

$$\beta = \sqrt[4]{\frac{Kd}{4E_d I_d}} = 0.384$$

Doweled Joint Stiffness = **70245** lb/in/in

Summer 2010

****Site 1-AC18(22) Doweled Contraction Joints, with un-cracked, locked…**

	LR	LTE	Avg Stiffness	
avg	175	76%	123899	
min	115	31%	7104	
max	410	97%	837632	
stdev	30	11%	101590	
Median	170	78%	96269	

% possibly un-cracked, LTE>88% = 9%

Sawed 2" dowels at 18"

Steel Area/ft = 2.094395

reinf. ratio = 0.970%

****Without un-cracked, locked…..**

	LR	LTE	Avg Stiffness
avg	175	76%	115945
min	115	31%	7104
max	410	97%	837632
stdev	30	10%	88894
Median	170	77%	94662

% locked/un-cracked, LTE>88% = 7

Probable Agg Interlock >24000 to 94000

$$k = \frac{1}{s\left(\frac{\varpi}{0.9G_d A_d} + \frac{\varpi^3}{12E_d I_d} + \frac{2+\beta\varpi}{2\beta^3 E_d I_d}\right)}$$

s is the dowel bar spacing =	18	in
w is the joint opening =	0.1	in
Dowel Diameter =	2	in
Ad is the dowel cross-sectional area =	3.14	sq in
Ed =	29000000	psi
Gd =	11153846.2	psi
Id =	0.785	in^4
Back-Calculated Dowel-Concrete Interaction modulus, DCI =	1487478	psi

$$\beta = \sqrt[4]{\frac{Kd}{4E_d I_d}} = 0.425$$

Doweled Joint Stiffness = **94662** lb/in/in

Site 1-AC18(22) ; Winter 2009

****Corners- No un-cracked or locked detected**

	LR, in.	LTE	Jt. Stiffness, lb/in/in
avg	195	62.3%	39325
median	196	62%	30561
min	130	36%	9769
max	322	84%	141311
stdev	36.1	10%	22776

Possible Un-cracked, LTE>89% = 0.0%

"Doweled on Both Joints"

Site 1-AC18(22) ; Summer 2010

All Corners, including locked/un-cracked joints

	LR	LTE	Avg Stiffness
avg	176	77%	117489
min	112	34%	7270
max	209	96%	598036
stdev	22	11%	98018
Median	178	79%	90267

% possibly un-cracked, LTE>88% = 13%

Doweled on Both Edges

All Corners, removed locked/un-cracked

	LR	LTE	Avg Stiffness
avg	176	77%	107916
min	112	34%	7270
max	209	95%	517574
stdev	22	11%	81776
Median	180	78%	87156

% possibly un-cracked, LTE>88% = 10%

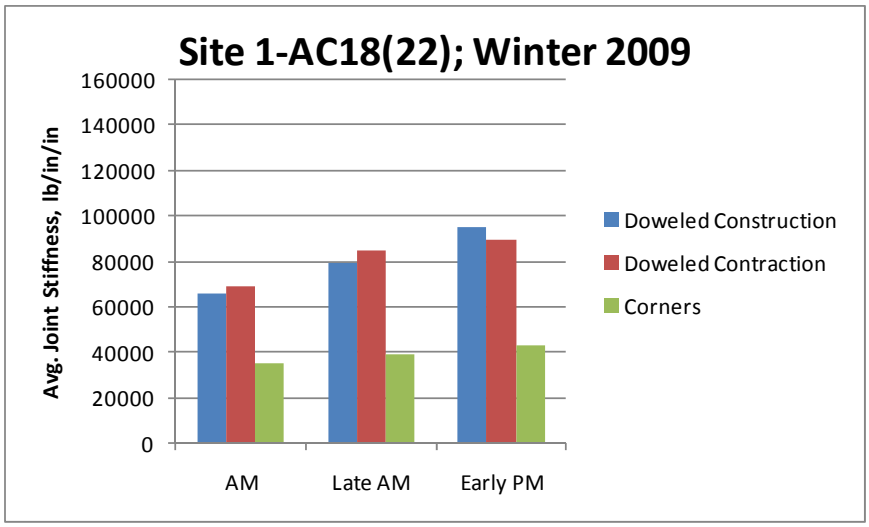

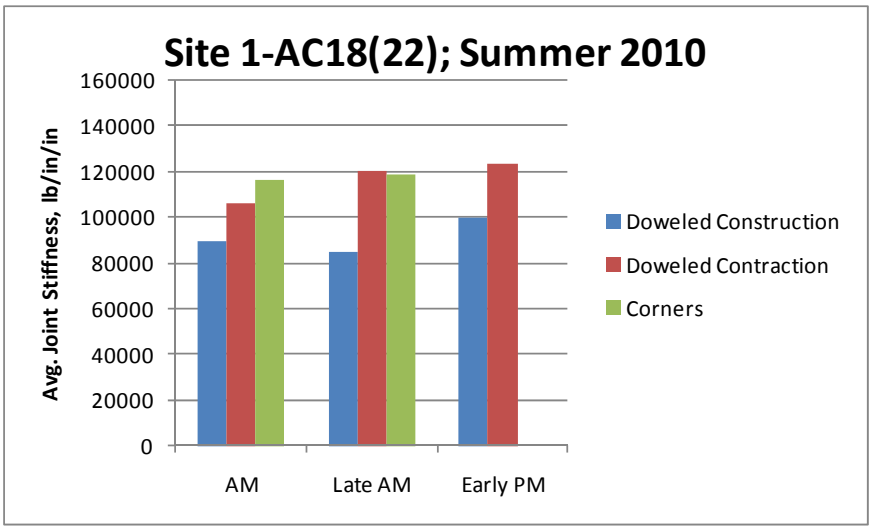

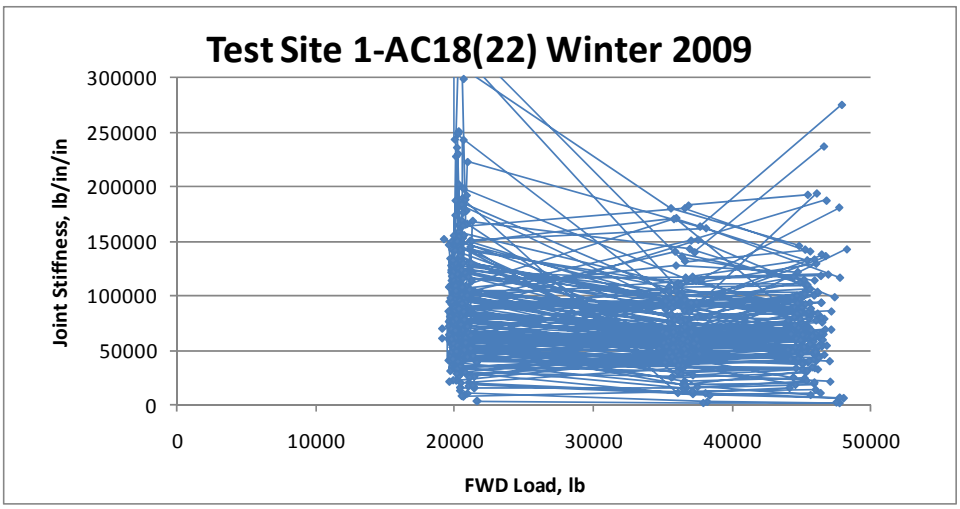
Test Site 1-AC18(22) Winter 2009
Joint Stiffness, lb/in/in
300000
250000
200000
150000
100000
50000
0
0
10000
20000
30000
40000
50000
FWD Load, lb

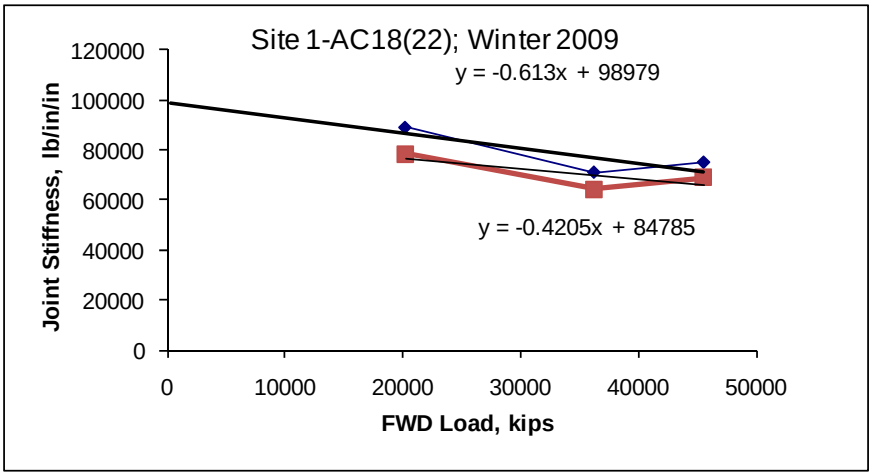
Site 1-AC18(22); Winter 2009
y = -0.613x + 98979
y = -0.4205x + 84785
Joint Stiffness, lb/in/in
120000
100000
80000
60000
40000
20000
0
0
10000
20000
30000
40000
50000
FWD Load, kips

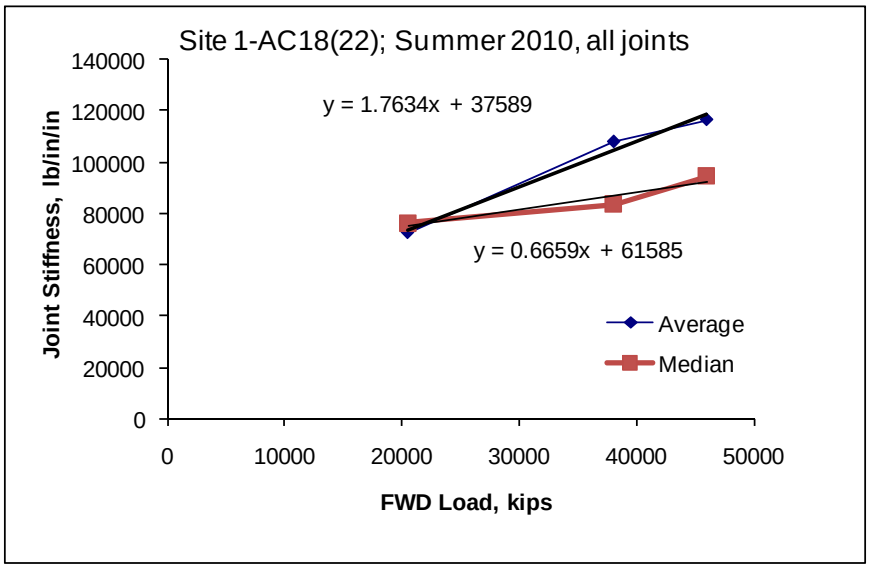
Site 1-AC18(22); Summer 2010, all joints
y = 1.7634x + 37589
y = 0.6659x + 61585
Average
Median
Joint Stiffness, lb/in/in
140000
120000
100000
80000
60000
40000
20000
0
0
10000
20000
30000
40000
50000
FWD Load, kips

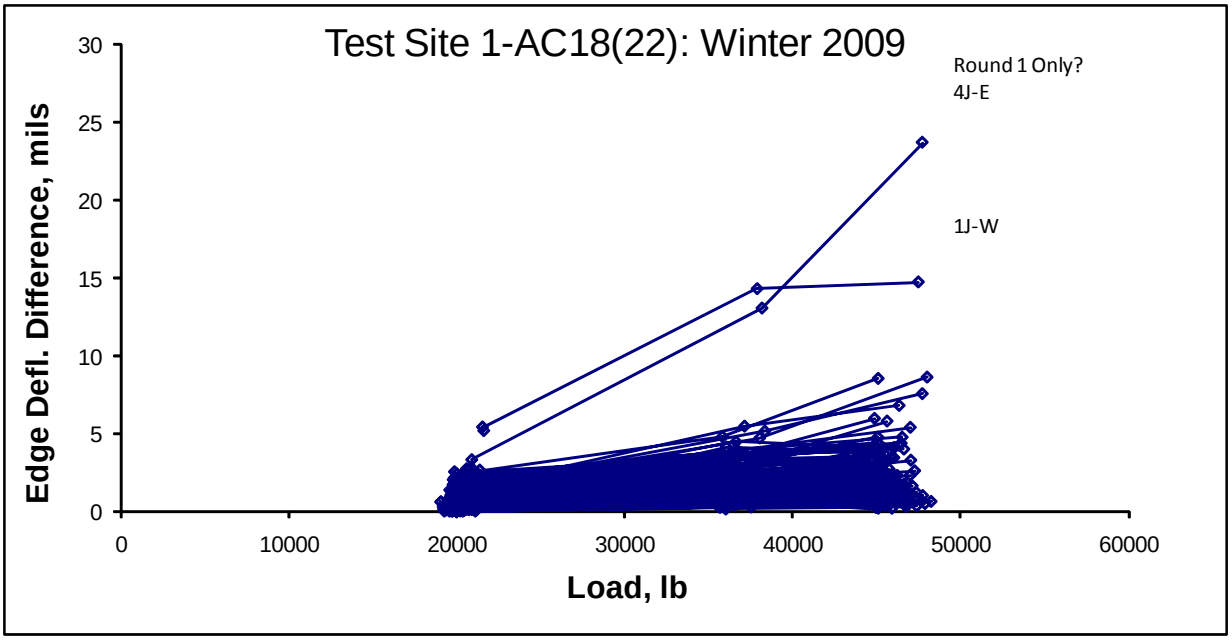
Test Site 1-AC18(22): Winter 2009
Round 1 Only?
4J-E
1J-W
Edge Defl. Difference, mils
Load, lb
0
5
10
15
20
25
30
0
10000
20000
30000
40000
50000
60000

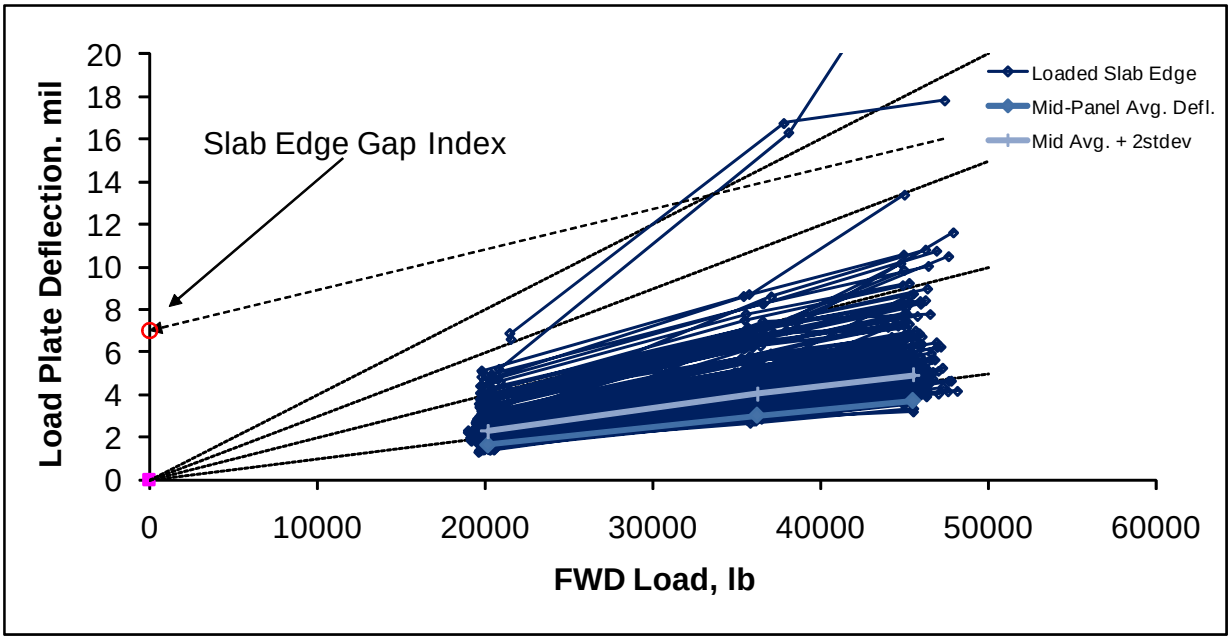
Slab Edge Gap Index
Loaded Slab Edge
Mid-Panel Avg. Defl.
Mid Avg. + 2stdev
Load Plate Deflection. mil
FWD Load, lb
0
2
4
6
8
10
12
14
16
18
20
0
10000
20000
30000
40000
50000
60000

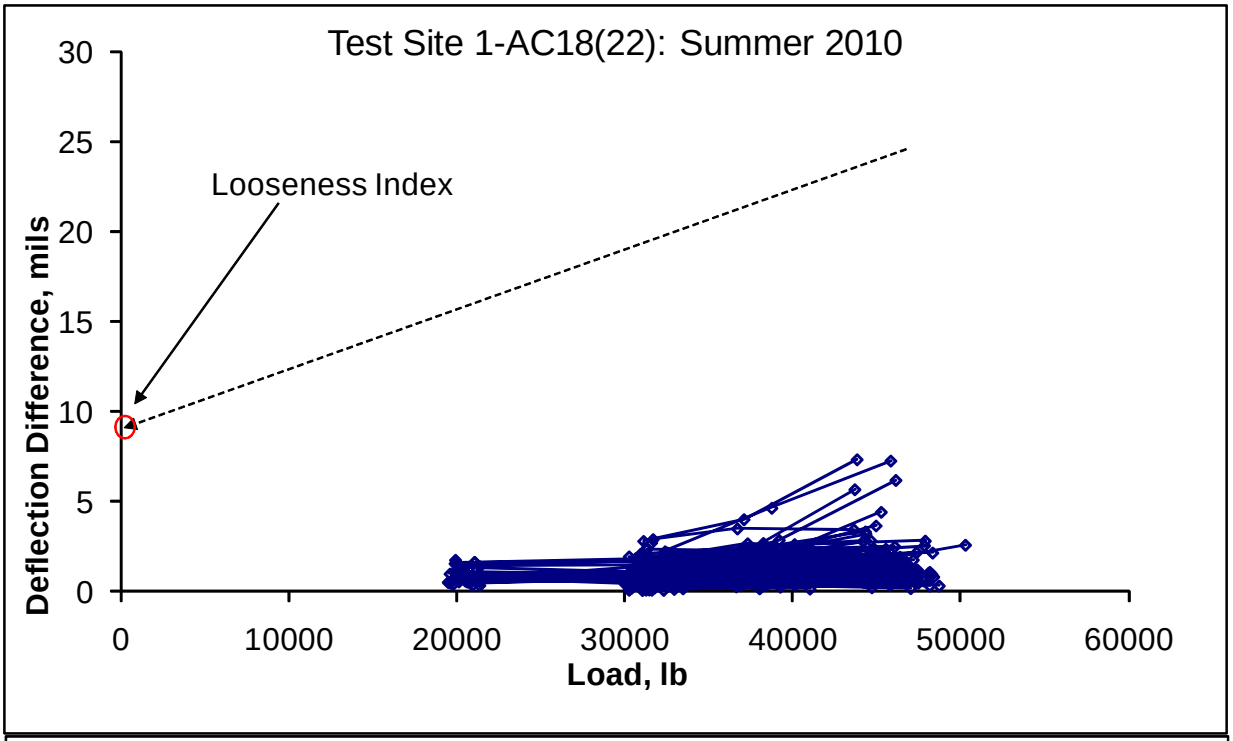
Test Site 1-AC18(22): Summer 2010
Looseness Index
Deflection Difference, mils
Load, lb
0
5
10
15
20
25
30
0
10000
20000
30000
40000
50000
60000

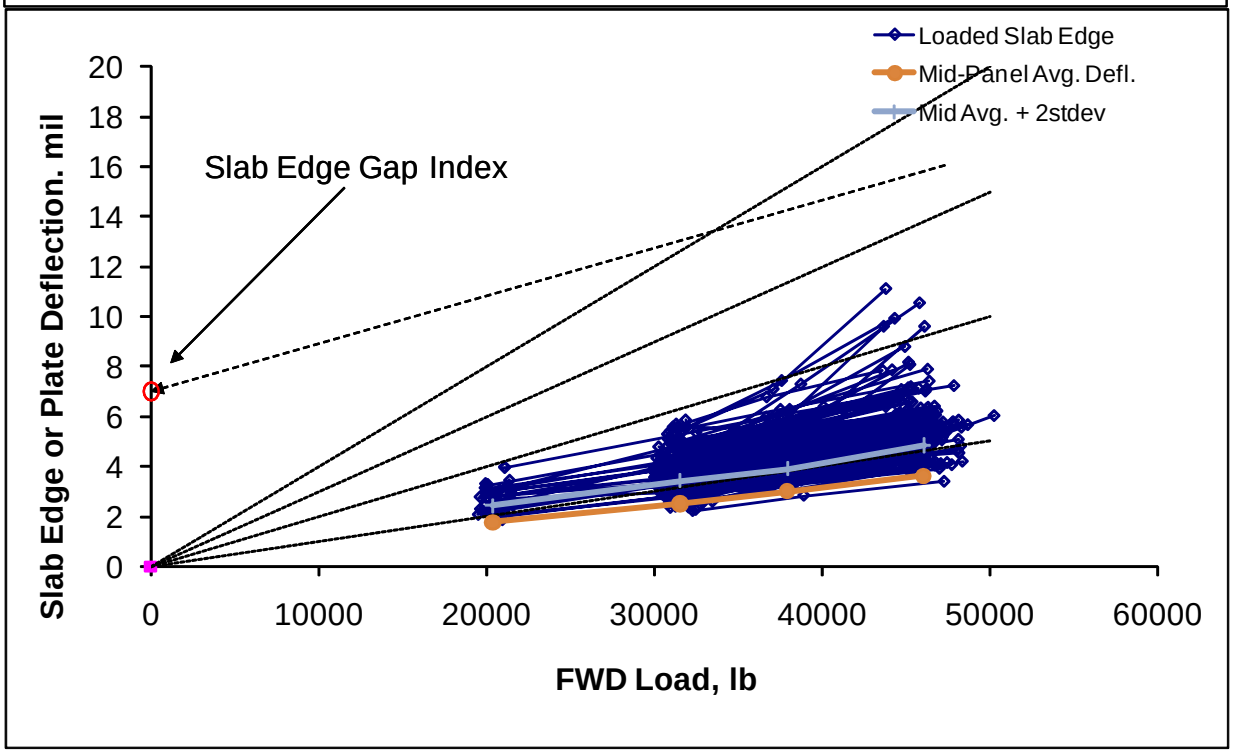
Loaded Slab Edge
Mid-Panel Avg. Defl.
Mid Avg. + 2stdev
Slab Edge Gap Index
Slab Edge or Plate Deflection. mil
FWD Load, lb
0
2
4
6
8
10
12
14
16
18
20
0
10000
20000
30000
40000
50000
60000

Site 1-AC18(22) Joint Looseness Data: Winter 2009

Looseness	All Good Data	N-S Joints	E-W Joints	Corners
Average	-0.21	-0.16	-0.25	-0.18
Maximum	2.73	0.89	2.73	0.67
Minimum	-4.17	-3.08	-4.17	-2.16
Std. Dev.	0.71	0.52	0.83	0.57
Count	211	59	113	36
20.2 kip %	-13%	-10%	-15%	-11%
36.3 kip %	-7%	-6%	-8%	-6%
45.6 kip %	-6%	-4%	-7%	-5%

Site 1-AC18(22) Slab Edge Gaps- All Joints

Edge Gap	*EW-Joints*	*NS-Joints*	*Corners*
Average	-0.20	-0.05	-0.04
Maximum	2.83	0.93	1.12
Minimum	-4.02	-3.03	-1.86
Std. Dev.	0.86	0.52	0.61
Count	104	55	36
20 kip %	-12%	-3%	-2%
36 kip %	-7%	-2%	-1%
45.5 kip %	-5%	-1%	-1%

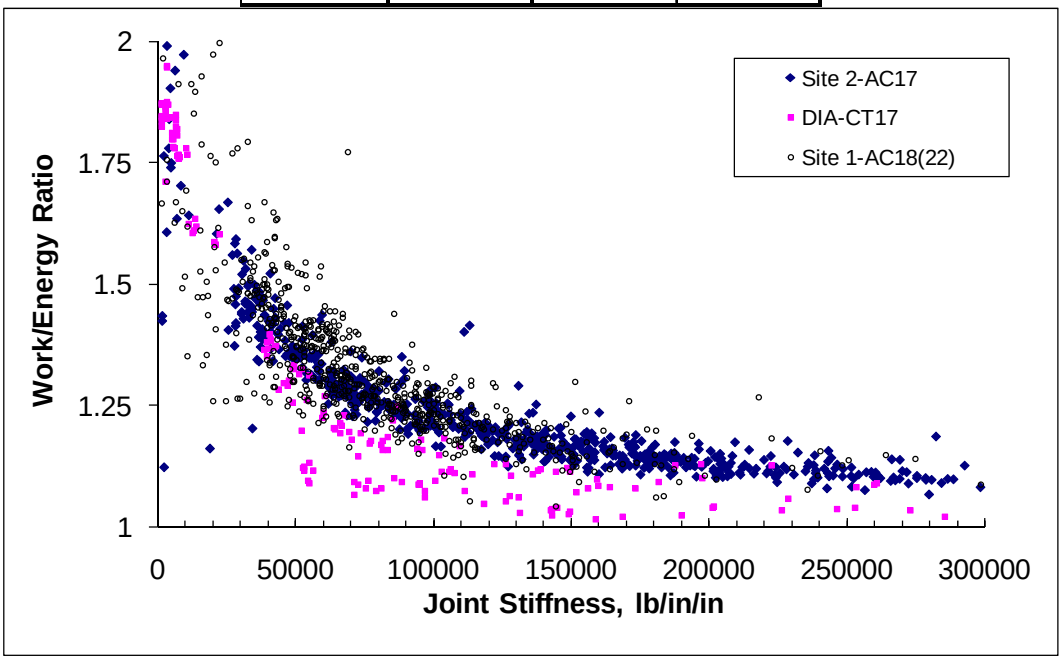

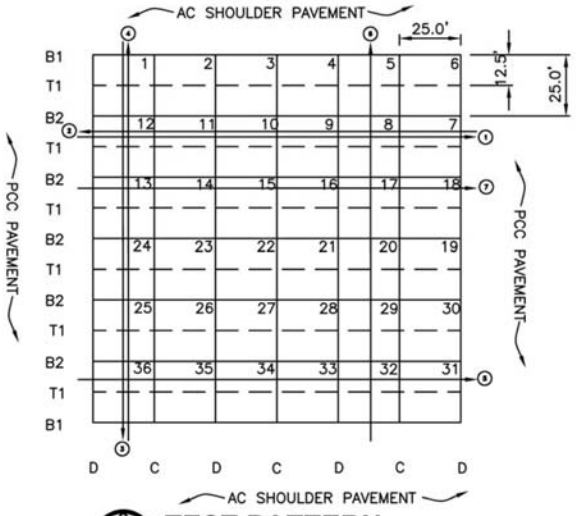

TEST PATTERN

LEGEND

(2) FWD TEST LANE NUMBER

T1 CONTRACTION JOINT: #6 DEFORMED BAR, 42" LONG, 20" SPACING.

B1 CONSTRUCTION JOINT: WITH KEY WAY, NO LOAD TRANSFER DEVICE.

B2 CONSTRUCTION JOINT: WITH KEY WAY, #6 DEFORMED BAR 42" LONG, 15" SPACING.

D CONTRACTION JOINT: NO LOAD TRANSFER DEVICE, AGGREGATE INTERLOCK ONLY.

C CONTRACTION JOINT: 1.5" SMOOTH DOWEL BAR, 20" LONG, 12"SPACING.

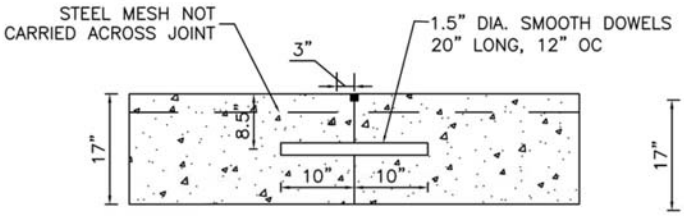

CONTRACTION JOINT - C

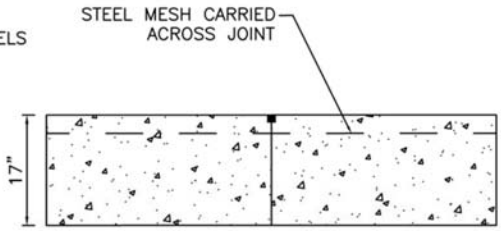

DUMMY CONTRACTION JOINT - D

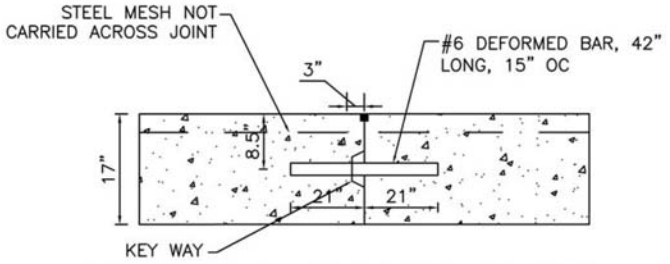

LONGITUDINAL CONSTRUCTION JOINT - B2

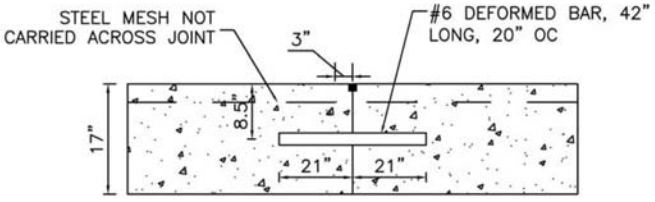

LONGITUDINAL CONSTRUCTION JOINT - T1

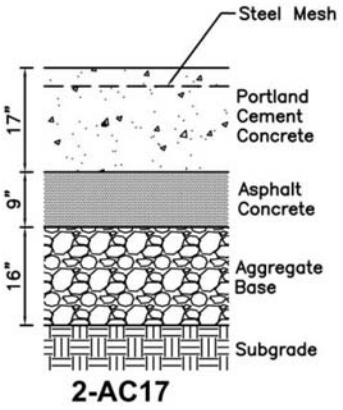

2-AC17

TEST SITE 2-AC17

2-AC17

Site Description: The site is located in the mid west of the United States. Elevations of the site, as indicated by USGS maps, are approximately 630 to 635 feet above sea level. Based on our observations, the pavement structure appears to be installed on natural subgrade soils. The typical natural subgrade as indicated by USDA soil maps is loamy sand over clay loam. The estimated PCI and SCI of the site is 73 and 78, respectively. The primary distress observed included low severity D-Cracking, occasional low severity linear cracking, and low severity corner spall.

Site Weather: The site is located in a wet/freeze climate zone. The below figures indicate the average temperature, average precipitation, average number of days above 90 degrees Fahrenheit, and average number of days below 32 degrees Fahrenheit.

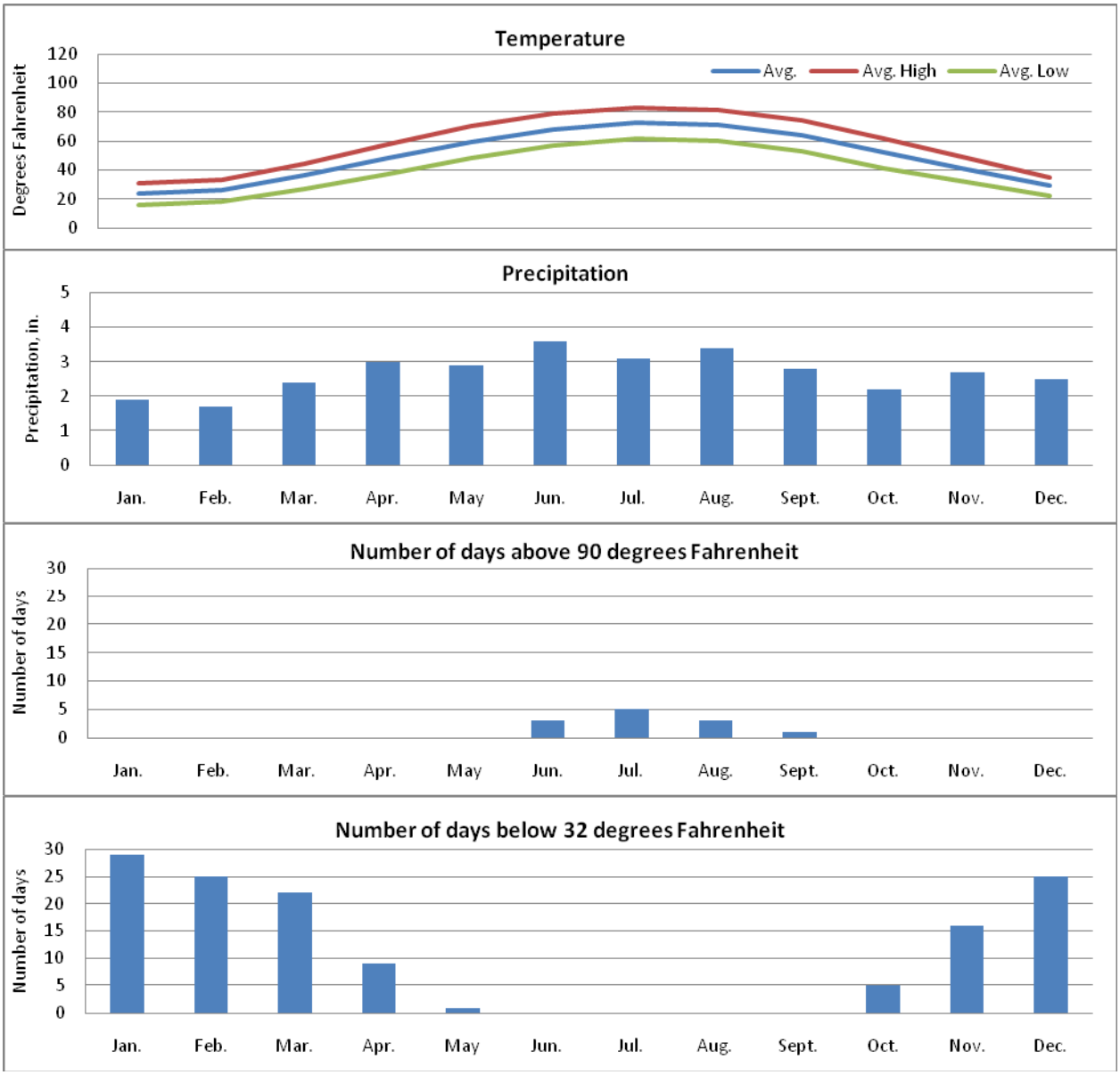

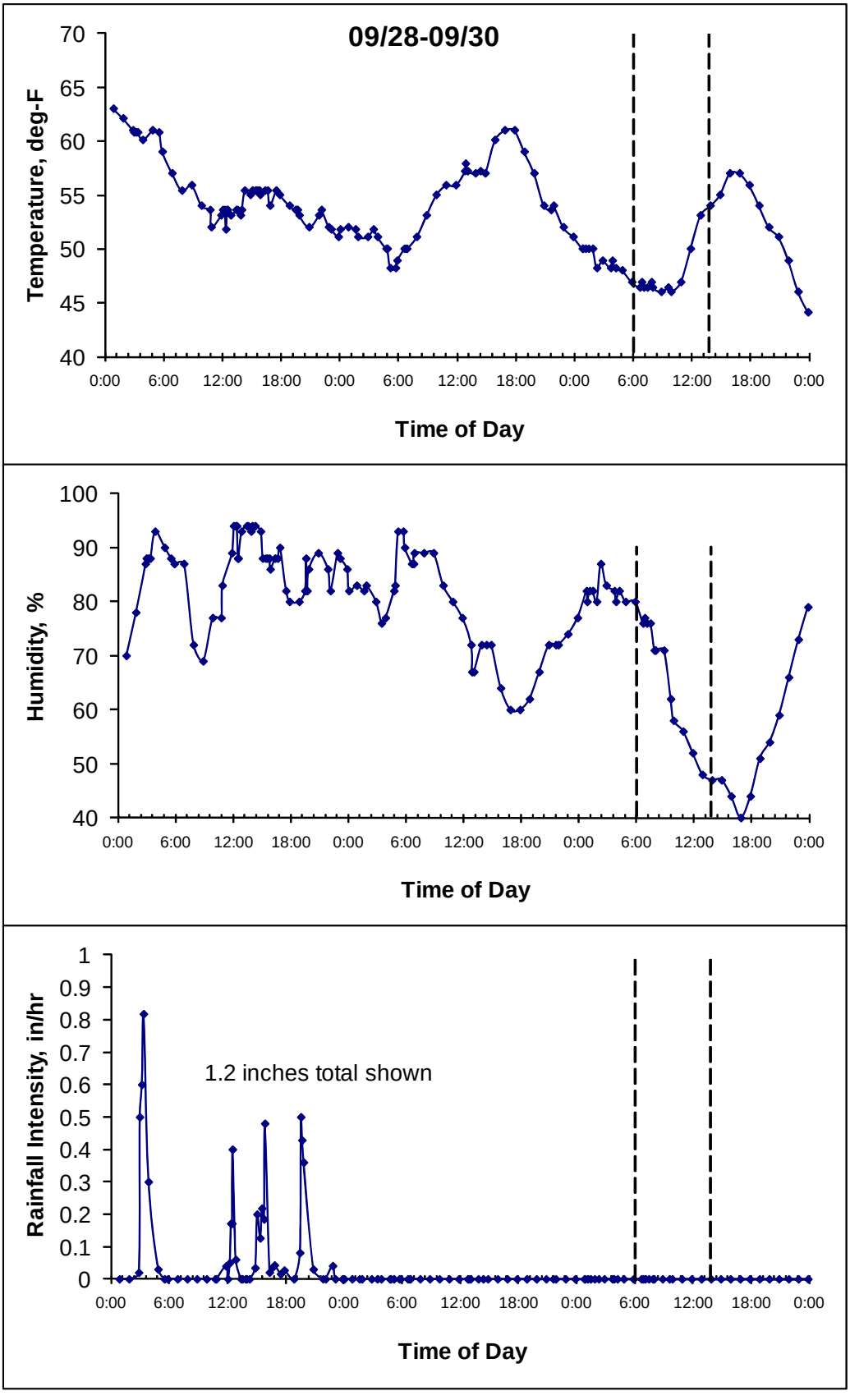
09/28-09/30
Temperature, deg-F
70
65
60
55
50
45
40
0:00
6:00
12:00
18:00
0:00
6:00
12:00
18:00
0:00
6:00
12:00
18:00
0:00
Time of Day
Humidity, %
100
90
80
70
60
50
40
0:00
6:00
12:00
18:00
0:00
6:00
12:00
18:00
0:00
6:00
12:00
18:00
0:00
Time of Day
Rainfall Intensity, in/hr
1
0.9
0.8
0.7
0.6
0.5
0.4
0.3
0.2
0.1
0
1.2 inches total shown
0:00
6:00
12:00
18:00
0:00
6:00
12:00
18:00
0:00
6:00
12:00
18:00
0:00
Time of Day

	Highway GPS3 55-3009	*Site 2-AC17* 8AM average	AM-PM Change
average curvature, ft^{-1}	0.000547	0.000224	0.000096
min. curvature	0.000203	-0.000072	0.000066
max. curvature	0.001077	0.000562	0.000119
st. dev. of curvature	0.00021	0.000177	0.000013
number of slabs	33	17	17

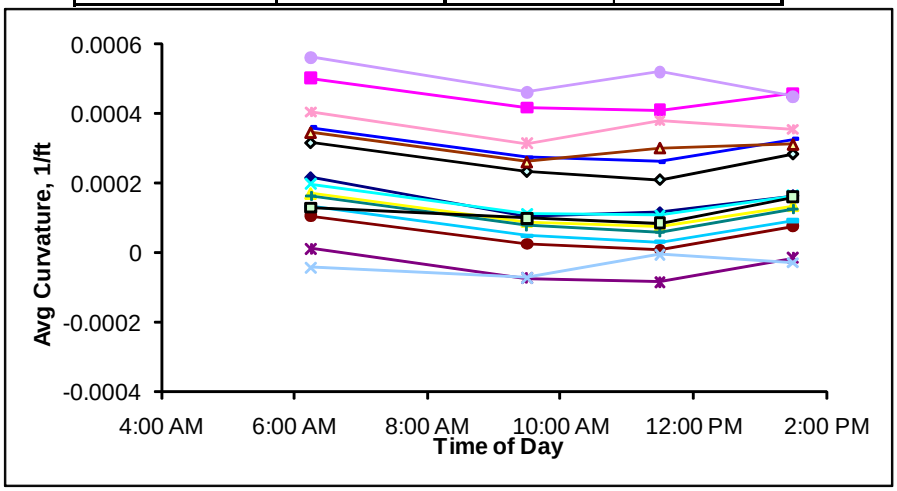

Site 2-AC17: ILLIBACK Summary

	Dense Liquid				*Elastic Solid*			
	***k*-value**	***k* stdev**	**Slab E_C**	**E_C Stdev**	**Subg. *E***	***E* stdev**	**Slab E_C**	**E_C Stdev**
Site Average =	470	49	5.48	0.53	79,343	4,857	4.10	0.25
Min Defl. =	490	38	6.80	0.51	85,523	3,580	5.17	0.22
Max Defl. =	433	50	4.72	0.51	72,263	5,230	3.52	0.25
AM Average =	***437***	***36***	***6.15***	***0.49***	***76,595***	***3,507***	***4.67***	***0.21***
Mid Average =	***423***	***30***	***6.73***	***0.45***	***75,995***	***2,813***	***5.15***	***0.19***
PM Average =	545	85	4.10	0.6	84,593	8,414	2.96	0.29
Best Guess	**430** *psi/in*		**6.44** *Msi*		**76295** *psi*		**4.91** *Msi*	

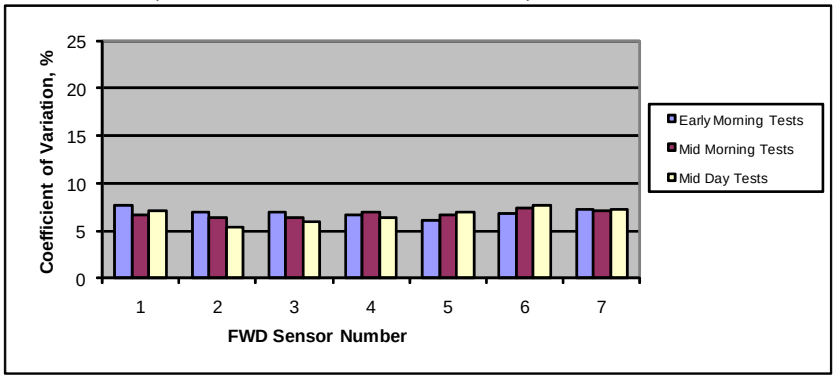

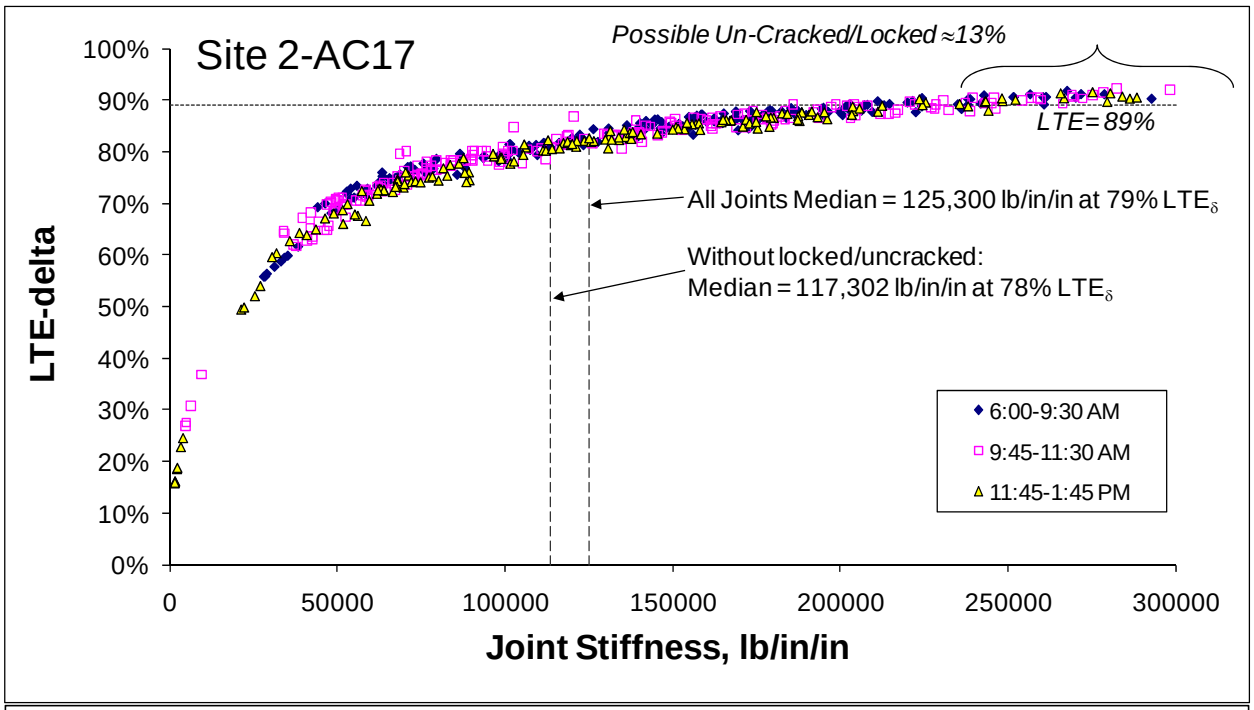
Site 2-AC17
Possible Un-Cracked/Locked ≈13%
LTE=89%
All Joints Median = 125,300 lb/in/in at 79% LTEδ
Without locked/uncracked:
Median = 117,302 lb/in/in at 78% LTEδ
6:00-9:30 AM
9:45-11:30 AM
11:45-1:45 PM
LTE-delta
Joint Stiffness, lb/in/in
100%
90%
80%
70%
60%
50%
40%
30%
20%
10%
0%
0
50000
100000
150000
200000
250000
300000

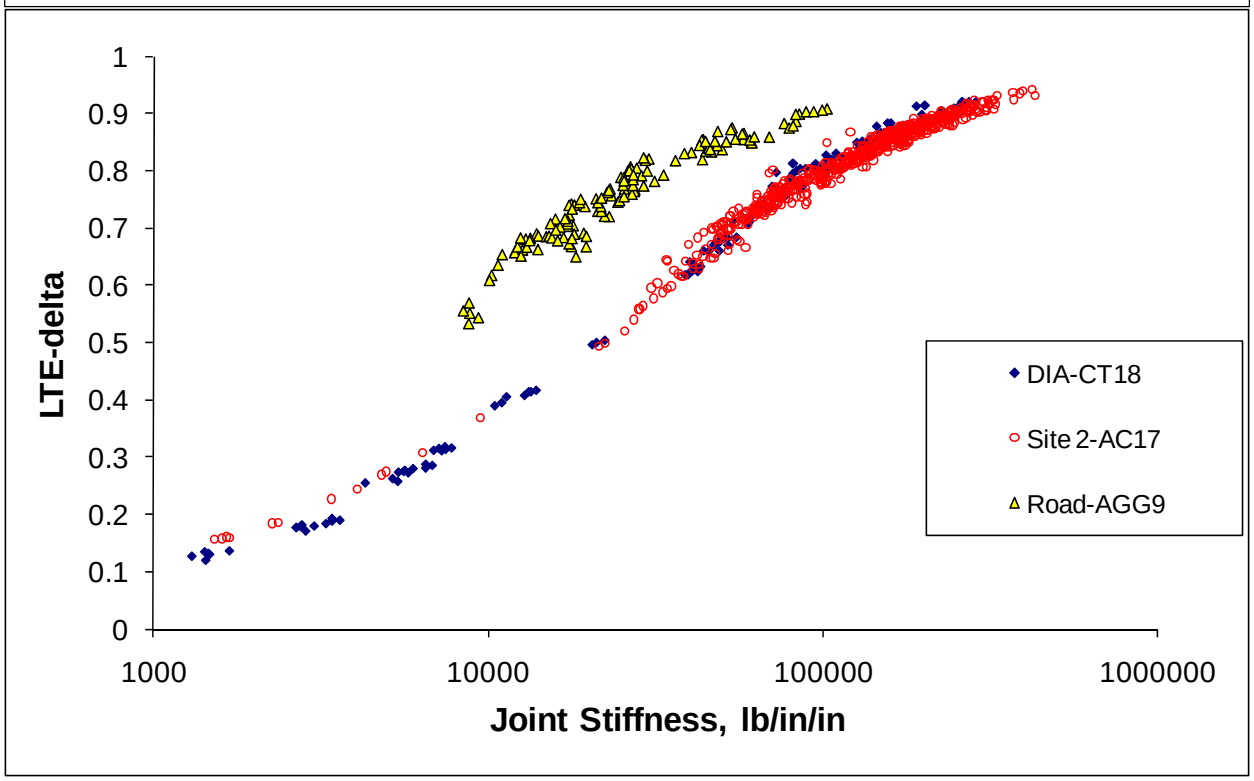
DIA-CT18
Site 2-AC17
Road-AGG9
LTE-delta
Joint Stiffness, lb/in/in
1
0.9
0.8
0.7
0.6
0.5
0.4
0.3
0.2
0.1
0
1000
10000
100000
1000000

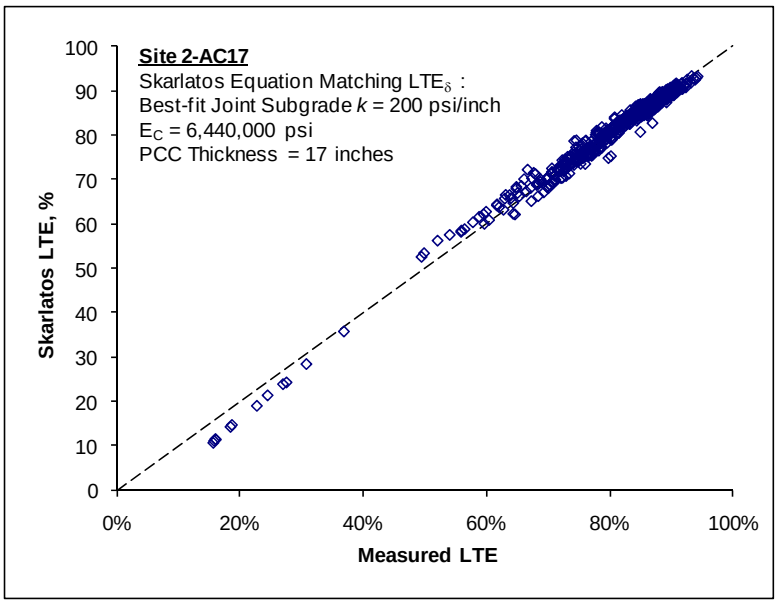
Site 2-AC17
Skarlatos Equation Matching LTE$_\delta$:
Best-fit Joint Subgrade k = 200 psi/inch
E_C = 6,440,000 psi
PCC Thickness = 17 inches
Skarlatos LTE, %
Measured LTE
0
10
20
30
40
50
60
70
80
90
100
0%
20%
40%
60%
80%
100%

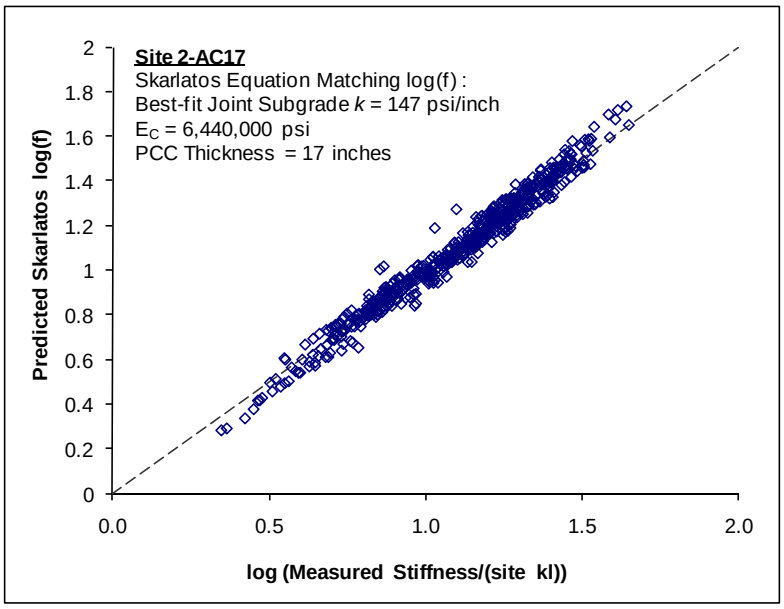
Site 2-AC17
Skarlatos Equation Matching log(f) :
Best-fit Joint Subgrade k = 147 psi/inch
E_C = 6,440,000 psi
PCC Thickness = 17 inches
Predicted Skarlatos log(f)
log (Measured Stiffness/(site kl))
0
0.2
0.4
0.6
0.8
1
1.2
1.4
1.6
1.8
2
0.0
0.5
1.0
1.5
2.0

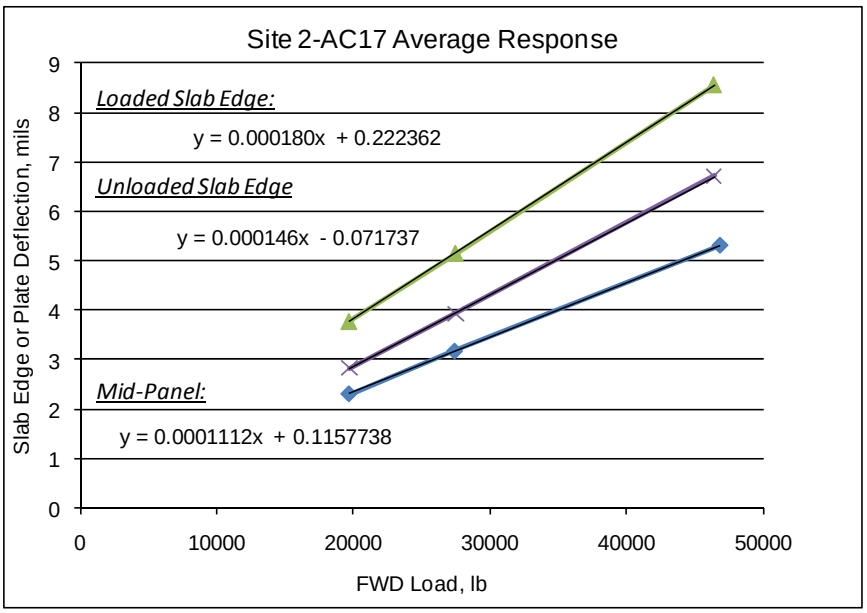

Site 2-AC17 L. Contraction Joints- including locked / un-cracked

	LR	LTE	Avg Stiffness
avg	**130**	**81%**	**155717**
min	**116**	**16%**	**1519**
max	**150**	**94%**	**420097**
stdev	**6**	**16%**	**69699**
Median	**129**	**85%**	**152603**

Possible Un-cracked, LTE>89% =11.4

#6Bars at 20" spacing, sawed

Steel Area/ft = 0.265072

reinf. ratio = 0.13%

Without locked / un-cracked joints

	LR	LTE	Avg Stiffness
avg	**130**	**80%**	**142451**
min	**116**	**16%**	**1519**
max	**150**	**91%**	**278603**
stdev	**6**	**17%**	**54422**
Median	**129**	**84%**	**147052**

% possibly un-cracked, LTE>89% = 3.6

at DCI = 5,000,000; kj = 36209

at DCI = 1,000,000; kj = 11164

Probable Agg Interlock = 110000 to 135000

$$k = \frac{1}{s\left(\frac{\varpi}{0.9 G_d A_d} + \frac{\varpi^3}{12 E_d I_d} + \frac{2+\beta\varpi}{2\beta^3 E_d I_d}\right)}$$

s is the dowel bar spacing =	20	in
w is the joint opening =	0.1	in
Dowel Diameter =	0.75	in
Ad is the dowel cross-sectional area =	0.44	sq in
Ed =	29000000	psi
Gd =	11153846	psi
Id =	0.016	in^4
Back-Calculated Dowel-Concrete Interaction modulus, DCI =	36450015	psi

$$\beta = \sqrt[4]{\frac{Kd}{4 E_d I_d}} = 1.974$$

Doweled Joint Stiffness = **147052** lb/in/in

Site 2-AC17 L. Construction Joints- including locked / un-cracked

	LR	LTE	Avg Stiffness
avg	119	82%	135359
min	106	67%	46425
max	131	94%	368047
stdev	6	7%	75303
Median	119	81%	111258

#6Bars at 15" spacing, formed possible small keyway

Possible Un-cracked, LTE>89% = 18.9

Steel Area/ft = 0.353429

reinf. ratio = 0.17%

lb/in/in

lb/in/in

psi

Without locked / un-cracked joints

	LR	LTE	Avg Stiffness
avg	119	80%	110792
min	106	67%	46425
max	131	91%	280780
stdev	6	6%	53718
Median	119	79%	93573

% possibly un-cracked, LTE>89% = 5.3

at DCI = 5,000,000; kj = 48278

at DCI = 1,000,000; kj = 14885

Probable Agg Interlock = 43000 to 80000

$$k = \frac{1}{s\left(\frac{\varpi}{0.9 G_d A_d} + \frac{\varpi^3}{12 E_d I_d} + \frac{2 + \beta\varpi}{2\beta^3 E_d I_d}\right)}$$

s is the dowel bar spacing =	15	in
w is the joint opening =	0.1	in
Dowel Diameter =	0.75	in
Ad is the dowel cross-sectional area =	0.44	sq in
Ed =	29000000	psi
Gd =	11153846	psi
Id =	0.016	in^4
Back-Calculated Dowel-Concrete Interaction modulus, DCI =	12583095	psi

$$\beta = \sqrt[4]{\frac{Kd}{4 E_d I_d}} = 1.513$$

Doweled Joint Stiffness = **93573** lb/in/in

Site 2-AC17 T. Doweled Contraction Joints- including locked / un-cracked

	LR	LTE	Avg Stiffness
avg	111	73%	81035
Median	110	73%	67030
min	102	49%	21411
max	126	91%	312789
stdev	6	9%	56025

1.5" dowels at 12", chairs, sawed

Possible Un-cracked, LTE>86% = 3.3

Steel Area/ft = 1.767146

reinf. ratio = 0.87%

Without locked / un-cracked joints

	LR	LTE	Avg Stiffness
avg	111	72%	74656
Median	110	73%	63529
min	102	49%	21411
max	124	88%	227176
stdev	5	9%	44598

Zero LTE > 89%

Probable Agg Interlock = 0 to 60000

$$k = \frac{1}{s\left(\frac{\varpi}{0.9 G_d A_d} + \frac{\varpi^3}{12 E_d I_d} + \frac{2 + \beta\varpi}{2\beta^3 E_d I_d}\right)}$$

s is the dowel bar spacing =	12	in
w is the joint opening =	0.3	in
Dowel Diameter =	1.5	in
Ad is the dowel cross-sectional area =	1.77	sq in
Ed =	29000000	psi
Gd =	11153846	psi
Id =	0.249	in^4
Back-Calculated Dowel-Concrete Interaction modulus, DCI =	1074867	psi

$$\beta = \sqrt[4]{\frac{Kd}{4 E_d I_d}} = 0.486$$

Doweled Joint Stiffness = **63529** lb/in/in

Site 2-AC17 T. Mesh-tied Contraction Joints, including possible un-cracked

	LR	LTE	Avg Stiffness
avg	123	84%	173403
Median	123	86%	171043
min	109	69%	49395
max	135	93%	427581
stdev	6	6%	74416

welded wire fabric, 0.204 sq in per ft, sawed

Possible Un-cracked, LTE>89% = 22.6

reinf. ratio = 0.10%

Without locked / un-cracked joints

	LR	LTE	Avg Stiffness
avg	123	84%	160987
Median	122	85%	163152
min	109	69%	49395
max	135	92%	322482
stdev	6	5%	64582

% possibly un-cracked, LTE>89% = 14.3

at DCI = 5,000,000; kj = 31978

at DCI = 1,000,000; kj = 10007

Probable Agg Interlock = 130000 to 150000

$$k = \frac{1}{s\left(\frac{\varpi}{0.9 G_d A_d} + \frac{\varpi^3}{12 E_d I_d} + \frac{2+\beta\varpi}{2\beta^3 E_d I_d}\right)}$$

s is the dowel bar spacing =	6	in
w is the joint opening =	0.1	in
Dowel Diameter =	0.36	in
Ad is the dowel cross-sectional area =	0.10	sq in
Ed =	29000000	psi
Gd =	11153846	psi
Id =	0.001	in^4
Back-Calculated Dowel-Concrete Interaction modulus, DCI =	5000000	psi

$$\beta = \sqrt[4]{\frac{Kd}{4 E_d I_d}} = 2.083$$

Doweled Joint Stiffness = **31978** lb/in/in

Site 2-AC17 Corner Tests, No un-cracked corners detected

	LR	LTE	Avg Stiffness
avg	118	71%	76174
min	102	22%	3286
max	149	93%	327350
stdev	9	16%	69936
Median	118	69%	37367

% possibly un-cracked, LTE>86% = 6.7

Dowels, Ties, or Mesh on all edges

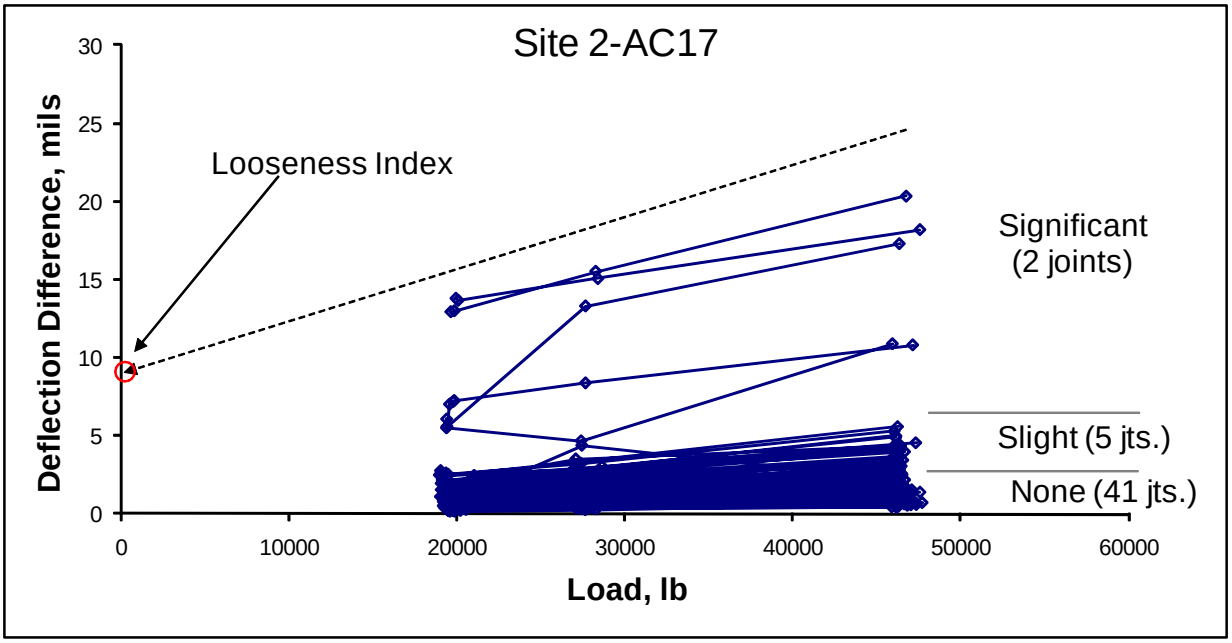

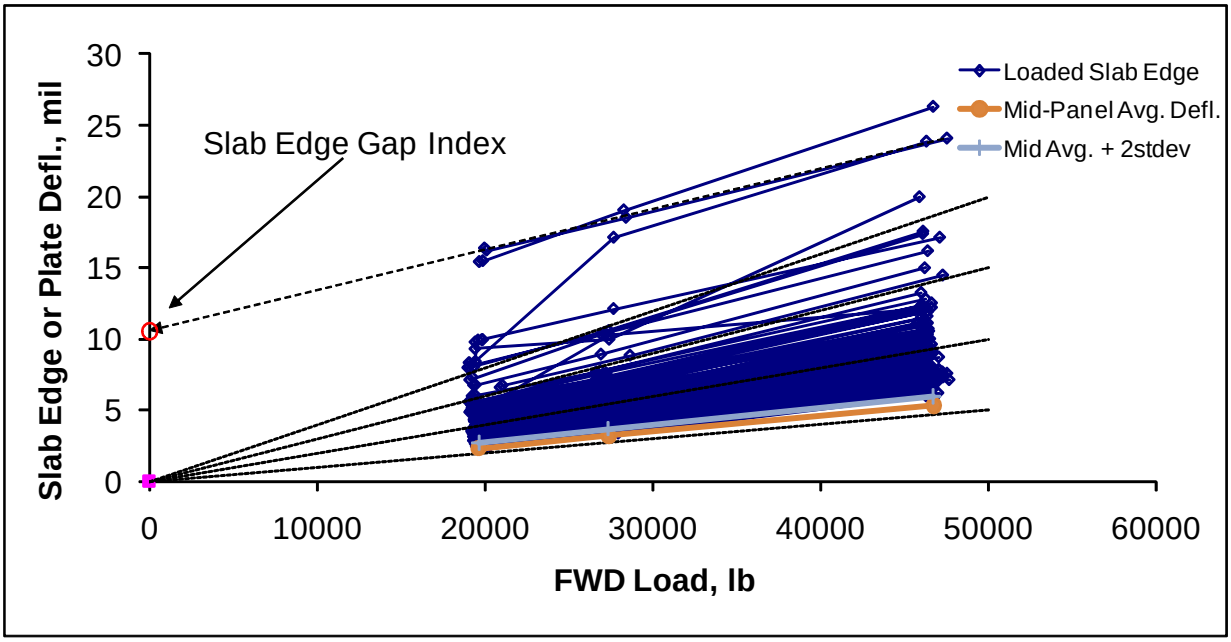

Site 2-AC17; Slab Edge Gaps, All Normal Joints

mils	All	AM	Mid	PM
Avg	0.11	0.15	0.15	0.01
Min	-1.03	-1.03	-0.39	-0.56
Max	1.37	1.37	1.07	0.54
Stdev	0.31	0.37	0.27	0.27

count = 163

Std. Error = 0.024453 mils

Site 2-AC17 Joint Looseness Data; without 1sdj, without locked/uncracked

Looseness	All Good Data	All Data, no un-cracked	Transverse	C-jt	D-jt	LongConst	LongContract	Corners
Average	0.22	0.22	0.22	0.18	0.28	0.22	0.11	0.35
Maximum	1.29	1.29	0.59	0.57	0.59	0.89	0.51	1.29
Minimum	-0.98	-0.98	-0.31	-0.31	-0.17	-0.06	-0.03	-0.98
Std. Dev.	0.29	0.29	0.26	0.27	0.24	0.20	0.11	0.55
Count	110	111	44	28	16	27	26	17
19.7 kip %	8%	8%	7%	6%	9%	8%	4%	12%
27.5 kip %	5%	5%	5%	4%	7%	5%	3%	9%
46.4 kip %	3%	3%	3%	3%	4%	3%	2%	5%

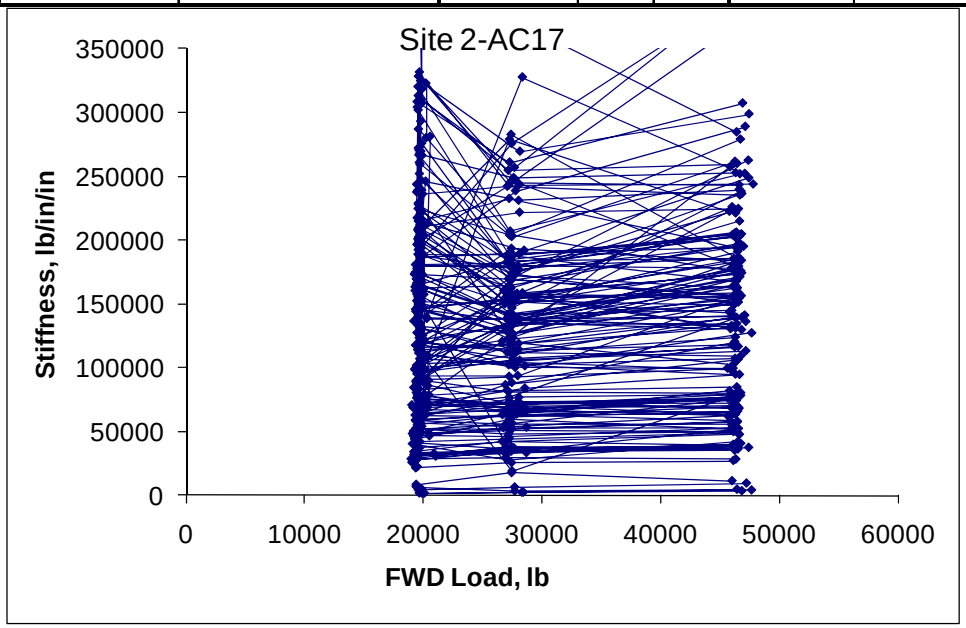

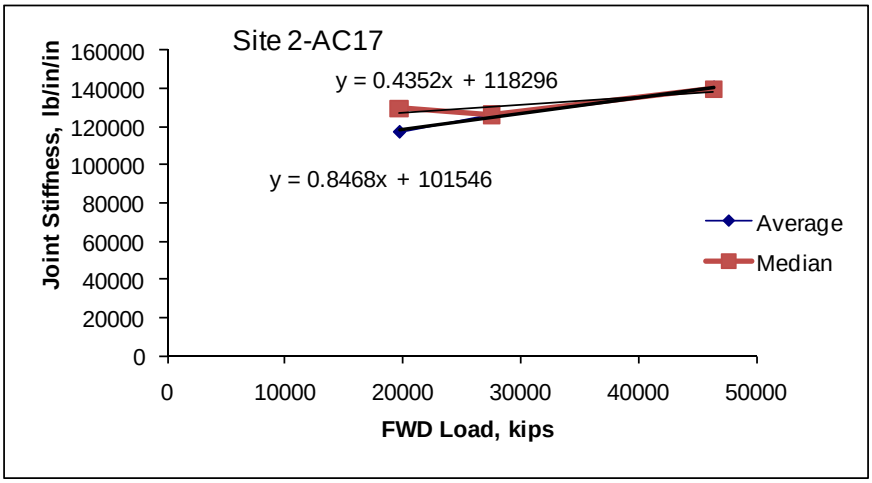

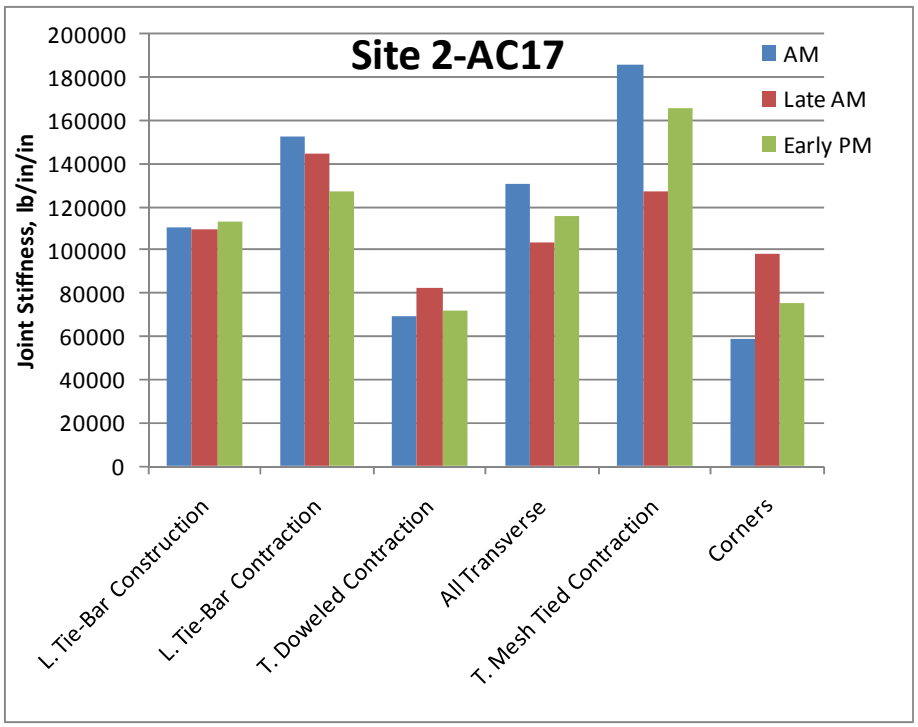
Site 2-AC17
AM
Late AM
Early PM
Joint Stiffness, lb/in/in
200000
180000
160000
140000
120000
100000
80000
60000
40000
20000
0
L. Tie-Bar Construction
L. Tie-Bar Contraction
T. Doweled Contraction
All Transverse
T. Mesh Tied Contraction
Corners

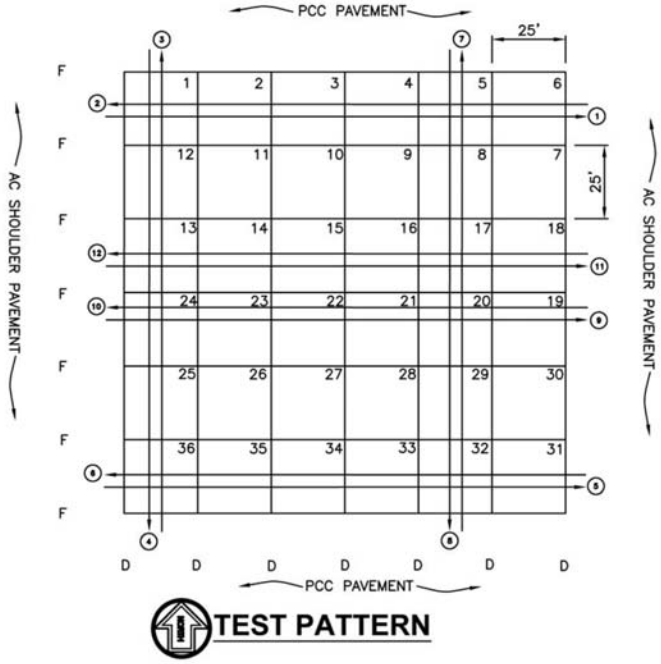

LEGEND

(2) FWD TEST LANE NUMBER

D CONSTRUCTION JOINT: 1 3/8" DIA. SMOOTH DOWEL, 20" LONG, 15" SPACING.

F CONTRACTION JOINT: 1 3/8" DIA. SMOOTH DOWEL BAR, 20" LONG, 15" SPACING.

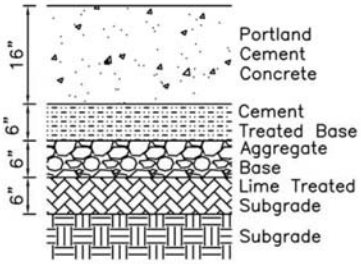

3-CT16

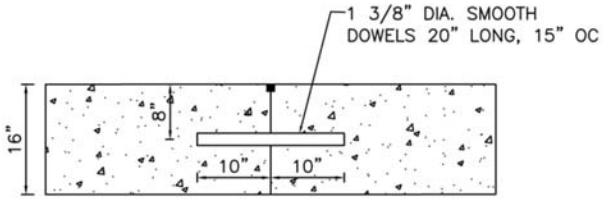

CONTRACTION JOINT - F

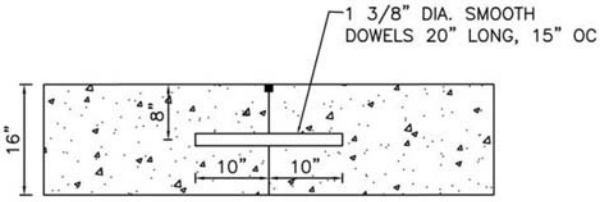

LONGITUDINAL CONSTRUCTION JOINT - D

TEST SITE 3-CT16

3-CT16

Site Description: The site is located in the south central region of the United States. Elevations of the site, as indicated by USGS maps, are approximately 490 to 500 feet above sea level at the base of a hill. Based on our observations, the pavement structure appears to be installed on natural subgrade soils. The typical natural subgrade as indicated by USDA soil maps is silty clay over silt loam. The estimated PCI and SCI of the site is 100 and 100, respectively. No significant distress was observed.

Site Weather: The site is located in a wet/no freeze climate zone. The below figures indicate the average temperature, average precipitation, average number of days above 90 degrees Fahrenheit, and average number of days below 32 degrees Fahrenheit.

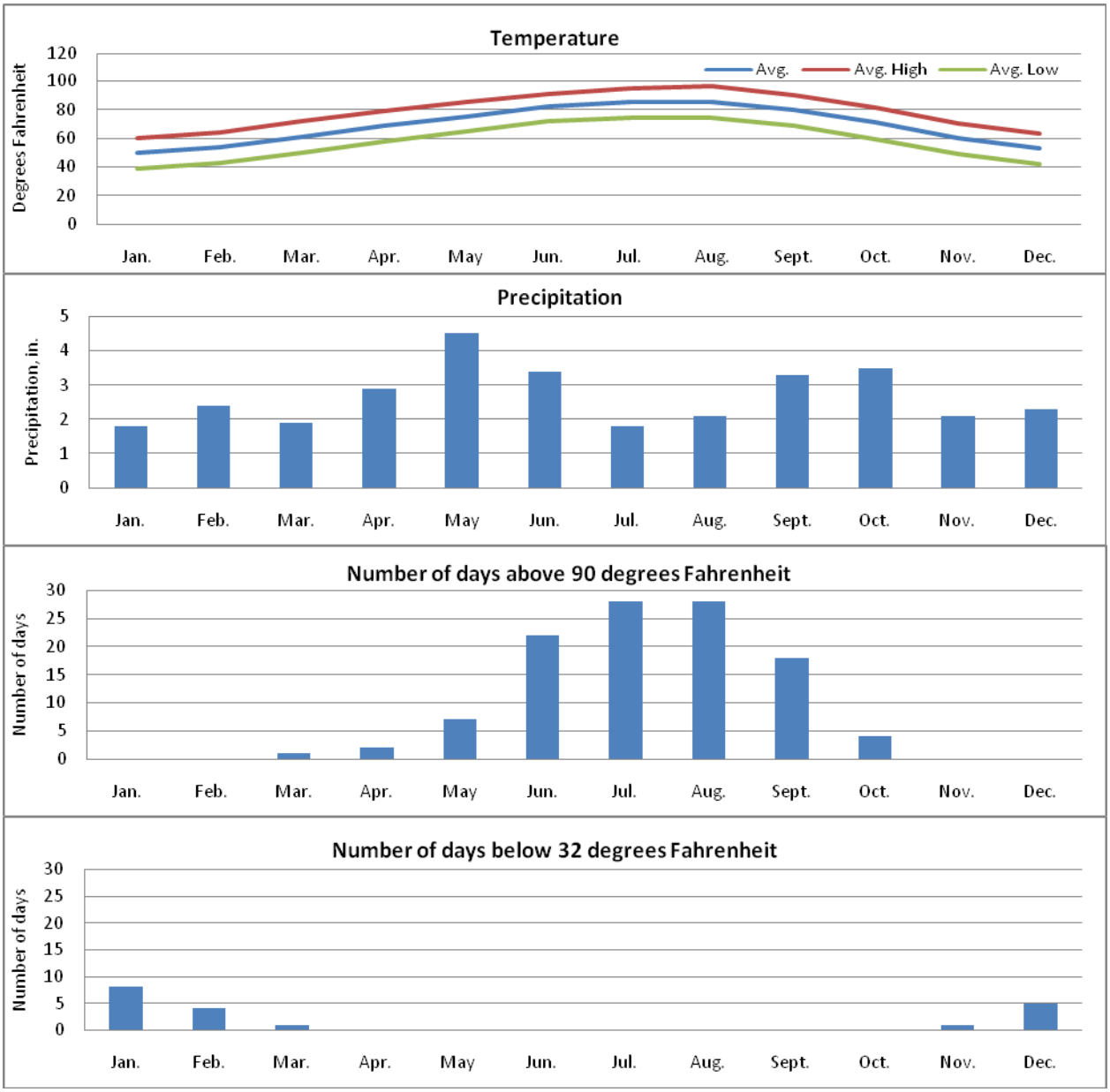

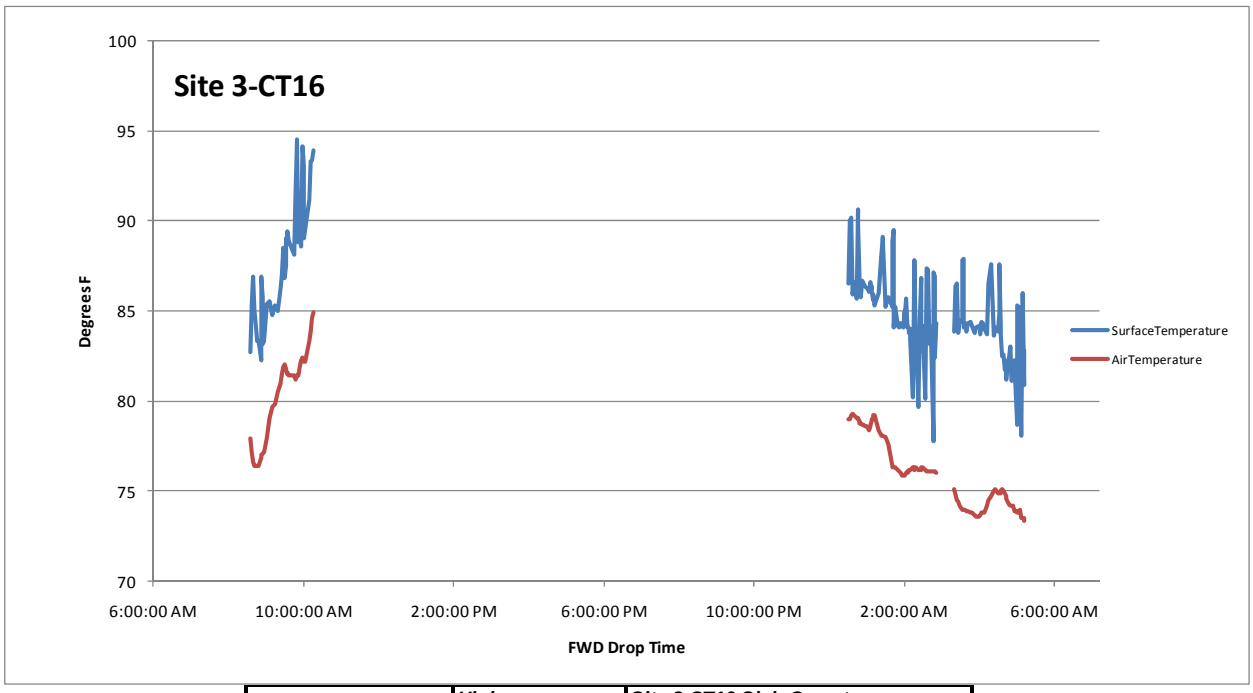

	Highway GPS3 55-3009	*Site 3-CT16 Slab Curvature* 8AM average	AM-PM Change
average curvature, ft^{-1}	0.000547	-0.000066	0.000025
min. curvature	0.000203	-0.000278	0.000010
max. curvature	0.001077	0.000076	0.000040
st. dev. of curvature	0.00021	0.000131	0.000011
number of slabs	33	7	7

-1

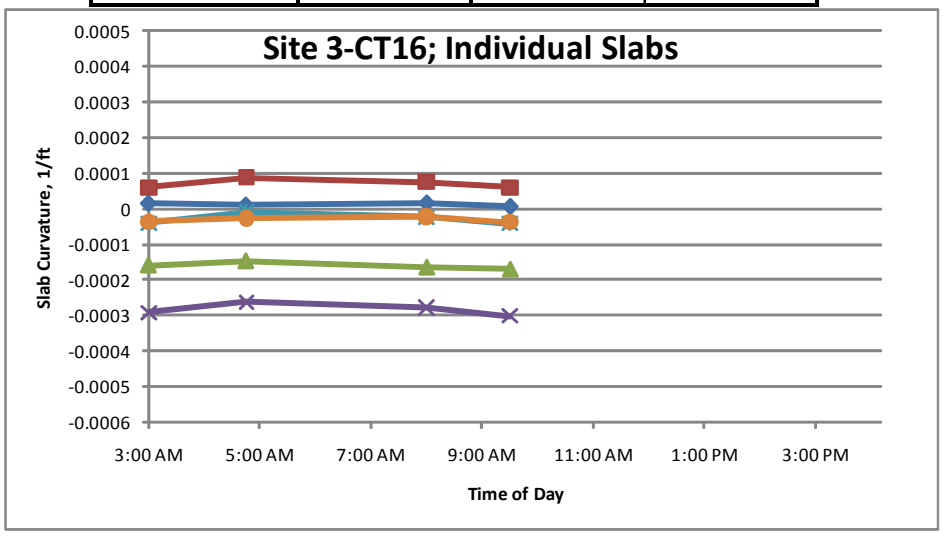

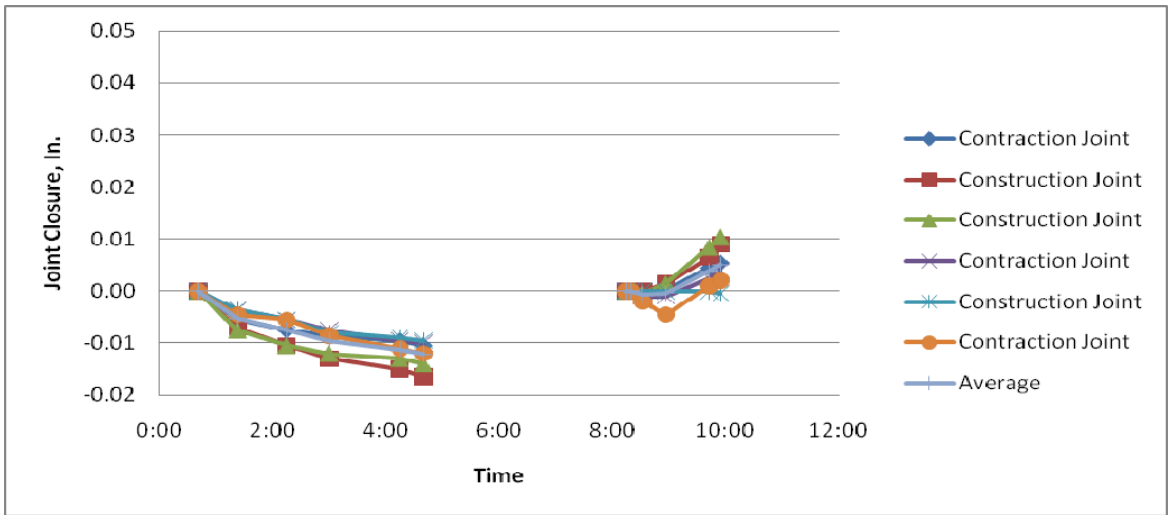

Test Site 3-CT16: ILLIBACK Summary

	Dense Liquid				*Elastic Solid*				Radius
	***k*-value**	***k* stdev**	**Slab E_C**	**E_C Stdev**	**Subg. *E***	***E* stdev**	**Slab E_C**	**E_C Stdev**	***f*-Values**
R1 Average =	***401***	***42***	***7.46***	***0.76***	***71,776***	***5,061***	***5.70***	***0.4***	***50.5***
R1 Min defl. =	443	45	8.81	0.87	80,331	5,503	6.76	0.46	51.3
R1 Max defl. =	342	33	6.74	0.63	61,951	3,959	5.17	0.33	51.2
R2 Average =	***395***	***36***	***6.70***	***0.58***	***69,355***	***3,715***	***5.10***	***0.27***	***49.3***
R2 Min defl. =	532	65	6.45	0.73	87,889	6,488	4.76	0.35	45.4
R2 Max defl. =	334	29	5.90	0.49	59,217	2,987	4.49	0.22	49.8
R3 Average =	***404***	***42***	***6.87***	***0.67***	***71,096***	***4,582***	***5.21***	***0.34***	***49.4***
R3 Min defl. =	448	43	7.83	0.72	79,279	4,640	5.96	0.35	49.7
R3 Max defl. =	356	32	6.07	0.51	62,671	3,187	4.62	0.23	49.4
Best Guess	**400**		**7.01**		**70,742**		**5.34**		**49.7**
	psi/in		*Msi*		*psi*		*Msi*		

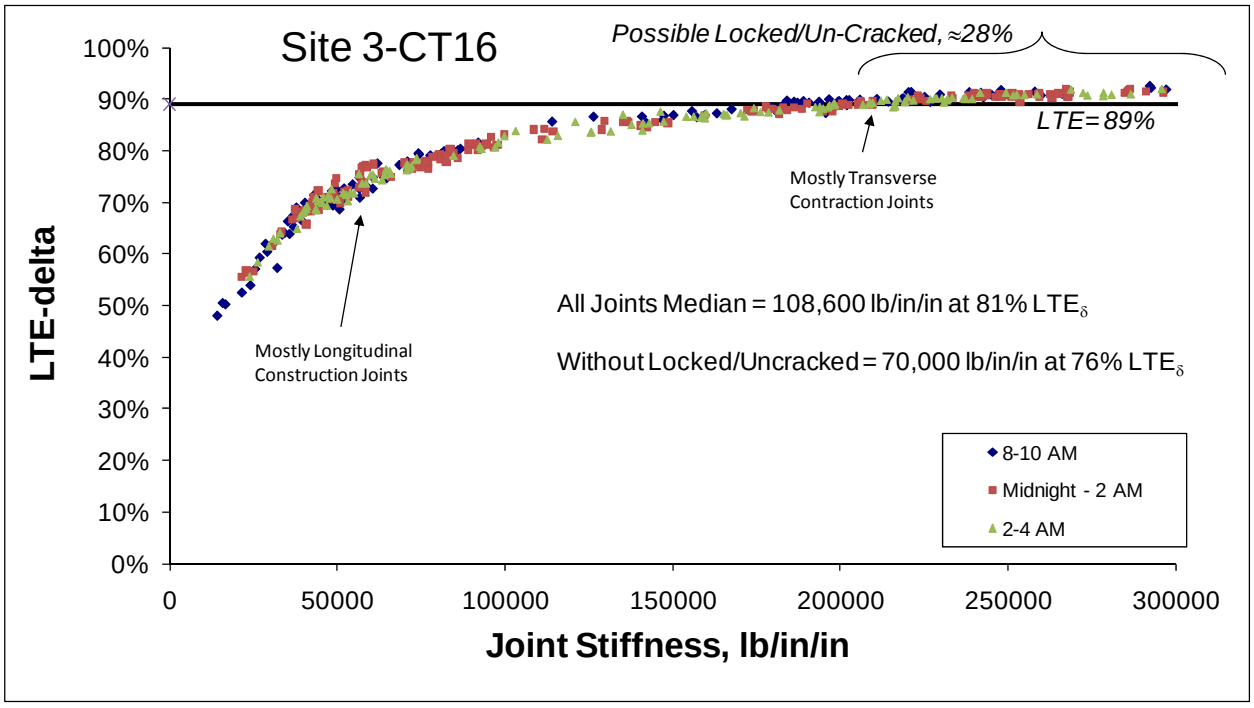

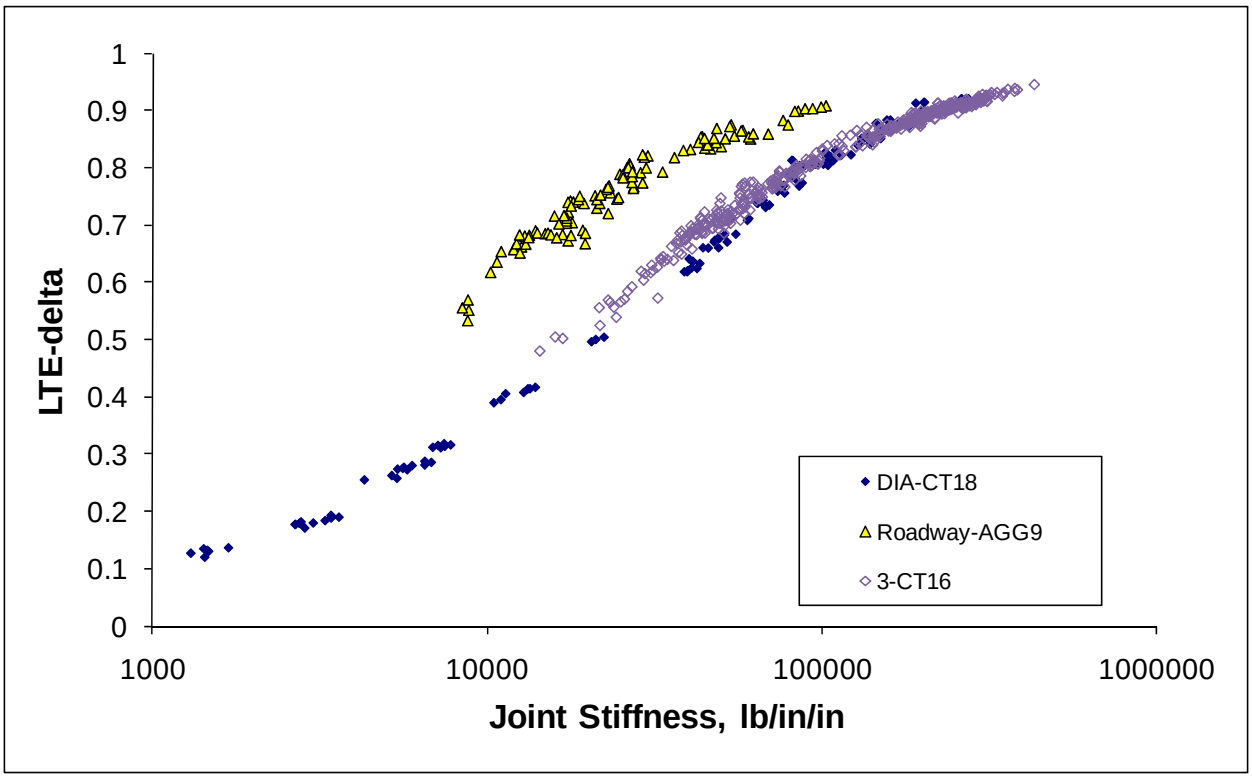
LTE-delta
Joint Stiffness, lb/in/in
1
0.9
0.8
0.7
0.6
0.5
0.4
0.3
0.2
0.1
0
1000
10000
100000
1000000
DIA-CT18
Roadway-AGG9
3-CT16

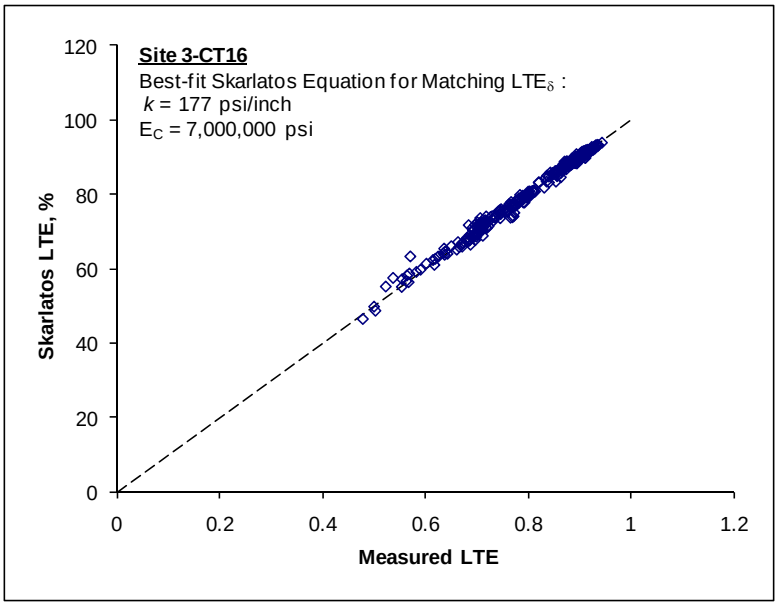
Site 3-CT16
Best-fit Skarlatos Equation for Matching LTEδ :
k = 177 psi/inch
EC = 7,000,000 psi
Skarlatos LTE, %
Measured LTE
120
100
80
60
40
20
0
0
0.2
0.4
0.6
0.8
1
1.2

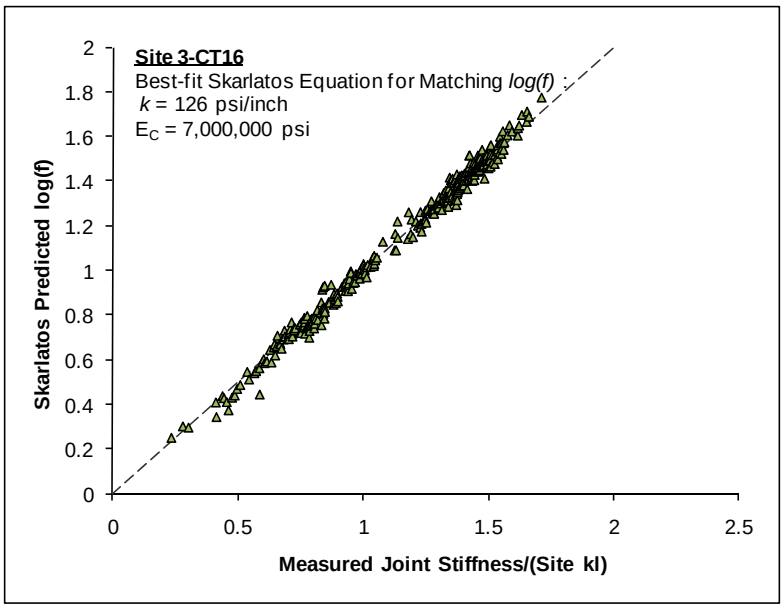
Site 3-CT16
Best-fit Skarlatos Equation for Matching log(f) :
k = 126 psi/inch
E_C = 7,000,000 psi
Skarlatos Predicted log(f)
Measured Joint Stiffness/(Site kl)
0
0.2
0.4
0.6
0.8
1
1.2
1.4
1.6
1.8
2
0
0.5
1
1.5
2
2.5

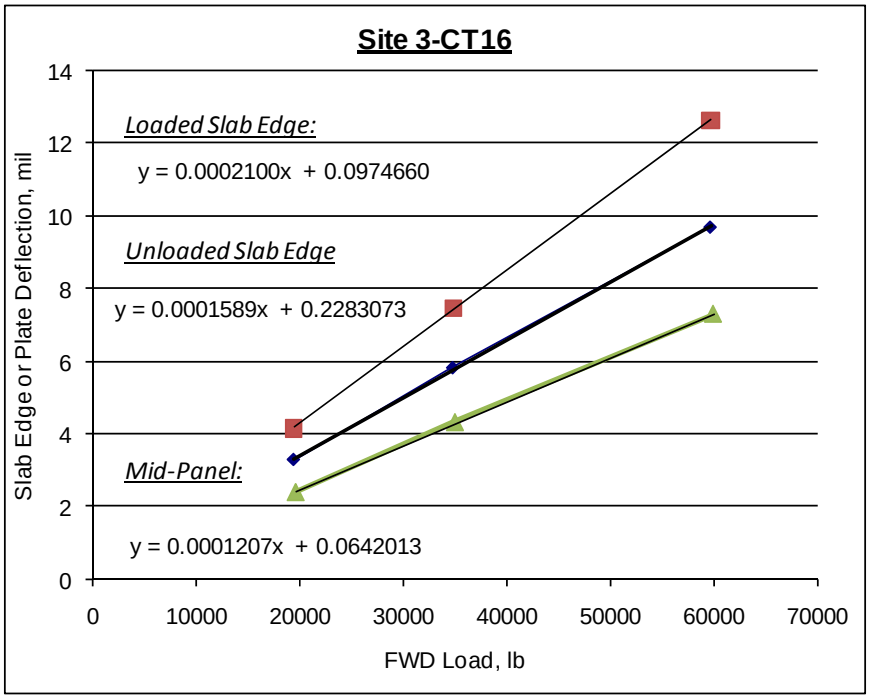
Site 3-CT16
Loaded Slab Edge:
y = 0.0002100x + 0.0974660
Unloaded Slab Edge
y = 0.0001589x + 0.2283073
Mid-Panel:
y = 0.0001207x + 0.0642013
Slab Edge or Plate Deflection, mil
FWD Load, lb
0
2
4
6
8
10
12
14
0
10000
20000
30000
40000
50000
60000
70000

Site 3-CT16: Doweled Construction Joints, No un-cracked joints detected

	LR	LTE	Avg Stiffness
avg	115	73%	62551
min	95	48%	14326
max	151	91%	241867
stdev	8	8%	29674
Median	114	73%	56684

% possibly un-cracked, LTE>89% = 1 drop, 0.5%

Formed 1.375" dowels at 15"

Steel Area/ft = 1.187915

reinf. ratio = 0.619%

Probable Agg Interlock = 0 to 50000

$$k = \frac{1}{s\left(\frac{\varpi}{0.9 G_d A_d} + \frac{\varpi^3}{12 E_d I_d} + \frac{2 + \beta\varpi}{2\beta^3 E_d I_d}\right)}$$

s is the dowel bar spacing =	15	in
w is the joint opening =	0.1	in
Dowel Diameter =	1.375	in
Ad is the dowel cross-sectional area =	1.48	sq in
Ed =	29000000	psi
Gd =	11153846	psi
Id =	0.175	in^4
Back-Calculated Dowel-Concrete Interaction modulus, DCI =	1424056	psi

$$\beta = \sqrt[4]{\frac{Kd}{4 E_d I_d}} = 0.557$$

Doweled Joint Stiffness = **56684** lb/in/in

Site 3-CT16; Doweled Contraction Joints, including locked / un-cracked

	LR	LTE	Avg Stiffness
avg	136	89%	223222
min	118	81%	97131
max	167	95%	428332
stdev	9	2%	55662
Median	137	90%	219422

% possibly un-cracked, LTE>89% = 64%

Sawed 1.375" dowels at 15"

Steel Area/ft = 1.187915

reinf. ratio = 0.619%

Without possible locked / un-cracked joints

	LR	LTE	Avg Stiffness
avg	134	88%	194767
min	118	81%	97131
max	154	95%	428332
stdev	9	2%	48043
Median	132	88%	193265

% possibly un-cracked, LTE>89% = 33.3

DCI = 1 msi, kj = 43640

DCI = 5 msi, kj = 121215

Probable Agg Interlock = 70000 to 150000

$$k = \frac{1}{s\left(\frac{\varpi}{0.9 G_d A_d} + \frac{\varpi^3}{12 E_d I_d} + \frac{2+\beta\varpi}{2\beta^3 E_d I_d}\right)}$$

s is the dowel bar spacing =	15	in
w is the joint opening =	0.1	in
Dowel Diameter =	1.375	in
Ad is the dowel cross-sectional area =	1.48	sq in
Ed =	29000000	psi
Gd =	11153846	psi
Id =	0.175	in^4
Back-Calculated Dowel-Concrete Interaction modulus, DCI =	5000000	psi

$$\beta = \sqrt[4]{\frac{Kd}{4 E_d I_d}} = 0.762$$

Doweled Joint Stiffness = **142698** lb/in/in

Site 3-CT16; All Corners, no locked / un-cracked detected

	LR	LTE	Avg Stiffness
avg	110	75%	70518
min	103	53%	16548
max	119	89%	168362
stdev	5	10%	39432
Median	110	78%	72265

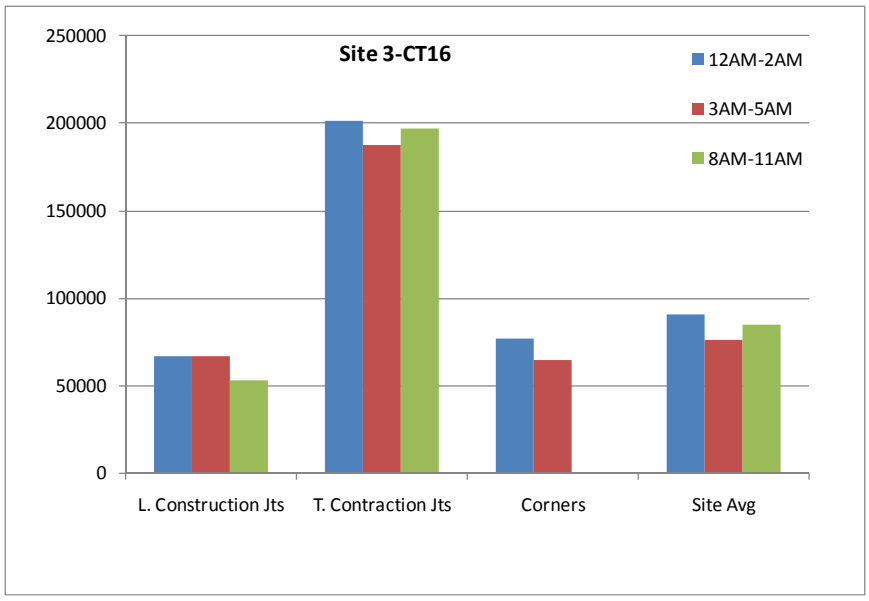
Site 3-CT16
12AM-2AM
3AM-5AM
8AM-11AM
250000
200000
150000
100000
50000
0
L. Construction Jts
T. Contraction Jts
Corners
Site Avg

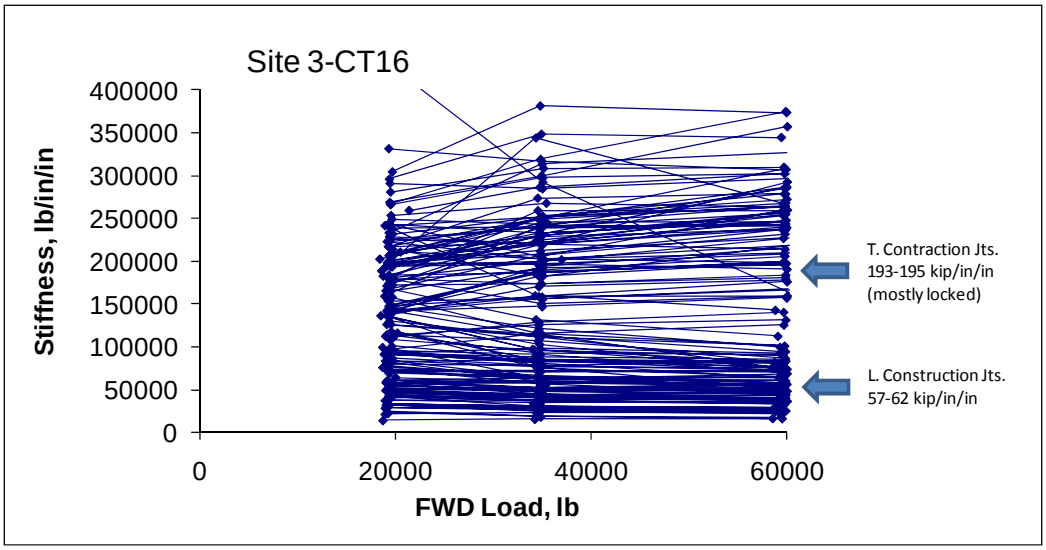
Site 3-CT16
Stiffness, lb/in/in
400000
350000
300000
250000
200000
150000
100000
50000
0
0
20000
40000
60000
FWD Load, lb
T. Contraction Jts.
193-195 kip/in/in
(mostly locked)
L. Construction Jts.
57-62 kip/in/in

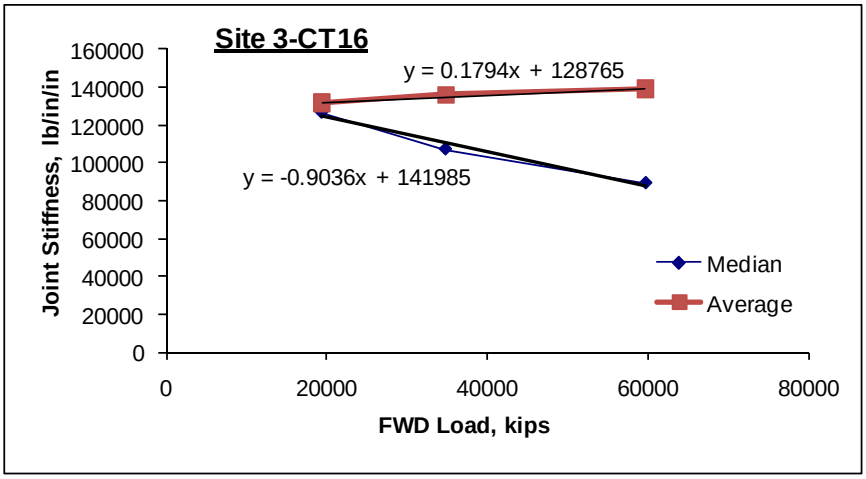
Site 3-CT16
y = 0.1794x + 128765
y = -0.9036x + 141985
Joint Stiffness, lb/in/in
160000
140000
120000
100000
80000
60000
40000
20000
0
0
20000
40000
60000
80000
FWD Load, kips
Median
Average

Site 3-CT16 Slab Edge Gaps- All Good Data

	All	AM	Mid	PM
Avg	0.10	0.11	0.05	0.13
Min	-0.59	-0.59	-0.51	-0.37
Max	0.39	0.38	0.37	0.39
Stdev	0.19	0.20	0.19	0.16

Site 3-CT16 Joint Looseness Data

Looseness	All Good Data	Constr. Jt	Contra. Jt	Corners
Average	-0.13	-0.25	0.07	0.28
Maximum	0.34	0.34	0.21	7.29
Minimum	-1.22	-1.22	-0.48	-1.15
Std. Dev.	0.31	0.32	0.08	2.01
Count	165	71	74	21
21.6 kip %	-2%	-4%	1%	5%
33.5 kip %	-1%	-3%	1%	3%
46.1 kip %	-1%	-2%	1%	2%

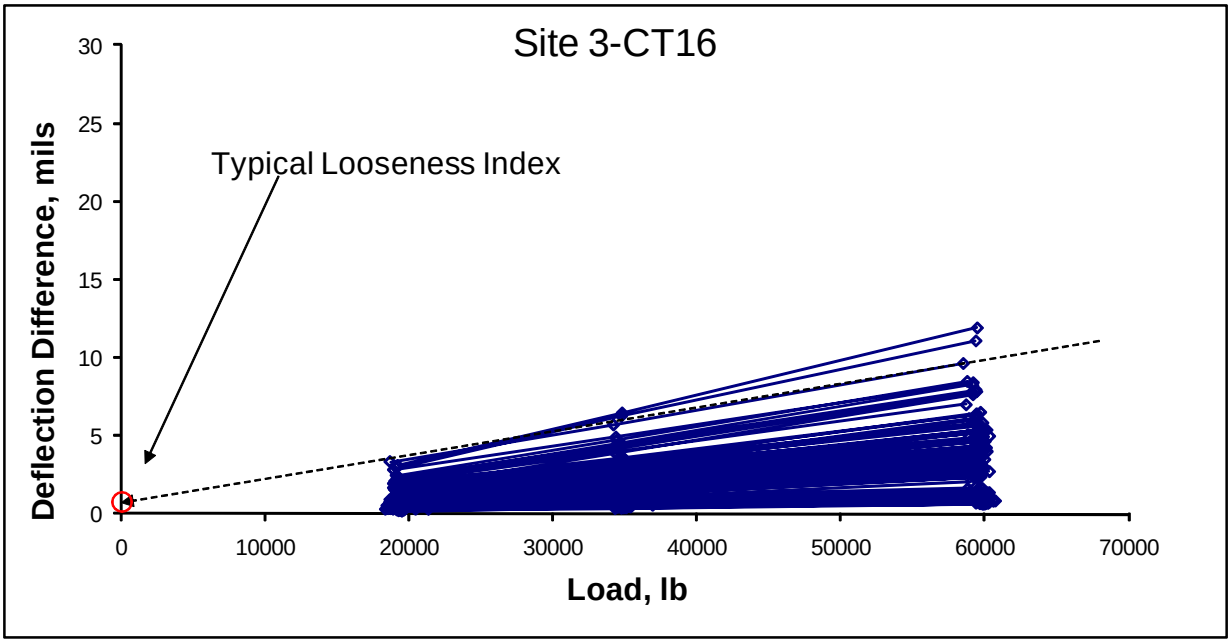
Site 3-CT16
Typical Looseness Index
Deflection Difference, mils
30
25
20
15
10
5
0
0
10000
20000
30000
40000
50000
60000
70000
Load, lb

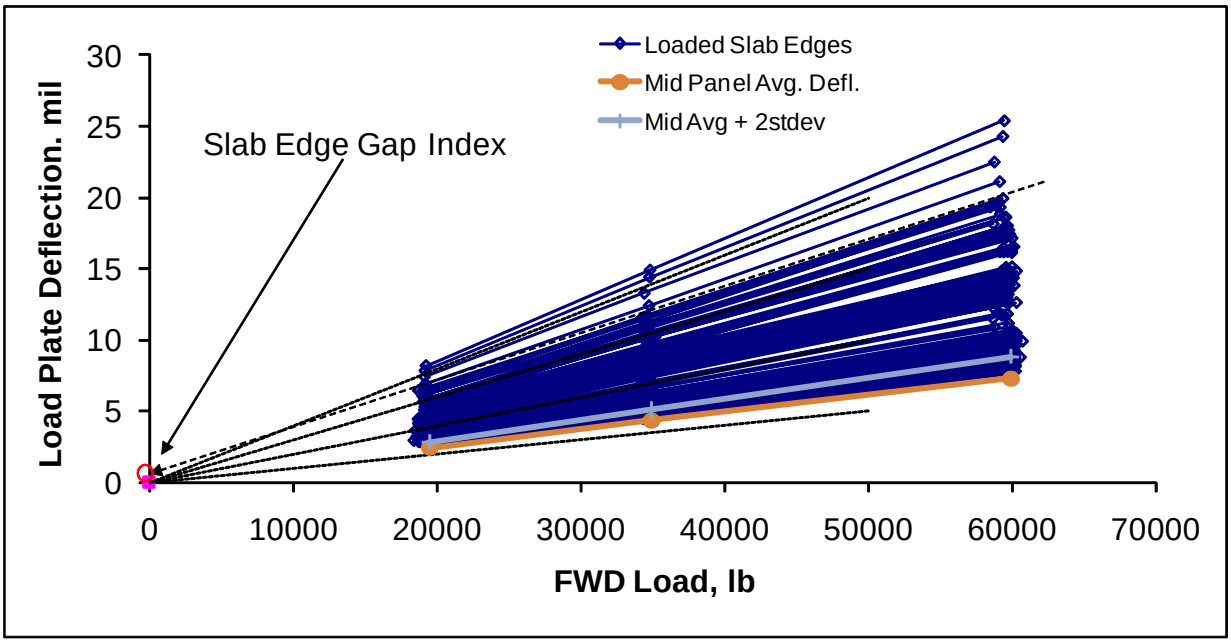
Loaded Slab Edges
Mid Panel Avg. Defl.
Mid Avg + 2stdev
Slab Edge Gap Index
Load Plate Deflection. mil
30
25
20
15
10
5
0
0
10000
20000
30000
40000
50000
60000
70000
FWD Load, lb

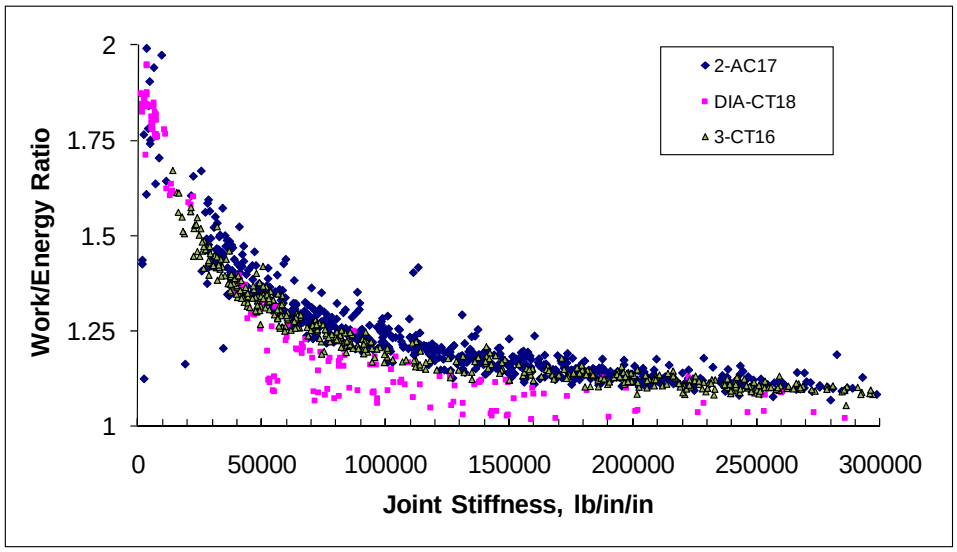
2
1.75
1.5
1.25
1
Work/Energy Ratio
0
50000
100000
150000
200000
250000
300000
Joint Stiffness, lb/in/in
2-AC17
DIA-CT18
3-CT16

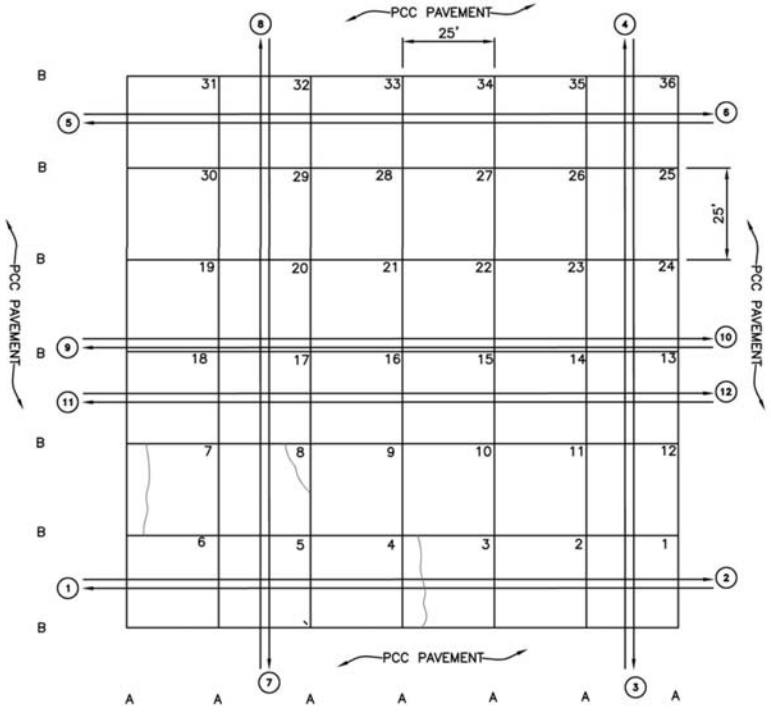

TEST PATTERN

LEGEND

(2) FWD TEST LANE NUMBER

A CONTRACTION JOINT: 2" DIA. SMOOTH DOWEL BAR, 24" LONG, 15" SPACING, ONE SIDE GREASED.

B CONSTRUCTION JOINT: 2" DIA. SMOOTH DOWEL BAR, 24" LONG, 15" SPACING, ONE SIDE GREASED, DRILLED AND EPOXIED INTO PLACE.

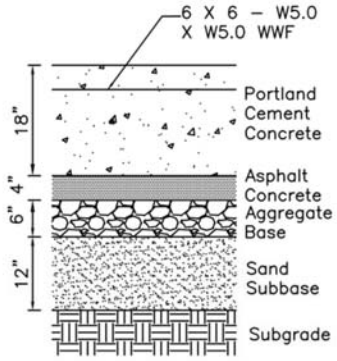

4-AC18

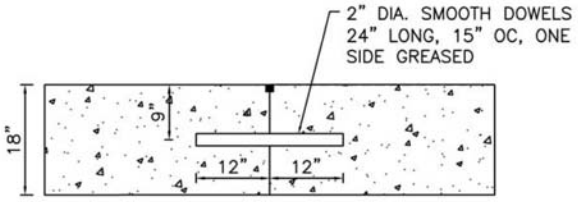

CONTRACTION JOINT - A

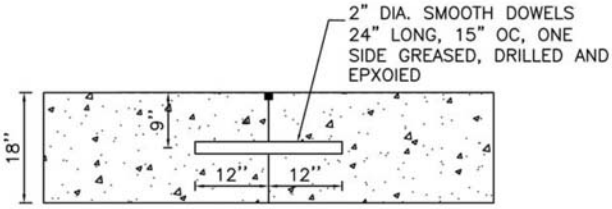

LONGITUDINAL CONSTRUCTION JOINT - B

TEST SITE 4-AC18

4-AC18

Site Description: The site is located on east coast of the United States. Elevations of the site, as indicated by USGS maps, are approximately 10 to 20 feet above sea level. The airport is surrounded by a rivers on three sides. Based on topographic information and observations, the site appears to be constructed on 5 to 10 feet of fill, overlying natural soils. The typical natural subgrade as indicated by USDA soil maps is 12 inches of material over 14 inches of gravelly sand, over 12 inches of loamy sand over gravelly loamy sand. The estimated PCI and SCI of the site is 79 and 79, respectively. The primary distress observed included low severity joint spall, and medium and high severity linear cracking.

Site Weather: The site is located in a wet/freeze climate zone. The below figures indicate the average temperature, average precipitation, average number of days above 90 degrees Fahrenheit, and average number of days below 32 degrees Fahrenheit.

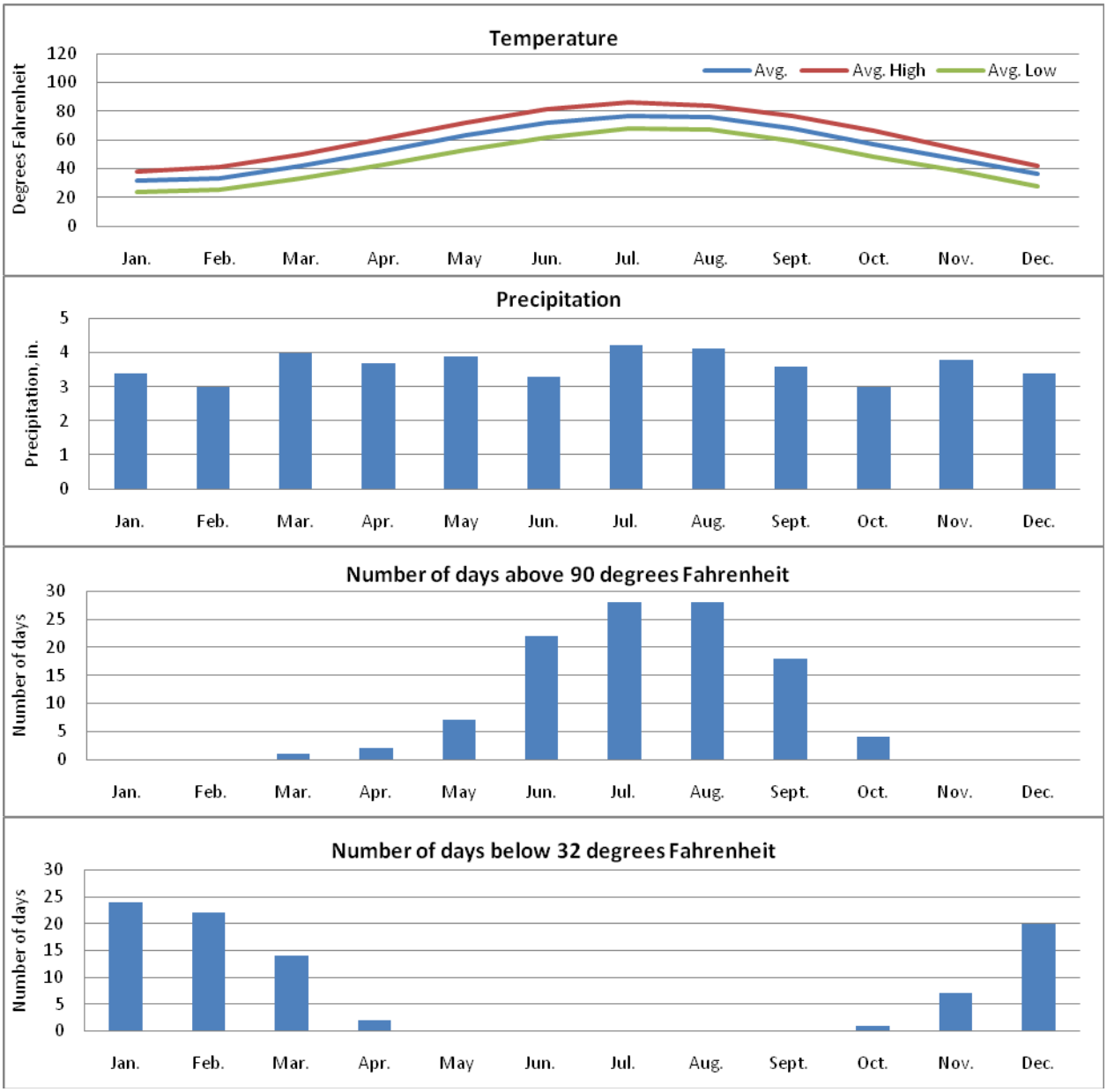

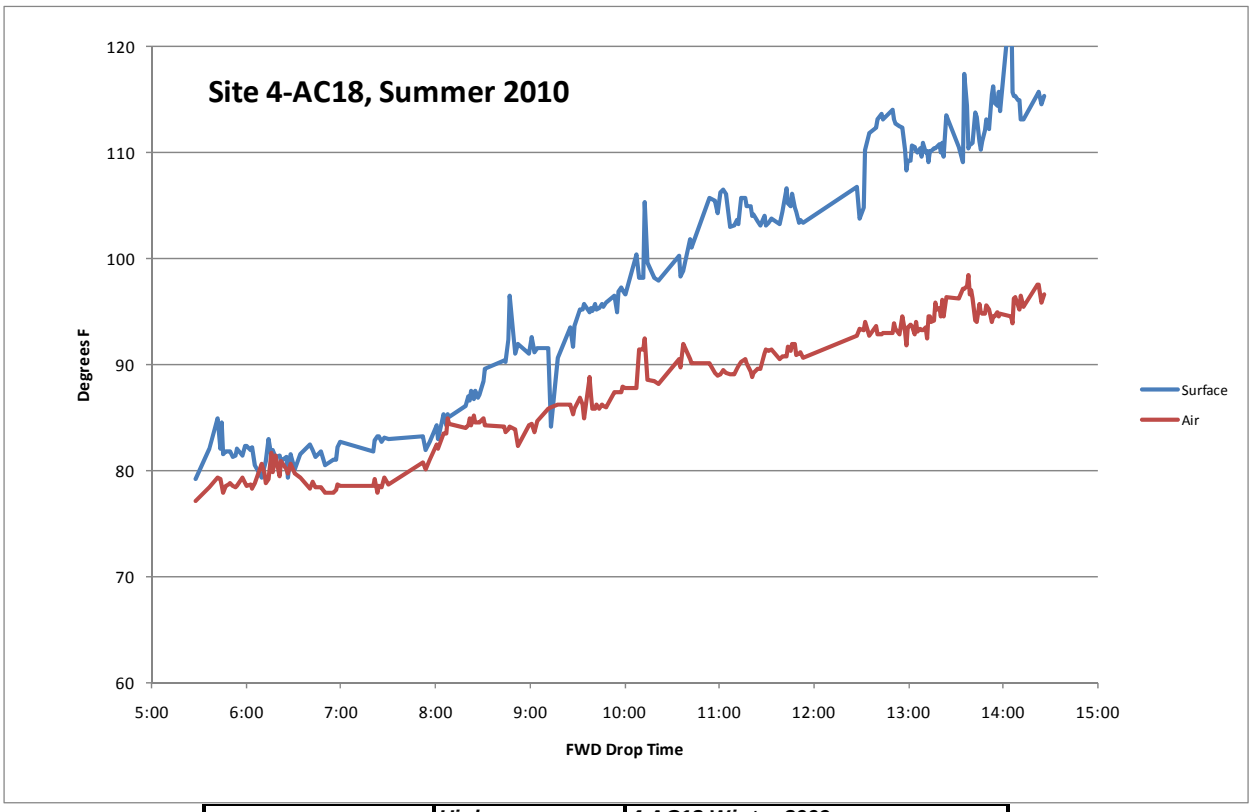

	Highway GPS3 55-3009	*4-AC18 Winter 2009* 8AM average	AM-PM Change
average curvature, ft^{-1}	0.000547	0.000040	0.000034
min. curvature	0.000203	-0.000310	0.000019
max. curvature	0.001077	0.000282	0.000045
st. dev. of curvature	0.00021	0.000214	0.000009
number of slabs	33	8	8

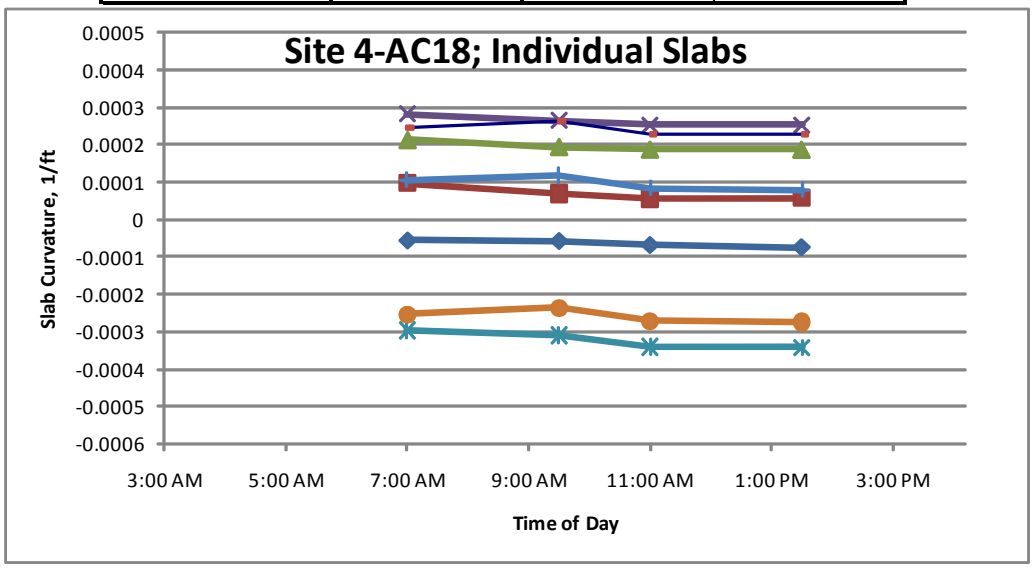

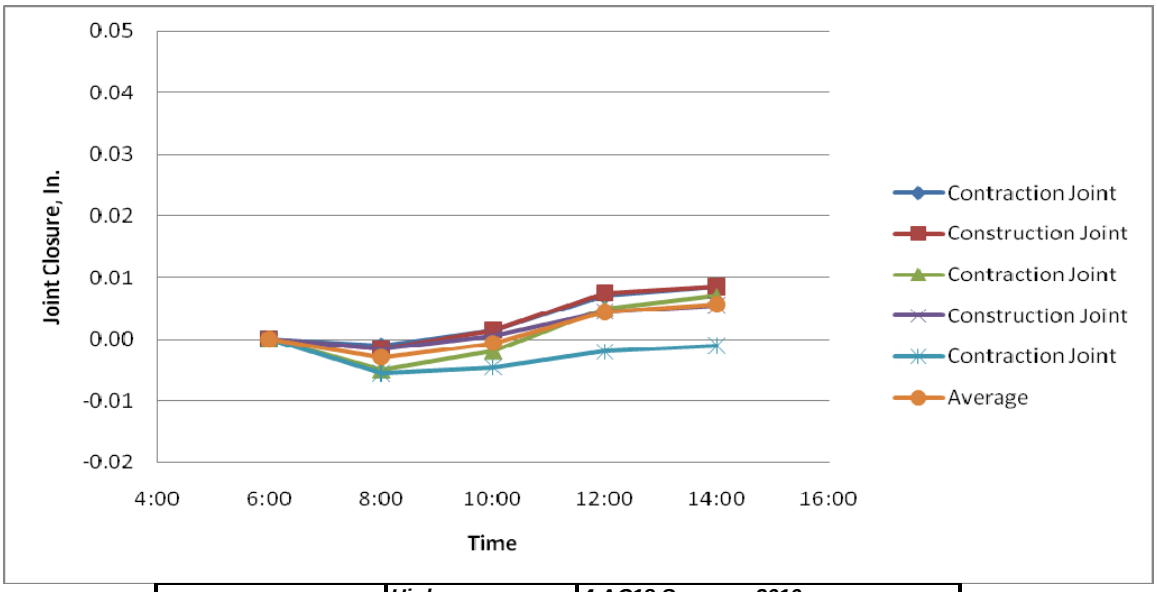

	Highway GPS3 55-3009	*4-AC18 Summer 2010* 8AM average	AM-PM Change
average curvature, ft^{-1}	0.000547	0.000005	0.000072
min. curvature	0.000203	-0.000342	0.000031
max. curvature	0.001077	0.000258	0.000097
st. dev. of curvature	0.00021	0.000238	0.000023
number of slabs	33	7	7

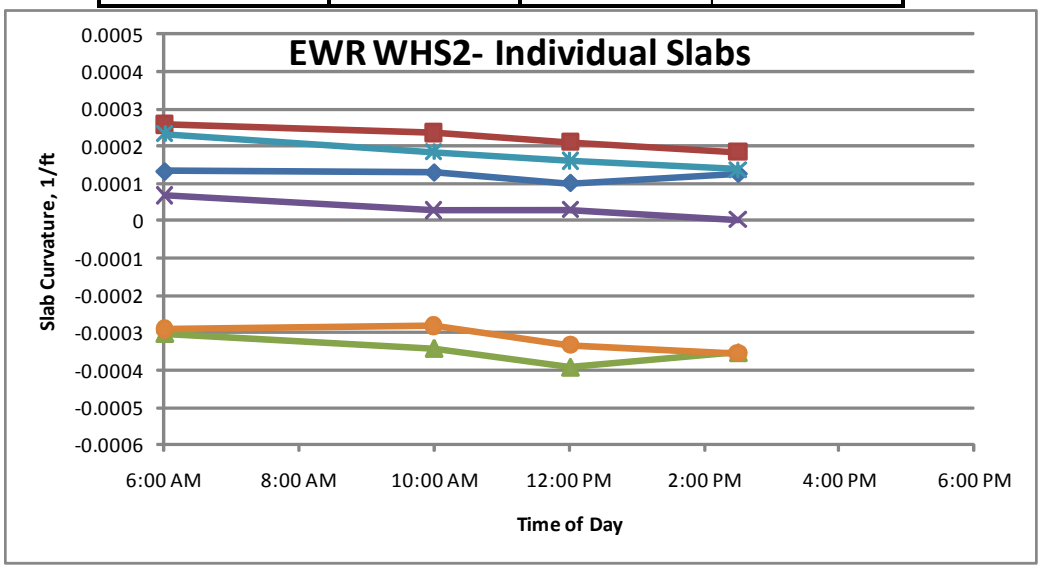

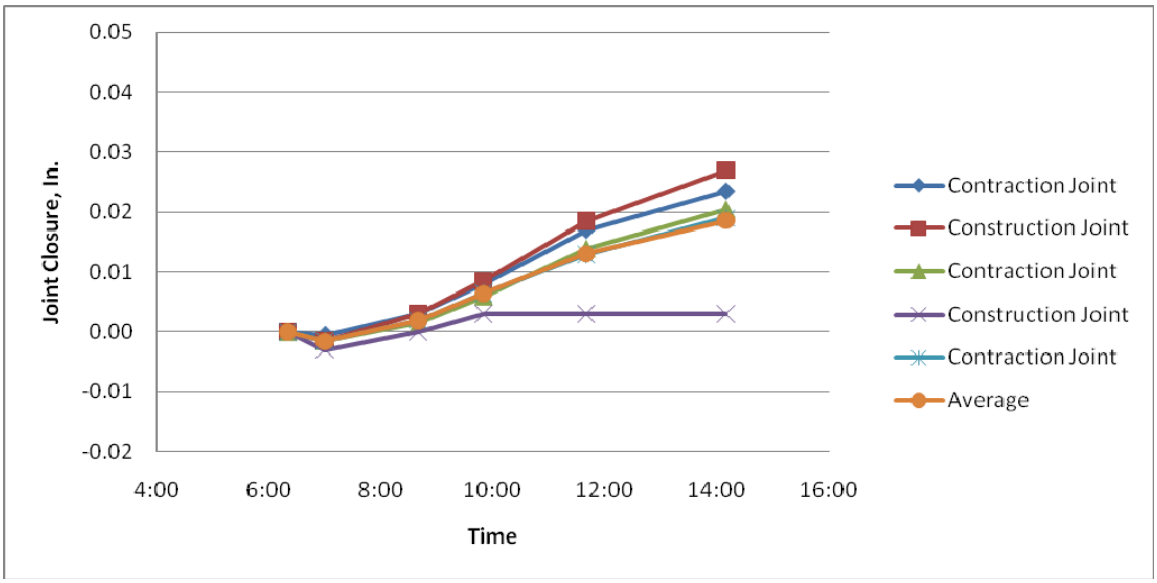

Site 4-AC18; ILLIBACK Summary Winter, 2009

	Dense Liquid				*Elastic Solid*				*Radius*
	***k*-value**	***k* stdev**	**Slab E_C**	**E_C Stdev**	**Subg. *E***	***E* stdev**	**Slab E_C**	**E_C Stdev**	**I-VALUES**
Min. Defl. =	342	30	8.14	0.65	69,854	4,108	6.43	0.38	58.7
Site Average	275	24	6.96	0.56	56,700	3,404	5.52	0.33	59.6
Max. Defl. =	236	21	5.97	0.5	48,743	3,133	4.74	0.3	59.6
Best Guess	**275** *psi/in*		**6.96** *Msi*		**56700** *psi*		**5.52** *Msi*		**59.56** *inches*

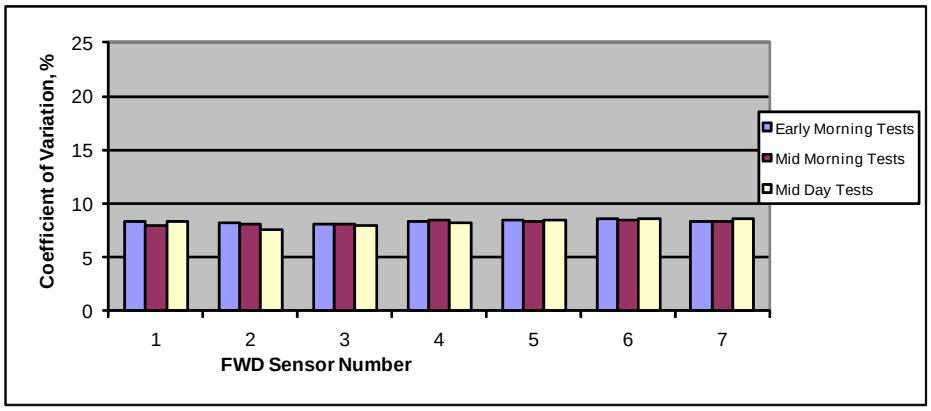

Site 4-AC18 ILLIBACK Summary- Summer 2010

	Dense Liquid				*Elastic Solid*				*Radius*
	***k*-value**	***k* stdev**	**Slab E_C**	**E_C Stdev**	**Subg. *E***	***E* stdev**	**Slab E_C**	**E_C Stdev**	**I-Values**
Site Average =	***305***	***28***	***6.27***	***0.53***	***60,178***	***3,725***	***4.93***	***0.31***	***56.5***
Site Min. =	332	24	9.28	0.64	69,831	3,471	7.42	0.37	61.1
Site Max =	273	27	4.84	0.45	52,159	3,539	3.77	0.26	54.5
Best Guess	**305**		**6.27**		**60178**		**4.93**		**56.5**
	psi/in		*Msi*		*psi*		*Msi*		*inches*

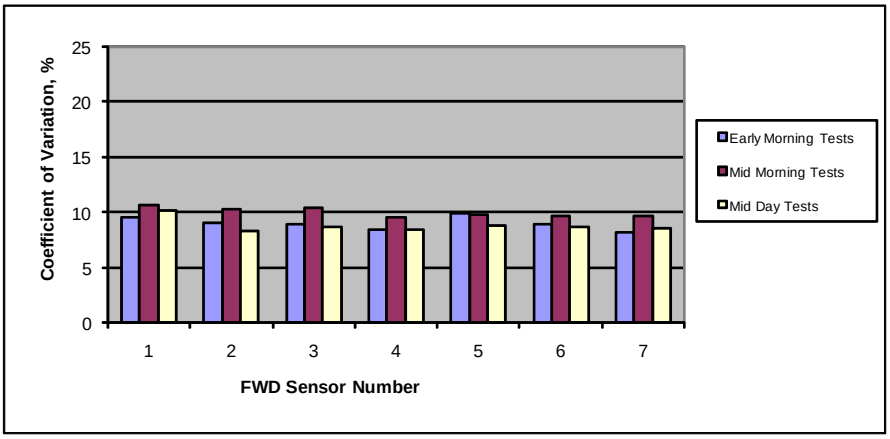

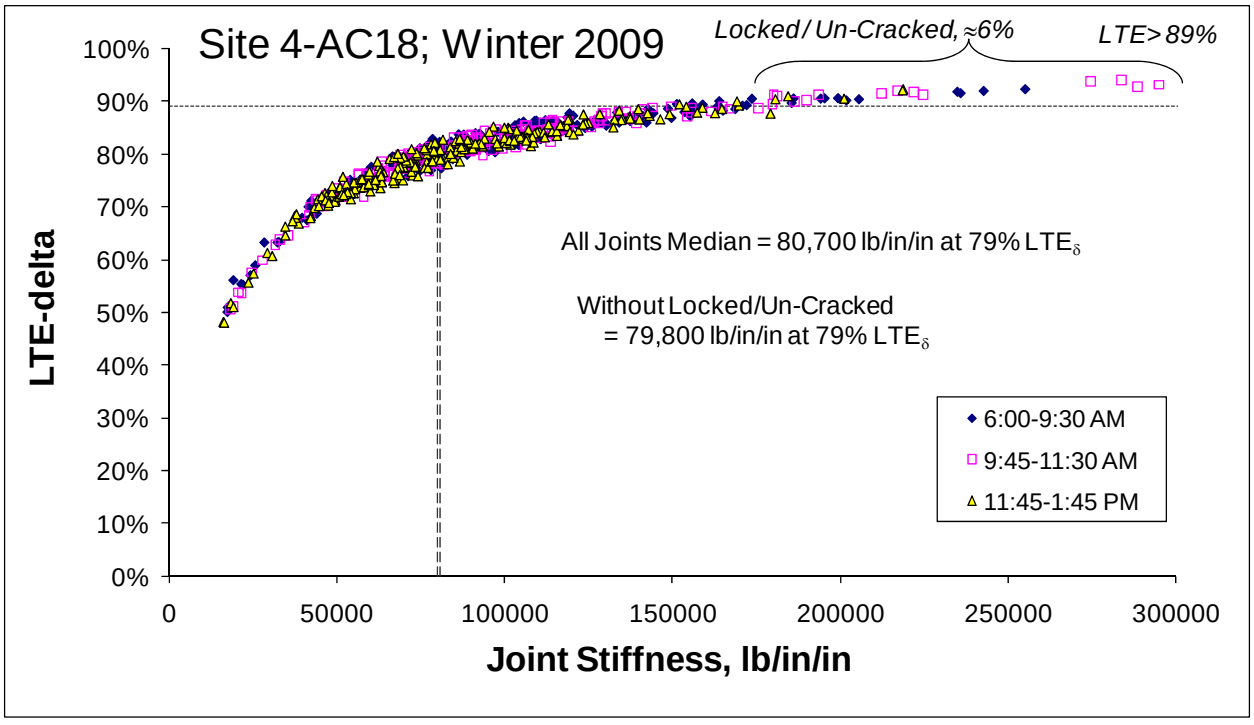

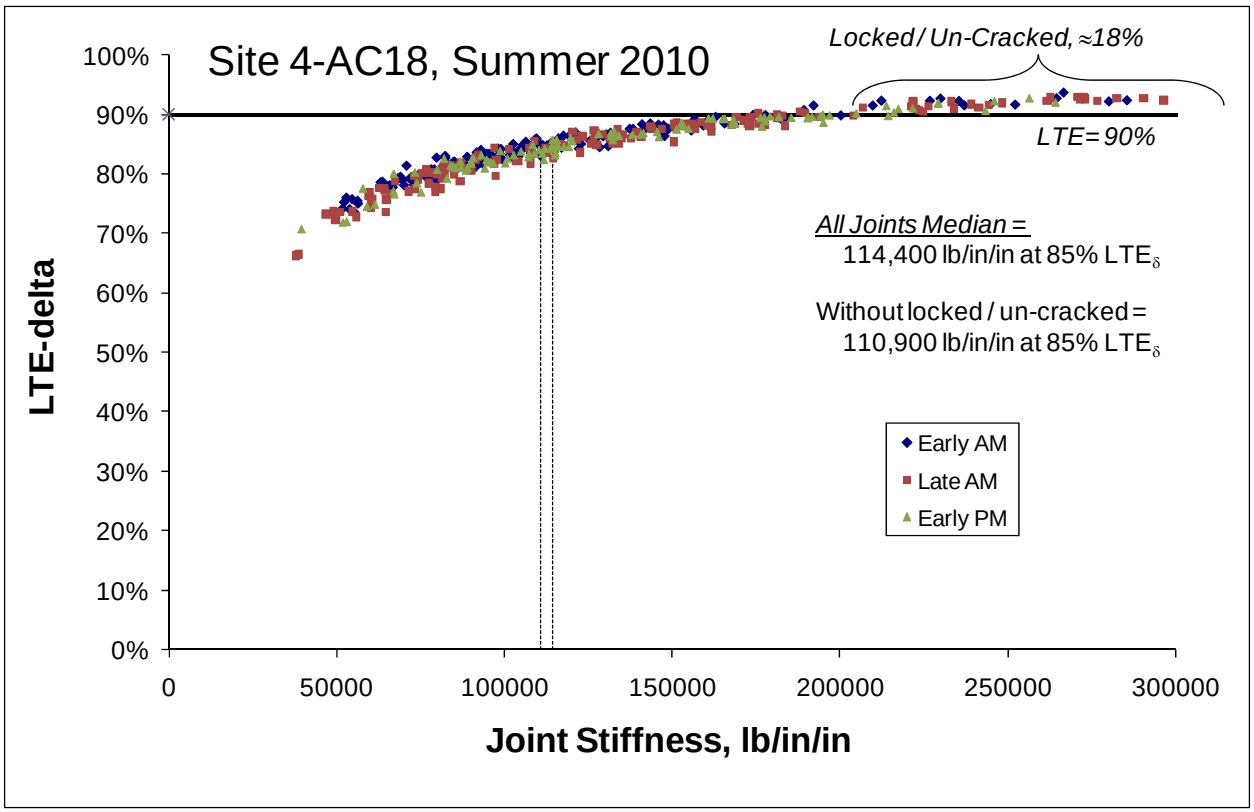
Site 4-AC18, Summer 2010
Locked / Un-Cracked, ≈18%
LTE = 90%
All Joints Median =
114,400 lb/in/in at 85% LTEδ
Without locked / un-cracked =
110,900 lb/in/in at 85% LTEδ
Early AM
Late AM
Early PM
LTE-delta
Joint Stiffness, lb/in/in
100%
90%
80%
70%
60%
50%
40%
30%
20%
10%
0%
0
50000
100000
150000
200000
250000
300000

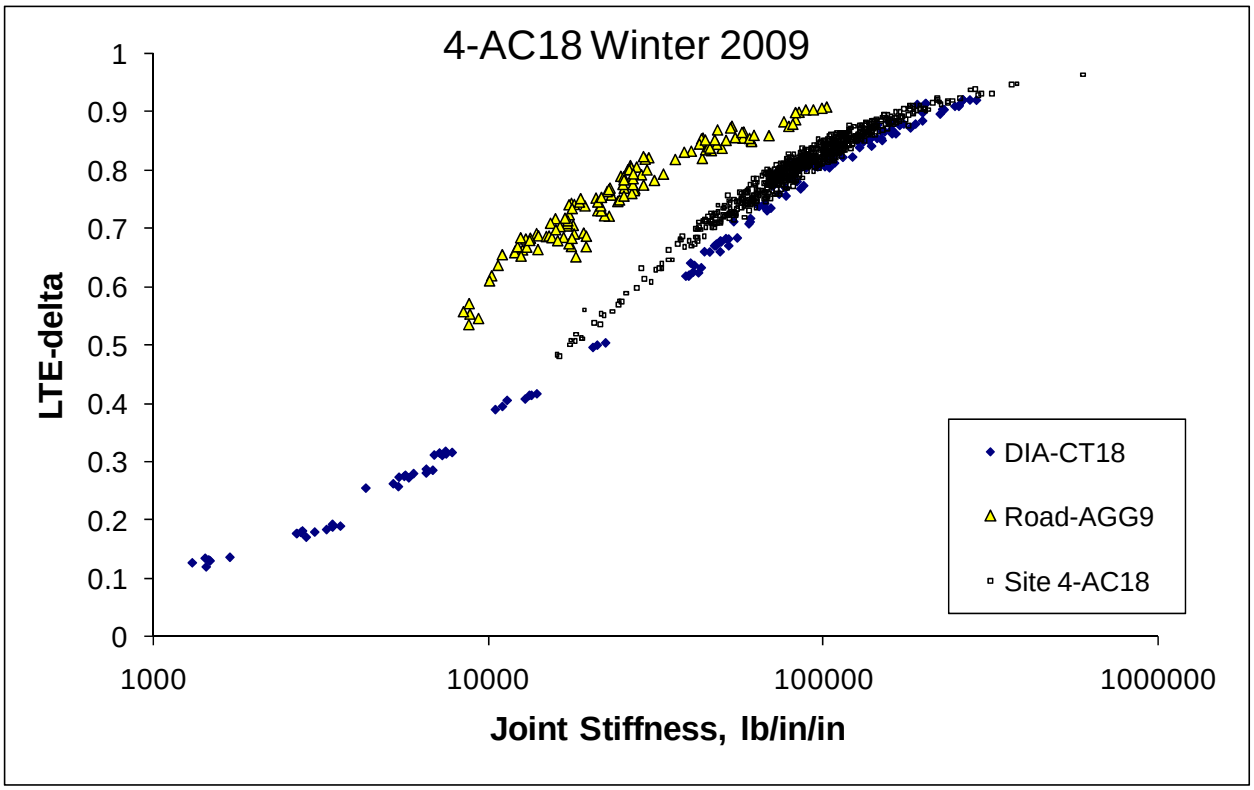
4-AC18 Winter 2009
DIA-CT18
Road-AGG9
Site 4-AC18
LTE-delta
Joint Stiffness, lb/in/in
1
0.9
0.8
0.7
0.6
0.5
0.4
0.3
0.2
0.1
0
1000
10000
100000
1000000

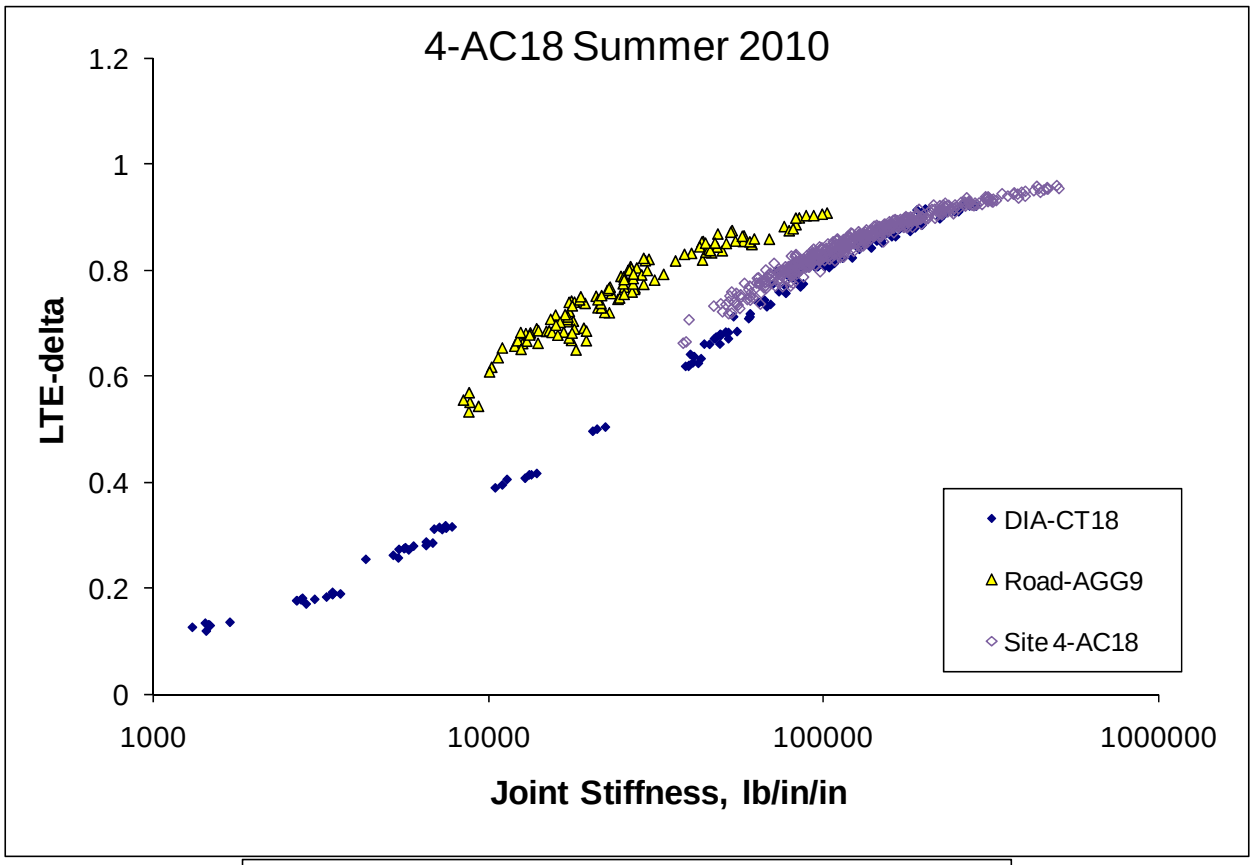
4-AC18 Summer 2010
LTE-delta
1.2
1
0.8
0.6
0.4
0.2
0
1000
10000
100000
1000000
Joint Stiffness, lb/in/in
DIA-CT18
Road-AGG9
Site 4-AC18

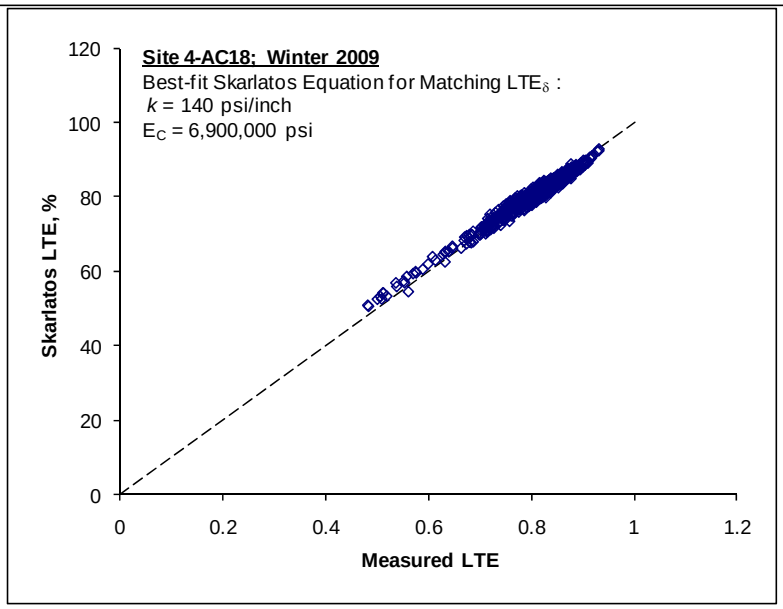
Site 4-AC18; Winter 2009
Best-fit Skarlatos Equation for Matching LTEδ :
k = 140 psi/inch
EC = 6,900,000 psi
Skarlatos LTE, %
120
100
80
60
40
20
0
0
0.2
0.4
0.6
0.8
1
1.2
Measured LTE

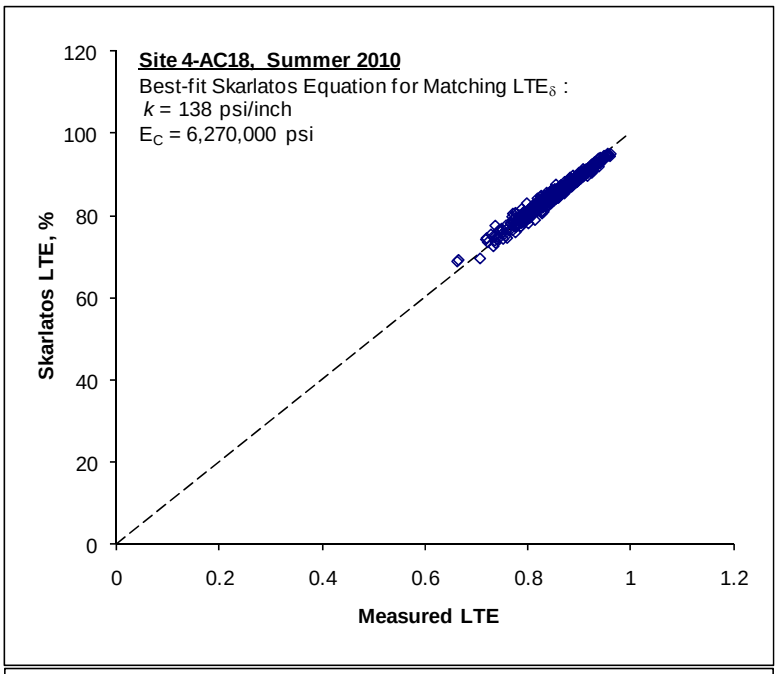
Site 4-AC18, Summer 2010
Best-fit Skarlatos Equation for Matching LTEδ :
k = 138 psi/inch
EC = 6,270,000 psi
Skarlatos LTE, %
Measured LTE
0
20
40
60
80
100
120
0
0.2
0.4
0.6
0.8
1
1.2

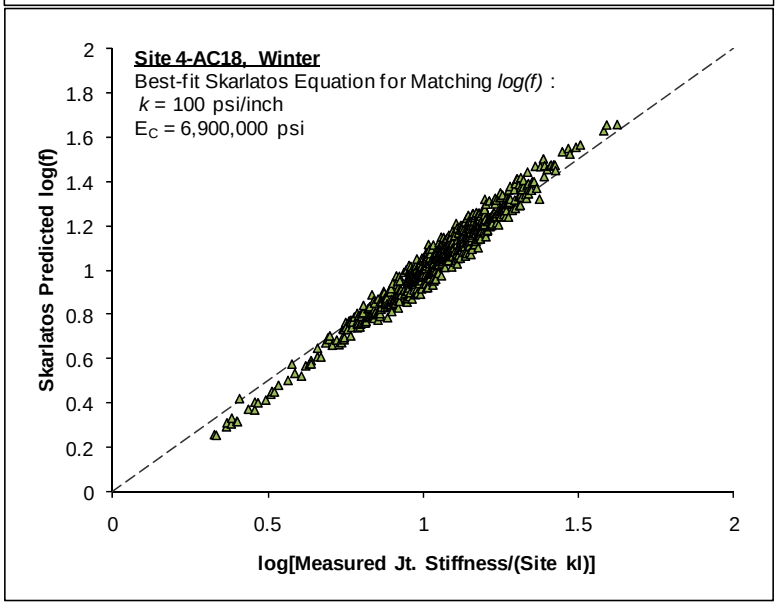
Site 4-AC18, Winter
Best-fit Skarlatos Equation for Matching log(f) :
k = 100 psi/inch
EC = 6,900,000 psi
Skarlatos Predicted log(f)
log[Measured Jt. Stiffness/(Site kl)]
0
0.2
0.4
0.6
0.8
1
1.2
1.4
1.6
1.8
2
0
0.5
1
1.5
2

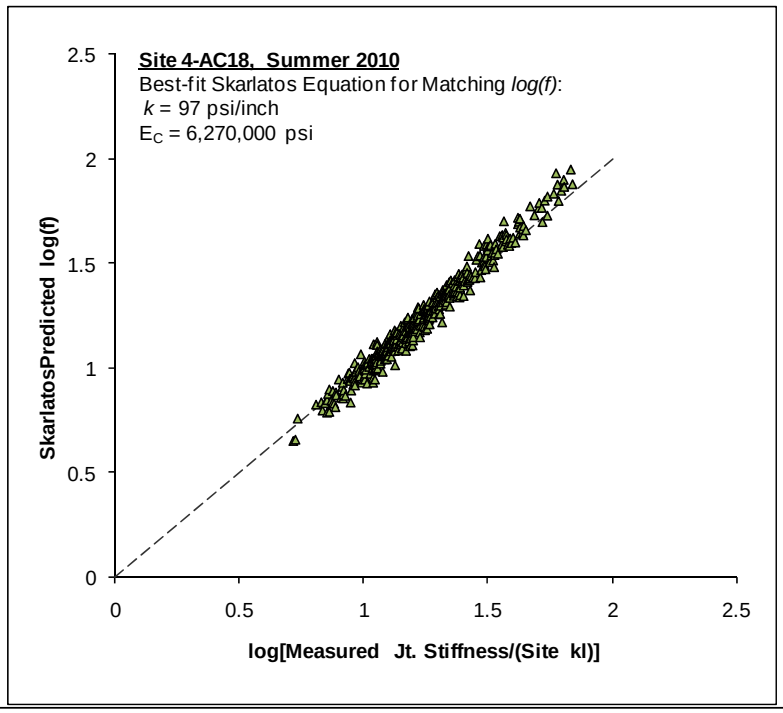
Site 4-AC18, Summer 2010
Best-fit Skarlatos Equation for Matching log(f):
k = 97 psi/inch
EC = 6,270,000 psi
SkarlatosPredicted log(f)
log[Measured Jt. Stiffness/(Site kl)]
0
0.5
1
1.5
2
2.5

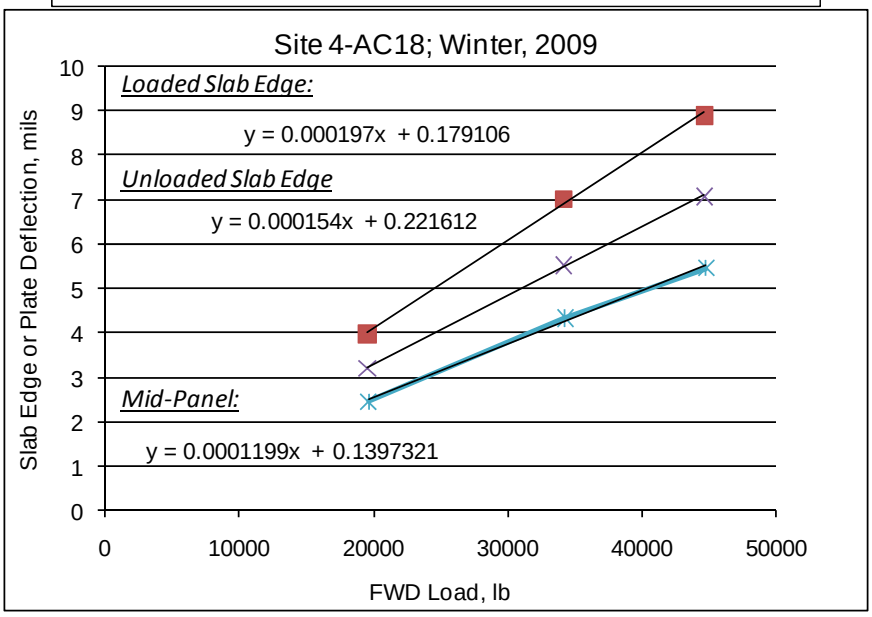
Site 4-AC18; Winter, 2009
Loaded Slab Edge:
y = 0.000197x + 0.179106
Unloaded Slab Edge
y = 0.000154x + 0.221612
Mid-Panel:
y = 0.0001199x + 0.1397321
Slab Edge or Plate Deflection, mils
FWD Load, lb
0
10000
20000
30000
40000
50000

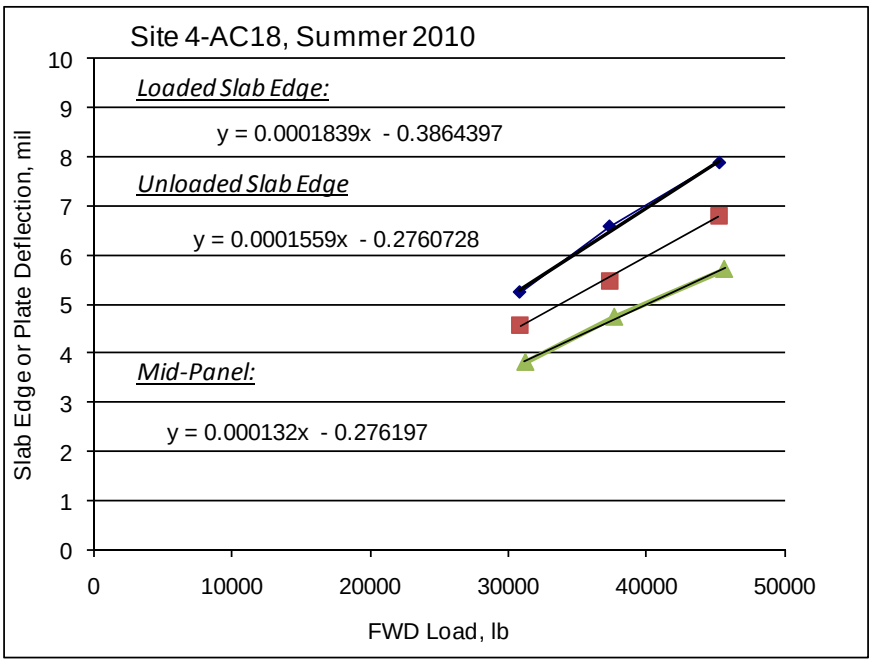

4-AC18 Winter 2009; Doweled Contraction Joints- including locked/un-cracked

	LR	LTE	Avg Stiffness
avg	148	84%	113380
Median	147	84%	103252
min	129	63%	31628
max	194	96%	596011
stdev	7	4%	50372

% possibly un-cracked, LTE>89% = 7%

Sawed, 2" dowels at 15"

Steel Area/ft = 2.513274
reinf. ratio = 1.16%

Without locked/un-cracked joints

	LR	LTE	Avg Stiffness
avg	148	83%	109027
Median	147	83%	101613
min	131	63%	31628
max	194	95%	377526
stdev	7	4%	41025

% possibly un-cracked, LTE>89% = 5%

Probable Agg Interlock = 0 to 100000

$$k = \frac{1}{s\left(\frac{\varpi}{0.9 G_d A_d} + \frac{\varpi^3}{12 E_d I_d} + \frac{2+\beta\varpi}{2\beta^3 E_d I_d}\right)}$$

s is the dowel bar spacing =	15	in
w is the joint opening =	0.1	in
Dowel Diameter =	2	in
Ad is the dowel cross-sectional area =	3.14	sq in
Ed =	29000000	psi
Gd =	11153846	psi
Id =	0.785	in^4
Back-Calculated Dowel-Concrete Interaction modulus, DCI =	1279760	psi

$$\beta = \sqrt[4]{\frac{Kd}{4 E_d I_d}} = 0.409$$

Doweled Joint Stiffness = **101613** lb/in/in

4-AC18 Summer 2010; Doweled Contraction Joints- including locked/un-cracked

	LR	LTE	Avg Stiffness
avg	155	86%	150102
min	137	66%	37957
max	190	96%	495578
stdev	10	5%	85148
Median	154	86%	126997

% possibly un-cracked, LTE>91% = 18%

Sawed, 2" dowels at 15"

Steel Area/ft = 2.513274

reinf. ratio = 1.16%

Without locked / un-cracked joints

	LR	LTE	Avg Stiffness
avg	155	85%	138472
min	137	66%	37957
max	190	96%	466039
stdev	10	5%	72672
Median	154	85%	117726

% possibly un-cracked, LTE>86% = 12%

Probable Agg Interlock = >17000 to 117000

$$k = \frac{1}{s\left(\frac{\varpi}{0.9G_dA_d} + \frac{\varpi^3}{12E_dI_d} + \frac{2+\beta\varpi}{2\beta^3E_dI_d}\right)}$$

s is the dowel bar spacing =	15	in
w is the joint opening =	0.1	in
Dowel Diameter =	2	in
Ad is the dowel cross-sectional area =	3.14	sq in
Ed =	29000000	psi
Gd =	11153846	psi
Id =	0.785	in^4
Back-Calculated Dowel-Concrete Interaction modulus, DCI =	1560993	psi

$$\beta = \sqrt[4]{\frac{Kd}{4E_dI_d}} = 0.430$$

Doweled Joint Stiffness = **117726** lb/in/in

4-AC18 Winter 2009; Doweled Construction Joints- No locked or un-cracked joints detected

	LR	LTE	Avg Stiffness
avg	146	75%	65720
Median	146	76%	66365
min	130	48%	16060
max	180	87%	155378
stdev	6	8%	24466

% possibly un-cracked, LTE>89% = 1%

Formed, 2" dowels at 15"

Steel Area/ft = 2.513274

reinf. ratio = 1.16%

Probable Agg Interlock = 0 to 60000

$$k = \frac{1}{s\left(\frac{\varpi}{0.9G_dA_d} + \frac{\varpi^3}{12E_dI_d} + \frac{2+\beta\varpi}{2\beta^3E_dI_d}\right)}$$

s is the dowel bar spacing =	15	in
w is the joint opening =	0.1	in
Dowel Diameter =	2	in
Ad is the dowel cross-sectional area =	3.14	sq in
Ed =	29000000	psi
Gd =	11153846	psi
Id =	0.785	in^4
Back-Calculated Dowel-Concrete Interaction modulus, DCI =	720971	psi

$$\beta = \sqrt[4]{\frac{Kd}{4E_dI_d}} = 0.355$$

Doweled Joint Stiffness = **66365** lb/in/in

4-AC18 Summer 2010; Doweled Construction Joints- Including locked or un-cracked joints

	LR	LTE	Avg Stiffness
avg	146	84%	137446
min	131	71%	39519
max	186	96%	503318
stdev	9	6%	83117
Median	144	84%	109224

% possibly un-cracked, LTE>89% = 18%

Formed, 2" dowels at 15"

Steel Area/ft = 2.513274

reinf. ratio = 1.16%

limiting dowel k = 1300000

Without locked / un-cracked joints

	LR	LTE	Avg Stiffness
avg	146	84%	130215
min	131	71%	39519
max	186	96%	503318
stdev	10	6%	78744
Median	144	84%	104306

% possibly un-cracked, LTE>86% = 14%

Probable Agg Interlock = >40000 to 100000

$$k = \frac{1}{s\left(\frac{\varpi}{0.9G_d A_d} + \frac{\varpi^3}{12E_d I_d} + \frac{2+\beta\varpi}{2\beta^3 E_d I_d}\right)}$$

s is the dowel bar spacing =	15	in
w is the joint opening =	0.1	in
Dowel Diameter =	2	in
Ad is the dowel cross-sectional area =	3.14	sq in
Ed =	29000000	psi
Gd =	11153846	psi
Id =	0.785	in^4

Back-Calculated Dowel-Concrete Interaction modulus, DCI = 1325730 psi (5-8 msi)

$$\beta = \sqrt[4]{\frac{Kd}{4E_d I_d}} = 0.413$$

Doweled Joint Stiffness = **104306** lb/in/in

Site 4-AC18 Winter 2009; Corners- No locked / un-cracked joints detected

	LR	LTE	Avg Stiffness
avg	137	74%	51771
min	119	26%	2082
max	213	87%	99006
stdev	15	11%	22465
Median	133	77%	48761

% possibly un-cracked, LTE>86% = 2%

Doweled on Both Edges

Site 4-AC18 Summer 2010; Corners- Including locked / un-cracked joints

	LR	LTE	Avg Stiffness
avg	149	86%	123081
min	127	67%	26683
max	183	96%	475071
stdev	12	5%	84295
Median	149	86%	98584

possibly un-cracked, LTE>91% = 16%

Doweled on all Edges

Without locked / un-cracked

	LR	LTE	Avg Stiffness
avg	149	85%	117355
min	127	67%	26683
max	183	96%	475071
stdev	12	5%	77550
Median	147	86%	96799

% possibly un-cracked, LTE>86% = 13

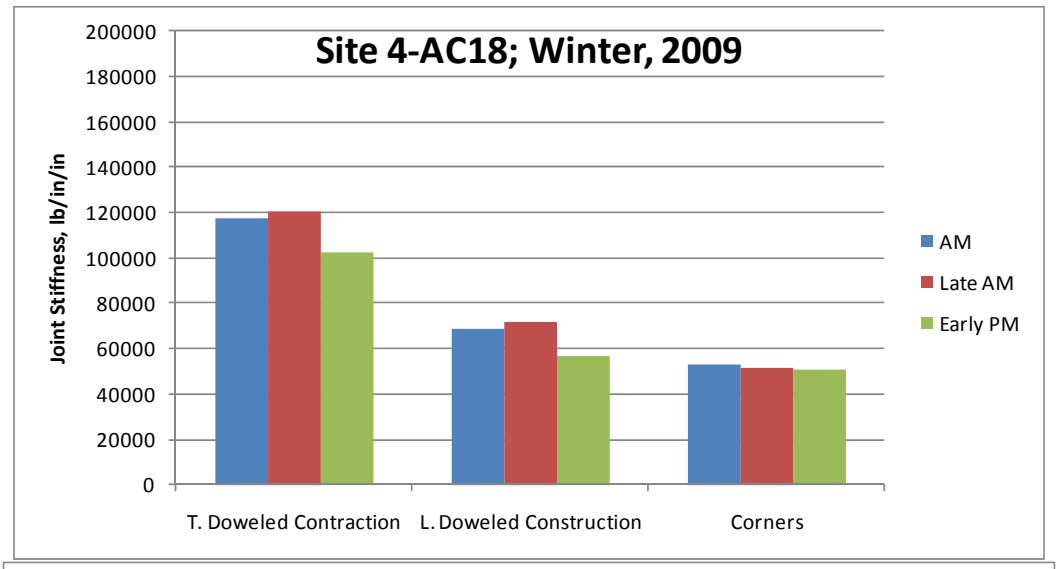
Site 4-AC18; Winter, 2009
Joint Stiffness, lb/in/in
200000
180000
160000
140000
120000
100000
80000
60000
40000
20000
0
T. Doweled Contraction
L. Doweled Construction
Corners
AM
Late AM
Early PM

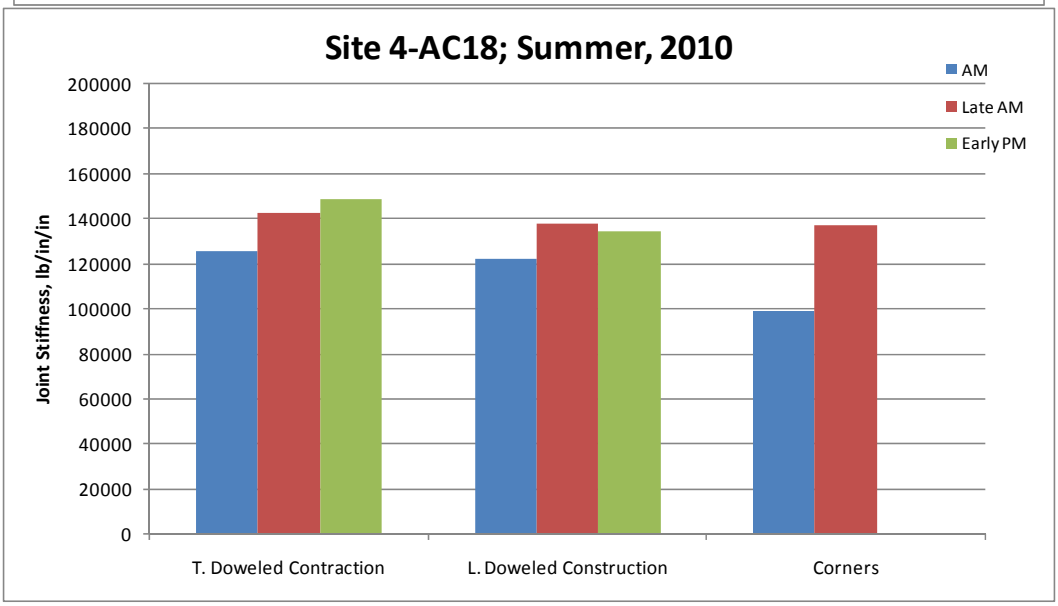
Site 4-AC18; Summer, 2010
Joint Stiffness, lb/in/in
200000
180000
160000
140000
120000
100000
80000
60000
40000
20000
0
T. Doweled Contraction
L. Doweled Construction
Corners
AM
Late AM
Early PM

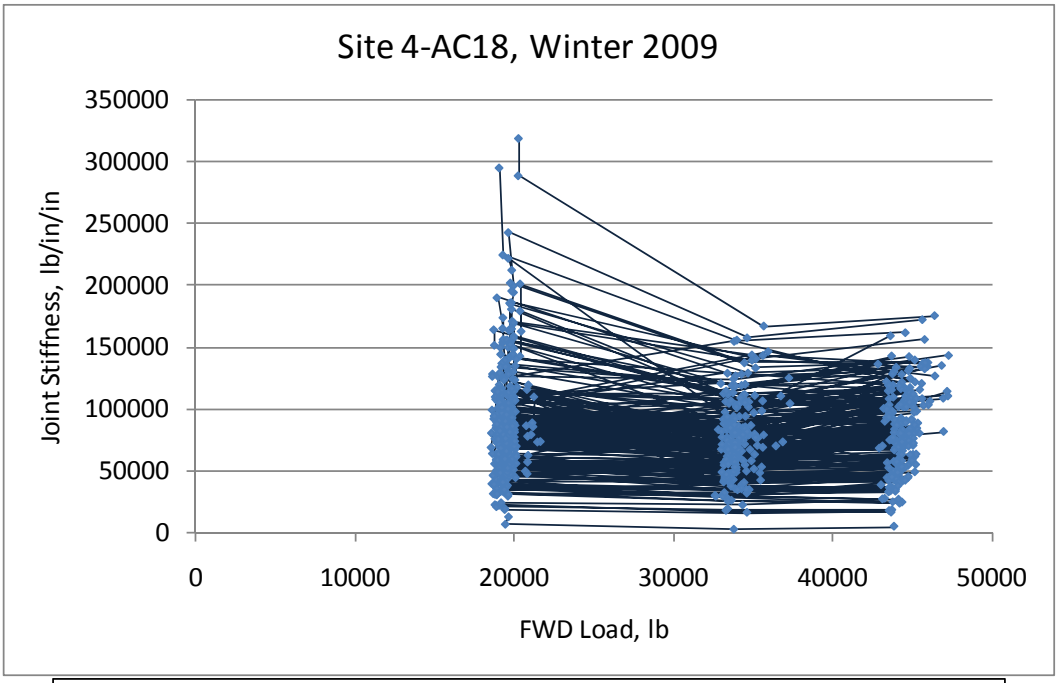
Site 4-AC18, Winter 2009
Joint Stiffness, lb/in/in
350000
300000
250000
200000
150000
100000
50000
0
0
10000
20000
30000
40000
50000
FWD Load, lb

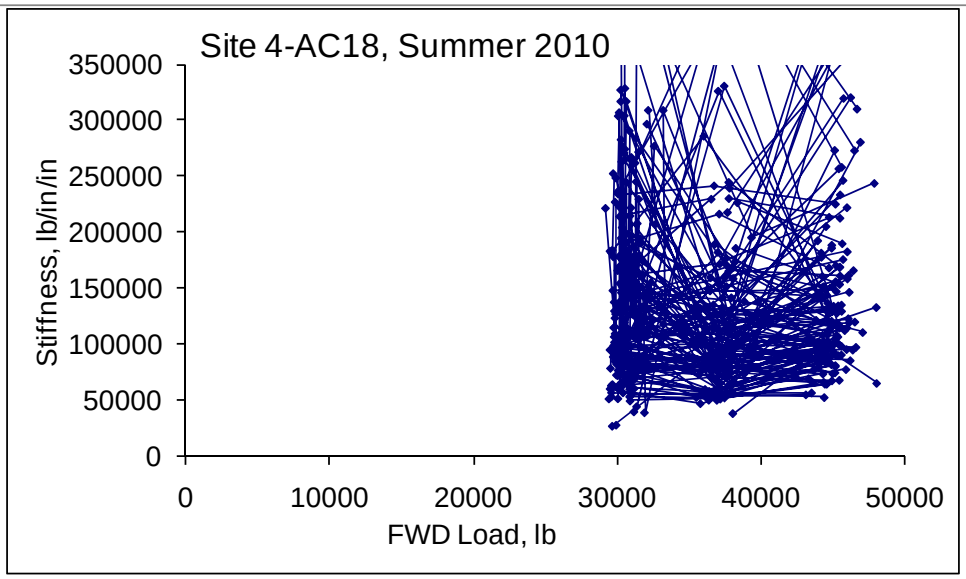
Site 4-AC18, Summer 2010
Stiffness, lb/in/in
350000
300000
250000
200000
150000
100000
50000
0
0
10000
20000
30000
40000
50000
FWD Load, lb

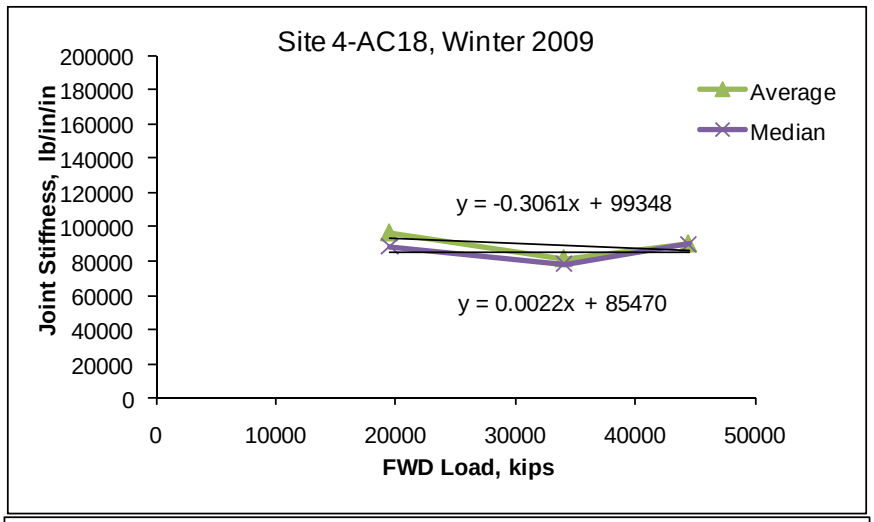

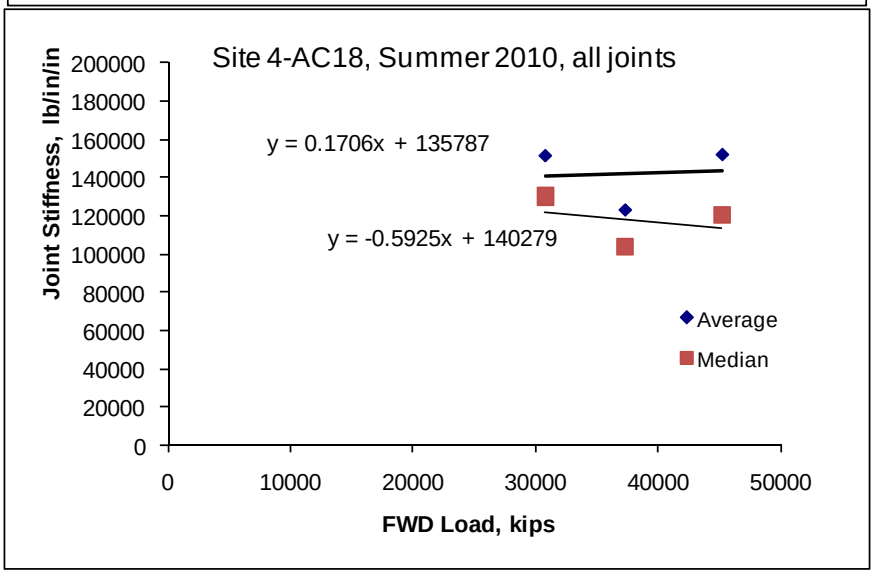

Site 4-AC18; Winter 2009, Edge Gaps- All Joints

	All	AM	Mid	PM
Avg	0.15	0.20	0.11	0.14
Min	-1.71	-0.26	-1.71	-0.78
Max	2.62	2.62	0.49	0.89
Stdev	0.32	0.35	0.29	0.32

Site 4-AC18, Summer 2010 Edge Gaps, all joints

	All	AM	Mid	PM
Avg	-0.25	-0.42	-0.10	-0.18
Min	-3.73	-1.88	-3.73	-2.55
Max	5.60	5.60	1.49	1.12
Stdev	1.07	1.11	1.07	0.97

Site 4-AC18; Winter 2009

Looseness	All Good Data	Contraction	Construction	Corners
Average	-0.06	-0.01	-0.21	-0.07
Maximum	2.60	0.53	0.47	0.46
Minimum	-1.63	-1.63	-0.78	-1.05
Std. Dev.	0.35	0.27	0.23	0.33
Count	203	96	60	24
19.5 kip %	-2%	0%	-6%	-2%
34.2 kip %	-1%	0%	-4%	-1%
44.5 kip %	-1%	0%	-3%	-1%

Site 4-AC18, Summer 2010

Looseness	*All Data*	*E-Joint*	*w-Joint*	*n-joint*	*s-joint*	*Corners*
Average	0.00	0.11735	-0.10	-0.42	0.03	0.37
Maximum	6.97	1.74	1.00	1.71	2.45	6.97
Minimum	-2.69	-1.62	-1.82	-1.97	-2.69	-1.42
Std. Dev.	1.13	0.79	0.74	1.04	1.15	1.65
Count	121	27	23	24	23	24

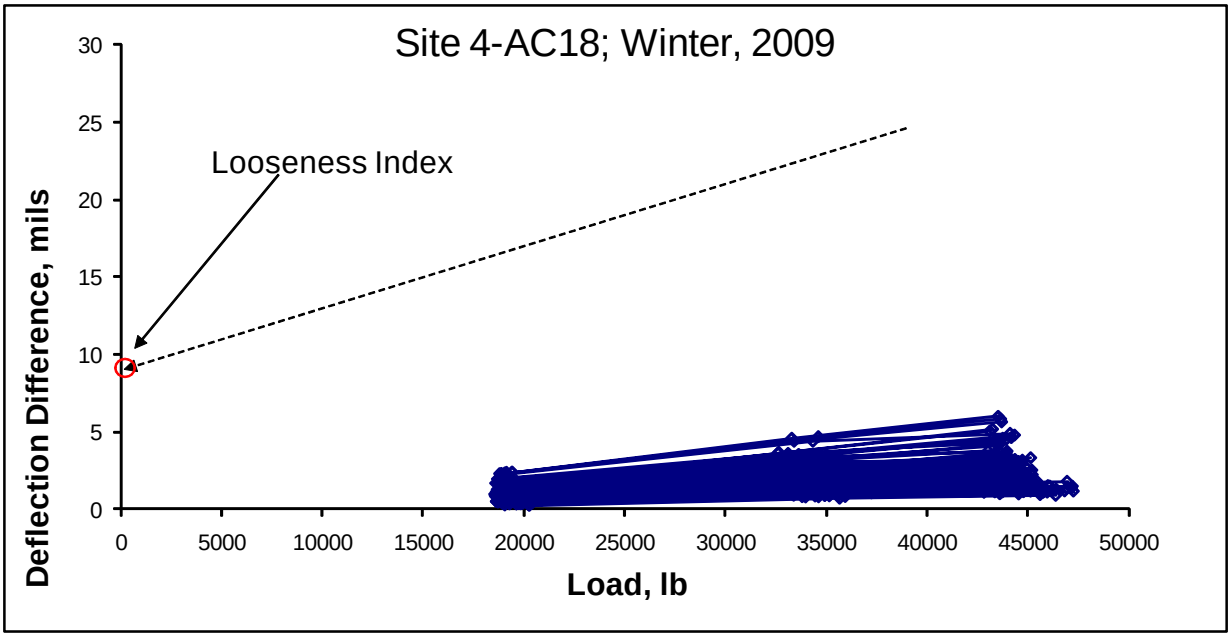
Site 4-AC18; Winter, 2009
Looseness Index
Deflection Difference, mils
Load, lb
0
5
10
15
20
25
30
0
5000
10000
15000
20000
25000
30000
35000
40000
45000
50000

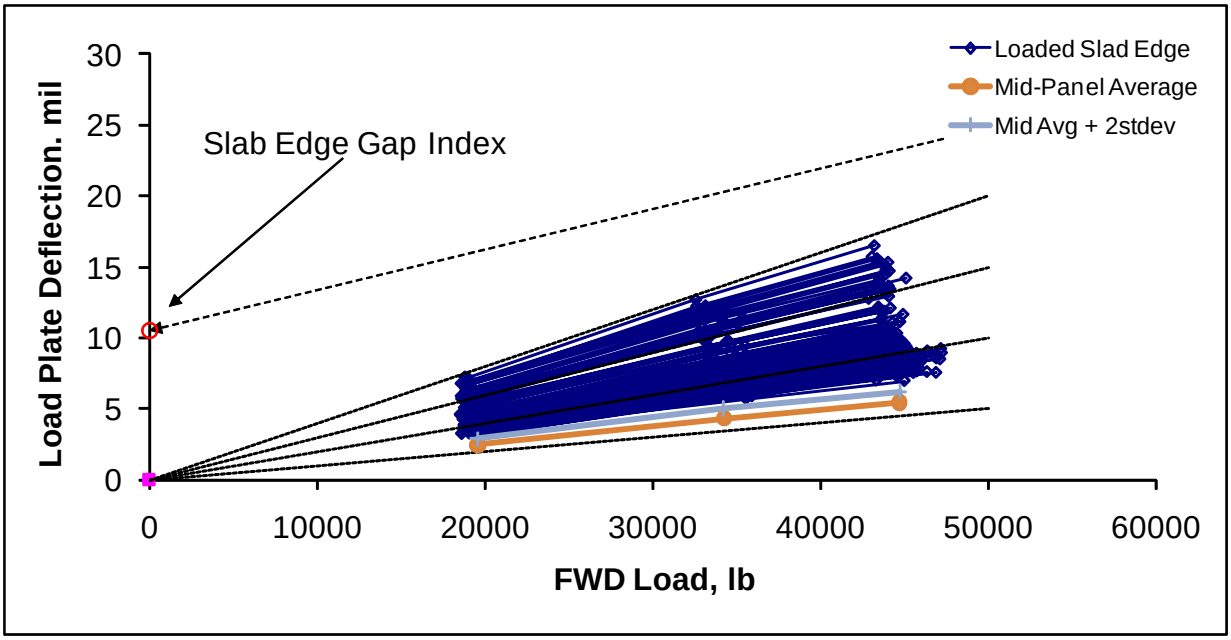
Loaded Slad Edge
Mid-Panel Average
Mid Avg + 2stdev
Slab Edge Gap Index
Load Plate Deflection. mil
FWD Load, lb
0
5
10
15
20
25
30
0
10000
20000
30000
40000
50000
60000

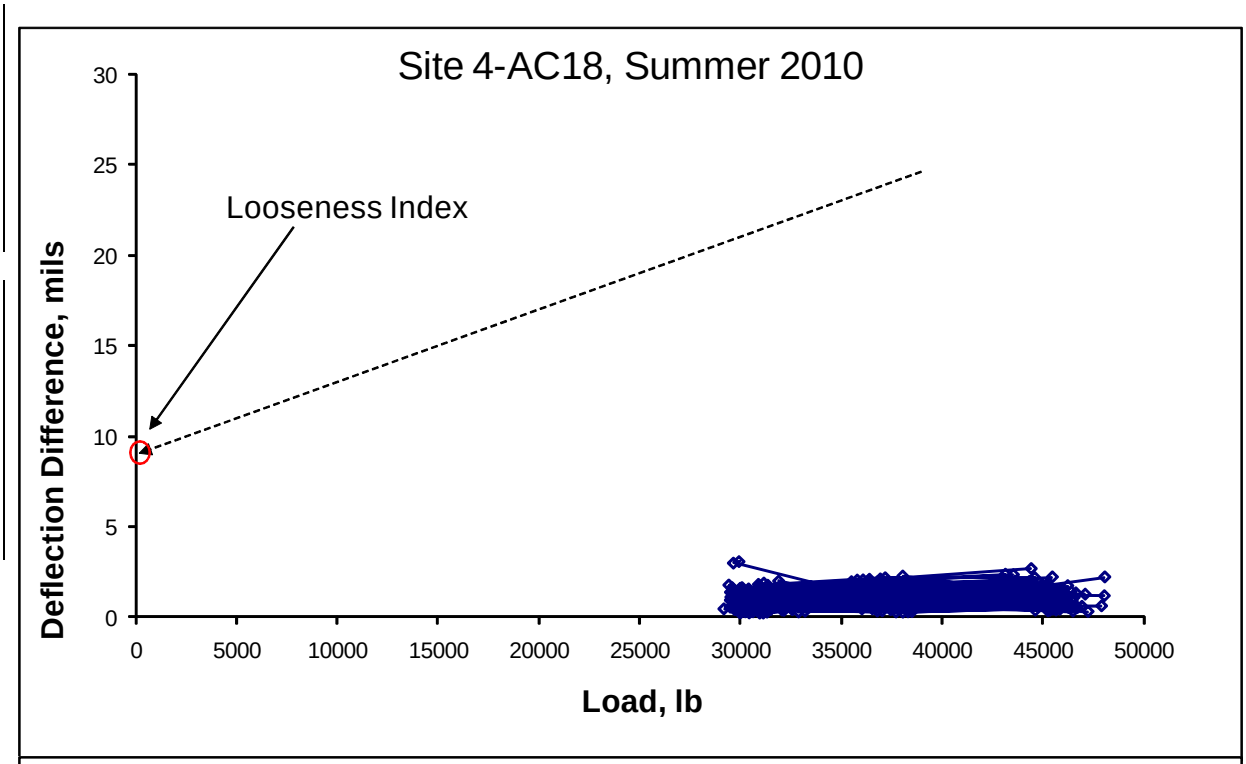
Site 4-AC18, Summer 2010
Looseness Index
Deflection Difference, mils
Load, lb
0
5
10
15
20
25
30
0
5000
10000
15000
20000
25000
30000
35000
40000
45000
50000

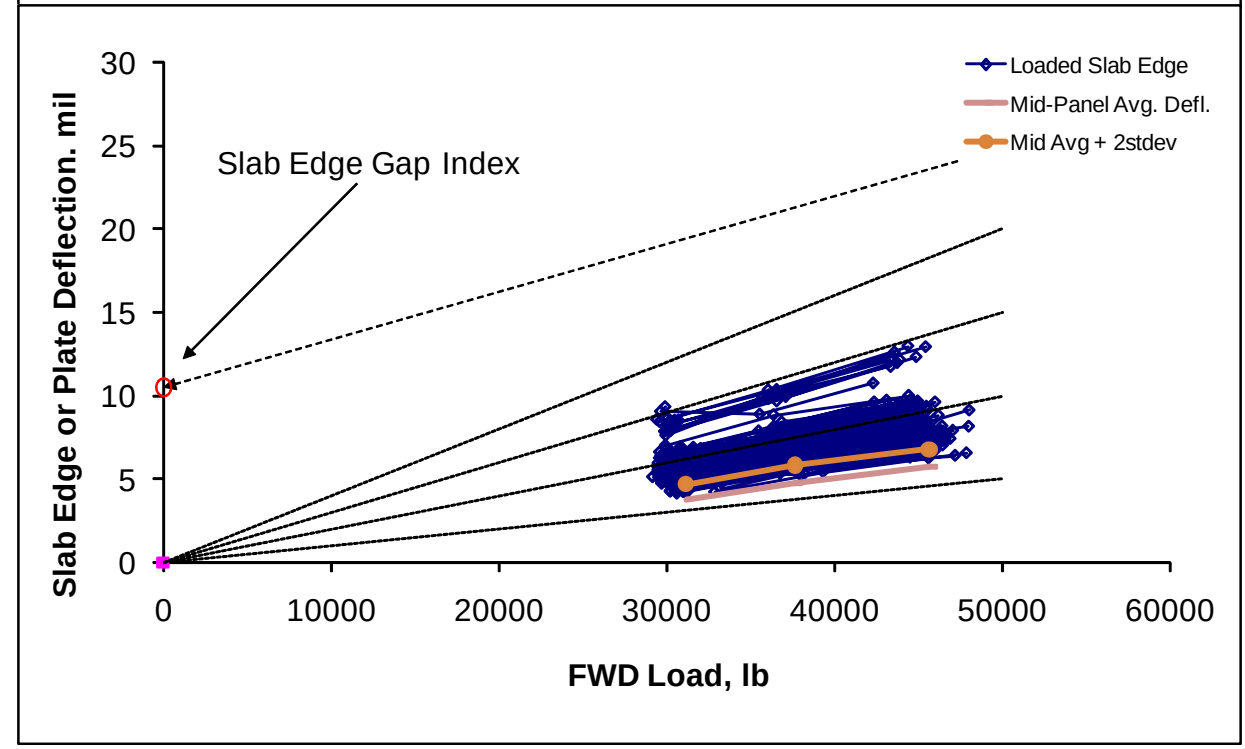
Slab Edge Gap Index
Loaded Slab Edge
Mid-Panel Avg. Defl.
Mid Avg + 2stdev
Slab Edge or Plate Deflection. mil
FWD Load, lb
0
5
10
15
20
25
30
0
10000
20000
30000
40000
50000
60000

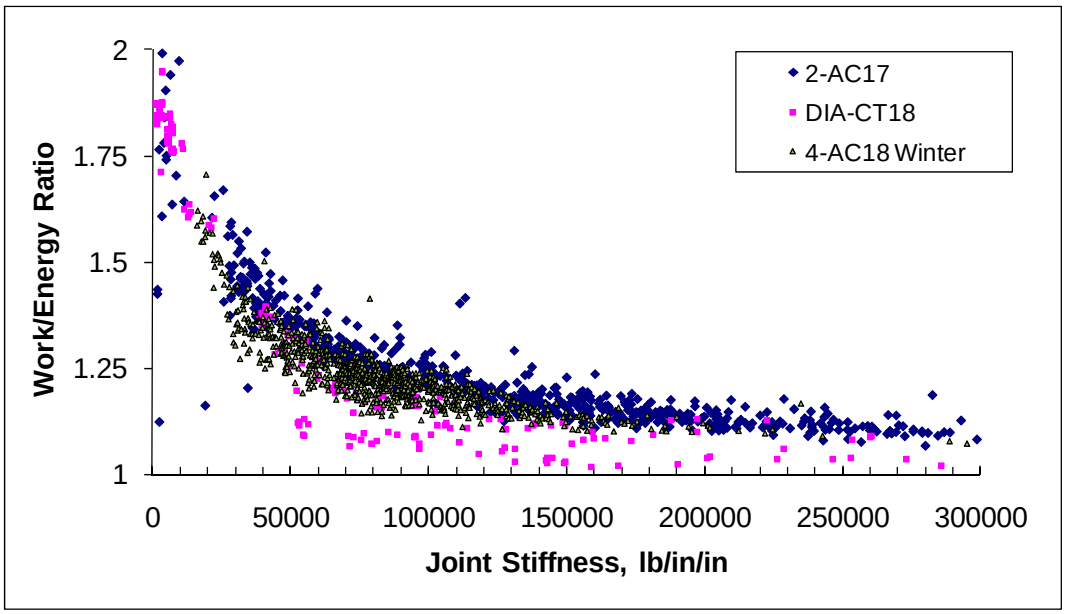
2
1.75
1.5
1.25
1
Work/Energy Ratio
0
50000
100000
150000
200000
250000
300000
Joint Stiffness, lb/in/in
2-AC17
DIA-CT18
4-AC18 Winter

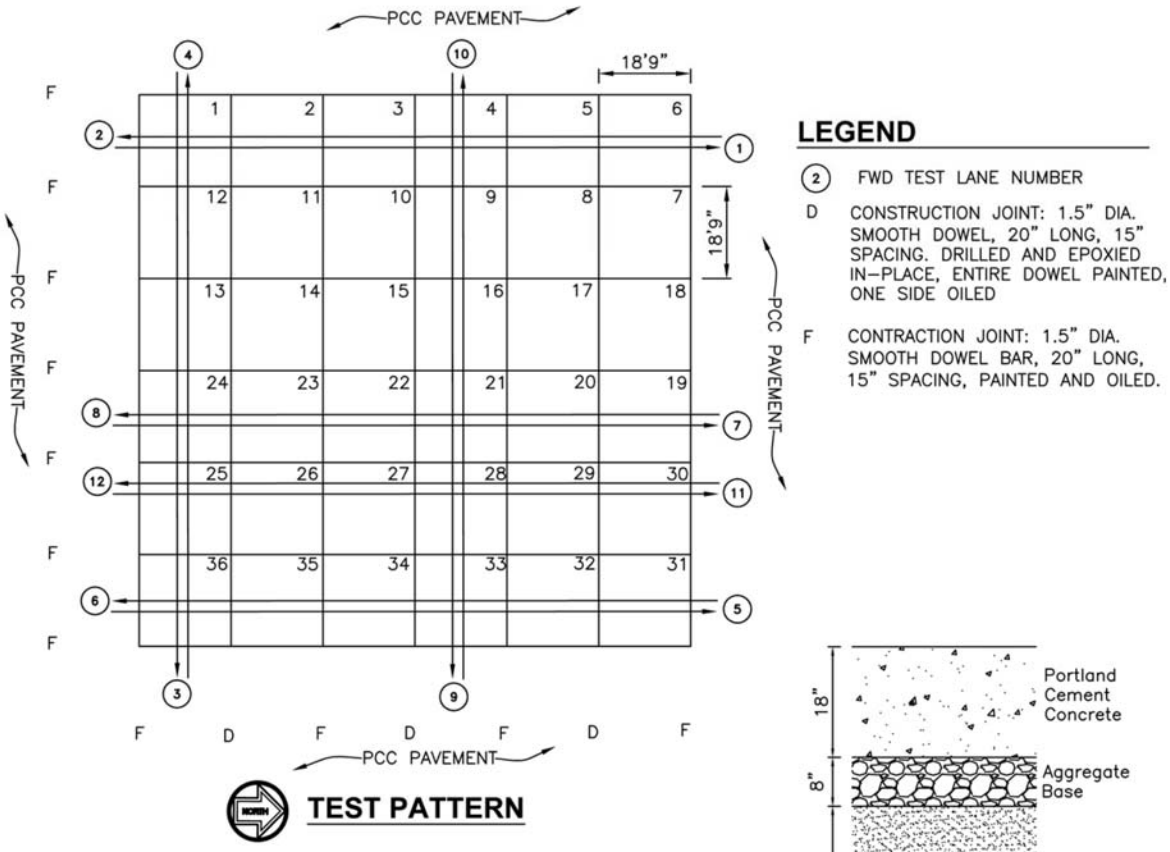

5-AGG18

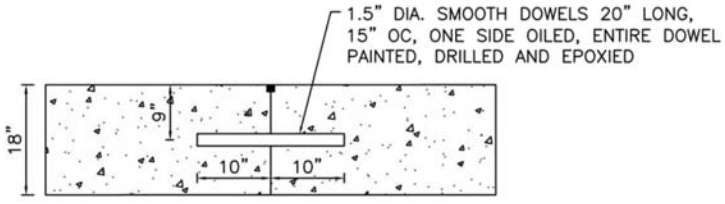

LONGITUDINAL CONSTRUCTION JOINT - D

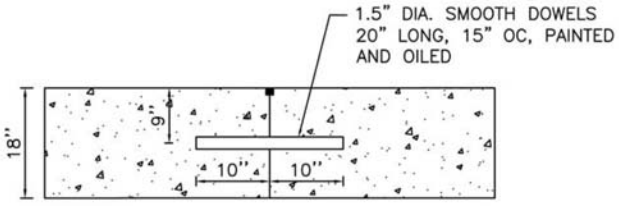

CONTRACTION JOINT - F

TEST SITE 5-AGG18

5-AGG18

Site Description: The site is located in the south west region of the United States. Elevations of the site, as indicated by USGS maps, are approximately 1110 to 1120 feet above sea level. The airport is located in a urban area near the top bank of a dry river bed. Based on topographic information and observations, the site appears to be constructed on natural subgrade soils. The typical natural subgrade soils as indicated by USDA soil maps is sandy loam. The estimated PCI and SCI of the site is 91 and 100, respectively. The primary distress observed included low and medium severity small patches.

Site Weather: The site is located in a dry/no freeze climate zone. The below figures indicate the average temperature, average precipitation, average number of days above 90 degrees Fahrenheit, and average number of days below 32 degrees Fahrenheit.

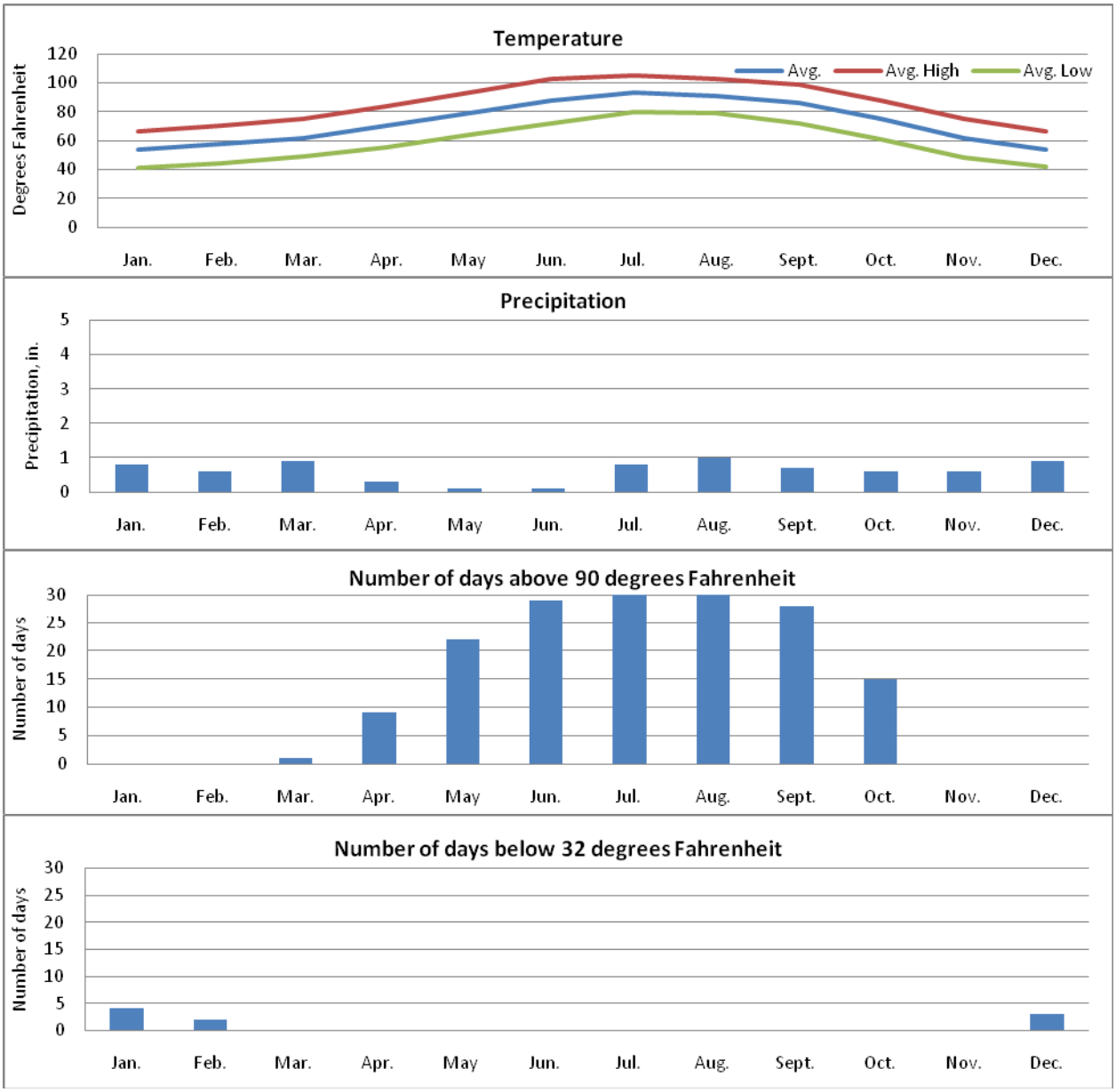

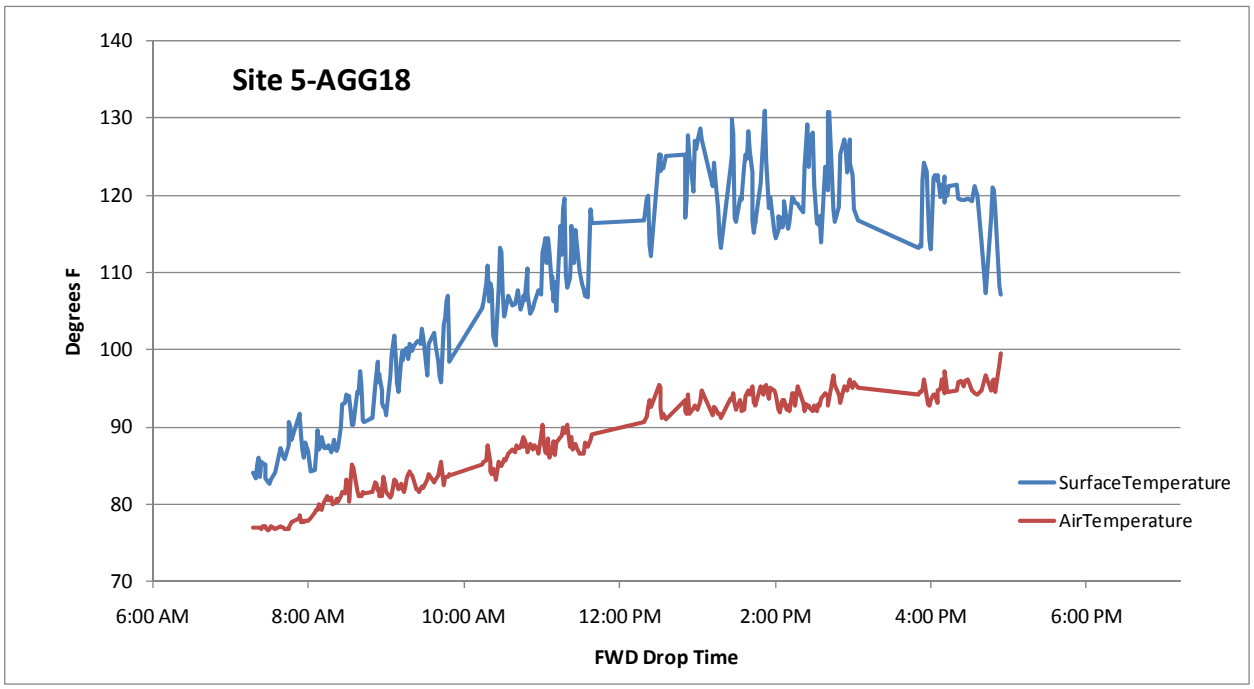

	500-ft Highway GPS3 55-3009	*Site 5-AGG18* ≈ 8AM average	AM-PM Change
average curvature, 1/ft	0.000547	0.000126	0.000111
min. curvature	0.000203	-0.000362	0.000089
max. curvature	0.001077	0.000555	0.000124
st. dev. of curvature	0.00021	0.000287	0.000012
number of slabs	33	7	7

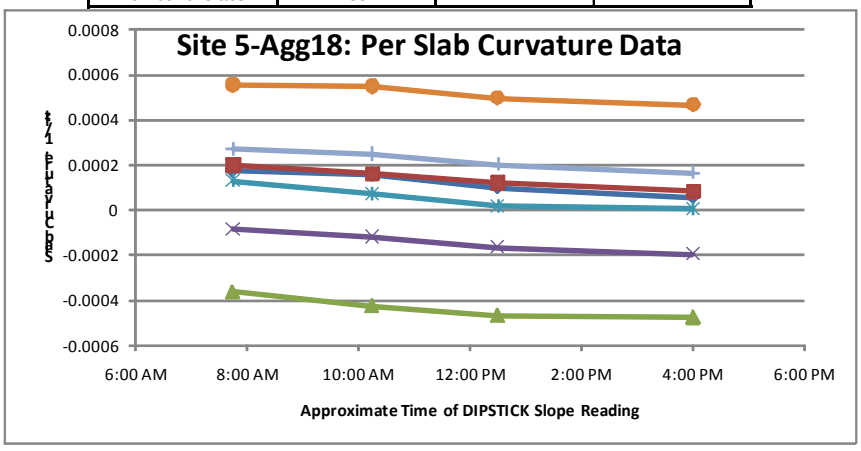

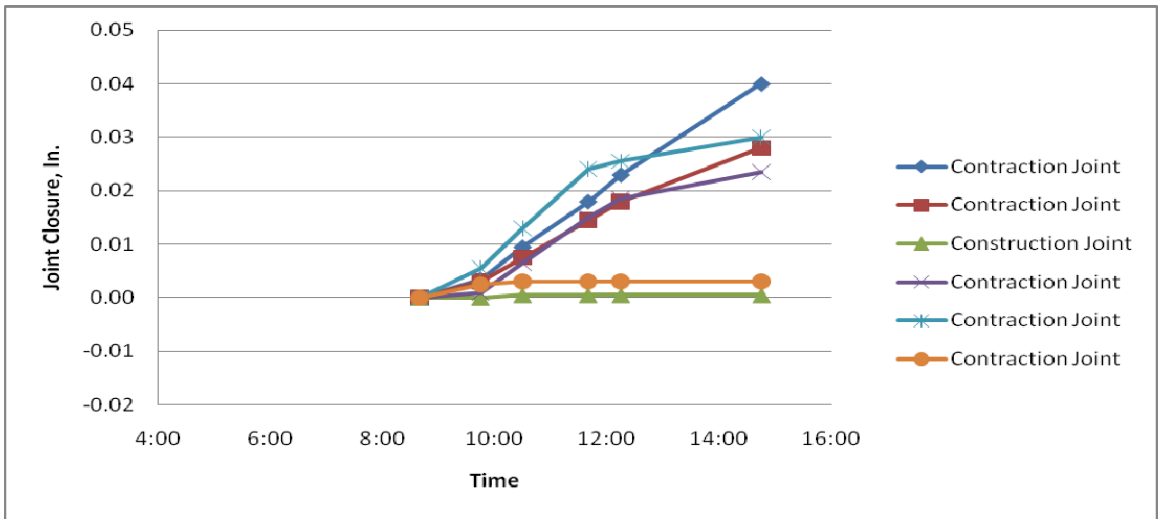
0.05
0.04
0.03
0.02
0.01
0.00
-0.01
-0.02
Joint Closure, In.
4:00
6:00
8:00
10:00
12:00
14:00
16:00
Time
Contraction Joint
Contraction Joint
Construction Joint
Contraction Joint
Contraction Joint
Contraction Joint

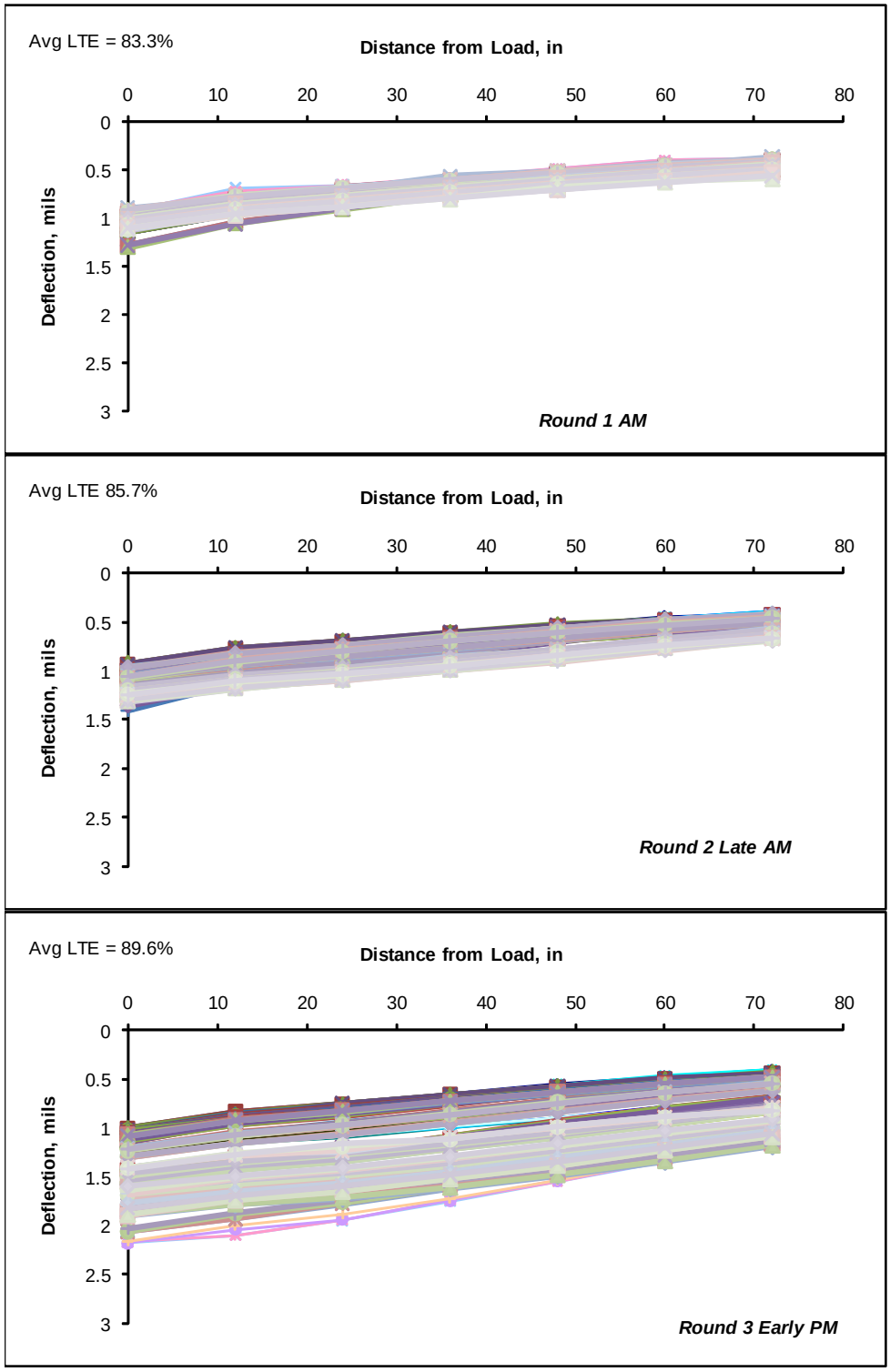
Avg LTE = 83.3%
Distance from Load, in
0
10
20
30
40
50
60
70
80
Deflection, mils
0
0.5
1
1.5
2
2.5
3
Round 1 AM
Avg LTE 85.7%
Distance from Load, in
Deflection, mils
Round 2 Late AM
Avg LTE = 89.6%
Distance from Load, in
Deflection, mils
Round 3 Early PM

Site 5-AGG18 ILLIBACK Summary- Site Averages without extreme 34M response

	Dense Liquid				*Elastic Solid*				*Radius of Relative*
	***k*-value**	***k* stdev**	**Slab E_C**	**E_C Stdev**	**Subg. *E***	***E* stdev**	**Slab E_C**	**E_C Stdev**	***stiffness (DL subg)***
Site Average =	488	59	3.49	0.4	77,380	5,371	2.55	0.18	43.4
Min. Defl. =	791	135	3.21	0.52	112,896	11,200	2.22	0.22	37.7
Max. Defl. =	300	29	2.96	0.27	50,615	2,784	2.22	0.12	47.1
Run 1 avg	671	114	3.10	0.49	98,307	9,973	2.17	0.22	38.9
Run 2 avg	557	75	3.47	0.44	86,173	6,721	2.50	0.2	42.0
Run 3 avg	330	25	3.84	0.27	57,653	2,208	2.91	0.11	49.0
Slab 34M Run1	390	38	3.69	0.34	65,261	3,772	2.76	0.16	46.6
Slab 34M Run2	133	3	4.31	0.09	28,731	455	3.49	0.06	63.4
Slab 34M Run3	86	1	4.01	0.05	20,083	344	3.31	0.06	69.4
Best Guess	**614**		**3.29**		**92240**		**2.34**		**40.4**
	psi/in		*Msi*		*psi*		*Msi*		*inches*

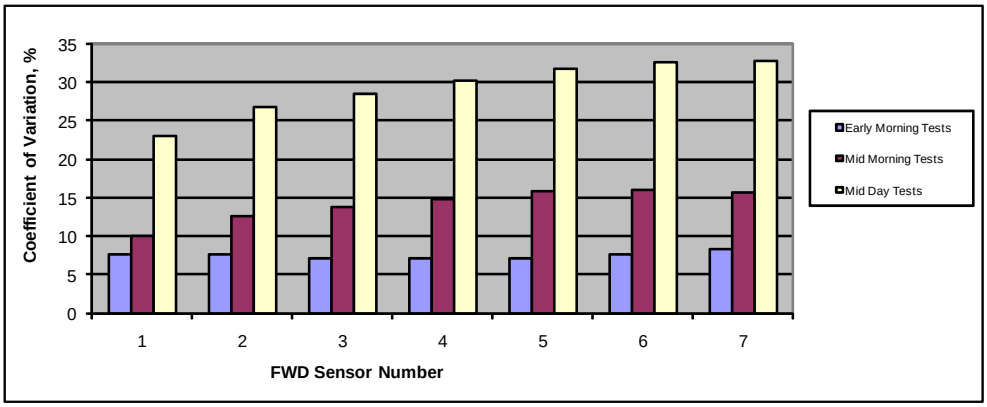

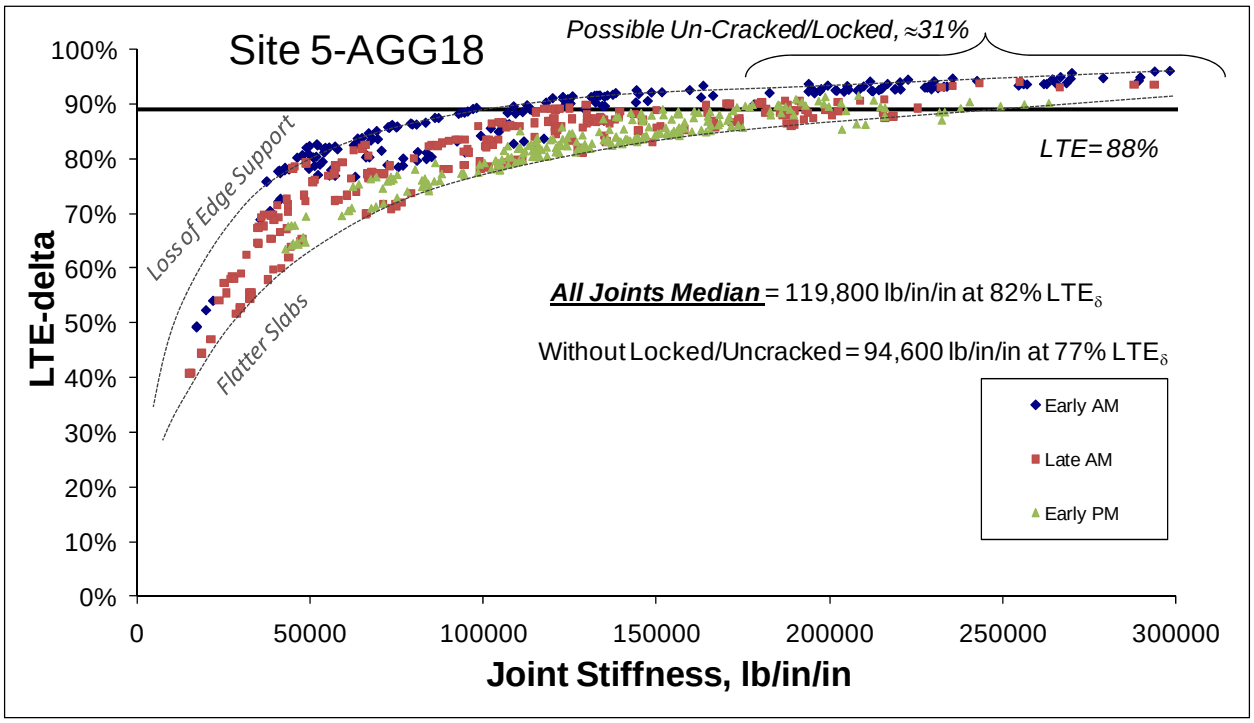

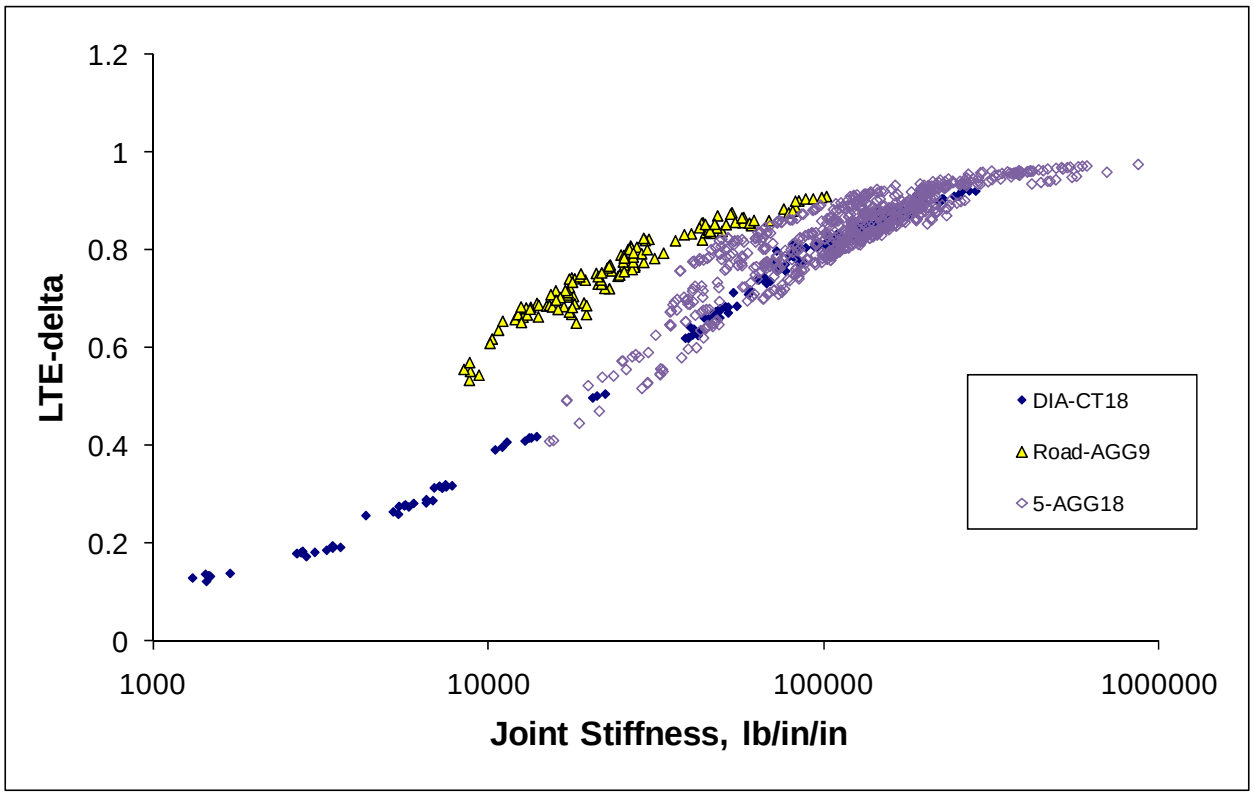
1.2
1
0.8
0.6
0.4
0.2
0
LTE-delta
1000
10000
100000
1000000
Joint Stiffness, lb/in/in
DIA-CT18
Road-AGG9
5-AGG18

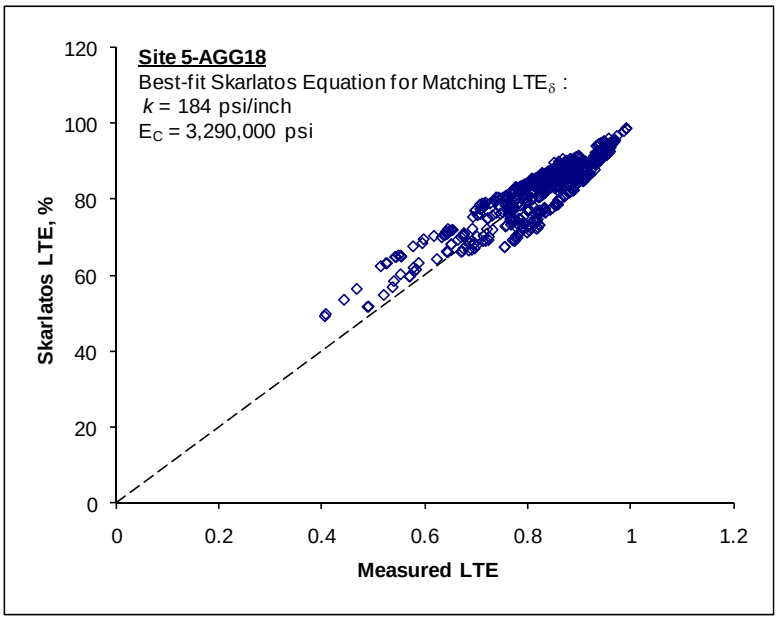
Site 5-AGG18
Best-fit Skarlatos Equation for Matching LTEδ :
k = 184 psi/inch
EC = 3,290,000 psi
120
100
80
60
40
20
0
Skarlatos LTE, %
0
0.2
0.4
0.6
0.8
1
1.2
Measured LTE

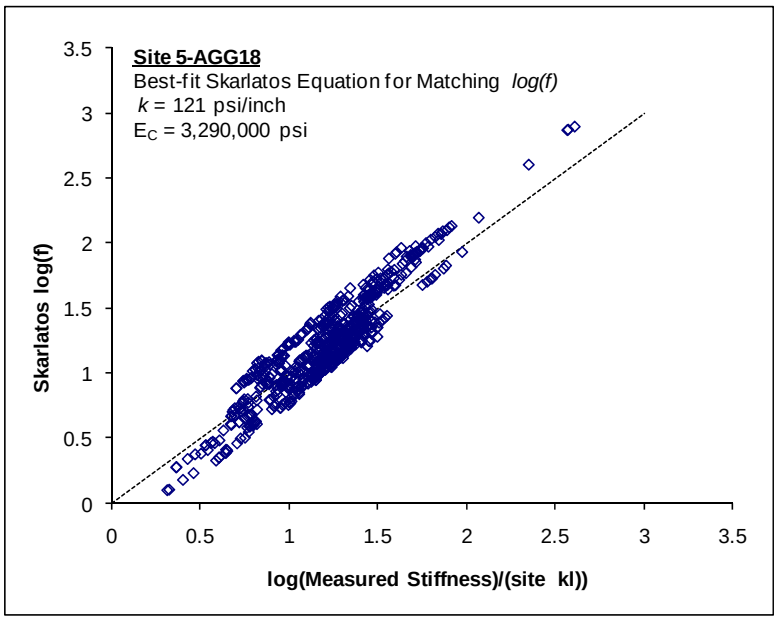
Site 5-AGG18
Best-fit Skarlatos Equation for Matching log(f)
k = 121 psi/inch
EC = 3,290,000 psi
Skarlatos log(f)
log(Measured Stiffness)/(site kl))
0
0.5
1
1.5
2
2.5
3
3.5

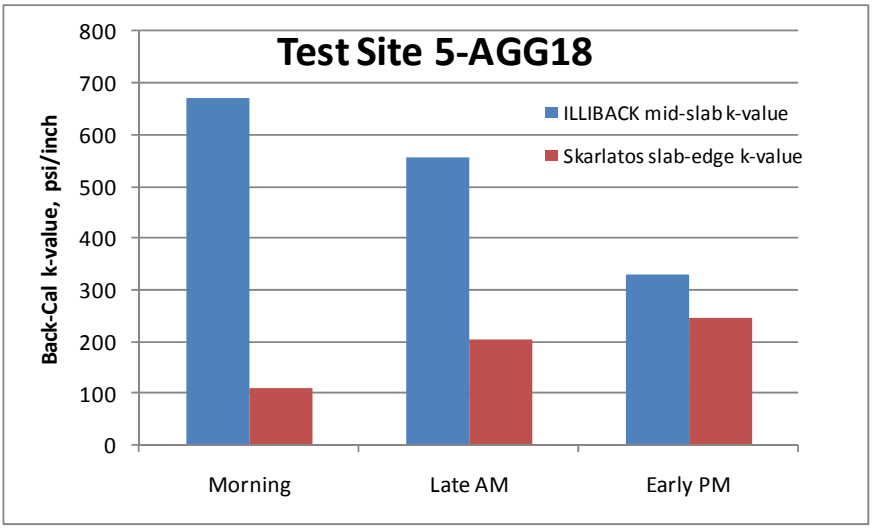
Test Site 5-AGG18
ILLIBACK mid-slab k-value
Skarlatos slab-edge k-value
Back-Cal k-value, psi/inch
800
700
600
500
400
300
200
100
0
Morning
Late AM
Early PM

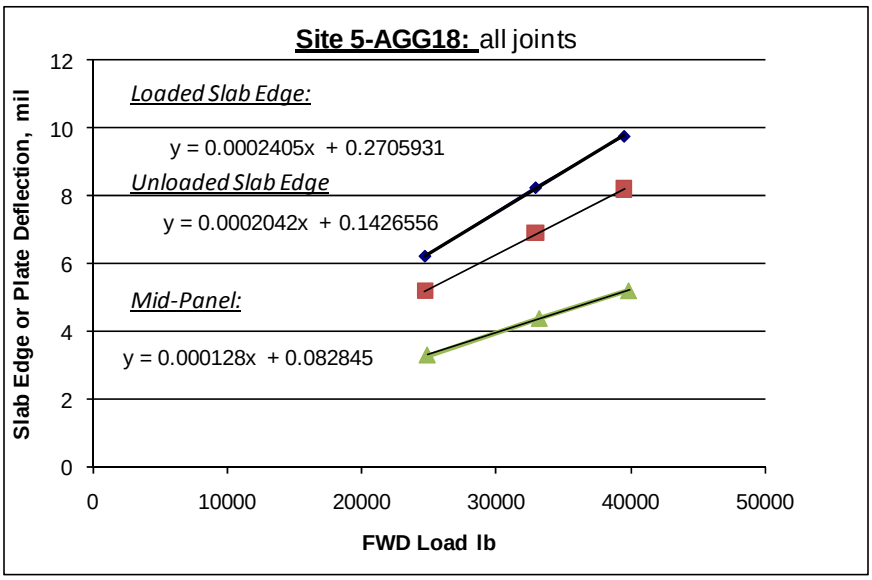

Site 5-AGG18 T. Doweled Contraction, including locked / un-cracked

	LR	LTE	Avg Stiffness	
avg	111	89%	242643	
min	94	80%	84350	
max	162	99%	3010155	
stdev	16	4%	299384	
Median	106	89%	186807	

trans Sawed 1.5" dowels at 15"

% possibly un-cracked, LTE>88% = 61

Steel Area/ft = 1.413717

reinf. ratio = 0.654%

Without locked / un-cracked

	LR	LTE	Avg Stiffness
avg	111	85%	148045
min	95	80%	84350
max	149	89%	233452
stdev	14	2%	35317
Median	111	86%	144139

% possibly un-cracked, LTE>88% = 13

at DCI = 1000000, kj = 51000

Probable Agg Interlock = 90000 to 140000

$$k = \frac{1}{s\left(\frac{\varpi}{0.9G_dA_d} + \frac{\varpi^3}{12E_dI_d} + \frac{2+\beta\varpi}{2\beta^3E_dI_d}\right)}$$

s is the dowel bar spacing =	15	in
w is the joint opening =	0.1	in
Dowel Diameter =	1.5	in
Ad is the dowel cross-sectional area =	1.77	sq in
Ed =	29000000	psi
Gd =	11153846	psi
Id =	0.249	in^4
Back-Calculated Dowel-Concrete Interaction modulus, DCI =	4102272	psi (maximum)

$$\beta = \sqrt[4]{\frac{Kd}{4E_dI_d}} = 0.680$$

Doweled Joint Stiffness = **144139** lb/in/in

Site 5-AGG18 L. Doweled Contraction, including locked / un-cracked

	LR	LTE	Avg Stiffness
avg	107	80%	96029
min	91	41%	15228
max	161	95%	235453
stdev	14	10%	43625
Median	102	81%	100835

long Sawed 1.5" dowels at 15"

% possibly un-cracked, LTE>88% = 17

Steel Area/ft = 1.413717

reinf. ratio = 0.654%

Without locked / un-cracked

	LR	LTE	Avg Stiffness
avg	108	78%	87434
min	91	41%	15228
max	161	89%	189840
stdev	15	9%	38034
Median	102	80%	83513

% possibly un-cracked, LTE>88% = 4

at DCI = 1000000, kj = 51000

Probable Agg Interlock = 33000 to 80000

$$k = \frac{1}{s\left(\frac{\varpi}{0.9G_dA_d} + \frac{\varpi^3}{12E_dI_d} + \frac{2+\beta\varpi}{2\beta^3E_dI_d}\right)}$$

s is the dowel bar spacing =	15	in
w is the joint opening =	0.1	in
Dowel Diameter =	1.5	in
Ad is the dowel cross-sectional area =	1.77	sq in
Ed =	29000000	psi
Gd =	11153846	psi
Id =	0.249	in^4

Back-Calculated Dowel-Concrete Interaction modulus, DCI = 1953236 psi (maximum)

$$\beta = \sqrt[4]{\frac{Kd}{4E_dI_d}} = 0.565$$

Doweled Joint Stiffness = **83513** lb/in/in

Site 5-AGG18 L. Doweled Construction; including locked / un-cracked

	LR	LTE	Avg Stiffness
avg	105	79%	103385
min	90	52%	23632
max	143	96%	699063
stdev	11	10%	86167
Median	101	81%	84213

Long Formed 1.5" dowels at 15"

% possibly un-cracked, LTE>88% = 19

Steel Area/ft = 1.413717

reinf. ratio = 0.654%

Without locked / un-cracked

	LR	LTE	Avg Stiffness
avg	105	77%	79607
min	90	52%	23632
max	143	90%	178122
stdev	11	9%	37351
Median	102	78%	69130

% possibly un-cracked, LTE>88% = 5.4

at DCI = 1000000, kj = 51000

Probable Agg Interlock = 19000 to 68000

$$k = \frac{1}{s\left(\frac{\varpi}{0.9G_dA_d} + \frac{\varpi^3}{12E_dI_d} + \frac{2+\beta\varpi}{2\beta^3E_dI_d}\right)}$$

s is the dowel bar spacing =	15	in
w is the joint opening =	0.1	in
Dowel Diameter =	1.5	in
Ad is the dowel cross-sectional area =	1.77	sq in
Ed =	29000000	psi
Gd =	11153846	psi
Id =	0.249	in^4

Back-Calculated Dowel-Concrete Interaction modulus, DCI = 1512173 psi

$$\beta = \sqrt[4]{\frac{Kd}{4E_dI_d}} = 0.530$$

Doweled Joint Stiffness = **69130** lb/in/in

Site 5-AGG18 Corners, including locked / un-cracked joints

	LR	LTE	Avg Stiffness
avg	115	77%	92519
min	98	24%	3304
max	152	96%	351629
stdev	12	16%	74810
Median	113	82%	68028

% possibly un-cracked, LTE>88% = 19

Doweled on All Edges

Without locked / un-cracked

	LR	LTE	Avg Stiffness
avg	115	73%	71524
min	98	24%	3304
max	152	89%	196110
stdev	13	16%	55670
Median	114	81%	46844

% possibly un-cracked, LTE>88% = 1

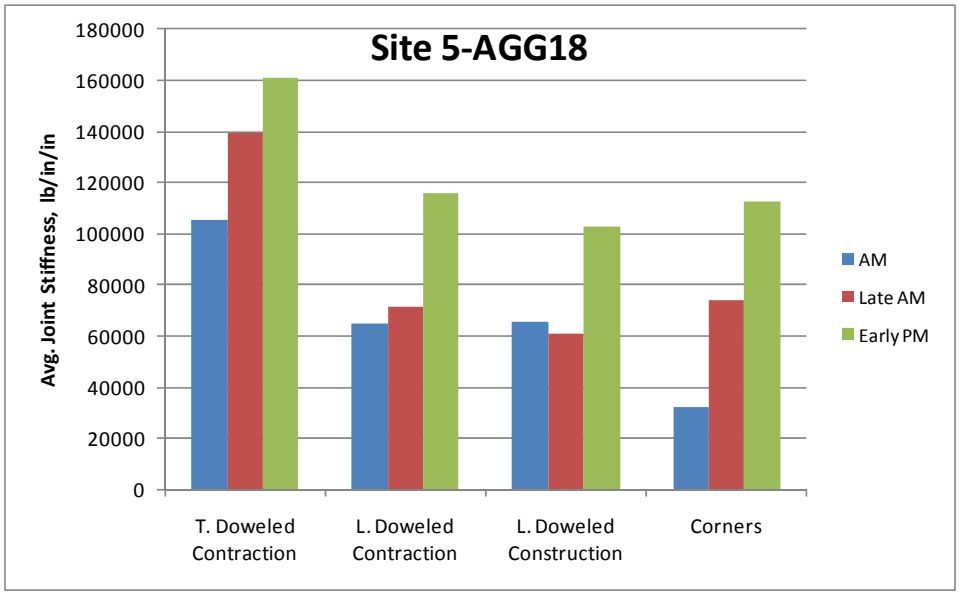

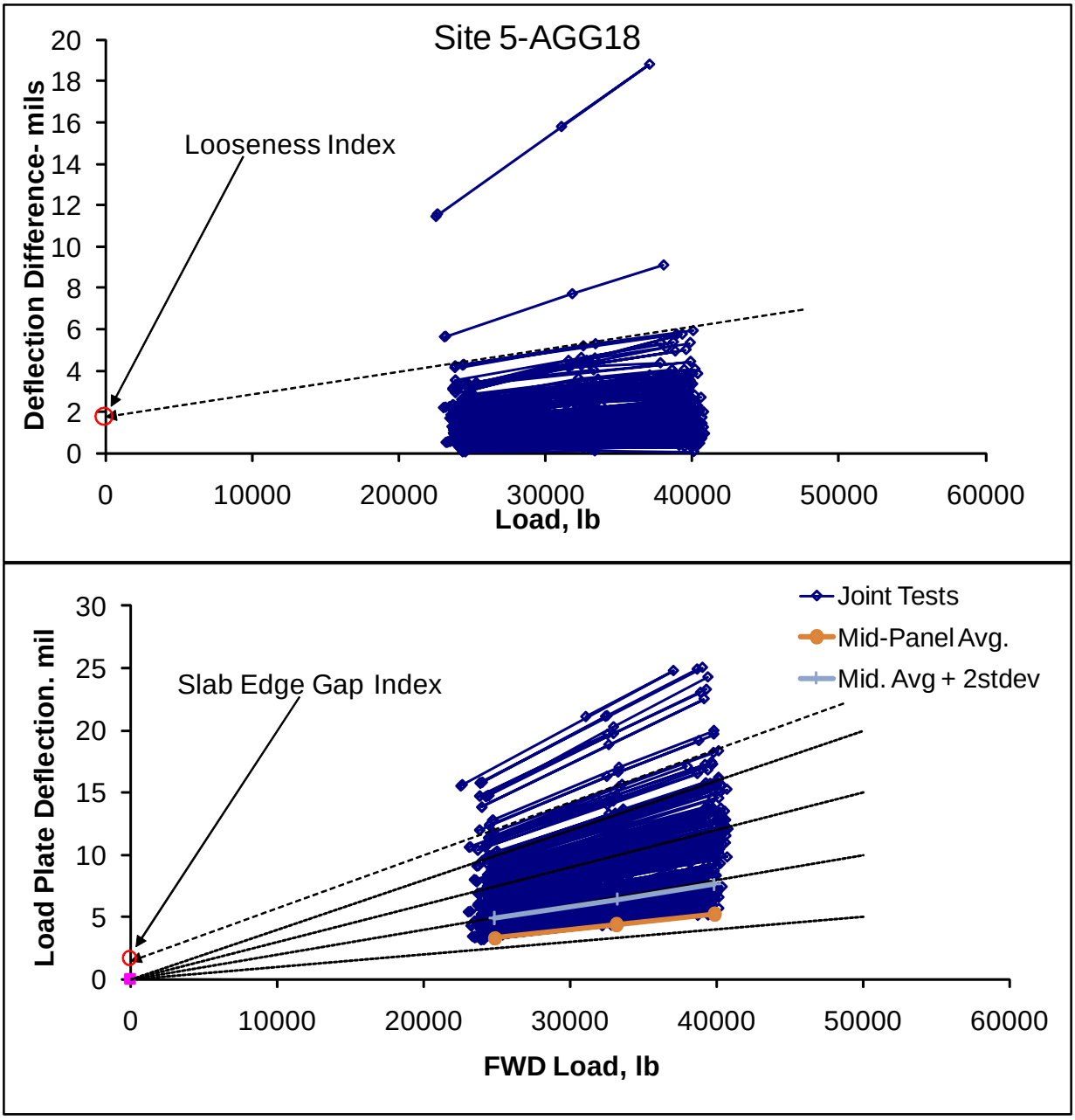

Looseness- All Good Data

	All	AM	Mid	PM
Avg	0.09	0.02	0.21	0.04
Min	-2.65	-2.65	-1.50	-0.56
Max	1.66	1.66	1.53	0.38
Stdev	0.43	0.56	0.43	0.18

Edge Gaps- All Good Data

	All	AM	Mid	PM
Avg	0.29	0.48	0.35	0.03
Min	-1.04	-1.04	-0.78	-0.59
Max	1.58	1.58	1.47	0.49
Stdev	0.44	0.48	0.47	0.19

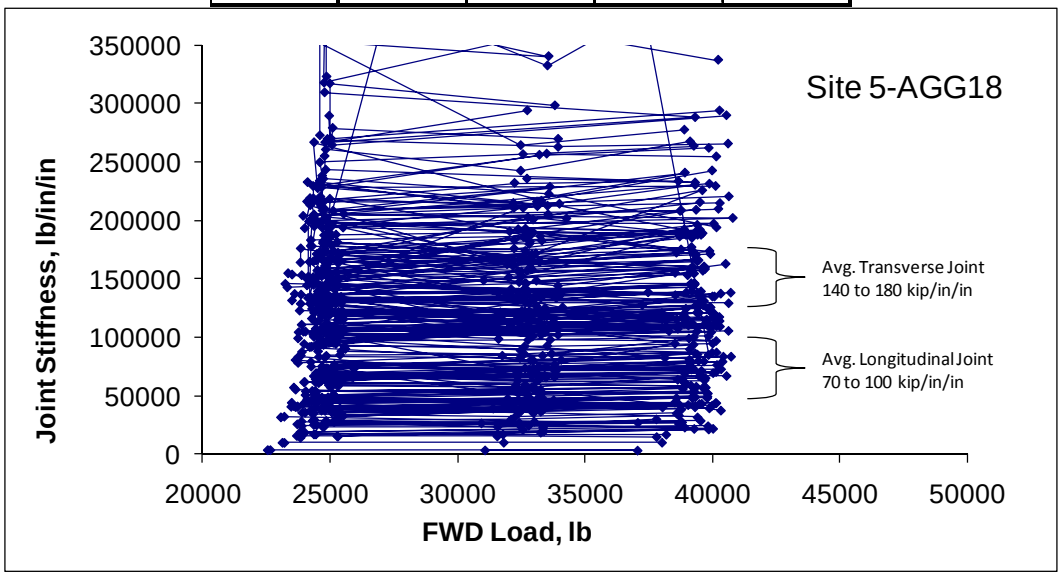

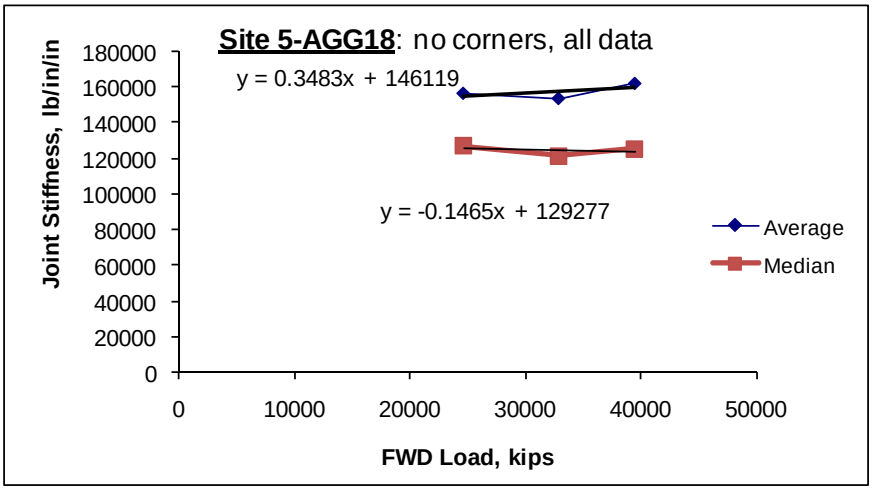

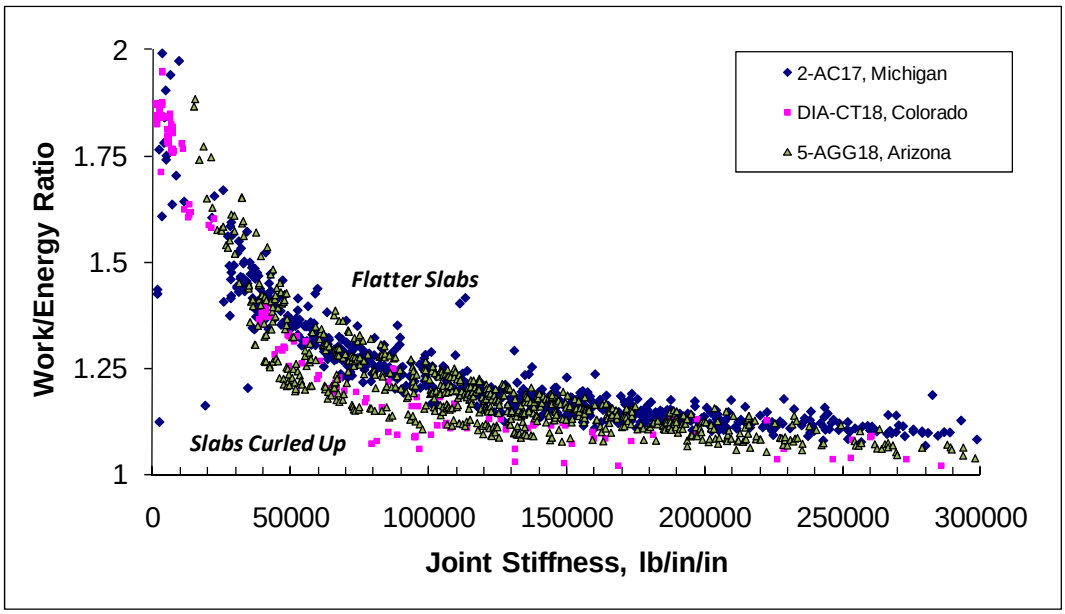
2
1.75
1.5
1.25
1
Work/Energy Ratio
0
50000
100000
150000
200000
250000
300000
Joint Stiffness, lb/in/in
2-AC17, Michigan
DIA-CT18, Colorado
5-AGG18, Arizona
Flatter Slabs
Slabs Curled Up

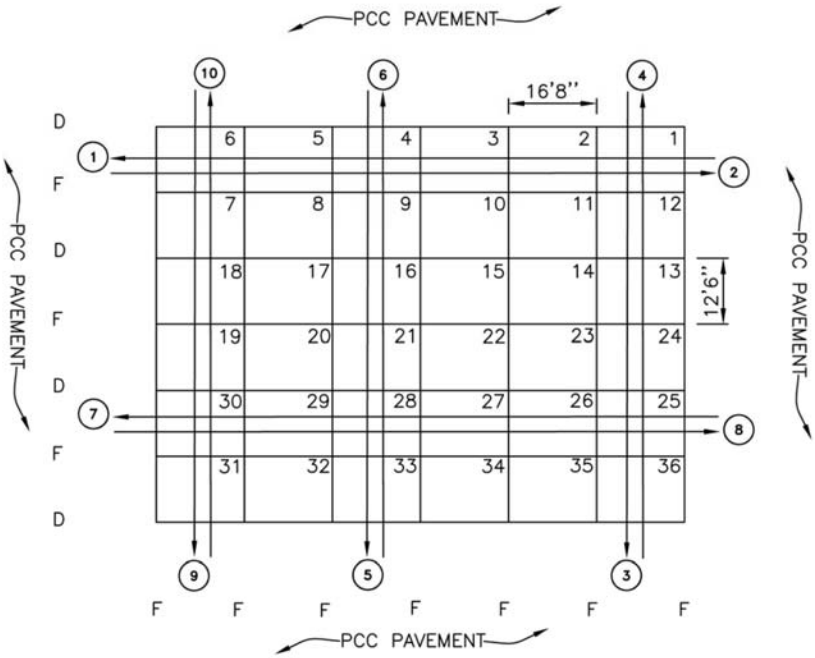

TEST PATTERN

LEGEND

(2) FWD TEST LANE NUMBER

D CONSTRUCTION JOINT: 1.25" DIA. SMOOTH DOWEL, 20" LONG, 15" SPACING.

F CONTRACTION JOINT: 1.25" DIA. SMOOTH DOWEL BAR, 20" LONG, 15" SPACING.

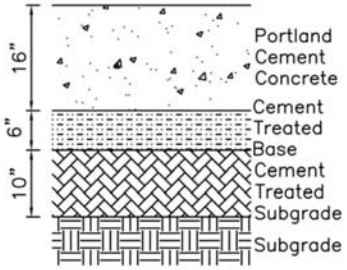

6-CT16

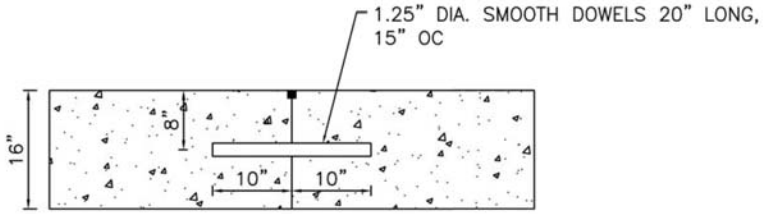

LONGITUDINAL CONSTRUCTION JOINT - D

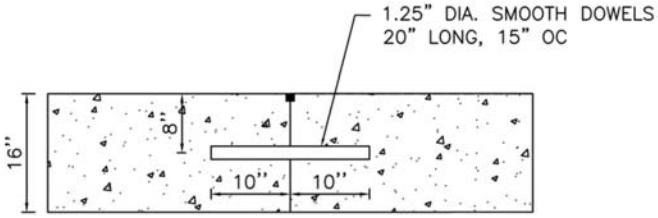

CONTRACTION JOINT - F

TEST SITE 6-CT16

6-CT16

Site Description: The site is located in the south west region of the United States. Elevations of the site, as indicated by USGS maps, are approximately 3920 to 3930 feet above sea level. The airport is located in a flat area with nearby buttes and hills. Based on topographic information and observations, the site appears to be constructed on natural subgrade soils. The typical natural subgrade as indicated by USDA soil maps is silt loam. The estimated PCI and SCI of the site is 94 and 94, respectively. The primary distress observed included low severity joint and corner spall.

Site Weather: The site is located in a dry/no freeze climate zone. The below figures indicate the average temperature, average precipitation, average number of days above 90 degrees Fahrenheit, and average number of days below 32 degrees Fahrenheit.

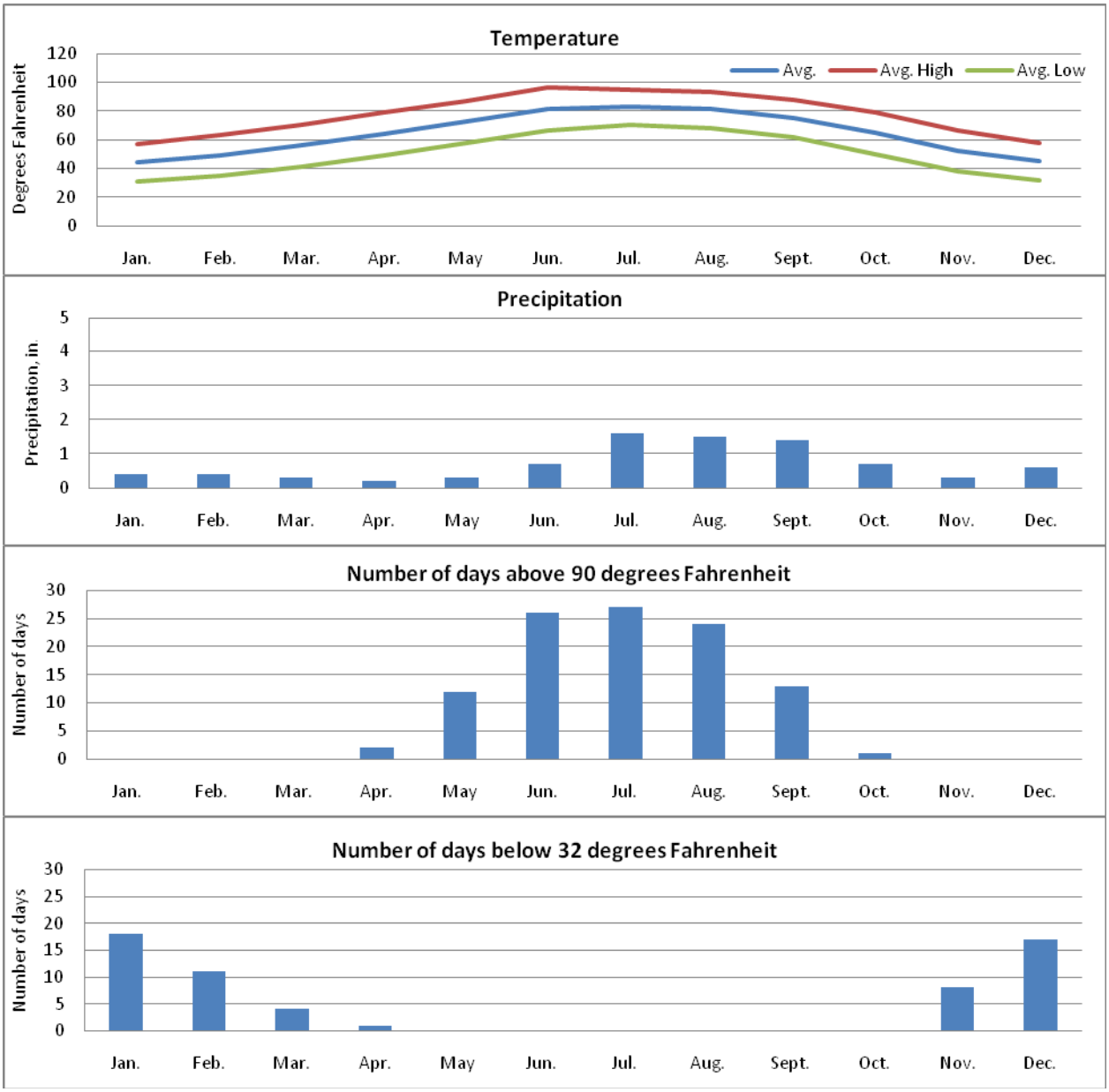

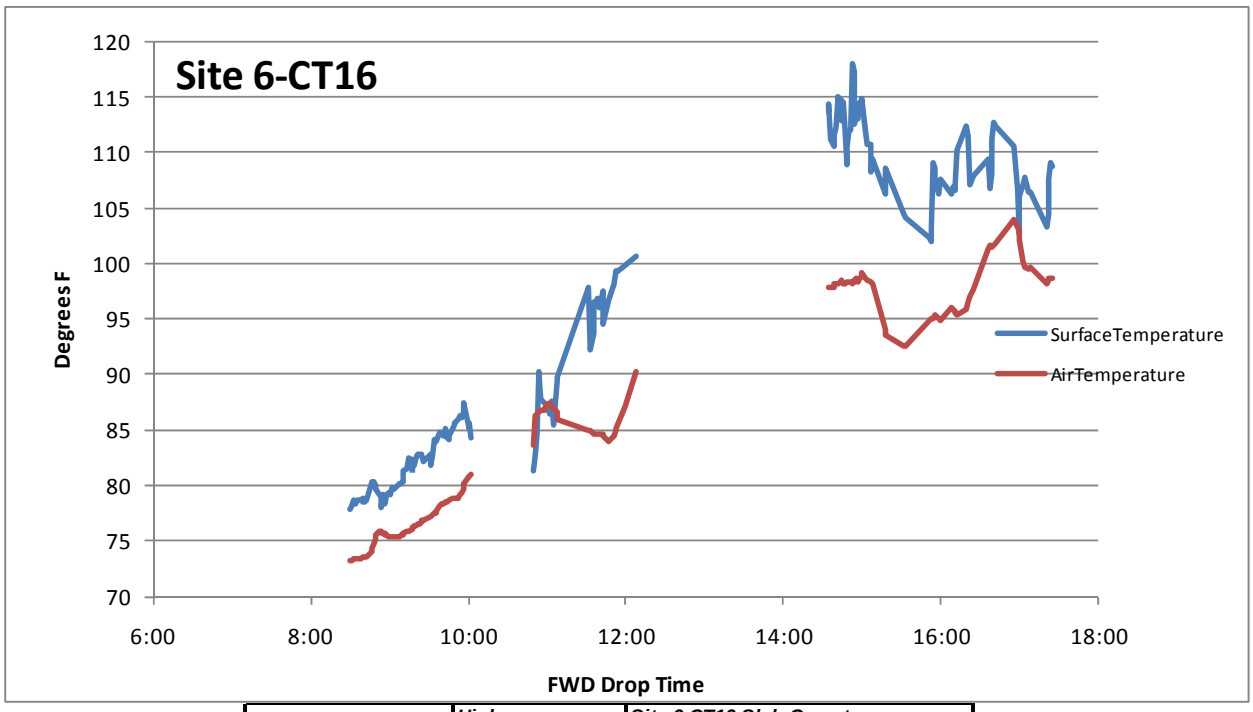

	Highway GPS3 55-3009	*Site 6-CT16 Slab Curvature* 8AM average	AM-PM Change
average curvature, ft^{-1}	0.000547	0.000098	0.000053
min. curvature	0.000203	-0.000279	0.000028
max. curvature	0.001077	0.000729	0.000066
st. dev. of curvature	0.00021	0.000333	0.000014
number of slabs	33	7	7

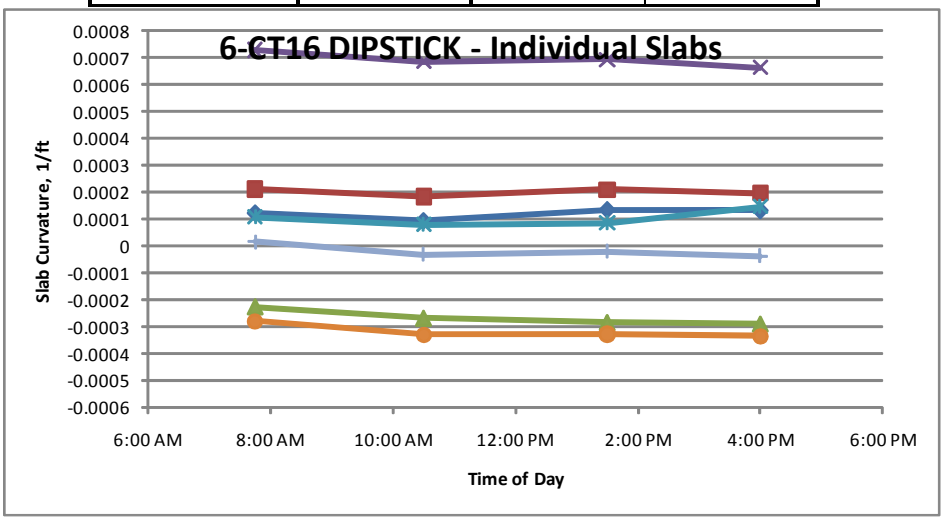

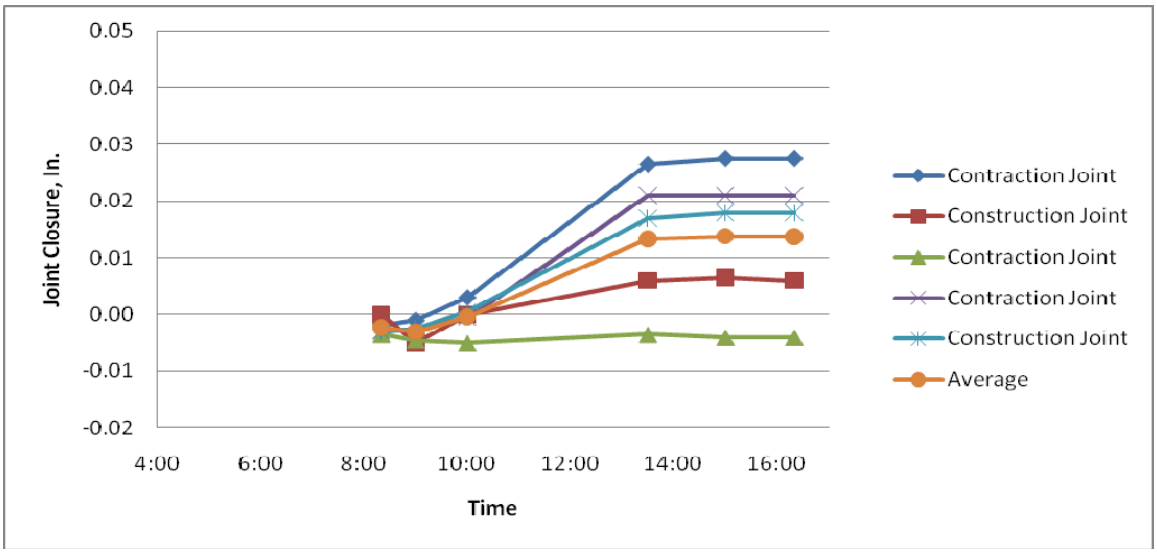

Site 6-CT16; ILLIBACK Summary

	Dense Liquid				*Elastic Solid*				*Radius*
	***k*-value**	***k* stdev**	**Slab E_C**	**E_C Stdev**	**Subg. *E***	***E* stdev**	**Slab E_C**	**E_C Stdev**	**I-VALUES**
Site Average =	***205***	***10***	***8.69***	***0.42***	***43,712***	***1,246***	***6.98***	***0.2***	***62.0***
Site Min. =	261	13.6	13.30	0.65	57,925	1,804	10.81	0.34	64.9
Site Max =	175	10.4	4.63	0.27	33,794	1,104	3.62	0.12	55.1
AM	191	11	9.09	0.5	41,782	1,514	7.36	0.27	63.8
mid	223	10.1	7.99	0.35	45,855	1,042	6.34	0.14	59.5
PM	202	9.6	9.06	0.42	43,560	1,169	7.30	0.2	62.9
30, 31, 33 R1	153	7.2	5.83	0.27	31,896	780	4.65	0.11	60.4
25-29 R1	181	8.9	7.57	0.36	38,439	1,063	6.08	0.17	61.8
33 R2	227	11	2.92	0.14	37,770	290	2.18	0.02	46.0
Best Guess	**205**		**8.69**		**43712**		**6.98**		**62.0**
	psi/in		*Msi*		*psi*		*Msi*		*inches*

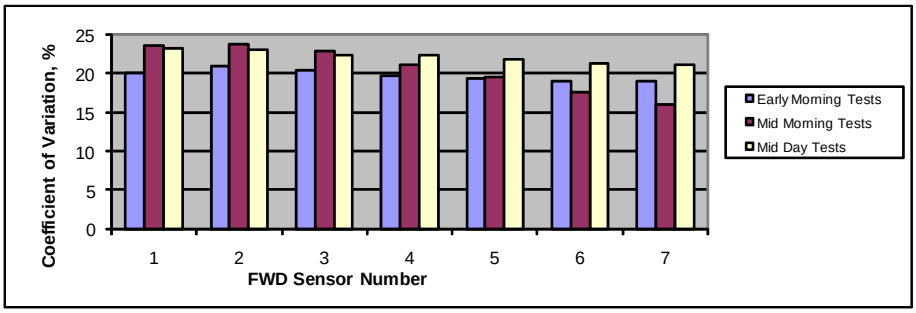

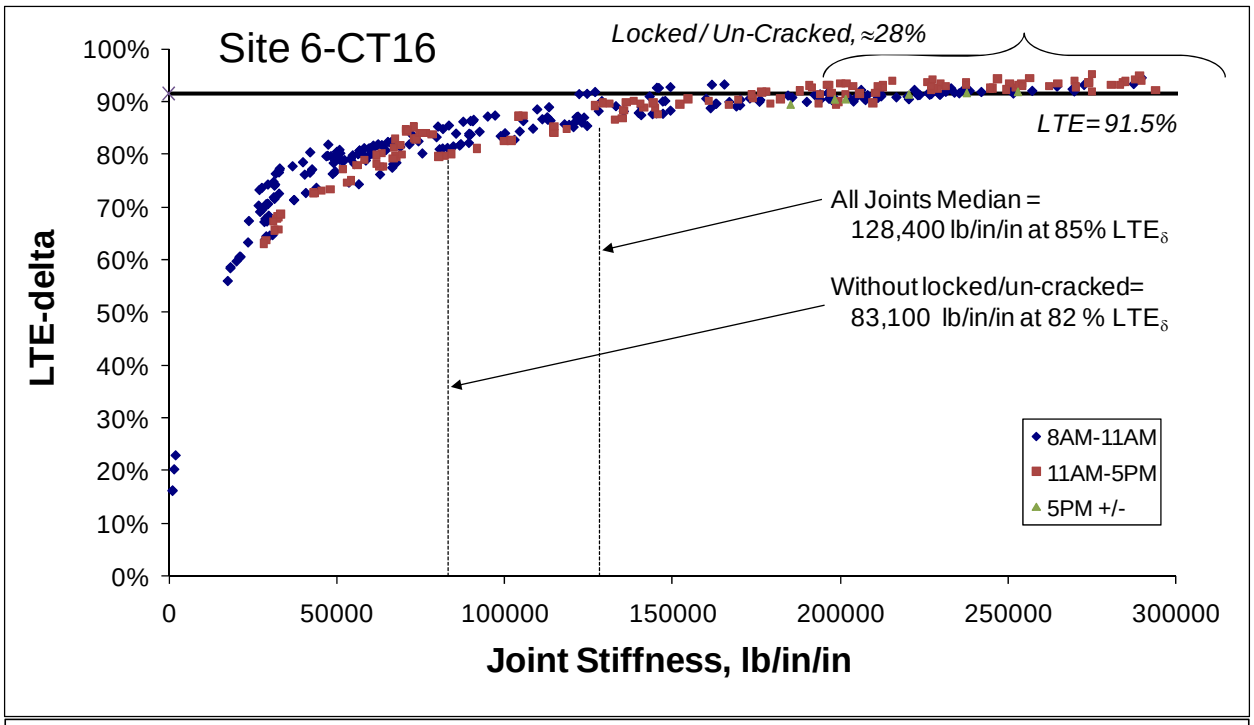
Site 6-CT16
Locked / Un-Cracked, ≈28%
LTE = 91.5%
All Joints Median = 128,400 lb/in/in at 85% LTE$_\delta$
Without locked/un-cracked= 83,100 lb/in/in at 82 % LTE$_\delta$
8AM-11AM
11AM-5PM
5PM +/-
LTE-delta
Joint Stiffness, lb/in/in
100%
90%
80%
70%
60%
50%
40%
30%
20%
10%
0%
0
50000
100000
150000
200000
250000
300000

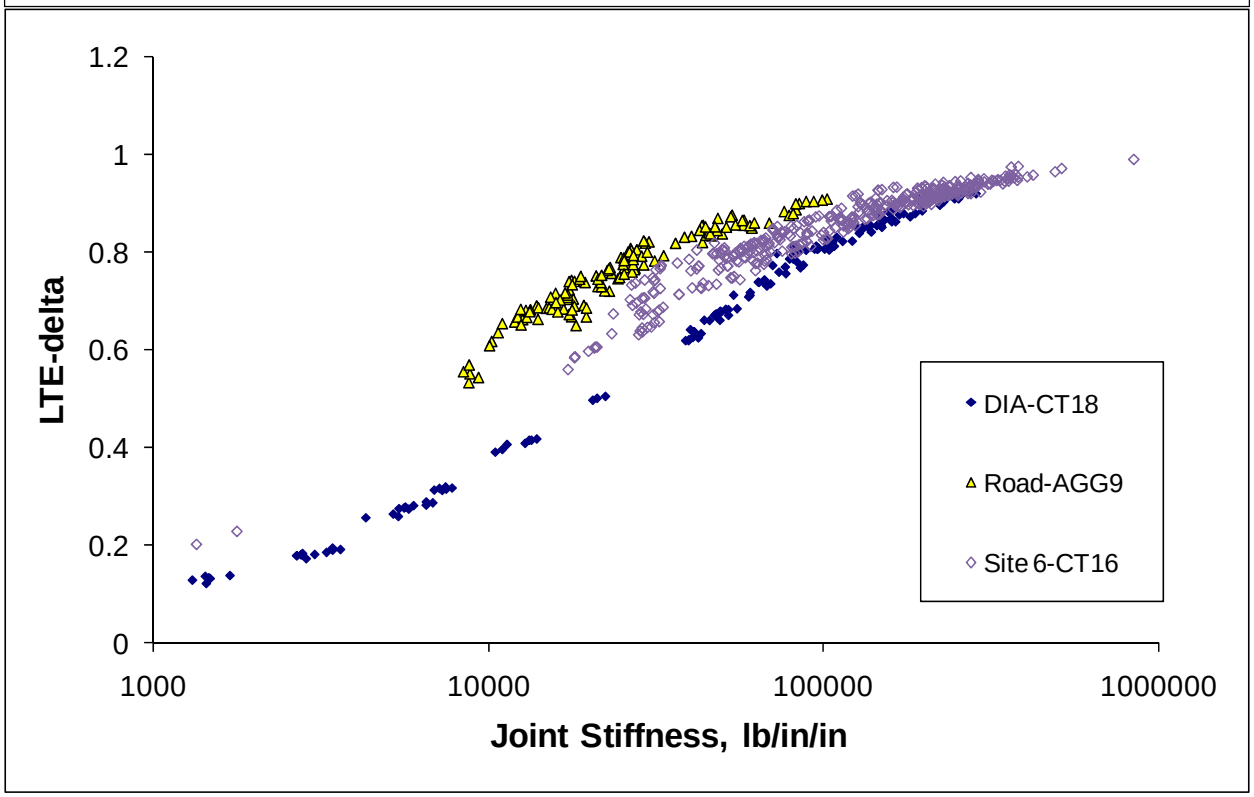
DIA-CT18
Road-AGG9
Site 6-CT16
LTE-delta
Joint Stiffness, lb/in/in
1.2
1
0.8
0.6
0.4
0.2
0
1000
10000
100000
1000000

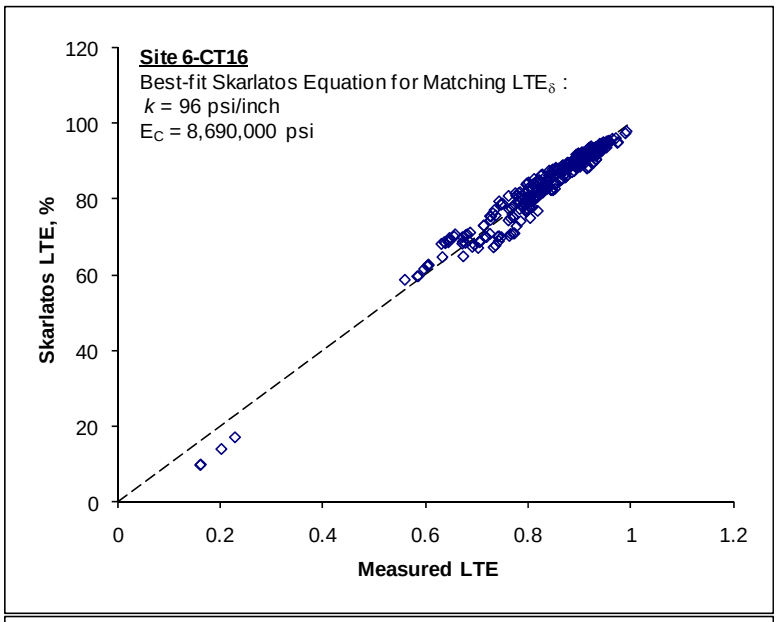
Site 6-CT16
Best-fit Skarlatos Equation for Matching LTEδ :
k = 96 psi/inch
EC = 8,690,000 psi
Skarlatos LTE, %
Measured LTE
0
20
40
60
80
100
120
0
0.2
0.4
0.6
0.8
1
1.2

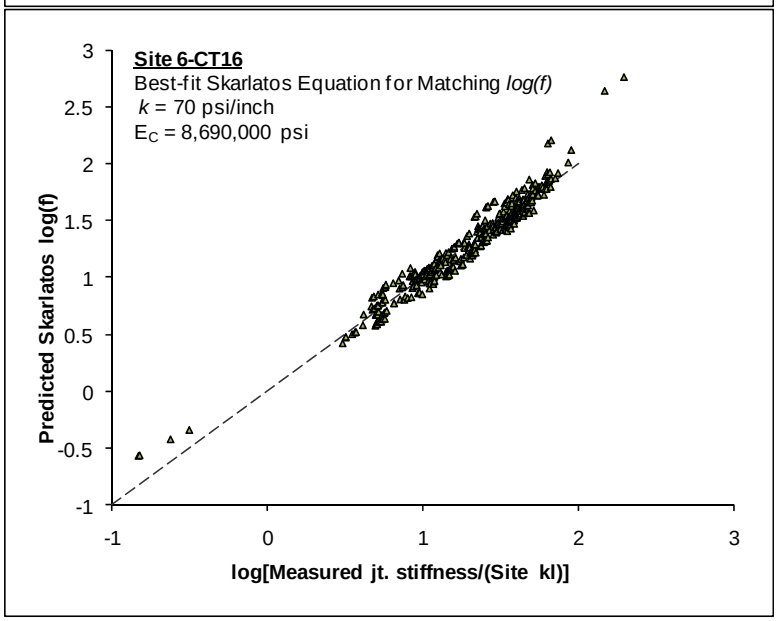
Site 6-CT16
Best-fit Skarlatos Equation for Matching log(f)
k = 70 psi/inch
EC = 8,690,000 psi
Predicted Skarlatos log(f)
log[Measured jt. stiffness/(Site kl)]
-1
-0.5
0
0.5
1
1.5
2
2.5
3
-1
0
1
2
3

Site 6-CT16 T. Doweled Contraction Joints; Including locked / un-cracked

	LR, in.	LTE	Jt. Stiffness, lb/in/in
avg	135	87%	165901
min	97	76%	31612
max	234	99%	1120261
stdev	23	6%	137577
Median	134	88%	134112

Sawed, 1.25" dowels at 15 inches

Possible Un-cracked, LTE>91% = 24%

Steel Area/ft = 0.981748
reinf. ratio = 0.51%

Without locked / un-cracked joints

	LR, in.	LTE	Jt. Stiffness, lb/in/in
avg	130	85%	111333
min	97	76%	31612
max	185	92%	269749
stdev	17	5%	58288
Median	131	85%	104110

Possible Un-cracked, LTE>91% = 6%

at DCI = 1000000, kj = 37000
Probable Agg Interlock = 70000 to 100000

$$k = \frac{1}{s\left(\frac{\varpi}{0.9G_dA_d} + \frac{\varpi^3}{12E_dI_d} + \frac{2+\beta\varpi}{2\beta^3E_dI_d}\right)}$$

s is the dowel bar spacing =	15	in
w is the joint opening =	0.1	in
Dowel Diameter =	1.25	in
Ad is the dowel cross-sectional area =	1.23	sq in
Ed =	29000000	psi
Gd =	11153846	psi
Id =	0.120	in^4
Back-Calculated Dowel-Concrete Interaction modulus, DCI =	4096965	psi

$$\beta = \sqrt[4]{\frac{Kd}{4E_dI_d}} = 0.779$$

Doweled Joint Stiffness = **104110** lb/in/in

Site 6-CT16 L. Doweled Contraction Joints; Including locked / un-cracked

	LR, in.	LTE	Jt. Stiffness, lb/in/in
avg	157	89%	187957
min	96	69%	26783
max	223	95%	405003
stdev	39	6%	82443
Median	178	92%	206824

Sawed, 1.25" dowels at 15 inches

Possible Un-cracked, LTE>91% = 54%

Steel Area/ft = 0.981748
reinf. ratio = 0.51%

Without locked / un-cracked joints

	LR, in.	LTE	Jt. Stiffness, lb/in/in
avg	146	86%	141216
min	97	69%	26783
max	223	92%	269213
stdev	42	7%	75559
Median	141	90%	143558

Possible Un-cracked, LTE>91% = 11%

at DCI = 1000000, kj = 37000
at DCI = 5000000, kj = 120000
Probable Agg Interlock = 23000 to 140000

$$k = \frac{1}{s\left(\frac{\varpi}{0.9G_dA_d} + \frac{\varpi^3}{12E_dI_d} + \frac{2+\beta\varpi}{2\beta^3E_dI_d}\right)}$$

s is the dowel bar spacing =	15	in
w is the joint opening =	0.1	in
Dowel Diameter =	1.25	in
Ad is the dowel cross-sectional area =	1.23	sq in
Ed =	29000000	psi
Gd =	11153846	psi
Id =	0.120	in^4
Back-Calculated Dowel-Concrete Interaction modulus, DCI =	6366013	psi

$$\beta = \sqrt[4]{\frac{Kd}{4E_dI_d}} = 0.870$$

Doweled Joint Stiffness = **143558** lb/in/in

Site 6-CT16 L. Doweled Construction Joints; Including locked / un-cracked

	LR, in.	LTE	Jt. Stiffness, lb/in/in
avg	130	74%	68895
min	104	16%	839
max	192	92%	294073
stdev	21	14%	55160
Median	126	78%	56195

Formed, 1.25" dowels at 15 inches

Possible Un-cracked, LTE>93% = 6%

Steel Area/ft = 0.981748

reinf. ratio = 0.51%

Without locked / un-cracked joints

	LR, in.	LTE	Jt. Stiffness, lb/in/in
avg	130	74%	68895
min	104	16%	839
max	192	92%	294073
stdev	21	14%	55160
Median	126	78%	56195

Possible Un-cracked, LTE>93% = 6%

at DCI = 1000000, kj = 37000

Probable Agg Interlock = 20000 to 55000

$$k = \frac{1}{s\left(\frac{\varpi}{0.9G_dA_d} + \frac{\varpi^3}{12E_dI_d} + \frac{2+\beta\varpi}{2\beta^3E_dI_d}\right)}$$

s is the dowel bar spacing =	15	in
w is the joint opening =	0.1	in
Dowel Diameter =	1.25	in
Ad is the dowel cross-sectional area =	1.23	sq in
Ed =	29000000	psi
Gd =	11153846	psi
Id =	0.120	in^4
Back-Calculated Dowel-Concrete Interaction modulus, DCI =	1769514	psi

$$\beta = \sqrt[4]{\frac{Kd}{4E_dI_d}} = 0.632$$

Doweled Joint Stiffness = **56195** lb/in/in

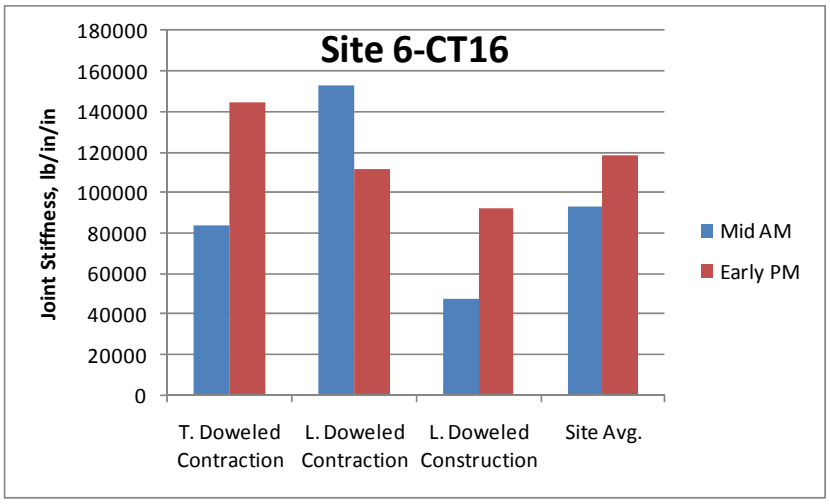

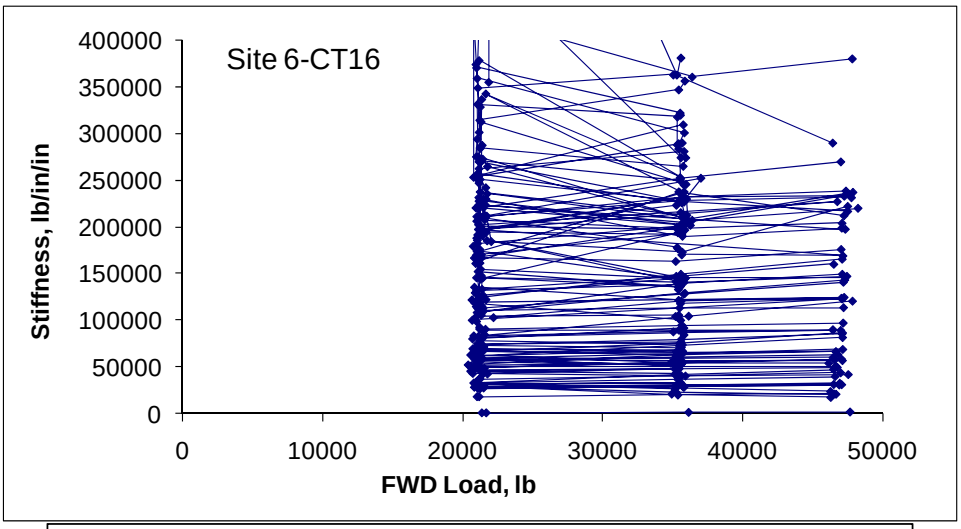

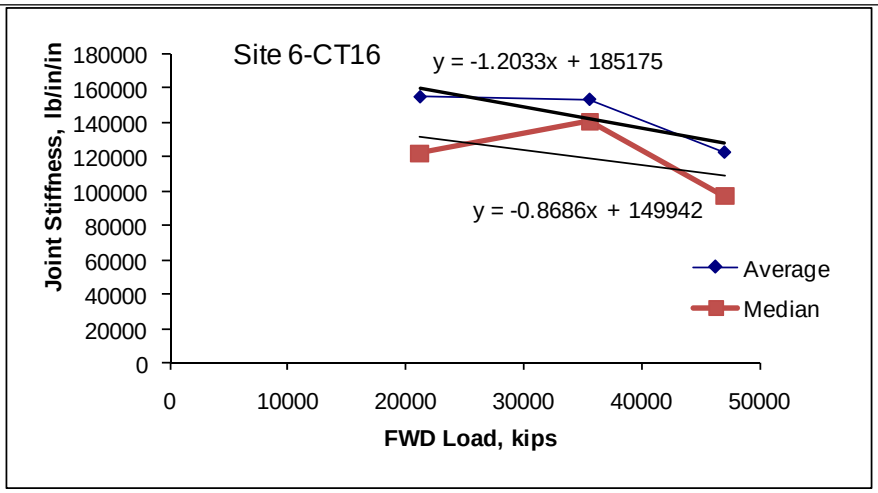

Site 6-CT16 Slab Edge Gaps

1 High Gap 21-mil 28N removed removed

	All	AM	Mid	PM
Avg	0.24	0.40	0.08	-0.07
Min	-0.82	-0.82	-0.37	-0.23
Max	2.69	2.69	0.67	0.03
Stdev	0.49	0.62	0.21	0.14

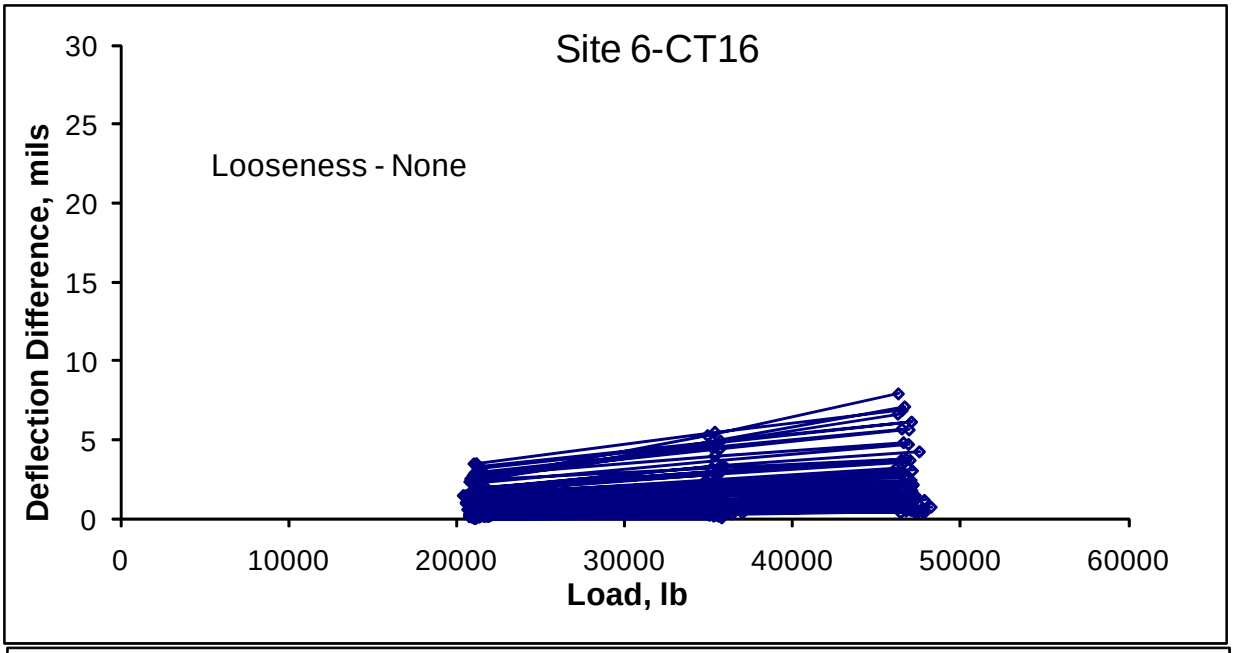
Site 6-CT16
Looseness - None
Deflection Difference, mils
Load, lb
0
5
10
15
20
25
30
0
10000
20000
30000
40000
50000
60000

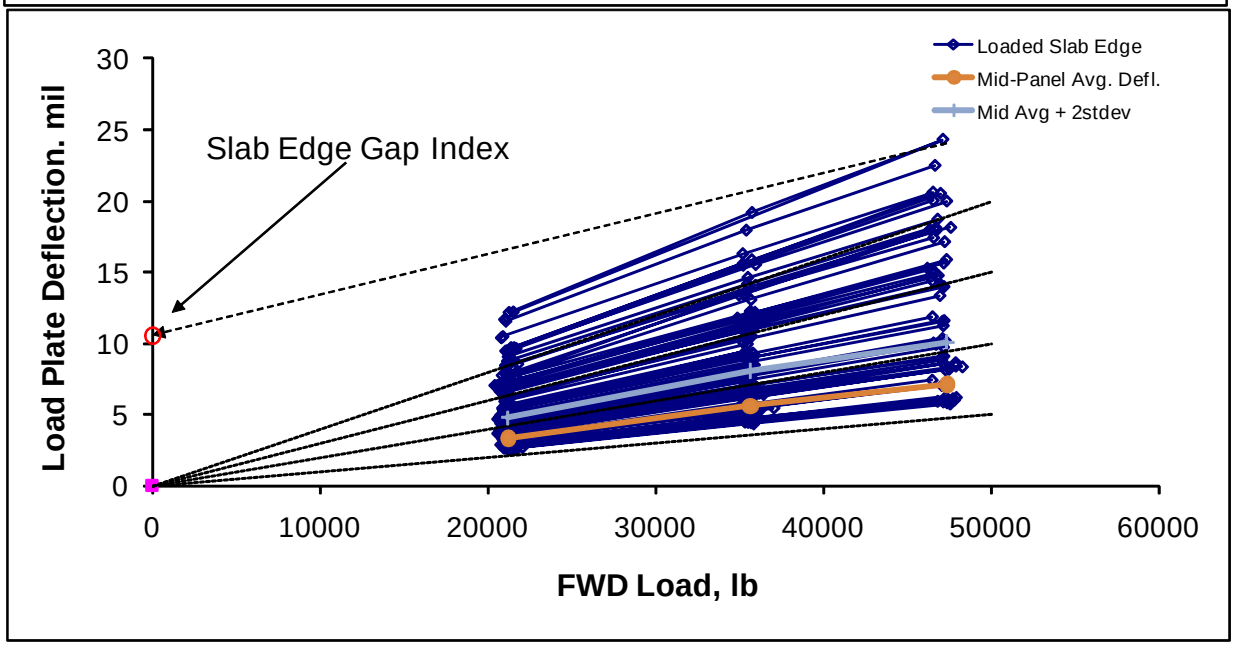
Loaded Slab Edge
Mid-Panel Avg. Defl.
Mid Avg + 2stdev
Slab Edge Gap Index
Load Plate Deflection. mil
FWD Load, lb
0
5
10
15
20
25
30
0
10000
20000
30000
40000
50000
60000

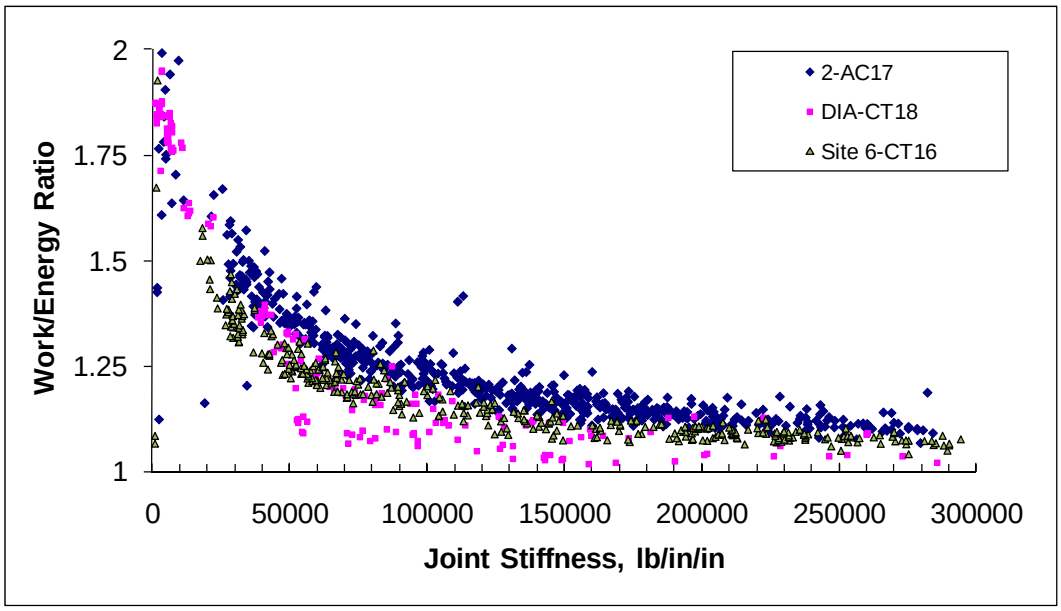
2
1.75
1.5
1.25
1
Work/Energy Ratio
0
50000
100000
150000
200000
250000
300000
Joint Stiffness, lb/in/in
2-AC17
DIA-CT18
Site 6-CT16

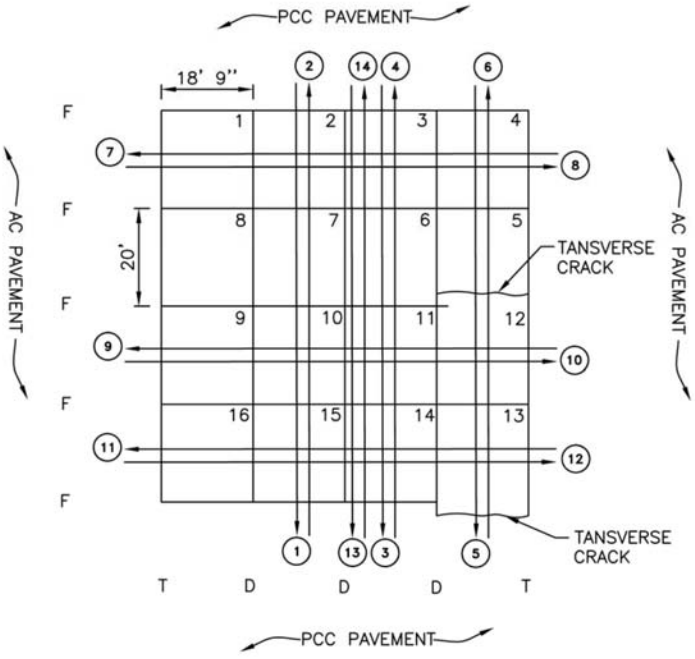

TEST PATTERN

LEGEND

(2) FWD TEST LANE NUMBER

D CONSTRUCTION JOINT: 1.25" DIA. SMOOTH DOWEL, 20" LONG, 18" SPACING, ONE SIDE OILED.

F CONTRACTION JOINT: NO LOAD TRANSFER ASSEMBLY, AGGREGATE INTERLOCK ONLY.

T THICKENED EDGE JOINT: SLAB THICKNESS INCREASED TO 16.8", NO LOAD TRANSFER ASSEMBLY, AGGREGATE INTERLOCK ONLY.

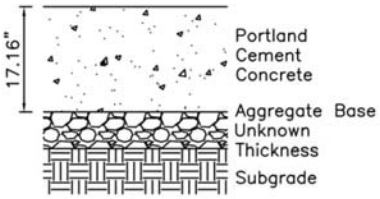

7-AGG17

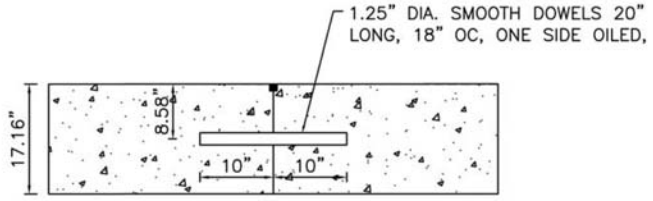

LONGITUDINAL CONSTRUCTION JOINT - D

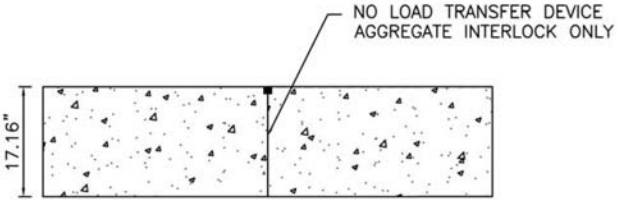

CONTRACTION JOINT - F

TEST SITE 7-AGG17

Site Description: The site is located in the north west region of the United States. Elevations of the site, as indicated by USGS maps, are approximately 2440 to 2450 feet above sea level. The airport is located in a flat area with nearby buttes and hills. Based on topographic information and observations, the site appears to be constructed on natural subgrade soils. The typical natural subgrade as indicated by USDA soil maps is silt loam. The estimated PCI and SCI of the site is 78 and 78, respectively. The primary distress observed included medium severity linear cracking.

Site Weather: The site is located in a dry/freeze climate zone. The below figures indicate the average temperature, average precipitation, average number of days above 90 degrees Fahrenheit, and average number of days below 32 degrees Fahrenheit.

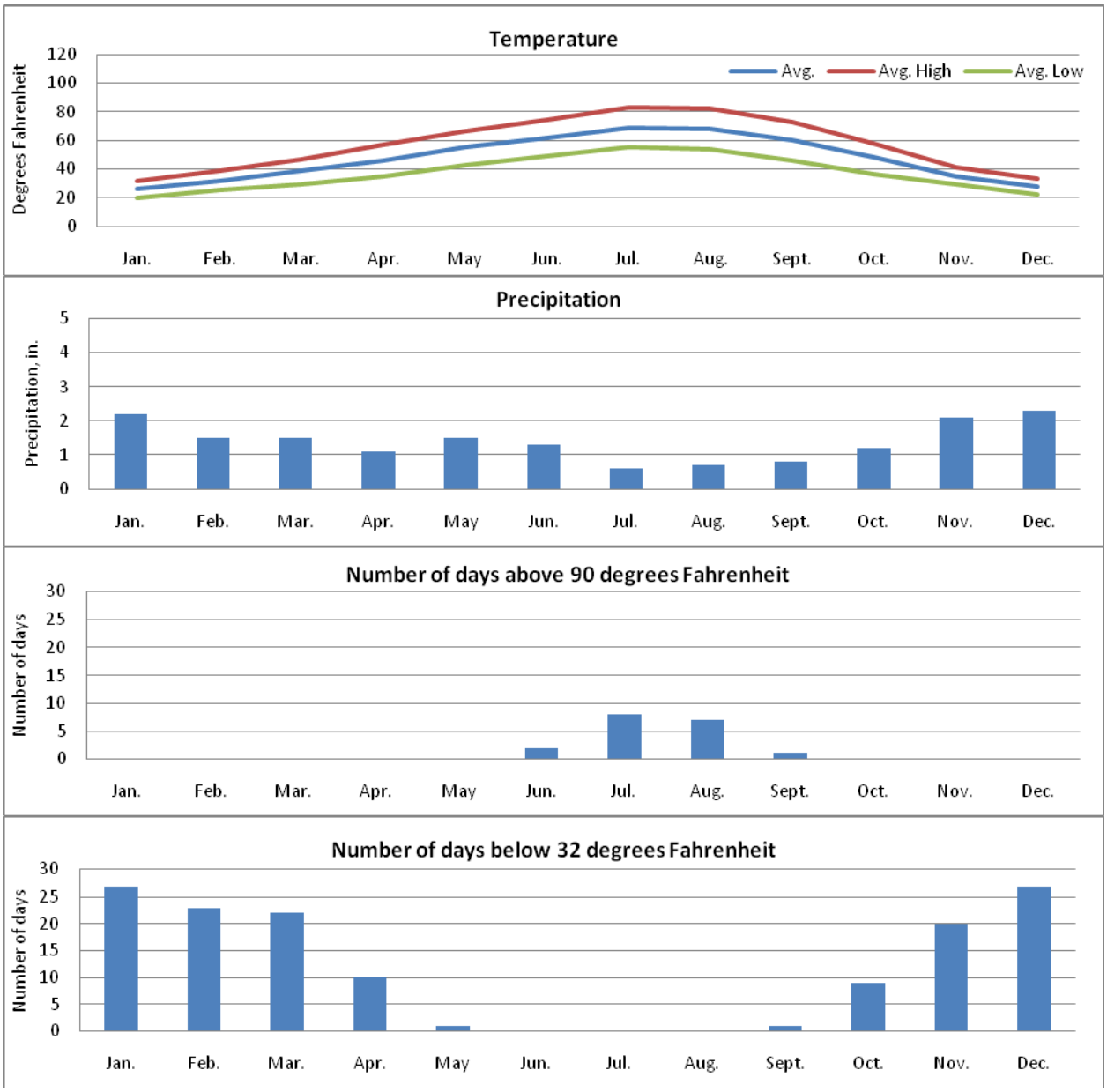

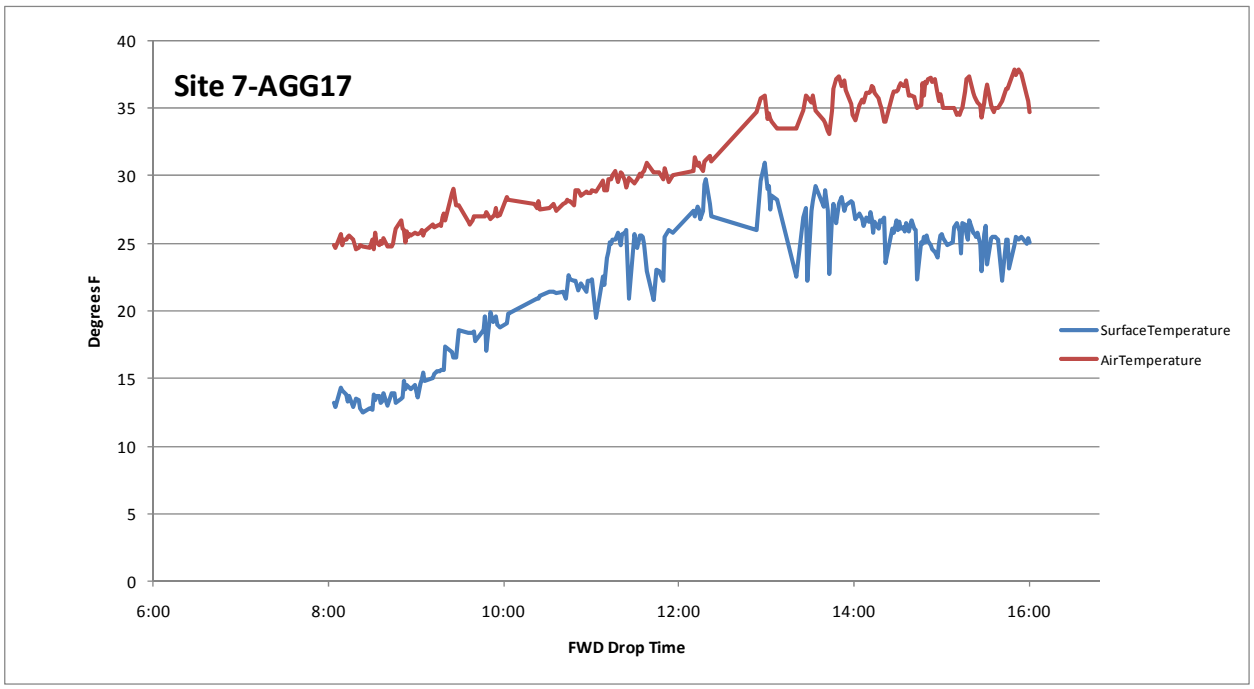

	Highway GPS3 55-3009	*Site 7-AGG17 Slab Curvature* 8AM average	AM-PM Change
average curvature, ft^{-1}	0.000547	0.000070	0.000043
min. curvature	0.000203	-0.000170	0.000024
max. curvature	0.001077	0.000247	0.000069
st. dev. of curvature	0.00021	0.000157	0.000016
number of slabs	33	7	7

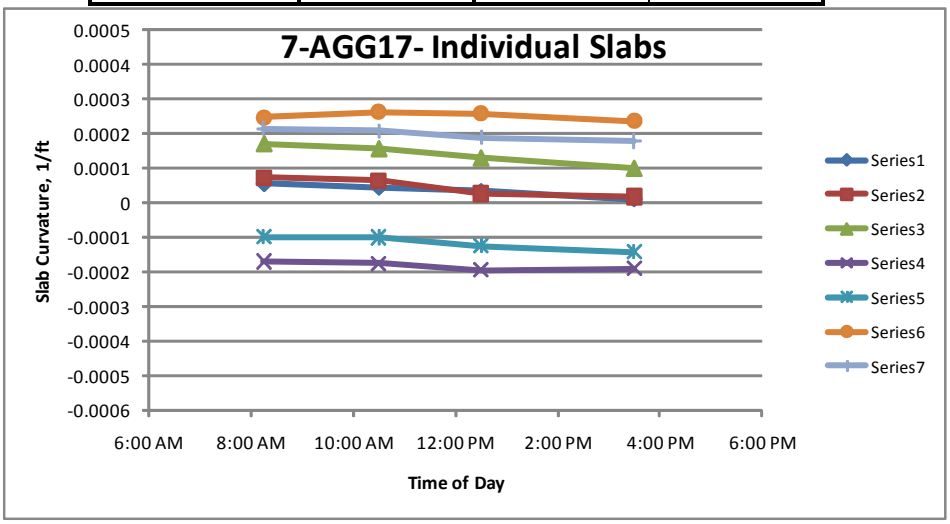

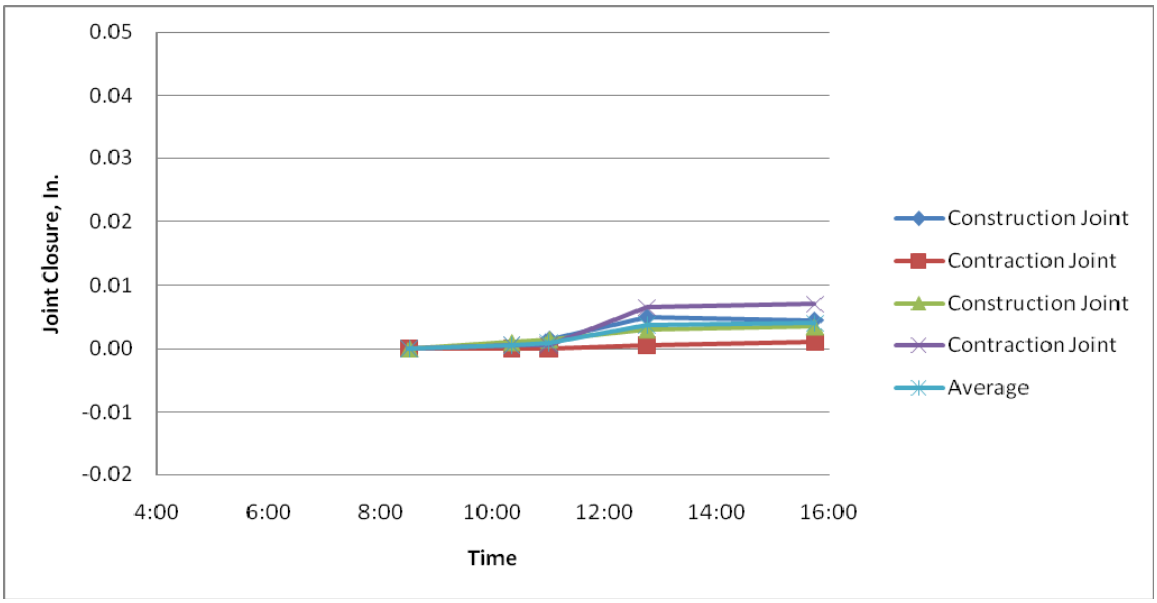

Site 7-AGG17 ILLIBACK Summary

	Dense Liquid				*Elastic Solid*			
	***k*-value**	***k* stdev**	**Slab E_C**	**E_C Stdev**	**Subg. *E***	***E* stdev**	**Slab E_C**	**E_C Stdev**
Site Average =	291	20.4	4.26	0.28	51,424	1,776	3.25	0.11
Site Min. =	426	37.1	4.47	0.36	70,427	3,021	3.31	0.14
Site Max =	248	21	3.86	0.32	44,283	2,358	2.95	0.16
R1 avg	312	22.8	4.37	0.3	54,646	1,985	3.32	0.12
R2 avg	285	19	4.27	0.27	50,542	1,643	3.26	0.11
R3 avg	278	19.4	4.15	0.27	49,316	1,710	3.17	0.11
Best Guess	**292**		**4.26**		**51501**		**3.25**	
	psi/in		*Msi*		*psi*		*Msi*	

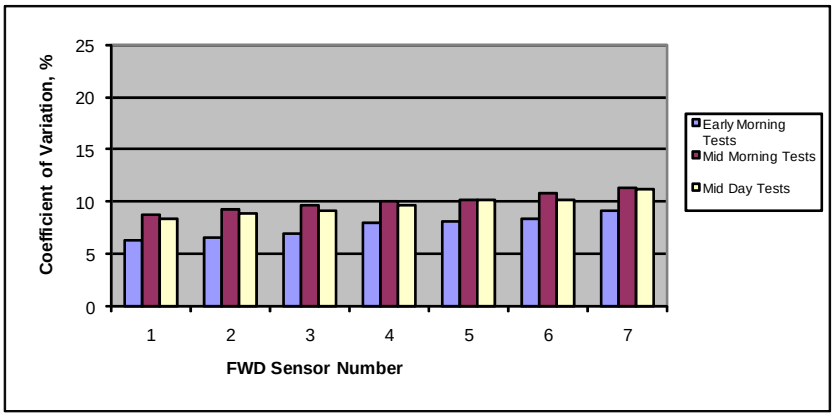

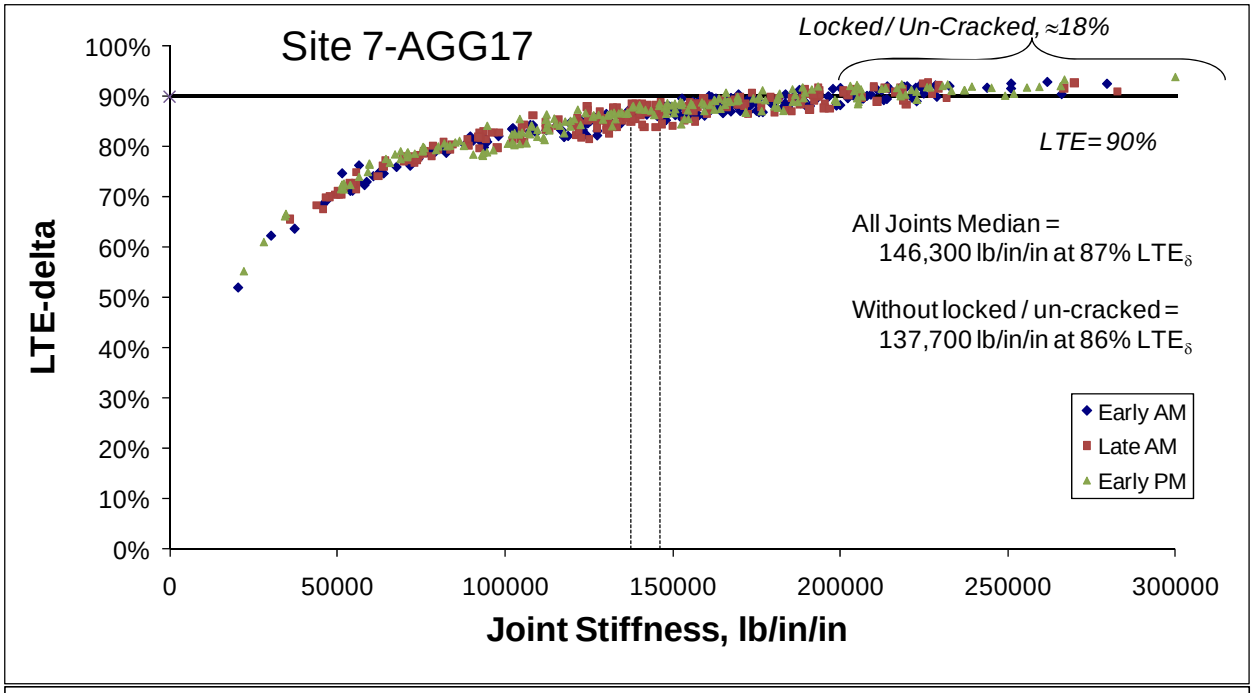
Site 7-AGG17
Locked / Un-Cracked, ≈18%
LTE = 90%
All Joints Median =
146,300 lb/in/in at 87% LTEδ
Without locked / un-cracked =
137,700 lb/in/in at 86% LTEδ
Early AM
Late AM
Early PM
LTE-delta
Joint Stiffness, lb/in/in
100%
90%
80%
70%
60%
50%
40%
30%
20%
10%
0%
0
50000
100000
150000
200000
250000
300000

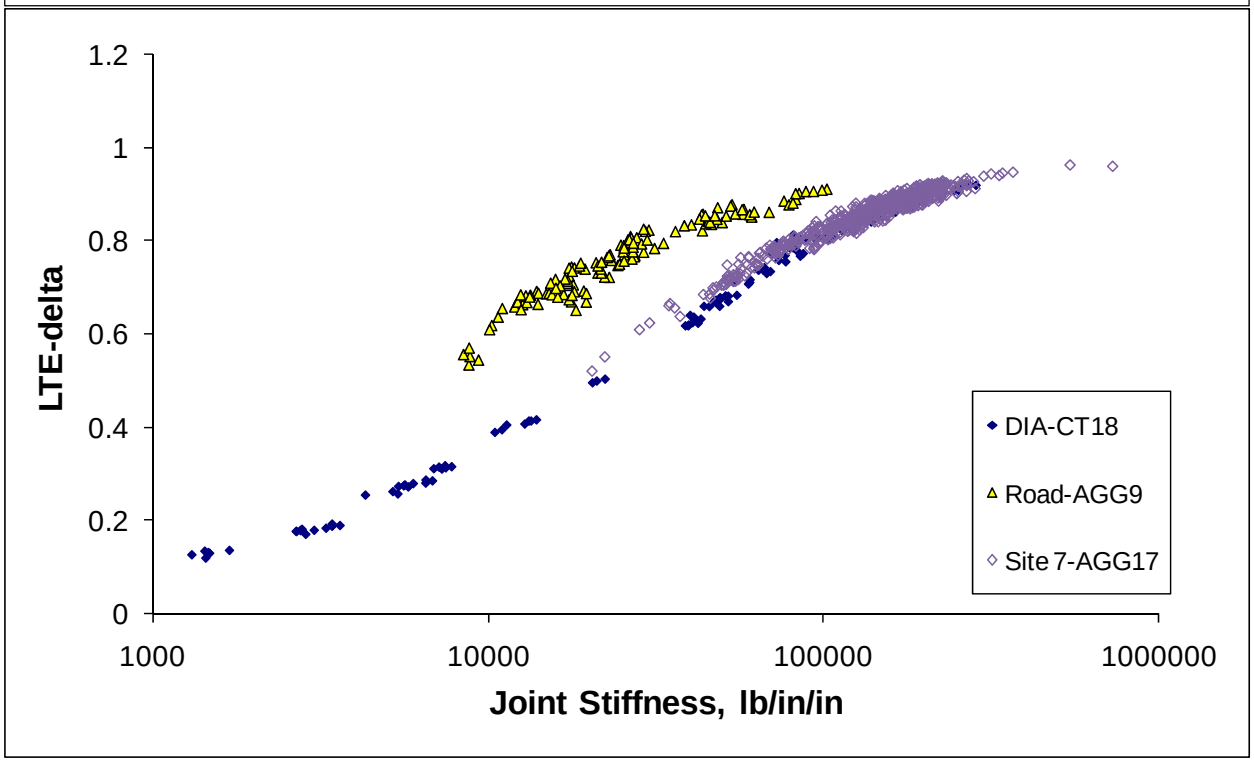
DIA-CT18
Road-AGG9
Site 7-AGG17
LTE-delta
Joint Stiffness, lb/in/in
1.2
1
0.8
0.6
0.4
0.2
0
1000
10000
100000
1000000

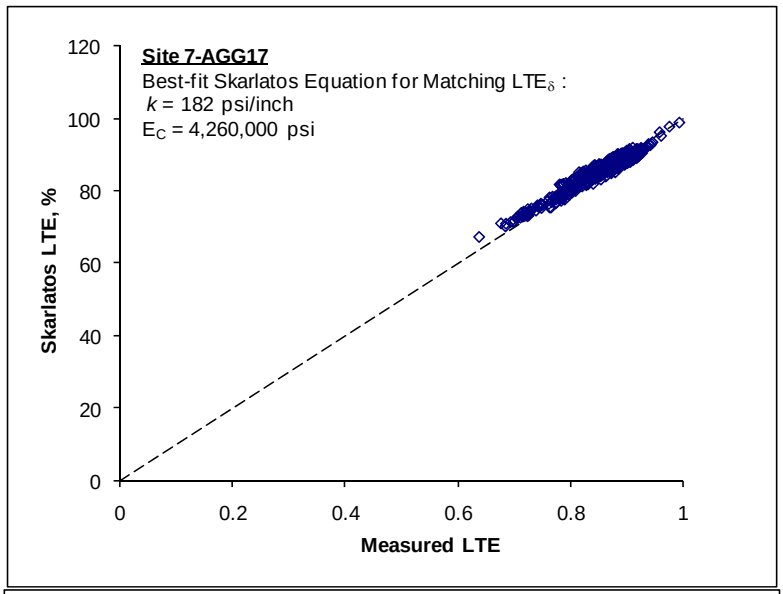
Site 7-AGG17
Best-fit Skarlatos Equation for Matching LTEδ :
k = 182 psi/inch
EC = 4,260,000 psi
Skarlatos LTE, %
Measured LTE
0
20
40
60
80
100
120
0
0.2
0.4
0.6
0.8
1

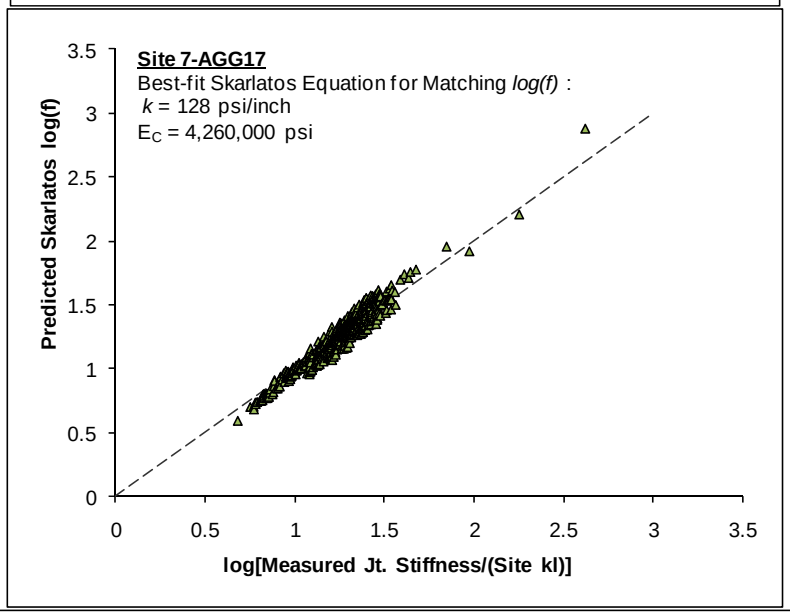
Site 7-AGG17
Best-fit Skarlatos Equation for Matching log(f) :
k = 128 psi/inch
EC = 4,260,000 psi
Predicted Skarlatos log(f)
log[Measured Jt. Stiffness/(Site kl)]
0
0.5
1
1.5
2
2.5
3
3.5

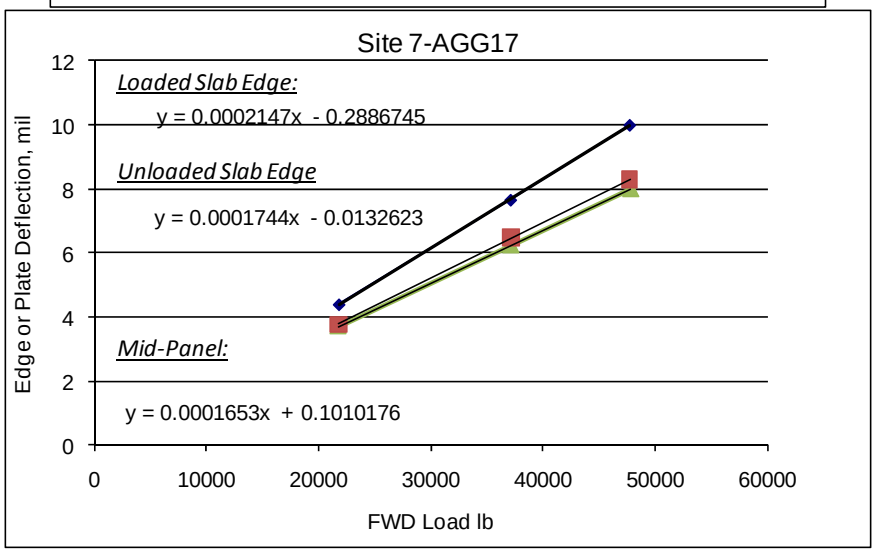
Site 7-AGG17
Loaded Slab Edge:
y = 0.0002147x - 0.2886745
Unloaded Slab Edge
y = 0.0001744x - 0.0132623
Mid-Panel:
y = 0.0001653x + 0.1010176
Edge or Plate Deflection, mil
FWD Load lb
0
2
4
6
8
10
12
0
10000
20000
30000
40000
50000
60000

Site 7-AGG17 T Agg. Interlock Contraction Joints, Including locked / un-cracked

	LR, in.	LTE	Jt. Stiffness, lb/in/in	Possible Un-cracked, LTE>90% = 23%
avg	130	87%	167092	
min	104	64%	37172	*Agg Interlock Joints*
max	171	98%	1379918	
stdev	12	5%	86589	
Median	129	88%	164029	

Without locked / un-cracked joints

	LR, in.	LTE	Jt. Stiffness, lb/in/in	Possible Un-cracked, LTE>90% = 12%
avg	128	86%	158559	
min	104	64%	37172	
max	171	98%	1379918	
stdev	11	5%	89600	
Median	127	87%	154202	

Site 7-AGG17 L. Doweled Construction Joints, Including locked / un-cracked

	LR, in.	LTE	Jt. Stiffness, lb/in/in	Possible Un-cracked, LTE>90% = 14%
avg	118	84%	138626	
min	105	68%	43635	
max	140	99%	3221449	**1" dowels at 18 inches**
stdev	8	6%	220963	Steel Area/ft = 0.523599
Median	118	85%	117473	reinf. ratio = 0.257%

Without locked / un-cracked joints

	LR, in.	LTE	Jt. Stiffness, lb/in/in	Possible Un-cracked, LTE>90% = 9%
avg	118	83%	114954	
min	105	68%	43635	kj @ DCI = 5 million; 67,369 lb/in/in
max	140	93%	279788	Probable Agg Interlock = 40,000 to 100000
stdev	8	6%	45081	
Median	117	84%	112282	

$$k = \frac{1}{s\left(\frac{\varpi}{0.9 G_d A_d} + \frac{\varpi^3}{12 E_d I_d} + \frac{2+\beta\varpi}{2\beta^3 E_d I_d}\right)}$$

s is the dowel bar spacing =	18	in
w is the joint opening =	0.1	in
Dowel Diameter =	1	in
Ad is the dowel cross-sectional area =	0.79	sq in
Ed =	29000000	psi
Gd =	11153846	psi
Id =	0.049	in^4
Back-Calculated Dowel-Concrete Interaction modulus, DCI =	10139227	psi

$$\beta = \sqrt[4]{\frac{Kd}{4 E_d I_d}} = 1.155$$

Doweled Joint Stiffness = **112282** lb/in/in

Data Not Significant
Only 2 or three joints

Site 7-AGG17 Thickened Edge AC Joint, with locked / un-cracked

	LR, in.	LTE	Jt. Stiffness, lb/in/in	Possible Un-cracked, LTE>86% = 65%
avg	90	78%	363438	
min	86	52%	20291	
max	98	99%	1932229	***Thickened free edge with AC shoulder***
stdev	3	15%	613260	un-loaded measured AC "stuck" to loaded PCC
Median	90	78%	69420	quite short response length

All Good Data- removed (negative LTE's), Removed possible un-cracked joints

	LR, in.	LTE	Jt. Stiffness, lb/in/in	Possible Un-cracked, LTE>90% = 85%
avg	90	81%	444412	
min	86	55%	22158	
max	98	99%	1932229	
stdev	3	15%	664342	
Median	90	86%	120301	

Site 7-AGG17; All Corners, including locked / un-cracked

	LR	LTE	Avg Stiffness	
avg	117	83%	128563	% possibly un-cracked, LTE>90% = 24
min	105	51%	16487	
max	132	92%	253517	
stdev	7	8%	61925	
Median	115	85%	122143	

Without locked / un-cracked

	LR	LTE	Avg Stiffness	
avg	117	82%	116680	% possibly un-cracked, LTE>90% = 15
min	105	51%	16487	
max	132	91%	252825	
stdev	8	8%	52997	
Median	116	85%	118191	

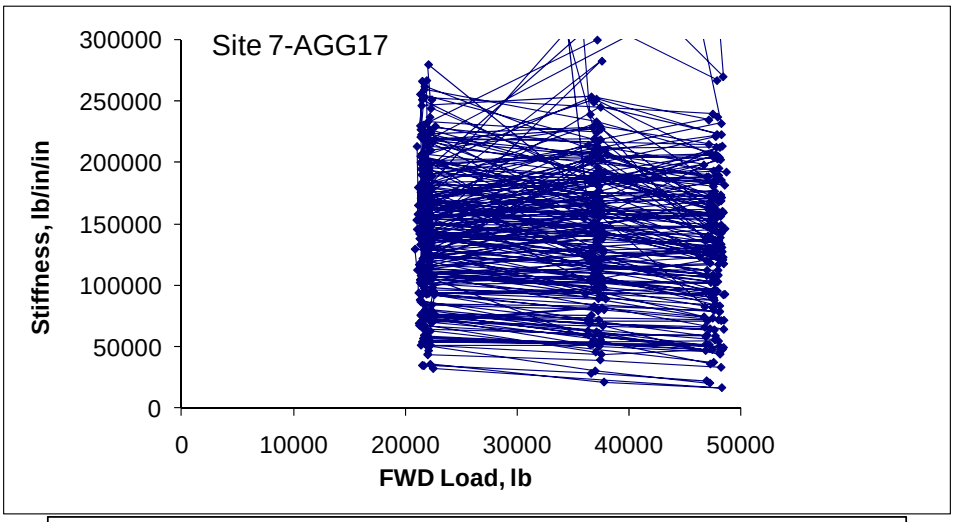
Site 7-AGG17
Stiffness, lb/in/in
300000
250000
200000
150000
100000
50000
0
0
10000
20000
30000
40000
50000
FWD Load, lb

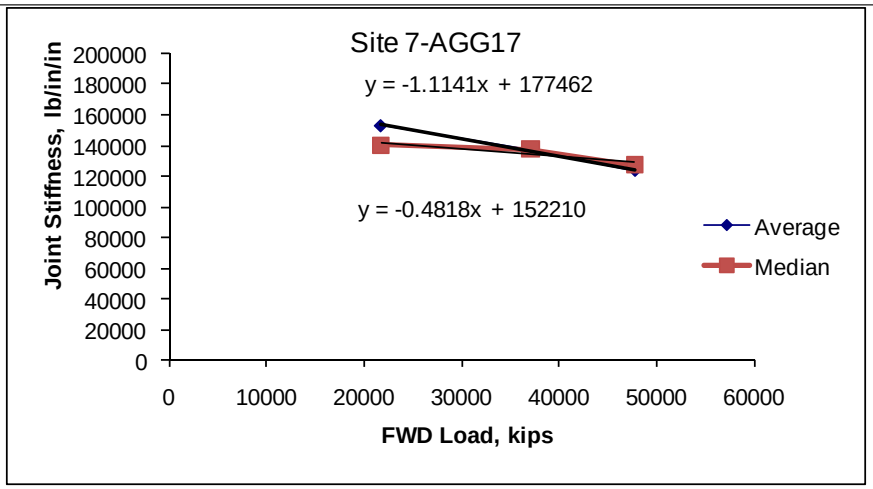
Site 7-AGG17
y = -1.1141x + 177462
y = -0.4818x + 152210
Average
Median
Joint Stiffness, lb/in/in
200000
180000
160000
140000
120000
100000
80000
60000
40000
20000
0
0
10000
20000
30000
40000
50000
60000
FWD Load, kips

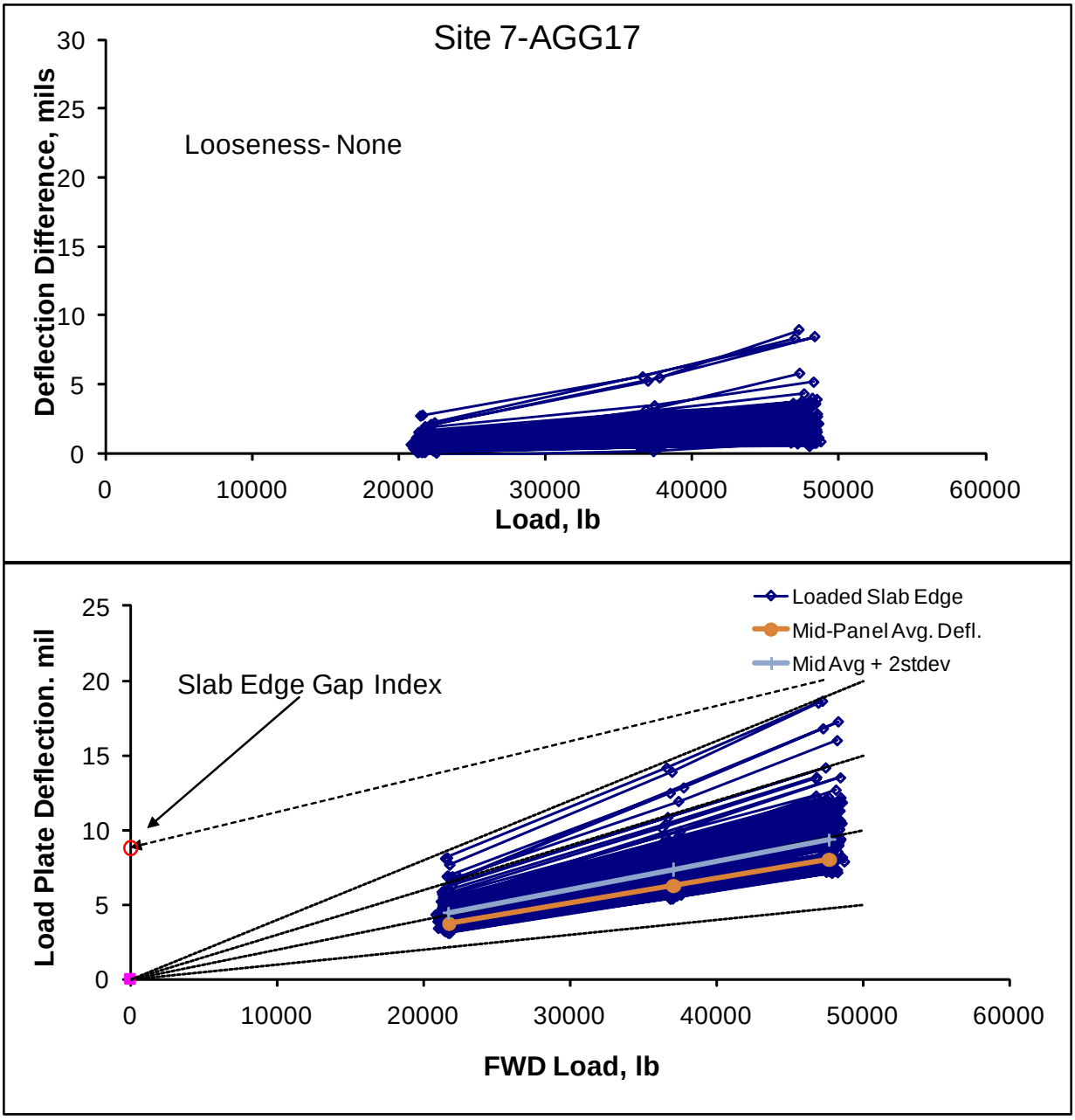

Site 7-AGG17; Slab Edge Gaps- All Good Data

	All	AM	Mid	PM
Avg	-0.34	-0.50	-0.31	-0.21
Min	-2.36	-2.36	-1.40	-0.71
Max	0.26	0.26	0.24	0.26
Stdev	0.39	0.49	0.34	0.23

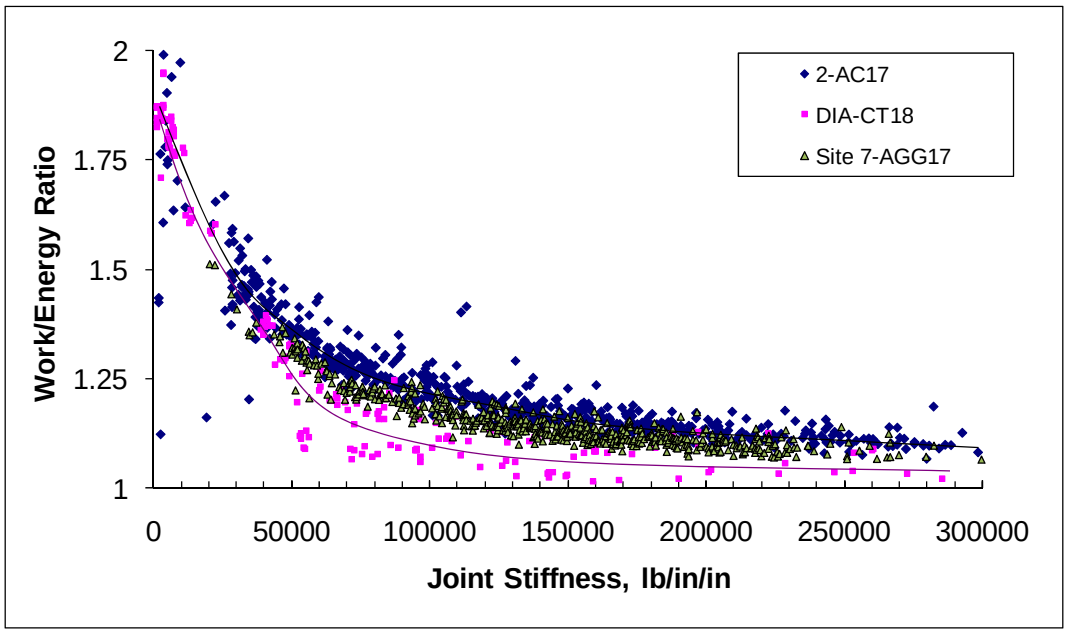
2
1.75
1.5
1.25
1
Work/Energy Ratio
0
50000
100000
150000
200000
250000
300000
Joint Stiffness, lb/in/in
2-AC17
DIA-CT18
Site 7-AGG17

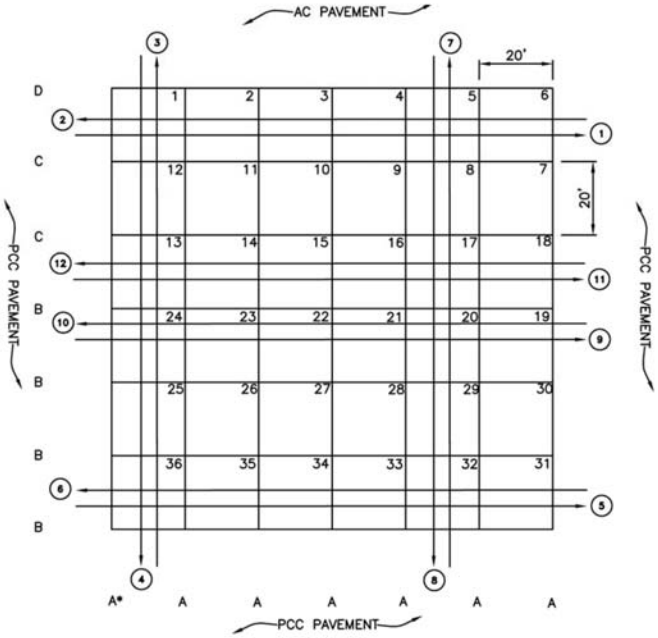

TEST PATTERN

LEGEND

(2) FWD TEST LANE NUMBER

A CONSTRUCTION JOINT: 1.25" DIA. SMOOTH DOWEL, 20" LONG, 15" SPACING, ONE SIDE PAINTED AND GREASED.

A* CONSTRUCTION JOINT: 1.25" DIA. SMOOTH DOWEL BAR, 20" LONG, 15" SPACING, ONE SIDE PAINTED AND OILED. EXCEPT SLABS 36 AND 25 HAVE #5 TIE BAR, 30" LONG, 30" SPACING, WITH KEYWAY.

B CONTRACTION JOINT: WEAKENED PLANE JOINT, NO LOAD TRANSFER ASSEMBLY.

C CONTRACTION JOINT: 1.25" DIA. SMOOTH DOWEL, 20" LONG, 15" SPACING, ONE SIDE PAINTED AND GREASED.

D THICKENED EDGE EXPANSION JOINT: 0.75" EXPANSION JOINT MATERIAL, NO LOAD TRANSFER ASSEMBLY.

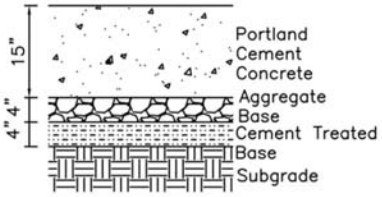

8-AGG15

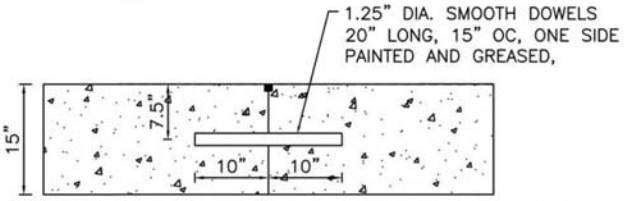

LONGITUDINAL CONSTRUCTION JOINT - A

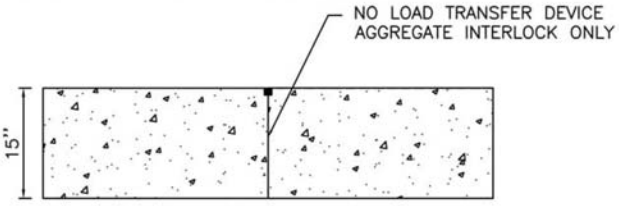

CONTRACTION JOINT - B

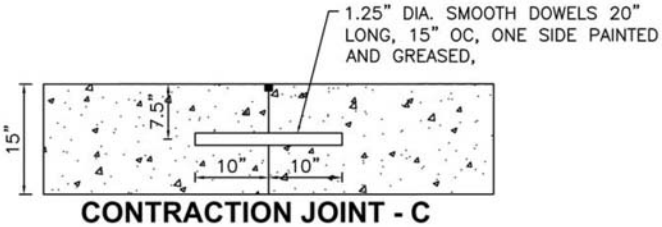

CONTRACTION JOINT - C

TEST SITE 8-AGG15

8-AGG15

Site Description: The site is located on the east coast of the United States. Elevations of the site, as indicated by USGS maps, are approximately 110 to 120 feet above sea level. Based on topographic information and observations, the site appears to be constructed on 1 to 3 feet of fill soils overlying natural subgrade soils. The typical natural subgrade as indicated by USDA soil maps is silt loam. The estimated PCI and SCI of the site is 94 and 95, respectively. The primary distress observed included low severity scaling and joint spall.

Site Weather: The site is located in a wet/freeze climate zone. The below figures indicate the average temperature, average precipitation, average number of days above 90 degrees Fahrenheit, and average number of days below 32 degrees Fahrenheit.

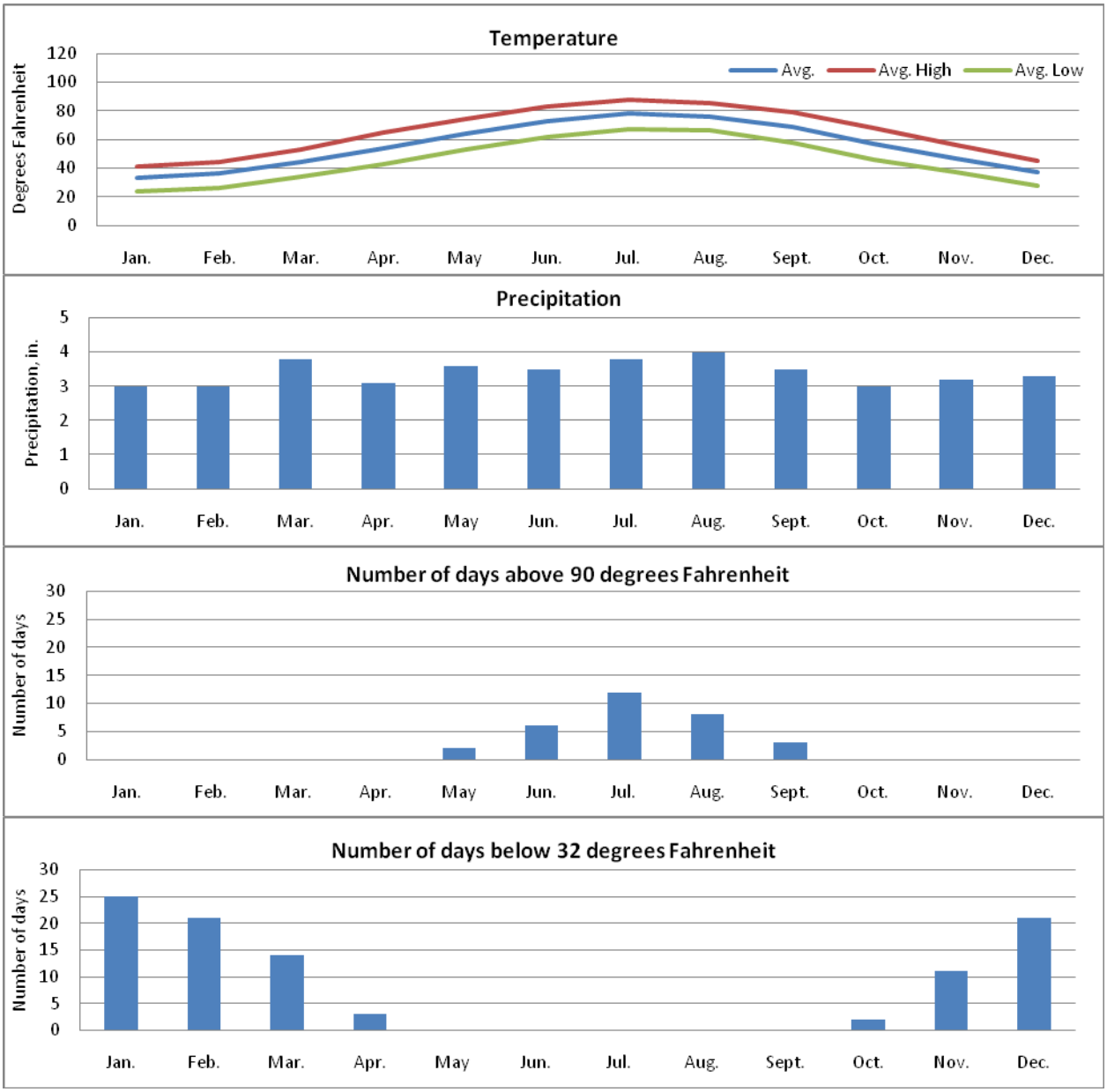

	Highway GPS3 55-3009	*Site 8-AGG15 Slab Curvature* 8AM average	AM-PM Change
average curvature, ft^{-1}	0.000547	-0.000062	0.000041
min. curvature	0.000203	-0.000358	0.000005
max. curvature	0.001077	0.000131	0.000055
st. dev. of curvature	0.00021	0.000152	0.000015
number of slabs	33	8	8

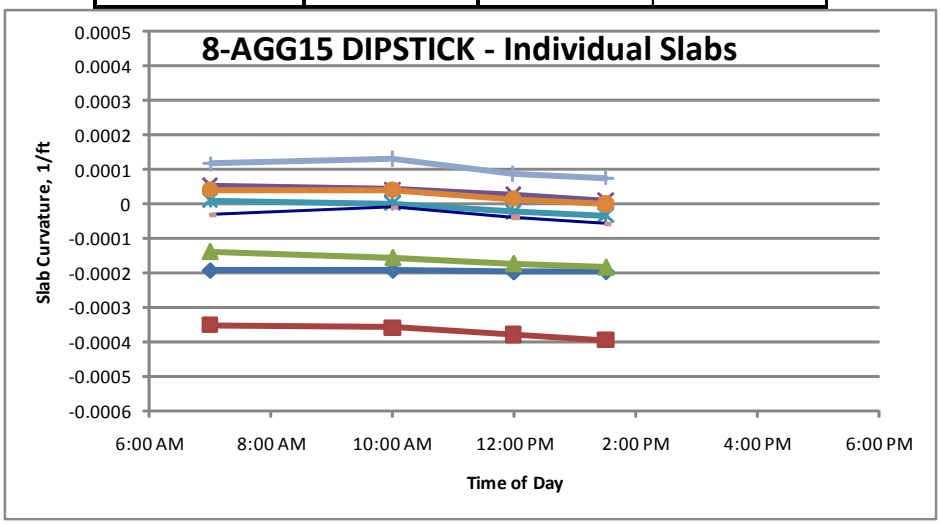

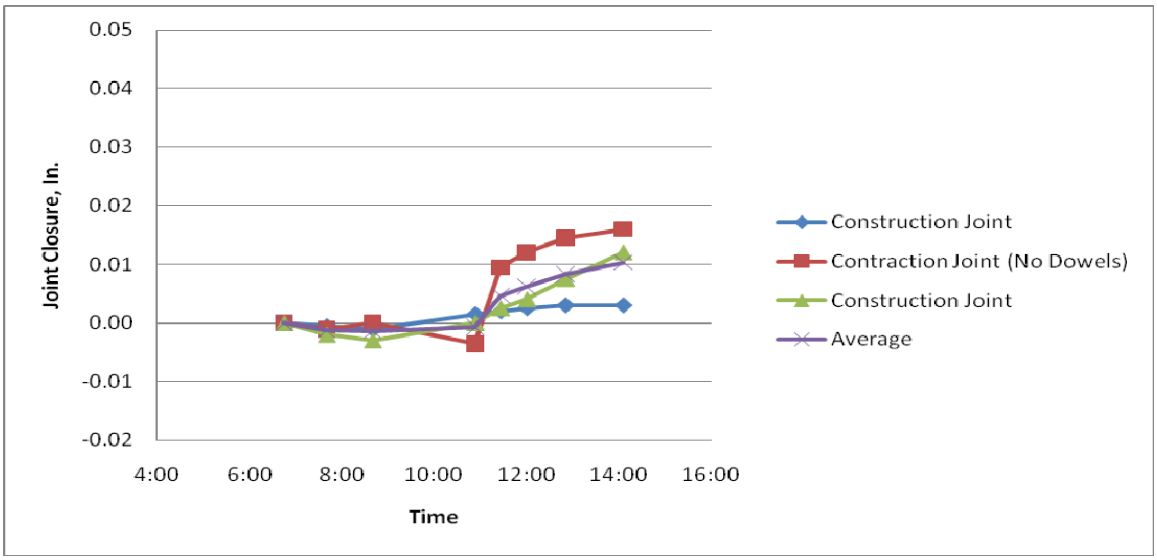

Site 8-AGG15 ILLIBACK Summary

	Dense Liquid				Elastic Solid				Radius
	k-value	*k* stdev	Slab E_C	E_C Stdev	Subg. *E*	*E* stdev	Slab E_C	E_C Stdev	l-values
Site Average =	190	11	6.81	0.37	37,492	1,189	5.35	0.17	56.7
Site Min. =	284	20	5.77	0.4	49,614	1,770	4.38	0.17	49.2
Site Max =	120	6	8.22	0.35	27,105	699	6.75	0.17	66.6
Best Guess	**190**		**6.80**		**37500**		**5.35**		**56.7**
	psi/in		*Msi*		*psi*		*Msi*		*inches*

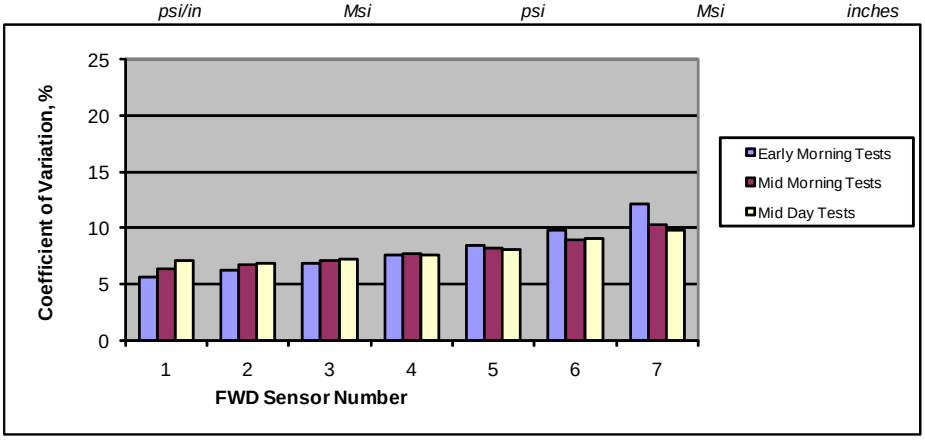

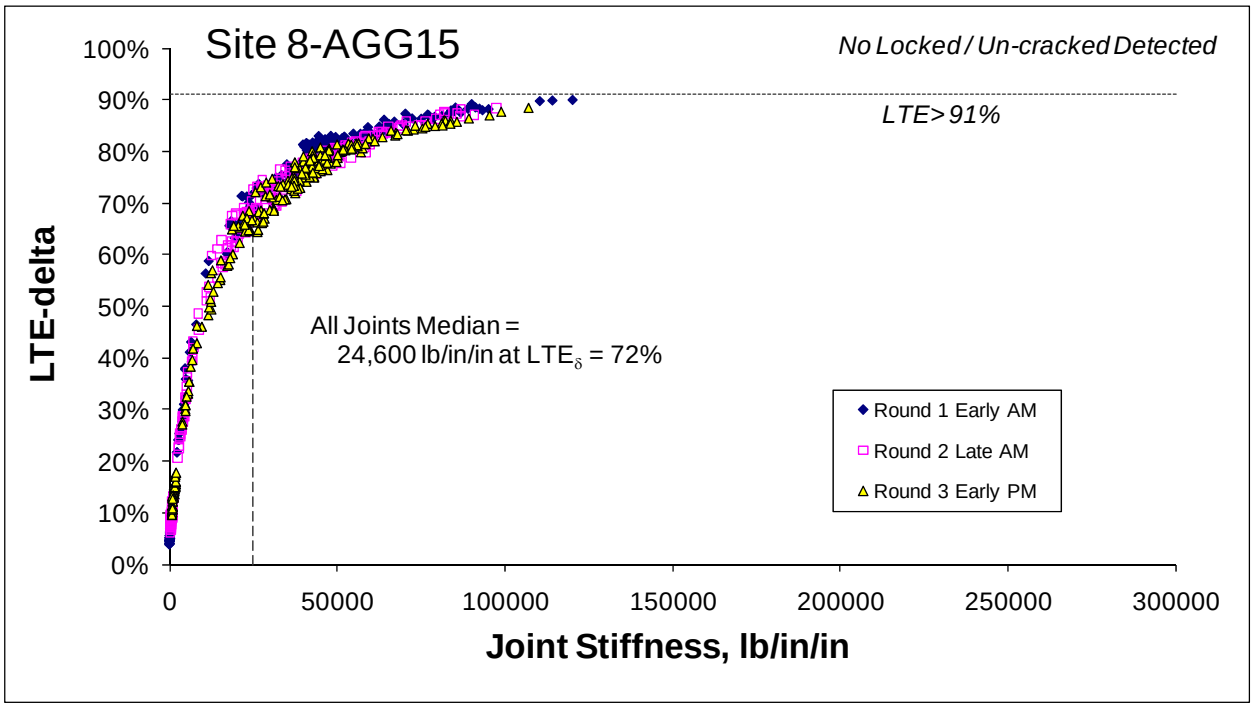

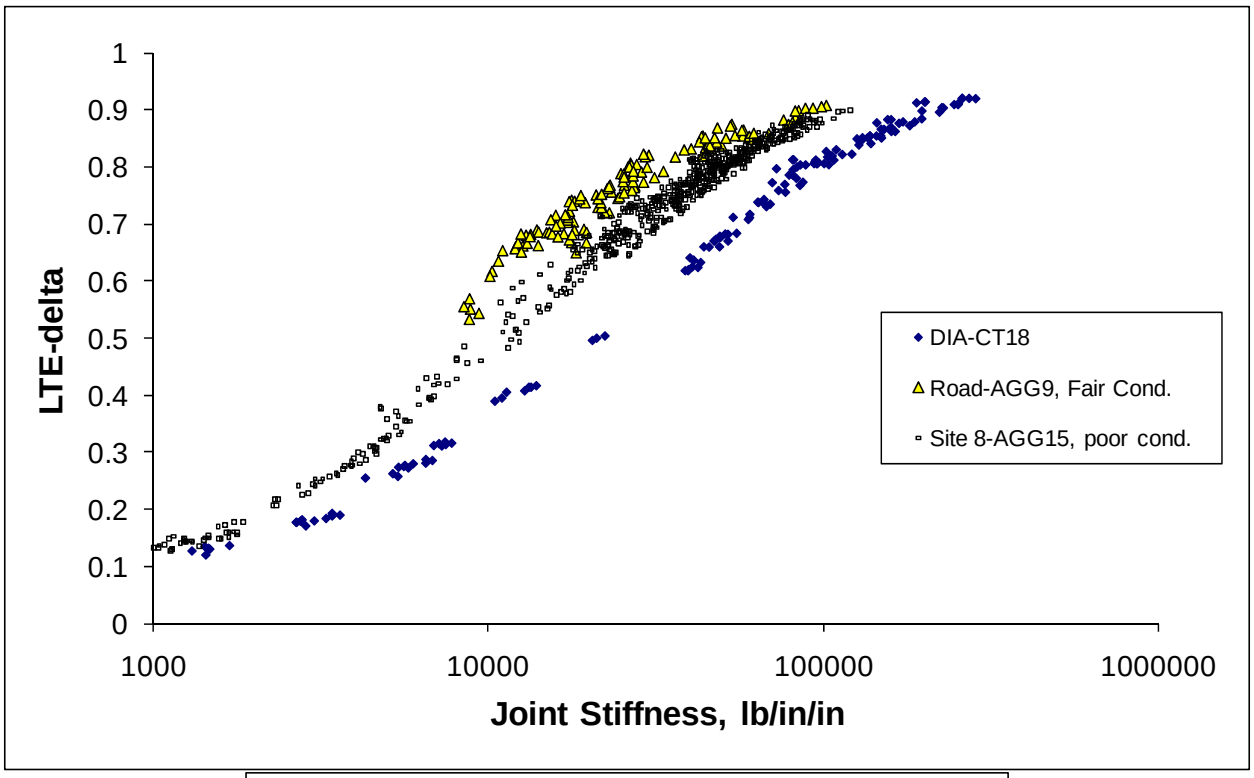
LTE-delta
1
0.9
0.8
0.7
0.6
0.5
0.4
0.3
0.2
0.1
0
1000
10000
100000
1000000
Joint Stiffness, lb/in/in
DIA-CT18
Road-AGG9, Fair Cond.
Site 8-AGG15, poor cond.

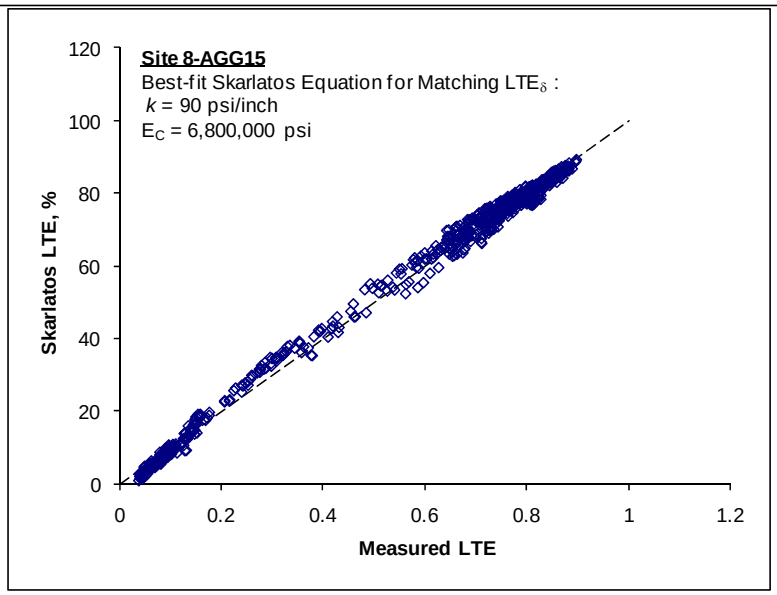
Site 8-AGG15
Best-fit Skarlatos Equation for Matching LTEδ :
k = 90 psi/inch
EC = 6,800,000 psi
Skarlatos LTE, %
120
100
80
60
40
20
0
0
0.2
0.4
0.6
0.8
1
1.2
Measured LTE

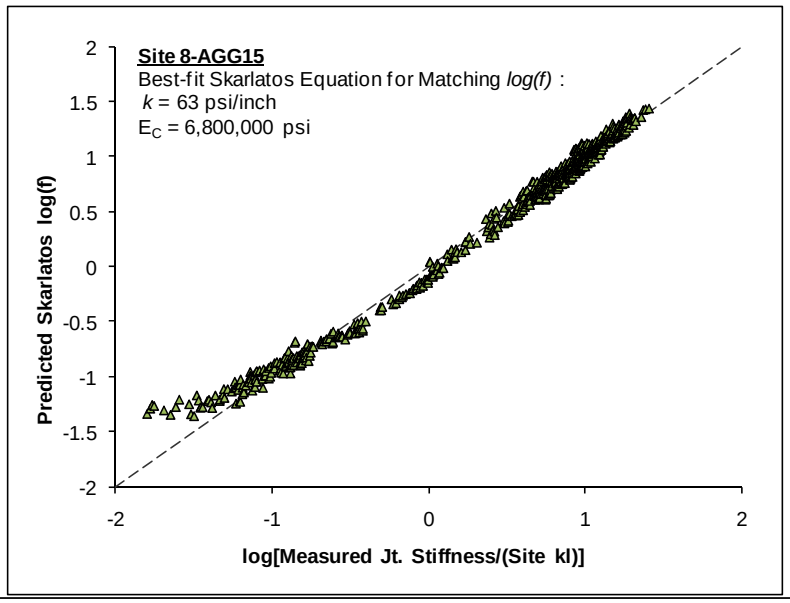
Site 8-AGG15
Best-fit Skarlatos Equation for Matching log(f) :
k = 63 psi/inch
E_C = 6,800,000 psi
Predicted Skarlatos log(f)
log[Measured Jt. Stiffness/(Site kl)]
2
1.5
1
0.5
0
-0.5
-1
-1.5
-2
-2
-1
0
1
2

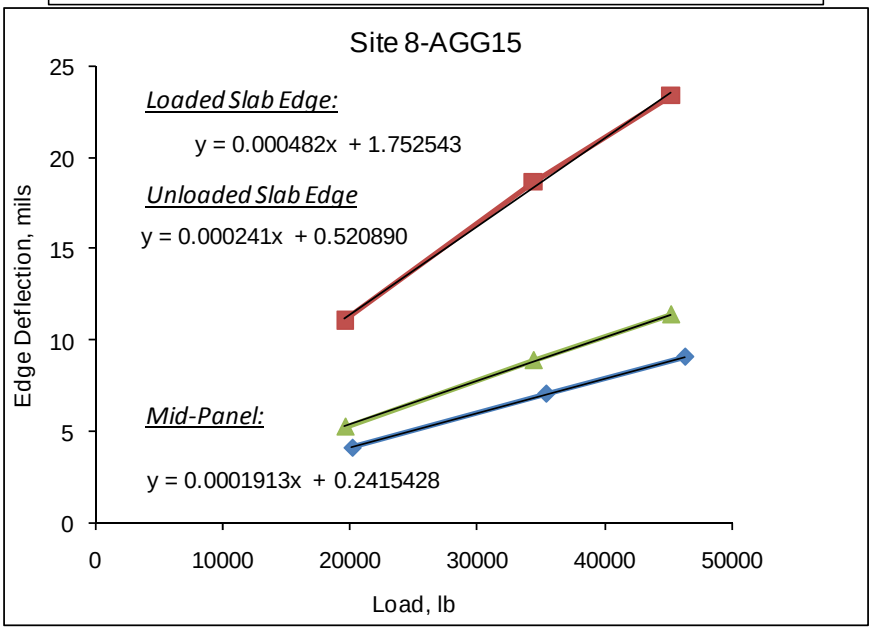
Site 8-AGG15
Loaded Slab Edge:
y = 0.000482x + 1.752543
Unloaded Slab Edge
y = 0.000241x + 0.520890
Mid-Panel:
y = 0.0001913x + 0.2415428
Edge Deflection, mils
Load, lb
25
20
15
10
5
0
0
10000
20000
30000
40000
50000

****Site 8-AGG15 Doweled Construction Joints, No locked / un-cracked Detected**

	LR, in.	LTE	Jt. Stiffness, lb/in/in	Possible Un-cracked, LTE>89% = 1.2%
avg	118	74.3%	43946	
Median	116	78%	41979	***Formed, 1.25" dowels at 15", near 3-slab reinforced edge***
min	107	21%	2276	
max	138	90%	120194	Steel Area/ft = 0.981748
stdev	5.9	13%	22181	reinf. ratio = 0.545%

Probable Agg. Interlock = 0 to 40000

$$k = \frac{1}{s\left(\frac{\varpi}{0.9 G_d A_d} + \frac{\varpi^3}{12 E_d I_d} + \frac{2+\beta\varpi}{2\beta^3 E_d I_d}\right)}$$

s is the dowel bar spacing =	15	in
w is the joint opening =	0.1	in
Dowel Diameter =	1.25	in
Ad is the dowel cross-sectional area =	1.23	sq in
Ed =	29000000	psi
Gd =	11153846	psi
Id =	0.120	in^4
Back-Calculated Dowel-Concrete Interaction modulus, DCI =	1192043	psi

$$\beta = \sqrt[4]{\frac{Kd}{4 E_d I_d}} = 0.572$$

Doweled Joint Stiffness = **41979** lb/in/in

****Site 8-AGG15 Aggregate Interlock Joints, No locked / un-cracked Detected**

	LR, in.	LTE	Jt. Stiffness, lb/in/in	Possible Un-cracked, LTE>89% = 1.5%
avg	217	9.4%	644	
Median	209	9%	562	***Agg Interlock Only- Gone***
min	149	4%	41	
max	438	18%	1856	
stdev	45.3	4%	446	

****Site 8-AGG15 Doweled Contraction Joints, No locked / un-cracked Detected**

	LR, in.	LTE	Jt. Stiffness, lb/in/in	Possible Un-cracked, LTE>89% = 1.5%
avg	122	50.4%	14232	
Median	120	53%	12208	***Sawed, 1.25" Dowels at 15", next to expansion jt!***
min	109	24%	3039	
max	137	82%	44135	Steel Area/ft = 0.981748
stdev	7.4	17%	10203	reinf. ratio = 0.545%

Probable Agg Interlock = 0 to 10000

$$k = \frac{1}{s\left(\frac{\varpi}{0.9 G_d A_d} + \frac{\varpi^3}{12 E_d I_d} + \frac{2+\beta\varpi}{2\beta^3 E_d I_d}\right)}$$

s is the dowel bar spacing =	15	in
w is the joint opening =	0.1	in
Dowel Diameter =	1.25	in
Ad is the dowel cross-sectional area =	1.23	sq in
Ed =	29000000	psi
Gd =	11153846	psi
Id =	0.120	in^4
Back-Calculated Dowel-Concrete Interaction modulus, DCI =	225666	psi

$$\beta = \sqrt[4]{\frac{Kd}{4 E_d I_d}} = 0.377$$

Doweled Joint Stiffness = **12208** lb/in/in

****Site 8-AGG15 Corner Load Tests, no locked / uncracked detected**

	LR, in.	LTE	Jt. Stiffness, lb/in/in
avg	136	58.8%	28256
median	121	72%	24578
min	106	4%	41
max	438	90%	120194
stdev	41.4	28%	24722

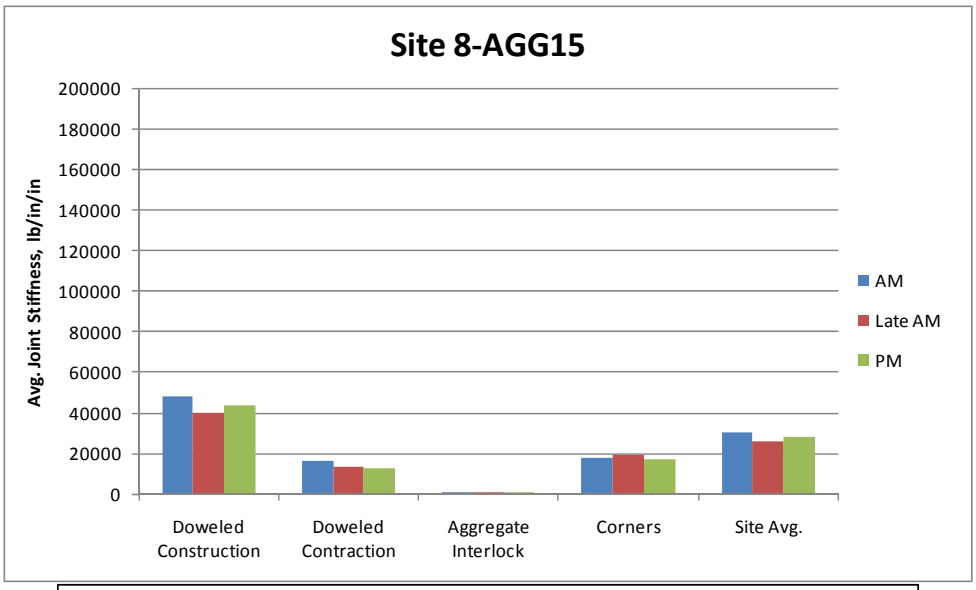

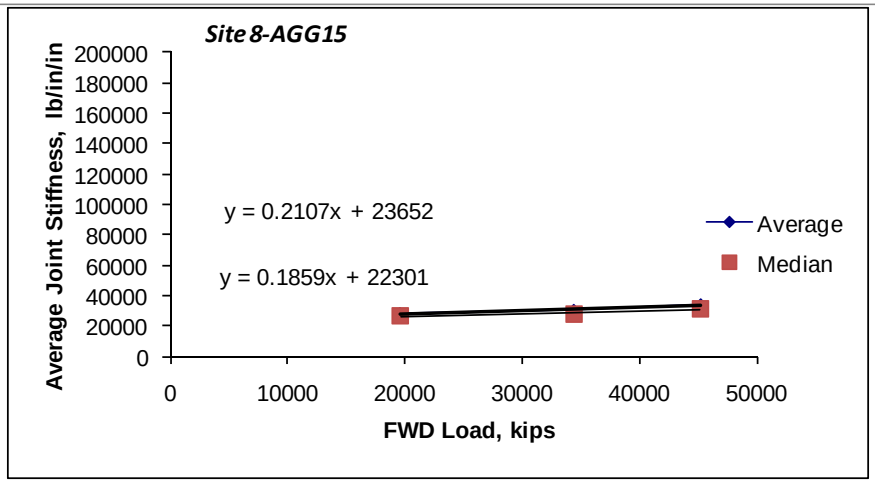

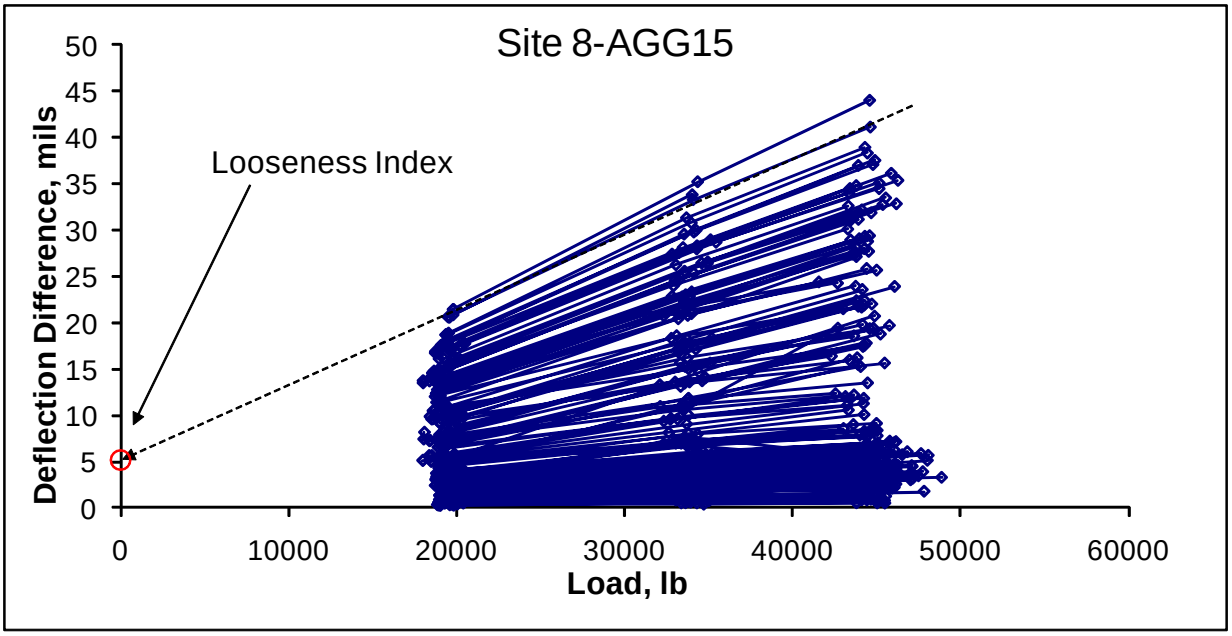

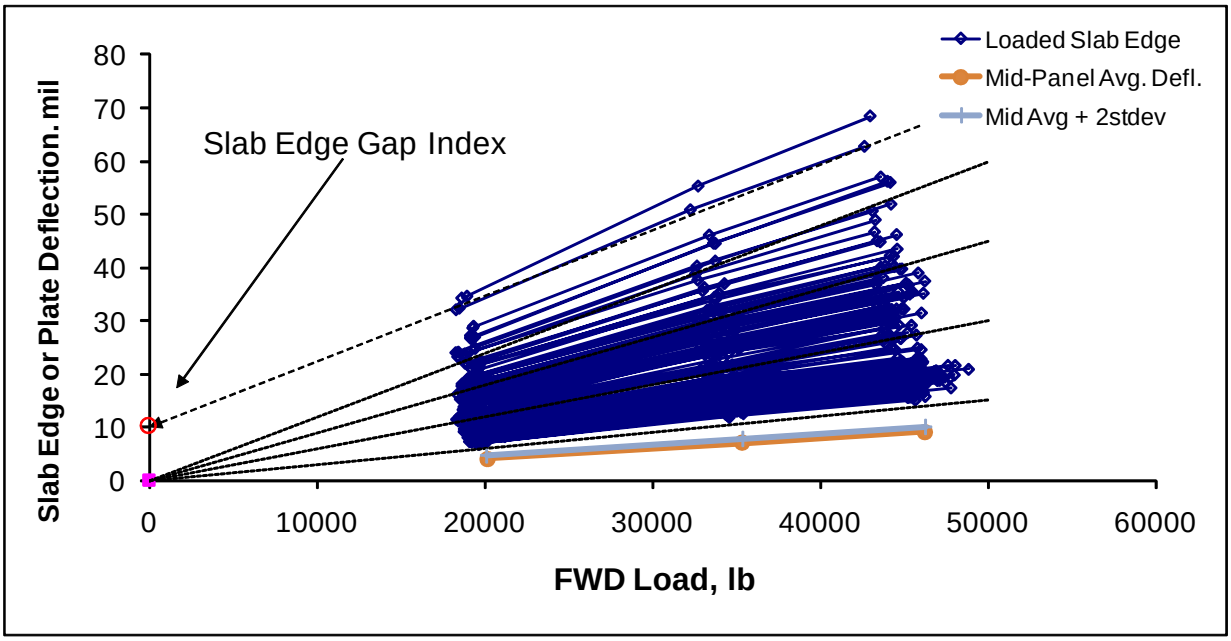

Site 8-AGG15; Slab Edge Gaps

	All	AM	Mid	PM	D-Constr.	Agg Interl.	D-Contra.	Corners
Avg	1.86	2.35	1.99	1.24	1.34	2.52	0.75	3.75
Min	-3.06	-1.75	-1.39	-3.06	0.09	0.01	-1.75	-3.06
Max	9.03	7.97	9.03	8.15	5.28	4.49	2.86	9.03
Stdev	1.57	1.55	1.53	1.44	0.84	1.14	1.10	2.35

Site 8-AGG15; Joint Looseness Data

Looseness	All Data	Agg Interlock	Doweled Contra.	Doweled Const.	Corners
Average	1.11	2.40	-0.09	0.75	1.72
Maximum	5.78	4.67	2.76	5.16	5.78
Minimum	-6.25	-0.34	-6.25	-0.14	-5.09
Std. Dev.	1.60	1.23	2.25	0.89	2.22
Count	210	35	20	113	31
19.5 kip %	20%	44%	-2%	14%	32%
34.2 kip %	12%	26%	-1%	8%	19%
44.9 kip %	10%	22%	-1%	7%	16%

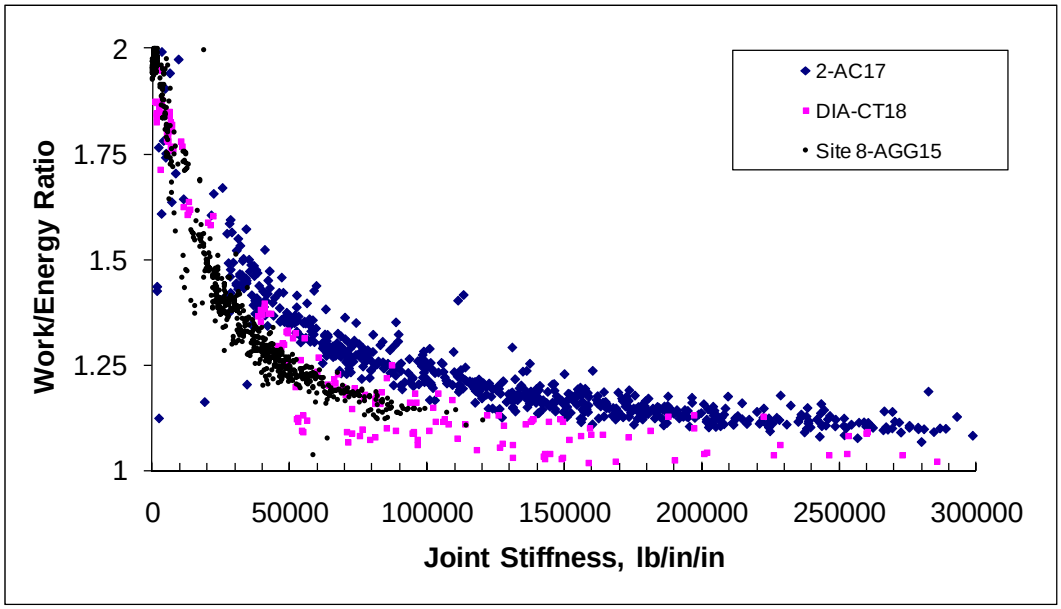

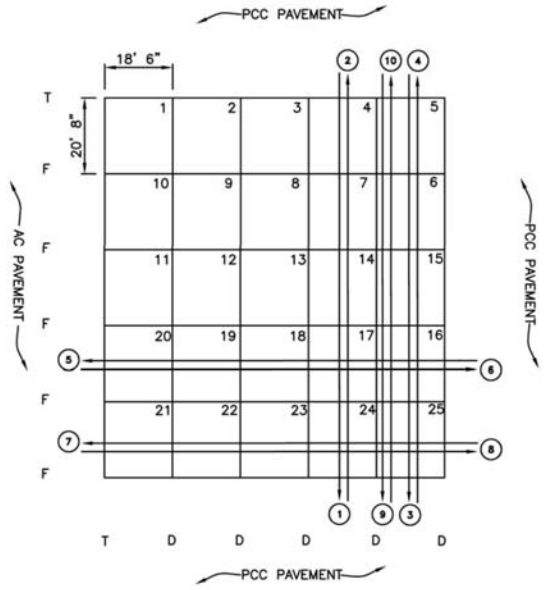

TEST PATTERN

LEGEND

(2) FWD TEST LANE NUMBER

D CONSTRUCTION JOINT: 1.0" DIA. SMOOTH DOWEL, 20" LONG, 18" SPACING, ONE SIDE OILED.

F CONTRACTION JOINT: NO LOAD TRANSFER ASSEMBLY, AGGREGATE INTERLOCK ONLY.

T THICKENED EDGE JOINT: SLAB THICKNESS INCREASED TO 16.8", NO LOAD TRANSFER ASSEMBLY, AGGREGATE INTERLOCK ONLY.

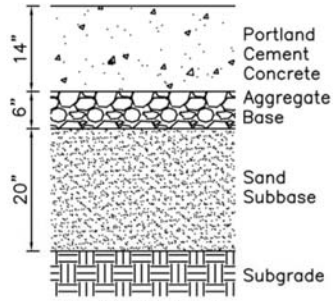

9-AGG14

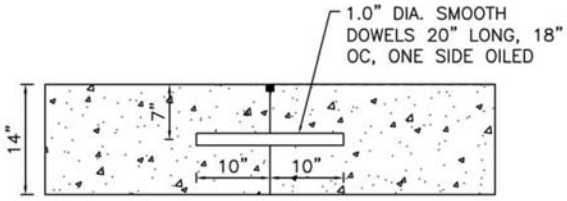

LONGITUDINAL CONSTRUCTION JOINT - D

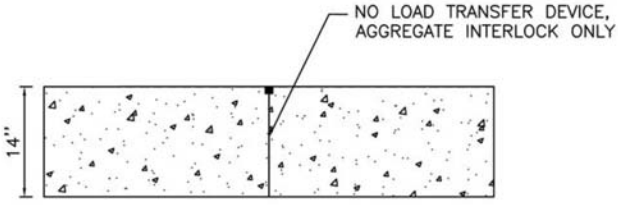

CONTRACTION JOINT - F

TEST SITE 9-AGG14

Site Description: The site is located in the northwest region of the United States. Elevations of the site, as indicated by USGS maps, are approximately 2440 to 2450 feet above sea level. The airport is located in a flat area with nearby buttes and hills. Based on topographic information and observations, the site appears to be constructed on natural subgrade soils. The typical natural subgrade as indicated by USDA soil maps is silt loam. The estimated PCI and SCI of the site is 92 and 92, respectively. The primary distress observed included low severity linear cracking and low severity joint spall.

Site Weather: The site is located in a dry/freeze climate zone. The below figures indicate the average temperature, average precipitation, average number of days above 90 degrees Fahrenheit, and average number of days below 32 degrees Fahrenheit.

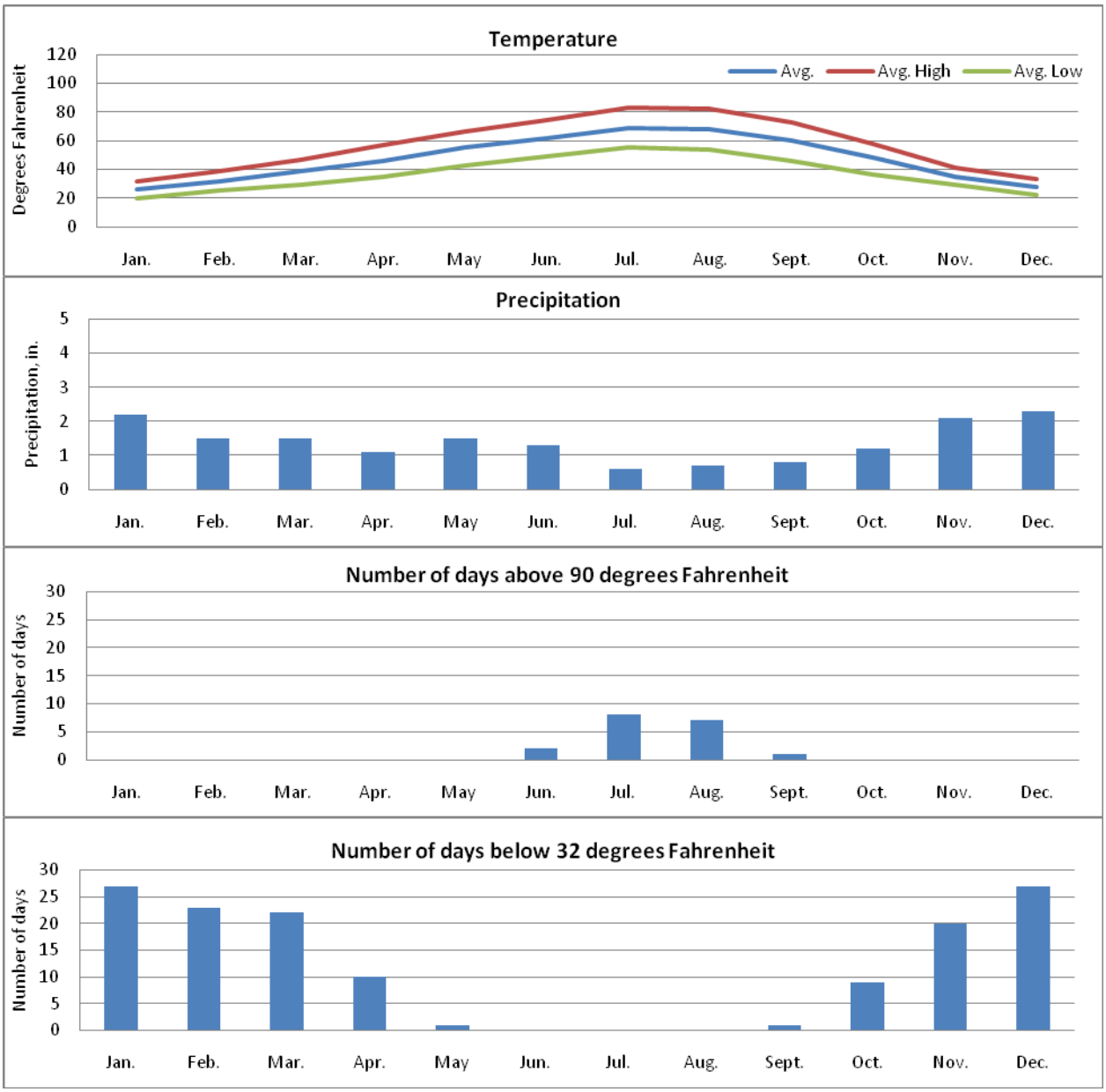

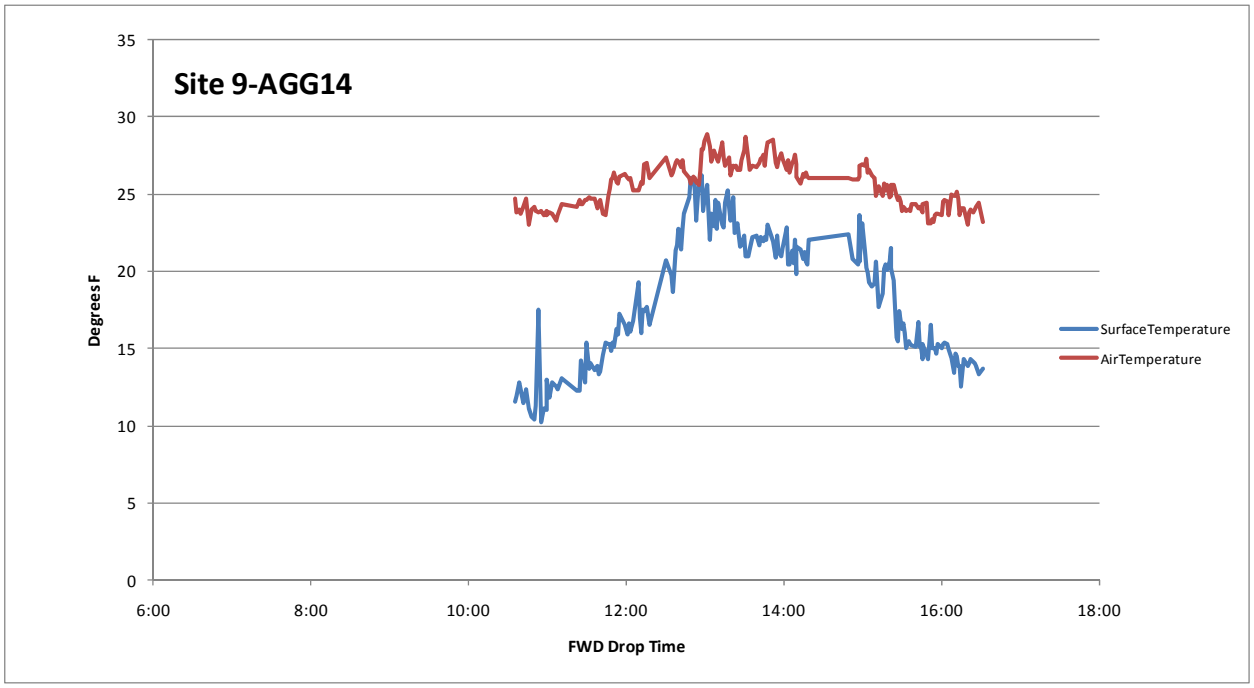

	Highway	*Site 9-AGG14 Slab Curvature*	
	GPS3 55-3009	8AM average	AM-PM Change
average curvature, ft^{-1}	0.000547	-0.000021	0.000042
min. curvature	0.000203	-0.000319	0.000027
max. curvature	0.001077	0.000231	0.000061
st. dev. of curvature	0.00021	0.000204	0.000013
number of slabs	33	7	7

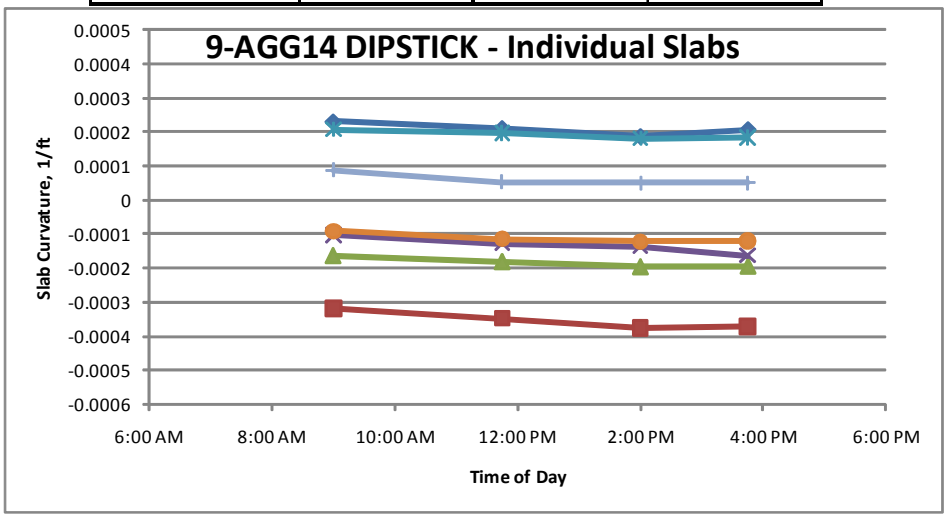

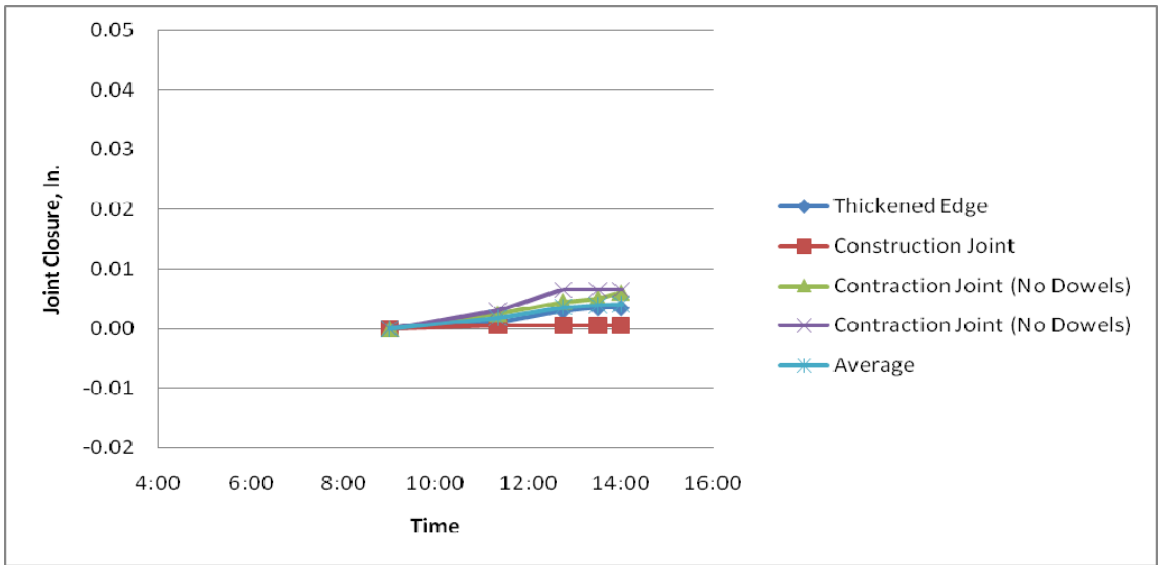

Site 9-AGG14; ILLIBACK Summary

	Dense Liquid				*Elastic Solid*			
	***k*-value**	***k* stdev**	**Slab E_C**	**E_C Stdev**	**Subg. *E***	***E* stdev**	**Slab E_C**	**E_C Stdev**
Site Average =	227	9.2	6.48	0.25	40,778	611	4.97	0.07
Site Min defl. =	452	26.7	5.64	0.32	68,875	1,653	4.05	0.1
Site Max defl. =	165	6.9	5.85	0.23	31,019	565	4.54	0.08
R1 avg	258	11.5	6.51	0.27	45,065	692	4.96	0.08
R2 avg	203	7.5	6.51	0.22	37,346	543	5.03	0.07
R3 avg	227	9.5	6.36	0.25	40,680	631	4.88	0.08
5M R1	163	6.1	12.58	0.45	36,191	704	10.26	0.2
5M R2	70	0.6	9.58	0.09	17,619	394	8.06	0.18
5M R3	88	1	8.19	0.09	20,334	368	6.75	0.12
Best Guess	**229**		**6.46**		**41030**		**4.96**	
	psi/in		*Msi*		*psi*		*Msi*	

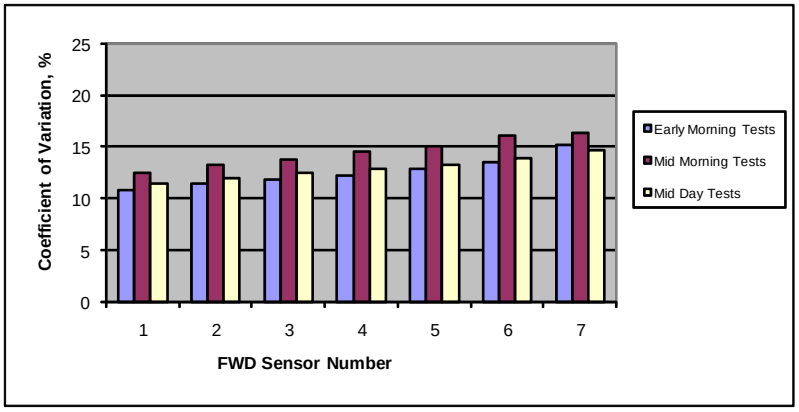

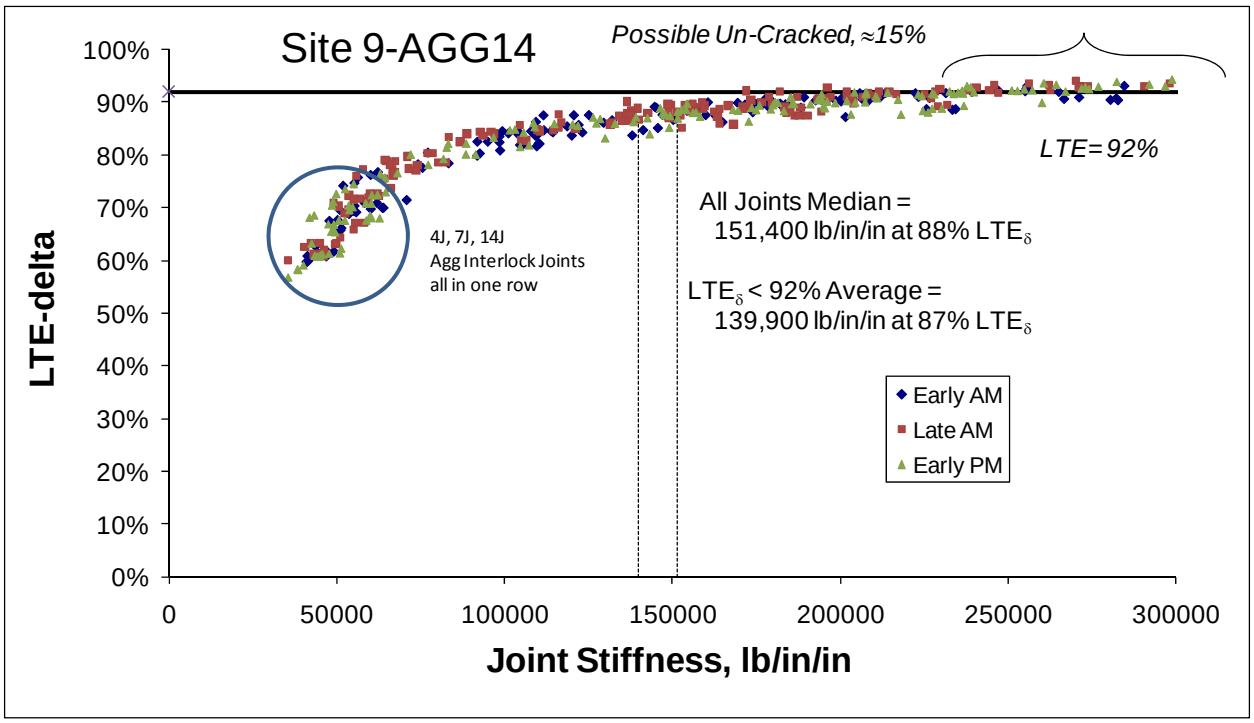
Site 9-AGG14
Possible Un-Cracked, ≈15%
LTE=92%
All Joints Median =
151,400 lb/in/in at 88% LTE$_\delta$
LTE$_\delta$ < 92% Average =
139,900 lb/in/in at 87% LTE$_\delta$
4J, 7J, 14J
Agg Interlock Joints
all in one row
Early AM
Late AM
Early PM
LTE-delta
Joint Stiffness, lb/in/in
100%
90%
80%
70%
60%
50%
40%
30%
20%
10%
0%
0
50000
100000
150000
200000
250000
300000

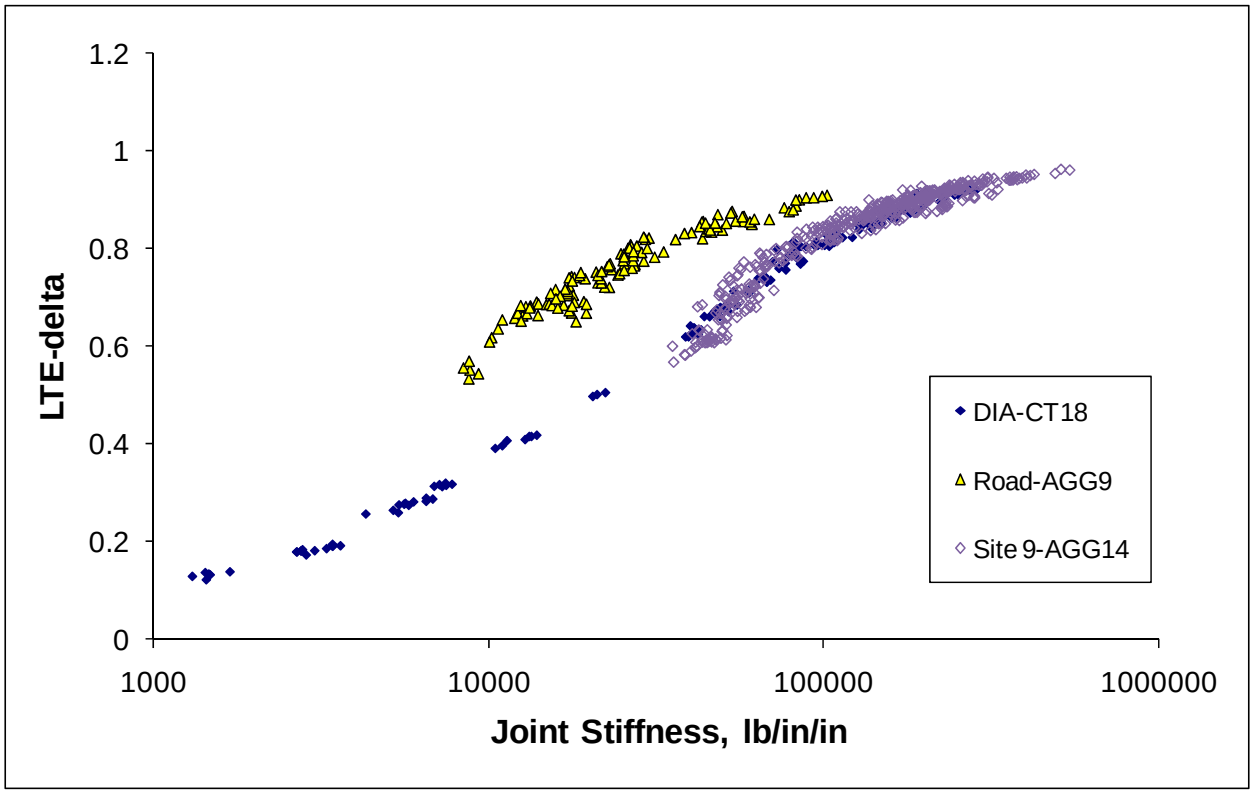
DIA-CT18
Road-AGG9
Site 9-AGG14
LTE-delta
Joint Stiffness, lb/in/in
1.2
1
0.8
0.6
0.4
0.2
0
1000
10000
100000
1000000

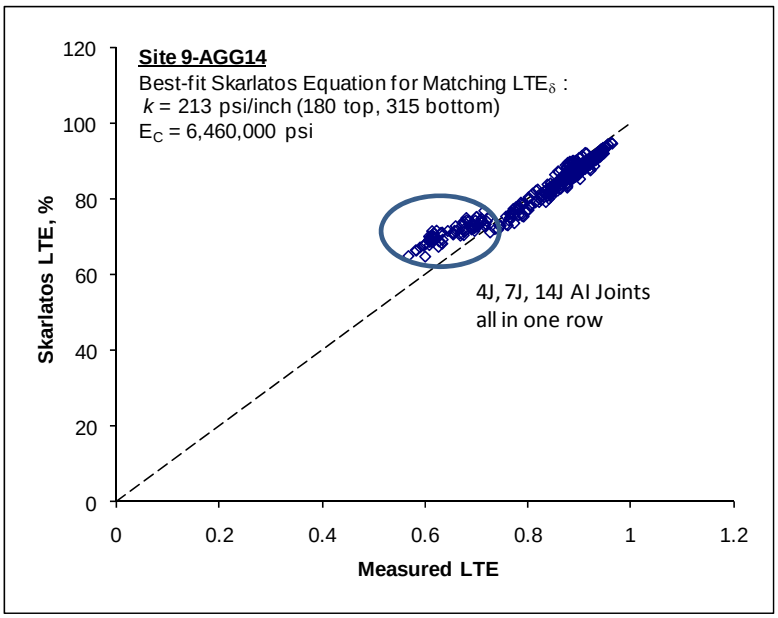
Site 9-AGG14
Best-fit Skarlatos Equation for Matching LTEδ :
k = 213 psi/inch (180 top, 315 bottom)
EC = 6,460,000 psi
4J, 7J, 14J AI Joints
all in one row
Skarlatos LTE, %
Measured LTE
120
100
80
60
40
20
0
0
0.2
0.4
0.6
0.8
1
1.2

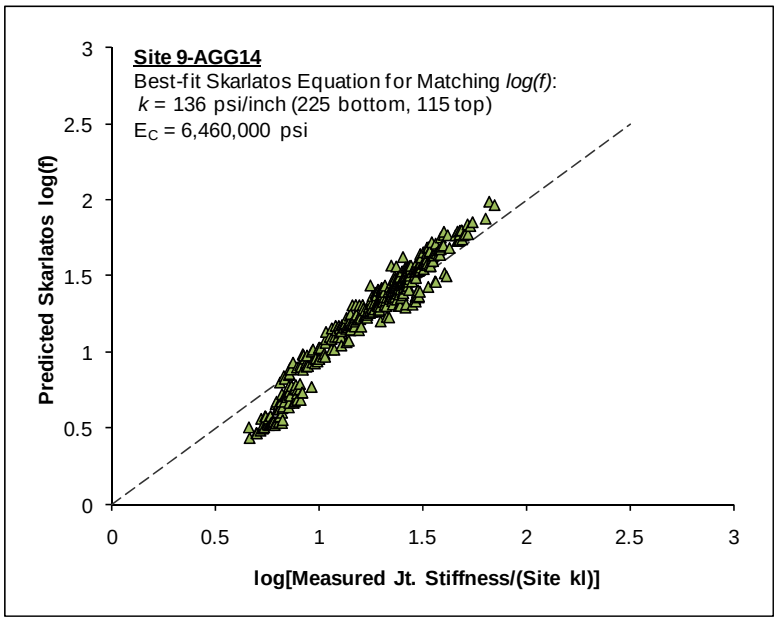
Site 9-AGG14
Best-fit Skarlatos Equation for Matching log(f):
k = 136 psi/inch (225 bottom, 115 top)
EC = 6,460,000 psi
Predicted Skarlatos log(f)
log[Measured Jt. Stiffness/(Site kl)]
3
2.5
2
1.5
1
0.5
0
0
0.5
1
1.5
2
2.5
3

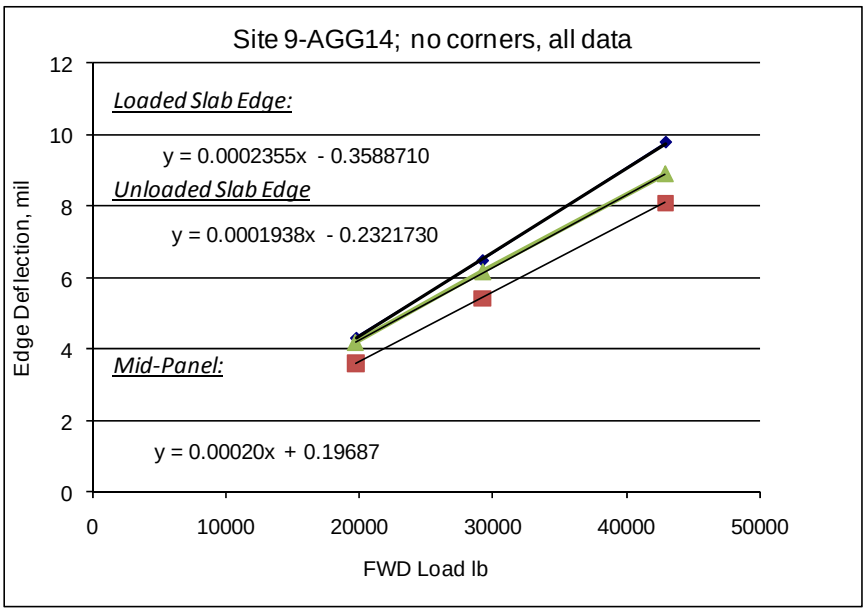

Site 9-AGG14 Aggregate Interlock Joints, including locked / un-cracked

	LR	LTE	Avg Stiffness	
avg	109	80%	143510	% possibly un-cracked, LTE>92% = 16%
min	88	57%	35299	
max	148	95%	492148	
stdev	11	12%	99356	
Median	110	84%	109553	

Without locked / un-cracked

	LR	LTE	Avg Stiffness	
avg	108	79%	123592	% possibly un-cracked, LTE>92% = 7%
min	88	57%	35299	
max	148	95%	322691	
stdev	11	11%	80264	
Median	109	80%	82584	

Site 9-AGG14 Doweled Construction Joints, including locked / un-cracked

	LR	LTE	Avg Stiffness
avg	124	89%	178388
min	107	74%	52078
max	156	96%	543938
stdev	8	3%	71151
Median	122	89%	172781

% possibly un-cracked, LTE>92% = 18%

1" Dowels at 18" centers

Steel Area/ft = 0.523599

reinf. ratio = 0.31%

Without locked / un-cracked

	LR	LTE	Avg Stiffness
avg	123	88%	166268
min	107	74%	52078
max	156	96%	512280
stdev	8	3%	58442
Median	122	89%	159437
	minus AGG =		*76854*

% possibly un-cracked, LTE>92% = 8.5%

"difference" DCI = 5500000

$$k = \frac{1}{s\left(\frac{\varpi}{0.9G_dA_d} + \frac{\varpi^3}{12E_dI_d} + \frac{2+\beta\varpi}{2\beta^3E_dI_d}\right)}$$

s is the dowel bar spacing =	18	in
w is the joint opening =	0.001	in
Dowel Diameter =	1	in
Ad is the dowel cross-sectional area =	0.79	sq in
Ed =	29000000	psi
Gd =	11153846	psi
Id =	0.049	in^4
Back-Calculated Dowel-Concrete Interaction modulus, DCI =	5500000	psi

$$\beta = \sqrt[4]{\frac{Kd}{4E_dI_d}} = 0.991$$

Doweled Joint Stiffness = **77003** lb/in/in

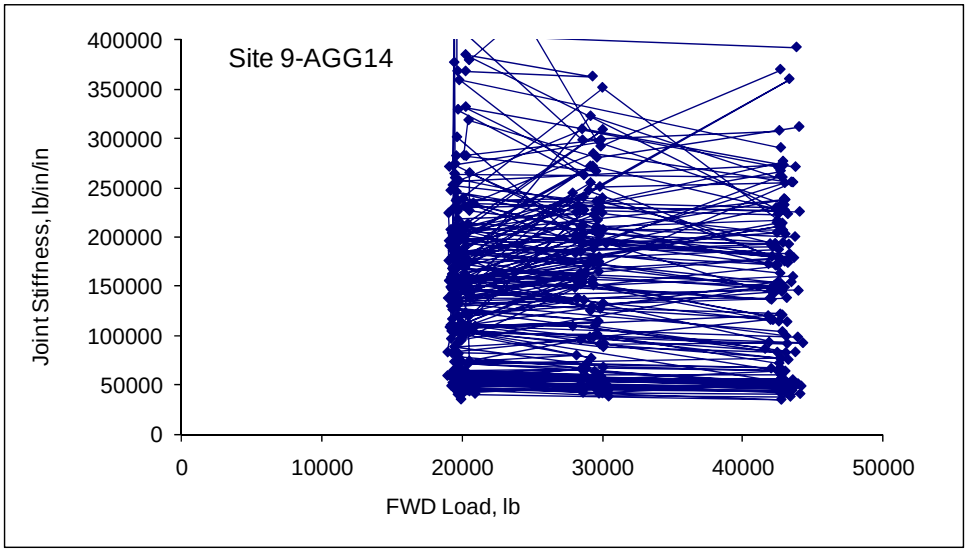

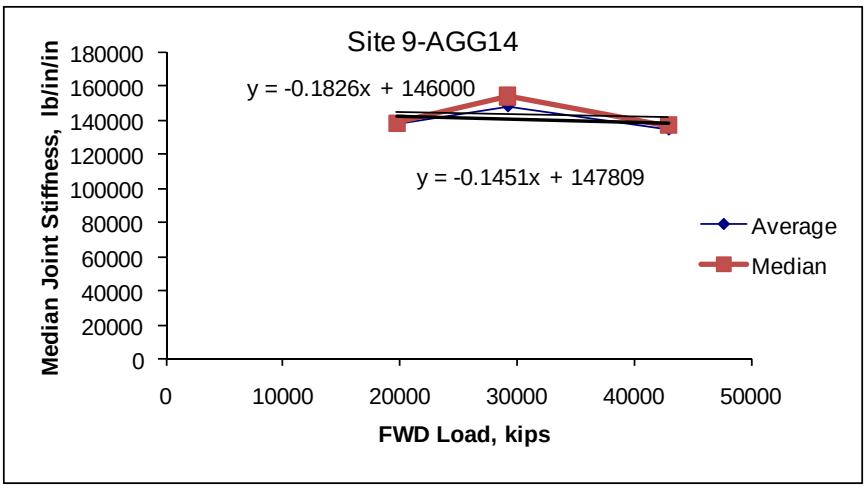

Site 9-AGG14 Slab Edge Gaps- All Joints

	All	AM	Mid	PM
Avg	-0.34	-0.39	-0.31	-0.31
Min	-0.93	-0.93	-0.67	-0.75
Max	0.27	0.19	0.27	0.13
Stdev	0.22	0.25	0.20	0.20

Site 9-AGG14 Joint Looseness Data

Looseness	All Good Data	Al-Joint	TE-Joint	DCN-Joint
Average	-0.11	-0.13	-0.09	-0.09
Maximum	0.41	0.41	0.33	0.37
Minimum	-1.19	-0.59	-0.45	-1.19
Std. Dev.	0.25	0.21	0.24	0.29
Count	120	61	12	47

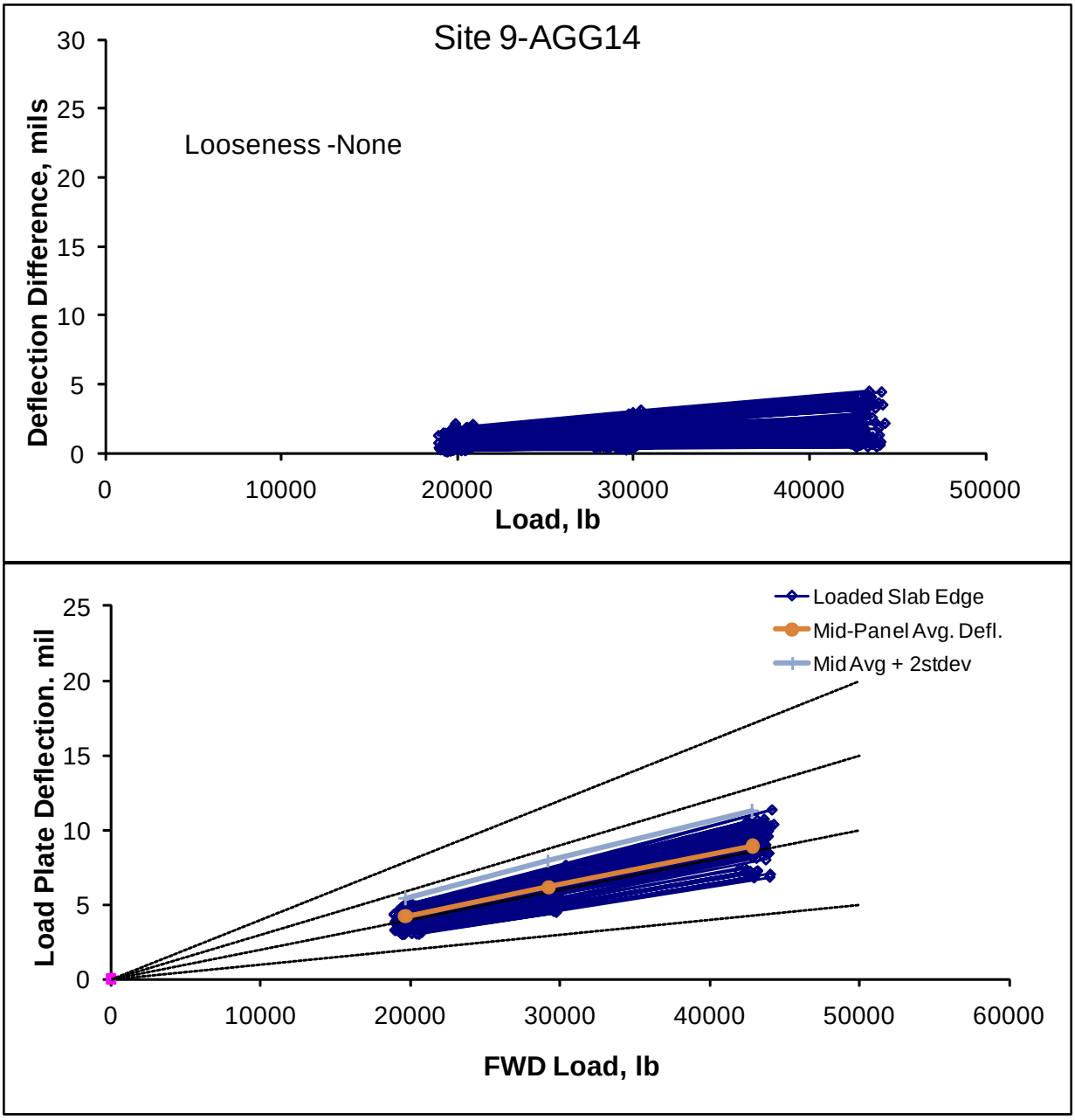
Site 9-AGG14
Looseness -None
Deflection Difference, mils
30
25
20
15
10
5
0
0
10000
20000
30000
40000
50000
Load, lb
Loaded Slab Edge
Mid-Panel Avg. Defl.
Mid Avg + 2stdev
Load Plate Deflection. mil
25
20
15
10
5
0
0
10000
20000
30000
40000
50000
60000
FWD Load, lb

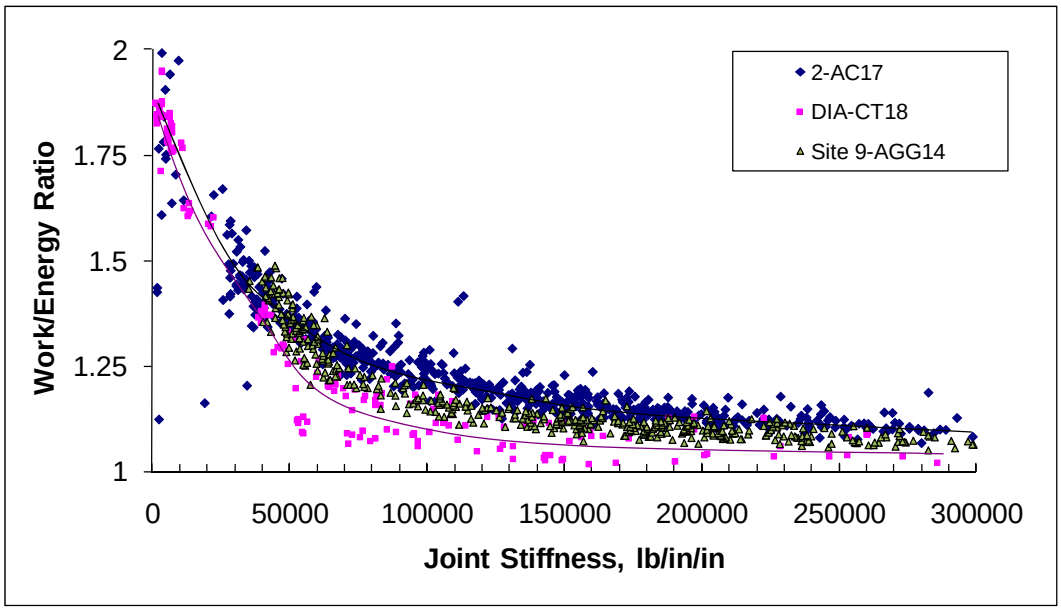
2
1.75
1.5
1.25
1
Work/Energy Ratio
0
50000
100000
150000
200000
250000
300000
Joint Stiffness, lb/in/in
2-AC17
DIA-CT18
Site 9-AGG14

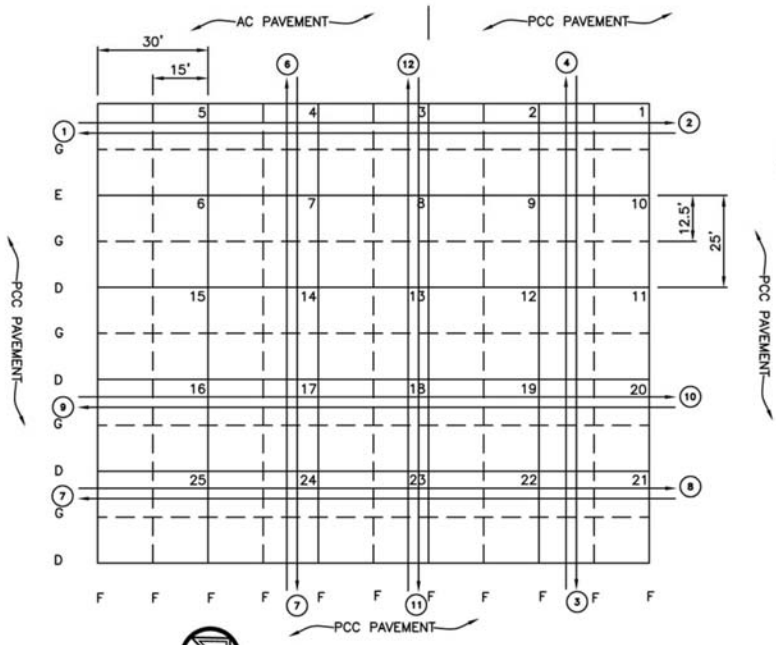

TEST PATTERN

LEGEND

(2)	FWD TEST LANE NUMBER
G	CONTRACTION JOINT: NO. 5 DEFORMED TIE BAR, 30" LONG, 30" SPACING.
F	CONTRACTION JOINT: 1.5" DIA. DOWEL BAR, 20" LONG, 15" SPACING, ONE SIDE GREASED.
E	CONSTRUCTION JOINT: 1" DIA. DEFORMED BAR, 30" LONG, 24" SPACING, ONE SIDE GREASED.
D	CONSTRUCTION JOINT: 1.5" DIA. DOWEL BAR, 20" LONG, 15" SPACING, ONE SIDE GREASED.

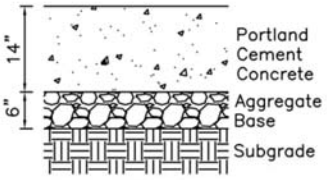

10-AGG14

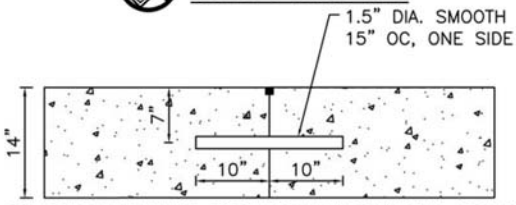

LONGITUDINAL CONSTRUCTION JOINT - D

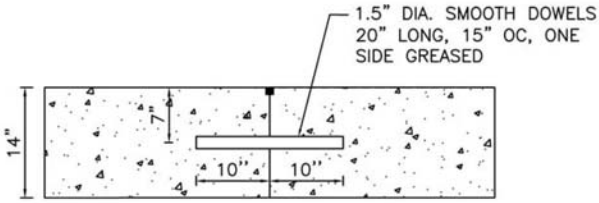

CONTRACTION JOINT - F

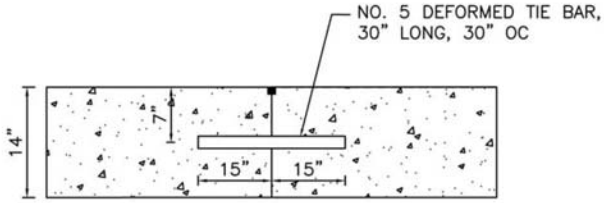

CONTRACTION JOINT - G

TEST SITE 10-AGG14

10-AGG14

Site Description: The site is located on the west coast of the United States. Elevations of the site, as indicated by USGS maps, are approximately 35 to 45 feet above sea level. The airport is located in a high density urban area. Based on topographic information and observations, the site appears to be constructed on 1 to 3 feet of fill soils overlying natural subgrade soils. The typical natural subgrade as indicated by USDA soil maps is sandy loam over sandy clay loam. The estimated PCI and SCI of the site is 96 and 98, respectively. The primary distress observed included low severity scaling and joint spall.

Site Weather: The site is located in a dry/no freeze climate zone. The below figures indicate the average temperature, average precipitation, average number of days above 90 degrees Fahrenheit, and average number of days below 32 degrees Fahrenheit.

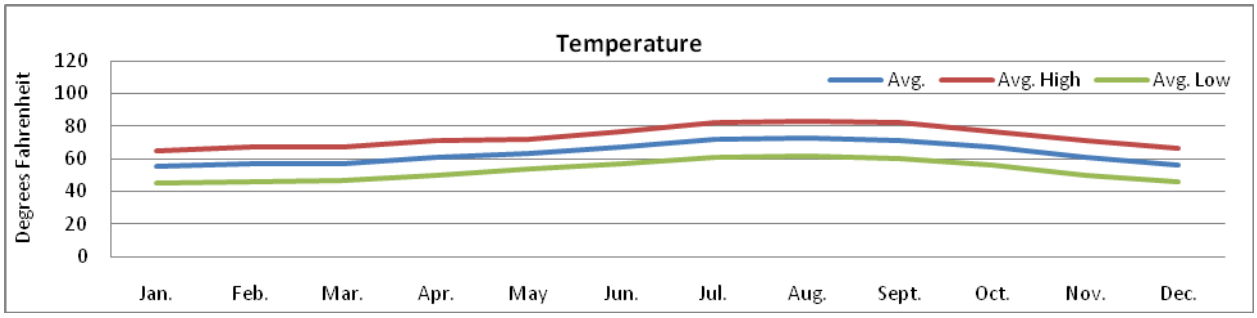

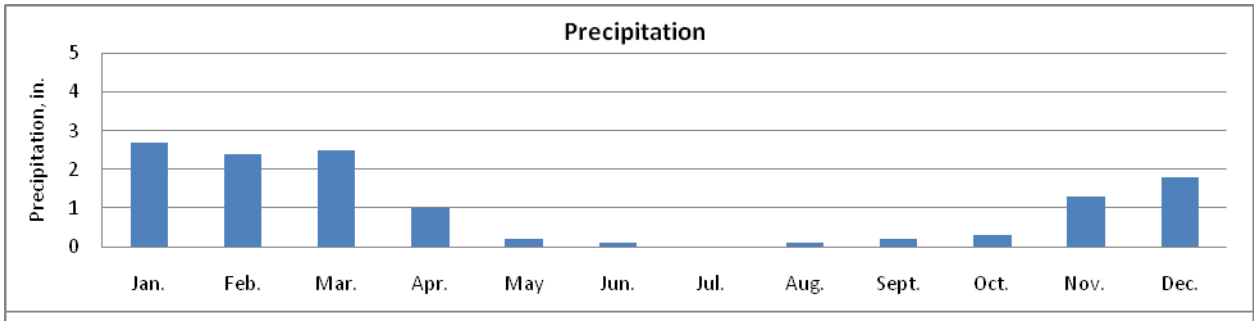

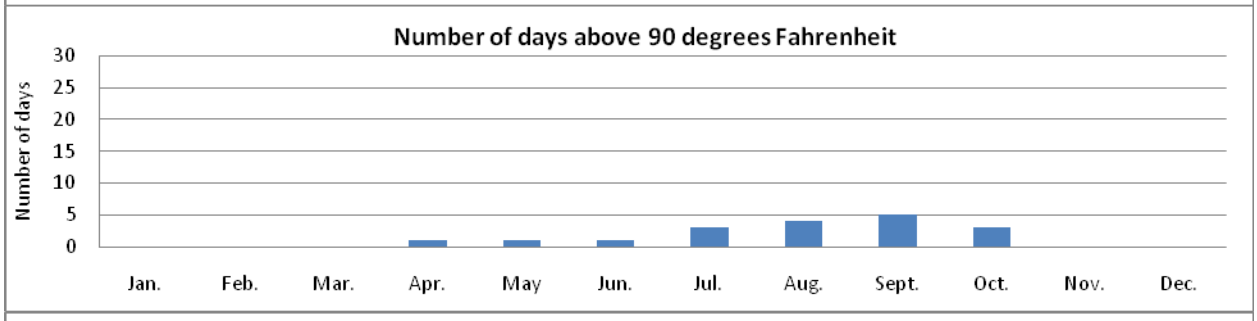

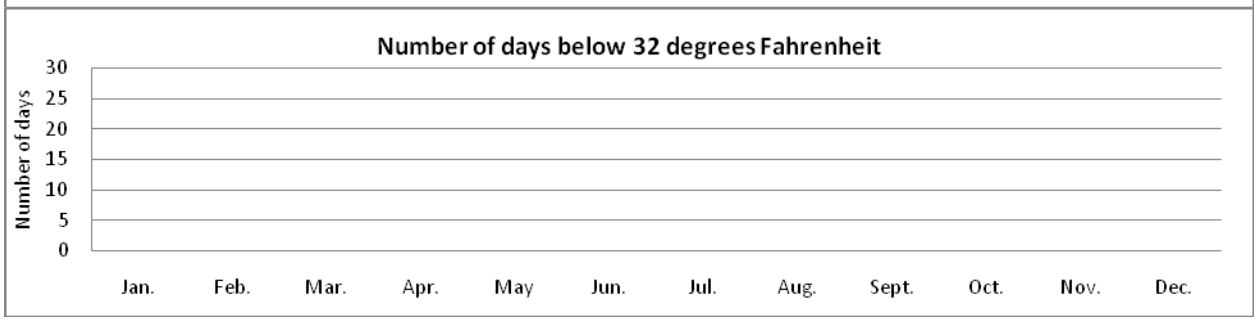

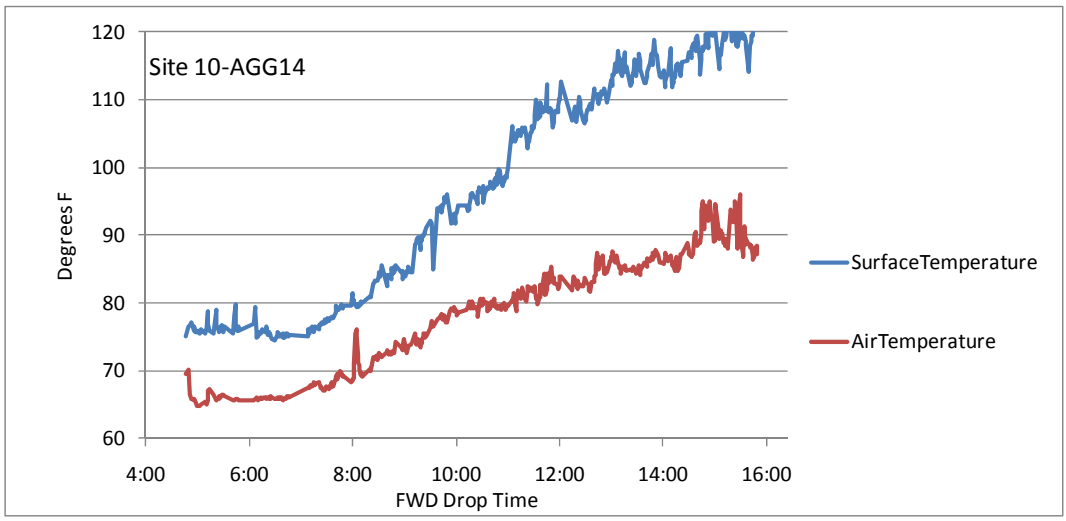

	Highway GPS3 55-3009	*Site 10-AGG14 Slab Curvature* 8AM average	AM-PM Change
average curvature, ft^{-1}	0.000547	0.000112	0.000134
min. curvature	0.000203	-0.000442	0.000096
max. curvature	0.001077	0.000383	0.000206
st. dev. of curvature	0.00021	0.000289	0.000037
number of slabs	33	8	8

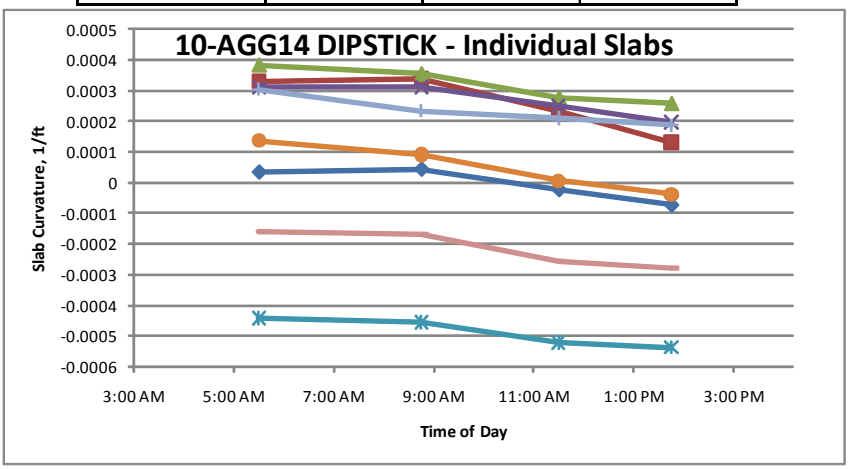

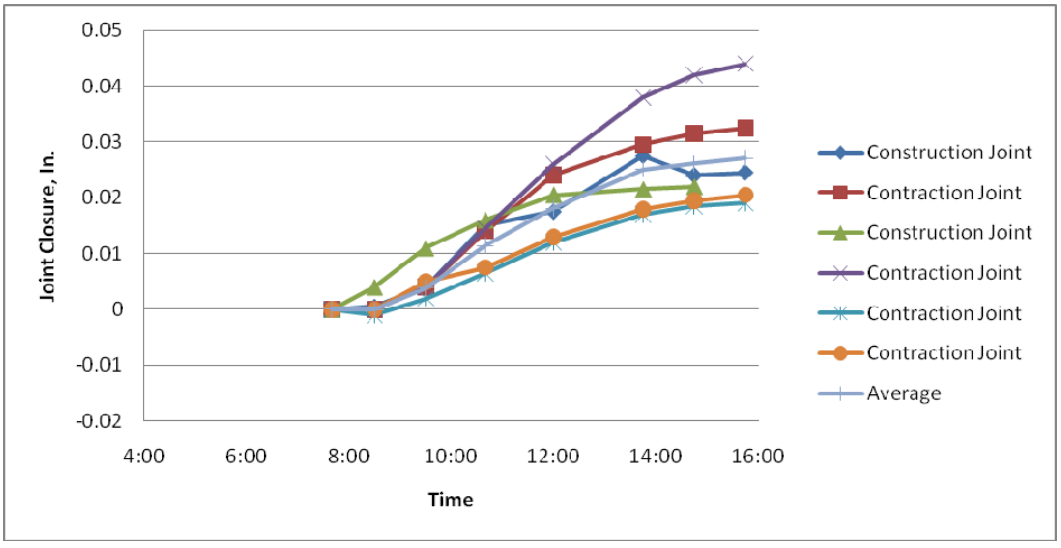

Site 10-AGG14 ILLIBACK Summary- Without soft basins at edge

	Dense Liquid				*Elastic Solid*			
	k-value	***k stdev***	**Slab EC**	**EC Stdev**	**Subg. E**	***E stdev***	**Slab EC**	**EC Stdev**
Site Average =	260	16	5.28	0.32	43,636	925	3.95	0.84
Site Min. =	283	15	6.57	0.34	48,706	869	4.97	0.89
Site Max =	248	24	3.79	0.35	39,401	1,824	2.77	1.28
AM Average =	266	19	4.92	0.33	43,878	1,179	3.64	0.98
Mid Average =	265	17	5.41	0.33	44,479	963	4.08	0.88
PM Average =	249	14	5.56	0.29	42,580	665	4.19	0.65
Best Guess	**260**		**5.28**		**43636**		**3.95**	
	psi/in		*Msi*		*psi*		*Msi*	

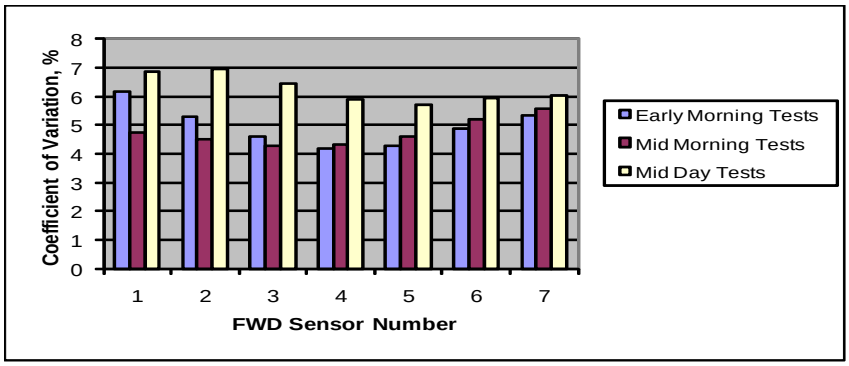

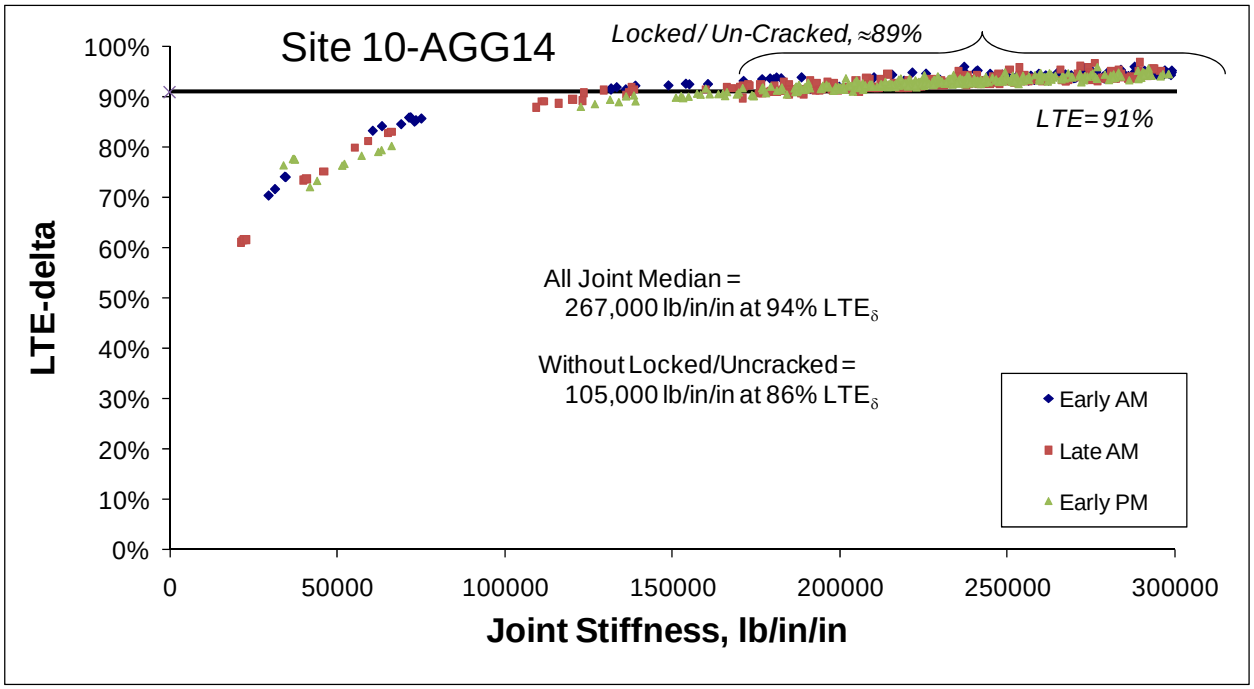

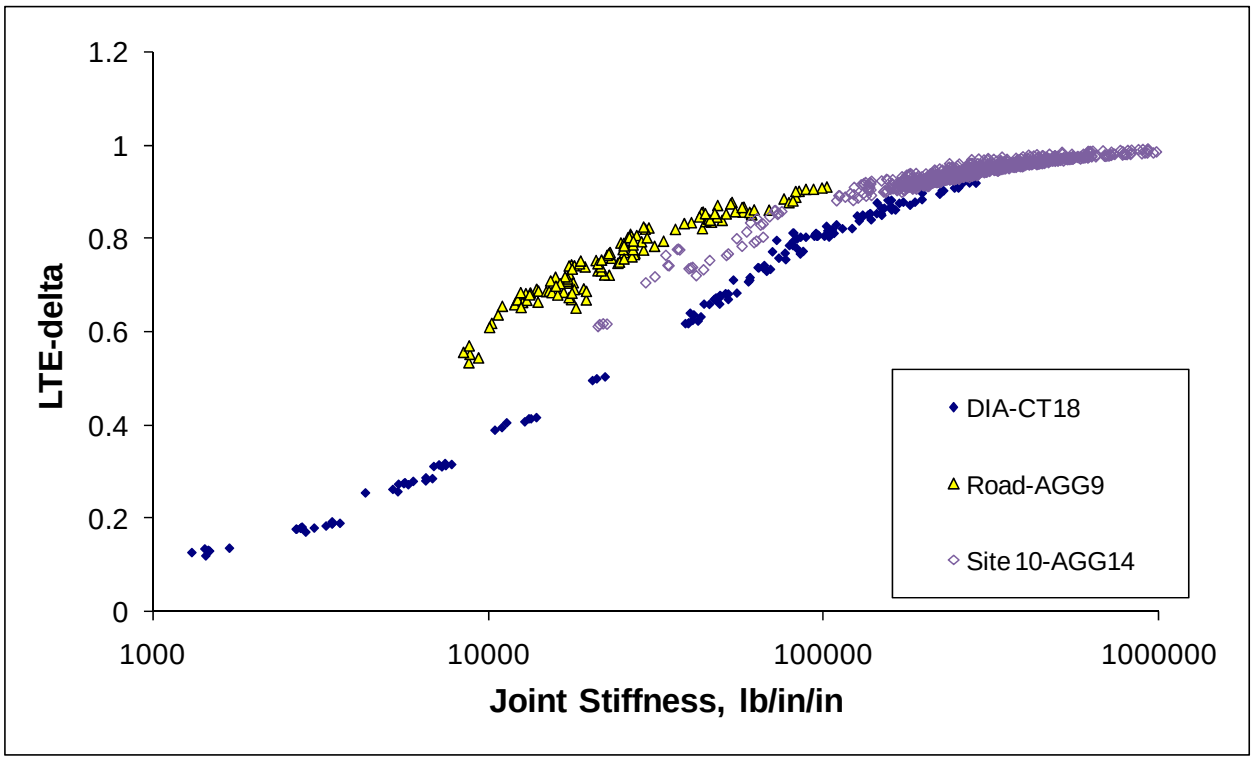
1.2
1
0.8
0.6
0.4
0.2
0
LTE-delta
1000
10000
100000
1000000
Joint Stiffness, lb/in/in
DIA-CT18
Road-AGG9
Site 10-AGG14

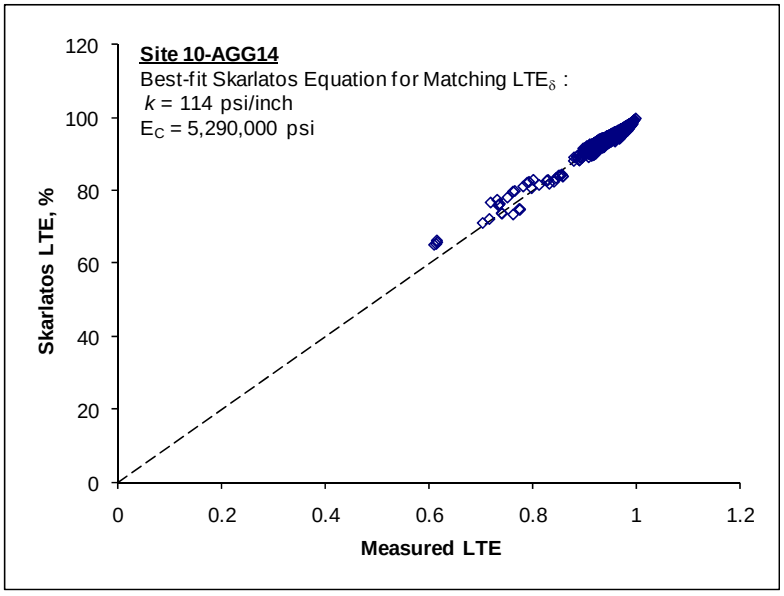
Site 10-AGG14
Best-fit Skarlatos Equation for Matching LTEδ :
k = 114 psi/inch
EC = 5,290,000 psi
120
100
80
60
40
20
0
Skarlatos LTE, %
0
0.2
0.4
0.6
0.8
1
1.2
Measured LTE

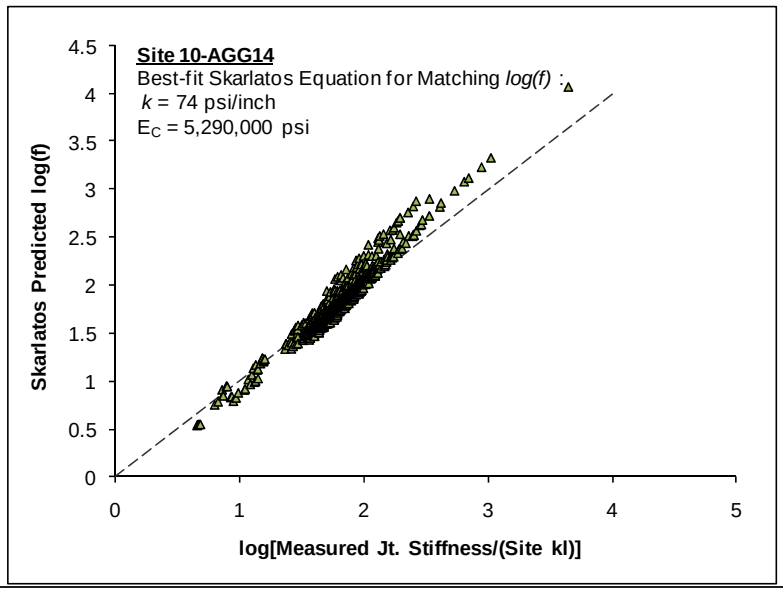
Site 10-AGG14
Best-fit Skarlatos Equation for Matching log(f) :
k = 74 psi/inch
EC = 5,290,000 psi
Skarlatos Predicted log(f)
log[Measured Jt. Stiffness/(Site kl)]
0
0.5
1
1.5
2
2.5
3
3.5
4
4.5
0
1
2
3
4
5

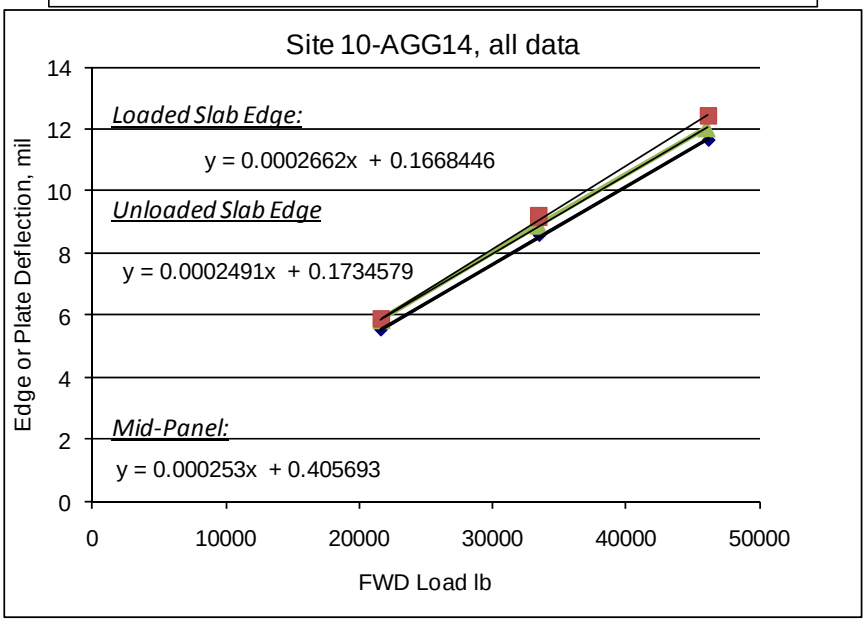
Site 10-AGG14, all data
Loaded Slab Edge:
y = 0.0002662x + 0.1668446
Unloaded Slab Edge
y = 0.0002491x + 0.1734579
Mid-Panel:
y = 0.000253x + 0.405693
Edge or Plate Deflection, mil
FWD Load lb
0
2
4
6
8
10
12
14
0
10000
20000
30000
40000
50000

10-AGG14 T. Doweled Contraction Joints, including locked / un-cracked

	LR	LTE	Avg Stiffness
avg	127	94%	366242
min	101	89%	131391
max	176	100%	20981619
stdev	15	2%	819757
Median	126	94%	262235

% possibly un-cracked, LTE>91% = 95

Sawed 1.5" dowels at 15"

Steel Area/ft = 1.413717
reinf. ratio = 0.841%

F-joints, removed possible un-cracked

	LR	LTE	Avg Stiffness
avg	130	91%	185987
min	118	89%	131391
max	153	94%	280749
stdev	9	1%	27499
Median	128	91%	185369

% possibly un-cracked, LTE>86% = 33

at DCI=5000000, kj = 167000
Probable Agg Interlock = 20000 to 100000

$$k = \frac{1}{s\left(\frac{\varpi}{0.9G_dA_d} + \frac{\varpi^3}{12E_dI_d} + \frac{2+\beta\varpi}{2\beta^3E_dI_d}\right)}$$

s is the dowel bar spacing =	15	in
w is the joint opening =	0.1	in
Dowel Diameter =	1.5	in
Ad is the dowel cross-sectional area =	1.77	sq in
Ed =	29000000	psi
Gd =	11153846	psi
Id =	0.249	in^4
Back-Calculated Dowel-Concrete Interaction modulus, DCI =	5000000	psi

$$\beta = \sqrt[4]{\frac{Kd}{4E_dI_d}} = 0.714$$

Doweled Joint Stiffness = **166602** lb/in/in

10-AGG14 L. Doweled Construction Joint, including locked / un-cracked

	LR	LTE	Avg Stiffness
avg	108	88%	161630
min	97	72%	39808
max	121	96%	344852
stdev	8	8%	99451
Median	109	91%	153138

% possibly un-cracked, LTE>91% = 50

Formed, 1" dowels at 24"

Steel Area/ft = 0.392699
reinf. ratio = 0.234%

Without locked / uncracked

	LR	LTE	Avg Stiffness
avg	108	83%	95049
min	97	72%	39808
max	121	93%	229902
stdev	9	7%	52374
Median	106	85%	73372

% possibly un-cracked, LTE>86% = 14

at DCI=5000000, kj = 51000
Probable Agg Interlock = 22000 to 100000

$$k = \frac{1}{s\left(\frac{\varpi}{0.9G_dA_d} + \frac{\varpi^3}{12E_dI_d} + \frac{2+\beta\varpi}{2\beta^3E_dI_d}\right)}$$

s is the dowel bar spacing =	24	in
w is the joint opening =	0.1	in
Dowel Diameter =	1	in
Ad is the dowel cross-sectional area =	0.79	sq in
Ed =	29000000	psi
Gd =	11153846	psi
Id =	0.049	in^4
Back-Calculated Dowel-Concrete Interaction modulus, DCI =	5000000	psi

$$\beta = \sqrt[4]{\frac{Kd}{4E_dI_d}} = 0.968$$

Doweled Joint Stiffness = **50527** lb/in/in

10-AGG14 L. Tied Contraction Joints, including locked / un-cracked

	LR	LTE	Avg Stiffness
avg	112	94%	377925
min	97	61%	21351
max	127	99%	1197075
stdev	7	6%	193406
Median	112	95%	337665

% possibly un-cracked, LTE>86% = 94

Sawed, #5 bars at 30"

Steel Area/ft = 0.122718
reinf. ratio = 0.073%

G-joints, with LTE>86% (un-cracked joints) removed

	LR	LTE	Avg Stiffness
avg	102	79%	89953
min	97	61%	21351
max	111	96%	332445
stdev	5	12%	84382
Median	101	84%	62065

% possibly un-cracked, LTE>86% = 7

at DCI=5000000, kj = 17000
Probable Agg Interlock = 40000 to 300000

$$k = \frac{1}{s\left(\frac{\varpi}{0.9 G_d A_d} + \frac{\varpi^3}{12 E_d I_d} + \frac{2+\beta\varpi}{2\beta^3 E_d I_d}\right)}$$

s is the dowel bar spacing =	30	in
w is the joint opening =	0.1	in
Dowel Diameter =	0.625	in
Ad is the dowel cross-sectional area =	0.31	sq in
Ed =	29000000	psi
Gd =	11153846	psi
Id =	0.007	in^4
Back-Calculated Dowel-Concrete Interaction modulus, DCI =	5000000	psi

$$\beta = \sqrt[4]{\frac{Kd}{4E_d I_d}} = 1.377$$

Doweled Joint Stiffness = **17389** lb/in/in

10-AGG14 L. Doweled Construction Joints, including locked / un-cracked

	LR	LTE	Avg Stiffness
avg	110	93%	273624
min	97	80%	55214
max	129	99%	1331308
stdev	9	3%	145097
Median	111	93%	240993

% possibly un-cracked, LTE>91% = 89

Formed, 1.5" dowels at 15"

Steel Area/ft = 1.413717
reinf. ratio = 0.841%

D-joints, removed possible un-cracked

	LR	LTE	Avg Stiffness
avg	115	88%	127454
min	103	80%	55214
max	129	91%	169783
stdev	9	4%	41631
Median	115	89%	145004

% possibly un-cracked, LTE>91% = zero

at DCI=5000000, kj = 167000
Probable Agg Interlock = 0 to 70000

$$k = \frac{1}{s\left(\frac{\varpi}{0.9 G_d A_d} + \frac{\varpi^3}{12 E_d I_d} + \frac{2+\beta\varpi}{2\beta^3 E_d I_d}\right)}$$

s is the dowel bar spacing =	15	in
w is the joint opening =	0.1	in
Dowel Diameter =	1.5	in
Ad is the dowel cross-sectional area =	1.77	sq in
Ed =	29000000	psi
Gd =	11153846	psi
Id =	0.249	in^4
Back-Calculated Dowel-Concrete Interaction modulus, DCI =	5000000	psi

$$\beta = \sqrt[4]{\frac{Kd}{4E_d I_d}} = 0.714$$

Doweled Joint Stiffness = **166602** lb/in/in

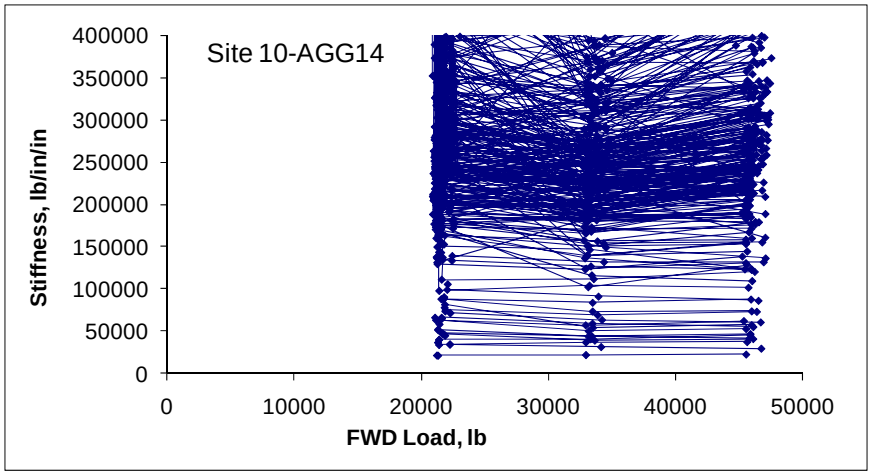
Site 10-AGG14
Stiffness, lb/in/in
400000
350000
300000
250000
200000
150000
100000
50000
0
0
10000
20000
30000
40000
50000
FWD Load, lb

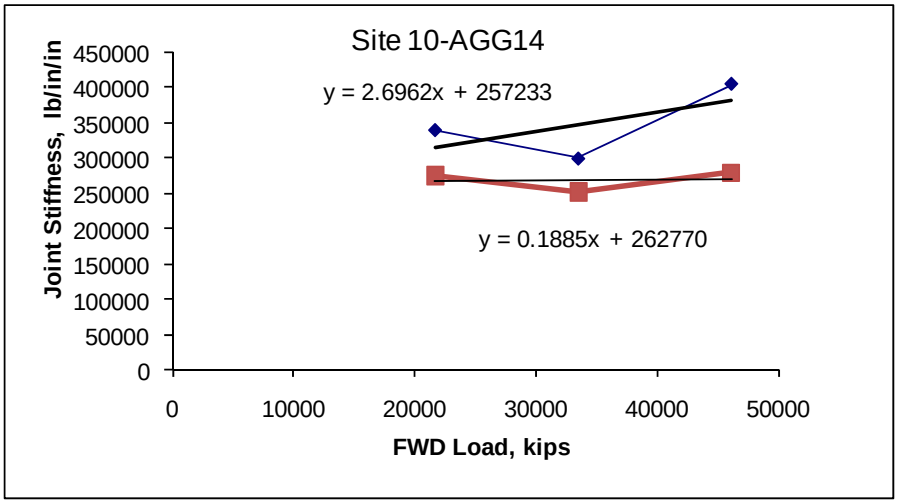
Site 10-AGG14
y = 2.6962x + 257233
y = 0.1885x + 262770
Joint Stiffness, lb/in/in
450000
400000
350000
300000
250000
200000
150000
100000
50000
0
0
10000
20000
30000
40000
50000
FWD Load, kips

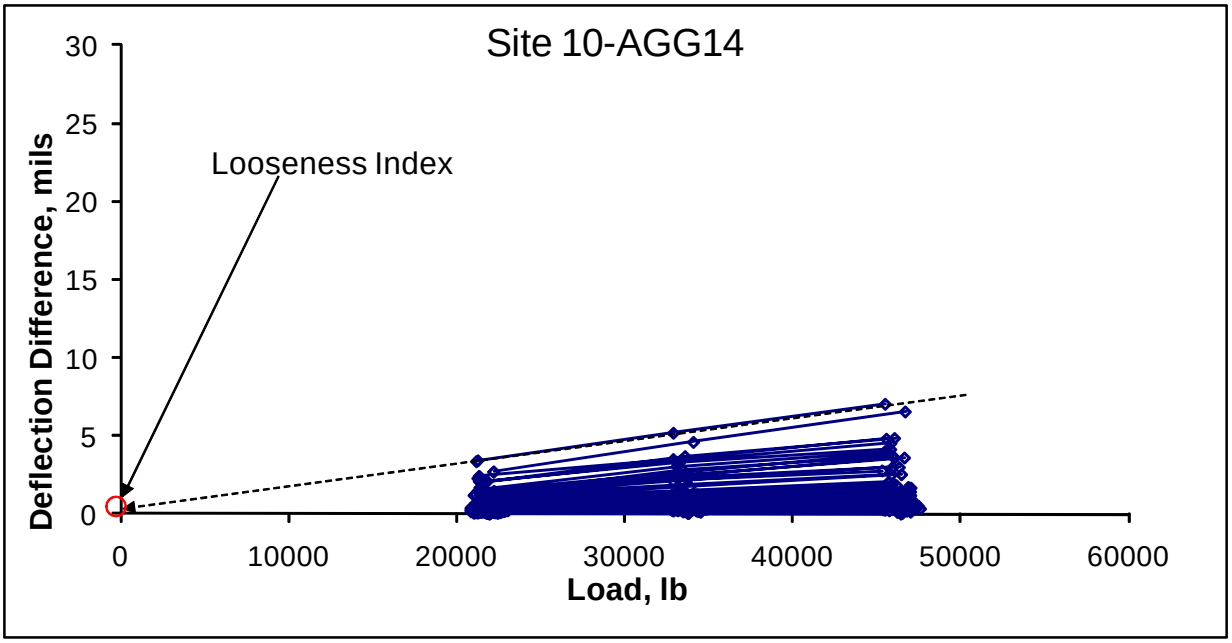

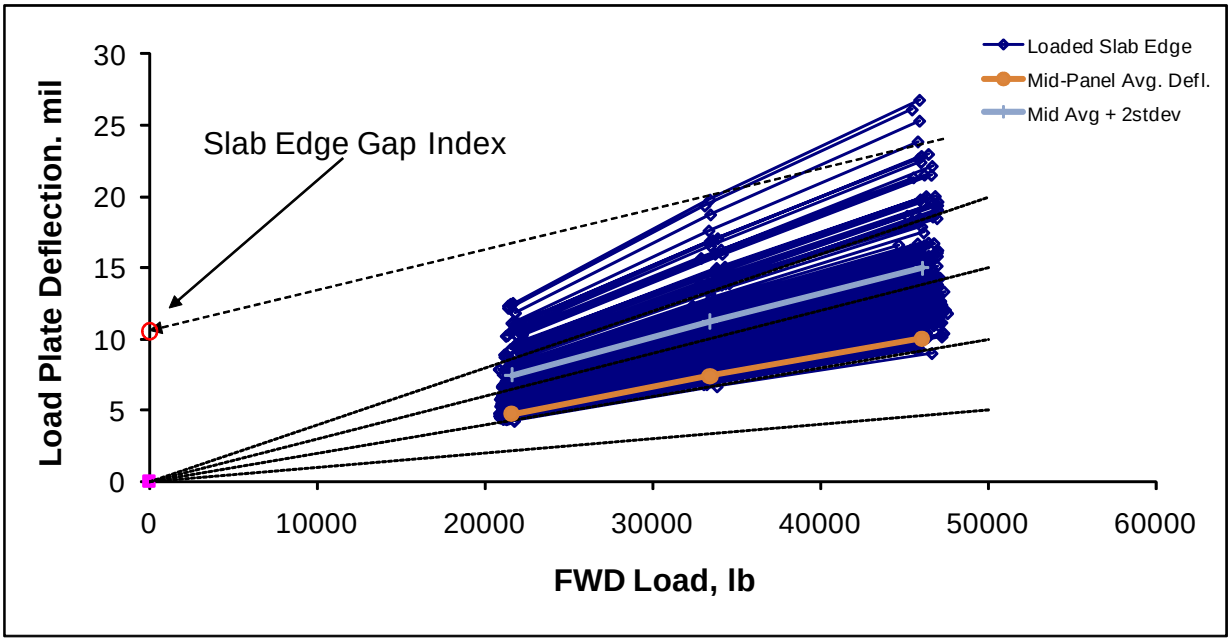

Site 10-AGG14 Slab Edge Gaps- All Joints

	All	AM	Mid	PM
Avg	0.11	0.16	0.11	0.06
Min	-0.36	-0.36	-0.26	-0.32
Max	0.96	0.70	0.96	0.48
Stdev	0.18	0.19	0.19	0.13

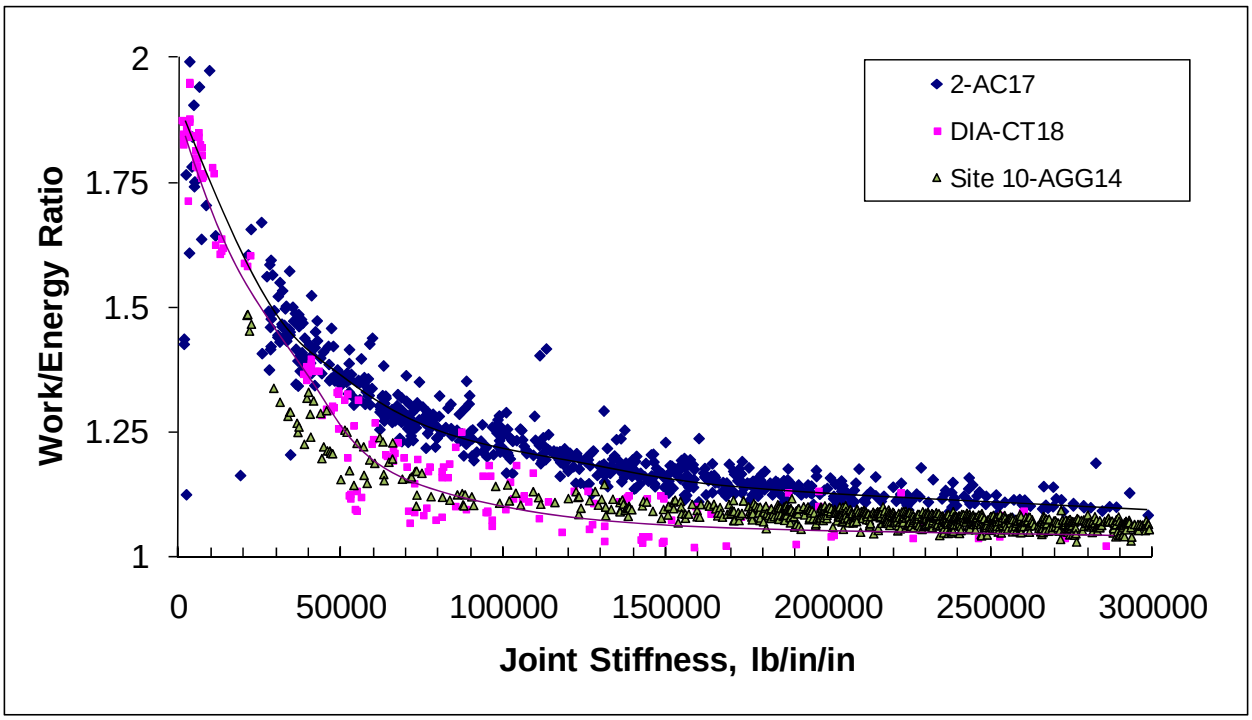
2
1.75
1.5
1.25
1
Work/Energy Ratio
0
50000
100000
150000
200000
250000
300000
Joint Stiffness, lb/in/in
2-AC17
DIA-CT18
Site 10-AGG14

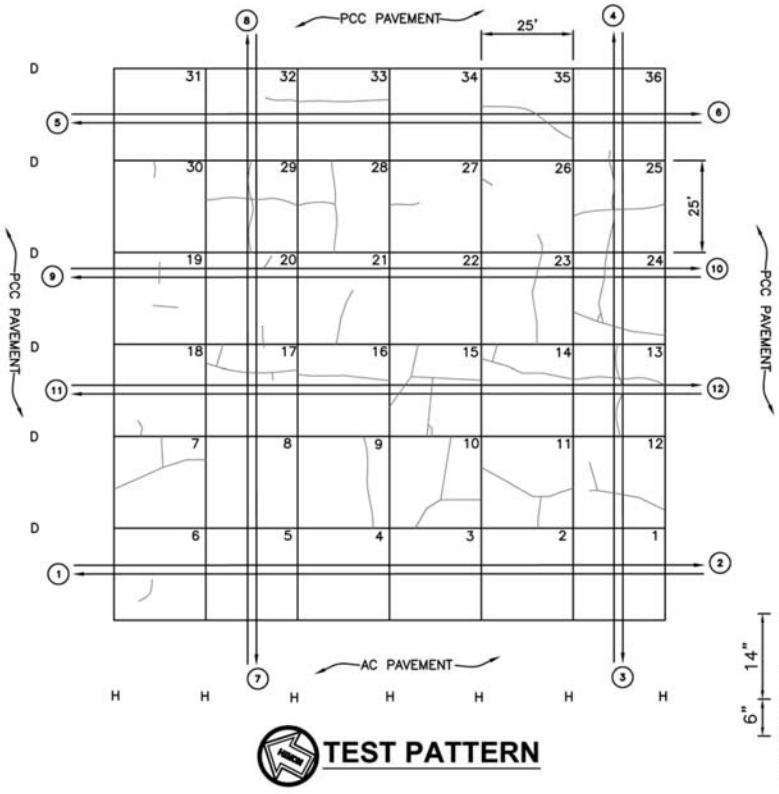

TEST PATTERN

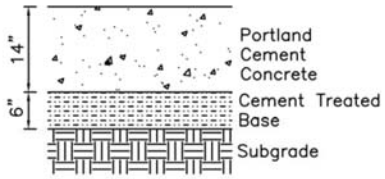

11-CT14

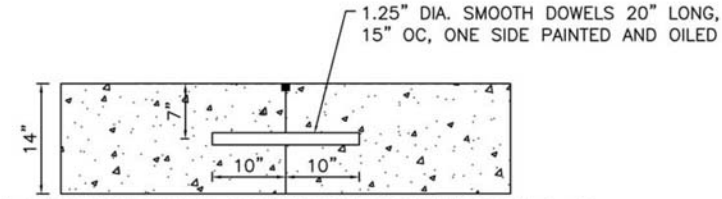

LONGITUDINAL CONSTRUCTION JOINT - D

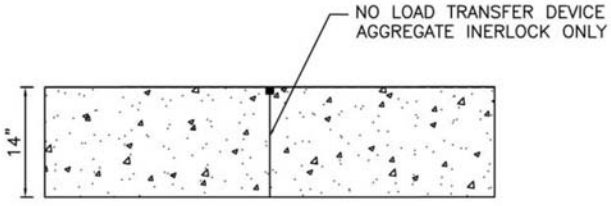

CONTRACTION JOINT - H

TEST SITE 11-CT14

Site Description: The site is located on the east coast of the United States. Elevations of the site, as indicated by USGS maps, are approximately 110 to 120 feet above sea level. Based on topographic information and observations, the site appears to be constructed on 1 to 3 feet of fill soils overlying natural subgrade soils. The typical natural subgrade as indicated by USDA soil maps is silt loam. The estimated PCI and SCI of the site is 52 and 54, respectively. The primary distress observed included frequent low and medium severity linear cracking, occasional low severity scaling, and occasional low and medium severity shattered slabs.

Site Weather: The site is located in a wet/freeze climate zone. The below figures indicate the average temperature, average precipitation, average number of days above 90 degrees Fahrenheit, and average number of days below 32 degrees Fahrenheit.

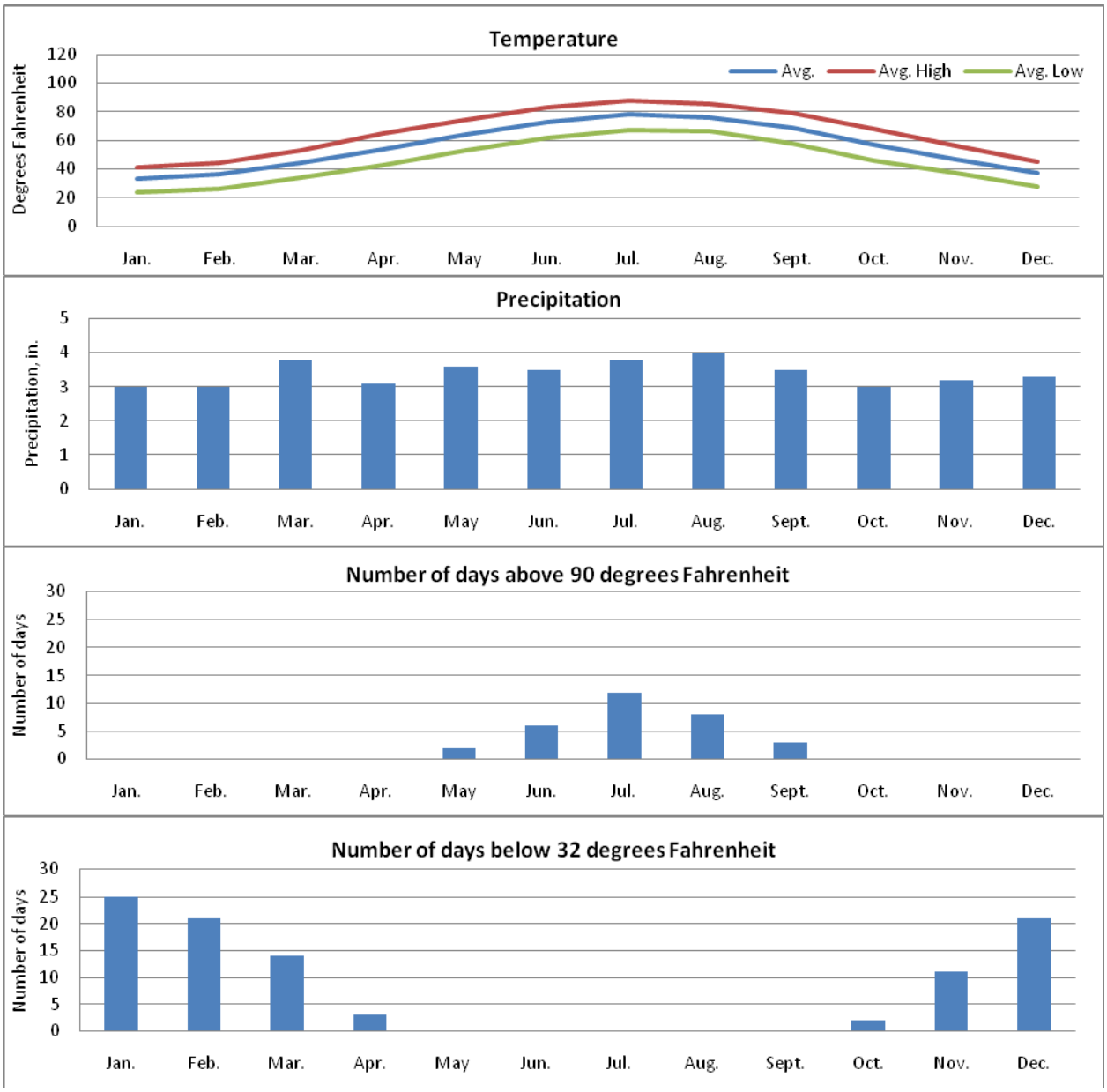

	Highway	11-CT14 Slab Curvature	
	GPS3 55-3009	8AM average	AM-PM Change
average curvature, ft^{-1}	0.000547	-0.000384	0.000023
min. curvature	0.000203	-0.000781	0.000014
max. curvature	0.001077	-0.000078	0.000029
st. dev. of curvature	0.00021	0.000237	0.000006
number of slabs	33	8	8

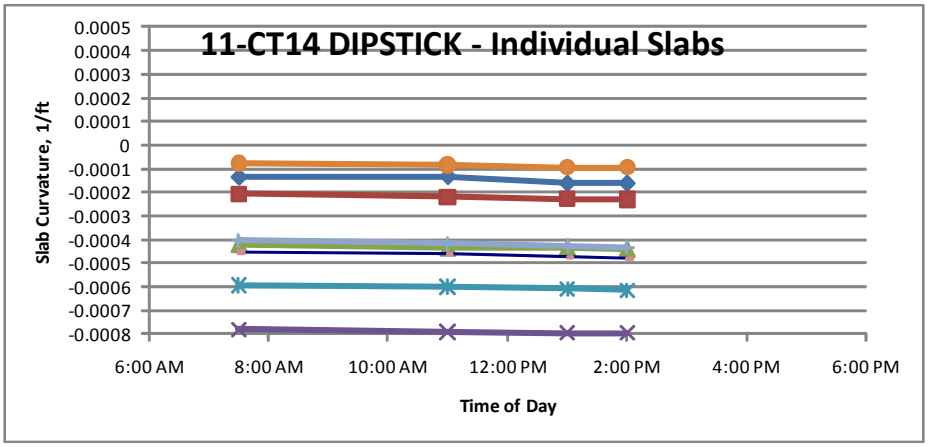

Site 11-CT14 ILLIBACK Summary

	Dense Liquid				Elastic Solid				Radius
	k-value	*k* stdev	Slab E_C	E_C Stdev	Subg. *E*	*E* stdev	Slab E_C	E_C Stdev	I-VALUES
Site Average =	198	14.9	4.87	0.34	34,450	1,279	3.69	0.14	49.0
Site Min. =	267	24	5.96	0.5	45,683	2,216	4.49	0.22	47.8
Site Max =	153	10	3.68	0.23	26,560	761	2.79	0.08	48.7
Best Guess	**200** *psi/in*		**4.90** *Msi*		**35000** *psi*		**3.70** *Msi*		**49.0** inches

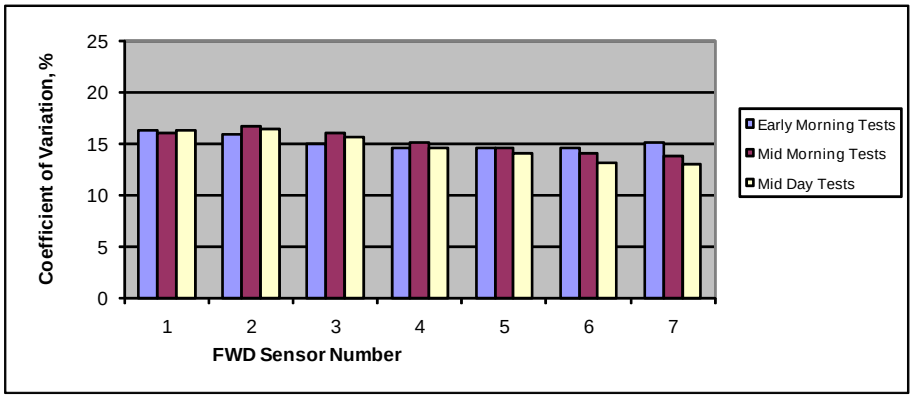

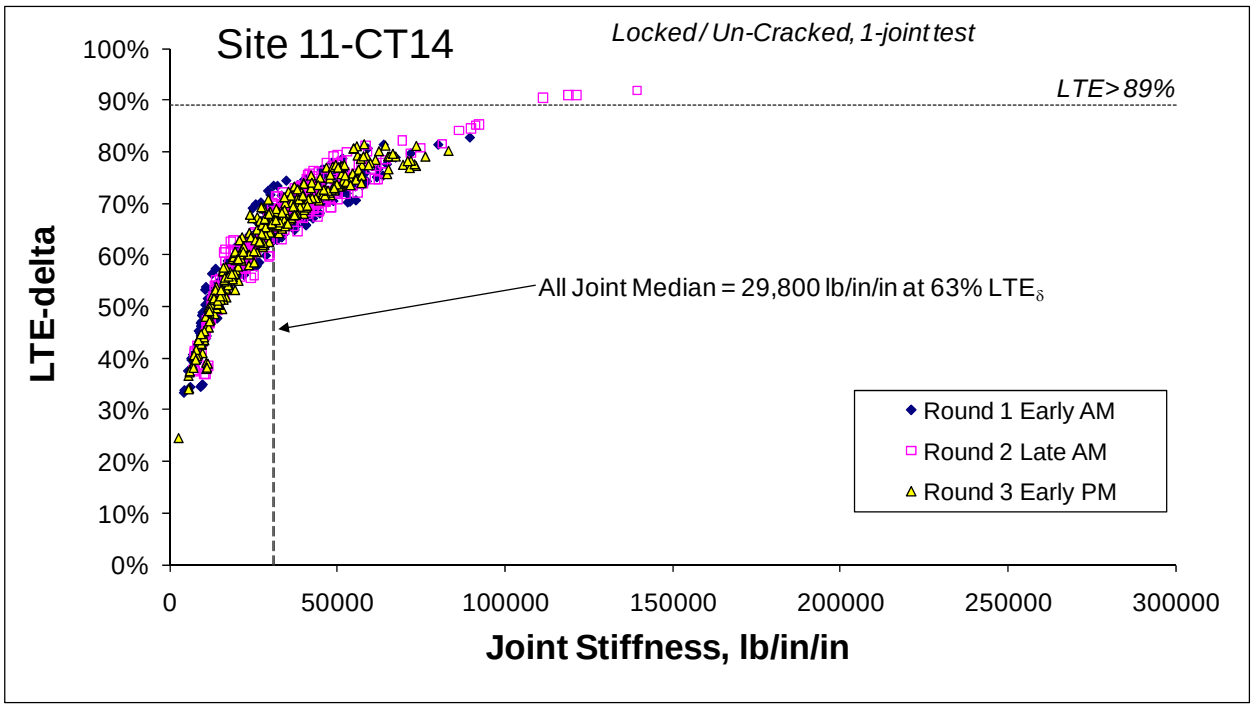
Site 11-CT14
Locked / Un-Cracked, 1-joint test
LTE> 89%
All Joint Median = 29,800 lb/in/in at 63% LTEδ
Round 1 Early AM
Round 2 Late AM
Round 3 Early PM
LTE-delta
Joint Stiffness, lb/in/in
100%
90%
80%
70%
60%
50%
40%
30%
20%
10%
0%
0
50000
100000
150000
200000
250000
300000

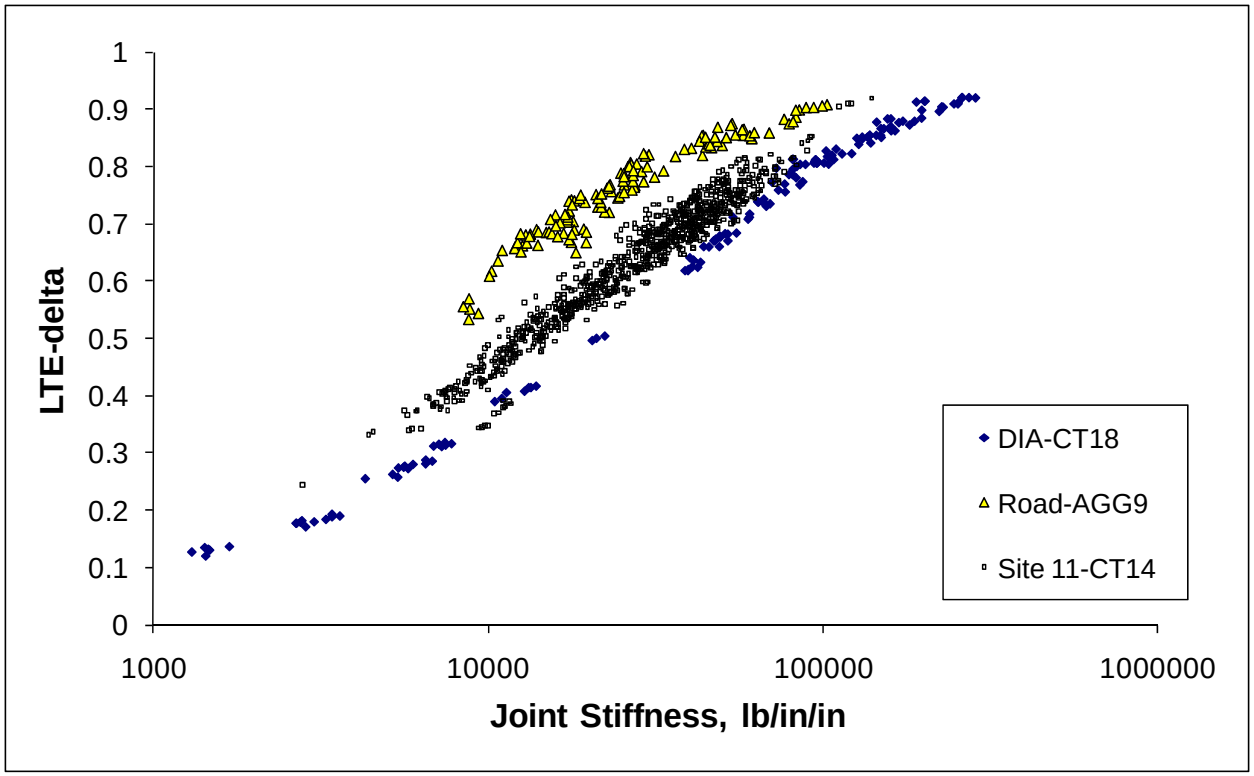
DIA-CT18
Road-AGG9
Site 11-CT14
LTE-delta
Joint Stiffness, lb/in/in
1
0.9
0.8
0.7
0.6
0.5
0.4
0.3
0.2
0.1
0
1000
10000
100000
1000000

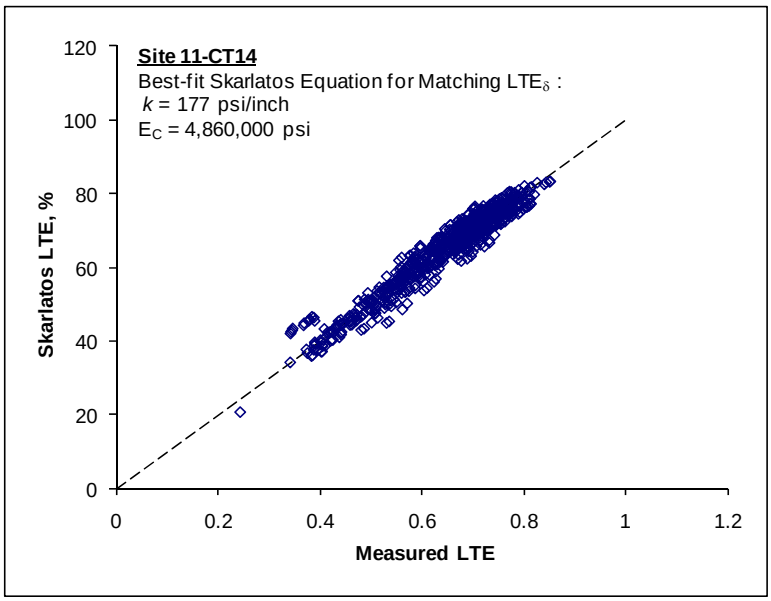
Site 11-CT14
Best-fit Skarlatos Equation for Matching LTEδ :
k = 177 psi/inch
EC = 4,860,000 psi
Skarlatos LTE, %
Measured LTE
0
20
40
60
80
100
120
0
0.2
0.4
0.6
0.8
1
1.2

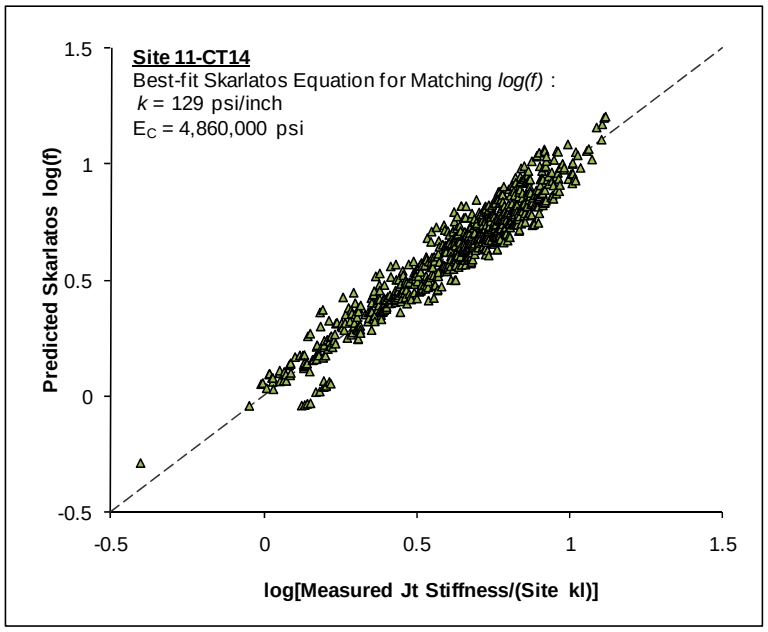
Site 11-CT14
Best-fit Skarlatos Equation for Matching log(f) :
k = 129 psi/inch
EC = 4,860,000 psi
Predicted Skarlatos log(f)
log[Measured Jt Stiffness/(Site kl)]
-0.5
0
0.5
1
1.5
-0.5
0
0.5
1
1.5

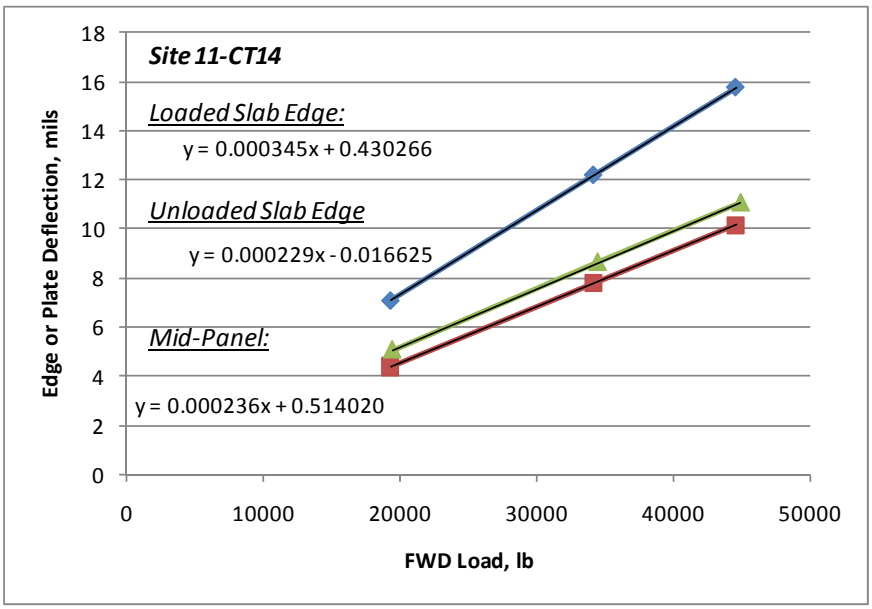

Site 11-CT14 T. Agg. Interlock Joints- No locked / uncracked detected

	LR, in.	LTE	Jt. Stiffness, lb/in/in
avg	121	63.8%	34792
Median	120	67%	34316
min	93	37%	6884
max	143	92%	139439
stdev	7.7	11%	19951

Site 11-CT14 L. Doweled Construction Joints, no un-cracked detected

	LR, in.	LTE	Jt. Stiffness, lb/in/in
avg	114	65.7%	32604
Median	115	68%	31544
min	86	24%	2776
max	136	82%	73735
stdev	8.3	11%	13830

Formed, 1.25" dowels at 15"

Steel Area/ft = 0.981748

reinf. ratio = 0.584%

Probable Agg Interlock = 0 to 30000

$$k = \frac{1}{s\left(\frac{\varpi}{0.9 G_d A_d} + \frac{\varpi^3}{12 E_d I_d} + \frac{2+\beta\varpi}{2\beta^3 E_d I_d}\right)}$$

s is the dowel bar spacing =	15	in
w is the joint opening =	0.1	in
Dowel Diameter =	1.25	in
Ad is the dowel cross-sectional area =	1.23	sq in
Ed =	29000000	psi
Gd =	11153846	psi
Id =	0.120	in^4
Back-Calculated Dowel-Concrete Interaction modulus, DCI =	800000	psi

$$\beta = \sqrt[4]{\frac{Kd}{4 E_d I_d}} = 0.518$$

Doweled Joint Stiffness = **31250** lb/in/in

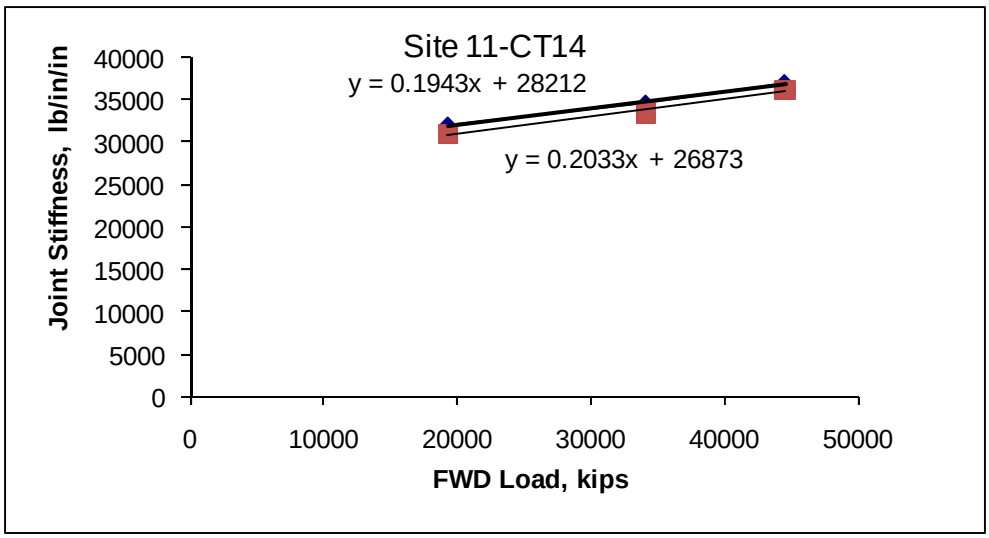
Site 11-CT14
y = 0.1943x + 28212
y = 0.2033x + 26873
Joint Stiffness, lb/in/in
40000
35000
30000
25000
20000
15000
10000
5000
0
0
10000
20000
30000
40000
50000
FWD Load, kips

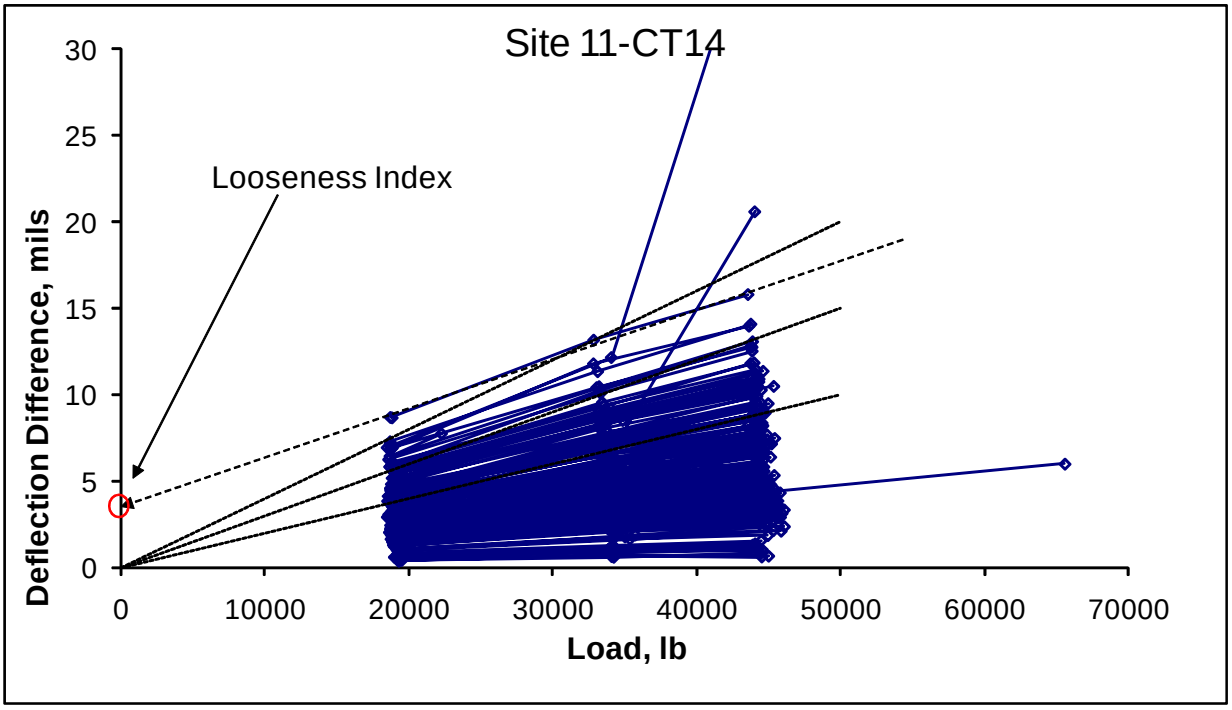

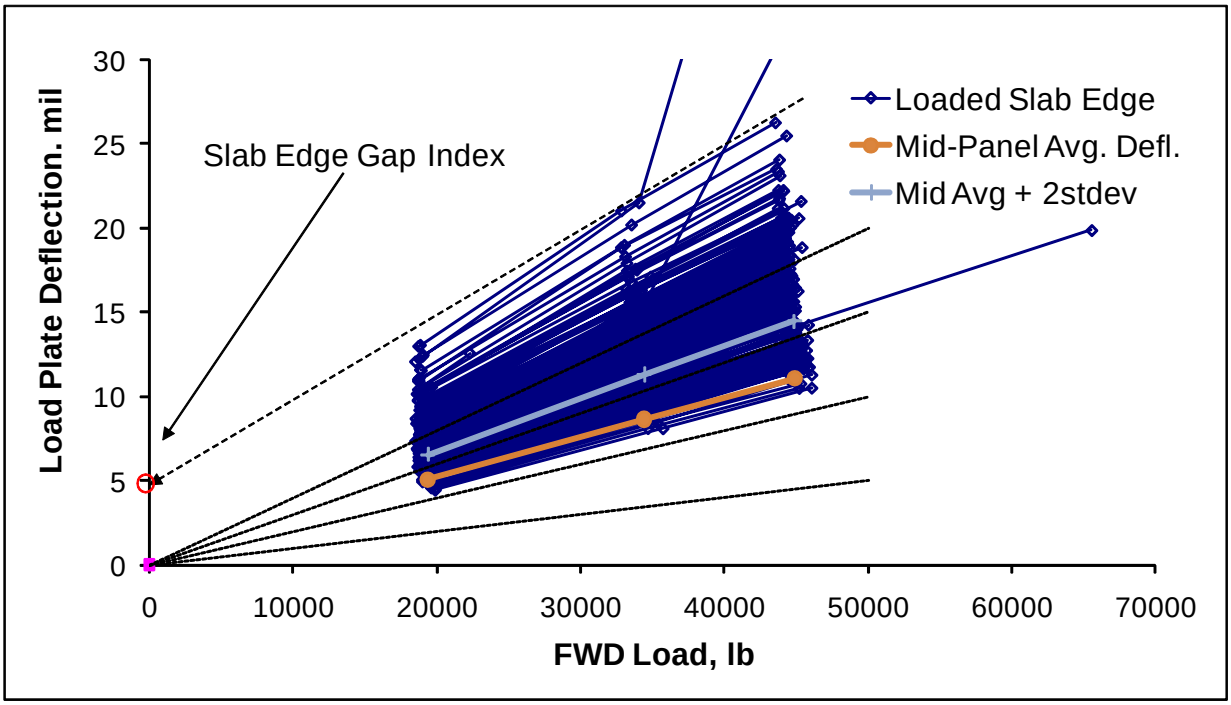

Site 11-CT14 Slab Edge Gaps- All Good Data

	All	AM	Mid	PM	Corners	Longit	Transv
Avg	0.64	0.88	0.50	0.53	1.05	0.60	0.54
Median	0.53	0.78	0.48	0.47	0.95	0.52	0.48
Min	-0.32	0.04	-0.08	-0.32	0.08	-0.03	-0.32
Max	2.93	2.93	1.43	1.70	2.93	2.58	1.85
Stdev	0.51	0.60	0.37	0.44	0.57	0.49	0.44

Site 11-CT14 Looseness- All Good Data

Looseness	All	AM	Mid	PM
Avg	0.678	0.873	0.553	0.609
Min	-0.131	0.030	-0.126	-0.131
Max	3.227	3.227	1.565	2.089
Stdev	0.521	0.632	0.344	0.493

Looseness	***All Good Data***	***Transverse***	***LongConst***	***Corners***
Average	0.68	0.62	0.57	1.31
Maximum	3.23	2.12	2.15	3.23
Minimum	-0.13	-0.13	-0.13	0.23
Std. Dev.	0.52	0.46	0.42	0.71
Count	213	100	63	18
19.3 kip %	0.096	0.087	0.081	0.185
34.1 kip %	0.056	0.050	0.047	0.107
44.5 kip %	0.043	0.039	0.036	0.083